

Discolouration by iron-phenolic interactions

Colourful insights into the
mechanisms and proposed
solutions for food
fortification

Discolouration by iron-phenolic interactions

Judith Bijlsma

2023

^{26}Fe



Judith Bijlsma

Propositions

1. Fe(III)-nucleotide salts are innovative iron fortificants for savoury foods.
(this thesis)
2. Reactivity of iron compounds is influenced by more than just their individual water solubilities.
(this thesis)
3. The food labelling information of micronutrients in meat analogues is misleading for consumers.
(Based on: Mayer Labba et al., Nutrients, 2022; 19: 3903)
4. Dehorning of cattle contradicts the basic principles of the animal welfare law.
(Based on: Menke et al., in Animal health and welfare in organic agriculture, 2004; 163-180 and Wet dieren; <https://wetten.overheid.nl/BWBR0030250/2022-12-22>)
5. Sharing layperson summaries of all scientific research output improves science communication.
6. Improved menstrual education for all empowers society to benefit from better time management throughout the menstrual cycle.
7. To 'let food be thy medicine' a 'fork to pharm(a)' strategy is required.

Propositions belonging to the thesis, entitled

Discolouration by iron-phenolic interactions

Colourful insights into the mechanisms and proposed solutions for food fortification

Judith Bijlsma

Wageningen, 14 September 2023

Discolouration by iron-phenolic interactions

Colourful insights into the mechanisms and proposed solutions for food fortification

Judith Bijlsma

Thesis committee

Promotor

Prof. Dr J.-P. Vincken
Professor at the Laboratory of Food Chemistry
Wageningen University & Research

Co-promotors

Dr W.J.C. de Bruijn
Assistant professor at the Laboratory of Food Chemistry
Wageningen University & Research

Prof. Dr K.P. Velikov
Senior Science & Program Leader
Unilever Innovation Centre Wageningen B.V.

Other members

Prof. Dr V. Fogliano, Wageningen University & Research
Prof. Dr A. Napolitano, University of Naples Federico II, Italy
Dr W.D.C. Schenkeveld, Wageningen University & Research
Dr L. Rossi, Delft University of Technology

This research was conducted under the auspices of the VLAG Graduate School (Biobased, Biomolecular, Chemical, Food and Nutrition Sciences).

Discolouration by iron-phenolic interactions

Colourful insights into the mechanisms and proposed solutions for food fortification

Judith Bijlsma

Thesis

submitted in fulfilment of the requirements for the degree of doctor
at Wageningen University

by the authority of the Rector Magnificus,

Prof. Dr A.P.J. Mol,

in the presence of the

Thesis Committee appointed by the Academic Board

to be defended in public

on Thursday 14 September 2023

at 1:30 p.m. in the Omnia Auditorium.

Judith Bijlsma

Discolouration by iron-phenolic interactions

Colourful insights into the mechanisms and proposed solutions for food fortification,
289 pages.

PhD thesis, Wageningen University, Wageningen, the Netherlands (2023)

With references, with summary in English

ISBN 978-94-6447-790-0

DOI <https://doi.org/10.18174/634568>

*Somewhere over the rainbow,
skies are blue, and the dreams
that you dare to dream
really do come true.*

Abstract

Food fortified with iron can effectively reduce the global prevalence of iron deficiency. However, when food is fortified with iron, its colour and the bioavailability of iron can be compromised by the reactivity of iron with phenolics. This research aimed to create insights into the chemistry of iron-phenolic interactions at the molecular level and to explore strategies to limit iron-phenolic mediated discolouration of fortified foods.

For the design of iron-fortified food products, it is important to understand the main factors that affect discolouration mediated by iron-phenolic interactions. To study this, a fractional factorial design was implemented. We concluded that the main factors affecting discolouration mediated by Fe(III)-catechol complexation were the type of iron salt, pH, and temperature. We created an integrated approach to unravel, for the first time, the combined contribution of three different iron-flavonoid interactions (*i.e.* complexation, oxidation, and the formation of networks) to discolouration in aqueous solution. Presence of the C2–C3 double bond in combination with the catechol B-ring (*i.e.* 3'-4' site) and either the 4-carbonyl or 3-hydroxyl group increased the intensity of discolouration, the extent of flavonoid oxidation, and the formation of metal-phenolic networks. We also investigated the effect of (acylated) 7-*O*-apiosylglucosyl substitution of naturally present flavones on the interaction with iron. The 7-*O*-apiosylglucosyl moiety led to increased discolouration for flavones possessing solely the 4-5 site, whereas a decrease in discolouration was observed for flavones with an additional 3'-4' site. Overall, the least discolouration was observed at low pH, for poorly water soluble phenolics without a catechol group, and when using a water insoluble iron salt.

To limit the discolouration mediated by iron-phenolic interactions, we designed water insoluble iron salts and compared these to the currently used ferric pyrophosphate (Fe_4PP_3). First, we synthesised mixed Ca-Fe(III) pyrophosphate salts with the general formula $\text{Ca}_{2(1-x)}\text{Fe}_{4x}(\text{P}_2\text{O}_7)_{(1+2x)}$ and $0 \leq x \leq 1$. The pH-dependent iron dissolution in aqueous model systems could be tuned by changing the *x*-value and was up to four times higher at gastric pH (*i.e.* improved bio-accessibility) and up to eight times lower at food pH (*i.e.* decreased reactivity) for the mixed salts with $x \leq 0.18$, compared to Fe_4PP_3 . Second, we synthesised Fe(III) salts with the taste enhancers inosine monophosphate (IMP) and guanosine monophosphate (GMP). The Fe_2IMP_3 and Fe_2GMP_3 salts were even more soluble at gastric pH and less soluble at food pH than the Ca-Fe(III) pyrophosphate salts. It was found in model phenolic systems at food pH that the colour changes for the $\text{Ca}_{2(1-x)}\text{Fe}_{4x}(\text{P}_2\text{O}_7)_{(1+2x)}$ salts with $x \leq 0.18$ and for the Fe_2IMP_3 and Fe_2GMP_3 salts remained acceptable for slightly water soluble and insoluble phenolics. We conclude that these newly designed Fe(III) salts can potentially serve as iron fortificants for food due to their increased iron solubility at gastric pH and decreased iron-phenolic reactivity at food pH.

Table of contents

Chapter 1	General introduction	1
Part I	Insights into iron-phenolic interactions	39
Chapter 2	Revealing the main factors and two-way interactions contributing to food discolouration caused by iron-catechol complexation	41
Chapter 3	Unravelling discolouration caused by iron-flavonoid interactions: Complexation, oxidation, and formation of networks	65
Chapter 4	Interactions of natural flavones with iron are affected by 7-O-glycosylation, but not by additional 6"-O-acylation	105
Part II	Strategies to limit iron-phenolic mediated discolouration	155
Chapter 5	Design and characterisation of Ca-Fe(III) pyrophosphate salts with tuneable pH-dependent solubility for dual-fortification of foods	157
Chapter 6	Reactivity of Fe(III)-containing pyrophosphate salts with phenolics: Complexation, oxidation, and surface interaction	185
Chapter 7	Interaction of iron(III) with taste enhancers: Potential of Fe(III) salts with inosine monophosphate or guanosine monophosphate for food fortification	217
Chapter 8	General discussion	247
Summary		273
Acknowledgements		279
About the author		285

CHAPTER 1

General introduction

General introduction

Food fortification to counter iron deficiency

•

Iron chemistry

•

Phenolics in fortified foods

•

Chemistry underlying iron-phenolic interactions

•

Iron fortification strategies to limit iron-phenolic interactions

•

Aim and outline of the thesis

1.1. Food fortification to counter iron deficiency

Current societal challenges are to fight hunger and combat all forms of (micronutrient) malnutrition, of which iron deficiency is one of the most prevalent forms. Iron fortification of food is an effective solution to counter iron deficiency. However, fortification of food with iron is challenging due to the reactivity of the iron ions with food ingredients (e.g. lipids, phenolics). Iron initiates lipid (per)oxidation and hereby induces rancidity. Additionally, iron-phenolic interactions in foods that contain plant material compromise product colour and impair the bioavailability of iron. The iron fortification compounds with the best bioavailability tend to be most reactive with the food matrix, leading to undesirable sensory changes of the product. In this thesis, we specifically focus on iron-phenolic interactions. Systematic knowledge of iron-phenolic chemistry and the main factors that influence iron-phenolic interactions and the resulting discolouration is lacking. This hampers the quest for strategies to optimise the design of stable iron-fortified foods. This thesis aims to create insights into the chemistry of iron-phenolic interactions at the molecular level and to explore strategies to limit iron-phenolic mediated discolouration.

1.1.1. Iron deficiency and anaemia

Iron is an essential micronutrient and a deficit of iron in the human body impairs health and quality of life. A deficit of iron causes fatigue and weakness, and results in poor work productivity and difficulty concentrating.^[1] Iron deficiency is defined as a decrease of total iron in the body, whereas iron deficiency anaemia occurs when iron deficiency is so severe that haemoglobin is no longer produced.^[1-3] Anaemia is defined by low levels of haemoglobin resulting in a lack of healthy red blood cells to deliver oxygen to the body's tissues. In addition to severe iron deficiency, anaemia can also be caused by other micronutrient deficits, immune disorders, hemoglobinopathies, or chronic-, gynaecological-, and infectious diseases. However, iron deficiency is the main cause of anaemia worldwide and accounts for at least half of the anaemia prevalence.^[1,4]

Anaemia is a global health problem, affecting one quarter of the world's population.^[5,6] The prevalence of anaemia differs per region and population group, and has the highest burden in women of reproductive age and children, especially in low- and middle-income countries.^[4,7] The prevalence of anaemia in women aged 15-49 is depicted in **Fig. 1.1**. The distribution of anaemia per region is similar for children but the total prevalence is even more severe. In total 40 % of the children (6-59 months) suffer from anaemia versus 30 % of women (15-49 years).^[7] Iron deficiency anaemia in women and children leads to increased maternal mortality, premature delivery, and increased infant mortality.^[9] The importance of micronutrients for children's health is underlined by the statement of Henrietta Fore from UNICEF: "*Although micronutrients may be micro, they are mighty for the world's children*".^[10]

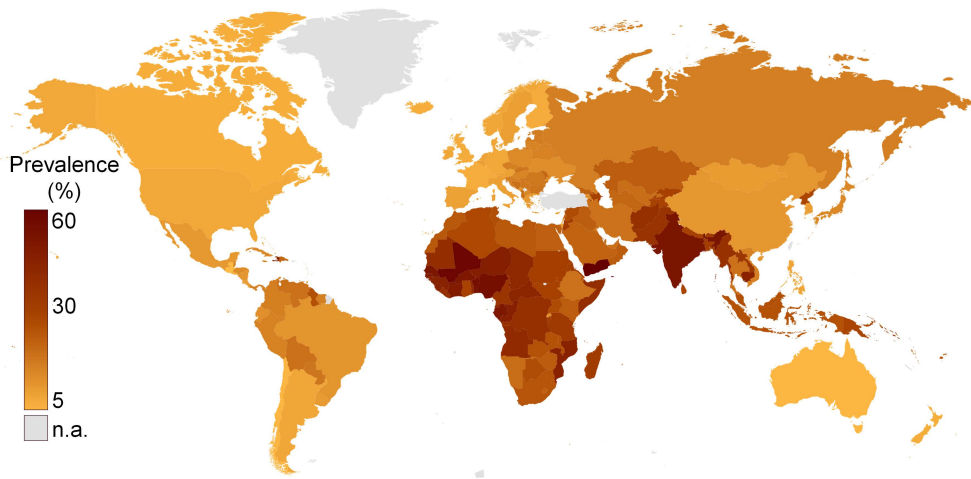


Figure 1.1. Overview of the prevalence (%) of anaemia in women of reproductive age (aged 15-49), n.a. data not available. Data extracted from the WHO Global anaemia estimates, 2021 edition.^[8] Iron deficiency is the main cause of anaemia worldwide and accounts for at least half of the anaemia prevalence.^[1,4]

Iron deficiency has multiple causes, amongst which poverty and malnutrition are the main causes in low- and middle-income countries. In high-income countries, well-known causes of iron deficiency are malabsorption, chronic blood loss during menstruation, and strict vegan and vegetarian diets.^[1,11,12]

The global nutrition target set by WHO in 2014, which is also one of the targets of the zero hunger sustainable development goal set by the UN, is to achieve a 50 % reduction of anaemia in women of reproductive age by 2025.^[13] However, the global prevalence of anaemia has not decreased since 2014 and even showed a slight increase (26.6 % vs. 27.3 %).^[8,14] Economic, food, and health system disruptions caused by the COVID-19 pandemic, and the energy and food insecurity due to the war in Ukraine will lead to a continuing increase in malnutrition and anaemia globally.^[15,16] Food fortification is one of the promising solutions to combat this growing burden of malnutrition.

1.1.2. Preventing iron deficiency through fortification of foods

The four main strategies to combat iron deficiency are supplementation (e.g. pills, capsules, syrups), dietary diversification, biofortification (i.e. improving the nutritional quality of food crops), and food fortification with iron.^[9,17] Of these four, food fortification offers the most cost-effective approach to deliver iron to the global population.^[5,18-20] Food fortification is the addition of one or more essential nutrients to food, aiming to prevent or correct a nutrient deficiency.^[5,9] Flour, sugar, and dairy products have traditionally been used as a vehicle for fortification. Additionally, condiments and seasonings, such as salts, bouillon cubes, soy sauce, curry, flavoured

salts, and flavouring agents such as monosodium glutamate, have also been investigated and/or implemented as fortification vehicles.^[21] These food stuffs are suitable fortification vehicles as they are consumed on regular basis in adequate amounts, as well as being widely available and affordable.^[5,19,22] Bouillon cubes in particular are a promising fortification vehicle as they reach large populations.^[22-25] Additionally, tea has also been investigated as a fortification vehicle as it is one of the most consumed beverages in the world.^[26]

1.1.3. The two types of dietary iron

In the diet, two types of iron can be distinguished: haem iron and non-haem iron. Haem iron originates from haemoglobin and myoglobin and is only present in animal-based sources, whereas non-haem iron is present in both vegetable and animal sources.^[27,28] The iron uptake from the two types of iron is different.^[29] Non-haem iron absorption occurs via the divalent metal transporter (DMT1) which is located at the proximal part of the duodenum and upper jejunum. Divalent (ferrous) iron can be transported directly and trivalent (ferric) iron is first reduced to the ferrous form by an enzyme and then transported by DMT1.^[29,30] The absorption of haem iron is to date still poorly understood.^[31] Generally, haem iron is better absorbed by the body (15-35 % absorbed) than non-haem iron (3-20 % absorbed), and dietary factors have less effect on its absorption.^[5,32,33] Haem iron is, however, less suitable for fortification because of its limited availability and affordability, its dark red to black colour, and its animal origin.^[34] Therefore, non-haem iron is mainly used for food fortification as it is cheap and easily available. Unfortunately, iron from these non-haem iron sources can have a negative impact on the sensory properties of the fortified product.

1.1.4. Challenges in iron fortification of foods

Iron is a highly challenging micronutrient for food fortification from the dietary perspective because the levels of added iron as fortificant should be regulated, and from the technological perspective because iron is so reactive.^[35]

Dietary challenges

The levels of iron to fortify food should be carefully balanced to ensure that consumers receive the necessary amounts of iron while minimising the risk of excessive iron intake.^[36] Iron catalyses a series of reactions (e.g. the Fenton reaction) in the body that result in the formation of reactive oxygen species (ROS).^[37] Thereby, excess levels of iron in the body can be toxic and may promote cancer, gastrointestinal distress, and cardiovascular diseases, and are linked to increased morbidity.^[12,20] An additional complicating factor is that an excess of iron can also increase the severity of malaria infection.^[38,39] Malaria is especially prevalent in low- and middle-income countries where iron fortification is most needed, thus warranting extra care in dosing iron to avoid excessive intake in these countries.^[40] It is challenging to ensure adequate iron levels due to the narrow range between the recommended intake (5-8 mg/day for children, 6-7 mg/day for adults) and the

maximum allowed intake for iron (40-45 mg/day for children, 45 mg/day for adults).^[36,41]

Additionally, other compounds present in the food may increase or decrease iron absorption, especially from non-haem iron. The main dietary enhancers for non-haem iron absorption are ascorbic acid and animal tissues (e.g. beef, chicken, fish, pork, and lamb).^[35,42] The nature of the enhancing effect of animal tissue is unclear but thought to be protein related, and is not related to the haem that is present in the animal tissue.^[43,44] Inhibitors for iron absorption are phytic acid and phenolics. These substances can form complexes with iron that are insoluble in the gut and therefore poorly absorbed.^[3,45] An excess of calcium (> 40 mg) in an iron containing meal can also lead to decreased absorption of non-haem iron.^[46] Calcium acts as a non-competitive inhibitor of iron transport with the DMT1.^[47,48]

Commercially fortified foods usually provide 15-30 % of the recommended iron intake per serving.^[49,50] It is also recommended that the fortification level is adjusted for the relative bioavailability of the iron compound.^[36,50] The effect of the food matrix on absorption should also be considered as differences in iron absorption, depending on the food matrix (i.e. bouillon, or a meal prepared from this bouillon), have previously been reported.^[23,51]

Technological challenges

Ideally, the sensory properties of a product (i.e. appearance, odour, taste, and texture) are not changed by iron fortification. However, iron fortification may cause unacceptable sensory changes due to rancidity as it initiates lipid (per)oxidation, undesirable colour changes, and metallic aftertaste.^[52] The adverse effect of iron fortification on the sensory properties of food results in poor acceptance of the fortified product by consumers.^[35,53] The undesirable colour changes and lipid (per)oxidation induced rancidity are the main factors limiting the successful introduction of iron-fortified foods to the market. The focus of this study is on the undesirable colour changes that are introduced upon iron fortification.

The main mechanism described for colour change in fortified foods is the complexation of iron to phenolics, resulting in blue or black products.^[54-56] An additional disadvantage, besides the discolouration caused by these iron-phenolic complexes, is the fact that these complexes are generally poorly soluble.^[3,45] The absorption of (non-haem) iron from these complexes can be reduced up to 90 %, although the extent of reduction depends on the phenolic backbone and quantity.^[57-59] Moreover, the oxidation of the phenolic and/or iron may also result in brown or red colour formation. To ensure the acceptance of fortified products and the bioavailability of iron, it is important to prevent the formation of strongly coloured products and/or insoluble iron-phenolic complexes. Consequently, the chemistry

underlying the formation of these coloured iron-phenolic interaction products should be understood and potential strategies to prevent its formation should be explored.

1.2. Iron chemistry

Iron is a chemical element with atomic number 26 and an atomic weight of 55.85. The four naturally occurring iron isotopes are Fe⁵⁶ (91.8 %), Fe⁵⁴ (5.8 %), Fe⁵⁷ (2.1 %), and Fe⁵⁸ (0.3 %).^[60] The electronic configuration of iron in the metal (0) oxidation state is [Ar] 3d⁶4s². The most common oxidation states of iron in nature and used for food fortification are 2+ (*i.e.* the ferrous form, Fe(II); [Ar] 3d⁶) and 3+ (*i.e.* the ferric form, Fe(III); [Ar] 3d⁵).^[52] The unpaired electrons in the 3d-orbitals give rise to the magnetic properties of iron, the spin state, and the reactivity of iron. Iron, in its native form, rapidly reacts with oxygen to form iron oxides, or with water or moist air to form iron hydrolysis products (**text box 1.1**).^[61]

Text box 1.1. Iron hydrolysis

When the iron ion is dissolved in water it will form aqua complexes [Fe(H₂O)₆]³⁺ and [Fe(H₂O)₆]²⁺. In aqueous media, the iron aqua complexes can undergo subsequent hydrolysis reactions that are represented by the following equation:

$$[\text{Fe}(\text{H}_2\text{O})_n]^{z+} + \text{H}_2\text{O} \rightleftharpoons [\text{Fe}(\text{H}_2\text{O})_{n-1}(\text{OH})]^{(z-1)+} + \text{H}_3\text{O}^+$$

Iron can be octahedrally coordinated (*i.e.* coordinated to six atoms) to O²⁻, OH⁻ or H₂O resulting in the formation of oxides and hydroxides.^[60,62] The species of iron that are present in an aqueous solution are dependent on pH and the redox potential (E_h) of the environment (**Fig. 1.2A**). At higher E_h Fe(II) oxidises to Fe(III). Fe(II) also oxidises to Fe(III) at higher pH to form insoluble iron (hydr)oxide species (*i.e.* Fe₂O₃ or Fe(OH)₃).^[62] Initially, these (hydr)oxide species are yellow, but due to polymerisation a red precipitate is formed in time (**Fig. 1.2B**).^[62-64]

As mentioned in **section 1.1.3**, iron exists in haem and non-haem forms that differ in their absorption, but also in their chemical structure and behaviour. In haem iron, iron is contained within the porphyrin ring structure (**Fig. 1.2C**). The Fe(II) contained in or bound to the porphyrin ring shows reduced (oxidative) reactivity. Non-haem iron (both as inorganic or organic iron compounds) is present in the diet as either the Fe(II) or Fe(III) form. Non-haem iron includes iron salts, iron in low-molecular-weight complexes, ferritin, and in catalytic sites of enzymes.^[27,69]

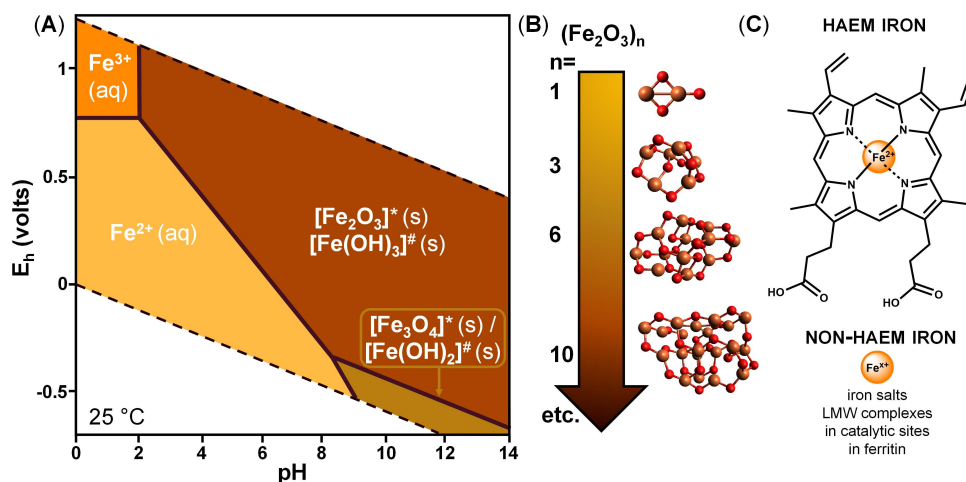


Figure 1.2. (A) Pourbaix (E_h -pH) diagram for iron, the diagram was produced using Geochemist's Workbench (Edition 17.0; $\text{Log} a_{\text{Fe}^{2+}} = -6$). *In a dry environment mainly oxides are formed. #In a humid environment mainly hydroxides are formed.^[52,65-67] Aqueous species are indicated by (aq) and solid species by (s). The dashed lines indicate the boundaries for oxidation and reduction of water. (B) The polymerisation of Fe_2O_3 to polynuclear species (Fe orange, O red) adapted from Erlebach *et al.*^[68] the arrow indicates the colour change from yellow to red due to polymerisation. (C) The structure of haem and non-haem iron.

1.3. Phenolics in fortified foods

Phenolic compounds are characterised by their structure, which contains at least one benzene ring substituted with one or more hydroxyl groups. Phenolics are secondary plant metabolites that are ubiquitous in vegetables, herbs, and fruits and are therefore present in many foods. In nature, more than 8,000 phenolics exist that are classified as (iso)flavonoids and non-flavonoids, the last group of which includes phenolic acids, lignans, and stilbenes.^[70,71] Savoury concentrates (e.g. bouillon cubes, soy sauce) and tea are examples of potential fortification vehicles that are rich in phenolic compounds (Fig. 1.3).

The main herbs and spices that are generally present in bouillon cubes are parsley, celery, and turmeric which contain phenolic compounds of the flavone (e.g. apigenin and luteolin) and curcuminoid (e.g. curcumin) subclasses.^[72,73] Soy sauce is especially rich in isoflavones, such as genistein.^[75] Green tea leaves mainly contain catechins which belong to the flavanol subclass but also contain some flavonols such as quercetin.^[76] Black tea phenolics are a mixture of dimeric, oligomeric, and polymeric oxidation products of flavanols.^[77] In nature, substitution of the phenolic backbone, e.g. by hydroxylation, methylation, methoxylation, acylation, glycosylation, or prenylation yields diverse phenolic structures with widely varying properties.^[78] For example, glycosylation of phenolic compounds reduces their reactivity and enhances their solubility in water.^[70,79,80]

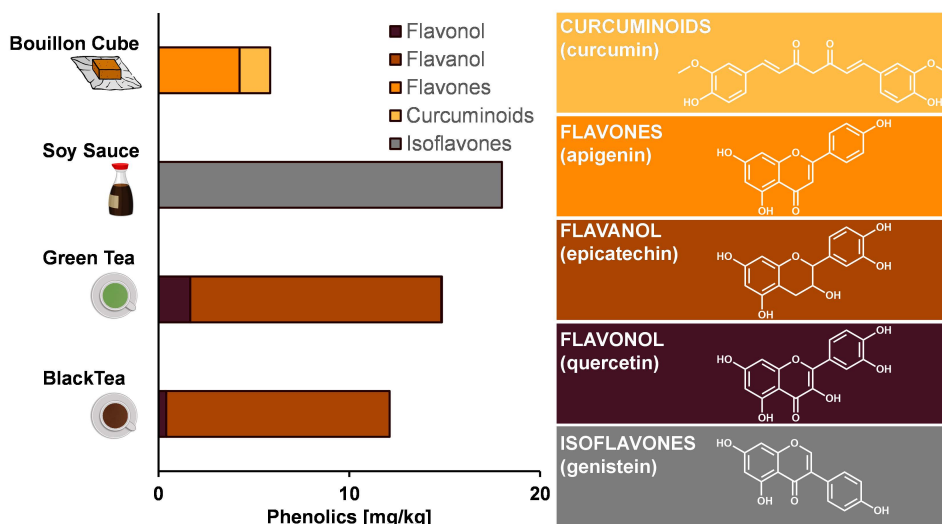


Figure 1.3. Chart indicating the phenolic content and composition of four potential fortification vehicles. The phenolic contents were obtained and calculated based on data from King *et al.*, Yashin *et al.*, Haytowitz *et al.*, and Fukutake *et al.*[72–75] Examples of phenolics belonging to the curcuminoid, flavone, flavanol, flavonol, and isoflavone subclasses are shown on the right.

1.4. Chemistry underlying iron-phenolic interactions

To date, the chemical interactions between iron and phenolics, which include complex formation and redox processes, and the resulting discolouration, have not been fully elucidated.^[81]

1.4.1. Formation of iron-phenolic coordination complexes

Iron has rich coordination chemistry and, as both Fe(II) and Fe(III) contain unfilled d-orbitals, it can form octahedral complexes with a large number of ligands.^[52,62,82,83] These coordination complexes, where a coordinate bond (*i.e.* dative covalent bond) is formed between a metal and ligand, are also known as Lewis acid-base complexes. Here, a Lewis acid is defined as a species that has empty orbitals and can accept an electron pair (electrophile), whereas a Lewis base is a species that can donate a lone electron pair (nucleophile). In these complexes, the bases react with acids to share an electron pair without a change in oxidation number. Lewis acids and bases are classified as being soft, borderline, or hard, based on their ionic radius, orbital energy, electronegativity, and polarisability.^[84] According to the concept of hard and soft acids and bases (HSAB), hard acids prefer to coordinate hard bases and soft acids prefer to coordinate soft bases.^[85,86] In this study, we work with iron as metal and phenolics as ligands. Fe(II) is a borderline acid and therefore favours coordination to borderline Lewis bases such as nitrogen and sulphur.^[86] Fe(III) is a hard Lewis acid, that favours coordination to hard Lewis bases such as oxygen, hydroxide, water, phosphate, and sulphate. The phenolate group of phenolics is particularly favoured as a coordination

site for hard Lewis acids as it is electron-rich and can therefore easily donate electrons to Fe(III).^[52,81,84,85]

Phenolics, especially those that possess two hydroxyl groups in the *ortho* position (*i.e.* *ortho*-diphenolic; catechol), often coordinate iron in a bidentate fashion, meaning that one phenolic can form two coordinate bonds with a single iron (**Fig. 1.4A**).^[87] The bidentate coordination of phenolics to Fe(III) results in the formation of stable chelation complexes.^[87] However, the catecholate group is not a prerequisite for Fe(III) complexation to phenolics, as Fe(III) can also coordinate to other oxygen containing groups of phenolic compounds. The complexation of phenolics to Fe(II) in presence of molecular oxygen (O_2) is followed by fast auto-oxidation to Fe(III) because of the higher stability of the Fe(III)-phenolic complex (**Fig. 1.4A**).^[88,89]

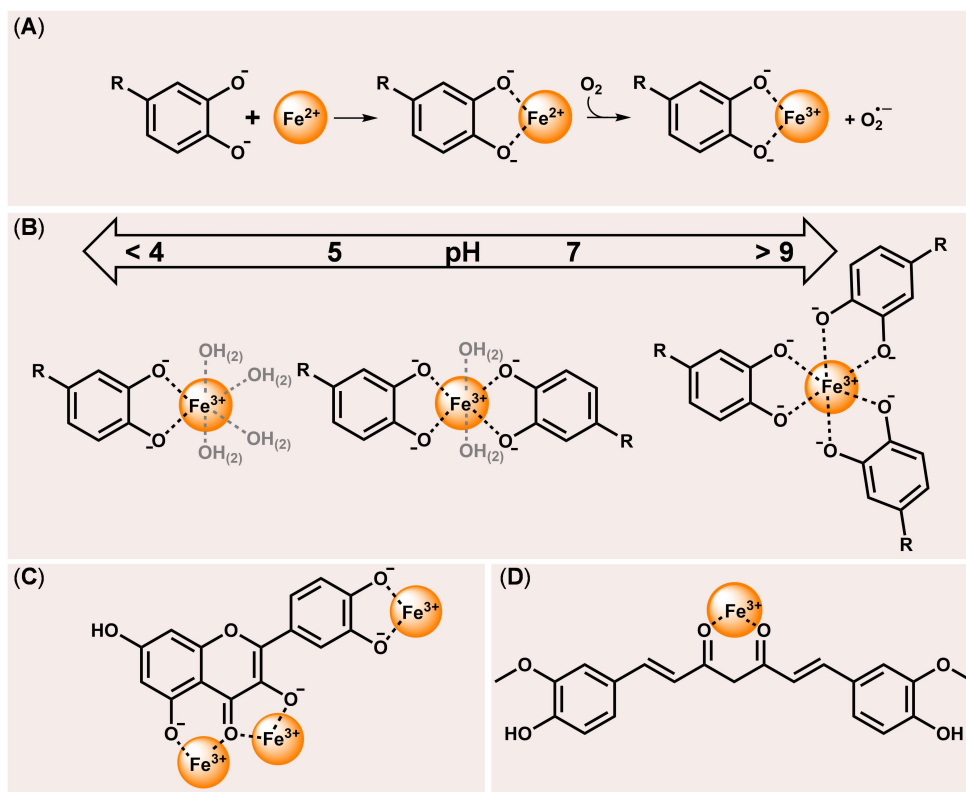


Figure 1.4. (A) Coordination of Fe(II) by phenolics and one of the proposed mechanisms for auto-oxidation generating the Fe(III)-phenolic complex.^[88] (B) The stoichiometry of iron-phenolic complexes with iron to phenolic ratios of 1:1, 1:2, and 1:3 as influenced by pH. The mixed hydroxo species ($OH_{(2)}$) for the 1:1 and 1:2 complex are indicated in grey. (C) Multiple iron complexation sites of quercetin. (D) Complexation of Fe(III) to curcumin.

The pH strongly influences the complexation of iron to phenolics because it affects the deprotonation of phenolics and the hydrolytic processes of iron. At elevated pH,

when the hydroxyl group is deprotonated, the anionic phenolates coordinate to the cationic iron. Typically, the pK_a of phenolics is 9-10.^[81] However, in presence of iron, the deprotonated state of the phenolic is stabilised and thermodynamically more favourable, leading to a decrease of the apparent pK_a to 5-8.^[87,90] Iron can coordinate up to three catecholate groups, creating an octahedral geometry around the iron centre (**Fig. 1.4B**).^[81] The stoichiometry of the iron-phenolic complexes is dependent on the ratio of iron and phenolic, the concentration of iron and phenolic, phenolic structure, solvent, and pH.^[81,91] The formation of mixed hydroxo complexes in an aqueous solution is also an option for Fe(III)-phenolic complexes with 1:1 or 1:2 iron to phenolic stoichiometry (**Fig. 1.4B**).^[92,93] Some phenolics, for example, the ones belonging to the flavonoid subclass, possess multiple iron chelation sites and can coordinate multiple Fe(III) ions (**Fig. 1.4C**).^[94] Additionally, Fe(III) can also form stable, dark-coloured, complexes with the diketone group of curcumin (**Fig. 1.4D**).^[95,96]

Coordination-driven network formation of iron and phenolics

More recently it has been reported that metal-phenolic complexation can also lead to the formation of self-assembled supramolecular network structures. These so-called metal-phenolic networks (MPNs) are formed as a result of the coordination-driven cross-linking of metals and phenolics.^[97,98] For example, the formation of such networks has been reported for the combination of Fe(III) with phenolics with multiple chelation sites (*e.g.* tannic acid).^[97,99-101] The formation of metal-phenolic networks on the surface of solid substrates (*e.g.* polystyrene) has also been demonstrated for flavonoids.^[98,102] It has not yet been investigated whether Fe(III) can also form these networks with dietary phenolics in aqueous food model solutions in absence of these substrates. MPNs are less straight forward to analyse compared to the mononuclear iron-phenolic complexes due to the complexity of their structure, larger molecular size, and the poor solubility of the networks. Thus, the structural requirements for the formation of MPNs of dietary phenolics with iron and its possible effect on discolouration and solubility in iron-fortified food are still unknown.

Stability of iron-phenolic complexes

The stability of iron-phenolic complexes is governed by two aspects; thermodynamic and kinetic stabilities. In general, the terms stable and unstable relate to thermodynamic stability. The thermodynamic stability of these complexes refers to the tendency of the complex to exist under equilibrium conditions. Complexation equilibria of metals and ligands in an aqueous solution, excluding the aquo ions, can be described by **equation 1.1**, in which M is the metal ion (*e.g.* iron), and L is the ligand type involved (*e.g.* phenolic), n represents the number of ligands, and ML_n is the complex.^[103] The expression of the overall stability constant, β , is defined by **equation 1.2**, in this expression the square brackets denote the concentration.



$$\beta = \frac{[ML_n]}{[M][L]^n} \quad (\text{Eq. 1.2})$$

It has been observed that the addition of ligands to the metal centre in solution occurs step-by-step as defined by the stepwise stability constant, K_n (equations 1.3 and 1.4).^[103] The overall stability constant (β) is the product of the stepwise stability constants ($\beta_n = K_1K_2K_3 \dots K_n$).



$$K_n = \frac{[ML_n]}{[ML_{n-1}][L]} \quad (\text{Eq. 1.4})$$

A higher Log β value indicates a more stable complex between the metal and ligand. If the value of Log β is more than 8, the complex is considered thermodynamically stable.^[104] The formed complexes of phenolics with Fe(III) have Log β values > 40 and are thermodynamically very stable (Table 1.1).^[105] For comparison, complexes of Fe(III) with the popular chelating agent EDTA have Log β values of 25.^[81,106,107] The fact that phenolics stabilise Fe(III) over Fe(II), as indicated in Fig. 1.4A, is also reflected by the higher stability constants of the Fe(III) complexes compared to the Fe(II) complexes (Table 1.1).^[81] It is important to note that the stability of a metal complex is dependent on several factors and the solution conditions (e.g. pH, temperature, ionic strength).

Table 1.1. Reported stability constants for catechol and selected food phenolics with Fe(II) and Fe(III). Note: the stability of the complex is dependent on the solution conditions (e.g. pH, temperature, ionic strength).

Phenolic	Iron	Log β	Log K_1	Log K_2	Log K_3	Reference
Catechol	Fe(II)	13.5	7.9	5.6	-	[107]
	Fe(II)	-	8.4	-	-	[110]
	Fe(III)	43.7	20.0	14.7	9.0	[106]
Catechin	Fe(III)	47.4	21.8	15.7	9.9	[54]
Curcumin	Fe(III)	41.4	-	-	-	[111]
Quercetin	Fe(II)	13.3	9.4	3.9	-	[112]
	Fe(III)	44.2	-	-	-	[92]

The stability constants of complexes provide insights into the strength of the complexation and can be used to perform speciation modelling. With the speciation modelling of metal-ligand complexes, the concentrations of metal-ligand species can be predicted over a pH range in solution. Although iron-phenolic complexation has long been studied, only a few stability constants have been reported and the determination of constants for poorly water soluble or water insoluble iron-phenolic complexes is difficult.^[108,109]

The kinetic stability of iron-phenolic complexes has also been explored previously. Thermodynamically stable complexes are not necessarily kinetically stable. Kinetic

stability is classified as labile or inert and is based on how fast a metal coordinates to the ligand. Metal complexes that react within 1 min are classified as labile complexes as they undergo rapid ligand substitution. Iron-phenolic complexation is fast (< 1 min),^[113,114] indicating that the complexes are kinetically labile.^[115] The lability of the complexes indicates that the exchange of the phenolic coordinate bond with other ligands (e.g. water or EDTA) can occur. Overall, iron-phenolic complexes are thermodynamically stable and kinetically labile, which is a common relationship for metal complexes.^[105]

1.4.2. Analytical challenge of iron-phenolic complexes: solving the insoluble

The analysis of iron-phenolic complexes is complicated due to the insoluble nature of many complexes and hydrolytic processes in aqueous solutions. Additionally, the lability of the complexes can cause exchange or continuation reactions before or during analysis. In this section, we provide an overview of the most common methods used to analyse iron-phenolic complexes. **Table 1.2** provides an overview of previously reported analyses of iron complexes with the main phenolics that are present in fortification vehicles (**Fig. 1.3**), *i.e.* apigenin, (epi)catechin, curcumin, genistein, luteolin, and quercetin. Quercetin has been most widely investigated due to its ubiquity in nature. Only a few studies have investigated multiple phenolic (sub)classes and compared the effect of the structural variation on their iron complexing ability. Water is the preferred solvent for analysis because we are interested in iron-phenolic complexes in food products. However, due to their limited water solubility, most of the iron-phenolic complexes of interest have been studied in organic solvents and only few studies have investigated iron-phenolic complexation in aqueous solution.

It is known that the presence of water molecules or other solvent molecules can have a strong influence on the structure of the formed (mixed hydroxo) complex, and its colour and stability.^[116-119] In studies in which measurements have been performed in an aqueous solution or mixed solvent system, buffer compounds have been used to set the pH. However, it is often overlooked that buffer compounds can interfere with the complexation reaction.^[120,121] Phosphates in particular demonstrate strong complexing ability with iron.^[122,123] Additionally, most studies did not investigate the full pH range that is relevant for food products (3-7), gastric (1-3), and intestinal (6-8) conditions.

Table 1.2. Overview of the analysed iron-phenolic complexes, the solvent used for analysis, its pH, and the characterisation methods.

Phenolic ^a	Solvent ^b	pH	Characterisation Method ^c	Ref.
Cat	Water	2, 4, 6, 8	UV-Vis, colourimeter	[26,55,124]
Curc	Methanol	1-9	UV-Vis, FT-IR	[125-128]
Curc	Methanol-Water	1.5-7	UV-Vis, FT-IR, Raman, potentiometry, ¹ H-NMR	[129,130]
Curc	Ethanol-Water	3.5-5.7	UV-Vis, ESI-MS, MALDI-TOF-MS	[111,131,132]
Curc	Propylene glycol-Water	n.d.	UV-Vis, MS, FT-IR	[95]
Lut	Ethanol	5.6	UV-Vis, FT-IR, ESI-MS	[133]
Lut	Hot water (90°C)	n.d.	ESI-MS	[134]
Lut	Water and Ethanol	n.d.	Potentiometry, UV-Vis	[135]
Quer	Methanol	n.d.	UV-Vis, ESI-MS, ¹ H-NMR, FT-IR, DFT, EPR	[119,136-140]
Quer	Methanol-Water	2-12	ESI-MS, UV-Vis, EPR	[114,141-144]
Quer	Dioxane-Water	n.d.	UV-Vis, potentiometry	[112]
Quer	Water	4 - 11	UV-Vis, potentiometry, ¹ H-NMR, ¹³ C-NMR	[92,145]
Cat, Quer	(DMSO-)phosphate buffer	7.2-7.4	UV-Vis, microcalorimetry	[113,144,146]
Cat, Quer	MES buffer	6	UV-Vis	[88]
Cat, Quer	(DMF-)acetate buffer	3 - 8	UV-Vis	[57,141,147]
Cat, Lut, Quer	Methanol-Water (0.1 % acetic acid)	< 5.5	ESI-MS	[148,149]
Api, Cat, Lut, Quer	DMSO-acetate, DMSO-HEPES	4.5, 5.5, 6.8, 7.5	Ferrozine assay	[150]
Api, Cat, Gen, Lut, Quer	Acetate buffer, MOPS buffer	5.5, 7.4	UV-Vis	[148]

^a Api: apigenin; Cat: (epi)catechin; Curc: curcumin; Gen: genistein Lut: luteolin; Quer: quercetin

^b DMSO: dimethyl sulfoxide; MES: 2-morpholin-4-ylthanesulfonic acid; DMF: dimethylformamide; MOPS: 3-(morpholin-4-yl)propane-1-sulfonic acid; HEPES: 2-[4-(2-hydroxyethyl)piperazin-1-yl]ethane-1-sulfonic acid

^c UV-Vis: ultraviolet-visible spectroscopy; MS: mass spectrometry; ESI-MS: electrospray ionisation ion trap mass spectrometry; NMR: nuclear magnetic resonance spectroscopy; FT-IR: Fourier transform infrared spectroscopy; DFT: density functional theory; EPR: electron paramagnetic resonance spectroscopy

The studies from **Table 1.2** indicated different stoichiometry, complex stability, phenolic oxidation, and colour of the phenolics with iron, depending on the oxidation state of iron, used solvent, pH, and analytical method. The various characterisation methods each provide specific information regarding the concentration, speciation, binding sites, molecular mass, or colour of the complex. In **Table 1.3** we provide an overview of the commonly used analytical techniques for the structural characterisation of iron-phenolic complexes, including the principle of the technique, the specific features it analyses, and the main drawbacks. This overview offers guidelines on which technique to employ for answering certain research questions. The required analysis time and state of the sample (e.g. solid, aqueous) are included as well.

Conventional techniques to obtain stability constants and to determine the stoichiometry of complexes in solution are potentiometry and spectrophotometry (UV-Vis). However, these techniques only provide indirect information about the stoichiometry and number of species (e.g. ML, ML₂, etc) formed, as the obtained data is often treated by speciation models where certain assumptions are made to obtain a model with the best fit.^[152,164,165]

Table 1.3. Common analytical methods for the structural characterisation of coordination complexes.

Characterisation Method	Potentiometry	UV-Vis ^a	¹ H-NMR, ¹³ C-NMR ^b	ESI-MS ^c	FT-IR or Raman ^d	MALDI-TOF-MS ^e	DFT ^f
Main principle	Determination of stability constants by measurement of pH upon titration of base. The competition of ligand for H ⁺ and metal is measured.	UV-Vis absorption provides insight in electronic transitions of parent compound and changes upon metal complexation (e.g. $\pi \rightarrow \pi^*$ or $\pi \rightarrow d_{sp}$).	Upon complexation chemical shifts of protons and carbons of the parent compound are indicative for where the metal binds.	Mass spectra provide insight in the stoichiometry of a complex and in the preferred binding site.	Metal complexation affects the vibrational energy of specific bonds in the parent compound, providing insight in preferred binding site.	Mass spectra provide insight in the molecular mass and stoichiometry of complexes in solid state.	Computational technique to predict molecular structure, vibrational frequencies, and electric and magnetic properties
Stability constants	✓	✓	✓	✓	X	X	✓
Stoichiometry	✓	✓	X	✓	X	✓	✓
Binding site	X	✓	✓	✓	✓	X	✓
Molecular weight	X	X	X	✓	X	✓	✓
Colour	X	✓	X	X	X	X	X
State	(Aqueous) Solution	Solution	Solution	Solution/Gas	Liquid, solid, gas	Solid	Vacuum, Solvent
Analysis time	3-24 hours	< 1 min	< 1 hour	< 30 min	< 10 min	< 10 min	Hours
Drawbacks	<ul style="list-style-type: none"> Indirect information only by treatment of the data with models using specific software packages. Only provides information about the soluble species. 	<ul style="list-style-type: none"> Absorption spectra influenced by solvent and pH. Determination of stoichiometry and binding sites only indirect (e.g. via Job's method). 	<ul style="list-style-type: none"> High cost of deuterated solvents and the equipment. The magnetic nature of iron will negatively affect the signal. 	<ul style="list-style-type: none"> Ionisation may change composition of the complex (e.g. by addition of solvent molecules or adduct formation). Ions can undergo reactions in the gas phase. 	<ul style="list-style-type: none"> Water vapor gives high signal, making measurement in aqueous solution more complex. Cannot distinguish individual species in mixtures. 	<ul style="list-style-type: none"> Ionisation may change composition of the complex Selecting the right matrix can be laborious and is analyte dependent. Identification of LMW species less reliable. 	<ul style="list-style-type: none"> Comparison with experimental data needed. Complications with reactions in solution due to errors with solvent modelling.
Reference	[151-153]	[81, 121, 154]	[130, 140, 144, 155]	[148, 152, 156, 157]	[158, 159]	[111, 160-162]	[111, 118, 119, 145, 163]

^a ultraviolet visible spectroscopy, ^b ¹H nuclear magnetic resonance, ¹³C nuclear magnetic resonance; ^c electrospray ionisation ion trap mass spectrometry; ^d Fourier transform infrared spectroscopy or Raman spectroscopy; ^e matrix assisted laser desorption ionisation time of flight mass spectrometry; ^f density functional theory

To obtain qualitative information about the complexes, additional information can be acquired by NMR, FT-IR, or Raman spectroscopy, or by ESI-MS and MALDI-TOF-MS. Most of these techniques require the complex to be in (aqueous) solution for characterisation, although some are suitable for analysis of insoluble complexes. Additionally, computational methods are widely used to study the structure of the formed complexes and to predict the IR and electronic spectroscopic properties. For the full characterisation of multiple structural features of iron-phenolic complexes and colour a combination of the methods mentioned in **Table 1.3** is required.

1.4.3. Oxidation of phenolics in presence of iron

Complex formation between Fe(III) and phenolics can be followed by an electron transfer (ET) from the phenolic to iron.^[143,166,167] In this process, Fe(III) is reduced to Fe(II) and simultaneously the phenolic is oxidised. In the case of bidentate coordination to an *ortho*-diphenolic compound, a semiquinone-type radical is formed after the first ET and upon a second ET an *ortho*-quinone will be formed (**Fig. 1.5A**).^[87,168,169] Additionally, the oxidation of phenolics has been reported after monodentate coordination and under non-complexing conditions (e.g. low pH, in presence of chelating agents) via a reversible direct electron transfer from the phenolic to Fe(III), (**Fig. 1.5B**).^[114,168,170] Both reactions depicted in **Fig. 1.5** yield *ortho*-quinones that are highly reactive and their continuation reactions can result in a plethora of reaction products.^[71]

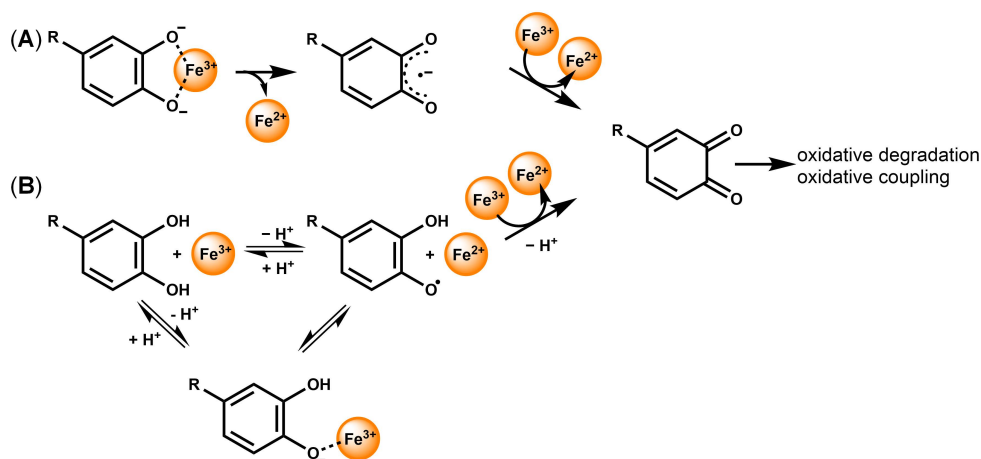


Figure 1.5. Schematic representation of the oxidation of a phenolic to a semiquinone-type radical and eventually to a quinone in presence of Fe(III) via **(A)** electron transfer after bidentate complexation, adapted from Perron *et al.*,^[81] or **(B)** direct electron transfer after monodentate coordination or in non-complexing conditions adapted from Hajji *et al.*, Hynes *et al.*, and Jameson *et al.*^[114,168,170]

Most of the studies on iron-phenolic interactions have focussed primarily on the analysis of iron-phenolic complexes and only a few studies have separately assessed the iron-mediated oxidation of phenolics.^[113,114,171] In those studies that have investigated iron-mediated oxidation of phenolics, it has been studied spectrophotometrically by use of UV-Vis. This method allows to determine the kinetics of the electron transfer reaction but does not allow identification and quantification of the reaction products that follow from continuation reactions of the *ortho*-quinones. Additionally, the corresponding mechanism for iron-mediated oxidation of the selected food phenolics that are of interest for the fortification vehicle (e.g. quercetin, luteolin, apigenin, catechin) is poorly documented. And so is the effect of iron-mediated oxidation of these selected phenolics and its products on colour. To obtain comprehensive insights into the oxidation of these phenolics by iron and its effect on colour, the reaction products should be identified and quantified. The identification of the oxidative degradation and oxidative coupling products can also be used to elucidate the iron-mediated oxidative mechanism of these phenolics.

1.4.4. Colour changes as a result of iron-phenolic interactions

Colour change by iron-phenolic complexation

The UV-Vis absorption properties of phenolics in absence of metals are generally attributed to electronic transitions between the delocalised π -type molecular orbitals.^[172,173] Complexation of Fe(III) to deprotonated phenolics leads to fast and intense discolouration and a bathochromic shift in the UV-Vis spectra.^[54,55,124] These shifts are attributed to either $\pi \rightarrow \pi^*$ transitions (**Fig. 1.6A**) or LMCT ($\pi \rightarrow d_\pi$) transitions (**Fig. 1.6B**).^[91,118,144]

The $\pi \rightarrow \pi^*$ transitions are a result of an electron that moves from the bonding π -orbitals in the highest occupied molecular orbital (HOMO) of the ligand to the antibonding π^* -orbitals in the lowest unoccupied molecular orbital (LUMO) of the ligand (**Fig. 1.6C**).^[118] Bathochromic shifting of these $\pi \rightarrow \pi^*$ transition bands upon Fe(III) complexation (**Fig. 1.6A**) has been reported to be a result of an increase in the size of the conjugated system, resulting in a decrease in the energy gap between the HOMO and LUMO states.^[118,121,141,174] The wavelength (λ) and energy gap (E) between the HOMO and LUMO are inversely related according to the Planck relation ($E = hc/\lambda$) (**Fig. 1.6C**).

Fig. 1.6D depicts one likely general representation of the molecular orbital energy diagram for octahedral Fe(III) complexes and provides further information about the various ligand-to-metal charge transfer (LMCT) transitions on the molecular orbital level. On the left the metal d-orbitals (i.e. Fe(III)) are depicted, on the right the ligand orbitals, and in between the molecular orbitals for the complex.

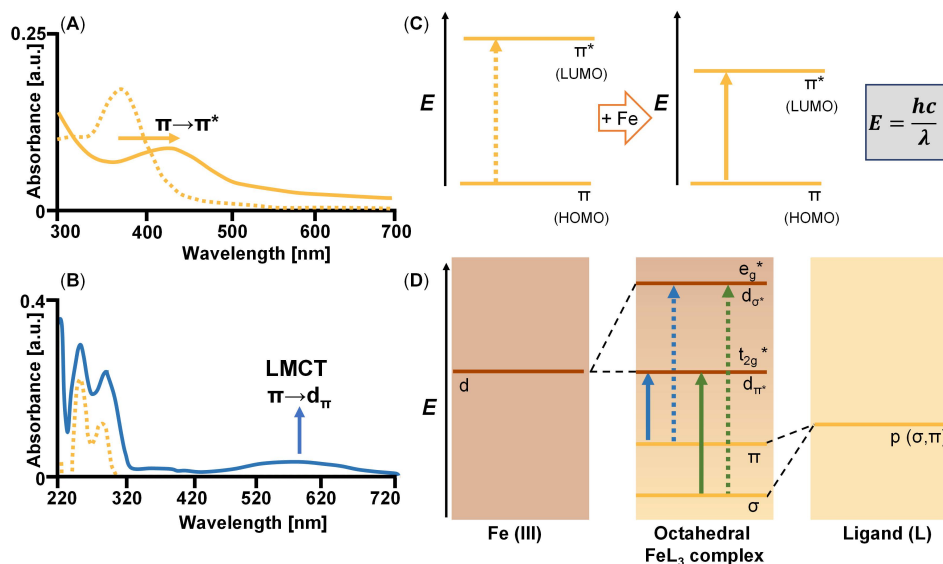


Figure 1.6. (A) Bathochromic shifting of the phenolic $\pi \rightarrow \pi^*$ transition absorption band from 372 nm (yellow dotted line) to ~425 nm (solid line) in presence of Fe(III), demonstrated here for quercetin at pH 7.2 based on data extracted from Guo *et al.*^[144] (B) Absorbance spectra of phenolic (yellow dotted line), in presence of Fe(III) the LMCT ($\pi \rightarrow d_\pi$) transition band appears as a broad band with a maximum at 550-600 nm (blue line), demonstrated here for dihydroxybenzoic acid (DHBA) at pH 7.4 based on data extracted from Andjelković *et al.*^[121] (C) Schematic overview of the $\pi \rightarrow \pi^*$ transitions in phenolic ligands, complexation with Fe moves the HOMO and LUMO states closer in energy.^[118] (D) Schematic molecular orbital energy diagram depicting possible ligand-to-metal charge transfer (LMCT) transitions for iron(III) in an octahedral environment of σ - and π -donor ligands, adapted from Reinen *et al.*^[175] The $\pi \rightarrow d$ transitions are indicated in blue and the $\sigma \rightarrow d$ transitions in green. The main transition that has been reported to be responsible for the absorption in the visible region upon Fe(III)-phenolic complexation is the $\pi \rightarrow d_\pi$ transition indicated by the solid blue line.^[54,176]

When an octahedral transition metal complex is formed, the 3d-orbitals of the free iron split into different energy levels indicated by the t_{2g} and e_g -orbitals in Fig. 1.6D.^[115] The three t_{2g} -orbitals (i.e. d_{xy} , d_{yz} , d_{zx}) have lower energy than the two e_g -orbitals (i.e. d_{z^2} , $d_{x^2-y^2}$). The ligand p-orbitals can form σ - and π -bonds (e.g. head-on overlap or lateral overlap of atomic orbitals). The bonding (σ and π) orbitals in the octahedral complex are lower in energy than the atomic orbitals because of the increased stability that is associated with the formation of the bond.^[177] The main mechanism that has been reported for off-colour formation upon Fe(III)-phenolic complexation is LMCT with a (partial) transfer of electrons from the p-orbitals of the phenolics to the d-orbitals of Fe(III). In the octahedral complexes, $\pi \rightarrow d$ and $\sigma \rightarrow d$ transitions are possible (Fig. 1.6D).^[54,176] The $\pi \rightarrow d_\pi$ LMCT transition has the smallest energy difference and the absorption in the visible region of Fe(III)-phenolic complexes is mostly attributed to these $\pi \rightarrow d_\pi$ transitions.^[175-178] Whereas, the $\sigma \rightarrow d$ transitions have a larger

energy difference and are therefore generally not associated with absorption of visible light.

These $\pi \rightarrow d_\pi$ transitions of Fe(III)-phenolic complexes result in the absorption of specific wavelengths and the formation of a broad absorbance band from 380–800 nm (**Fig. 1.6B**).^[54,121] Formation of a broad band is due to excitation of the electrons to various vibrational states. It has been demonstrated that Fe(II)-phenolic complexes display bands of higher frequency (*i.e.* in the UV range) compared to Fe(III)-phenolic complexes and are typically not coloured.^[110,179,180]

Although the terms electron transfer and charge transfer are often used interchangeably, they are not the same process.^[181,182] Electron transfer is the correct term for the process in which an electron is transferred from the ligand to the metal, thereby changing the oxidation states of both. Charge transfer (*e.g.* electron donor–electron acceptor complex), on the other hand, is the process of transferring a fraction of the electronic charge between the ligand and metal (*i.e.* partial charge transfer), providing stabilisation of the complex.^[181]

The λ_{\max} value of the LMCT depends on the structure of the phenolic and stoichiometry of the complex. Upon increasing the Fe(III)-phenolic stoichiometry from 1:1 to 1:3, the LMCT band shifts to a lower wavelength. The energy gap between the p- and d-orbitals increases due to a decrease of Lewis acidity of the metal centre upon substitution of water by ligand, leading to destabilisation of the d-orbitals.^[54]

The $\pi \rightarrow \pi^*$ and $\pi \rightarrow d_\pi$ transitions are sensitive to the coordination environment. Therefore, the colour of Fe(III)-phenolic complexes depends on the inherent properties of the ligand and external factors.^[183] For both transitions, solvatochromism can occur, *i.e.* a change in the absorption spectra (λ_{\max} , intensity) in solvents of different polarity.^[116,117]

Colour change by phenolic oxidation

Iron-induced electron transfer reactions, resulting in the reduction of Fe(III) to Fe(II) and oxidation of the phenolic, have been reported to result in the decomposition of the iron-phenolic complex and a decrease in colour at acidic pH (1–3).^[56,167,168] However, continuation reactions of quinones can yield oxidative coupling or oxidative degradation products of the phenolics. Since most research on iron-mediated oxidation products thus far did not identify the oxidation products, it is unclear what the effect of these products is on the overall colour. Oxidative coupling of phenolics can lead to an extension of the conjugated system, which decreases the energy gap between the HOMO and LUMO orbitals and in this way can contribute to brown colour formation.^[56,184] However, upon oxidative degradation, the size of the conjugated system of the phenolic may decrease, resulting in a decrease in colour. Additionally,

both types of oxidative reaction products may also form coloured complexes with Fe(III), although it is still unclear in what way this will affect the colour.

The combined contribution of complexation and oxidation on Fe(III)-phenolic mediated discolouration in food model systems has not previously been studied. In this thesis, we will investigate the chemistry underlying the formation of coloured Fe(III)-phenolic interaction products by use of model phenolic systems. The chosen model systems in this thesis mainly resemble the phenolics present in bouillon cubes as it is a promising iron fortification vehicle. Besides this, we have also investigated the water soluble tea phenolics as a model system, in order to expand the scope of phenolic structures beyond the water insoluble flavones and curcuminoids that are present in bouillon cubes .

1.4.5. Factors affecting iron-phenolic interactions

Iron-phenolic complexation and oxidation can be affected by the inherent properties of the ligand and by external factors. This section provides an overview of the effect of the individual factors that have been reported to affect iron-phenolic interactions and discolouration. Because the food production chain is a dynamic process, where multiple factors can change at the same time, further understanding of the interplay between these factors on iron-phenolic interaction and discolouration is required to improve the design of iron-fortified foods.

Phenolic structure

The *ortho*-diphenolic group (catechol motif) has been recognised as a good iron complexation site and is responsible for the iron-mediated discolouration of monomeric phenolics.^[124] However, it is not a prerequisite for iron complexation and discolouration of phenolics. Fe(III) can also form stable, dark-coloured, complexes with the diketone group of curcumin.^[95,96] The presence of more binding sites on flavonoids also increases iron complexation,^[147,148,150] and possibly also influences discolouration. The effect of the presence of multiple iron coordination sites, as is the case for certain flavonoids, on colour in an aqueous solution remains unclear to date.

As mentioned in **section 1.3**, phenolics in nature are often substituted to yield diverse structures.^[78] The flavones in bouillon cubes, which originate from celery and parsley, are likely acylated and glycosylated at the O7 position.^[185] Most studies investigating iron-phenolic interactions and discolouration have been performed with phenolic aglycones.^[81,118,124,177] A few studies have compared the complexation ability of quercetin and its 3-O-glucoside rutin.^[92,113,136,140,144] Presence of glucose at the O3 position blocks the complexation of iron to the 3-4 binding site. No studies have been performed to date that investigate the effect of glycosylation on the O7 position, and the influence of other types of glycosyl residues besides glucose (*e.g.* hexose, pentose, furanose type monosaccharides and monosaccharide vs. disaccharide). The effect of additional acylation of these 7-O-glycosyl residues on the complexation of

flavones to iron has also not been investigated previously. The effect of acylation has only been investigated for the anthocyanin subclass of flavonoids.^[186-188] Anthocyanins are not abundant in the aforementioned fortification vehicles. However, they are present as a supramolecular metal complex *in planta* and responsible for blue flower colour development.^[186,187] In these highly associated complexes, acylation by an aromatic acid moiety (e.g. hydroxybenzoic, coumaric, caffeic acid) results in the stabilisation of the complex. The effect of acylation by simple acids (e.g. malonyl or acetyl) on iron interaction with simple phenolics has not been explored previously.

External factors

Several external factors influence iron-phenolic complexation, oxidation, and subsequent discolouration. The **pH** has a profound influence on iron-phenolic complexation and oxidation. The pH directly affects the deprotonation of the phenolic and the hydrolytic processes of the iron ion.^[81,124] Especially, complexation and subsequent oxidation of iron-phenolic at pH 3-7 are important determinants of discolouration of iron-fortified foods. The effect of pH on the formation of coloured Fe(III)-catechol species (section 1.4.4) and Fe(III) hydroxides in aqueous solution is visualised in (Fig. 1.7).

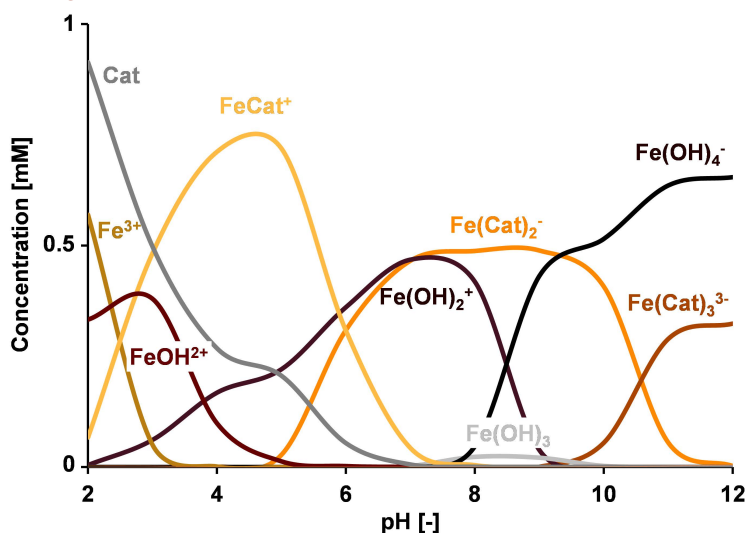


Figure 1.7. Predicted speciation diagram of a system containing 1 mM Fe(III) and 1 mM catechol, indicating the effect of increasing pH from 2 to 12. Visual MINTEQ (version 3.1) was used for the simulation. Catechol, Fe(III)-catechol, and Fe(III) hydrolysis species and stability constants (Log *K*) were obtained from the standard database in Visual MINTEQ 3.1 and were not fixed to a constant ionic strength. The colours of the lines are for illustrative purposes only and are not linked to the colour of the species.

For Fe(III)-catechol the 1:1 complex is formed at pH 2 and the stoichiometry increases to 1:2 and 1:3 upon increasing the pH.^[54,189] This indicates that coloured Fe(III)-catechol complexes are present in the relevant pH range for food (3-7). Additionally, the presence of ferric hydroxides also increases over pH. The changing stoichiometry of the Fe(III)-catechol complex and the presence of Fe(III) hydroxides will lead to a change in colour upon an increase in pH.^[124] If Fe(II) is used for fortification, the auto-oxidation of Fe(II) to Fe(III) is also enhanced at higher pH, thereby favouring the formation of more stable and coloured Fe(III)-phenolic complexes.^[62]

The pH is also suggested to affect the Fe-mediated oxidation of the phenolic. It has been reported that at acidic pH (1-3), when iron is not coordinated to phenolics, the direct electron transfer reactions are fast.^[56,167-169] At pH 7.4, no iron-induced oxidation of phenolics has been observed after 1 hour,^[113,114] the effect over longer time and in absence of buffering compounds has not been reported. It has been suggested that, at neutral pH, the formation of a stable Fe(III) complex is favoured over electron transfer and oxidation.^[56,87,170,171,190] The current studies on iron-phenolic interactions have not investigated the complexation and subsequent oxidation of phenolics with iron at pH 6.5, which is most relevant for savoury food.

Temperature has also been reported to affect iron-phenolic interactions. An increase in temperature in the range of 15-45 °C leads to more complexation and discolouration.^[191,192] However, one study reported that a further increase in temperature to 100 °C resulted in decreased iron-phenolic complexation and discolouration.^[124] The Fe(III)-mediated oxidation rate of phenolics is suggested to strongly increase with increasing temperature (95 °C), similarly as for auto-oxidation of phenolics.^[55,193]

The presence of **oxygen** plays a key role in complexation, oxidation and discolouration. As mentioned in **section 1.4.1** oxygen is required to auto-oxidise the colourless Fe(II)-phenolic complex to create the more stable coloured Fe(III)-phenolic complex.^[124] Additionally, the presence of oxygen is linked to increased metal-mediated oxidation of flavonoids.^[87,194]

The **ionic strength** is a factor that may differ widely, depending on the fortification vehicle. Electrostatic screening of the charges on iron and the phenolics by the counterions of salts (2 M NaCl) has been reported.^[195] This electrostatic screening may lead to the destabilisation of metal-ligand complexes, resulting in an increased energy gap, and thus a shift of the LMCT band to lower wavelengths (hypsochromic shift).^[196-198] Contrary to this, another study reports bathochromic shifting for metal-ligand complexes upon increasing the salt concentration.^[199] To date, no reports mention the effect of ionic strength on the LMCT transition of Fe(III)-phenolic complexes. Lastly, a positive correlation between the ionic strength (up to 2 M NaCl)

and Fe(III)-mediated oxidation rate of structures containing a catechol motif has been reported.^[200]

An overview of the aforementioned external factors on iron-phenolic complexation, oxidation, and discolouration is provided in **Table 1.4**. This overview indicates that the effect of some factors on iron-phenolic complexation, oxidation, and discolouration is unknown or unclear due to contradictory reports. Additionally, all of these studies have only investigated the effect of one factor at a time and the (combined) interaction effects of the factors have not been investigated.

Table 1.4. Overview of the effect of the individual factors on iron-phenolic complexation, oxidation, and discolouration. + indicates a positive correlation; - indicates a negative correlation; ± indicates contradicting findings in literature; and n.d. that the effect is not determined to date.

Factor	Complexation	Oxidation	Discolouration	Ref.
pH	+	-	+	[56,81,87,124,167-171,190]
Temperature	±	+	±	[54,55,124,191-193,201]
Oxygen	+	+	+	[87,124,194]
Ionic strength	-	+	n.d.	[196-200]
Interplay of factors	n.d.	n.d.	n.d.	

It remains unclear what the interplay between the aforementioned factors on iron-phenolic interactions is and what factors are the main contributors to discolouration. It is important to understand this interplay because the external factors may change multiple times during the various steps in food production, storage, preparation, and consumption.

The effect of macronutrients and other food ingredients

The interactions between iron and phenolics can also be affected by macronutrients (*i.e.* carbohydrates, fat, and protein) or other ingredients in the fortification vehicle. The iron-phenolic complexes show much higher stability constants than complexes of iron with the other macronutrients.^[107,202-205] Therefore, these macronutrients have been suggested to have no direct effect on iron-phenolic complexation. However, the currently used fortification vehicles may also contain taste enhancers (*e.g.* condiments and seasonings) that can affect iron-phenolic interactions. The presence of the taste enhancer monosodium glutamate (MSG) in an iron-fortified savoury food concentrate has previously been associated with significant negative effects on discolouration.^[206] Other taste enhancers, the 5'-ribonucleotides, have also been identified to coordinate metals,^[207-209] although the effect of iron complexation to nucleotides on iron-phenolic interactions has not yet been investigated.

1.5. Iron fortification strategies to limit iron-phenolic interactions

Based on the overview provided in **Table 1.4**, iron-phenolic mediated discolouration can be decreased by lowering the pH and avoiding oxygen. However, lowering the pH to prevent iron-phenolic complexation will introduce undesirable sensory changes (sourness).^[55] Additionally, it is technically difficult and expensive to completely avoid oxygen from the food product upon production, storage, preparation, and consumption. In this section, several other strategies to limit undesirable iron-phenolic interactions whilst maintaining the sensory properties and iron bioavailability in iron-fortified food will be discussed.

1.5.1. Selection of iron compound

A wide variety of iron salts exists, as the iron cation will form salts with almost all anions (e.g. chloride, sulphate, phosphate).^[60] For food fortification, it is important to select a suitable food-grade iron compound (e.g. ferrous sulphate, ferric pyrophosphate).^[210] It is preferred to select those iron compounds that possess the highest relative bioavailability, have minimal effect on the sensory properties of the food, and are affordable. Several iron compounds are currently used as fortificant and they are divided into four main categories: (i) water soluble, (ii) poorly water soluble but soluble in dilute acid, (iii) water insoluble and poorly soluble in dilute acid, and (iv) chelated iron compounds. The relative bioavailability, reactivity expressed as the colour change, and cost of one example iron compound per category are provided in **Table 1.5**.

Table 1.5. Examples of commonly used iron compounds per category and their typical bioavailability, reactivity, and cost, based on data from Allen *et al.*, Habeych *et al.*, Douglas *et al.*, Hurrell *et al.*, and Wegmüller *et al.*^[5,55,211-213]

Iron compounds	Bioavailability ^a	Reactivity ^b	Cost ^c
(i) Water soluble Ferrous sulphate	1	6-25	1
(ii) Poorly water soluble, soluble in dilute acid Ferrous fumarate	1	1-23	2
(iii) Water insoluble, poorly soluble in dilute acid Ferric pyrophosphate	0.2-0.7	1-2	4
(iv) Chelated iron compounds Sodium iron EDTA	2-3	3	13

^a Relative bioavailability compared to ferrous sulphate; ^b Reactivity of iron compound in condiments after two months storage expressed as average colour change (ΔE): no visually perceivable change ($\Delta E = 1-3$); minor visually perceivable change ($\Delta E = 3-10$); unacceptable visually observable change ($\Delta E > 10$)^[212,214]; ^c Relative cost per g iron compared to ferrous sulphate, *n.b.* cost in 2019.^[213]

In general, the water soluble compounds (i) possess high bioavailability but are also the most reactive compounds. They are especially suitable for dry products and products with fast turnover. The compounds that are poorly soluble in water but soluble in dilute acid (ii) are soluble in gastric acids. Therefore, they display similar bioavailability as water soluble compounds but tend to be slightly less reactive because they are poorly soluble at the pH of food. The water insoluble compounds

that display poor solubility in dilute acid (iii) show reduced bioavailability, but are widely used in industry due to their lower reactivity and good price. Chelated iron compounds (iv) are compounds where iron is bound (in a bidentate fashion) to the ligand. These chelated iron compounds possess good bioavailability and are also less reactive, but the production of these compounds is expensive, making them less attractive for fortification due to their impact on the price of the product. Examples of chelated iron compounds are sodium iron EDTA, ferrous bisglycinate, and ferric ammonium citrate,^[5] but also the more recently developed ferric phytate compounds,^[24,25] and iron-casein complex.^[215-217]

None of the currently available iron fortificants is bioavailable, showing little reactivity, and available at low cost. Depending on the fortification vehicle and purpose, the most suitable iron compound should be selected.

Current state-of-the-art iron fortificant for bouillon: ferric pyrophosphate

Due to its decreased reactivity, affordable price, and white appearance, the preferred iron compound for bouillon cubes is the water insoluble, and poorly soluble in dilute acid ferric pyrophosphate $[\text{Fe}_4(\text{P}_2\text{O}_7)_3; \text{Fe}_4\text{PP}_3]$.^[5,218] Micronised or colloidal Fe_4PP_3 can be used for food fortification as the reduction in particle size to micro-scale or nano-scale improves the solubility and bioavailability (Fig. 1.8).^[218-222] However, sensory changes upon fortification of bouillon cubes and other foods by micronised Fe_4PP_3 may arise due to the increased solubility of micronised Fe_4PP_3 .^[5,206] In addition to micronisation, the addition of tetrasodium pyrophosphate $[\text{Na}_4\text{P}_2\text{O}_7; \text{NaPP}]$ has also been suggested to enhance iron bioavailability of Fe_4PP_3 -fortified bouillon cubes,^[23] but a follow-up study did not confirm these findings.^[51]

Another option to improve Fe_4PP_3 bioavailability is by incorporating secondary minerals in a mixed system (Fig. 1.8). An example of a natural mixed phosphate is anastaseikoite $[\text{CaFe(II)P}_2\text{O}_7]$.^[223] The addition of zinc in a mixed Fe(III) phosphate system has been proven to increase the iron bioavailability of iron in these compounds.^[224-226] Additionally, the inclusion of a fifty-times excess of magnesium in a mixed Fe_4PP_3 system has been demonstrated to reduce its reactivity with phenolics compared to Fe_4PP_3 .^[227] Although magnesium and zinc metal cations can be used for this purpose, calcium is preferred due to its higher recommended intake and, consequently, less risk of overdosing.^[36] Additionally, the doping of calcium on insoluble Fe(III)-oxide $[\text{Fe}_2\text{O}_3]$ and Fe(III)-phosphate $[\text{FePO}_4]$ compounds has previously been shown to improve the solubility of iron in dilute acid and to improve the sensory properties of fortified foods.^[225,228] It is unknown whether the incorporation of calcium in Fe_4PP_3 can yield compounds with low iron dissolution at food relevant pH, thereby decreasing reactivity, whilst maintaining or increasing solubility at gastric pH, and improving bioavailability. Additionally, the ideal composition of x in such a compound $[\text{Ca(II)}_{2(1-x)}\text{Fe(III)}_{4x}(\text{P}_2\text{O}_7)_{(1+x)}]$ remains to be explored. Inclusion of a second metal in a mixed compound is preferred over

micronisation, as it is suggested to maintain the sensorial properties and provide bioavailable iron.

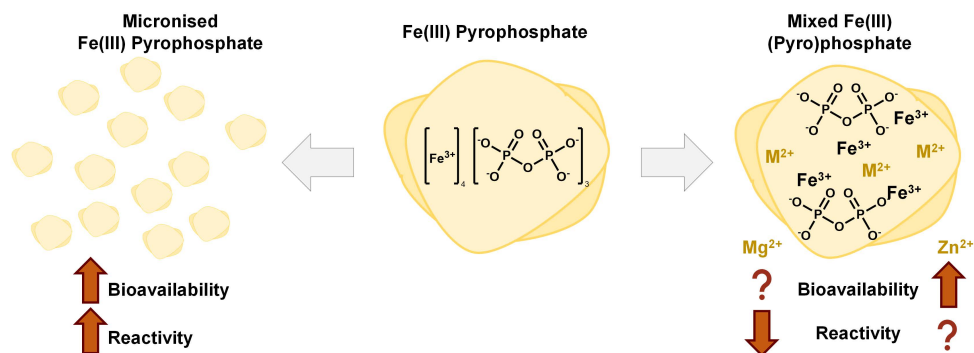


Figure 1.8. Schematic representation of micronisation of Fe(III) pyrophosphate or the inclusion of divalent metal in the inorganic (pyro)phosphate matrix based on van Leeuwen *et al.* and Zimmermann and Hilty.^[224,225,227]

1.5.2. Other approaches to limit iron-phenolic mediated discolouration

Reducing agents

Fe(II) complexes with phenolics are colourless, therefore the addition of reducing agents is another potential strategy for iron fortification as it can reduce complexed Fe(III)-phenolics to Fe(II)-phenolics. One example of a reducing agent that has been widely investigated is ascorbic acid. Ascorbic acid addition has been demonstrated to prevent discolouration of Fe(III) in presence of phenolics (*e.g.* chlorogenic acid).^[124] Additionally, ascorbic acid can reduce *ortho*-quinones back to their *ortho*-diphenolic precursors, thereby limiting oxidative browning.^[229] Moreover, the presence of reducing agents, especially ascorbic acid, has been demonstrated to increase iron absorption in general,^[19,35,124,230] either by reducing Fe(III) to Fe(II) thereby facilitating uptake via DMT1, or by the formation of a soluble iron-ascorbate complex with improved bioavailability. There are, however, some limitations to this approach. At pH 5 the formation of coloured Fe(III)-phenolic complexes has been demonstrated to decrease in presence of ascorbate, but at pH 7 this is no longer the case.^[177] At this pH, the discolouration can even increase because of the high solubility of the iron-ascorbate complex. Also, the rapid oxidation of ascorbic acid to dehydroascorbic acid occurs in presence of Fe(III).^[231-234] After depletion of ascorbic acid the discolouration will still occur. Additionally, presence of ascorbic acid can introduce sourness to the fortified food product.^[55]

Sulphite, cysteine, and glutathione are examples of sulphur-containing compounds that are mild reducing agents. One study reports prevention of Fe(III)-phenolic mediated discolouration by sodium bisulphite, although it is not indicated if this is a pH effect or due to reduction of Fe(III) to Fe(II).^[124] The effect of cysteine and glutathione on Fe(III)-phenolic complexation has, to date, not been reported. It has

been reported that the addition of all three compounds can prevent the formation of coloured phenolic oxidation products via a reaction with *ortho*-quinones that are formed upon oxidation of *ortho*-diphenols.^[235-237] This reaction leads to the formation of colourless addition products that cannot be further oxidised and do not participate in browning reactions.

Competing ligands and competing metals

The labile nature of the Fe(III)-phenolic complexes, allows the exchange of the dative bonds with other competing ligands or metals. A prerequisite for the competing ligand or metal to inhibit iron-phenolic interactions is that either it forms a more (thermodynamically) stable complex in the used pH range compared to the iron-phenolic complex or that it is present in excess.^[55]

Acetate, citrate, and EDTA are examples of competing ligands that have previously been investigated in model systems with gallic acid and iron at pH 4.4.^[55] In this pH range, all three chelating agents can (partially) prevent iron-phenolic mediated discolouration. At pH 7, which is more similar to the pH of bouillon cubes, EDTA is the most promising chelating agent when compared to citrate, glycine, and hexametaphosphate.^[26,124] This is in line with the reported stability constants (Log β) of the ligands, which were respectively 25, 11, and 10 for EDTA, citrate, and glycine.^[107] However, even when present in high excess (*i.e.* 1:500 molar ratio iron:EDTA) it could not fully prevent the formation of the highly stable Fe(III)-phenolic complexes (**Table 1.1**) at pH 7.^[26] At pH 5, a 1:2 molar ratio iron:EDTA has been proven to be sufficient to fully prevent Fe(III)-phenol complex formation. This reveals the high dependency of this approach on pH.^[26,238] Other drawbacks of this approach using EDTA are the high cost, the suggested interference with the absorption of other minerals, and the synthetic nature limiting consumer acceptance.^[5] To improve consumer acceptance, it would be most suitable to choose a competing ligand that is already inherent to the fortification vehicle. In **section 1.4.5** taste enhancers (MSG and 5'-ribonucleotides) were mentioned as ingredients that are present in the product and could potentially coordinate Fe(III). To test if these taste enhancers can act as competing ligands, the stability of Fe(III) taste enhancer complexes should be investigated.

In addition to their reducing capacity, sulphur-containing compounds may also act as competing ligands for Fe(III)-phenolic complexation. Cysteine can form complexes with Fe(II) (Log β = 6.7) and Fe(III) (Log β = 10.9).^[204] Taking into account the higher stability constants of Fe-phenolic complexes (**Table 1.1**), cysteine may be able to compete with Fe(II)-phenolic complexes or with Fe(III)-phenolic complexes when present in excess.^[55] However, the effect of sulphur-containing compounds on competing for iron-phenolic complexation has not been explored to date.

Another strategy is the use of competing metals that form complexes with phenolics such as Zn(II), Mg(II), or Ca(II). These metals do not show LMCT transitions in presence

of phenolics. For Zn(II) this is because the 3d-orbitals are filled and for Mg(II) and Ca(II) because they do not contain 3d-orbitals.^[55,239] The major limiting factor of this approach is that the Fe(III) complexes with phenolics typically have higher stability constants compared to complexes with these divalent metals.^[107,240] Complexes of catechol with Fe(III), Zn(II), Mg(II), and Ca(II) have Log β values of respectively 43.8, 9.9, 5.7, and 3.4.^[106,240] Therefore, the formation of the Fe(III)-phenolic complexes can only be hindered by adding an excess of these divalent metals, which may potentially lead to excessive intake and limitation of iron uptake by competing for the DMT1 receptor.^[29,46]

1.6. Aim and outline of this thesis

Iron fortification of foods is compromised by the reactivity of iron with phenolics, causing undesirable sensory changes in the fortified food. Systematic knowledge of iron-phenolic chemistry and the main factors that influence iron-phenolic interactions and the resulting discolouration in aqueous (food-like) systems is lacking. Furthermore, current strategies to limit iron reactivity in fortified foods are not yet sufficiently effective at preventing discolouration and typically involve the use of insoluble iron compounds that are also less bioavailable. Therefore, potential strategies to solve the balancing act of limiting reactivity and maximizing bioavailability should be identified and developed. The main aims of this thesis are: (i) to obtain insights into the chemistry of iron-phenolic interactions at the molecular level, and (ii) to explore strategies to limit the iron-phenolic mediated discolouration. A visual outline of this thesis is depicted in **Fig. 1.9**.

In **part I** of this thesis (**Chapters 2, 3, and 4**) we obtained a better understanding of the molecular interactions between iron and phenolics in aqueous model systems. In **Chapter 2** we studied the main factors and two-way interactions that contributed to food discolouration caused by iron-catechol complexation by the implementation of a three-level fractional factorial design. In **Chapter 3** we assessed the effect of the structural features of ten different flavonoids on discolouration caused by complexation, oxidation, and the formation of metal-phenolic networks. The work described in this chapter provides insight into the reactivity of iron with flavonoid aglycons. However, in nature and food products, the majority of flavonoids are glycosylated. Therefore, we have also purified nine differentially (acylated) flavone glycosides in **Chapter 4** and comprehensively investigated the effect of (acylated) 7-O-apiosylglucose substitution of flavones on their interaction with iron.

In **part II** of this thesis (**Chapters 5, 6, and 7**), we explored potential strategies to limit discolouration caused by iron-phenolic interactions. In **Chapter 5** we examined whether the incorporation of calcium in a mixed calcium-iron(III) pyrophosphate results in pH-dependent dissolution (*i.e.* increased dissolution at gastric pH (1-3) and decreased dissolution at food pH (3-7)), and what the ideal composition of such a salt would be. Additionally, the work presented in **Chapter 6** aimed to establish how these

newly developed calcium-iron(III) pyrophosphate salts react with a set of structurally diverse phenolics. In **Chapter 7** we investigated the interaction of Fe(III) with taste enhancers that are present in food and explored the potential of these interactions to be exploited for synthesis of iron compounds with improved pH-dependent dissolution behaviour and decreased reactivity with poorly soluble phenolics. The most important outcomes of this research are put in perspective and discussed in a broader context in **Chapter 8**.

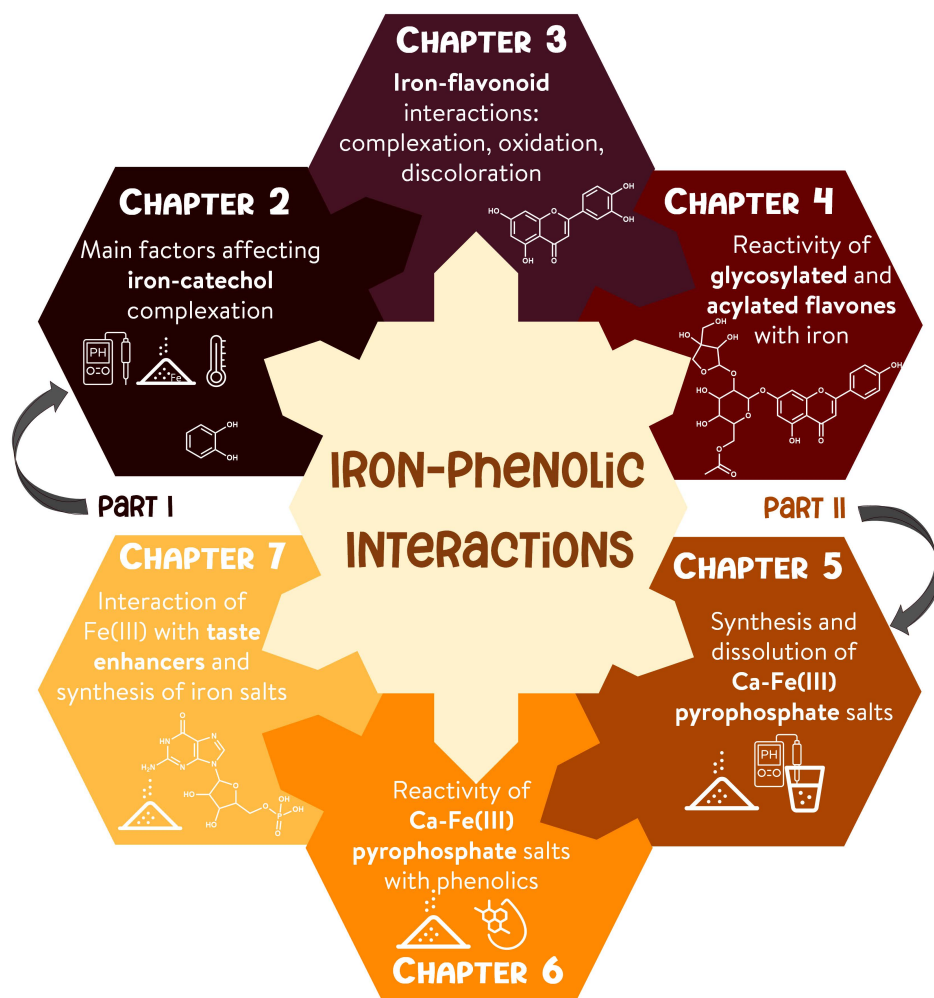


Figure 1.9. Visual outline of this thesis. Chemical insights into the iron-phenolic interactions are described in **part I** in **Chapter 2, 3, and 4**. Strategies to limit iron-phenolic interactions are explored in **part II** in **Chapter 5, 6, and 7**.

1.7. References

- 1 Camaschella, C. (2015). Iron-deficiency anemia. *New England Journal of Medicine*, 372(19), 1832-1843.
- 2 Bermejo, F., & García-López, S. (2009). A guide to diagnosis of iron deficiency and iron deficiency anemia in digestive diseases. *World Journal Gastroenterology*, 15(37), 4638-4643.
- 3 Shubham, K., Anukiruthika, T., Dutta, S., Kashyap, A. V., Moses, J. A., & Anandharamkrishnan, C. (2020). Iron deficiency anemia: A comprehensive review on iron absorption, bioavailability and emerging food fortification approaches. *Trends in Food Science & Technology*, 99, 58-75.
- 4 Kassebaum, N. J., Jasrasaria, R., Naghavi, M., Wulf, S. K., Johns, N., Lozano, R., Regan, M., Weatherall, D., Chou, D. P., Eisele, T. P., Flaxman, S. R., Pullan, R. L., Brooker, S. J., & Murray, C. J. L. (2014). A systematic analysis of global anemia burden from 1990 to 2010. *Blood*, 123(5), 615-624.
- 5 Allen, L. H., De Benoist, B., Dary, O., & Hurrell, R. (2006). Guidelines on food fortification with micronutrients. World Health Organization.
- 6 McLean, E., Cogswell, M., Egli, I., Wojdyla, D., & De Benoist, B. (2009). Worldwide prevalence of anaemia. WHO vitamin and mineral nutrition information system, 1993–2005. *Public Health Nutrition*, 12(4), 444-454.
- 7 WHO. (2021). Global anaemia estimates. Retrieved from: https://www.who.int/data/gho/data/themes/topics/anaemia_in_women_and_children Accessed 09/12/2022.
- 8 WHO. (2021). Prevalence of anaemia in women of reproductive age (aged 15-49) (%). Retrieved from: [https://www.who.int/data/gho/data/indicators/indicator-details/GHO/prevalence-of-anaemia-in-women-of-reproductive-age\(-\)](https://www.who.int/data/gho/data/indicators/indicator-details/GHO/prevalence-of-anaemia-in-women-of-reproductive-age(-)) Accessed 17/01/2023.
- 9 Huma, N., Salim-Ur-Rehman, Anjum, F. M., Murtaza, M. A., & Sheikh, M. A. (2007). Food fortification strategy—preventing iron deficiency anemia: A review. *Critical Reviews in Food Science and Nutrition*, 47(3), 259-265.
- 10 Fore, H. (2020). The micronutrient forum 5th global conference 2020. *CONNECTED 2020*.
- 11 Pawlak, R., Berger, J., & Hines, I. (2018). Iron status of vegetarian adults: A review of literature. *American Journal of Lifestyle Medicine*, 12(6), 486-498.
- 12 Martínez-Navarrete, N., Camacho, M. M., Martínez-Lahuerta, J., Martínez-Monzó, J., & Fito, P. (2002). Iron deficiency and iron-fortified foods—a review. *Food Research International*, 35(2), 225-231.
- 13 WHO. (2014). Global nutrition targets 2025: Anaemia policy brief. Geneva: World Health Organization.
- 14 WHO. (2021). Global nutrition targets tracking tool WHO, UNICEF, EC - version 2.0. Retrieved from: <https://www.who.int/tools/global-targets-tracking-tool>. Accessed 07/12/2022.
- 15 Headey, D., Heidkamp, R., Osendarp, S., Ruel, M., Scott, N., Black, R., Shekar, M., Bouis, H., Flory, A., & Haddad, L. (2020). Impacts of COVID-19 on childhood malnutrition and nutrition-related mortality. *The Lancet*, 396(10250), 519-521.
- 16 Osendarp, S., Verburg, G., Bhutta, Z., Black, R. E., de Pee, S., Fabrizio, C., Headey, D., Heidkamp, R., Laborde, D., & Ruel, M. T. (2022). Act now before Ukraine war plunges millions into malnutrition. *Nature*, 604, 620-624.
- 17 Vishwakarma, S., Genu Dalbhagat, C., Mandliya, S., & Niwas Mishra, H. (2022). Investigation of natural food fortificants for improving various properties of fortified foods: A review. *Food Research International*, 156, 11186.
- 18 Hurrell, R. F., Lynch, S., Bothwell, T., Cori, H., Glahn, R., Hertrampf, E., Kratky, Z., Miller, D., Rodenstein, M., Streekstra, H., Teucher, B., Turner, E., Yeung, C. K., & Zimmermann, M. B. (2004). Enhancing the absorption of fortification iron. *International Journal for Vitamin and Nutrition Research*, 74(6), 387-401.
- 19 Hurrell, R. F. (1997). Preventing iron deficiency through food fortification. *Nutrition Reviews*, 55(6), 210-222.
- 20 Zuidam, N. J. (2012). An industry perspective on the advantages and disadvantages of iron micronutrient delivery systems. In N. Garti & D. J. McClements (Eds.), *Encapsulation technologies and delivery systems for food ingredients and nutraceuticals*, (pp. 505-540): Woodhead Publishing.
- 21 de Mejia, E. G., Aguilera-Gutiérrez, Y., Martín-Cabrejas, M. A., & Mejia, L. A. (2015). Industrial processing of condiments and seasonings and its implications for micronutrient fortification. *Annals of the New York Academy of Sciences*, 1357(1), 8-28.
- 22 Moretti, D., Hurrell, R. F., & Cercamondi, C. I. (2018). Bouillon cubes. In M. G. V. Mannar & R. F. Hurrell (Eds.), *Food fortification in a globalized world*, (pp. 159-165): Elsevier.
- 23 Cercamondi, C. I., Duchateau, G. S., Harika, R. K., van den Berg, R., Murray, P., Koppenol, W. P., Zeder, C., Zimmermann, M. B., & Moretti, D. (2016). Sodium pyrophosphate enhances iron bioavailability from bouillon cubes fortified with ferric pyrophosphate. *British Journal of Nutrition*, 116(3), 496-503.
- 24 Gupta, S., Habeych, E., Scheers, N., Merinat, S., Rey, B., Galaffu, N., & Sandberg, A.-S. (2020). The development of a novel ferric phytate compound for iron fortification of bouillons (part I). *Scientific Reports*, 10(1), 1-10.
- 25 Dold, S., Zimmermann, M. B., Jeroense, F., Zeder, C., Habeych, E., Galaffu, N., Grathwohl, D., Foman, J. T., Merinat, S., & Rey, B. (2020). Iron bioavailability from bouillon fortified with a novel ferric phytate compound: A stable iron isotope study in healthy women (part II). *Scientific Reports*, 10(1), 1-9.
- 26 McGee, E. J. T., & Diosady, L. L. (2018). Prevention of iron-polyphenol complex formation by chelation in black tea. *LWT - Food Science and Technology*, 89, 756-762.
- 27 Anderson, G. J., & Frazer, D. M. (2017). Current understanding of iron homeostasis. *The American Journal of Clinical Nutrition*, 106, 1559S-1566S.

- 28 Hurrell, R., & Egli, I. (2010). Iron bioavailability and dietary reference values. *The American Journal of Clinical Nutrition*, 91(5), 1461S-1467S.
- 29 Zimmermann, M. B., & Hurrell, R. F. (2007). Nutritional iron deficiency. *The Lancet*, 370(9586), 511-520.
- 30 Gunshin, H., Mackenzie, B., Berger, U. V., Gunshin, Y., Romero, M. F., Boron, W. F., Nussberger, S., Gollan, J. L., & Hediger, M. A. (1997). Cloning and characterization of a mammalian proton-coupled metal-ion transporter. *Nature*, 388(6641), 482-488.
- 31 Dutt, S., Hamza, I., & Bartnikas, T. B. (2022). Molecular mechanisms of iron and heme metabolism. *Annual Review of Nutrition*, 42, 311-335.
- 32 Monsen, E. R., Hallberg, L., Layrisse, M., Hegsted, D. M., Cook, J., Mertz, W., & Finch, C. A. (1978). Estimation of available dietary iron. *The American Journal of Clinical Nutrition*, 31(1), 134-141.
- 33 Bothwell, T. H., & Macphail, A. P. (2004). The potential role of NaFeEDTA as an iron fortificant. *International Journal for Vitamin and Nutrition Research*, 76(6), 421-434.
- 34 Miret, S., Tascioglu, S., van der Burg, M., Frenken, L., & Klaffke, W. (2010). In vitro bioavailability of iron from the heme analogue sodium iron chlorophyllin. *Journal of Agricultural and Food Chemistry*, 58(2), 1327-1332.
- 35 Blanco-Rojo, R., & Vaquero, M. P. (2019). Iron bioavailability from food fortification to precision nutrition. A review. *Innovative Food Science & Emerging Technologies*, 51, 126-138.
- 36 Allen, L. H., Carriquiry, A. L., & Murphy, S. P. (2019). Perspective: Proposed harmonized nutrient reference values for populations. *Advances in Nutrition*, 11(3), 469-483.
- 37 Zhang, Y., Tian, X., Teng, A., Li, Y., Jiao, Y., Zhao, K., Wang, Y., Li, R., Yang, N., & Wang, W. (2022). Polyphenols and polyphenols-based biopolymer materials: Regulating iron absorption and availability from spontaneous to controllable. *Critical Reviews in Food Science and Nutrition*, 1-19.
- 38 Hurrell, R. (2010). Iron and malaria: Absorption, efficacy and safety. *International Journal for Vitamin and Nutrition Research*, 80(45), 279-292.
- 39 Prentice, A. M. (2008). Iron metabolism, malaria, and other infections: What is all the fuss about? *The Journal of Nutrition*, 138(12), 2537-2541.
- 40 Hurrell, R. F. (2011). Safety and efficacy of iron supplements in malaria-endemic areas. *Annals of Nutrition and Metabolism*, 59(1), 64-66.
- 41 Meltzer, H. M., Aro, A., Andersen, N. L., Koch, B., & Alexander, J. (2003). Risk analysis applied to food fortification. *Public Health Nutrition*, 6(3), 281-290.
- 42 Piskin, E., Cianciosi, D., Gulec, S., Tomas, M., & Capanoglu, E. (2022). Iron absorption: Factors, limitations, and improvement methods. *ACS Omega*, 7(24), 20441-20456.
- 43 Hurrell, R. F., Reddy, M. B., Juillat, M., & Cook, J. D. (2006). Meat protein fractions enhance nonheme iron absorption in humans. *The Journal of Nutrition*, 136(11), 2808-2812.
- 44 Cook, J. D., & Monsen, E. R. (1976). Food iron absorption in human subjects. III. Comparison of the effect of animal proteins on nonheme iron absorption. *The American Journal of Clinical Nutrition*, 29(8), 859-867.
- 45 Zijp, I. M., Korver, O., & Tijburg, L. B. (2000). Effect of tea and other dietary factors on iron absorption. *Critical Reviews in Food Science and Nutrition*, 40(5), 371-398.
- 46 Hallberg, L. (1998). Does calcium interfere with iron absorption? *The American Journal of Clinical Nutrition*, 68, 3-4.
- 47 Cegarra, L., Aguirre, P., Nuñez, M. T., Gerdtsen, Z. P., & Salgado, J. C. (2022). Calcium is a noncompetitive inhibitor of DMT1 on the intestinal iron absorption process: Empirical evidence and mathematical modeling analysis. *American Journal of Physiology-Cell Physiology*, 323(6), C1791-C1806.
- 48 Shawki, A., & Mackenzie, B. (2010). Interaction of calcium with the human divalent metal-ion transporter-1. *Biochemical and Biophysical Research Communications*, 393(3), 471-475.
- 49 Klassen-Wigger, P., Geraets, M., Messier, M. C., Detzel, P., Lenoble, H. P., Barclay, D. V., Mannar, M. G. V., & Hurrell, R. F. (2018). Micronutrient fortification of bouillon cubes in Central and West Africa. In M. G. V. Mannar & R. F. Hurrell (Eds.), *Food fortification in a globalized world*, (pp. 363-372): Elsevier.
- 50 Hurrell, R. F. (2022). Ensuring the efficacious iron fortification of foods: A tale of two barriers. *Nutrients*, 14(8), 1609.
- 51 Eilander, A., Funke, O. M., Moretti, D., Zimmermann, M. B., Owujuyigbe, T. O., Blonk, C., Murray, P., & Duchateau, G. S. (2019). High bioavailability from ferric pyrophosphate-fortified bouillon cubes in meals is not increased by sodium pyrophosphate: A stable iron isotope study in young Nigerian women. *The Journal of Nutrition*, 149(5), 723-729.
- 52 Mehansho, H. (2006). Iron fortification technology development: New approaches. *The Journal of Nutrition*, 136(4), 1059-1063.
- 53 Bovell-Benjamin, A. C., & Guinard, J.-X. (2003). Novel approaches and application of contemporary sensory evaluation practices in iron fortification programs. *Critical Reviews in Food Science and Nutrition*, 43(4), 379-400.
- 54 Elhabiri, M., Carrère, C., Marmolle, F., & Traboulsi, H. (2007). Complexation of iron(III) by catecholate-type polyphenols. *Inorganica Chimica Acta*, 360(1), 353-359.
- 55 Habeych, E., van Kogelenberg, V., Sagalowicz, L., Michel, M., & Galaffu, N. (2016). Strategies to limit colour changes when fortifying food products with iron. *Food Research International*, 88, 122-128.
- 56 Janssen, R. H., Canelli, G., Sanders, M. G., Bakx, E. J., Lakemond, C. M., Fogliano, V., & Vincken, J.-P. (2019). Iron-polyphenol complexes cause blackening upon grinding *Hermetia illucens* (black soldier fly) larvae. *Scientific Reports*, 9(1), 2967.

- 57 Brune, M., Hallberg, L., & Skanberg, A.-B. (1991). Determination of iron-binding phenolic groups in foods. *Journal of Food Science*, 56(1), 128-131.
- 58 Brune, M., Rossander, L., & Hallberg, L. (1989). Iron absorption and phenolic compounds: Importance of different phenolic structures. *European Journal of Clinical Nutrition*, 43(8), 547-557.
- 59 Hurrell, R. F., Reddy, M., & Cook, J. D. (1999). Inhibition of non-haem iron absorption in man by polyphenolic-containing beverages. *British Journal of Nutrition*, 81(4), 289-295.
- 60 Silver, J. (1993). Introduction to iron chemistry. In J. Silver (Ed.), *Chemistry of iron*, (pp. 1-29): Springer.
- 61 Esmaeilbeig, M. A., Khorram, M., Ayatollahi, S., & Zolghadr, A. R. (2022). On the hydrolysis of iron ions: DFT-based molecular dynamics perspective. *Journal of Molecular Liquids*, 367, 120323.
- 62 Flynn, C. M. (1984). Hydrolysis of inorganic iron(III) salts. *Chemical Reviews*, 84(1), 31-41.
- 63 Cornell, R. M., Giovanoli, R., & Schneider, W. (1989). Review of the hydrolysis of iron(III) and the crystallization of amorphous iron(III) hydroxide hydrate. *Journal of Chemical Technology & Biotechnology*, 46(2), 115-134.
- 64 Scheinost, A. C., & Schwertmann, U. (1999). Color identification of iron oxides and hydroxysulfates. *Soil Science Society of America Journal*, 63(5), 1463-1471.
- 65 Bethke, C. M. (2022). Geochemist's workbench. In C. M. Bethke (Ed.), *Geochemical and biogeochemical reaction modeling*, (pp. 439-449): University Press.
- 66 Weinrich, H., Durmus, Y. E., Tempel, H., Kungl, H., & Eichel, R.-A. (2019). Silicon and iron as resource-efficient anode materials for ambient-temperature metal-air batteries: A review. *Materials*, 12(13), 2134.
- 67 Russell, M. J., & Hall, A. J. (2009). A hydrothermal source of energy and materials at the origin of life. *Chemical evolution II: from origins of life to modern society*, 45-62.
- 68 Erlebach, A., Kurland, H.-D., Grabow, J., Müller, F. A., & Sierka, M. (2015). Structure evolution of nanoparticulate Fe₂O₃. *Nanoscale*, 7(7), 2960-2969.
- 69 Salim-Ur-Rehman, Huma, N., Tarar, O. M., & Shah, W. H. (2010). Efficacy of non-heme iron-fortified diets: A review. *Critical Reviews in Food Science and Nutrition*, 50(5), 403-413.
- 70 Crozier, A., Jaganath, I. B., & Clifford, M. N. (2009). Dietary phenolics: Chemistry, bioavailability and effects on health. *Natural Product Reports*, 26(8), 1001-1043.
- 71 Lund, M. N. (2021). Reactions of plant polyphenols in foods: Impact of molecular structure. *Trends in Food Science & Technology*, 112, 241-251.
- 72 King, A. M. Y., & Young, G. (1999). Characteristics and occurrence of phenolic phytochemicals. *Journal of the American Dietetic Association*, 99(2), 213-218.
- 73 Yashin, A., Yashin, Y., Xia, X., & Nemzer, B. (2017). Antioxidant activity of spices and their impact on human health: A review. *Antioxidants*, 6(3), 70.
- 74 Haytowitz, D. B., Wu, X., & Bhagwat, S. (2018). USDA database for the flavonoid content of selected foods, release 3.3. *US Department of Agriculture*, 173.
- 75 Fukutake, M., Takahashi, M., Ishida, K., Kawamura, H., Sugimura, T., & Wakabayashi, K. (1996). Quantification of genistein and genistin in soybeans and soybean products. *Food and Chemical Toxicology*, 34(5), 457-461.
- 76 Wang, H., Provan, G. J., & Helliwell, K. (2000). Tea flavonoids: Their functions, utilisation and analysis. *Trends in Food Science & Technology*, 11(4-5), 152-160.
- 77 Harbowy, M. E., Balentine, D. A., Davies, A. P., & Cai, Y. (1997). Tea chemistry. *Critical Reviews in Plant Sciences*, 16(5), 415-480.
- 78 Cheynier, V. (2005). Polyphenols in foods are more complex than often thought. *The American Journal of Clinical Nutrition*, 81(1), 223S-229S.
- 79 Markham, K., Chari, V., & Mabry, T. (1982). The flavonoids: Advances in research. *London: Chapman and Hall*, 19-134.
- 80 Cuyckens, F., & Claeys, M. (2004). Mass spectrometry in the structural analysis of flavonoids. *Journal of Mass Spectrometry*, 39(1), 1-15.
- 81 Perron, N. R., & Brumaghim, J. L. (2009). A review of the antioxidant mechanisms of polyphenol compounds related to iron binding. *Cell Biochemistry and Biophysics*, 53(2), 75-100.
- 82 Sánchez, M., Sabio, L., Gálvez, N., Capdevila, M., & Domínguez-Vera, J. M. (2017). Iron chemistry at the service of life. *IUBMB Life*, 69(6), 382-388.
- 83 Kumari, A., & Chauhan, A. K. (2021). Iron nanoparticles as a promising compound for food fortification in iron deficiency anemia: A review. *Journal of Food Science and Technology*, 59(9), 3319-3335.
- 84 Pearson, R. G. (1987). Recent advances in the concept of hard and soft acids and bases. *Journal of Chemical Education*, 64(7), 561.
- 85 Pearson, R. G. (1968). Hard and soft acids and bases, HSAB, part 1: Fundamental principles. *Journal of Chemical Education*, 45(9), 581.
- 86 Pearson, R. G. (1963). Hard and soft acids and bases. *Journal of the American Chemical Society*, 85(22), 3533-3539.
- 87 Hider, R. C., Liu, Z. D., & Khodr, H. H. (2001). Metal chelation of polyphenols. *Methods in Enzymology*, 335, 190-203.
- 88 Perron, N. R., Wang, H. C., DeGuire, S. N., Jenkins, M., Lawson, M., & Brumaghim, J. L. (2010). Kinetics of iron oxidation upon polyphenol binding. *Dalton Transactions*, 39(41), 9982-9987.
- 89 Chvátalová, K., Slaninová, I., Březinová, L., & Slanina, J. (2008). Influence of dietary phenolic acids on redox status of iron: Ferrous iron autoxidation and ferric iron reduction. *Food Chemistry*, 106(2), 650-660.

- 90 Parkin, G. (2004). Synthetic analogues relevant to the structure and function of zinc enzymes. *Chemical Reviews*, 104(2), 699-768.
- 91 Kasprzak, M. M., Erxleben, A., & Ochocki, J. (2015). Properties and applications of flavonoid metal complexes. *RSC Advances*, 5(57), 45853-45877.
- 92 Escandar, G. M., & Sala, L. F. (1991). Complexing behavior of rutin and quercetin. *Canadian Journal of Chemistry*, 69(12), 1994-2001.
- 93 Malešev, D., & Kuntić, V. (2007). Investigation of metal-flavonoid chelates and the determination of flavonoids via metal-flavonoid complexing reactions. *Journal of the Serbian Chemical Society*, 72(10), 921-939.
- 94 Uivarosi, V., Munteanu, A. C., Sharma, A., & Singh Tuli, H. (2019). Metal complexation and patent studies of flavonoid. In H. Singh Tuli (Ed.), *Current aspects of flavonoids: Their role in cancer treatment*, (pp. 39-89): Springer Singapore.
- 95 Hieu, T. Q., & Thao, D. T. T. (2019). Enhancing the solubility of curcumin metal complexes and investigating some of their biological activities. *Journal of Chemistry*, 2019, 8082195.
- 96 Gordon, O. N., Luis, P. B., Sintim, H. O., & Schneider, C. (2015). Unraveling curcumin degradation autoxidation proceeds through spiroepoxide and vinyl ether intermediates en route to the main bicyclopentadiene. *Journal of Biological Chemistry*, 290(8), 4817-4828.
- 97 Ejima, H., Richardson, J. J., & Caruso, F. (2017). Metal-phenolic networks as a versatile platform to engineer nanomaterials and biointerfaces. *Nano Today*, 12, 136-148.
- 98 Rahim, M. A., Björnalm, M., Bertleff-Zieschang, N., Ju, Y., Mettu, S., Leeming, M. G., & Caruso, F. (2017). Multiligand metal-phenolic assembly from green tea infusions. *ACS Applied Materials & Interfaces*, 10(9), 7632-7639.
- 99 Rahim, M. A., Ejima, H., Cho, K. L., Kempe, K., Müllner, M., Best, J. P., & Caruso, F. (2014). Coordination-driven multistep assembly of metal-polyphenol films and capsules. *Chemistry of Materials*, 26(4), 1645-1653.
- 100 Rahim, M. A., Kempe, K., Müllner, M., Ejima, H., Ju, Y., van Koeven, M. P., Suma, T., Braunger, J. A., Leeming, M. G., Abrahams, B. F., & Caruso, F. (2015). Surface-confined amorphous films from metal-coordinated simple phenolic ligands. *Chemistry of Materials*, 27(16), 5825-5832.
- 101 Rahim, M. A., Björnalm, M., Suma, T., Faria, M., Ju, Y., Kempe, K., Müllner, M., Ejima, H., Stickland, A. D., & Caruso, F. (2016). Metal-phenolic supramolecular gelation. *Angewandte Chemie*, 128(44), 14007-14011.
- 102 Bertleff-Zieschang, N., Rahim, M. A., Ju, Y., Braunger, J. A., Suma, T., Dai, Y., Pan, S., Cavalieri, F., & Caruso, F. (2017). Biofunctional metal-phenolic films from dietary flavonoids. *Chemical Communications*, 53(6), 1068-1071.
- 103 Bjerrum, J. (1950). On the tendency of the metal ions toward complex formation. *Chemical Reviews*, 46(2), 381-401.
- 104 Dalal, M. (2017). Metal-ligand equilibria in solution. In M. Dalal (Ed.), *A textbook of inorganic chemistry*, vol. 1(pp. 44-69): Dalal Institute.
- 105 Laurie, S. (1972). Kinetic stability versus thermodynamic stability. *Journal of Chemical Education*, 49(11), 746.
- 106 Avdeef, A., Sofen, S. R., Bregante, T. L., & Raymond, K. N. (1978). Coordination chemistry of microbial iron transport compounds. 9. Stability constants for catechol models of enterobactin. *Journal of the American Chemical Society*, 100(17), 5362-5370.
- 107 Martell, A. E., & Smith, R. M. (1982). *Critical stability constants: First supplement* (Vol. 1) Springer.
- 108 Ahmedova, A., Paradowska, K., & Wawer, I. (2012). ¹H, ¹³C MAS NMR and DFT GIAO study of quercetin and its complex with Al(III) in solid state. *Journal of Inorganic Biochemistry*, 110, 27-35.
- 109 de Souza, R. F. V. d., & de Giovanni, W. F. (2005). Synthesis, spectral and electrochemical properties of Al(III) and Zn(II) complexes with flavonoids. *Spectrochimica Acta Part A: Molecular and Biomolecular Spectroscopy*, 61(9), 1985-1990.
- 110 Kipton, H., Powell, J., & Taylor, M. C. (1982). Interactions of iron(II) and iron(III) with gallic acid and its homologues: A potentiometric and spectrophotometric study. *Australian Journal of Chemistry*, 35(4), 739-756.
- 111 Beneduci, A., Corrente, G. A., Marino, T., Aiello, D., Bartella, L., Di Donna, L., Napoli, A., Russo, N., Romeo, I., & Furia, E. (2019). Insight on the chelation of aluminum(III) and iron(III) by curcumin in aqueous solution. *Journal of Molecular Liquids*, 296, 111805.
- 112 G. Erdogan, R. Karadag, & E. Dolen. (2005). Potentiometric and spectrophotometric determination of the stability constants of quercetin complexes with aluminium(III) and iron(II). *Reviews in Analytical Chemistry*, 24(4), 247-262.
- 113 Nkhili, E., Loonis, M., Mihai, S., El Hajji, H., & Dangles, O. (2014). Reactivity of food phenols with iron and copper ions: Binding, dioxygen activation and oxidation mechanisms. *Food & Function*, 5(6), 1186-1202.
- 114 Hajji, H. E., Nkhili, E., Tomao, V., & Dangles, O. (2006). Interactions of quercetin with iron and copper ions: Complexation and autoxidation. *Free Radical Research*, 40(3), 303-320.
- 115 Miessler, G. L., & Tarr, D. A. (2000). Coordination chemistry IV: Reactions and mechanisms. In G. L. Miessler & D. A. Tarr (Eds.), *Inorganic chemistry*, (pp. 412-453): Pearson Education International.
- 116 Atkins, P. W., Overton, T. I., Rourke, J. P., Weller, M. T., & Armstrong, F. A. (2014). d-Metal complexes: Electronic structure and properties. In D. Shriver, M. Weller, T. Overton, J. Rourke & F. Armstrong (Eds.), *Inorganic chemistry 6th edition*. New York, NY: W.H. Freeman and Company.

- 117 Kreno, L. E., Leong, K., Farha, O. K., Allendorf, M., Van Duyne, R. P., & Hupp, J. T. (2012). Metal-organic framework materials as chemical sensors. *Chemical Reviews*, 112(2), 1105-1125.
- 118 Ren, J., Meng, S., Lekka, C. E., & Kaxiras, E. (2008). Complexation of flavonoids with iron: Structure and optical signatures. *The Journal of Physical Chemistry B*, 112(6), 1845-1850.
- 119 Leopoldini, M., Russo, N., Chiodo, S., & Toscano, M. (2006). Iron chelation by the powerful antioxidant flavonoid quercetin. *Journal of Agricultural and Food Chemistry*, 54(17), 6343-6351.
- 120 Ferreira, C. M., Pinto, I. S., Soares, E. V., & Soares, H. M. (2015). (Un)suitability of the use of pH buffers in biological, biochemical and environmental studies and their interaction with metal ions—a review. *RSC Advances*, 5(39), 30989-31003.
- 121 Andjelković, M., Van Camp, J., De Meulenaer, B., Depaemelaere, G., Socaciu, C., Verloo, M., & Verhe, R. (2006). Iron-chelation properties of phenolic acids bearing catechol and galloyl groups. *Food Chemistry*, 98(1), 23-31.
- 122 Ferguson, W. J., Braunschweiger, K. I., Braunschweiger, W. R., Smith, J. R., McCormick, J. J., Wasmann, C. C., Jarvis, N. P., Bell, D. H., & Good, N. E. (1980). Hydrogen ion buffers for biological research. *Analytical Biochemistry*, 104(2), 300-310.
- 123 Jiang, C., Wang, X., Parekh, B., & Leonard, J. (1998). Pyrite depression by phosphates in coal flotation. *Mining, Metallurgy & Exploration*, 15(1), 1-7.
- 124 Mellican, R. I., Li, J., Mehansho, H., & Nielsen, S. S. (2003). The role of iron and the factors affecting off-color development of polyphenols. *Journal of Agricultural and Food Chemistry*, 51(8), 2304-2316.
- 125 Bicer, N., Yildiz, E., Yegani, A. A., & Aksu, F. (2018). Synthesis of curcumin complexes with iron(III) and manganese(II), and effects of curcumin-iron(III) on alzheimer's disease. *New Journal of Chemistry*, 42(10), 8098-8104.
- 126 Bagchi, A., Mukherjee, P., Bhowmick, S., & Raha, A. (2015). Synthesis, characterization and antibacterial activity of a novel curcumin metal complex. *International Journal of Drug Development and Research*, 7(2), 0-0.
- 127 Khalil, M. I., Al-Zahem, A. M., & Al-Qunaibit, M. H. (2013). Synthesis, characterization, mössbauer parameters, and antitumor activity of Fe(III) curcumin complex. *Bioinorganic Chemistry and Applications*, 2013.
- 128 Özbolat, G., Alizadeh Yegani, A., & Tuli, A. (2018). Synthesis, characterization and electrochemistry studies of iron(III) complex with curcumin ligand. *Clinical and Experimental Pharmacology and Physiology*.
- 129 Refat, M. S. (2013). Synthesis and characterization of ligational behavior of curcumin drug towards some transition metal ions: Chelation effect on their thermal stability and biological activity. *Spectrochimica Acta Part A: Molecular and Biomolecular Spectroscopy*, 105, 326-337.
- 130 Borsari, M., Ferrari, E., Grandi, R., & Saladini, M. (2002). Curcuminoids as potential new iron-chelating agents: Spectroscopic, polarographic and potentiometric study on their Fe(III) complexing ability. *Inorganica Chimica Acta*, 328(1), 61-68.
- 131 Baum, L., & Ng, A. (2004). Curcumin interaction with copper and iron suggests one possible mechanism of action in alzheimer's disease animal models. *Journal of Alzheimer's Disease*, 6(4), 367-377.
- 132 Modi, G., & Pitre, K. (2009). The role of Fe(II) in the increased medicinal potency of curcumin analyzed by electrochemical methods. *Journal of Coordination Chemistry*, 62(6), 931-939.
- 133 Yang, S., Bai, G., Chen, L., Shen, Q., Diao, X., & Zhao, G. (2014). The interaction of phenolic acids with Fe(III) in the presence of citrate as studied by isothermal titration calorimetry. *Food Chemistry*, 157, 302-309.
- 134 Zheng, K., Xiong, Y., Li, Z., Peng, L., Guo, Q., Li, X., & Deng, X. (2020). ESI-TOF MS analysis and DNA cleavage activity of complexes formed by luteolin and five metal ions in hot water. *Inorganic and Nano-Metal Chemistry*, 50(11), 1181-1188.
- 135 Malacaria, L., Bruno, R., Corrente, G. A., Armentano, D., Furia, E., & Beneduci, A. (2022). Experimental insights on the coordination modes of coumarin-3-carboxylic acid towards Cr(III)-, Co(II)-, Ni(II)-, Cu(II)- and Zn(II): A detailed potentiometric and spectroscopic investigation in aqueous media. *Journal of Molecular Liquids*, 346, 118302.
- 136 de Souza, R. F. V., & De Giovanni, W. F. (2004). Antioxidant properties of complexes of flavonoids with metal ions. *Redox Report*, 9(2), 97-104.
- 137 Trifunski, S., & Munteanu, M. F. (2018). Synthesis, characterization and antioxidant activity of cooper-quercetin complex and iron-quercetin complex. *Revista de Chimie*, 69(10), 2621-2624.
- 138 Liu, Y., & Guo, M. (2015). Studies on transition metal-quercetin complexes using electrospray ionization tandem mass spectrometry. *Molecules*, 20(5), 8583-8594.
- 139 Raza, A., Xu, X., Xia, L., Xia, C., Tang, J., & Ouyang, Z. (2016). Quercetin-iron complex: Synthesis, characterization, antioxidant, DNA binding, DNA cleavage, and antibacterial activity studies. *Journal of Fluorescence*, 26(6), 2023-2031.
- 140 de Souza, R. F. V., Sussuchi, E. M., & De Giovanni, W. F. (2003). Synthesis, electrochemical, spectral, and antioxidant properties of complexes of flavonoids with metal ions. *Synthesis and Reactivity in Inorganic and Metal-Organic Chemistry*, 33(7), 1125-1144.
- 141 Dimitrić Marković, J. M., Marković, Z. S., Brdarić, T. P., Pavelkić, V. M., & Jadranin, M. B. (2011). Iron complexes of dietary flavonoids: Combined spectroscopic and mechanistic study of their free radical scavenging activity. *Food Chemistry*, 129(4), 1567-1577.

- 142 Papan, P., Kantapan, J., Sangthong, P., Meepowpan, P., & Dechsupa, N. (2020). Iron (III)-quercetin
complex: Synthesis, physicochemical characterization, and MRI cell tracking toward potential
143 applications in regenerative medicine. *Contrast Media & Molecular Imaging*, 2020.
- 144 Ryan, P., & Hynes, M. J. (2008). The kinetics and mechanisms of the reactions of iron(III) with quercetin
and morin. *Journal of Inorganic Biochemistry*, 102(1), 127-136.
- 145 Guo, M., Perez, C., Wei, Y., Rapoza, E., Su, G., Bou-Abdallah, F., & Chasteen, N. (2007). Iron-binding
properties of plant phenolics and cranberry's bio-effects. *Dalton Transactions*(43), 4951-4961.
- 146 Corrente, G. A., Malacaria, L., Beneduci, A., Furia, E., Marino, T., & Mazzone, G. (2021). Experimental and
theoretical study on the coordination properties of quercetin towards aluminum(III), iron(III) and
copper(II) in aqueous solution. *Journal of Molecular Liquids*, 325, 115171.
- 147 Horniblow, R. D., Henesy, D., Iqbal, T. H., & Tselepis, C. (2017). Modulation of iron transport, metabolism
and reactive oxygen status by quercetin-iron complexes in vitro. *Molecular Nutrition & Food
Research*, 61(3), 1600692.
- 148 Khokhar, S., & Owusu Apenten, R. K. (2003). Iron binding characteristics of phenolic compounds: Some
tentative structure-activity relations. *Food Chemistry*, 81(1), 133-140.
- 149 Mira, L., Tereza Fernandez, M., Santos, M., Rocha, R., Helena Florêncio, M., & Jennings, K. R. (2002).
Interactions of flavonoids with iron and copper ions: A mechanism for their antioxidant activity. *Free
Radical Research*, 36(11), 1199-1208.
- 150 Fernandez, M. T., Mira, M. L., Florêncio, M. H., & Jennings, K. R. (2002). Iron and copper chelation by
flavonoids: An electrospray mass spectrometry study. *Journal of Inorganic Biochemistry*, 92(2), 105-
111.
- 151 Mladěnka, P., Macáková, K., Filipský, T., Zatloukalová, L., Jahodář, L., Bovicelli, P., Silvestri, I. P., Hrdina,
R., & Saso, L. (2011). In vitro analysis of iron chelating activity of flavonoids. *Journal of Inorganic
Biochemistry*, 105(5), 693-701.
- 152 Gans, P., Sabatini, A., & Vacca, A. (1996). Investigation of equilibria in solution. Determination of
equilibrium constants with the HYPERQUAD suite of programs. *Talanta*, 43(10), 1739-1753.
- 153 Di Marco, V. B., & Bombi, G. G. (2006). Electrospray mass spectrometry (ESI-MS) in the study of metal-
ligand solution equilibria. *Mass Spectrometry Reviews*, 25(3), 347-379.
- 154 Reijenga, J., van Hoof, A., van Loon, A., & Teunissen, B. (2013). Development of methods for the
determination of pKa values. *Analytical Chemistry Insights*, 8, 53-71.
- 155 Jovanovic, S. V., Simic, M. G., Steenken, S., & Hara, Y. (1998). Iron complexes of gallic catechins.
Antioxidant action or iron regulation? *Journal of the Chemical Society, Perkin Transactions 2*(11), 2365-
2370.
- 156 Rusu, A., Hancu, G., & Imre, S. (2018). Essential guide of analysis methods applied to silver complexes
with antibacterial quinolones. *Advanced Pharmaceutical Bulletin*, 8(2), 181-189.
- 157 Di Marco, V. B., Bombi, G. G., Ranaldo, M., & Traldi, P. (2007). Metal-ligand solution equilibria studied
by electrospray ionization mass spectrometry: Correlation between ion intensity and acid-base
equilibria in solution. *Rapid Communications in Mass Spectrometry*, 21(23), 3825-3832.
- 158 Keith-Roach, M. J. (2010). A review of recent trends in electrospray ionisation-mass spectrometry for
the analysis of metal-organic ligand complexes. *Analytica Chimica Acta*, 678(2), 140-148.
- 159 Stuart, B. H. (2004). Inorganic molecules. In B. H. Stuart (Ed.), *Infrared spectroscopy: Fundamentals and
applications*, (pp. 95-110): John Wiley & Sons.
- 160 Smith, B. C. (2011). Introduction to infrared spectroscopy. In B. C. Smith (Ed.), *Fundamentals of Fourier
transform infrared spectroscopy*, (pp. 1-17): CRC press.
- 161 Petković, M., Petrović, B., Savić, J., Bugarčić, Ž. D., Dimitrić-Marković, J., Momić, T., & Vasić, V. (2010).
Flavonoids as matrices for MALDI-TOF mass spectrometric analysis of transition metal complexes.
International Journal of Mass Spectrometry, 290(1), 39-46.
- 162 Wyatt, M. F. (2011). MALDI-TOFMS analysis of coordination and organometallic complexes: A niche
area to work in. *Journal of Mass Spectrometry*, 46(7), 712-719.
- 163 Bailey, G. A., & Fogg, D. E. (2016). Confronting neutrality: Maximizing success in the analysis of
transition-metal catalysts by MALDI mass spectrometry. *ACS Catalysis*, 6(8), 4962-4971.
- 164 Casasnovas, R., Ortega-Castro, J., Donoso, J., Frau, J., & Munoz, F. (2013). Theoretical calculations of
stability constants and pK_a values of metal complexes in solution: Application to pyridoxamine-
copper(II) complexes and their biological implications in age inhibition. *Physical Chemistry Chemical
Physics*, 15(38), 16303-16313.
- 165 Buglyó, P., Nagy, E. M., Farkas, E., Sóvágó, I., Sanna, D., & Micera, G. (2007). New insights into the metal
ion-peptide hydroxamate interactions: Metal complexes of primary hydroxamic acid derivatives of
common dipeptides in aqueous solution. *Polyhedron*, 26(8), 1625-1633.
- 166 Martell, A. E., & Motekaitis, R. J. (1988). Formation and degradation of an oxalato- and peroxo-bridged
dicobalt bisdien dioxxygen complex: Binuclear complexes as hosts for the activation of two
coordinated guests. *Journal of the American Chemical Society*, 110(24), 8059-8064.
- 167 Ryan, P., & Hynes, M. J. (2008). The kinetics and mechanisms of the reactions of iron(III) with
naringenin, hesperetin, 3-hydroxychromone and 3-hydroxyflavone. A comparison of the coordination
power of 3-hydroxychromone and 5-hydroxychromone. *Journal of Coordination Chemistry*, 61(23),
3711-3726.
- 168 Hynes, M. J., & O'Coinceanainn, M. n. (2004). The kinetics and mechanisms of reactions of iron(III) with
caffeic acid, chlorogenic acid, sinapic acid, ferulic acid and naringin. *Journal of Inorganic Biochemistry*,
98(8), 1457-1464.

- 168 Hynes, M. J., & Ó Coinneainn, M. n. (2001). The kinetics and mechanisms of the reaction of iron(III) with gallic acid, gallic acid methyl ester and catechin. *Journal of Inorganic Biochemistry*, 85(2), 131-142.
- 169 Jameson, G. N., Kudryavtsev, A. B., & Linert, W. (2001). The oxidation of 6-hydroxydopamine in aqueous solution. Part 1. The formation of three metastable quinones at low pH. *Journal of the Chemical Society, Perkin Transactions 2*(4), 557-562.
- 170 Jameson, G. N. L., & Linert, W. (2001). The oxidation of 6-hydroxydopamine in aqueous solution. Part 3. Kinetics and mechanism of the oxidation with iron(III). *Journal of the Chemical Society, Perkin Transactions 2*(4), 569-575.
- 171 Linert, W., Jameson, R., & Herlinger, E. (1991). Complex formation followed by internal electron transfer: The reaction between L-dopa and iron(III). *Inorganica Chimica Acta*, 187(2), 239-247.
- 172 Anouar, E. H., Gierschner, J., Duroux, J.-L., & Trouillas, P. (2012). UV/visible spectra of natural polyphenols: A time-dependent density functional theory study. *Food Chemistry*, 131(1), 79-89.
- 173 García, G., Atilhan, M., & Aparicio, S. (2016). Flavonol-carbon nanostructure hybrid systems: a DFT study on the interaction mechanism and UV/vis features. *Physical Chemistry Chemical Physics*, 18(6), 4760-4771.
- 174 Jurd, L., & Geissman, T. (1956). Absorption spectra of metal complexes of flavonoid compounds. *Journal of Organic Chemistry*, 21(12), 1395-1401.
- 175 Reinen, D. (2014). The correlation between structure and color of iron oxide-type solids, sustainable pigments with gentle hues. *Zeitschrift für Anorganische und Allgemeine Chemie*, 640(14), 2677-2683.
- 176 Alhashmialameer, D., Collins, J., Hattenhauer, K., & Kerton, F. M. (2016). Iron amino-bis(phenolate) complexes for the formation of organic carbonates from CO₂ and oxiranes. *Catalysis Science & Technology*, 6(14), 5364-5373.
- 177 McGee, E. J. T. (2017). *Prevention of iron-polyphenol complex formation in iron-fortified tea: PhD thesis*. University of Toronto, Canada.
- 178 Cherrak, S. A., Mokhtari-Soulimane, N., Berroukeche, F., Bensenane, B., Cherbonnel, A., Merzouk, H., & Elhabiri, M. (2016). In vitro antioxidant versus metal ion chelating properties of flavonoids: A structure-activity investigation. *PLoS one*, 11(10), e0165575-e0165575.
- 179 Perron, N. R., Hodges, J. N., Jenkins, M., & Brumaghim, J. L. (2008). Predicting how polyphenol antioxidants prevent DNA damage by binding to iron. *Inorganic Chemistry*, 47(14), 6153-6161.
- 180 Jewett, S. L., Eggling, S., & Geller, L. (1997). Novel method to examine the formation of unstable 2: 1 and 3: 1 complexes of catecholamines and iron (III). *Journal of Inorganic Biochemistry*, 66(3), 165-173.
- 181 Cho, Y.-J., Lee, A.-R., Kim, S.-Y., Cho, M., Han, W.-S., Son, H.-J., Cho, D. W., & Kang, S. O. (2016). The influence of π -conjugation on competitive pathways: Charge transfer or electron transfer in new D- π -A and D- π -Si- π -A dyads. *Physical Chemistry Chemical Physics*, 18(33), 22921-22928.
- 182 Kochi, J. K. (1988). Electron transfer and charge transfer: Twin themes in unifying the mechanisms of organic and organometallic reactions. *Angewandte Chemie International Edition in English*, 27(10), 1227-1266.
- 183 Yuen, A. K., Hutton, G. A., Masters, A. F., & Maschmeyer, T. (2012). The interplay of catechol ligands with nanoparticulate iron oxides. *Dalton Transactions*, 41(9), 2545-2559.
- 184 Tan, J., de Bruijn, W. J. C., van Zadelhoff, A., Lin, Z., & Vincken, J.-P. (2020). Browning of epicatechin (EC) and epigallocatechin (EGC) by auto-oxidation. *Journal of Agricultural and Food Chemistry*, 68(47), 13879-13887.
- 185 Hostettler, G. L., Riedl, K. M., & Schwartz, S. J. (2012). Endogenous enzymes, heat, and pH affect flavone profiles in parsley (*Petroselinum crispum* var. *neapolitanum*) and celery (*Apium graveolens*) during juice processing. *Journal of Agricultural and Food Chemistry*, 60(1), 202-208.
- 186 Yoshida, K., Mori, M., & Kondo, T. (2009). Blue flower color development by anthocyanins: From chemical structure to cell physiology. *Natural Product Reports*, 26(7), 884-915.
- 187 Trouillas, P., Sancho-Garcia, J. C., De Freitas, V., Gierschner, J., Otyepka, M., & Dangles, O. (2016). Stabilizing and modulating color by copigmentation: Insights from theory and experiment. *Chemical Reviews*, 116(9), 4937-4982.
- 188 Alluis, B., & Dangles, O. (1999). Acylated flavone glucosides: Synthesis, conformational investigation, and complexation properties. *Helvetica Chimica Acta*, 82(12), 2201-2212.
- 189 Sever, M. J., & Wilker, J. J. (2004). Visible absorption spectra of metal-catecholate and metal-trionate complexes. *Dalton Transactions*, 7, 1061-1072.
- 190 Xu, H., Nishida, J., Ma, W., Wu, H., Kobayashi, M., Otsuka, H., & Takahara, A. (2012). Competition between oxidation and coordination in cross-linking of polystyrene copolymer containing catechol groups. *ACS Macro Letters*, 1(4), 457-460.
- 191 Lu, L.-L., Li, Y.-H., & Lu, X.-Y. (2009). Kinetic study of the complexation of gallic acid with Fe(III). *Spectrochimica Acta Part A: Molecular and Biomolecular Spectroscopy*, 74(3), 829-834.
- 192 Singh, K., & Kumar, A. (2019). Kinetics of complex formation of Fe(III) with caffeic acid: Experimental and theoretical study. *Spectrochimica Acta Part A: Molecular and Biomolecular Spectroscopy*, 211, 148-153.
- 193 Li, N., Taylor, L. S., Ferruzzi, M. G., & Mauer, L. J. (2012). Kinetic study of catechin stability: Effects of pH, concentration, and temperature. *Journal of Agricultural and Food Chemistry*, 60(51), 12531-12539.
- 194 Photiades, A., Grigorakis, S., & Makris, D. P. (2020). Kinetics and modeling of L-cysteine effect on the Cu(II)-induced oxidation of quercetin. *Chemical Engineering Communications*, 207(2), 139-152.

- 195 Guo, J., Richardson, J. J., Besford, Q. A., Christofferson, A. J., Dai, Y., Ong, C. W., Tardy, B. L., Liang, K.,
Choi, G. H., & Cui, J. (2017). Influence of ionic strength on the deposition of metal–phenolic networks.
196 *Langmuir*, 33(40), 10616–10622.
- 197 Czerwinski, K. R., Kim, J. I., Rhee, D. S., & Buckau, G. (1996). Complexation of trivalent actinide ions
(Am³⁺, Cm³⁺) with humic acid: The effect of ionic strength. *Radiochimica Acta*, 72(4), 179–188.
- 198 Fang, K., Yuan, D., Zhang, L., Feng, L., Chen, Y., & Wang, Y. (2015). Effect of environmental factors on
the complexation of iron and humic acid. *Journal of Environmental Sciences*, 27, 188–196.
- 199 Moyà, M. L., Rodriguez, A., & Sanchez, F. (1991). Salt effects on charge-transfer transitions. *Inorganica
Chimica Acta*, 188(2), 185–189.
- 200 Warner, L. W., Hoq, M. F., Myser, T. K., Henderson, W. W., & Shepherd, R. E. (1986). Influence of closed-
shell cations on the LMCT transition of pentacyanoferrate (III) complexes. *Inorganic Chemistry*, 25(11),
1911–1914.
- 201 El-Ayaan, U., Herlinger, E., Jameson, R. F., & Linert, W. (1997). Anaerobic oxidation of dopamine by
iron (III). *Journal of the Chemical Society, Dalton Transactions*(16), 2813–2818.
- 202 Sun, Y.-X., & Sun, W.-Y. (2014). Influence of temperature on metal-organic frameworks. *Chinese
Chemical Letters*, 25(6), 823–828.
- 203 Tian, L., Kejing, Y., Zhang, S., Yi, J., Zhu, Z., Decker, E. A., & McClements, D. J. (2021). Impact of tea
polyphenols on the stability of oil-in-water emulsions coated by whey proteins. *Food Chemistry*, 343,
128448.
- 204 Charley, P. J., Sarkar, B., Stitt, C. F., & Saltman, P. (1963). Chelation of iron by sugars. *Biochimica et
Biophysica Acta*, 69, 313–321.
- 205 Perrin, D. (1958). The stability of complexes of ferric ion and amino-acids. *Journal of the Chemical
Society*, 3125–3128.
- 206 Smith, R. M., & Martell, A. E. (1989). *Critical stability constants: Second supplement* (Vol. 6) Springer.
- 207 Jansen, F. J. H. M., & Velikov, K. P. (2014). Fortified savoury food concentrate. *European Patent Office,
EP2774497B1*(13157731.4).
- 208 Thakur, N., Sharma, B., Bishnoi, S., Mishra, S. K., Nayak, D., Kumar, A., & Sarma, T. K. (2018).
Multifunctional inosine monophosphate coordinated metal–organic hydrogel: Multistimuli
responsiveness, self-healing properties, and separation of water from organic solvents. *ACS
Sustainable Chemistry & Engineering*, 6(7), 8659–8671.
- 209 Lopez, A., & Liu, J. (2017). Self-assembly of nucleobase, nucleoside and nucleotide coordination
polymers: From synthesis to applications. *ChemNanoMat*, 3(10), 670–684.
- 210 Zhou, P., Shi, R., Yao, J.-F., Sheng, C.-F., & Li, H. (2015). Supramolecular self-assembly of nucleotide–
metal coordination complexes: From simple molecules to nanomaterials. *Coordination Chemistry
Reviews*, 292, 107–143.
- 211 Commission regulation (ec) no 1925/2006 of the European Parliament and of the Council of 20
212 december 2006 on the addition of vitamins and minerals and of certain other substances to foods.
(2006). Retrieved from: <https://eur-lex.europa.eu/legal-content/EN/TXT/PDF/?uri=CELEX:02006R1925-20221221&from=EN> Accessed 19/01/2023.
- 213 Douglas, F. W., Rainey, N. H., Wong, N. P., Edmondson, L. F., & LaCroix, D. E. (1981). Color, flavor, and
iron bioavailability in iron-fortified chocolate milk. *Journal of Dairy Science*, 64(9), 1785–1793.
- 214 Wegmüller, R., Zimmermann, M. B., & Hurrell, R. F. (2003). Dual fortification of salt with iodine and
encapsulated iron compounds: Stability and acceptability testing in Morocco and Côte d'Ivoire.
215 *Journal of Food Science*, 68(6), 2129–2135.
- 216 Hurrell, R. F. (2021). Iron fortification practices and implications for iron addition to salt. *The Journal of
Nutrition*, 151, 3S–14S.
- 217 Ghidouche, S., Rey, B., Michel, M., & Galaffu, N. (2013). A rapid tool for the stability assessment of
natural food colours. *Food Chemistry*, 139(1), 978–985.
- 218 Sabatier, M., Rytz, A., Husny, J., Dubascoux, S., Nicolas, M., Dave, A., Singh, H., Bodis, M., & Glahn, R. P.
(2020). Impact of ascorbic acid on the in vitro iron bioavailability of a casein-based iron fortificant.
219 *Nutrients*, 12(9), 2776.
- 220 Henare, S. J., Nur Singh, N., Ellis, A. M., Moughan, P. J., Thompson, A. K., & Walczyk, T. (2019). Iron
bioavailability of a casein-based iron fortificant compared with that of ferrous sulfate in whole milk:
A randomized trial with a crossover design in adult women. *The American Journal of Clinical Nutrition*,
110(6), 1362–1369.
- 221 Turck, D., Castenmiller, J., De Henauw, S., Hirsch-Ernst, K. I., Maciuk, A., Mangelsdorf, I., McArdle, H. J.,
Naska, A., Pelaez, C., Pentieva, K., Siani, A., Thies, F., Tsabouri, S., Vinceti, M., Cubadda, F., Frenzel, T.,
Heinonen, M., Prieto Maradona, M., Marchelli, R., Neuhäuser-Berthold, M., Poulsen, M., Schlatter, J. R.,
van Loveren, H., Ackert, R., & Knutsen, H. K. (2022). Safety of iron milk proteinate as a novel food
pursuant to Regulation (EU) 2015/2283 and bioavailability of iron from this source in the context of
Directive 2002/46/EC. *EFSA Journal*, 20(9), e07549.
- 222 van Leeuwen, Y. M., Velikov, K. P., & Kegel, W. K. (2012). Morphology of colloidal metal pyrophosphate
salts. *RSC Advances*, 2(6), 2534–2540.
- 223 Velikov, K. P., & Pelan, E. (2008). Colloidal delivery systems for micronutrients and nutraceuticals. *Soft
Matter*, 4(10), 1964–1980.
- 224 Sakaguchi, Rao, Nakata, Nanbu, & Juneja. (2004). Iron absorption and bioavailability in rats of
micronized dispersible ferric pyrophosphate. *International Journal for Vitamin and Nutrition Research*,
74(1), 3–9.

- 221 Fidler, M. C., Walczyk, T., Davidsson, L., Zeder, C., Sakaguchi, N., Juneja, L. R., & Hurrell, R. F. (2004). A micronised, dispersible ferric pyrophosphate with high relative bioavailability in man. *British Journal of Nutrition*, 91(1), 107-112.
- 222 Rossi, L., Velikov, K. P., & Philipse, A. P. (2014). Colloidal iron (III) pyrophosphate particles. *Food Chemistry*, 151, 243-247.
- 223 Miyawaki, R., Hatert, F., Pasero, M., & Mills, S. J. (2020). IMA commission on new minerals, nomenclature and classification (CNMNC)–newsletter 52. *European Journal of Mineralogy*, 32(1), 1-11.
- 224 Hilty, F. M., Arnold, M., Hilbe, M., Teleki, A., Knijnenburg, J. T. N., Ehrensperger, F., Hurrell, R. F., Pratsinis, S. E., Langhans, W., & Zimmermann, M. B. (2010). Iron from nanocompounds containing iron and zinc is highly bioavailable in rats without tissue accumulation. *Nature Nanotechnology*, 5(5), 374-380.
- 225 Zimmermann, M. B., & Hilty, F. M. (2011). Nanocompounds of iron and zinc: Their potential in nutrition. *Nanoscale*, 3(6), 2390-2398.
- 226 Scheuchzer, P., Syryamina, V. N., Zimmerman, M. B., Zeder, C., Nyström, L., Yulikov, M., & Moretti, D. (2023). Ferric pyrophosphate forms soluble iron coordination complexes with zinc compounds and solubilizing agents in extruded rice and predicts increased iron solubility and bioavailability in young women. *The Journal of Nutrition*, 153(3), 636-644.
- 227 van Leeuwen, Y. M., Velikov, K. P., & Kegel, W. K. (2014). Colloidal stability and chemical reactivity of complex colloids containing Fe^{3+} . *Food Chemistry*, 155, 161-166.
- 228 Hilty, F. M., Knijnenburg, J. T. N., Teleki, A., Krumeich, F., Hurrell, R. F., Pratsinis, S. E., & Zimmermann, M. B. (2011). Incorporation of Mg and Ca into nanostructured Fe_2O_3 improves Fe solubility in dilute acid and sensory characteristics in foods. *Journal of Food Science*, 76(1), N2-N10.
- 229 Kuijpers, T. F., Narváez-Cuenca, C.-E., Vincken, J.-P., Verloop, A. J., van Berkel, W. J., & Gruppen, H. (2012). Inhibition of enzymatic browning of chlorogenic acid by sulfur-containing compounds. *Journal of Agricultural and Food Chemistry*, 60(13), 3507-3514.
- 230 Pollack, S., Kaufman, R., Crosby, W. H., & Butkiewicz, J. E. (1963). Reducing agents and absorption of iron. *Nature*, 199(4891), 384-384.
- 231 Martinez, P., & Uribe, D. (1982). Study of the complexes of the ascorbic acid-iron (III) system. *Zeitschrift für Naturforschung B*, 37(11), 1446-1449.
- 232 Teucher, Olivares, & Cori. (2004). Enhancers of iron absorption: Ascorbic acid and other organic acids. *International Journal for Vitamin and Nutrition Research*, 74(6), 403-419.
- 233 Timoshnikov, V. A., Kobzeva, T. V., Polyakov, N. E., & Kontoghiorghes, G. J. (2020). Redox interactions of vitamin C and iron: Inhibition of the pro-oxidant activity by deferiprone. *International Journal of Molecular Sciences*, 21(11).
- 234 Shen, J., Griffiths, P. T., Campbell, S. J., Utinger, B., Kalberer, M., & Paulson, S. E. (2021). Ascorbate oxidation by iron, copper and reactive oxygen species: Review, model development, and derivation of key rate constants. *Scientific Reports*, 11(1), 7417.
- 235 Narváez-Cuenca, C.-E., Kuijpers, T. F. M., Vincken, J.-P., de Waard, P., & Gruppen, H. (2011). New insights into an ancient antibrowning agent: Formation of sulfophenolics in sodium hydrogen sulfite-treated potato extracts. *Journal of Agricultural and Food Chemistry*, 59(18), 10247-10255.
- 236 Richard, F. C., Goupy, P. M., Nicolas, J. J., Lacombe, J. M., & Pavia, A. A. (1991). Cysteine as an inhibitor of enzymic browning. 1. Isolation and characterization of addition compounds formed during oxidation of phenolics by apple polyphenol oxidase. *Journal of Agricultural and Food Chemistry*, 39(5), 841-847.
- 237 Fujimoto, A., & Masuda, T. (2012). Chemical interaction between polyphenols and a cysteinyl thiol under radical oxidation conditions. *Journal of Agricultural and Food Chemistry*, 60(20), 5142-5151.
- 238 Dueik, V., Chen, B. K., & Diosady, L. L. (2017). Iron-polyphenol interaction reduces iron bioavailability in fortified tea: Competing complexation to ensure iron bioavailability. *Journal of Food Quality*, 2017, 1-8.
- 239 Guo, J., Ping, Y., Ejima, H., Alt, K., Meissner, M., Richardson, J. J., Yan, Y., Peter, K., Von Elverfeldt, D., & Hagemeyer, C. E. (2014). Engineering multifunctional capsules through the assembly of metal-phenolic networks. *Angewandte Chemie International Edition*, 53(22), 5546-5551.
- 240 Martell, A. E., & Smith, R. M. (1977). *Critical stability constants: Other organic ligands* (Vol. 3) Springer.

PART I

Insights into iron-phenolic interactions

Chapter 2

Chapter 3

Chapter 4

CHAPTER 2

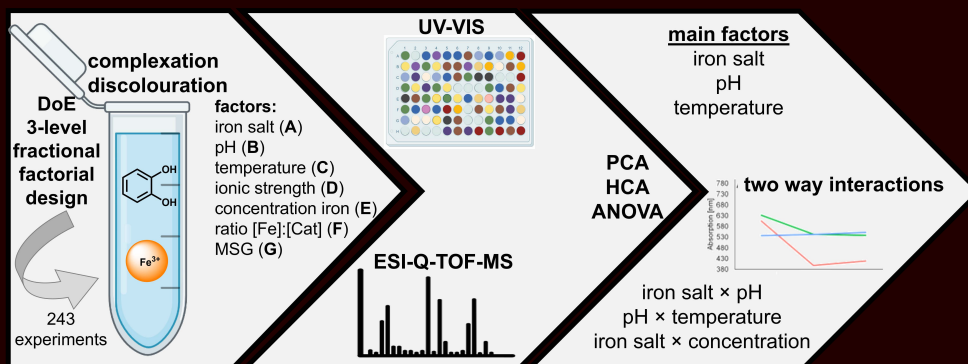
Revealing the main factors and two-way interactions contributing to food discolouration caused by iron-catechol complexation

Judith Bijlsma, Wouter J.C. de Bruijn,
Jos A. Hageman, Peter Goos,
Krassimir P. Velikov, and Jean-Paul Vincken

Based on: *Scientific Reports*, 2020, 10:8288.

Abstract

Fortification of food with iron is considered to be an effective approach to counter the global health problem caused by iron deficiency. However, reactivity of iron with the catechol moiety of food phenolics leads to discolouration and impairs bioavailability. In this study, we investigated the interplay between intrinsic and extrinsic factors on food discolouration caused by iron-catechol complexation. To this end, a three-level fractional factorial design was implemented. Absorbance spectra were analysed using statistical methods, including PCA, HCA, and ANOVA. Furthermore, a direct link between absorbance spectra and stoichiometry of the iron-catechol complexes was confirmed by ESI-TOF-MS. All statistical methods confirm that the main effects affecting discolouration were type of iron salt, pH, and temperature. Additionally, several two-way interactions, such as type of iron salt \times pH, pH \times temperature, and type of iron salt \times concentration significantly affected iron-catechol complexation. Our findings provide insights into iron-phenolic complexation-mediated discolouration, and facilitate the design of iron-fortified foods.



2.1. Introduction

Iron deficiency is a global health problem, affecting one quarter of the world's population.^[1] Iron fortification of food is an effective solution to counter iron malnutrition.^[2] However, due to the reactivity of the 'free' iron ion, iron fortification of food is notoriously difficult. Especially in food that contains plant material, complexation between iron and phenolic compounds can compromise product colour and impair the bioavailability of iron.^[3,4] Savoury concentrates (e.g. bouillon cubes) are an example of a phenolic-containing food product that is a promising vehicle for iron fortification, as they are widely available, frequently consumed, and affordable.^[5,6] Discolouration of iron-fortified bouillon cubes is currently limiting their successful introduction to the market, as colour is one of the critical sensory parameters of food.^[7]

To date, chemical interactions between phenolics and iron, combining redox processes and complex formation, have not been fully elucidated.^[8] Oxidation of the 1,2-dihydroxybenzene (i.e. catechol) moiety of phenolics in presence of ferric iron (Fe(III)) leads to the formation of quinones that polymerise to form brown-coloured compounds.^[4,8] However, Fe(III)-catalysed oxidation reactions of phenolic derivatives and catechol are very slow.^[9-11] On the other hand, complexation reactions by the formation of a coordinate bond between Fe(III) and deprotonated catechol, lead to fast and intense discolouration. Discolouration upon iron-catechol complexation results from the intense ligand-to-metal charge transfer (LMCT) absorbance band, typically observed between 380-800 nm.^[12] Deprotonation of the catechol moiety is required for iron binding, thus stoichiometry and colour of the iron-catechol complexes are pH dependent, as the complexing capacity of catechol increases at higher pH (Fig. 2.1).^{[8],[10,12]} The pK_a for the first hydroxyl group of catechol is 9.3 and of the second hydroxyl group 13.0.^[13] However, if iron is present, the deprotonated state is stabilised and thermodynamically more favourable, leading to an apparent pK_a of 5-8.^[14,15]

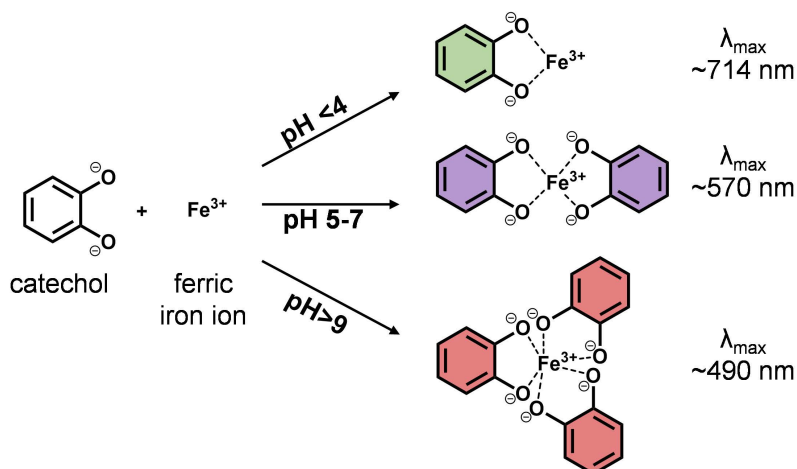


Figure 2.1. Coordination of ferric iron to deprotonated catechol at different pH values and corresponding maximum absorbance (λ_{max}) resulting from ligand-to-metal charge transfer, based on Perron *et al.*, and Elhabiri *et al.*^[8,12]

Iron-mediated oxidation of catechol is a slow process.^[9] Therefore, the main mechanism responsible for the discolouration of iron-fortified, phenolic-rich food products is expected to be iron-catechol complex formation. This study, therefore, focuses on discolouration resulting from fast complexation between iron and catechol.

Understanding the interplay between intrinsic and extrinsic factors on iron-catechol complexation is required to design iron-fortified products while preventing discolouration and ensuring the bioavailability of iron. The extrinsic factors of interest for food systems are temperature and humidity.^[3,4] Intrinsic factors expected to influence the iron-catechol complexation are: pH, the type of iron salt, iron concentration, ratio iron:catechol, ionic strength, and presence of taste enhancers.^[4,16] The effect of several factors (e.g. temperature and ionic strength) on iron-catechol complexation is currently unknown or unclear due to contradictory reports in literature.^[3,4,17-19] Additionally, two-way interactions between the aforementioned factors have not yet been investigated.

The goal of this study is to understand the effect of seven factors on iron-catechol complexation and discolouration to facilitate the optimisation of conditions in iron-fortified food. To obtain systematic insights into the effect of the seven factors at three levels, and their combined effects, a model system of aqueous mixtures of catechol (1,2-dihydroxybenzene) was studied using a duplicated regular 3^{8-3} fractional factorial design (FrFD). It is hypothesised that the main effects contributing to iron-catechol complexation are type of iron salt, pH, and temperature. Additionally, two-way interactions between these factors, or with other factors are expected to contribute to iron-catechol complexation.

2.2. Materials & methods

2.2.1. Materials

Ferric pyrophosphate (Fe_4PP_3) was obtained from Dr. Paul Lohmann GmbH KG (Emmerthal, Germany). All other chemicals used were purchased from Sigma Aldrich (St. Louis, MO, USA). Water was prepared using a Milli-Q water purification system (Merck Millipore, Billerica, MA, USA).

2.2.2. Experimental design

The combined effect of 7 different factors at 3 levels was investigated in this study. To limit the required number of experiments, while maximising the information obtained, a duplicated regular 3^{8-3} fractional factorial design (FrFD) with resolution V was implemented. This FrFD allowed us to estimate the main independent effects and the two-factor interactions that affect discolouration by iron-catechol complexation. The orthogonal array $L_{243}(3^{8-3})$ was designed according to design 8-3.1.^[20] The first factor in the design was the well plate in which the sample was tested. The seven other factors studied were: **(A)** type of iron salt, **(B)** pH, **(C)** temperature, **(D)** ionic

strength, (**E**) concentration of iron, (**F**) iron:catechol ratio, and (**G**) presence of MSG. The factor humidity was not taken into account as aqueous mixtures were tested. Each factor was studied at 3 levels; the factors with their respective levels are shown in **Table 2.1**. A total of 243 test combinations were investigated. Each of these were duplicated independently.

Table 2.1. Seven experimental factors and the corresponding three levels tested using the fractional factorial design.

Factors	Code	Level 0	Level 1	Level 2
Type of iron salt	A	FeCl ₃	FePO ₄	Fe ₄ PP ₃
pH	B	3	5	8
Temperature (°C)	C	23	40	100
Ionic strength (mM NaCl)	D	0	100	1000
Concentration iron (mM)	E	1	5	10
Ratio [Fe]:[Cat]	F	1:1	1:2	1:3
MSG (mM)	G	0	125	250

2.2.3. Preparation of iron-catechol mixtures

Mixtures of FeCl₃, FePO₄, and Fe₄PP₃ (final concentration iron ion 10 mM) were prepared in Eppendorf tubes and combined with catechol, sodium chloride, and MSG solutions according to the orthogonal array. Concentrated HCl and NaOH were used to adjust the pH as buffer usage is known to interfere with the complexation reaction.^[21,22] Samples were incubated at 23, 40, or 100 °C for 1 hour under constant shaking at 1000 rpm.

2.2.4. Colour assessment

After centrifugation for 5 min at 15,000 × *g*, colour of the samples was optically assessed and supernatant (200 µL) was transferred to a flat bottom 96 well-plate. Samples were diluted with water if needed. Dilution of sample was found to have a negligible effect on the absorbance spectra, except for the expected decrease in intensity (data not shown). Visible light spectra were recorded in the range from 380 to 800 nm in a SpectraMax iD3 (Molecular Devices, Sunnyvale, CA, USA), at room temperature.

Statistical data analysis

To analyse the acquired absorbance spectra, multivariate statistical analyses were performed. Prior to analysis, sum of squares normalisation was performed on the raw absorbance spectra to normalise signal intensity. Principal component analysis (PCA) was carried out to reduce the data dimensionality and to visualise relations between the experimental factors and normalised absorbance spectra. In addition, hierarchical cluster analysis (HCA) using Euclidean distance and Ward's linkage method^[23] was applied to depict similarities between the normalised absorbance spectra. HCA is an unsupervised clustering method where individual samples are combined into clusters based on similarity of their absorbance spectra. Normalisation, PCA, and HCA were performed by using the R statistical software package (R Core Team, 2013). The average maximum absorbance wavelength (λ_{\max}) of each hierarchical cluster was

determined in SPSS, outliers (z -score > 3.0 or z -score < -3.0) were removed from the dataset.

In addition to the exploratory statistical methods described above, the significance of the individual factors and interactions were investigated quantitatively using analysis of variance (ANOVA). PCA and HCA were performed on the complete normalised absorbance spectra. ANOVA requires a quantitative dependent variable. Therefore, the λ_{\max} value of the normalised spectra ($n=486$) was used instead of the complete spectra. For statistical purposes, a λ_{\max} of 380 nm (iron) or 410 nm (in presence of MSG) was used for the samples without a clear LMCT band. Tukey's *post hoc* comparisons (significant at $p < 0.05$) were carried out to create better insights into the effect of the different levels for the significant factors. ANOVA analysis was performed using IBM SPSS Statistic v.23 software (SPSS Inc., Chicago, IL, USA).

2.2.5. Evaluation of iron-catechol complexes by electrospray ionisation time of flight mass spectrometry (ESI-Q-TOF-MS)

Three samples per hierarchical cluster were randomly selected to be evaluated by ESI-Q-TOF-MS to further investigate the molecular structure of the iron-catechol complexes. Sample was introduced by direct infusion (2 mL h^{-1}) on a Synapt G2-Si high definition time of flight mass spectrometer equipped with a z-spray electrospray ionisation (ESI) source (Waters, Milford, MA, USA). The instrument was externally calibrated with sodium iodide and operated in normal resolution mode. The capillary voltage was set to 3.0 kV and 1.8 kV in positive (PI) and negative ionisation mode (NI), respectively. The sample cone was operated at 30 V and 40 V for PI and NI, respectively, with the source temperature set at 150°C . MS and MS^2 spectra were acquired between m/z 25-800 for 2 min at a 0.3 s scan time. The trap collision energy was 6 V in single MS mode and 22 V in MS^2 mode. Data acquisition and analysis were carried out by MassLynx v.4.1 (Waters, Milford, MA, USA).

2.3. Results & discussion

2.3.1. Exploratory analysis of factors affecting complexation

The combined effect of 7 factors at 3 levels (**Table 2.1**) on iron-catechol complexation was assessed by measuring the absorbance spectra for all 243 combinations obtained by the FrFD. In this study, the iron salts ferric phosphate (FePO_4) and ferric pyrophosphate ($\text{Fe}_4(\text{P}_2\text{O}_7)_3$, hereafter Fe_4PP_3), which are commonly used for food fortification, were compared to the well-documented iron salt ferric chloride (FeCl_3). For the other factors, the levels were chosen based on relevance for food applications. To create a concise overview of the different absorbance spectra, two exploratory statistical analyses were performed: principal component analysis (PCA) and hierarchical cluster analysis (HCA). Analysis by PCA provides an unbiased overview of the absorbance spectra and simplifies the different factors and levels by reducing the data dimensionality. The first two principal components accounted for

95 % of the total variance. In the plot of PC1 vs. PC2, the three levels of each factor were defined and evaluated. The PCA plots indicated that the factors type of iron salt (A), pH (B), temperature (C), and presence of MSG (G) were the main effects defining the location of the sample in the PC1-PC2 plane (Fig. 2.2). However, the three levels could not be discriminated entirely for these factors. For the factors ionic strength (D), iron concentration (E), and ratio iron:catechol (F), no clear differences between the levels were observed (Fig. S2.1).

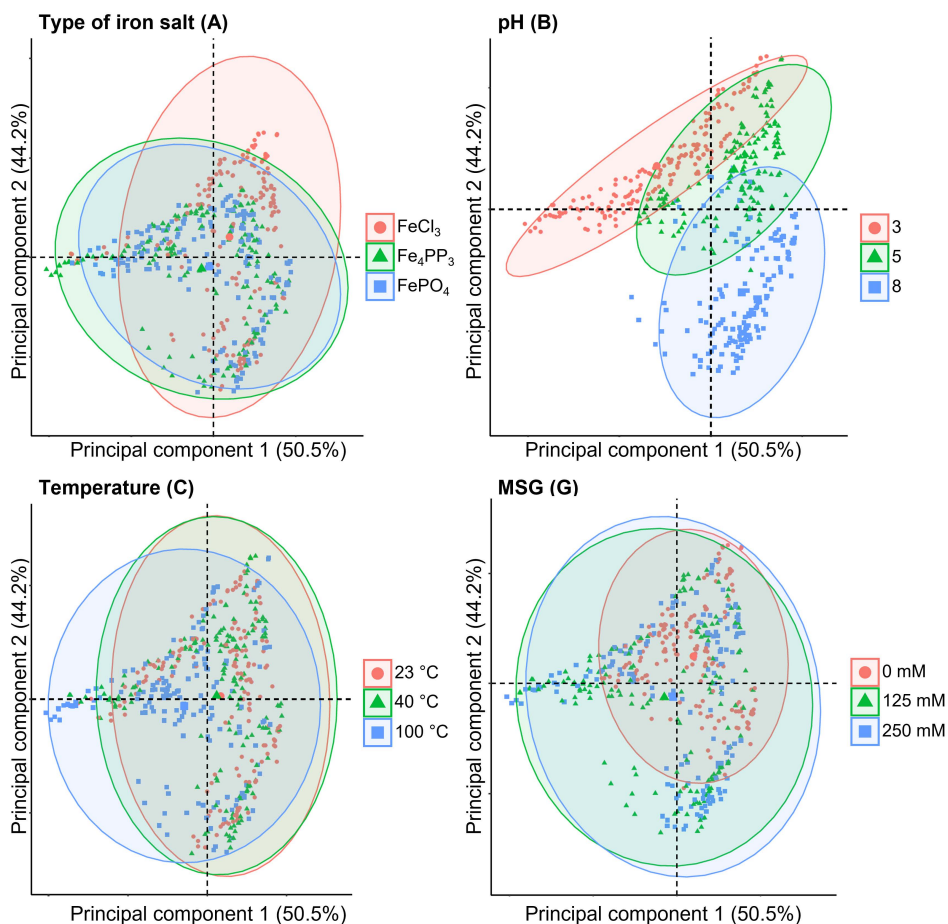


Figure 2.2. PCA biplots showing the principal component scores based on the normalised absorbance spectra, with colour indication for the different levels of the factors: type of iron salt (A), pH (B), temperature (C), and MSG (G).

For better interpretation of the PCA data, and to visualise which factors were most influential, HCA was used to cluster the normalised absorbance spectra. **Fig. 2.3** represents the dendrogram obtained from HCA, which depicts the relationships between absorbance spectra and experimental factors. These results indicated that the samples could be objectively grouped into 8 distinct clusters with similar absorbance spectra (**Fig. S2.2**). Colours in the heatmap below the dendrogram, correspond with the different factors and levels as indicated in **Fig. 2.3**.

Based on HCA, differences among the clusters were mainly the result of varying levels in the factors pH and type of iron salt. After clustering the average λ_{\max} value per cluster was calculated to obtain additional information regarding colour and complexation for each specific cluster. Typically, the LMCT absorbance band for iron-catechol complexes is from 380–800 nm.^[12] Based on the λ_{\max} values of the clusters, 1:1 complexes (~714 nm) were expected in cluster **5**, **7** and **8**, 1:2 complexes (~570 nm) in cluster **1**, **2** and **4**, and a mixture of 1:2 (~570 nm) and 1:3 (~490 nm) in cluster **3**.^[8,10] For the samples in cluster **6** no LMCT absorbance was observed (**Fig. S2.2**). The heatmap in **Fig. 2.3** shows that cluster **6** mainly contains samples at pH 3. This observation is explained by the reduced complexation affinity of catechol at pH < pK_a . In addition to this, some samples in cluster **6** showed presence of white sediment, most likely due to the poor water solubility of the iron salts under the acidic conditions present in this cluster.

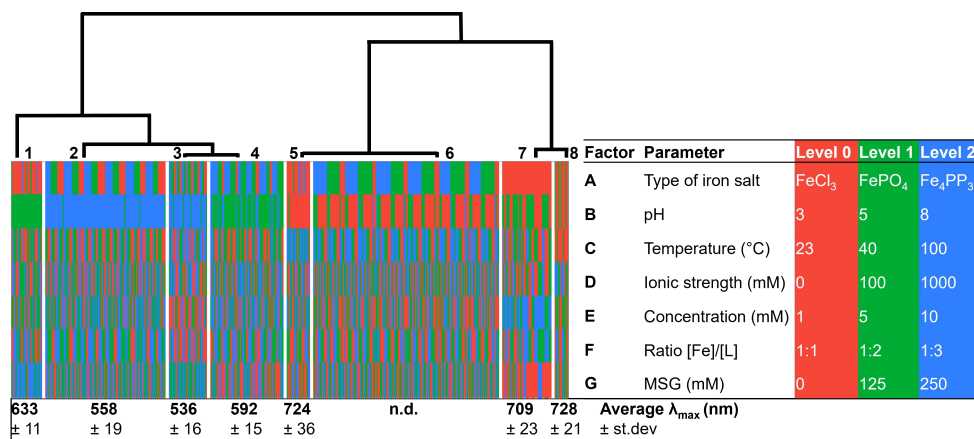


Figure 2.3. Dendrogram of samples hierarchically clustered based on the normalised absorbance spectra. The heatmap indicates the different levels of factors for each cluster as shown in the table. The average maximum absorbance wavelength (λ_{\max}) for each cluster is indicated below the heatmap. n.d. indicates that no LMCT band was detected.

2.3.2. Stoichiometry in the clusters confirmed by ESI-Q-TOF-MS

Analysis by ESI-Q-TOF-MS was used to investigate whether the maximum absorbance of each hierarchical cluster could indeed be linked to the stoichiometry of the complexes present in the samples from that cluster. To this end, three samples from each cluster were measured in negative (NI) and positive ionisation (PI) mode mass spectrometry. It was previously shown that due to the soft character of ESI, iron-phenolic complexes remain intact.^[16,24] Complexes of catechol with iron were detected at m/z 233.89, and 271.98 in NI (**Fig. 2.4A**) and m/z 163.96, 164.96, 273.99, and 275.00 in PI mode (**Fig. 2.4B**). These signals were absent in the FeCl_3 , Fe_4PP_3 , FePO_4 , catechol, and MSG blanks.

The iron-catechol complexes were tentatively identified based on the m/z value and isotope pattern (**Table 2.2**). Monocatecholate complexes were annotated in NI as chloride adduct at an m/z of 233.89 $[\text{Fe}^{3+} + (\text{catechol} - 2\text{H}^+) + 2\text{Cl}^-]^-$ and in PI at m/z 163.96 $[\text{Fe}^{3+} + (\text{catechol} - 2\text{H}^+)]^+$ or m/z 164.96 $[\text{Fe}^{2+} + (\text{catechol} - \text{H}^+)]^+$. Dicatecholate complexes were annotated in NI at m/z 271.98 $[\text{Fe}^{3+} + 2(\text{catechol} - 2\text{H}^+)]^-$ and in PI at m/z 273.99 $[\text{Fe}^{3+} + 2(\text{catechol} - \text{H}^+)]^+$ or at m/z 275.00 $[\text{Fe}^{2+} + \text{catechol} + (\text{catechol} - \text{H}^+)]^+$. These annotations are in agreement with previously reported complexes of Fe(III) with phenolic ligands such as catechol^[25] or flavonoids,^[26,27] using ESI-MS.^[25-27] It is suggested that the complexes with Fe(II), as observed in PI, are a result of in-source charge reduction. In-source charge reduction reactions during ESI-MS in positive ion mode were reported previously for metal complexes.^[28,29] Reduction of metal complexes in PI is a result of charge-transfer reactions between the iron complex and solvent molecules in the gas phase. Charge reduction was not observed for the iron-catechol complexes in NI.

Based on the results of ESI-Q-TOF-MS analysis, an overview was made of the distribution of stoichiometry of the complexes in each cluster (**Fig. 2.4C**). Samples in clusters **5**, **7**, and **8** showed mainly 1:1 stoichiometry, these outcomes are in agreement with the average λ_{max} value of those clusters between 709 and 728 nm (**Fig. 2.1**). The samples in clusters **1**, **2**, and **4** were mainly 1:2 with minor amounts of 1:1, which matches with their average λ_{max} (between 558 and 633 nm). Samples in cluster **3** showed only 1:2 stoichiometry, consistent with the average λ_{max} of 536 nm. Generally, a mixture of 1:2 and 1:3 metal to ligand species is present in the pH range of 7-9.^[8] However, no tricatecholate complexes were detected in any of our samples. Based on the average λ_{max} values of our clusters a mixture of 1:2 and 1:3 complexes was only expected in cluster **3** (average λ_{max} 536 \pm 16). For the samples of cluster **6**, only trace amounts of the 1:1 complex could be observed, which is in agreement with the absence of an LMCT band in the absorbance spectra (**Fig. S2.2**).

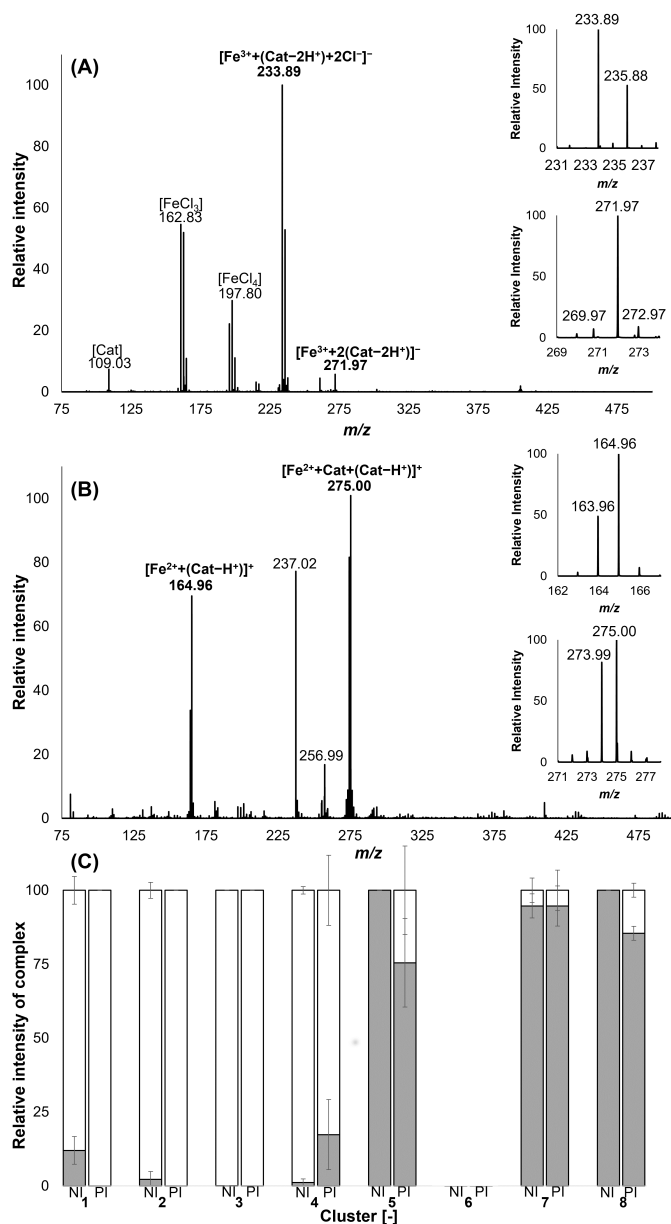
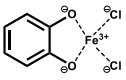
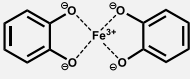
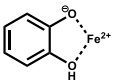
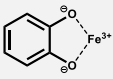
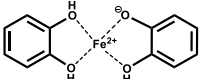
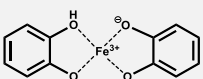


Figure 2.4. Electrospray ionisation mass spectra of a solution of ferric chloride (FeCl_3) and catechol, recorded in (A) negative (NI) and (B) positive (PI) ionisation mode. The insets represent the isotopic patterns of the monocatechol and dicatechol complexes. (C) Relative intensities of monocatechol (grey) and dicatechol (white) iron complexes in each of the hierarchical clusters (Figure 2.3) as measured in negative (NI) and positive (PI) ionisation mode ($n=3$, error bar is relative standard deviation). For cluster 6 only traces of complex/or no complex at all was observed in the mass spectra.

Table 2.2. Tentative structures of iron-catechol complexes with corresponding experimental and theoretical mass-to-charge ratios (m/z) and isotope abundance.

Tentative Structures	Isotopes	m/z		Isotope abundance (%)	
		Exp.	Theoretical	Exp.	Theoretical
$[\text{Fe}^{3+} + (\text{Cat} - 2\text{H}^+) + 2\text{Cl}^-]^-$ 	$^{12}\text{C}_6\text{H}_4\text{O}_2^{35}\text{Cl}_2^{54}\text{Fe}$	231.89	231.90	2.3	6.4
	$^{12}\text{C}_6\text{H}_4\text{O}_2^{35}\text{Cl}_2^{56}\text{Fe}$	233.89	233.89	100	100
	$^{12}\text{C}_5^{13}\text{CH}_4\text{O}_2^{35}\text{Cl}_2^{56}\text{Fe}$ and $^{12}\text{C}_6\text{H}_4\text{O}_2^{35}\text{Cl}_2^{57}\text{Fe}$	234.89	234.90	4	6.5
	$^{12}\text{C}_6\text{H}_4\text{O}_2^{35}\text{Cl}^{37}\text{Cl}^{56}\text{Fe}$	235.88	235.89	51.9	63.9
	$^{12}\text{C}_5^{13}\text{CH}_4\text{O}_2^{35}\text{Cl}^{37}\text{Cl}^{56}\text{Fe}$	236.89	236.89	2.1	4.1
	$^{12}\text{C}_6\text{H}_4\text{O}_2^{37}\text{Cl}_2^{56}\text{Fe}$	237.88	237.89	4.5	10.2
$[\text{Fe}^{3+} + 2(\text{Cat} - 2\text{H}^+)]^-$ 	$^{12}\text{C}_{12}\text{H}_8\text{O}_4^{54}\text{Fe}$	269.97	269.98	7.3	6.4
	$^{12}\text{C}_{12}\text{H}_8\text{O}_4^{56}\text{Fe}$	271.97	271.97	100	100
	$^{12}\text{C}_{11}^{13}\text{CH}_8\text{O}_4^{56}\text{Fe}$ and $^{12}\text{C}_{12}\text{H}_8\text{O}_4^{57}\text{Fe}$	272.97	272.98	13.4	13
$[\text{Fe}^{2+} + (\text{Cat} - \text{H}^+)]^+$ 	$^{12}\text{C}_6\text{H}_5\text{O}_2^{54}\text{Fe}$	162.97	162.97	3.2	6.4
	$^{12}\text{C}_6\text{H}_5\text{O}_2^{56}\text{Fe}$	164.96	164.96	100	100
	$^{12}\text{C}_5^{13}\text{CH}_5\text{O}_2^{56}\text{Fe}$ and $^{12}\text{C}_6\text{H}_5\text{O}_2^{57}\text{Fe}$	165.97	165.96	4.2	6.5
$[\text{Fe}^{3+} + (\text{Cat} - 2\text{H}^+)]^+$ 	$^{12}\text{C}_6\text{H}_4\text{O}_2^{54}\text{Fe}$	161.96	161.96	3	6.4
	$^{12}\text{C}_6\text{H}_4\text{O}_2^{56}\text{Fe}$	163.96	163.96	100	100
	$^{12}\text{C}_5^{13}\text{CH}_4\text{O}_2^{56}\text{Fe}$ and $^{12}\text{C}_6\text{H}_4\text{O}_2^{57}\text{Fe}$	164.96	164.96	8.8	6.5
$[\text{Fe}^{2+} + \text{Cat} + (\text{Cat} - \text{H}^+)]^+$ 	$^{12}\text{C}_{12}\text{H}_{11}\text{O}_4^{54}\text{Fe}$	272.99	273.00	8.1	6.4
	$^{12}\text{C}_{12}\text{H}_{11}\text{O}_4^{56}\text{Fe}$	275.00	275.00	100	100
	$^{12}\text{C}_{11}^{13}\text{CH}_{11}\text{O}_4^{56}\text{Fe}$ and $^{12}\text{C}_{12}\text{H}_{11}\text{O}_4^{57}\text{Fe}$	276.00	276.00	10	13
$[\text{Fe}^{3+} + (2\text{Cat} - \text{H}^+)]^+$ 	$^{12}\text{C}_{12}\text{H}_{10}\text{O}_4^{54}\text{Fe}$	271.98	272.00	7.3	6.4
	$^{12}\text{C}_{12}\text{H}_{10}\text{O}_4^{56}\text{Fe}$	273.99	273.99	100	100
	$^{12}\text{C}_{11}^{13}\text{CH}_{10}\text{O}_4^{56}\text{Fe}$ and $^{12}\text{C}_{12}\text{H}_{10}\text{O}_4^{57}\text{Fe}$	275.00	275.00	15.3	13

2.3.3. Factors affecting iron-catechol complexation

The results from PCA and HCA provide an unbiased overview of the main factors that affect the full absorbance spectra. To gain more in-depth insight concerning the influence of the 7 factors' main effects and 21 two-way interactions on iron-catechol complexation, analysis of variance (ANOVA) was performed (**Table 2.3**). ANOVA requires a quantitative dependent variable, to this end, the λ_{\max} value of each independent sample was used. Absorbance intensity was not taken into account. The ANOVA results (**Table 2.3**) confirmed that several two-way interactions significantly ($p < 0.05$) contributed to changes in λ_{\max} , and therefore affected discolouration.

Table 2.3. Analysis of variance of the 7 main effects and 21 interaction effects affecting iron-catechol complexation, significant factors and corresponding p -values are indicated in bold ($R^2 = 0.76$ and $R^2_{\text{adj}} = 0.70$).

Factor	Sum of Squares	Mean Square	F Value	p -value	Contribution (%)
A (type of iron salt)	937383	468691	115	6.68×10^{-40}	19
B (pH)	811126	405563	99	1.42×10^{-35}	16
C (temperature)	509469	254735	62	3.11×10^{-24}	10
D (ionic strength)	16304	8152	2	0.14	0
E (concentration iron)	100814	50407	12	6.27×10^{-6}	2
F (ratio [Fe]:[Cat])	869	434	0	0.90	0
G (MSG)	59483	29742	7	7.78×10^{-4}	1
A \times B	780182	195045	48	1.15×10^{-32}	16
A \times C	90012	22503	6	2.50×10^{-4}	2
A \times D	73998	18500	5	1.36×10^{-3}	1
A \times E	442251	110563	27	7.57×10^{-20}	9
A \times F	2235	559	0	0.97	0
A \times G	9240	2310	1	0.69	0
B \times C	357090	89272	22	2.66×10^{-16}	7
B \times D	32866	8216	2	0.09	1
B \times E	7930	1982	0	0.75	0
B \times F	11954	2989	1	0.57	0
B \times G	26167	6542	2	0.17	1
C \times D	5424	1356	0	0.86	0
C \times E	193111	48278	12	4.41×10^{-9}	4
C \times F	33035	8259	2	0.09	1
C \times G	121354	30338	7	8.83×10^{-6}	2
D \times E	8845	2211	1	0.70	0
D \times F	157640	39410	10	1.86×10^{-7}	3
D \times G	40674	10169	2	0.04	1
E \times F	10606	2651	1	0.63	0
E \times G	81992	20498	5	5.86×10^{-4}	2
F \times G	16030	4008	1	0.42	0

Significant two-way interactions were observed for **AB**, **AC**, **AD**, **AE**, **BC**, **CE**, **CG**, **DF**, **DG**, and **EG**. Together the two-way interactions explained 51 % of the variance observed in λ_{max} value. Interaction plots for these significant two-way interactions are shown in **Fig. 2.5**.

The two-way interactions that explained more than 5 % of the variance (**AB**, **AE**, and **BC**) are further discussed in the sections below. For the other significant two-way interactions, the mechanisms underlying their effect have not yet been elucidated. To the best of our knowledge, previous studies on the effect of various factors on discolouration caused by iron-phenolic complexation did not take two-way interactions into account.^[3,4] The obtained ANOVA model can be used to predict the λ_{max} value of unknown combinations of factors ($R^2_{\text{adj}} = 0.70$). The parameter estimates of the prediction model are presented in **Supplementary II (Table SII-1)**.

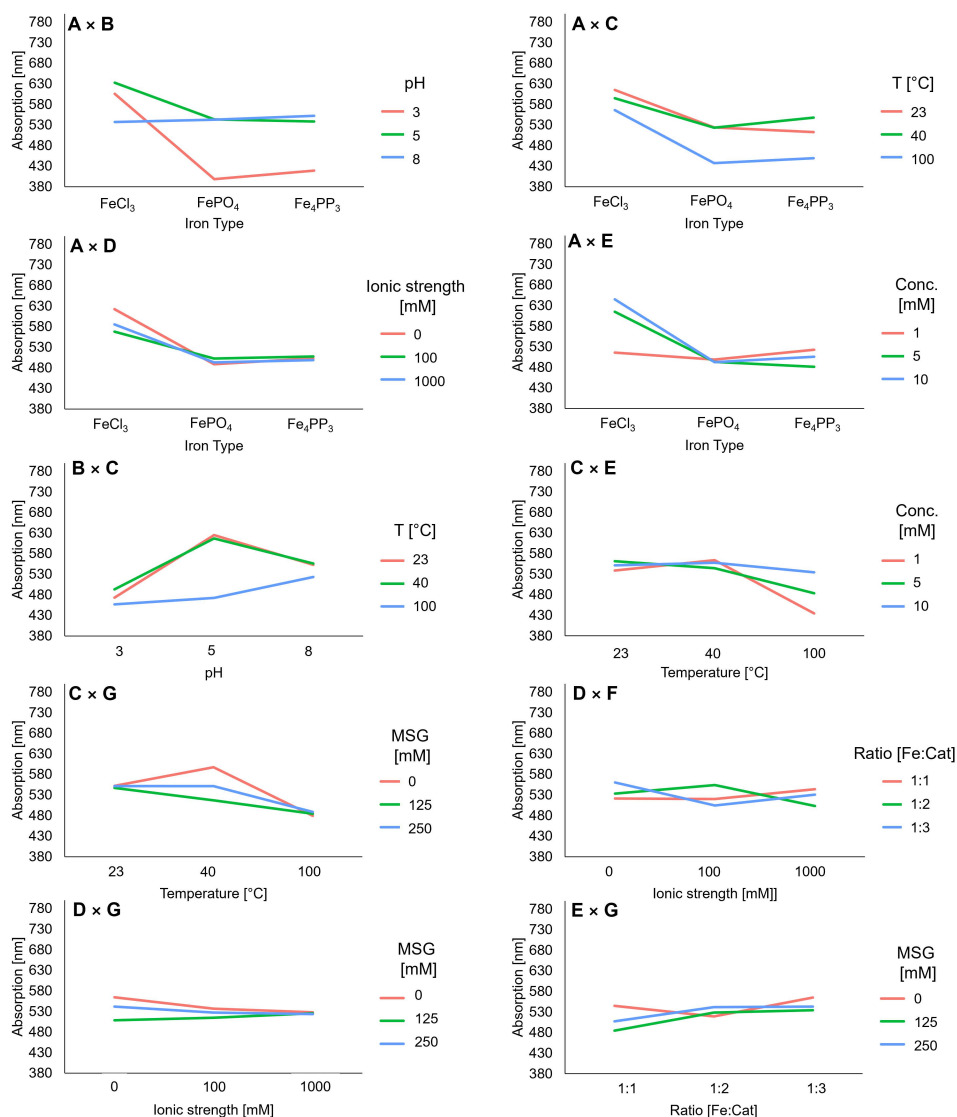


Figure 2.5. Interaction plots for the significant two-way interactions ($p < 0.05$) given by ANOVA ($n=486$), average maximum absorption wavelength is indicated on the y-axis. Letters indicate the factors corresponding with **Table 2.1**.

Effect of iron salt, pH, and temperature on discolouration

Significant interaction effects were observed between the type of iron salt (**A**) and pH (**B**). Generally, it was observed that mixtures with FeCl₃ resulted in discolouration at all pH values, although the λ_{\max} varied depending on pH. At pH 8 a significant decrease in λ_{\max} was observed compared to pH 3 or 5 (Tukey p -values of 1.18×10^{-4} and 1.03×10^{-7} , respectively). This is in line with the enhanced complexing capacity at $\text{pH} > \text{pK}_a$.

For Fe_4PP_3 and FePO_4 , a significant increase in discolouration was observed at $\text{pH} > 3$ (**Fig. 2.5; Supplementary II, Table SII-2**). To verify this conclusion, confirmatory experiments were performed with only the iron salt and pH as variable factors. In these experiments, iron-catechol mediated discolouration was observed for FeCl_3 at all pH values. For the Fe_4PP_3 and FePO_4 samples at pH 3, no colour was observed and white sediment (*i.e.* precipitate from undissolved iron salt) was present (**Fig. S2.3**). We believe that the interplay between the type of iron salt and pH (**AB**) could be explained by the enhanced dissolution of the iron ion from Fe_4PP_3 and FePO_4 upon an increase in $\text{pH}^{[30,31]}$, whereas the iron ion from FeCl_3 is readily soluble at pH 3. Enhanced dissolution of the iron ion from Fe_4PP_3 and FePO_4 upon increasing pH may either result from weaker interactions of phosphate and pyrophosphate ions with Fe(III) at elevated pH and/or from the formation of soluble complexes with deprotonated catechol.^[32,33] Tukey's *post hoc* comparison (**Supplementary II, Table SII-2**) also showed that, at pH 3 and 5, FeCl_3 significantly differed from Fe_4PP_3 and FePO_4 (Tukey, $p < 0.05$). On the other hand, no significant difference between the two poorly soluble iron salts Fe_4PP_3 and FePO_4 was observed at any pH. These outcomes indicate the importance of the type of iron salt used for food fortification in relation to the pH of the food product.

The interaction $\text{pH} \times \text{temperature}$ (**BC**) also significantly affected complexation. This is contrary to a previous report in which the temperature effect did not depend on pH for a combination of Fe(II) and flavonols.^[3] Habeych and co-authors state that colour development and formation of a dark precipitate was observed after heat treatment at 95°C , independently of pH. To further investigate the combined effect of pH and temperature, we performed additional experiments with pH and temperature as the only two independent variables, which showed a hypochromic shift in absorbance at pH 3 and 5 upon an increase in temperature and a hypsochromic shift at pH 8 (**Fig. S2.4**). *Post hoc* comparisons show no significant difference between the temperatures at pH 3 and 8. At pH 5 no significant difference was observed between 23°C and 40°C , but the results at 100°C were significantly different (**Supplementary II, Table SII-3**), in agreement with PCA results (**Fig. 2.2**). In some of the samples treated at 100°C , a dark precipitate was observed (**Fig. S2.5**). Likely, this precipitate results from iron-catalysed oxidation reactions that occur in parallel to, or as a continuation on the complexation reaction. Besides temperature, the oxidation of phenolics is influenced by pH,^[34] possibly explaining the interaction between pH and temperature observed in this study. In a previous study, Fe(III) -catalysed oxidation of phenolic derivatives at room temperature was shown to be slow.^[9] Faster oxidation at elevated temperatures is expected, as oxidation is a first-order reaction following a direct relation with temperature, as dictated by the Arrhenius equation. Further studies are necessary to gain more in-depth mechanistic insights into the effect of the two-way interaction of pH and temperature on iron-catechol complexation and the possible oxidation in iron-fortified food under various conditions. The outcomes of this study implicate that iron-catechol complexation may not be affected in regions with warmer climates ($\sim 40^\circ\text{C}$), but is affected upon boiling (100°C).

Effect of iron and catechol concentration on absorbance

The interaction effect between concentration and type of iron salt (**AE**) significantly contributed to discolouration. Colour development (intensity) was previously shown to be proportional to the iron concentration.^[4] However, the λ_{\max} was not expected to vary with the iron salt concentration. Tukey's test showed significant differences for FeCl_3 at the lowest concentration tested (**Supplementary II, Table SII-4**). The mechanism behind this effect is unclear.

Addition of MSG affects iron-catechol complexation

Interestingly, monosodium glutamate (MSG) showed significant interaction effects with temperature, ionic strength and concentration. PCA also showed that the addition of MSG affected the absorption spectra (**Fig. 2.2**). Binding of glutamate to Fe(III) was reported previously.^[35,36] However, the effect was expected to be minimal as Fe(III) has a lower overall binding stability constant for glutamate ($\text{Log } \beta = 5.5$) compared to the catechol groups of phenolics ($\text{Log } \beta = 43.8$).^[35-37]

Competitive or ternary complexation between iron, catechol, and MSG was further investigated using ESI-Q-TOF-MS. In these analyses, a peak was observed at m/z 308.98 in negative ionisation mode, which was only present in the samples that contained the combination of iron, catechol, and MSG. Based on the m/z , isotope pattern, and fragmentation spectra, this peak was tentatively identified as a ternary complex of catechol and iron with glutamate (**Table S2.1**). Glutamate most likely interacts with iron via the carboxylate oxygen and the amino nitrogen.^[38] The difference in absorbance (λ_{\max}) upon formation of the ternary complex may be due to the weaker interaction of glutamate with Fe(III) compared to catechol. Because of this, the λ_{\max} value of the ternary complex is expected to be between that of a 1:1 and 1:2 complex.^[12] In line with this hypothesis, the λ_{\max} of cluster **1**, which mainly contains the samples with high concentrations of MSG (**Fig. 2.3**) shows a hypsochromic shift compared to 1:1 and a bathochromic shift compared to 1:2 complexes. Further research regarding the apparent stability of the ternary complex is needed to confirm this hypothesis.

2.3.4. Mechanism of discolouration by iron-catechol reactions

The focus of this study was on the formation of water soluble iron-catechol complexes, under a wide variety of conditions, and the influence of this phenomenon on discolouration. Besides iron-catechol complexation, discolouration could also originate from iron-catalysed oxidation and polymerisation of catechol^[8] or from the formation of the strongly light absorbing iron (hydr)oxides upon Fe(III) hydrolysis.^[39] The latter is expected to be limited in the tested samples, as fast complexation of catechol to Fe(III) stabilises against the formation of Fe(III) hydrolysis products.^[40,41] Moreover, neither ferric (hydr)oxides, nor polymeric catechol oxidation products, were detected in the UV-Vis and MS spectra. Despite this, after incubation for 1 hour, black precipitate formation was observed in some samples, especially at elevated

temperatures (**Fig. S2.5**). Precipitate formation is suggested to result from the formation of insoluble products upon iron-catalysed catechol oxidation. In absence of iron, catechol can undergo autooxidation reactions in aqueous solution around neutral pH.^[13] The autooxidation products formed in the absence of iron are soluble and brown-coloured, whereas a clear black colour was observed of the precipitate in presence of iron (**Fig. S2.5**), indicating that different products were formed upon iron-catalysed oxidation. The observation that catechol is already oxidised after 1 hour in presence of iron is contrary to our initial expectations based on previous reports, which describe slow Fe(III)-catalysed oxidation rates of phenolic derivatives.^[9] The faster catechol oxidation rate observed in this study may result from elevated temperatures or different pH. Alternatively, the precipitate could be a result of the formation of iron-catechol networks.^[42] These networks between Fe(III) and phenolic derivatives can be formed thermodynamically at elevated temperature or due to kinetic assembly at low temperature.^[43] The findings of this study indicate that precipitation might occur, depending on intrinsic and extrinsic factors, which warrants further research on the parallel occurrence of iron-phenolic complexation and oxidation.

2.3.5. Implications for iron fortification of foods

As many common food phenolics also contain a catechol moiety, the findings of this study can be applied to the design of iron-fortified food formulations. The outcomes in this study indicate that the combined effect of factors on iron-phenolic complexation should not be neglected in the development of iron-fortified food. Food production, storage, and preparation are dynamic processes during which intrinsic (e.g. pH) and extrinsic factors (e.g. temperature) continuously change, resulting in discolouration depending on product properties, as shown by the findings of this study. Implementation of the parameter estimates from the ANOVA model that was generated by this study (**Supplementary II, Table SII-1**) can be useful to predict the λ_{\max} value of previously untested combinations of factors in the design of novel iron-fortified foods. Nevertheless, it should be considered that this prediction model is based on a model system and should be validated for real food formulations.

Our results indicate that usage of a combination of poorly soluble iron salts and low pH is a promising approach to limit discolouration due to iron-phenolic complexation. However, the effect of low pH on the sensory properties of food and the bioavailability of iron should also be considered. Even though the iron salts Fe_4PP_3 and FePO_4 show poor solubility and low reactivity at pH 3, the bioavailability of the iron ion is not necessarily affected by low pH. In the gastric pH range (pH < 3), the solubility of the iron ion from Fe_4PP_3 and FePO_4 is increased, enhancing the iron bio-accessibility.^[31,44] In this study, bouillon cubes are mentioned as an example of iron-fortified food. Besides, the findings provided can also be implemented in the design of other iron-fortified phenolic containing food products.

2.4. Conclusion

In this study, we successfully implemented a fractional factorial design to gain systematic insights into the combined effect of 7 experimental factors at 3 levels on iron-catechol complexation reactions and resulting discolouration in an iron-fortified food model system. HCA was used to identify 8 hierarchical clusters, each with different absorbance spectra resulting from varying stoichiometries of iron-catechol complexes, as confirmed by ESI-Q-TOF-MS. All three statistical methods revealed that the most important factors in iron-catechol complexation were the type of iron salt, pH, and temperature. Additionally, the interactions of several factors, such as type of iron salt \times pH, pH \times temperature, and type of iron salt \times concentration significantly affect iron-catechol complexation and are of practical importance. These interaction effects should not be neglected in the development of iron-fortified food. To minimise discolouration in food due to iron-phenolic complexation, application of the iron salts Fe_4PP_3 or FePO_4 in combination with low pH seems most promising.

2.5. Acknowledgements

Part of the presented results were obtained using a Synapt G2-Si high definition time of flight mass spectrometer which is owned by WUR-Shared Research Facilities. Investment by WUR-Shared Research Facility was made possible by the 'Regio Deal Foodvalley' of the province of Gelderland, The Netherlands.

2.6. References

- 1 McLean, E., Cogswell, M., Egli, I., Wojdyla, D., & De Benoist, B. (2009). Worldwide prevalence of anaemia, WHO vitamin and mineral nutrition information system, 1993–2005. *Public Health Nutrition*, 12(4), 444–454.
- 2 Allen, L. H., De Benoist, B., Dary, O., & Hurrell, R. (2006). Guidelines on food fortification with micronutrients. World Health Organization.
- 3 Habeych, E., van Kogelenberg, V., Sagalowicz, L., Michel, M., & Galaffu, N. (2016). Strategies to limit colour changes when fortifying food products with iron. *Food Research International*, 88, 122–128.
- 4 Mellican, R. I., Li, J., Mehansho, H., & Nielsen, S. S. (2003). The role of iron and the factors affecting off-color development of polyphenols. *Journal of Agricultural and Food Chemistry*, 51(8), 2304–2316.
- 5 Hurrell, R. F. (1997). Preventing iron deficiency through food fortification. *Nutrition Reviews*, 55(6), 210–222.
- 6 Moretti, D., Hurrell, R. F., & Cercamondi, C. I. (2018). Bouillon cubes. In M. G. V. Mannar & R. F. Hurrell (Eds.), *Food fortification in a globalized world*, vol. 1(pp. 159–165): Elsevier.
- 7 Bovell-Benjamin, A. C., & Guinard, J.-X. (2003). Novel approaches and application of contemporary sensory evaluation practices in iron fortification programs. *Critical Reviews in Food Science and Nutrition*, 43(4), 379–400.
- 8 Perron, N. R., & Brumaghim, J. L. (2009). A review of the antioxidant mechanisms of polyphenol compounds related to iron binding. *Cell Biochemistry and Biophysics*, 53(2), 75–100.
- 9 Nkhili, E., Loonis, M., Mihai, S., El Hajji, H., & Dangles, O. (2014). Reactivity of food phenols with iron and copper ions: Binding, dioxygen activation and oxidation mechanisms. *Food & Function*, 5(6), 1186–1202.
- 10 Sever, M. J., & Wilker, J. J. (2004). Visible absorption spectra of metal–catecholate and metal–tironate complexes. *Dalton Transactions*, 7, 1061–1072.
- 11 Pierpont, C. G. (2001). Studies on charge distribution and valence tautomerism in transition metal complexes of catecholate and semiquinonate ligands. *Coordination Chemistry Reviews*, 216–217, 99–125.
- 12 Elhabiri, M., Carrère, C., Marmolle, F., & Trahouls, H. (2007). Complexation of iron(III) by catecholate-type polyphenols. *Inorganica Chimica Acta*, 360(1), 353–359.
- 13 Maier, G. P., Bernt, C. M., & Butler, A. (2018). Catechol oxidation: Considerations in the design of wet adhesive materials. *Biomaterials Science*, 6(2), 332–339.
- 14 Hider, R. C., Liu, Z. D., & Khodr, H. H. (2001). Metal chelation of polyphenols. *Methods in Enzymology*, 335, 190–203.
- 15 Parkin, G. (2004). Synthetic analogues relevant to the structure and function of zinc enzymes. *Chemical Reviews*, 104(2), 699–768.
- 16 Janssen, R. H., Canelli, G., Sanders, M. G., Bakx, E. J., Lakemond, C. M., Fogliano, V., & Vincken, J.-P. (2019). Iron-polyphenol complexes cause blackening upon grinding *Hermetia illucens* (black soldier fly) larvae. *Scientific Reports*, 9(1), 2967.
- 17 Lu, L.-L., Li, Y.-h., & Lu, X.-y. (2009). Kinetic study of the complexation of gallic acid with Fe(III). *Spectrochimica Acta Part A: Molecular and Biomolecular Spectroscopy*, 74(3), 829–834.
- 18 Guo, J., Richardson, J. J., Besford, Q. A., Christofferson, A. J., Dai, Y., Ong, C. W., Tardy, B. L., Liang, K., Choi, G. H., & Cui, J. (2017). Influence of ionic strength on the deposition of metal–phenolic networks. *Langmuir*, 33(40), 10616–10622.
- 19 Fang, K., Yuan, D., Zhang, L., Feng, L., Chen, Y., & Wang, Y. (2015). Effect of environmental factors on the complexation of iron and humic acid. *Journal of Environmental Sciences*, 27, 188–196.
- 20 Xu, H. (2005). A catalogue of three-level regular fractional factorial designs. *Metrika*, 62(2–3), 259–281.
- 21 Andjelković, M., Van Camp, J., De Meulenaer, B., Depaemelaere, G., Socaciu, C., Verloo, M., & Verhe, R. (2006). Iron-chelation properties of phenolic acids bearing catechol and galloyl groups. *Food Chemistry*, 98(1), 23–31.
- 22 Ferreira, C. M., Pinto, I. S., Soares, E. V., & Soares, H. M. (2015). (Un)suitability of the use of pH buffers in biological, biochemical and environmental studies and their interaction with metal ions – a review. *RSC Advances*, 5(39), 30989–31003.
- 23 Ward, J. H. (1963). Hierarchical grouping to optimize an objective function. *Journal of the American Statistical Association*, 58(301), 236–244.
- 24 Di Marco, V. B., & Bombi, G. G. (2006). Electrospray mass spectrometry (ESI-MS) in the study of metal–ligand solution equilibria. *Mass Spectrometry Reviews*, 25(3), 347–379.
- 25 Orłowska, E., Roller, A., Pignitter, M., Jirsa, F., Krachler, R., Kandjoller, W., & Keppler, B. K. (2017). Synthetic iron complexes as models for natural iron–humic compounds: Synthesis, characterization and algal growth experiments. *Science of The Total Environment*, 577, 94–104.
- 26 Mira, L., Tereza Fernandez, M., Santos, M., Rocha, R., Helena Florêncio, M., & Jennings, K. R. (2002). Interactions of flavonoids with iron and copper ions: A mechanism for their antioxidant activity. *Free Radical Research*, 36(11), 1199–1208.
- 27 Fernandez, M. T., Mira, M. L., Florêncio, M. H., & Jennings, K. R. (2002). Iron and copper chelation by flavonoids: An electrospray mass spectrometry study. *Journal of Inorganic Biochemistry*, 92(2), 105–111.

- 28 Gianelli, L., Amendola, V., Fabbri, L., Pallavicini, P., & Mellerio, G. G. (2001). Investigation of reduction of Cu(II) complexes in positive-ion mode electrospray mass spectrometry. *Rapid Communications in Mass Spectrometry*, 15(23), 2347-2353.
- 29 Pei, J., Hsu, C.-C., Zhang, R., Wang, Y., Yu, K., & Huang, G. (2017). Unexpected reduction of iminoquinone and quinone derivatives in positive electrospray ionization mass spectrometry and possible mechanism exploration. *Journal of The American Society for Mass Spectrometry*, 28(11), 2454-2461.
- 30 Priambodo, R., Tan, Y.-L., Shih, Y.-J., & Huang, Y.-H. (2017). Fluidized-bed crystallization of iron phosphate from solution containing phosphorus. *Journal of the Taiwan Institute of Chemical Engineers*, 80, 247-254.
- 31 Tian, T., Blanco, E., Smoukov, S. K., Velez, O. D., & Velikov, K. P. (2016). Dissolution behaviour of ferric pyrophosphate and its mixtures with soluble pyrophosphates: Potential strategy for increasing iron bioavailability. *Food Chemistry*, 208, 97-102.
- 32 Lijklema, L. (1980). Interaction of orthophosphate with iron(III) and aluminum hydroxides. *Environmental Science & Technology*, 14(5), 537-541.
- 33 Altundogan, H. S., & Tumen, F. (2002). Removal of phosphates from aqueous solutions by using bauxite. I: Effect of pH on the adsorption of various phosphates. *Journal of Chemical Technology & Biotechnology*, 77(1), 77-85.
- 34 Kumamoto, M., Sonda, T., Nagayama, K., & Tabata, M. (2001). Effects of pH and metal ions on antioxidative activities of catechins. *Bioscience, biotechnology, and biochemistry*, 65(1), 126-132.
- 35 Djurdjević, P., & Jelić, R. (1997). Solution equilibria in L-glutamic acid and L-serine + iron(III) systems. *Transition Metal Chemistry*, 22(3), 284-293.
- 36 Perrin, D. (1958). The stability of complexes of ferric ion and amino acids. *Journal of the Chemical Society*, 3125-3128.
- 37 Avdeef, A., Sofen, S. R., Bregante, T. L., & Raymond, K. N. (1978). Coordination chemistry of microbial iron transport compounds. 9. Stability constants for catechol models of enterobactin. *Journal of the American Chemical Society*, 100(17), 5362-5370.
- 38 Sajadi, S. (2010). Metal ion-binding properties of L-glutamic acid and L-aspartic acid, a comparative investigation. *Natural Science*, 2(02), 85.
- 39 Flynn, C. M. (1984). Hydrolysis of inorganic iron(III) salts. *Chemical Reviews*, 84(1), 31-41.
- 40 Kosman, D. J. (2013). Iron metabolism in aerobes: Managing ferric iron hydrolysis and ferrous iron autoxidation. *Coordination Chemistry Reviews*, 257(1), 210-217.
- 41 Xiao, J., Wang, C., Lyu, S., Liu, H., Jiang, C., & Lei, Y. (2016). Enhancement of Fenton degradation by catechol in a wide initial pH range. *Separation and Purification Technology*, 169, 202-209.
- 42 Ejima, H., Richardson, J. J., & Caruso, F. (2017). Metal-phenolic networks as a versatile platform to engineer nanomaterials and biointerfaces. *Nano Today*, 12, 136-148.
- 43 Zhong, Q. Z., Li, S., Chen, J., Xie, K., Pan, S., Richardson, J. J., & Caruso, F. (2019). Oxidation-mediated kinetic strategies for engineering metal-phenolic networks. *Angewandte Chemie International Edition*, 58(36), 12563-12568.
- 44 Stumm, W., & Morgan, J. J. (2012). *Aquatic chemistry: Chemical equilibria and rates in natural waters* (Vol. 126) John Wiley & Sons.

2.7. Supplementary information

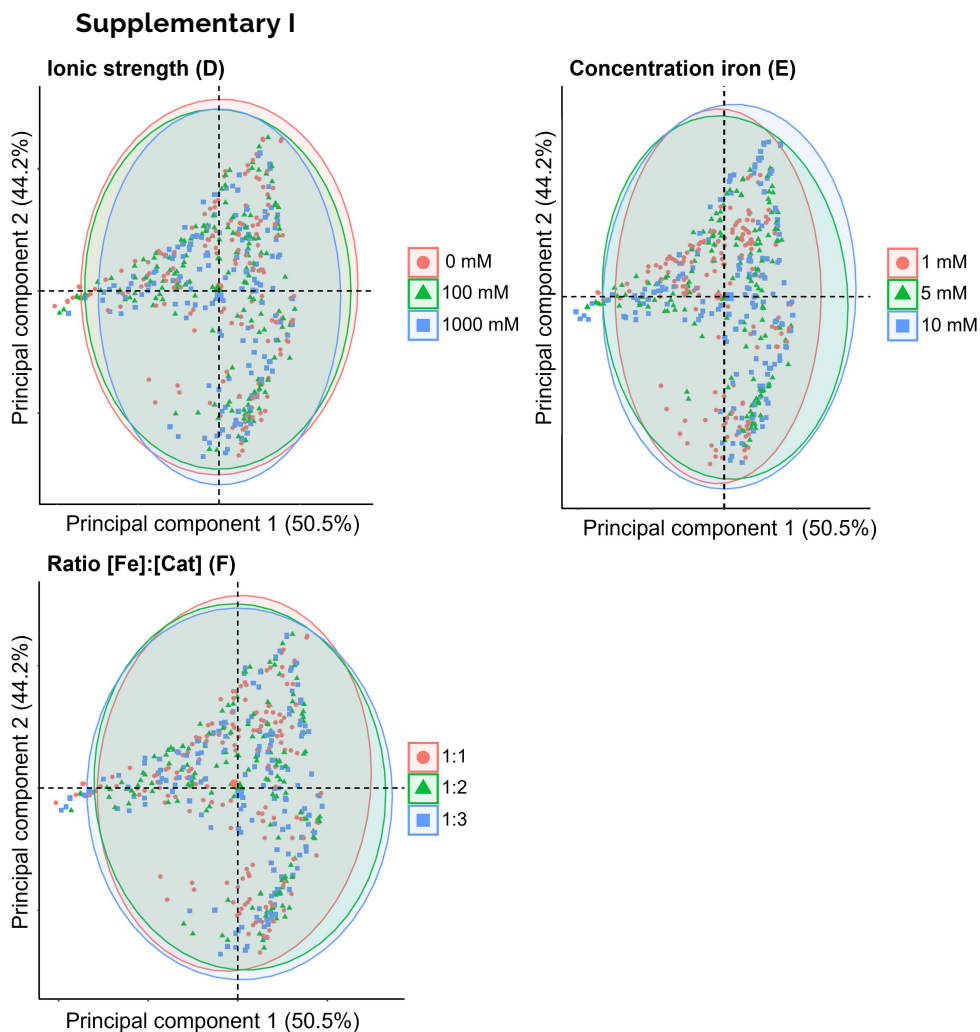


Figure S2.1. Biplots showing the principal component scores based on the absorbance spectra, with colour indicating different levels of the corresponding factors: ionic strength (D), concentration of iron (E), and ratio [Fe]:[Cat] (F).

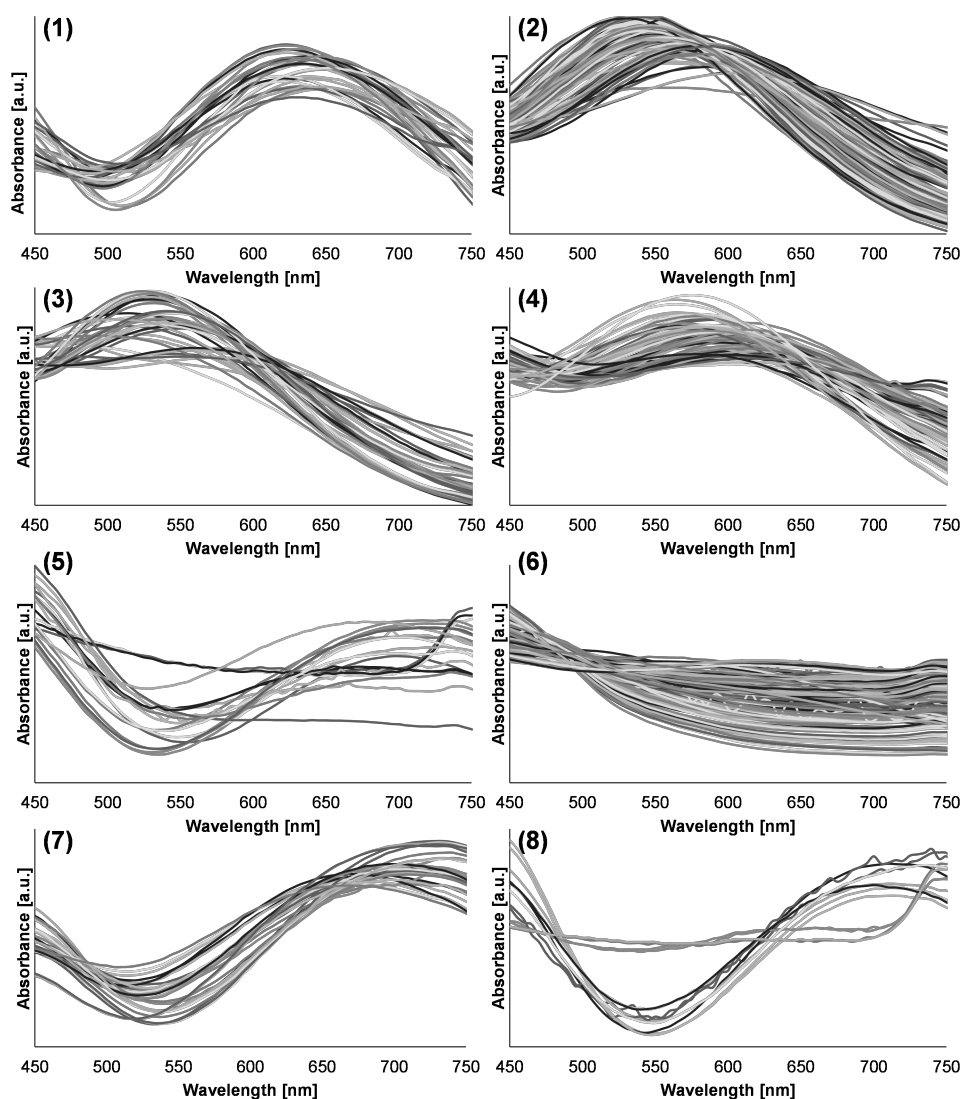


Figure S2.2. Overview of the clustered absorbance spectra after normalisation and HCA, the numbers 1-8 correspond with the cluster numbers of the dendrogram obtained by HCA (Figure 2.3).

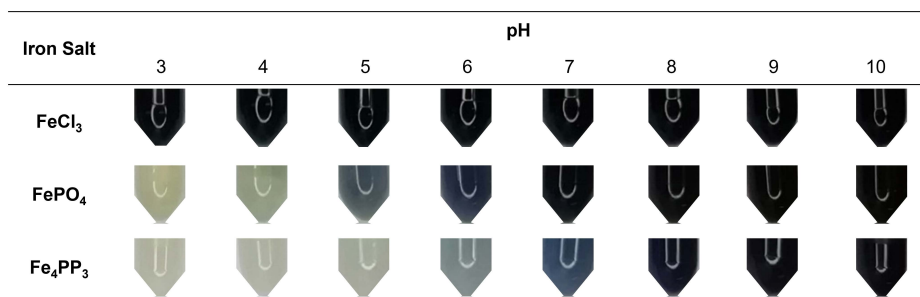


Figure S2.3. Photographs of Eppendorf showing colour formation of catechol in combination with the different iron salts at pH ranging from 3-10 after 1 hour incubation at 23 °C.

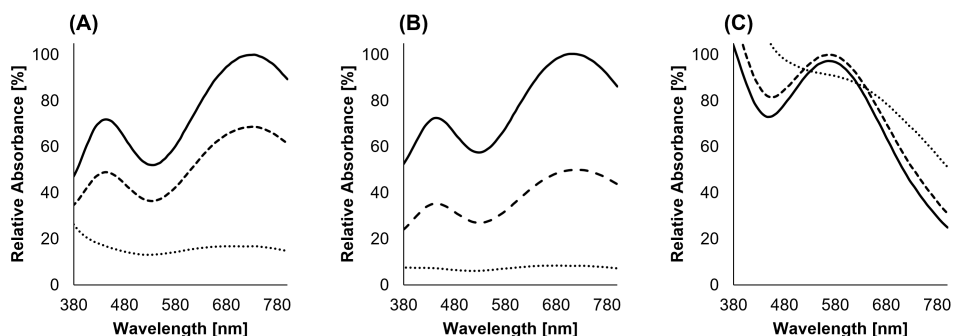


Figure S2.4. Absorbance spectra of FeCl_3 -Catechol mixtures at (A) pH 3, (B) pH 5, and (C) pH 8 after incubation at 23 °C (solid line), 40 °C (dashed line), and 100 °C (dotted line) for 1 hour.

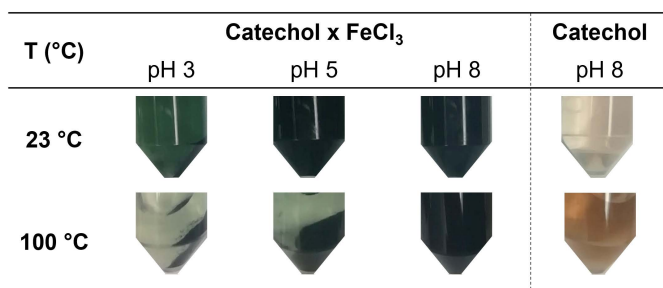
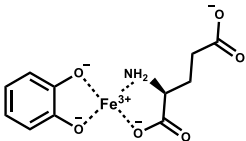


Figure S2.5. Photographs of Eppendorf tubes showing colour formation and precipitation of iron-catechol mixtures (10 mM) at pH 3, 5, and 8 after 1 hour incubation at 23 °C or 100 °C. A catechol solution without iron (pH 8) after 1 hour incubation is shown as a reference.

Table S2.1. Tentative structure of the iron-catechol-glutamate complex with experimental and theoretical mass-to-charge ratios (m/z) and isotope abundance.

Tentative Structure	Isotopes	m/z		Isotope abundance (%)	
		Exp.	Theoretical	Exp.	Theoretical
	$^{12}\text{C}_{11}\text{H}_{11}\text{NO}_6^{54}\text{Fe}$	306.99	307.00	3.6	6.4
	$^{12}\text{C}_{11}\text{H}_{11}\text{NO}_6^{56}\text{Fe}$	308.99	308.99	100	100
	$^{12}\text{C}_{11}\text{H}_{11}\text{NO}_6^{57}\text{Fe}$ or	309.99	310.00	9.8	14.2
	$^{12}\text{C}_{10}^{13}\text{C}_1\text{H}_{11}\text{NO}_6^{56}\text{Fe}$				
	$^{12}\text{C}_{10}^{13}\text{C}_1\text{H}_{11}\text{NO}_6^{57}\text{Fe}$	310.99	311.00	1.6	1.2
	or $^{12}\text{C}_9^{13}\text{C}_2\text{H}_{11}\text{NO}_6^{56}\text{Fe}$				

Supplementary II

The full **supplementary information II** file can be found on the publisher's website (<https://doi.org/10.1038/s41598-020-65171-1>) the table numbers in the text refer to the corresponding table numbers in the tab of the excel file.

CHAPTER 3

Unravelling discolouration caused by iron-flavonoid interactions:

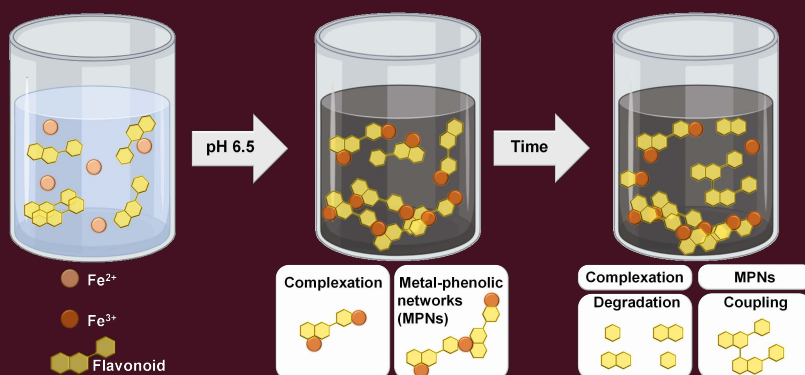
complexation, oxidation, and formation of networks

Judith Bijlsma, Wouter J.C. de Bruijn,
Krassimir P. Velikov, and Jean-Paul Vincken

Based on: *Food Chemistry*, 2022, 370:131292.

Abstract

Iron-flavonoid interactions in iron-fortified foods lead to undesirable discolouration. This study aimed to investigate iron-mediated complexation, oxidation, and resulting discolouration of flavonoids by spectrophotometric and mass spectrometric techniques. At pH 6.5, iron complexation to the 3-4 or 4-5 site instantly resulted in bathochromic shifting of the $\pi \rightarrow \pi^*$ transition bands, and complexation to the 3'-4' site (*i.e.* catechol moiety) induced a $\pi \rightarrow d_{\pi}$ transition band. Over time, iron-mediated oxidative degradation and coupling reactions led to the formation of hydroxybenzoic acid derivatives and dehydrodimers, respectively resulting in a decrease or increase in discolouration. Additionally, we employed XRD, SEM, and TEM to reveal the formation of insoluble black metal-phenolic networks (MPNs). This integrated study on iron-mediated complexation and oxidation of flavonoids showed that the presence of the C2-C3 double bond in combination with the catechol moiety and either the 4-carbonyl or 3-hydroxyl increased the intensity of discolouration, extent of oxidation, and formation of MPNs.



3.1. Introduction

Food fortified with iron can effectively reduce the global prevalence of iron deficiency.^[1] However, when food is fortified with iron, its colour and iron bioavailability can be compromised by the reactivity of the iron ion with flavonoids.^[2] Flavonoids are secondary plant metabolites that are ubiquitous in vegetables, herbs, and fruits. These compounds affect food colour and flavour, and possess a broad range of biological activities. The class of flavonoids includes several subclasses that share the same flavan (2-phenylchromen-4-one) backbone but possess different structural features based on the degree of oxidation of the pyran C-ring (**Fig. 3.1A**).

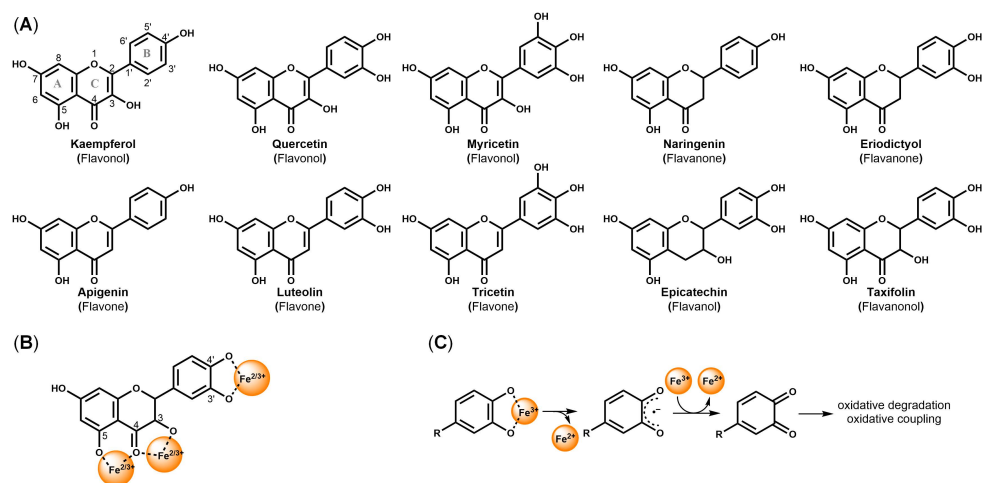


Figure 3.1. (A) Overview of the dietary flavonoids investigated in this study, the corresponding flavonoid subclass is indicated between brackets; (B) possible binding sites of iron ions (in ferrous or ferric state) on flavonoids; (C) oxidation of the flavonoid 3'-4' site to a semiquinone-type radical and eventually to a quinone in presence of ferric iron.

Hydroxyl and carbonyl groups on the flavan backbone can coordinate metal ions to form stable complexes. Flavonoids possess several structural moieties that can bind metal ions via coordinate bonds: (i) the 3-hydroxy-4-ketone moiety in the C-ring (3-4 site), (ii) 5-hydroxy-4-ketone moiety (4-5 site), and (iii) the 3'-4'-dihydroxy moiety located in the B-ring (3'-4' site) (**Fig. 3.1B**).^[3] The stoichiometry of iron-flavonoid complexes (e.g. 1:1, 1:2, and 2:1) and preferred iron-binding sites are dependent on the solvent, the pH of the sample, iron source, and flavonoid structure.^[4] Ferrous sulphate (FeSO_4) is used as iron source, since it is the most common iron fortificant in food owing to affordability, bioavailability, and (regulatory) acceptance by authorities and consumers.^[1] Complexation of flavonoids to Fe(II) is followed by fast auto-oxidation to Fe(III) because phenolic ligands stabilise Fe(III) over Fe(II) .^[5]

Complexation of metals to flavonoids changes the flavonoids' absorbance spectra, resulting in a bathochromic (red) shift.^[4] Complexation of Fe(III) to the catechol moiety

(i.e. 3'-4' site in flavonoids) causes intense off-colour development resulting from ligand-to-metal charge transfer (LMCT) phenomena, also referred to as $\pi \rightarrow d_{\pi}$ transitions.^[6,7] Typically, these $\pi \rightarrow d_{\pi}$ transitions result in a bathochromic shift of the absorbance and formation of a broad absorbance band ranging from 380-800 nm. Besides this, bathochromic shifting of the $\pi \rightarrow \pi^*$ transitions to around 425 nm has also been reported for flavonoids due to an increase in the size of the conjugated system upon Fe(III) complexation.^[8,9] Such a shift of $\pi \rightarrow \pi^*$ transitions was also reported for flavonoids, that contained solely a 4-5 binding site.^[10] Iron complexation to flavonoids that contain solely a 3-4 site has hitherto not been reported and its effects on absorbance spectra, including the underlying transition mechanisms, are yet unknown. Thus far, it remains unclear whether the shift in absorbance upon complexation of iron to either one or all three of the different binding sites of flavonoids is due to LMCT ($\pi \rightarrow d_{\pi}$ transitions), increased size of the conjugated system ($\pi \rightarrow \pi^*$ transitions), or a combination thereof.^[4]

Coordinate bond formation between Fe(III) and flavonoids can be followed by a redox reaction, via electron transfer (ET) from the flavonoid to iron.^[11] In this process, the complexed Fe(III) is reduced to Fe(II) and the flavonoid is thereby oxidised to a semiquinone-type radical, and a quinone upon a second ET (**Fig. 3.1C**). Subsequent reactions of the flavonoid quinones yield a plethora of products arising from degradation and oxidative coupling. Extension of the conjugated system of the flavonoid upon oxidative coupling contributes to browning.^[12] Additionally, the resulting degradation and oxidative coupling products may form complexes with iron, and thereby further affect the colour.

Iron-mediated complexation and oxidation are affected by the structural features of flavonoids as previously demonstrated by the structure-activity relationships established for iron complexation and radical scavenging, both measures of the antioxidant activity of flavonoids. Flavonoids possessing the catechol or pyrogallol moieties are generally stronger antioxidants because of the stability constants for binding of the 3'-4' site to iron.^[5,13] Furthermore, the presence of the 3-OH and/or the 5-OH in combination with the C4 keto group and the C2-C3 double bond is also associated with Fe(III)-complexation and reported to confer increased Fe(III)-reducing capacity.^[14,15] The Fe(III)-mediated oxidation of catechol and other phenolics at neutral pH is reported to be slow.^[16-18] However, in these reports, the interaction between Fe(III) and phenolics was usually measured over a short timespan (e.g. 1 h). Longer-term effects should be considered to more realistically mimic the iron-flavonoid interactions that can take place during food processing, storage, and preparation.

The aforementioned studies have focussed primarily on separately assessing either iron-mediated complexation or oxidation of flavonoids, and not the combined and interconnected effect of these two interactions on discolouration. Therefore, we

aimed to comprehensively investigate the combination of iron-mediated complexation and oxidation on the discolouration of a set of structurally different flavonoids. Ten different flavonoids were incubated with iron (FeSO_4) and the influence of structural features on discolouration was assessed. The contribution of complexation and oxidation to discolouration was elucidated via spectrophotometric and mass spectrometric techniques. Because complexation is known to affect iron bioavailability, the proportion of water soluble iron at pH 6.5 was investigated as a first indicator for iron bio-accessibility in presence of our broad set of flavonoids.^[19]

We hypothesised that (i) fast discolouration is caused by iron-flavonoid complexation; (ii) oxidation of flavonoids over time affects discolouration; (iii) structural features of the flavonoid, specifically the hydroxylation of the B-ring, the C2-C3 double bond, and the 3-hydroxy-4-keto moiety, and combinations thereof contribute to complexation and oxidation; and (iv) that the catechol moiety on the B-ring is prerequisite for LMCT. To the best of the authors' knowledge, this is the first integrated study investigating the combined effect of iron-mediated complexation and oxidation on the discolouration of a structurally diverse set of flavonoids.

3.2. Materials & methods

3.2.1. Materials

Quercetin hydrate (≥ 95 wt. %), 4-hydroxybenzoic acid (≥ 99 wt. %), 3,4,5-trihydroxybenzoic acid (≥ 98 wt. %), iron(II) sulphate heptahydrate (≥ 99 wt. %), and 3-(2-pyridyl)-5,6-diphenyl-1,2,4-triazine-p,p'-disulfonic acid monosodium salt hydrate (≥ 97 wt. %; ferrozine) were obtained from Sigma Aldrich (St. Louis, MO, USA). Myricetin (≥ 97 wt. %), naringenin (≥ 93 wt. %), epicatechin (≥ 97 wt. %), 3,4-dihydroxybenzoic acid (≥ 98 wt. %) and 2,4,6-trihydroxybenzoic acid (≥ 98 wt. %) were purchased from TCI Europe NV (Zwijndrecht, Belgium). Kaempferol (≥ 99 wt. %), luteolin (≥ 98 wt. %), eriodictyol (≥ 99 wt. %), and taxifolin (≥ 98 wt. %) were purchased from Extrasynthese (Genay, France), apigenin (≥ 98 wt. %) from Indofine Chemical Company (Hillsborough, NJ, USA), and tricetin (≥ 95 wt. %) from Specs (Delft, The Netherlands). Ascorbic acid (≥ 99 wt. %) was obtained from VWR International (Radnor, PA, USA). Dimethylsulfoxide (DMSO) was obtained from Merck Millipore (Billerica, MA, USA). ULC-MS grade acetonitrile (ACN) and water, both containing 0.1 vol. % formic acid (FA) were purchased from Biosolve (Valkenswaard, the Netherlands). Water for other purposes than UHPLC was prepared using a Milli-Q water purification system (Merck Millipore, Billerica, MA, USA).

3.2.2. Incubation of flavonoids with or without iron

Stock solutions of each flavonoid were made by dissolving them in DMSO to a 20 mM concentration. Subsequently, each flavonoid stock solution was diluted either in water (flavonoid blank; final concentration flavonoid 1 mM; pH 6.0-7.5) or in a freshly prepared FeSO_4 solution (iron-flavonoid; final concentration flavonoid 1 mM; final

concentration Fe(II) 1 mM; pH 4.5-5.0), for the iron blank a solution of 1mM FeSO₄ was prepared (pH 5.0). The final volume of all samples was 10 mL, containing 5 vol. % DMSO. An aliquot of 0.5 mL was taken from the sample immediately after adding the flavonoid (*t₀*). Subsequently, each sample was adjusted to pH 6.5 by using a pH-stat device (Metrohm, Herisau, Switzerland), and during the experiment the pH was maintained at 6.5 with automated titration using 0.05 M HCl and 0.05 M NaOH. This approach of maintaining pH with concentrated HCl and NaOH was chosen as buffer compounds can cause interference with complexation and oxidation reactions.^[20,21] After pH adjustment, the samples were incubated at 40 °C under magnetic stirring (300 rpm) and aliquots (0.5 mL) were taken after 0, 1, 2, 4, and 24 h. During incubation, no measures were taken to reduce oxygen and light levels. The 0.5 mL samples were centrifuged (5 min, 15,000 × *g*) and the supernatant was separated to obtain the water soluble (WS) fraction. The pellet was solubilised with DMSO (100 vol. %), which is known to be a suitable solvent for metal:ligand systems.^[22] The resulting suspension was centrifuged once more (5 min, 15,000 × *g*) and the supernatant was separated to obtain the DMSO soluble (DS) fraction. The DMSO insoluble pellet was freeze-dried to remove any remaining DMSO. Subsequently, 200 µL of 25 mM aqueous ascorbic acid was added to the freeze-dried pellet, which was then sonicated for 15 minutes, diluted 20 times with DMSO for a final DMSO concentration of 95 vol. %, and sonicated for an additional 15 min. After sonication, the sample was centrifuged for 5 min (15,000 × *g*) and the supernatant was collected as the ascorbic acid soluble (AAS) fraction. The remaining pellet was not analysed further. The colour of the samples was recorded and assessed by spectrophotometric analysis and by taking pictures (Samsung-G960F, Seoul, South Korea) against a white background.

3.2.3. Monitoring complexation, oxidation, and discolouration by UV-Vis spectroscopy

The effect of FeSO₄ addition on complexation and oxidation reactions, and their effect on discolouration was monitored using UV-Vis spectroscopy according to a method adapted from.^[16] In short, the UV-Vis spectra of the WS and DS fractions were obtained directly after sampling and centrifugation, 200 µL sample was transferred to a Corning UV-transparent flat-bottom polystyrene 96 well-plate (Sigma Aldrich, St. Louis, MO, USA). Spectra were recorded in the range from 250 – 750 nm in a SpectraMax iD3 (Molecular Devices, Sunnyvale, CA, USA), at room temperature. The lower relative polarity of DMSO in the DS fractions (0.44) in comparison to water in the WS fractions (1.00) can affect electronic transitions and absorbance spectra.^[23] In this study, a maximum bathochromic shift of the $\pi \rightarrow \pi^*$ and $\pi \rightarrow d_{\pi}$ bands of 30 nm was observed in presence of DMSO.

3.2.4. Flavonoid quantification and identification of reaction products by RP-UHPLC-PDA-ESI-ITMSⁿ

DS, WS, and AAS fractions were immediately analysed by reversed-phase ultra-high performance liquid chromatography coupled to electrospray ionisation ion trap mass spectrometry (RP-UHPLC-PDA-ESI-ITMSⁿ). Flavonoids and their oxidation products were separated on a Thermo Vanquish UHPLC system (Thermo Scientific, San Jose, CA, USA) equipped with an autosampler, a pump, a photodiode array (PDA) detector, and coupled *in-line* to an LTQ Velos Pro ion trap mass spectrometer (Thermo Scientific). The temperature of the autosampler was controlled at 25 °C to prevent solidification of DMSO ($T_m = 18.5$ °C). Sample (1 µL) was injected on an Acquity UPLC BEH C18 column (150 mm × 2.1 mm i.d., 1.7 µm) with a VanGuard (5 mm × 2.1 mm i.d., 1.7 µm) guard column of the same material (Waters, Milford, MA). Water (A) and acetonitrile (B), both acidified with 0.1 vol. % formic acid, were used as eluents. The flow rate was 400 µL min⁻¹, and the temperature of the column oven was 45 °C with the post-column cooler set to 40 °C. The following elution profile was used: 0.00 – 1.09 min, isocratic on 1 vol. % B; 1.09 – 20.72 min, linear gradient from 1 to 55 vol. % B; 20.72 – 21.81 min linear gradient from 55 to 100 vol. % B; 21.81 – 27.26 min isocratic on 100 vol. % B; 27.26 – 28.35 min linear gradient from 100 to 1 vol. % B; 28.35 – 33.81 min isocratic on 1 vol. % B. The PDA detector was set to measure the wavelength range of 190 – 680 nm. Mass spectrometric data were acquired using an ion trap mass spectrometer equipped with a heated electrospray ionisation probe (ESI-ITMSⁿ). Nitrogen was used as a sheath gas (50 arbitrary units) and auxiliary gas (13 arbitrary units). Data were collected over the m/z range of 100 – 1,500 in negative and positive ionisation mode by using source voltages of 2.5 and 3.5 kV, respectively. For both modes, the S-lens RF level was set at 67 %, the ion transfer tube temperature was 263 °C and the source heater temperature 425 °C. Data-dependent MS² analysis was performed on the most intense ion by collision-induced dissociation (CID) with normalised collision energy of 35 %. A dynamic mass exclusion approach was used, in which the most intense ion was fragmented 3 times and was subsequently excluded from fragmentation for the following 5 seconds, allowing data-dependent MS² of less intense co-eluting compounds. Data acquisition and processing were performed using Xcalibur (version 4.1, Thermo Scientific). Quantification of each flavonoid in the WS, DS, and AAS fraction was performed based on PDA peak area (280 nm) and an external calibration curve of the corresponding authentic standard (0.03 – 1 mM, in duplicate, $R^2 \geq 0.99$). The quantity of flavonoid over time was defined as recovery, in which the starting concentration of flavonoid (1 mM) was set as 100 % recovery. To test if the trend in flavonoid decrease over time was statistically significant, ANOVA analysis was performed using IBM SPSS Statistic v23 software (SPSS Inc., Chicago, IL, USA). Tukey's *post hoc* comparisons (significant at $p < 0.05$) were carried out to evaluate differences per time point in the total flavonoid recovery and recovery of flavonoid in the WS, DS, and AAS fraction.

3.2.5. Determination of iron concentration by ferrozine-based colourimetric assay

The total amount of iron in the WS, DS, and AAS fractions obtained at the different time points was quantified using a ferrozine-based colourimetric assay.^[24] Binding of ferrous iron by 3-(2-pyridyl)-5-6-(bis(4-phenylsulfonic acid)-1,2,4-triazine (*i.e.* ferrozine) results in the formation of a complex with λ_{max} at 565 nm. To ensure the reduction of ferric iron to its ferrous state, an excess of ascorbic acid (50 μL , 100 mM) was added to 50 μL sample (*i.e.* WS, DS, AAS fractions). After 1 h incubation with ascorbic acid, an excess of ferrozine (50 μL , 10 mM) was added. Ferrozine is a highly ferrous-stabilising ligand, therefore all ferrous iron binds to ferrozine to yield a ferrous iron-ferrozine complex.^[25] Samples were transferred to 96-well microplates and the absorbance at 565 nm was measured in a SpectraMax iD3, at room temperature. All measurements were performed in duplicate, quantification of total iron was performed based on intensity (565 nm) and a calibration curve of FeSO_4 (0.00625 – 0.5 mM, in duplicate, $R^2 \geq 0.99$). Measurements were corrected for the flavonoid blank and it was confirmed that the presence of DMSO did not interfere with the quantification of soluble iron.

3.2.6. Characterisation of the nature and morphology of iron-flavonoid reaction products

The nature and morphological characteristics of naringenin and quercetin samples prior to and after reaction with FeSO_4 but before fractionation to WS, DS, and AAS were analysed using X-ray powder diffraction (XRD), scanning electron microscopy (SEM), and transmission electron microscopy (TEM). The iron-flavonoid samples were prepared as described in **section 3.2.2** and a sample was taken before (t_0) and after adjustment of pH to 6.5 (t_6). XRD measurements were performed with a Bruker D8 Advance diffractometer (Bruker, Karlsruhe, Germany). The source consisted of Cu $K\alpha$ radiation ($\lambda = 1.54 \text{ \AA}$). XRD patterns were recorded from 5° to 60° 2θ , with a step size of 0.01° and a scan speed of 0.1 s/step. The XRD data was processed using the Bruker DIFFRAC.EVA software and the obtained patterns were identified by comparison with reference patterns in the Crystallography Open Database (COD). Optical analysis was carried out at the Wageningen Electron Microscopy Centre (WEMC). Prior to SEM, iron-flavonoid sample was applied to a 1 μm filter and air-dried. The sample was attached on a sample holder using carbon adhesive tabs and sputter-coated with 12 nm tungsten using a Leica SCD 500 (Vienna, Austria). SEM analysis was performed on FEI Magellan 400 (FEI, Eindhoven, The Netherlands). For TEM analysis, 1 mM samples were added to a 400 mesh formvar/carbon grid and air-dried before measurement using a JEM-1400Plus (JEOL, MA, USA), operating at 120 kV.

3.3. Results & discussion

3.3.1. Effect of flavonoid structure on iron-mediated discolouration

Absorbance spectra of the flavonoid samples were recorded in the absence and presence of iron. **Fig. 3.2A** shows the λ_{\max} values and colour of the flavonoid and flavonoid + iron samples at pH 6.5. Full absorbance spectra of the water soluble (WS) and DMSO soluble (DS) fractions of all ten flavonoids are shown in the supplementary information (**Fig. S3.1 to S3.4**).

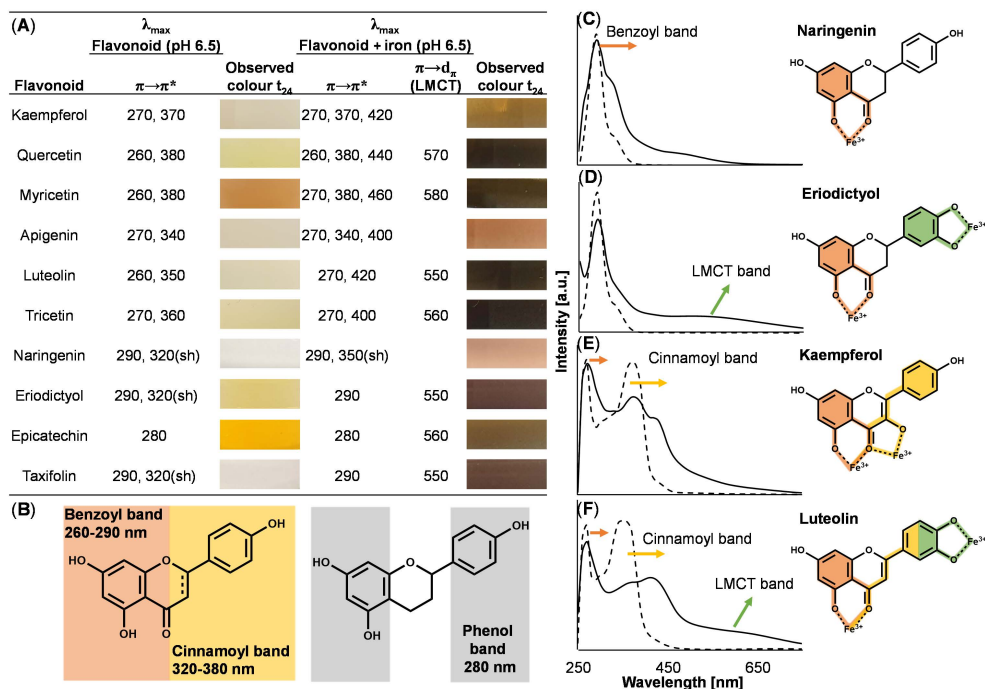


Figure 3.2. (A) Maximum absorbance wavelength (λ_{\max}) of the flavonoids in the presence and absence of FeSO_4 at pH 6.5, and pictures of the observed colour in the sample after 24 h incubation; (B) structural moieties of flavonoids responsible for the main $\pi \rightarrow \pi^*$ absorbance bands: the benzoyl band (orange), cinnamoyl band (yellow), and phenol band (grey). Combined WS and DS absorbance spectra of (C) naringenin; (D) eriodictyol; (E) kaempferol; and (F) luteolin in presence of FeSO_4 before pH adjustment (t_0 ; dotted line) and after adjusting pH to 6.5 (t_6 ; solid line), the conjugated system responsible for LMCT is marked in green; the conjugated system responsible for the benzoyl band is marked in orange; the conjugated system responsible for the cinnamoyl band in yellow.

Two characteristic $\pi \rightarrow \pi^*$ bands were observed in absorbance spectra of all flavonoids possessing a 4-keto group in conjugation with the C2-C3 double bond, namely the benzoyl (A-ring) and cinnamoyl (B-ring) bands with λ_{\max} values ranging from 260-290 nm and 320-380 nm, respectively (**Fig. 3.2B**). The absence of the C2-C3 double bond in the flavanones (*i.e.* naringenin, eriodictyol, and taxifolin) resulted in weak

absorbance of the cinnamoyl band as a shoulder (sh) band.^[26] Additionally, the larger conjugated system of flavonols and flavones led to a λ_{max} of the cinnamoyl band at higher wavelengths. Epicatechin lacks the 4-keto and C2-C3 double bond and therefore only showed a phenol band at 280 nm. Before adjustment of the pH to 6.5 (t_0), no changes in the absorbance spectra of flavonoids were observed in the presence of FeSO_4 compared to the spectra of flavonoids in absence of FeSO_4 .

Generally, the iron-flavonoid samples at t_0 were transparent or yellow and showed the same benzoyl, cinnamoyl, and phenol bands compared to the flavonoid blanks (**Fig. S3.3** and **S3.4**). Upon adjusting the pH to 6.5, a bathochromic shift to wavelengths in the visible spectrum was observed (**Fig. 3.2C-F**). These findings indicate that deprotonation of the hydroxyl substituents is a prerequisite for complexation, which subsequently leads to fast discolouration. Normally, the pK_a value of the most acidic phenol moiety of flavonoids is around 9 but, because iron stabilises the deprotonated state, the apparent pK_a is in the range of 5-8 in the presence of iron.^[5,27]

The structural features of flavonoids affected the electronic transition and the observed colour in presence of iron. The benzoyl $\pi \rightarrow \pi^*$ transition band broadened to higher wavelengths for naringenin (**Fig. 3.2C**). This flavanone contains only the 4-5 binding site and does not possess a C2-C3 double bond. Peak broadening resulted in an increased absorbance from 350 – 550 nm, which led to a light red-brown colour of these samples. Mellican *et al.* (2003) incubated similar concentrations of naringenin with ferric sulphate in pure water at pH 7. However, they reported that no colour formation was observed, even though their absorbance spectra also indicate an increase in absorbance from 400-650 nm, albeit at relatively low intensities.

Formation of a broad absorbance band (**Fig. 3.2D**) with a λ_{max} ranging from 550-560 was observed for flavonoids possessing the 3'-4' binding site (*i.e.* catecholate) but lacking the C2-C3 double bond (*i.e.* eriodictyol, epicatechin, and taxifolin). This wavelength is typical for LMCT in Fe(III)-catecholate complexes at pH ranging from 5-7 and caused the purplish appearance of these samples.^[6,16] Besides their 3'-4' binding site, eriodictyol and taxifolin also possess the 3-4 and 4-5 iron-binding sites. However, the absence of the C2-C3 double bond does not allow electron delocalisation through the whole structure, as a result, absorbance spectra of these flavonoids were dominated by the LMCT band (**Fig. 3.2D**, **Fig. S3.4**).

Bathochromic shifting of the benzoyl and cinnamoyl $\pi \rightarrow \pi^*$ band was observed for kaempferol and apigenin, both of which contain the 4-5 binding site in conjugation with the C2-C3 double bond (**Fig. 3.2E**). This bathochromic shifting was previously assigned to an extension of the conjugated π - π system induced by the positively charged metal.^[8] Discolouration of these samples resulted from the extended conjugated system, leading to increased absorbance in the visible spectrum. The

bathochromic shift of the cinnamoyl band of kaempferol was more intense than that of apigenin and shifted to higher wavelengths, as kaempferol possesses the 3-4 binding site in addition to the 4-5 binding site

Bathochromic shifting of the benzoyl band and cinnamoyl band was also observed for flavonoids containing the 3'-4' binding site, and the 4-5 binding site in conjugation with the C2-C3 double bond (*i.e.* quercetin, myricetin, luteolin, tricetin) (**Fig. 3.2F**). Additionally, for these flavonoids a broad absorbance band was observed at higher wavelengths, resulting from $\pi \rightarrow d_{\pi}$ transitions (*i.e.* LMCT) of the catechol or pyrogallol moiety and the complexed iron. The combination of the bathochromic shift of the cinnamoyl band ($\pi \rightarrow \pi^*$) band and LMCT band ($\pi \rightarrow d_{\pi}$) resulted in intense discolouration (**Fig. 3.2A**).

To summarise, discolouration was observed for all tested flavonoids in presence of iron at pH 6.5. Moreover, the electronic transition responsible for discolouration was defined by the structural features of the flavonoid. The presence of the combination of the catechol moiety, the 4-keto, and the C2-C3 double bond resulted in the most intense colour by a combination of bathochromic shifting of the cinnamoyl band ($\pi \rightarrow \pi^*$) and LMCT phenomena ($\pi \rightarrow d_{\pi}$). Presence of the 3-hydroxy group provided an additional binding site and therefore resulted in more intense discolouration.

3.3.2. Solubility and stability of flavonoids in presence of iron

The recovery of flavonoid over time in presence of iron was quantified by RP-UHPLC-PDA-MSⁿ (**Fig. 3.3**). An overview of the mass spectrometric and spectroscopic data used to identify the flavonoids is provided in the supplementary information (**Table S3.1**). Total recovery of flavonoid was followed over time in three different fractions, water soluble (WS), DMSO soluble (DS), and ascorbic acid soluble (AAS).

Iron-flavonoid complexes were unstable in the LC mobile phase (*i.e.* water/acetonitrile with 0.1 vol. % formic acid) because of protonation of the flavonoid at the acidic conditions.^[28] Therefore, only free flavonoids were identified and quantified, which could directly be linked to the solubility and extent of oxidation. Before adjustment of the pH (t_0), high recoveries were found for all flavonoids. Flavonoids with the C2-C3 double bond showed poor water solubility, as evidenced by their recovery in DS compared to WS, due to their planar ring structure facilitating hydrophobic interaction by π - π stacking of the aromatic nuclei in aqueous environments.

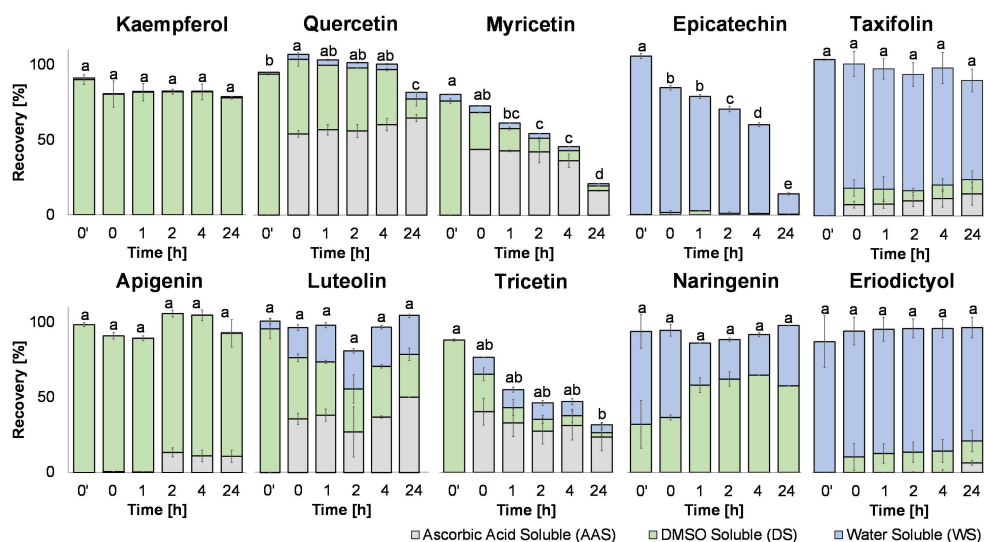


Figure 3.3. Recovery of kaempferol, quercetin, myricetin, epicatechin, taxifolin, apigenin, luteolin, tricetin, naringenin, and eriodictyol in the WS (blue), DS (green), and AAS (grey) fractions in presence of iron before adjustment of the pH (t_0) and after 0, 1, 2, 4, and 24 h of incubation at pH 6.5. Error bars indicate the standard deviation of independent duplicates. Different letters indicate a significant difference in total recovery compared to other time points for the same flavonoid (Tukey's test, $p < 0.05$). Significance of differences in the three individual fractions (*i.e.* WS, DS, and AAS) per time point for each flavonoid is indicated in the supplementary information, **Table S3.3**.

For the flavonoids with a pyrogallol moiety on the B-ring, *i.e.* myricetin and tricetin, a decreased recovery was observed over time, with respective losses of 78 % and 70 % of the initial amount after 24 h incubation. Pyrogallol moieties generally have a lower pK_a than catechol moieties, resulting in a higher phenoxide concentration at pH 6.5, making the flavonoid more prone to oxidation.^[2,29] For quercetin also a significant decrease of 14 % was observed after 24 h incubation. The iron-mediated oxidation rate increased due to the presence of the 3-hydroxy group (quercetin vs. luteolin) as well as the C2-C3 double bond (quercetin vs. taxifolin). For epicatechin, which lacks the 4-keto moiety, a loss of 87 % was observed over time. It is well-established that epicatechin can easily be oxidised to brown-coloured coupling products by enzymatic oxidation and auto-oxidation.^[12] The absence of the 4-keto group on epicatechin likely results in reduced oxidative stability compared to the other flavonoids tested.

For kaempferol, taxifolin, apigenin, luteolin, naringenin, and eriodictyol, no significant decrease was observed over 24 h of incubation in presence of iron ($p > 0.05$). For some flavonoids, in particular those that possess multiple iron-binding sites, adjustment to pH 6.5 led to the formation of black precipitate that was only soluble after the addition

of an excess of ascorbic acid (AAS). In **section 3.3.4** this phenomenon will be further discussed.

As a control, all flavonoids were also incubated at pH 6.5 over time in absence of iron (**Fig. S3.5**). Most flavonoids were stable over 24 h aqueous incubation in absence of iron. However, myricetin and epicatechin showed decreases of 45 % and 22 % in total recovery after 24 h incubation, respectively. Auto-oxidation of flavonoids in an aqueous solution occurs via electron transfer (ET) reactions. Myricetin possesses all structural features essential for oxidation (*i.e.* 3-OH, 4'-OH, and C2-C3 double bond) and is therefore also prone to auto-oxidation. However, the 78 % decrease in myricetin recovery in presence of iron shows that the oxidation reaction is accelerated by iron. In presence of iron, the degradation of tricetin was similar to myricetin (70 % vs. 78 % in 24 h). In absence of iron, no significant decrease was observed for tricetin. Tricetin lacks the 3-OH group, and cannot form quinone methides, which are chemically more reactive and unstable than *ortho*-quinones.^[30]

3.3.3. Flavonoid oxidation in the presence of iron

The complexation reaction can be followed up by ET reactions that cause oxidation of flavonoids, as evidenced by the decreased recovery of flavonoids over time (**Fig. 3.3**). These ET reactions yield a plethora of oxidation products by degradation or oxidative coupling reactions. The formation of flavonoid oxidation products was monitored by RP-UHPLC-PDA-MSⁿ.

The major oxidation products present in the WS and DS fractions were tentatively identified based on spectrometric and spectroscopic data (**Table S3.2**). The RP-UHPLC-PDA chromatograms of quercetin with FeSO₄ before and after 24 h of incubation (**Fig. 3.4A**) show that aqueous incubation of quercetin with FeSO₄ resulted in the formation of several oxidation products. Chromatograms of the other flavonoids before pH adjustment (*t*₀) and after 24 h incubation at pH 6.5 are provided in the supplementary information (**Fig. S3.6** and **S3.7**).

An overview was created of the main characteristic degradation end products and coupling products formed per flavonoid after 24 h of incubation (**Fig. 3.4B**). The oxidation products could not be quantified because the molar extinction coefficients of some of the formed compounds were unknown. However, the cumulative PDA (250 to 400 nm) peak areas of the chromatograms were used as an indication for the total amount of oxidation products formed (**Fig. 3.4C**), as all oxidation products showed λ_{max} values within this range.

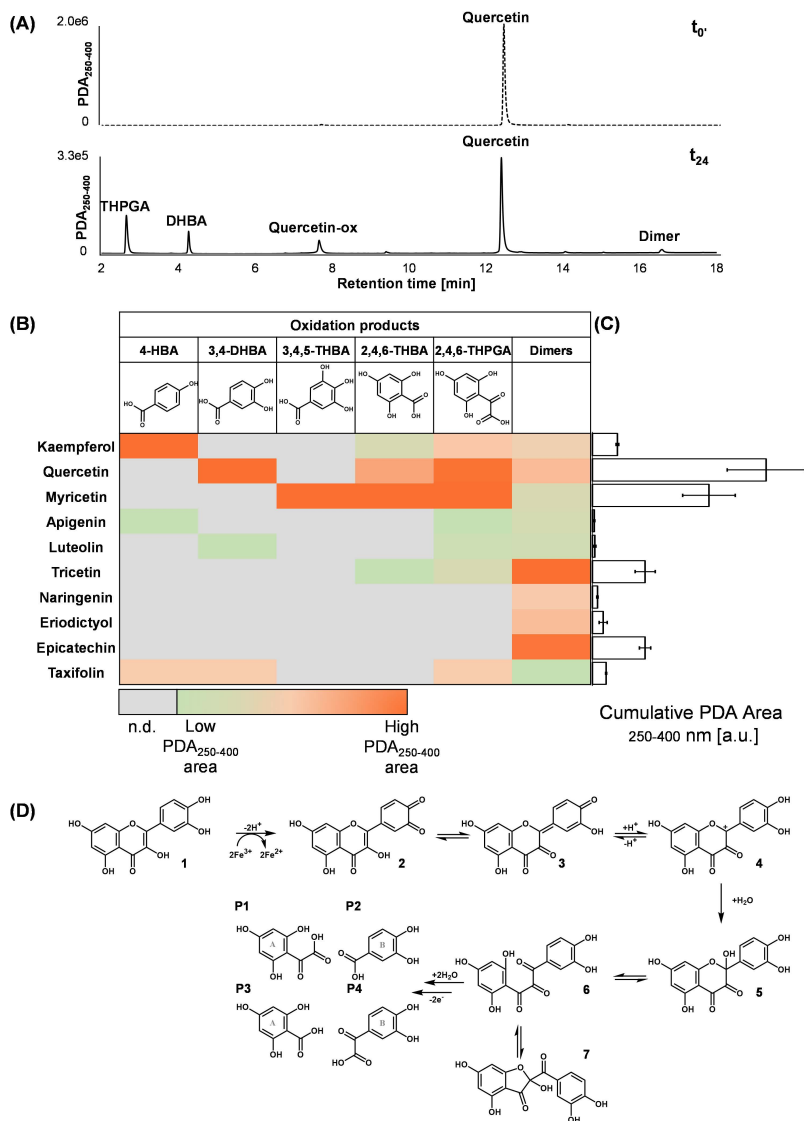


Figure 3.4. (A) RP-UHPLC-PDA (250-400 nm) profiles of quercetin \times FeSO_4 samples before incubation and pH adjustment (t_0) and after 24 h incubation pH 6.5, 40 °C (t_{24}). (B) Heatmap indicating the type and relative quantity of individual oxidation products formed per flavonoid after incubation for 24 h. Tentative identification of these compounds is based on Table S3.2, colour indicates the relative levels per oxidation product (grey = n.d., not detected; green = low $\text{PDA}_{250-400}$ area; and orange = high $\text{PDA}_{250-400}$ area). (C) Cumulative area of PDA peaks for oxidation products after 24 h of incubation, detected in the wavelength range of 250-400 nm. (D) Proposed pathway of Fe(III)-mediated oxidative cleavage of flavonols illustrated for quercetin. HBA = hydroxybenzoic acid, DHBA = dihydroxybenzoic acid, THBA = trihydroxybenzoic acid, THPGA = trihydroxyphenylglyoxylic acid.

Degradation reactions

The main characteristic degradation products formed by iron-mediated oxidation of flavonoids in aqueous solution were 4-hydroxybenzoic acid (4-HBA), 3,4-dihydroxybenzoic acid (3,4-DHBA; protocatechuic acid), or 3,4,5-trihydroxybenzoic acid (3,4,5-THBA; gallic acid), 2,4,6-THBA (*i.e.* phloroglucinol carboxylic acid), and 2,4,6-trihydroxyphenylglyoxilic acid (2,4,6-THPGA). The proposed pathway of Fe(III)-mediated oxidative degradation of quercetin is illustrated in **Fig. 3.4D**. The interaction of quercetin (**1**) with Fe(III), is followed by an ET from quercetin to Fe(III), leading to formation of a semiquinone (not shown) and upon a second ET an *ortho*-quinone (**2**) is formed. This *ortho*-quinone readily isomerises to a *para*-quinone methide intermediate (**3**), which is converted to a flavylum cation upon protonation (**4**). Subsequent hydroxylation at the C2 position leads to formation of an unstable 2,5,7,3'-4'-pentahydroxy-3,4-flavandione (**5**). Via ring-opening the intermediate 5,7,9,3'-4'-pentahydroxy-2,3,4-chalcantrione (**6**) is formed, this molecule is also unstable, and may rearrange to form the intermediate 2-(3'-4'-dihydroxybenzoyl)-2,4,6-trihydroxybenzofuran-3(2H)-one (**7**).^[31] Moreover, product **6** can undergo hydrolysis resulting in formation of lower molecular weight products. Cleavage of the C2-C3 bond upon hydrolysis results in formation of the A-ring derived 2,4,6-THPGA (**P1**) and B-ring derived 3,4-DHBA (**P2**). Moreover, cleavage of the C3-C4 bond upon hydrolysis results in the formation of A-ring derived 2,4,6-THBA (**P3**) and B-ring derived 3,4-DHPGA (**P4**) (**Fig. 3.4D**). For all investigated flavonoids, except epicatechin, a distinct peak was observed in RP-UHPLC-PDA-MSⁿ with a difference in *m/z* of 16 amu, probably this corresponds to one of the hydroxylated intermediates. Based on the mass spectrometric data and the fragmentation profile, which show RDA fragmentation typical for (oxidised) flavonoids. It seems unlikely that this peak was chalcantrione (**6**), as we would expect to observe a distinct MS² fragmentation profile resulting from cleavage between the more labile C2 and C3 or C3 and C4 positions in the MS. Therefore, it is expected that this peak corresponds to either the flavandione (**5**) or benzofuranone (**7**) (**Table S3.2**). We cannot presently distinguish between these two intermediate oxidation products.^[32]

If the 3-OH group was present in conjugation with the C2-C3 double bond (flavonols), degradation to hydroxybenzoic acid derivatives was more prominent compared to the other flavonoid subclasses. The presence of these functional moieties enables keto-enol tautomerisation and results in the formation of the *para*-quinone and highly reactive quinone methides.^[30,33] As a result, oxidative degradation was preferred over oxidative coupling for flavonols, which is in line with previous findings regarding flavonol oxidation in aqueous environments.^[34] In absence of the 3-OH group (*i.e.* flavones) only *ortho*-quinones can be formed, which are relatively more stable in aqueous solution than quinone methides, resulting in slower oxidation.^[30] In absence of the C2-C3 double bond (*i.e.* taxifolin) also limited formation of degradation products was observed as keto-enol tautomerism is not present in taxifolin and formation of

the quinone methides is less likely.^[33] If both of these moieties were absent (*i.e.* naringenin, eriodictyol, and epicatechin), no degradation products were observed.

Formation of degradation products over time lowered the absorbance in the visible range, as shown in the absorbance spectra of quercetin and myricetin (**Fig. S3.3**). A decrease was observed in the absorbances of both the LMCT band and the cinnamoyl-iron bands. Simultaneously, a new peak with λ_{max} at 290 nm appeared, resulting from the formed hydroxybenzoic acid derivatives that possess one phenolic moiety and a limited conjugated system. This decrease in absorbance in the visible range due to oxidation is in line with previous research on fading of the colour of aluminium-flavonoid complexes due to metal-mediated oxidation.^[35] Preliminary experiments (results not shown) indicated that incubation of quercetin with iron under the same conditions for an extended time (*i.e.* weeks) prompted the formation of a new LMCT band, most likely resulting from complexation of the hydroxybenzoic acid derivatives to iron.

Oxidative coupling reactions

Oxidative coupling of the flavonoids in presence of Fe(III) was also followed by RP-UHPLC-PDA-MS. Dimers were detected by creating extracted ion chromatograms with a dimer mass range of $((M_w \times 2) - 2) \pm 5$, and were tentatively identified based on their mass spectra. Detailed mass spectrometric and spectroscopic data of the dimers is provided in the supplementary information (**Table S3.2**). All identified dimers were dehydro-type dimers. Extracted ion chromatograms for specific m/z values that correspond to benzotropolone-type dimers (e.g. theaflavins) indicated that none of these types of dimers was formed. These findings are in line with recent work on the auto-oxidative browning mechanism of epicatechin, in which it was shown that dehydrodicatichins were the main products of epicatechin auto-oxidation.^[12] Thus, the iron-mediated dimerisation pathway is hypothesised to follow a similar mechanism as auto-oxidative dimerisation. Dimer formation was more prominent in the flavonoids lacking the C2-C3 double bond. Additionally, dimerisation was also observed for tricetin, which does possess the C2-C3 double bond. Thus, we suggest that the absence of the 3-OH group stabilised tricetin against undergoing degradation reactions, thereby directing the reaction towards oxidative coupling, resulting in dimer formation. Extracted ion chromatograms were also screened for trimers and oligomers. Except for epicatechin trimers, no tri- or oligomers were detected.

Flavonoid oxidative coupling is hypothesised to contribute to discolouration in two ways: (i) the dimers' extended conjugated systems give a brownish colour; and (ii) the dimers can form coloured complexes with iron. Most of the flavonoid dimers that were identified by UHPLC-PDA-MS had a λ_{max} ranging from 350-400 nm and thus showed absorbance in the visible light range (380-750 nm). However, even after 24 h, the relatively small amount of dimers formed via oxidative coupling did not affect the full absorbance spectra of the iron-flavonoid samples, except for epicatechin. The UV-Vis

absorbance spectra of epicatechin in presence of iron (**Fig. S3.8**) indicated increased absorbance between 400 and 500 nm, resulting from the formation of brown coloured epicatechin dimers and trimers. In addition to this broad absorbance "hump", the LMCT band with a λ_{max} around 550 nm was also still present, indicating the presence of iron-flavonoid complexes. Interaction of the epicatechin with iron resulted in a purplish colour, whereas interaction of the dimers and trimers with iron resulted in black colour formation due to the extended conjugated system and a combination of $\pi \rightarrow \pi^*$ and $\pi \rightarrow d_{\pi}$ transitions (**Fig. S3.8**). Furthermore, the number of iron-binding sites increases with the degree of polymerisation, as additional binding sites arise from hydroxyl/carbonyl groups.

Overall, iron-mediated oxidation reactions of flavonoids led to degradation or oxidative coupling, that resulted in a decrease or increase in visible light absorbance, respectively. Considering the trends observed here, it is expected that upon incubation for more than 24 h, these colour changes will become more pronounced.

3.3.4. Formation of iron-flavonoid networks

The samples of quercetin, myricetin, luteolin, and tricetin with FeSO_4 showed the formation of black particles with poor solubility and the flavonoids were only recovered after the addition of an excess of ascorbic acid (AAS) (**Fig. 3.5**). Recovery of flavonoids in the AAS fraction indicated that the poor solubility of flavonoids in presence of iron was caused by a reversible interaction (*i.e.* complexation). Disruption of the reversible iron-flavonoid interactions by addition of ascorbic acid can be due to protonation of the hydroxyl groups at low pH, reduction of Fe(III) to Fe(II) , competition by ascorbic acid for iron complexation, or a combination thereof. Exploratory experiments with concentrated HCl indicated that solely lowering the pH was sufficient to disrupt the iron-flavonoid interactions (results not shown). The main flavonoids that showed precipitation in our study (*i.e.* quercetin, myricetin, luteolin, and tricetin) possessed the 3-4 site and/or the 4-5 site in combination with the 3'-4' site. We, therefore, concluded that multiple iron-binding sites on flavonoids were a prerequisite for the formation of poorly soluble interaction products. Habeych and co-authors also observed precipitate formation of phenolic compounds with multiple binding sites in presence of FeSO_4 .^[2] These authors interpreted precipitation as either oxidation of phenolics to polymers, or formation of high molecular size networks by bridging of phenolics with iron, though neither of these mechanisms were confirmed.^[2] Based on the reversibility of our iron-flavonoid interactions by the addition of ascorbic acid, we hypothesise that precipitation was mainly the result of the formation of insoluble complexes or networks rather than covalent oxidative coupling. In another study, it was also reported that myricetin, quercetin, and luteolin can form Fe(III) -coordinated metal-phenolic networks (MPN).^[36] MPNs are supramolecular networks of metal ions coordinated to phenolic ligands and are commonly characterised by an amorphous nature.^[37,38] To confirm that MPNs were formed, the nature and morphology of the iron-flavonoid interaction products were

analysed by powder X-ray diffraction (XRD). For these experiments, we selected two samples: iron-quercetin, representing flavonoids with two binding sites, and iron-naringenin, representing flavonoids with one binding site (**Fig. 3.5**).

The XRD patterns of quercetin (**Fig. 3.5A**) and naringenin (**Fig. 3.5D**) showed crystalline patterns that were respectively identified as triclinic quercetin dihydrate and monoclinic naringenin. XRD patterns of mixed iron-flavonoid samples at t_0 showed crystalline peaks indicative for a mixture of the flavonoid and FeSO_4 without any interaction (**Fig. 3.5B** and **3.5E**). The XRD pattern of the iron-flavonoid samples after pH adjustment to 6.5 (**Fig. 3.5C** and **3.5F**) showed a broad "hump" caused by diffuse scattering. This broad "hump" is indicative for the disordered nature of an amorphous material. This is in line with previously reported results on the amorphous nature of the reaction product of iron with quercetin at pH 12.^[39] The XRD patterns of the iron-flavonoid samples after pH adjustment to 6.5 (**Fig. 3.5C** and **3.5F**) were distinctly different from those obtained for FeSO_4 on its own after pH adjustment to 6.5 (**Fig. S3.9**). Thus, we confirmed that the observed amorphousness is caused by an interaction between iron and the flavonoid and not by the formation of iron (oxy)hydroxide species. Also naringenin, for which no AAS fraction was observed, yielded an XRD pattern corresponding to an amorphous material. The amorphousness of iron-flavonoid reaction products can be a result of the formation of MPNs. Wang (2013) also showed that amorphousness may indicate the formation of iron-phenolic complex nanoparticles with a 1:3 stoichiometry.^[37,40] The existence of coordination-driven bridging interactions between iron and flavonoids via μ -oxo/hydroxo-bridged Fe(III) species can also result in amorphous MPNs (**Fig. S3.10**).^[37,41] Although the amorphous nature of the samples was a clear indication of the formation of more intricate iron-flavonoid interaction products, the XRD patterns on their own did not provide sufficient insights into these products' exact structural characteristics. To further investigate the potential presence of MPNs in our iron-flavonoid samples, electron microscopic measurements were performed. SEM images of quercetin showed rod-like or needle-like shapes representing its high crystallinity (**Fig. 3.5A**). After the addition of FeSO_4 and adjustment of pH, the surface morphology became a dense, uniform, smooth film with an amorphous nature (**Fig. 3.5C**), further supporting the hypothesis that insoluble MPNs were present in the sample.^[39] For naringenin, the morphology also changed after the addition of FeSO_4 and pH adjustment (**Fig. 3.5E**). The surface morphologies of the iron-quercetin and iron-naringenin samples was distinctively different. The higher surface roughness and fracturing observed in the iron-naringenin sample compared to the iron-quercetin sample are indicative for discontinuous MPNs or nanoparticle deposition, rather than continuous extended MPNs.

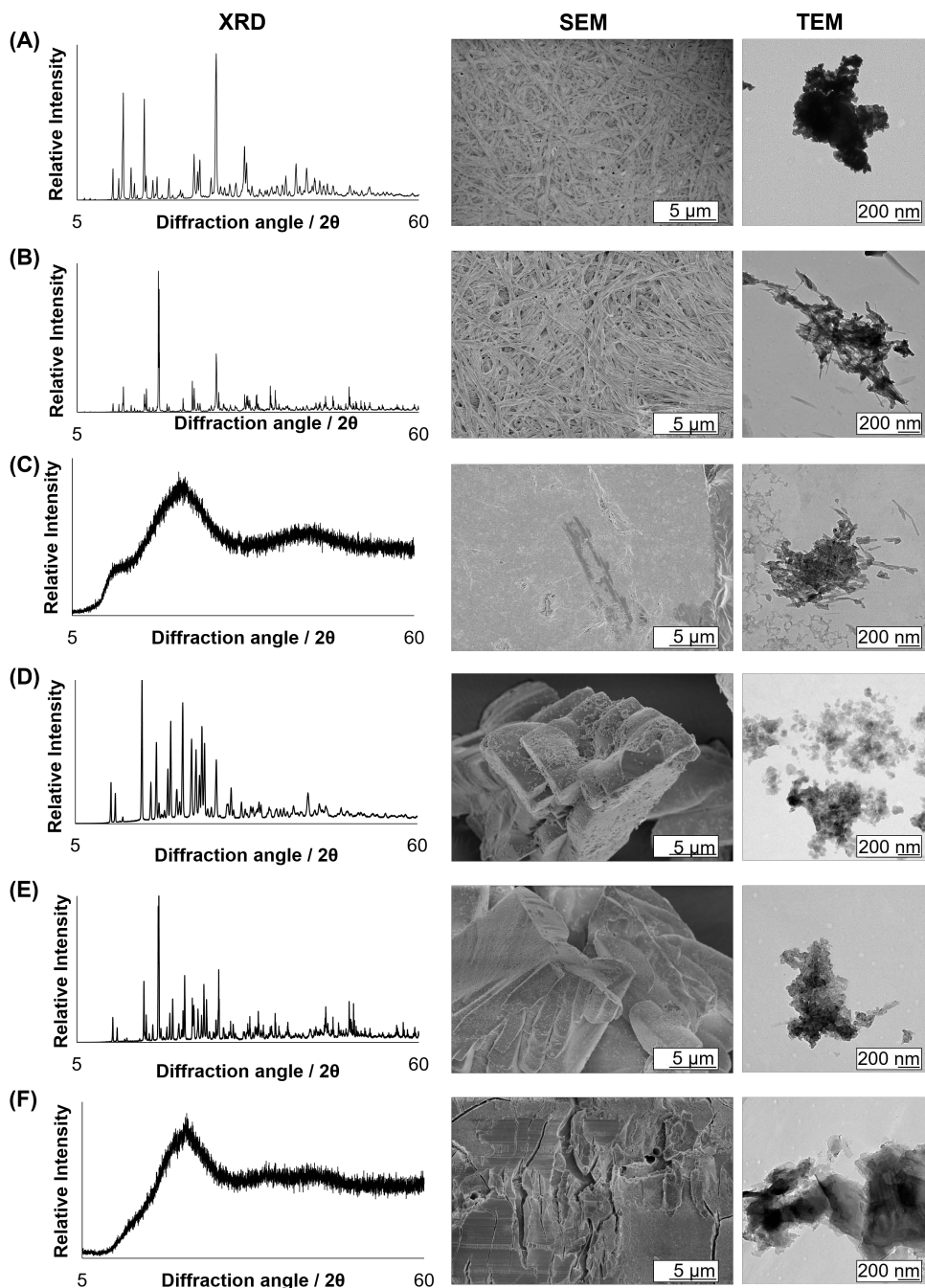


Figure 3.5. Powder XRD patterns, SEM images, and TEM images for (A) quercetin; (B) quercetin \times FeSO₄ (before pH adjustment, t_0); (C) quercetin \times FeSO₄ (pH = 6.5, t_0); (D) naringenin; (E) naringenin \times FeSO₄ (before pH adjustment, t_0); and (F) naringenin \times FeSO₄ (pH = 6.5, t_0).

TEM was performed on the iron-flavonoid samples in suspension. TEM images of pure quercetin show aggregation (**Fig. 3.5A**). High electron density led to intense Bragg reflections and dark contrast in the TEM image. Upon addition of FeSO_4 and before pH adjustment, the structure of quercetin still appeared needle-like and crystalline in SEM, but particles showed less aggregation in TEM (**Fig. 3.5B**). After adjustment to pH 6.5 characteristic needle-shaped structures were visible representing precipitated quercetin.^[42] In addition to that, irregularly shaped particles with morphologies in accordance with those of MPNs were revealed (**Fig. 3.5C**). This formation of networks was not observed for quercetin on its own. For naringenin, TEM revealed the presence of large aggregates, and the addition of FeSO_4 did not have much influence on their size or morphology (**Fig. 3.5D** and **3.5E**). The addition of iron to naringenin and pH adjustment to 6.5 led to the formation of amorphous particles of increased size (**Fig. 3.5F**).

Based on these results obtained for quercetin and naringenin, we concluded that formation of MPNs occurred in both samples upon addition of iron and adjustment of pH to 6.5. The presence of a binding site on the 3-4 site and/or the 4-5 site in combination with the 3'-4' site, as in quercetin, was a prerequisite to form continuous extended MPNs. Moreover, the higher AAS recovery of the flavone and flavonol subclasses compared to the flavan subclasses (**Fig. 3.3**) indicated that the presence of the C2-C3 double bond enhanced the formation of insoluble extended MPNs. Based on the results obtained for naringenin, we propose that even flavonoids with only one iron-binding site can form MPNs. The number of interactions per flavonoid and molecular size of the resulting amorphous interaction products of these flavonoids with only one iron-binding site is expected to be much lower compared to MPNs from flavonoids with multiple iron-binding sites. Therefore, flavonoids with only one iron-binding site had higher solubility, as shown by the fact that they were mainly recovered in the WS and DS fractions, rather than the AAS fractions. We suggest that the large conjugated system of insoluble, extended MPNs is responsible for the strong black discolouration of the observed precipitate (*i.e.* AAS fraction). Furthermore, we speculate that the reduced solubility of these MPNs may also lead to decreased bio-accessibility compared to smaller, soluble complexes.

3.3.5. Implications of iron-flavonoid interactions on bio-accessibility of iron

In addition to flavonoid solubility, total iron solubility (as defined by **Equation 3.1**) was assessed.

$$[\text{Fe}]_{\text{total}} = [\text{Fe}]^{2+} + [\text{Fe}]^{3+} + \sum[\text{Soluble products of Fe}^{2+} \text{ and Fe}^{3+}] \quad (\text{Eq. 3.1})$$

An overview of the recovery of iron, as determined by the ferrozine-based colourimetric assay, in the WS, DS, and AAS fractions are provided in the supplementary information (**Fig. S3.11**). The recovery of total iron in the water soluble (WS) fraction (**Fig. 3.6**) indicates its bio-accessibility.^[19] The total iron solubility of the

FeSO₄ control after pH adjustment to 6.5 decreased by 99 % due to the formation of poorly soluble iron (oxy)hydroxide species and hydrolytic polymers upon Fe(III) hydrolysis around neutral pH.^[19,43]

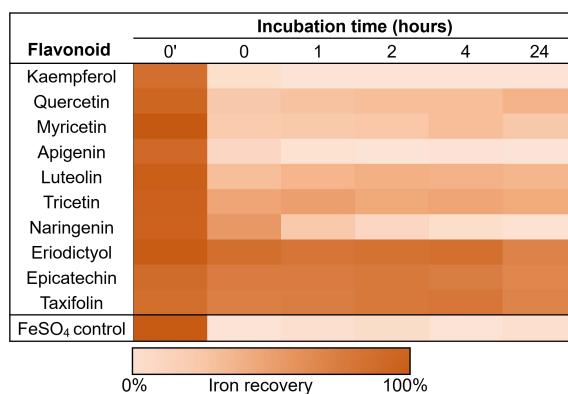


Figure 3.6. Heatmap showing total iron solubility over time in the WS fraction for the FeSO₄ control and after incubation of FeSO₄ with different flavonoids.

The total solubility of iron in water at pH 6.5 was enhanced for most flavonoids in comparison to the control. The highest iron recovery was observed for the less planar flavonoids (*i.e.* flavonoids without the C2-C3 double bond), which also had a relatively high recovery of flavonoid in the WS fraction (**Fig. 3.6**). Moreover, it was observed that iron solubility was enhanced if two or more hydroxyl groups were present on the flavonoid B-ring. Complexation of Fe(III) to catechol stabilises Fe(III) against the formation of hydrolysis products.^[16] On the other hand, combining iron with poorly water soluble flavonoids (*i.e.* kaempferol, quercetin, myricetin, apigenin, and naringenin) leads to precipitation of the complexes and/or MPNs, and thereby to low iron recovery in the WS fraction. The slight increase in iron solubility in the presence of some poorly water soluble flavonoids (*e.g.* quercetin and myricetin) over time indicates that their oxidative degradation products (*i.e.* hydroxybenzoic acid derivatives) may form water soluble complexes with iron. Most iron absorption occurs in the duodenum (pH 6-6.5) and the upper jejunum (pH 7-9).^[19] Therefore, higher total recoveries of iron in the WS fraction in presence of flavonoids at pH 6.5 are indicative for better bio-accessibility, which is defined as the quantity of iron in solution and available for absorption in the gastrointestinal tract. It should be noted that although bio-accessibility of iron is a prerequisite for bioavailability, iron bio-accessibility cannot directly be correlated to iron bioavailability, which also includes digestion, absorption, and metabolism.^[19] Nonetheless, based on these results, we expect that the formation of soluble iron-flavonoid complexes can still negatively affect iron bioavailability. Previous research on iron homeostasis in presence of quercetin and epigallocatechin gallate indicated an increase in apical uptake for the complexed iron, but a decrease in basolateral transport, leading to an overall reduction in iron bioavailability.^[44]

3.4. Conclusion

This is the first time that the combined effect of complexation, oxidation, and formation of networks on iron-mediated flavonoid discolouration, and the effect of flavonoids' structural features thereon, was investigated. Complexation of iron to all investigated flavonoids resulted in fast discolouration in aqueous samples at pH 6.5. Binding of iron to the 3-4 site or 4-5 site resulted in bathochromic shifting of the cinnamoyl and/or benzoyl ($\pi \rightarrow \pi^*$) bands. In accordance with the hypothesis, the presence of the 3'-4' site (*i.e.* catechol or pyrogallol moiety) was a prerequisite for the formation of an LMCT ($\pi \rightarrow d_n$) band. Flavonoids possessing the 3'-4' site in conjugation with the C2-C3 double bond, and the 4-5 site showed the most intense discolouration, resulting from a combination of bathochromic shifting of the cinnamoyl band and LMCT phenomena. In addition to more intense discolouration, the presence of the C2-C3 double bond and more hydroxyl groups on the B-ring also led to a greater extent of iron-mediated oxidation reactions. The presence of the 3-hydroxy group also enhanced oxidative degradation by the formation of highly reactive quinone methides as reaction intermediates. Oxidative degradation or oxidative coupling of the flavonoid, respectively resulted in a decrease or increase in visible light absorbance. With XRD, SEM, and TEM, we confirmed that the black precipitate formed when iron was incubated with flavonoids that possess multiple iron-binding sites, was the result of the formation of extended MPNs. These extended MPNs likely possessed a higher number of interactions and molecular size compared to MPNs from flavonoids with only one iron-binding site. Additionally, the water solubility of iron in the presence of flavonoids was enhanced by flavonoids that possessed the 3'-4' binding site but lacked the C2-C3 double bond. This study shows that the structural features of flavonoids strongly influence their interactions with iron via complexation and oxidation, thereby affecting the resulting discolouration and formation of networks. In future work, it should be explored how these mechanistic insights into iron-flavonoid interactions can be used to develop approaches to prevent discolouration in novel mineral-fortified foods.

3.5. Acknowledgements

We would like to thank Marcel Giesbers and Jelmer Vroom from the Wageningen Electron Microscopy Centre (WEMC) for carrying out TEM and SEM data collection. Ilse Gerrits is kindly acknowledged for her help with the X-Ray powder diffraction measurements. The authors are thankful to Cas Geerits for his contribution to the preliminary data processing. The graphical abstract was made with content from BioRender.com. Part of the presented results were obtained using advanced microscopy, mass spectrometry, and XRD equipment which is owned by WUR-Shared Research Facilities. Investment by WUR-Shared Research Facility was made possible by the 'Regio Deal Foodvalley' of the province of Gelderland, The Netherlands.

3.6. References

- 1 Allen, L. H., De Benoist, B., Dary, O., & Hurrell, R. (2006) *Guidelines on food fortification with micronutrients*: World Health Organization.
- 2 Habeych, E., van Kogelenberg, V., Sagalowicz, L., Michel, M., & Galaffu, N. (2016). Strategies to limit colour changes when fortifying food products with iron. *Food Research International*, 88, 122-128.
- 3 Uivarosi, V., Munteanu, A. C., Sharma, A., & Singh Tuli, H. (2019). Metal complexation and patent studies of flavonoid. In H. Singh Tuli (Ed.), *Current aspects of flavonoids: Their role in cancer treatment*, (pp. 39-89): Springer Singapore.
- 4 Kasprzak, M. M., Erxleben, A., & Ochocki, J. (2015). Properties and applications of flavonoid metal complexes. *RSC Advances*, 5(57), 45853-45877.
- 5 Perron, N. R., & Brumaghim, J. L. (2009). A review of the antioxidant mechanisms of polyphenol compounds related to iron binding. *Cell Biochemistry and Biophysics*, 53(2), 75-100.
- 6 Elhabiri, M., Carrère, C., Marmolle, F., & Traboulsi, H. (2007). Complexation of iron(III) by catecholate-type polyphenols. *Inorganica Chimica Acta*, 360(1), 353-359.
- 7 Mellican, R. I., Li, J., Mehansho, H., & Nielsen, S. S. (2003). The role of iron and the factors affecting off-color development of polyphenols. *Journal of Agricultural and Food Chemistry*, 51(8), 2304-2316.
- 8 Guo, M., Perez, C., Wei, Y., Rapoza, E., Su, G., Bou-Abdallah, F., & Chasteen, N. (2007). Iron-binding properties of plant phenolics and cranberry's bio-effects. *Dalton Transactions*(43), 4951-4961.
- 9 Ren, J., Meng, S., Lekka, C. E., & Kaxiras, E. (2008). Complexation of flavonoids with iron: Structure and optical signatures. *The Journal of Physical Chemistry B*, 112(6), 1845-1850.
- 10 Dowling, S., Regan, F., & Hughes, H. (2010). The characterisation of structural and antioxidant properties of isoflavone metal chelates. *Journal of Inorganic Biochemistry*, 104(10), 1091-1098.
- 11 Ryan, P., & Hynes, M. J. (2008). The kinetics and mechanisms of the reactions of iron(III) with quercetin and morin. *Journal of Inorganic Biochemistry*, 102(1), 127-136.
- 12 Tan, J., de Bruijn, W. J. C., van Zadelhoff, A., Lin, Z., & Vincken, J.-P. (2020). Browning of epicatechin (EC) and epigallocatechin (EGC) by auto-oxidation. *Journal of Agricultural and Food Chemistry*, 68(47), 13879-13887.
- 13 Mladěnka, P., Macáková, K., Filipický, T., Zatloukalová, L., Jahodář, L., Bovicelli, P., Silvestri, I. P., Hrdina, R., & Saso, L. (2011). In vitro analysis of iron chelating activity of flavonoids. *Journal of Inorganic Biochemistry*, 105(5), 693-701.
- 14 Mira, L., Tereza Fernandez, M., Santos, M., Rocha, R., Helena Florêncio, M., & Jennings, K. R. (2002). Interactions of flavonoids with iron and copper ions: A mechanism for their antioxidant activity. *Free Radical Research*, 36(11), 1199-1208.
- 15 Khokhar, S., & Owusu Apenten, R. K. (2003). Iron binding characteristics of phenolic compounds: Some tentative structure-activity relations. *Food Chemistry*, 81(1), 133-140.
- 16 Bijlsma, J., de Bruijn, W. J. C., Hageman, J. A., Goos, P., Velikov, K. P., & Vincken, J.-P. (2020). Revealing the main factors and two-way interactions contributing to food discolouration caused by iron-catechol complexation. *Scientific Reports*, 10(1), 8288.
- 17 Hajji, H. E., Nkhili, E., Tomao, V., & Dangles, O. (2006). Interactions of quercetin with iron and copper ions: Complexation and autooxidation. *Free Radical Research*, 40(3), 303-320.
- 18 Nkhili, E., Loonis, M., Mihai, S., El Hajji, H., & Dangles, O. (2014). Reactivity of food phenols with iron and copper ions: Binding, dioxygen activation and oxidation mechanisms. *Food & Function*, 5(6), 1186-1202.
- 19 Wienk, K., Marx, J., & Beynen, A. (1999). The concept of iron bioavailability and its assessment. *European Journal of Nutrition*, 38(2), 51-75.
- 20 Andjelković, M., Van Camp, J., De Meulenaere, B., Depaemelaere, G., Socaciu, C., Verloo, M., & Verhe, R. (2006). Iron-chelation properties of phenolic acids bearing catechol and galloyl groups. *Food Chemistry*, 98(1), 23-31.
- 21 Ferreira, C. M., Pinto, I. S., Soares, E. V., & Soares, H. M. (2015). (Un)suitability of the use of pH buffers in biological, biochemical and environmental studies and their interaction with metal ions—a review. *RSC Advances*, 5(39), 30989-31003.
- 22 El-Sherif, A. A., Shoukry, M. M., & Abd-Elgawad, M. M. A. (2013). Protonation equilibria of some selected α -amino acids in DMSO–water mixture and their Cu(II)-complexes. *Journal of Solution Chemistry*, 42(2), 412-427.
- 23 Reichardt, C., & Welton, T. (2011). *Solvents and solvent effects in organic chemistry*. New York John Wiley & Sons.
- 24 Stookey, L. L. (1970). Ferrozine: A new spectrophotometric reagent for iron. *Analytical Chemistry*, 42(7), 779-781.
- 25 Berker, K. I., Güçlü, K., Demirata, B., & Apak, R. (2010). A novel antioxidant assay of ferric reducing capacity measurement using ferrozine as the colour forming complexation reagent. *Analytical Methods*, 2(11), 1770-1778.
- 26 Dobashi, Y., Hirano, T., Hirano, M., & Ohkatsu, Y. (2008). Antioxidant and photo-antioxidant abilities of catechins. *Journal of Photochemistry and Photobiology A: Chemistry*, 197(2), 141-148.
- 27 Hider, R. C., Liu, Z. D., & Khodr, H. H. (2001). Metal chelation of polyphenols. *Methods in Enzymology*, 335, 190-203.

- 28 Krabbe, J. G., Lingeman, H., Niessen, W. M. A., & Irth, H. (2005). Screening for metal ligands by liquid chromatography-ligand-exchange-electrospray mass spectrometry. *Journal of Chromatography A*, 1093(1), 36-46.
- 29 Jovanovic, S. V., Simic, M. G., Steenken, S., & Hara, Y. (1998). Iron complexes of gallic catechins. Antioxidant action or iron regulation? *Journal of the Chemical Society, Perkin Transactions 2*(11), 2365-2370.
- 30 Stepanic, V., Gasparovic, A. C., Troselj, K. G., Amic, D., & Zarkovic, N. (2015). Selected attributes of polyphenols in targeting oxidative stress in cancer. *Current Topics in Medicinal Chemistry*, 15(5), 496-509.
- 31 Sokolová, R., Ramešová, Š., Kocábová, J., Kolivoška, V., Degano, I., & Pitzalis, E. (2016). On the difference in decomposition of taxifolin and luteolin vs. fisetin and quercetin in aqueous media. *Monatshefte für Chemie - Chemical Monthly*, 147(8), 1375-1383.
- 32 Zhou, A., & Sadik, O. A. (2008). Comparative analysis of quercetin oxidation by electrochemical, enzymatic, autooxidation, and free radical generation techniques: A mechanistic study. *Journal of Agricultural and Food Chemistry*, 56(24), 12081-12091.
- 33 Trouillas, P., Marsal, P., Siri, D., Lazzaroni, R., & Duroux, J.-L. (2006). A DFT study of the reactivity of OH groups in quercetin and taxifolin antioxidants: The specificity of the 3-OH site. *Food Chemistry*, 97(4), 679-688.
- 34 Pinelo, M., Manzocco, L., José Nuñez, M., & Cristina Nicoli, M. (2004). Solvent effect on quercetin antioxidant capacity. *Food Chemistry*, 88(2), 201-207.
- 35 Smith, G. J., Thomsen, S. J., Markham, K. R., Andary, C., & Cardon, D. (2000). The photostabilities of naturally occurring 5-hydroxyflavones, flavonols, their glycosides and their aluminium complexes. *Journal of Photochemistry and Photobiology A: Chemistry*, 136(1), 87-91.
- 36 Bertleff-Zieschang, N., Rahim, M. A., Ju, Y., Braunger, J. A., Suma, T., Dai, Y., Pan, S., Cavalieri, F., & Caruso, F. (2017). Biofunctional metal-phenolic films from dietary flavonoids. *Chemical Communications*, 53(6), 1068-1071.
- 37 Rahim, M. A., Kempe, K., Müllner, M., Ejima, H., Ju, Y., van Koeverden, M. P., Suma, T., Braunger, J. A., Leeming, M. G., Abrahams, B. F., & Caruso, F. (2015). Surface-confined amorphous films from metal-coordinated simple phenolic ligands. *Chemistry of Materials*, 27(16), 5825-5832.
- 38 Ejima, H., Richardson, J. J., & Caruso, F. (2017). Metal-phenolic networks as a versatile platform to engineer nanomaterials and biointerfaces. *Nano Today*, 12, 136-148.
- 39 Papan, P., Kantapan, J., Sangthong, P., Meepowpan, P., & Dechsupa, N. (2020). Iron (III)-quercetin complex: Synthesis, physicochemical characterization, and MRI cell tracking toward potential applications in regenerative medicine. *Contrast Media & Molecular Imaging*, 2020.
- 40 Wang, Z. (2013). Iron complex nanoparticles synthesized by eucalyptus leaves. *ACS Sustainable Chemistry & Engineering*, 1(12), 1551-1554.
- 41 Zhong, Q. Z., Li, S., Chen, J., Xie, K., Pan, S., Richardson, J. J., & Caruso, F. (2019). Oxidation-mediated kinetic strategies for engineering metal-phenolic networks. *Angewandte Chemie International Edition*, 58(36), 12563-12568.
- 42 Patel, A. R., Heussen, P. C. M., Hazekamp, J., Drost, E., & Velikov, K. P. (2012). Quercetin loaded biopolymeric colloidal particles prepared by simultaneous precipitation of quercetin with hydrophobic protein in aqueous medium. *Food Chemistry*, 133(2), 423-429.
- 43 Flynn, C. M. (1984). Hydrolysis of inorganic iron(III) salts. *Chemical Reviews*, 84(1), 31-41.
- 44 Lesjak, M., & Srai, S. K. S. (2019). Role of dietary flavonoids in iron homeostasis. *Pharmaceuticals*, 12(3), 119.
- 45 Jungbluth, G., & Ternes, W. (2000). HPLC separation of flavonols, flavones and oxidized flavonols with UV-, DAD-, electrochemical and ESI-ion trap MS detection. *Fresenius' Journal of Analytical Chemistry*, 367(7), 661-666.
- 46 Fuentes, J., Atala, E., Pastene, E., Carrasco-Pozo, C., & Speisky, H. (2017). Quercetin oxidation paradoxically enhances its antioxidant and cytoprotective properties. *Journal of Agricultural and Food Chemistry*, 65(50), 11002-11010.
- 47 Verloop, A. J. W., Gruppen, H., & Vincken, J.-P. (2016). Annotation of different dehydrocatechin oligomers by MS/MS and their occurrence in black tea. *Journal of Agricultural and Food Chemistry*, 64(30), 6011-6023.
- 48 Huvaere, K., Sinnaeve, B., Van Bocxlaer, J., & Skibsted, L. H. (2012). Flavonoid deactivation of excited state flavins: Reaction monitoring by mass spectrometry. *Journal of Agricultural and Food Chemistry*, 60(36), 9261-9272.

3.7. Supplementary information

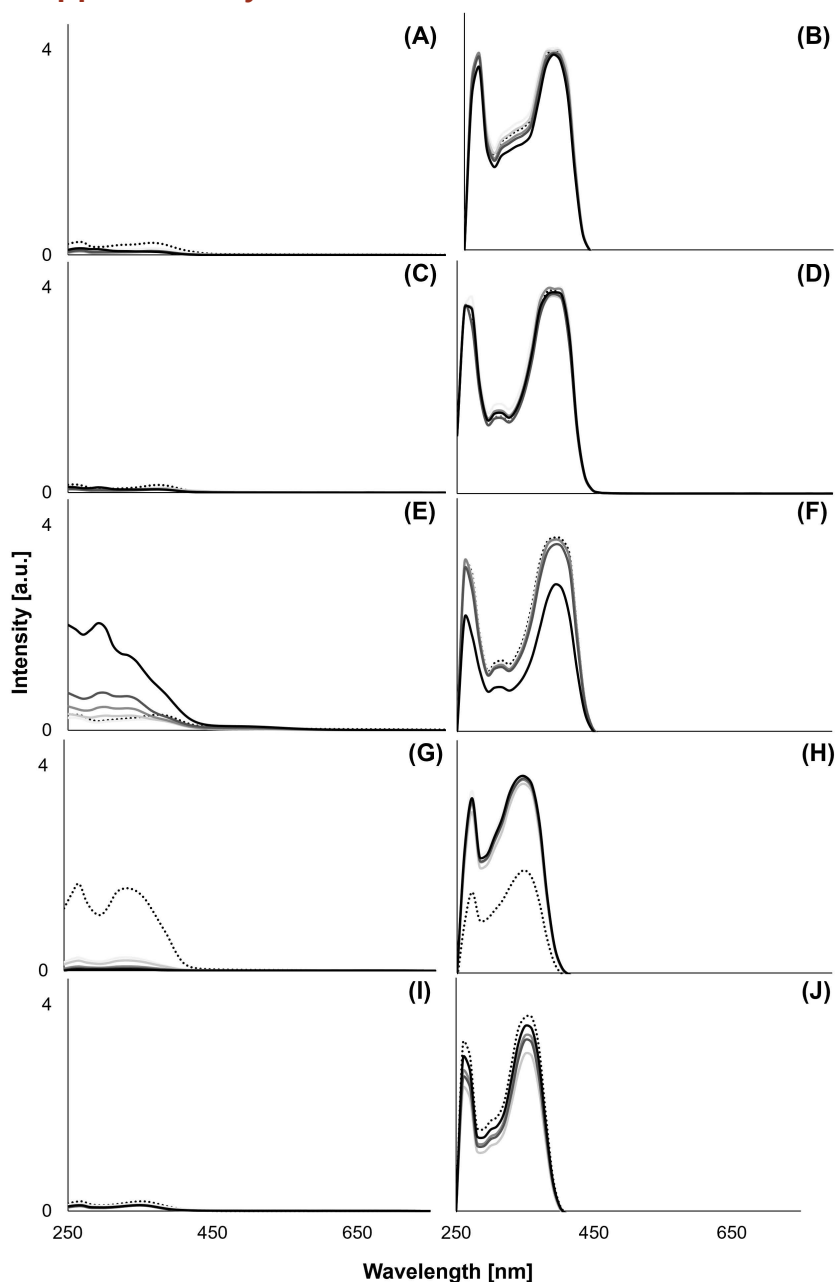


Figure S3.1. Absorbance spectra of flavonoid blanks at t_0 (dotted line), and after pH adjustment for the different timepoints: t_0 , t_1 , t_2 , t_4 to t_{24} (gradient light to dark) (A) kaempferol WS; (B) kaempferol DS; (C) quercetin WS; (D) quercetin DS; (E) myricetin WS; (F) myricetin DS; (G) apigenin WS; (H) apigenin DS; (I) luteolin WS; (J) luteolin DS.

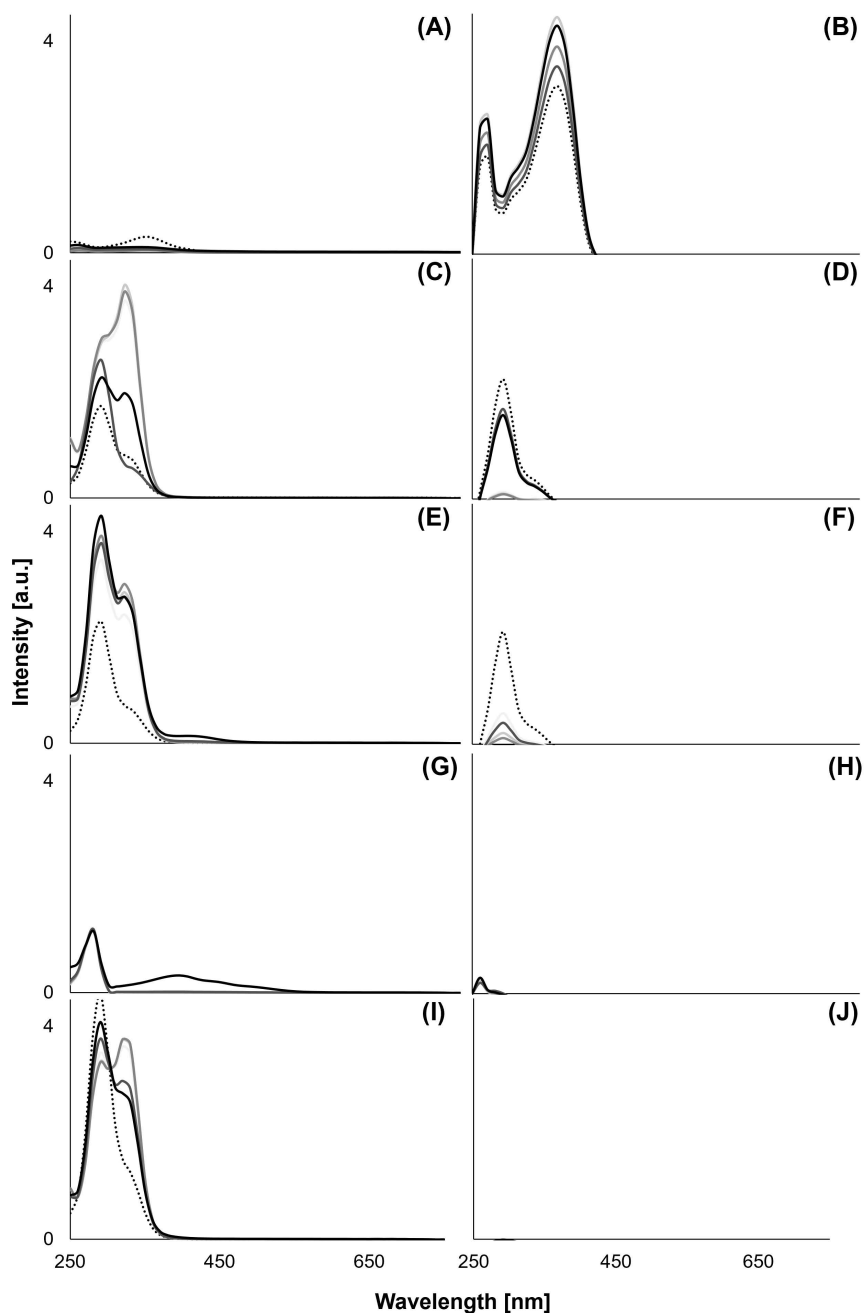


Figure S3.2. Absorbance spectra of flavonoid blanks at t_0 (dotted line), and after pH adjustment for the different timepoints: t_0, t_1, t_2, t_4 to t_{24} (gradient light to dark) (A) tricetin WS; (B) tricetin DS; (C) naringenin WS; (D) naringenin DS; (E) eriodictyol WS; (F) eriodictyol DS; (G) epicatechin WS; (H) epicatechin DS; (I) taxifolin WS; (J) taxifolin DS.

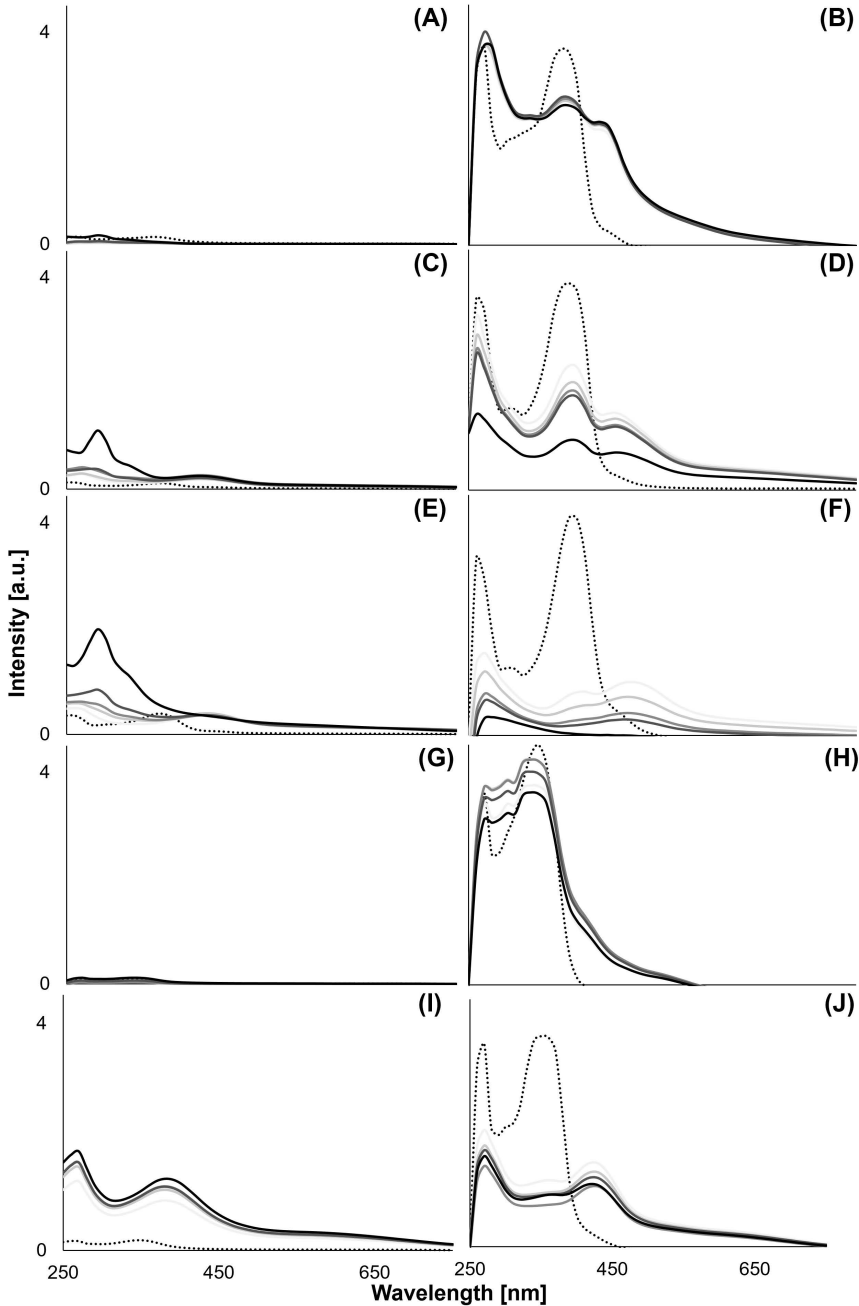


Figure S3.3. Absorbance spectra of iron-flavonoid samples at t_0 (dotted line), and after pH adjustment for the different timepoints: t_0 , t_1 , t_2 , t_4 to t_{24} (gradient light to dark) (A) kaempferol WS; (B) kaempferol DS; (C) quercetin WS; (D) quercetin DS; (E) myricetin WS; (F) myricetin DS; (G) apigenin WS; (H) apigenin DS; (I) luteolin WS; (J) luteolin DS.

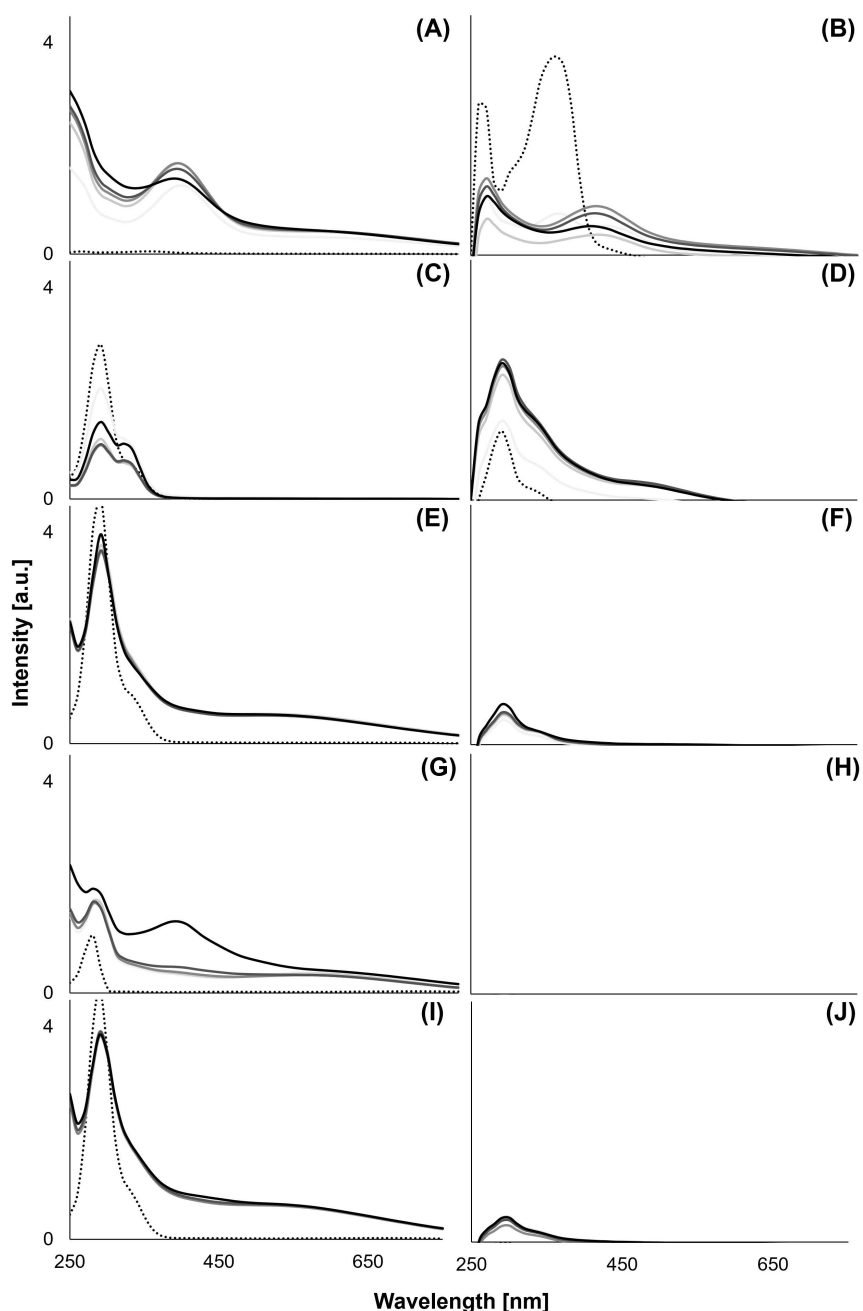


Figure S3.4. Absorbance spectra of iron-flavonoid samples at t_0 (dotted line), and after pH adjustment for the different timepoints: t_0 , t_1 , t_2 , t_4 to t_{24} (gradient light to dark) (A) tricetin WS; (B) tricetin DS; (C) naringenin WS; (D) naringenin DS; (E) eriodictyol WS; (F) eriodictyol DS; (G) epicatechin WS; (H) epicatechin DS; (I) taxifolin WS; (J) taxifolin DS.

Table S3.1. Flavonoid identification by RP-UHPLC-PDA-MS².

Rt (min)	λ_{max} (nm)	$[\text{M}-\text{H}]^-$ m/z	MS ² product ion m/z (relative abundance) ^a	$[\text{M}+\text{H}]^+$ m/z	MS ² product ion m/z (relative abundance) ^a	Identification ^b
7.35	278	289	<u>245</u> , 205 (36), 179 (13)	291	<u>139</u> , 123 (93), 165 (54), 273 (31)	Epicatechin
9.13	290	303	<u>285</u> , 177 (12)	305	<u>287</u> , 259 (85), 153 (45), 195 (22)	Taxifolin
10.56	374	317	<u>179</u> , 151 (37), 288 (11)	319	<u>273</u> , 301 (44), 165 (42), 245 (33), 153 (32), 290 (25), 263 (26)	Myricetin
10.90	266, 350	301	<u>301</u> , 239 (56), 255 (54), 283 (34), 215 (31), 191 (34), 151 (20)	303	<u>303</u> , 153 (13)	Tricetin
12.14	286	287	<u>151</u>	289	<u>163</u> , 153 (23), 271 (20), 179 (18)	Eriodictyol
12.40	370	301	<u>179</u> , 151 (74), 273 (18), 257 (13)	303	<u>257</u> , 229 (60), 165 (60), 285 (54), 247 (36), 274 (20), 303 (21)	Quercetin
12.41	346	285	<u>241</u> , 285 (91), 175 (71), 217 (61), 243 (63), 199 (52), 151 (30)	287	<u>287</u> , 258 (8), 153 (24)	Luteolin
13.79	290	271	<u>151</u> , 177 (21)	273	<u>153</u> , 147 (96)	Naringenin
13.83	266, 338	269	<u>225</u> , 149 (41), 269 (52), 201 (25)	271	<u>271</u> , 153 (22)	Apigenin
14.05	266, 366	285	<u>285</u> , 151 (36), 229 (17), 257 (16), 213 (16), 169 (12)	287	<u>287</u> , 165 (77), 241 (65), 213 (62), 258 (38), 231 (26), 153 (26), 121(16)	Kaempferol

n.d. not detected; ^a relative intensity threshold for fragments was $\geq 10\%$. The most intense fragment is underlined; ^b all identifications were confirmed with authentic standards.

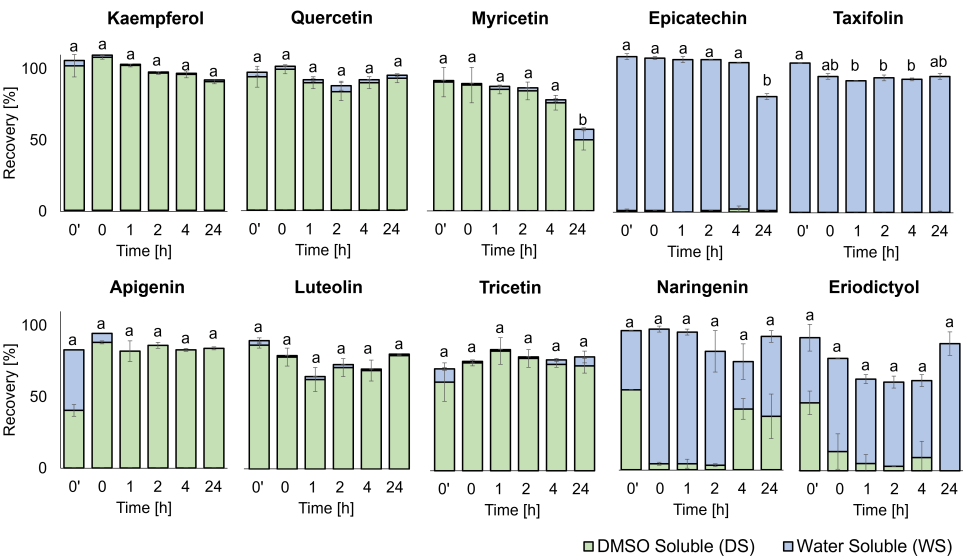


Figure S3.5. Recovery of kaempferol, quercetin, myricetin, epicatechin, taxifolin, apigenin, luteolin, tricetin, naringenin, eriodictyol in the WS (blue) and DS (green) before adjustment of the pH (t_0) and after 0, 1, 2, 4, and 24 hours of incubation at pH 6.5. Error bars indicate the standard deviation of independent duplicates. Different letters indicate a significant difference in total recovery compared to other time points for the same flavonoid (Tukey's test, $p < 0.05$). Significance of differences in the three individual fractions (*i.e.* WS, DS, and AAS) per time point for each flavonoid is indicated in supplementary information, **Table S3.3**.

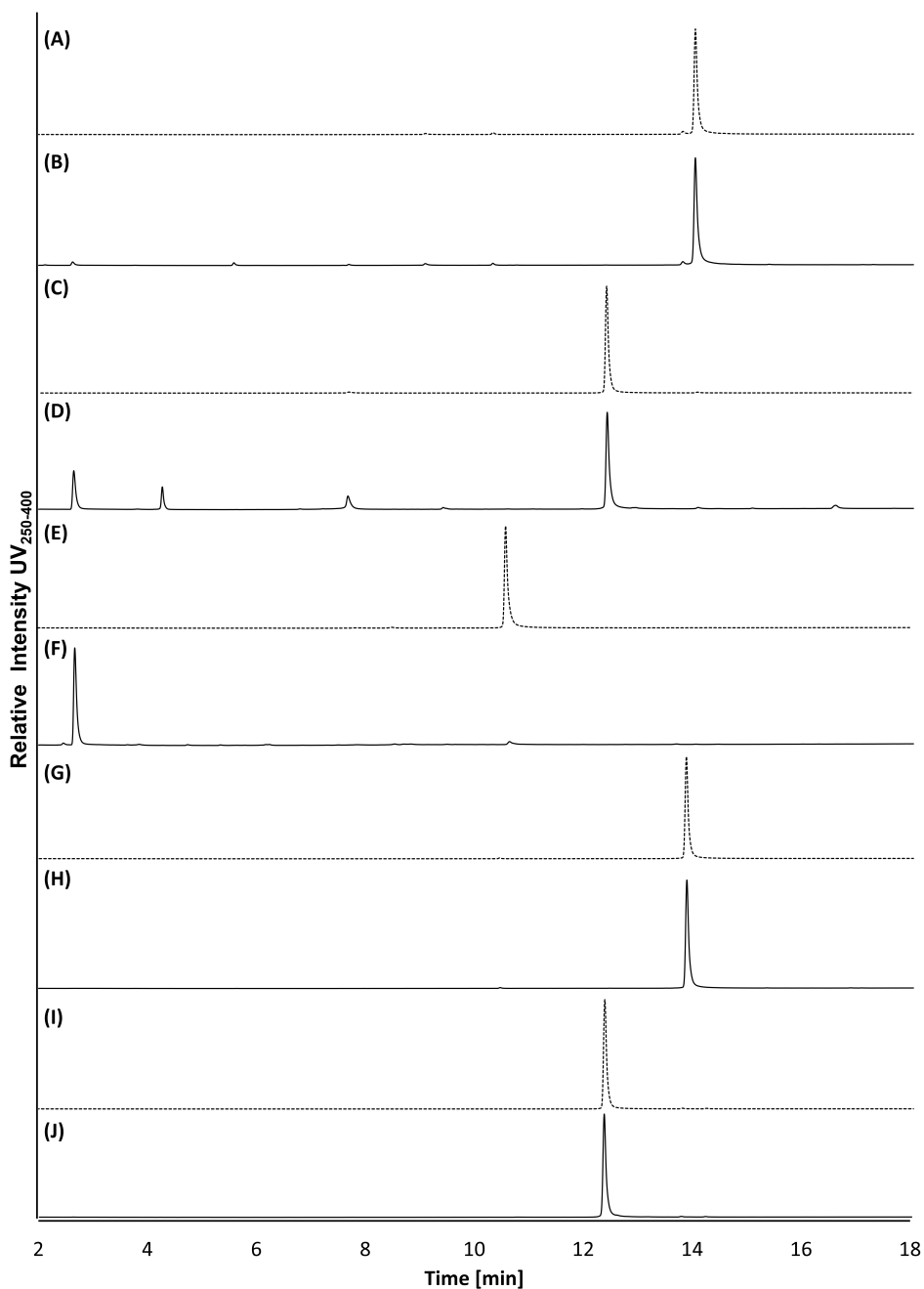


Figure S3.6. Combined RP-UHPLC-PDA (250-400 nm) chromatograms from the WS and DS fractions of (A) kaempferol \times FeSO₄ (t₀); (B) kaempferol \times FeSO₄ (t₂₄); (C) quercetin \times FeSO₄ (t₀); (D) quercetin \times FeSO₄ (t₂₄); (E) myricetin \times FeSO₄ (t₀); (F) myricetin \times FeSO₄ (t₂₄); (G) apigenin \times FeSO₄ (t₀); (H) apigenin \times FeSO₄ (t₂₄); (I) luteolin \times FeSO₄ (t₀); and (J) luteolin \times FeSO₄ (t₂₄).

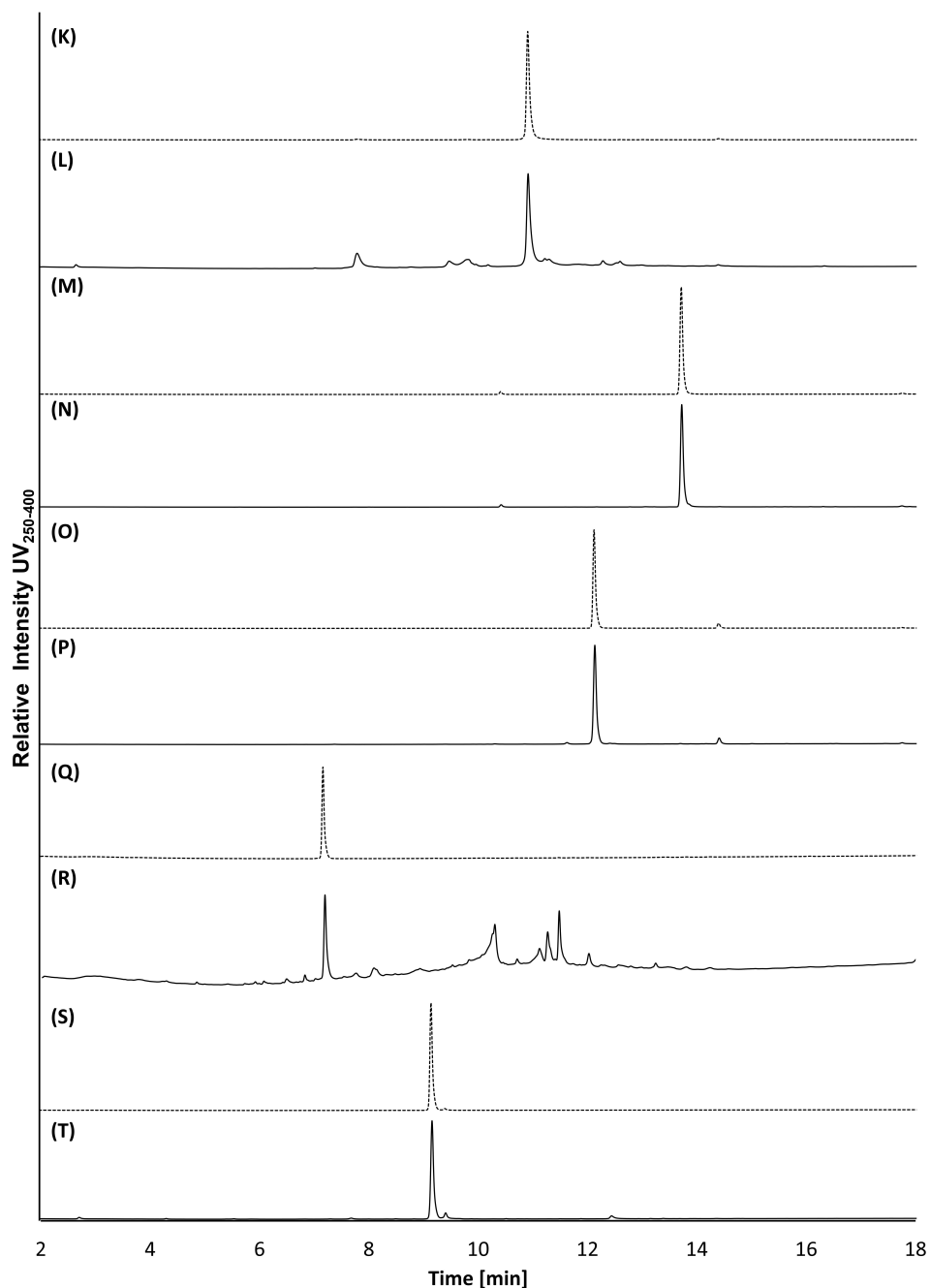


Figure S3.7. Combined RP-UHPLC-PDA (250-400 nm) chromatograms from the WS and DS fractions of **(K)** tricetin \times FeSO_4 (t_0); **(L)** tricetin \times FeSO_4 (t_{24}); **(M)** naringenin \times FeSO_4 (t_0); **(N)** naringenin \times FeSO_4 (t_{24}); **(O)** eriodictyol \times FeSO_4 (t_0); **(P)** eriodictyol \times FeSO_4 (t_{24}); **(Q)** epicatechin \times FeSO_4 (t_0); **(R)** epicatechin \times FeSO_4 (t_{24}); **(S)** taxifolin \times FeSO_4 (t_0); and **(T)** taxifolin \times FeSO_4 (t_{24}).

Table S3.2. Flavonoid oxidation products tentatively identified by RP-UHPLC-PDA-MS².

Rt (min)	λ_{\max} (nm)	[M-H] ⁻ m/z	MS ² product ion m/z (relative intensity) ^a	[M+H] ⁺ m/z	MS ² product ion m/z (relative intensity) ^a	Tentatively identified	Ref.
Intermediate oxidation products							
6.22	298	333	207, 315 (10)	335	n.d.	Myricetin-ox	d, e
7.37	290	319	n.d.	n.d.	n.d.	Taxifolin-ox	d, e
7.74	294	317	191, 299 (57), 207 (45), 163 (24), 273 (17)	319	n.d.	Quercetin-ox	d, e
7.82	282	317	273, 299 (26), 255 (10)	n.d.	n.d.	Tricetin-ox	d, e
9.13	294	301	273, 207 (16), 257 (13)	303	n.d.	Kaempferol-ox	d, e
10.24	n.d.	303	n.d.	n.d.	n.d.	Eriodictyol-ox	d, e
10.92	362	301	n.d.	n.d.	n.d.	Luteolin-ox	d, e
12.22	286	287	151	289	n.d.	Naringenin-ox	d, e
12.51	354	285	241, 285 (75), 217 (70), 175 (66), 199 (46), 243 (41), 267 (39), 151 (25)	287	n.d.	Apigenin-ox	d, e
Cleavage products							
2.46	270	169	125	n.d.	n.d.	3,4,5-Trihydroxybenzoic acid ^b	e
2.65	294	197	153	n.d.	n.d.	2,4,6-Trihydroxyphenylglyoxylic acid ^b	e
3.83	254, 294	169	151	n.d.	n.d.	2,4,6-Trihydroxybenzoic acid ^b	e
4.27	260, 294	153	109	n.d.	n.d.	3,4-Dihydroxybenzoic acid ^b	e
5.58	254	137	93	n.d.	n.d.	4-Hydroxybenzoic acid ^b	
Coupling products^c							
6.80	278, 394	577	439, 393 (91), 425 (76), 533 (54), 559 (54), 269 (32), 367 (14), 541 (13)	579	n.d.	β_{AB} -Type dehydrodicatechin	f
7.79	386	863	725, 425 (34), 449 (33), 845 (24), 819 (19), 413 (19), 801 (10), 407 (10)	865	n.d.	(δ - β)/ ϵ_{AB} -Type dehydrotricatechin ^f	f
8.92	385	577	439, 533 (67), 425 (37), 559 (38), 425 (36), 329 (27)	579	n.d.	β -Type dehydrodicatechin	f
10.29	378	575	449, 287 (50), 437 (38), 407 (24), 394 (22), 531 (13), 243 (13), 229 (12), 513 (11)	577	n.d.	δ_{AB} -Type dehydrodicatechin	f
10.31	378	861	680, 723 (54), 735 (32), 529 (20), 699 (19), 693 (16), 407 (16), 423 (10), 7099 (13)	863	n.d.	(δ - γ)/ δ_{AB} -Type dehydrotricatechin	f
10.68	378	575	449, 287 (57), 394 (32), 437 (30), 431 (22), 407 (26), 243 (14), 229 (14)	577	n.d.	δ_{AB} -Type dehydrodicatechin	f
11.11	370	575	449, 287 (59), 437 (38), 407 (34), 393 (27), 431 (24), 228 (16)	577	n.d.	δ_{AB} -Type dehydrodicatechin	f
11.29	334	601	323, 475 (51), 449 (18), 301 (13)	603	n.d.	Dehydrodicitricetin	

n.d. not detected; ^a relative intensity threshold for fragments was ≥ 10 . The most intense fragment is underlined; ^b identification confirmed with authentic standard; ^c only oxidative coupling products with a UV₂₅₀₋₄₀₀ area > 1000 after 24 h incubation in presence of FeSO₄ were shown; d [31, 45, 46], e [32], f [12, 47], g [48].

Table S3.2. Continued

Rt (min)	λ_{max} (nm)	[M-H] ⁻ <i>m/z</i>	MS ¹ product ion <i>m/z</i> (relative intensity) ^a	[M+H] ⁺ <i>m/z</i>	MS ² product ion <i>m/z</i> (relative intensity) ^a	Tentatively identified	Ref.
Coupling products^c							
11.47	378	575	449, 287 (62), 394 (40), 407 (29), 431 (27), 437 (26), 229 (16)	577	425, 245 (23), 397 (12)	δ_{AB} -Type dehydrodicatechin	f
12.90	346	603	487, 559 (25), 531 (21), 459 (19), 585 (21)	605	n.d.	Dehydroditricetin	
11.49	378	605	n.d.	607	n.d.	Dehydroditaxifolin	
13.15	366	603	n.d.	n.d.	n.d.	Dehydroditaxifolin	
13.24	374	861	n.d.	863	n.d.	Dehydrotricatechin	
14.17	278	573	405, 447 (46), 311 (27), 411 (27), 421 (19)	575	n.d.	Dehydrodieriodictyol	
14.71	362	603	n.d.	605	n.d.	Dehydroditaxifolin	
15.01	286	573	447, 421 (70), 411 (27)	575	n.d.	Dehydrodieriodictyol	
15.32	342	537	375, 443 (74), 417 (11)	539	n.d.	Dehydrodiapigenin	
15.36	358	541	311, 395 (56), 497 (23), 353 (16)	543	n.d.	Dehydrodinaringenin	
15.41	358	541	311, 395 (57), 497 (23), 353 (15)	543	n.d.	Dehydrodinaringenin	
15.60	358	541	311, 395 (58), 497 (21), 353 (15)	543	n.d.	Dehydrodinaringenin	
15.71	294, 358	541	311, 395 (54), 497 (21), 353 (15)	543	n.d.	Dehydrodinaringenin	
16.07	294, 354	541	311, 395 (55), 497 (21), 353 (15)	543	n.d.	Dehydrodinaringenin	
16.30	294, 350	541	311, 395 (57), 497 (22), 353 (16)	543	n.d.	Dehydrodinaringenin	
16.52	294, 354	541	311, 395 (53), 497 (21), 353 (15)	543	n.d.	Dehydrodinaringenin	
16.58	366	601	299, 271 (10)	603	n.d.	BC-type dehydroquercetin	e, g
17.07	366	569	n.d.	571	n.d.	Dehydrodikaempferol	g
17.27	366	569	417, 525 (24), 541 (20), 551 (20), 443 (22)	571	n.d.	BC-type dehydrokaempferol	g
17.49	350	569	n.d.	571	n.d.	Dehydrodiluteolin	

n.d. not detected; ^a relative intensity threshold for fragments was ≥ 10 . The most intense fragment is underlined; ^b identification confirmed with authentic standard; ^c only oxidative coupling products with a UV₂₅₀₋₄₀₀ area > 1000 after 24 h incubation in presence of FeSO₄ were shown; d [31, 45, 46], e [32], f [12, 47], g [48].

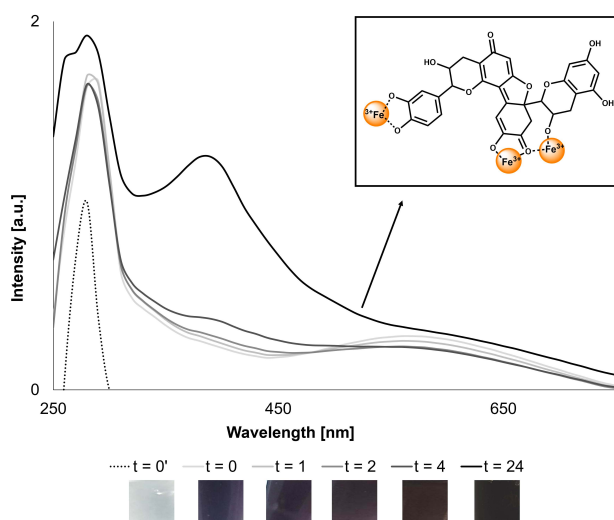


Figure S3.8. Absorbance spectra of epicatechin \times FeSO_4 over time upon incubation at 40°C and pH 6.5, including images of the colour of the sample at the different time points. The inset shows proposed binding sites of iron to a δ -type dehydrodicatechin.

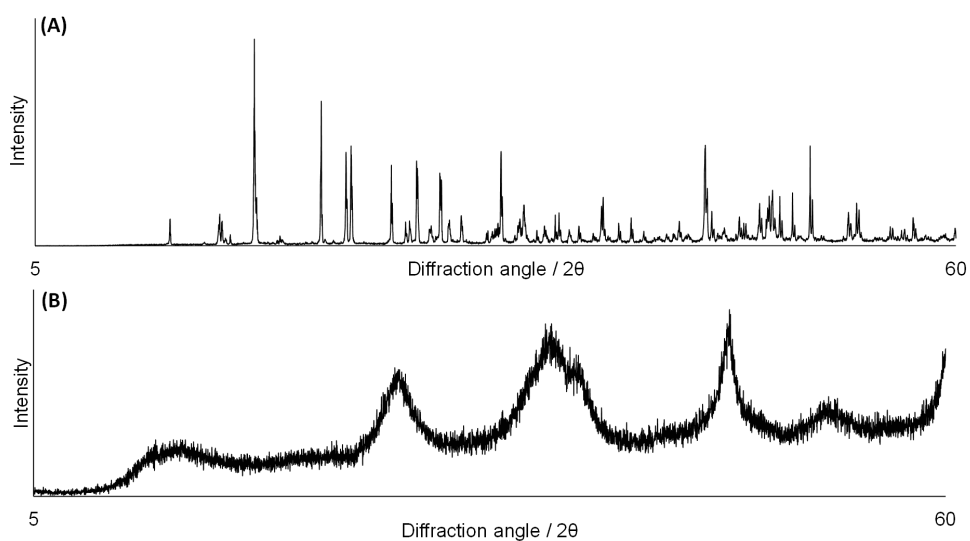


Figure S3.9. Powder XRD pattern of (A) ferrous sulphate blank, pattern was identified as monoclinic $\text{FeH}_{14}\text{O}_{11}\text{S}$ and (B) ferrous sulphate blank after incubation for 1 hour at pH 6.5, pattern was identified as orthombic iron oxyhydroxide $[\text{FeO}(\text{OH})]$, e.g. lepidocrocite.

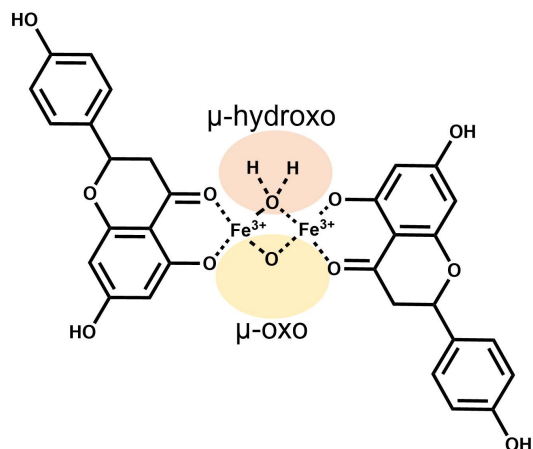


Figure S3.10. Schematic illustration of coordination of Fe(III) to naringenin via μ -oxo/hydroxo-bridged species in aqueous solution, based on μ -oxo-bridged species reported previously by Zhong *et al.*^[41]

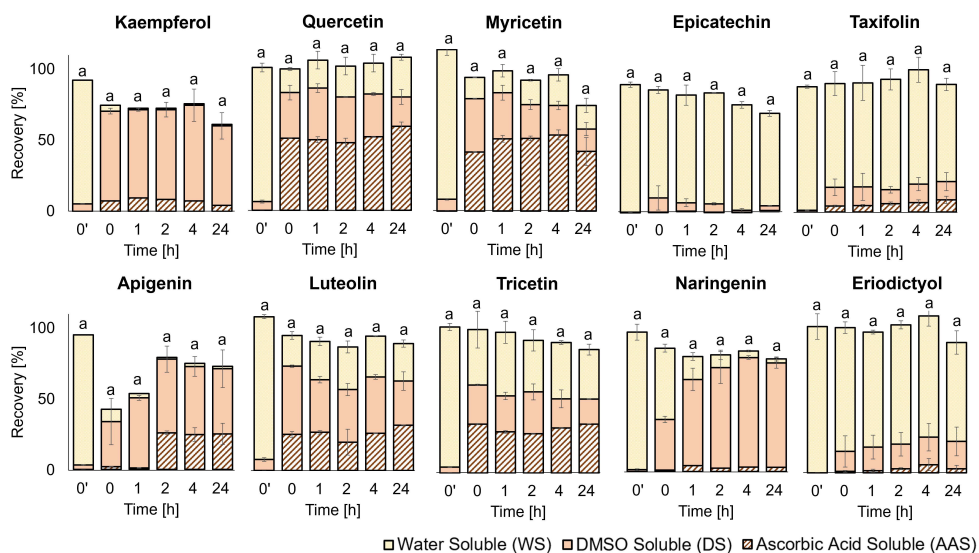


Figure S3.11. Recovery of iron in the WS (yellow), DS (orange) and AAS (brown hashed) fractions of samples containing kaempferol, quercetin, myricetin, apigenin, luteolin, tricetin, naringenin, eriodictyol, epicatechin, and taxifolin before adjustment of the pH (t_0) and after 0, 1, 2, 4, and 24 hours of incubation at pH 6.5. Error bars indicate the standard deviation of independent duplicates. Different letters indicate a significant difference in total iron recovery compared to other time points for the same flavonoid (Tukey's test, $p < 0.05$). Significance of differences in the three individual fractions (*i.e.* WS, DS, and AAS) per time point for each flavonoid is indicated in supplementary information, **Table S3.3**.

Table S3.3. Statistical analysis of the flavonoid and iron recovery in total and for the recovery in each of the three different fractions: water soluble (WS), DMSO soluble (DS), and ascorbic acid soluble (AAS) fractions. The quantitative differences were assessed by Tukey's *post hoc* comparison ($p < 0.05$). Significant differences in recovery compared to the other time points for the same flavonoid are indicated with a different letter.

Flavonoid	Time	Flavonoid recovery in presence of FeSO ₄				Flavonoid recovery in absence of FeSO ₄				Iron recovery in presence of flavonoid			
		Tot.	WS	DS	AAS	Tot.	WS	DS	AAS	Tot.	WS	DS	AAS
Kaempferol	0'	a	a	a	a	a	a	a	n.a.	a	a	b	c
	0	a	b	a	a	a	a	a	n.a.	a	b	a	ab
	1	a	bc	a	a	a	a	a	n.a.	a	b	a	ab
	2	a	bc	a	a	a	a	a	n.a.	a	b	a	b
	4	a	bc	a	a	a	a	a	n.a.	a	b	a	ab
	24	a	c	a	a	a	a	a	n.a.	a	b	a	b
Quercetin	0'	b	b	a	b	a	a	a	n.a.	a	a	b	a
	0	a	a	bc	a	a	a	a	n.a.	a	b	a	a
	1	ab	a	bc	a	a	a	a	n.a.	a	b	a	a
	2	ab	a	bc	a	a	a	a	n.a.	a	b	a	a
	4	ab	a	c	a	a	a	a	n.a.	a	b	a	a
	24	c	a	d	a	a	a	a	n.a.	a	b	a	a
Myricetin	0'	a	a	a	c	a	a	a	n.a.	a	a	c	b
	0	ab	a	b	a	a	a	a	n.a.	a	b	a	a
	1	bc	b	c	a	a	a	a	n.a.	a	b	ab	a
	2	c	c	d	a	a	a	a	n.a.	a	b	abc	a
	4	c	c	d	a	a	a	a	n.a.	a	b	abc	a
	24	d	d	e	b	b	b	a	n.a.	a	b	bc	a
Epicatechin	0'	a	a	a	a	a	a	a	n.a.	a	a	a	a
	0	b	b	a	a	a	a	a	n.a.	a	ab	a	a
	1	b	c	a	a	a	a	a	n.a.	a	ab	a	a
	2	c	d	a	a	a	a	a	n.a.	a	ab	a	a
	4	d	e	a	a	a	a	a	n.a.	a	ab	a	a
	24	e	f	a	a	b	b	a	n.a.	a	b	a	a
Taxifolin	0'	a	a	a	a	a	a	a	n.a.	a	a	a	b
	0	ab	ab	a	a	ab	b	a	n.a.	a	a	a	ab
	1	ab	ab	a	a	b	b	a	n.a.	a	a	a	ab
	2	ab	ab	a	a	b	b	a	n.a.	a	a	a	ab
	4	ab	ab	a	a	b	b	a	n.a.	a	a	a	ab
	24	b	b	a	a	ab	b	a	n.a.	a	a	a	a

n.a. not applicable, no ascorbic acid soluble fraction was present.

Table S3.3. Continued

Flavonoid	Time	Flavonoid recovery in presence of FeSO ₄				Flavonoid recovery in absence of FeSO ₄				Iron recovery in presence of flavonoid			
		Tot.	WS	DS	AAS	Tot.	WS	DS	AAS	Tot.	WS	DS	AAS
Apigenin	0'	a	a	a	b	a	a	b	n.a.	a	a	a	b
	0	a	a	a	b	a	b	a	n.a.	a	b	a	b
	1	a	a	a	b	a	c	a	n.a.	a	b	a	b
	2	a	a	a	a	a	c	a	n.a.	a	b	a	a
	4	a	a	a	a	a	c	a	n.a.	a	b	a	a
	24	a	a	a	a	a	c	a	n.a.	a	b	a	a
Luteolin	0'	a	b	a	b	a	a	a	n.a.	a	a	b	b
	0	a	a	b	a	a	a	a	n.a.	a	b	a	a
	1	a	a	b	a	a	a	a	n.a.	a	b	a	a
	2	a	a	b	a	a	a	a	n.a.	a	b	a	ab
	4	a	a	b	a	a	a	a	n.a.	a	b	a	a
	24	a	a	b	a	a	a	a	n.a.	a	b	a	a
Tricetin	0'	a	c	a	b	a	a	a	n.a.	a	a	b	d
	0	ab	a	b	a	a	a	a	n.a.	a	b	a	a
	1	ab	a	c	ab	a	a	a	n.a.	a	b	a	bc
	2	ab	ab	c	ab	a	a	a	n.a.	a	b	a	c
	4	ab	ab	c	ab	a	a	a	n.a.	a	b	ab	b
	24	b	b	c	ab	a	a	a	n.a.	a	b	ab	a
Naringenin	0'	a	a	b	a	a	b	a	n.a.	a	a	c	c
	0	a	ac	ab	a	a	a	b	n.a.	a	b	b	b
	1	a	b	ab	a	a	a	b	n.a.	a	c	ab	a
	2	a	b	a	a	a	a	b	n.a.	a	c	a	ab
	4	a	b	a	a	a	b	ab	n.a.	a	c	a	ab
	24	a	bc	ab	a	a	ab	ab	n.a.	a	c	a	ab
Eriodictyol	0'	a	a	a	b	a	b	ab	n.a.	a	a	a	a
	0	a	a	a	b	a	ab	ab	n.a.	a	a	a	a
	1	a	a	a	b	a	ab	ab	n.a.	a	a	a	a
	2	a	a	a	b	a	ab	ab	n.a.	a	a	a	a
	4	a	a	a	b	a	b	ab	n.a.	a	a	a	a
	24	a	a	a	a	a	a	b	n.a.	a	a	a	a

n.a. not applicable, no ascorbic acid soluble fraction was present.

CHAPTER 4

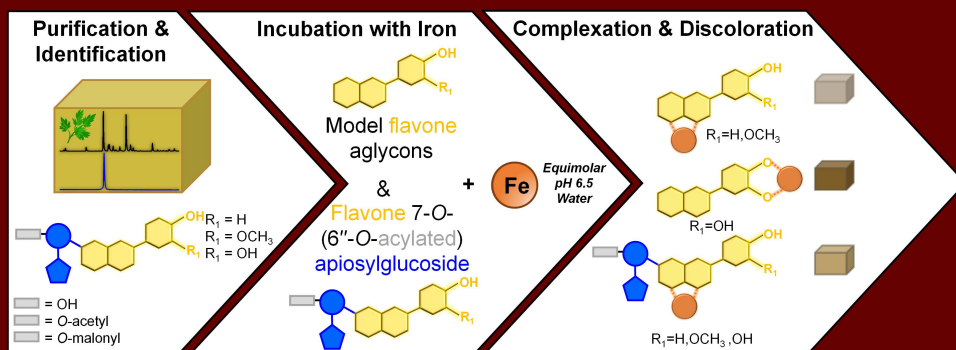
Interaction of natural flavones with iron are affected by 7-O-glycosylation, but not by additional 6"-O-acylation

Judith Bijlsma, Wouter J.C. de Bruijn, Jamie Koppelaar, Mark G. Sanders, Krassimir P. Velikov, and Jean-Paul Vincken

Based on: *ACS Food Science & Technology*, 2023, 3:1111-1121

Abstract

In iron-fortified bouillon cubes, reactivity of the iron ion with (acylated) flavone glycosides from herbs can affect product colour and bioavailability of iron. This study investigates the influence of 7-*O*-glycosylation and additional 6''-*O*-acetylation or 6''-*O*-malonylation of flavones on their interaction with iron. Nine (6''-*O*-acylated) flavone 7-*O*-apiosylglucosides were purified from celery (*Apium graveolens*) and their structures were elucidated by MS and NMR. In presence of iron, a bathochromic shift and darker colour was observed for the 7-*O*-apiosylglucosides compared to the aglycon of flavones that only possess the 4–5 site. Thus, the ability of iron to coordinate to the flavone 4–5 site is increased by 7-*O*-glycosylation. For flavones with an additional 3'–4' site, less discolouration was observed for the 7-*O*-apiosylglucoside compared to the aglycon. Additional 6''-*O*-acylation did not affect the colour. These findings indicate that model systems used to study discolouration in iron-fortified foods should also comprise (acylated) glycosides of flavonoids.



4.1. Introduction

Food fortified with iron can effectively reduce the global prevalence of iron deficiency.^[1] Bouillon cubes and other types of savoury concentrates are promising vehicles for iron fortification, as they are widely available, frequently consumed, and affordable.^[2,3] However, when bouillon cubes are fortified with iron, the colour and the bioavailability of iron can be compromised by the reactivity of the iron ion with phenolics.^[4] Bouillon cubes typically contains salt, carbohydrates, starch, fats, proteins, herbs, and spices.^[3] The phenolics that react with iron mainly originate from the herbs and spices. Common herbs in bouillon cubes are parsley (*Petroselinium crispum*) and celery (*Apium graveolens*).^[5] These herbs are especially rich in flavones, a subclass of flavonoids that possess a 2-phenylchromen-4-one backbone (Fig. 4.1A).^[6] Apigenin, chrysoeriol, diosmetin, and luteolin are examples of common flavone backbones that are present in celery and parsley.^[7] Iron can coordinate to the 5-hydroxy-4-ketone moiety (4–5 site) of flavones, as shown in Fig. 4.1A. Additionally, iron coordination to the 3'-4'-dihydroxy moiety located in the B-ring (3'-4' site) of flavones can occur, such as the B-ring of luteolin.^[8]

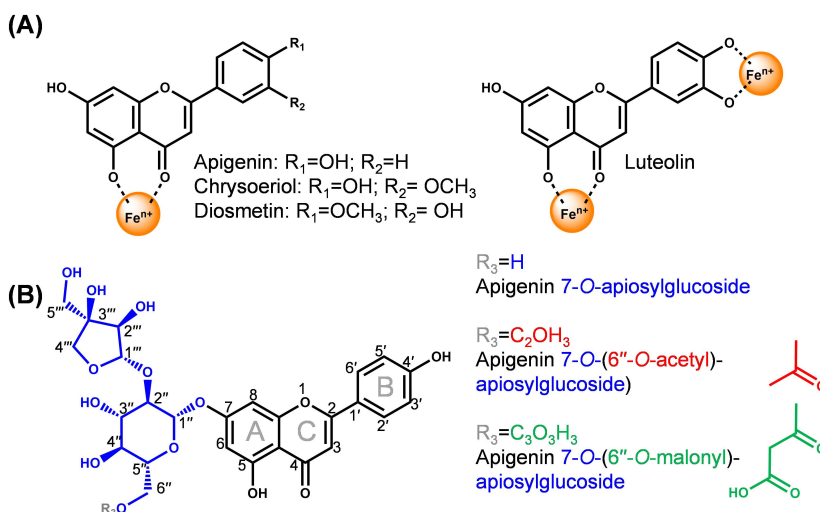


Figure 4.1. (A) Structures of common flavone aglycons present in celery and parsley including the proposed iron coordination to the 4–5 site for apigenin, chrysoeriol, and diosmetin and additional coordination to the 3'-4' site for luteolin. (B) The structure of apigenin 7-O-apiosylglucoside (i.e. apiin), apigenin 7-O-(6''-O-acetyl)-apiosylglucoside (i.e. 6''-acetylapiin), and apigenin 7-O-(6''-O-malonyl)-apiosylglucoside (i.e. 6''-malonylapiin).^[9,10]

In plants and plant-derived ingredients, the majority of flavones are glycosylated. Glycosylation of flavones reduces their reactivity and enhances their solubility in water.^[11,12] Glycosylated flavones from celery and parsley can also possess additional acylation of the glycoside moiety's hydroxyl groups by acetyl or malonyl groups.^[7,9,10,13] So far, only the structures of apigenin 7-O-apiosylglucoside (also known as apiin), apigenin 7-O-(6''-O-acetyl)-apiosylglucoside (also known as 6''-

acetylapiin) and apigenin 7-*O*-(6''-*O*-malonyl)-apiosylglucoside (also known as 6''-malonylapiin) have been confirmed by NMR (**Fig. 4.1B**).^[9,10] For the other (acylated) flavone glycosides in celery and parsley, identification was tentative and based solely on mass spectrometry.^[7,13] Detailed structural elucidation of these other (acylated) flavone glycosides has to be performed to confirm these tentative identifications.

To date, all research on understanding iron-phenolic interactions (*i.e.* complexation, oxidation, formation of networks) and its resulting discolouration in fortified foods has focused on model systems using simple phenolic and/or flavonoid aglycons.^[8,14–18] These studies show that flavonoid aglycons can form complexes with ferrous [Fe(II)] or ferric [Fe(III)] iron. Due to the higher stability of the Fe(III) complexes, the complexes with Fe(II) autoxidise to form coloured Fe(III) iron complexes.^[15] Moreover, the complexation of Fe(III) to flavonoids can lead to oxidative coupling or oxidative degradation of flavonoids and the formation of iron-phenolic networks.^[8]

The influence of 7-*O*-glycosylation and additional acylation on the interactions of flavones with iron is not yet understood. To be able to extrapolate the knowledge obtained using studies on flavonoid aglycons to real food fortification vehicles, such as bouillon cubes, it is important to investigate the effect of flavone glycosylation and additional acylation on iron interaction. It has already been shown that 3-*O* and 5-*O* glucosylation affects metal coordination to the anthocyanin subclass of flavonoids and quercetin.^[19–24] However, because the 7-OH group of the flavone is not normally involved in iron complexation, we expect that 7-*O*-glycosylation of the flavone does not affect iron complexation and oxidation reactions. On the other hand, the addition of a malonyl group to the glycoside could potentially increase the stability of metal-flavonoid complexes due to the coordination of iron by the free carboxylate group.^[21] For acetylation, no such effect on complexation with iron is expected since there is no free carboxylate group.

In this study, we aimed to comprehensively investigate the effect of 7-*O* substitution of different flavone backbones with (acylated) apiosylglucosyl moieties. We first isolated and purified the flavones that are naturally present in bouillon cubes and herbs, by methanolic extraction and preparative chromatography, respectively. Structural elucidation was performed by employing ion trap mass spectrometry (ITMS), high resolution Orbitrap MS (FTMS), and nuclear magnetic resonance (NMR) spectroscopy. Subsequently, these purified compounds were incubated with iron(II) sulfate (FeSO₄), and the influence of the flavones' structural features on their interaction with iron in terms of complexation, oxidation, and discolouration was assessed via spectrophotometric and mass spectrometric techniques.

4.2. Materials & methods

4.2.1. Materials

From a local supermarket we purchased chicken bouillon cubes (Knorr, Unilever), containing the following ingredients as declared on the label: salt, vegetable fat (palm, shea butter, salt butter), flavour enhancer (E621, E627, E631), potato starch, sugar, onion powder, chicken fat (2 %) (chicken fat, antioxidant E392), spices (turmeric, celery seed), carrot 1 %, yeast extract, parsley, aroma, chicken meat extract (0.1 %), caramel syrup, maltodextrin. Dried celery leaves (*Apium graveolens*, Apiaceae) and dried parsley leaves (*Petroselinum crispum*, Apiaceae) (Verstegen Spices and Sauces BV) were also purchased at a local supermarket. Iron(II) sulfate heptahydrate (≥ 99 wt. %), 3-(2-pyridyl)-5,6-diphenyl-1,2,4-triazine-*p,p'*-disulfonic acid monosodium salt hydrate (≥ 97 wt. %; ferrozine), formic acid (≥ 98 vol. %), and deuterium oxide (D_2O) were obtained from Merck Life Science (Darmstadt, Germany). Luteolin (≥ 98 wt. %) was purchased from Santa Cruz Biotechnology Inc. (Santa Cruz, CA, USA), apigenin (≥ 98 wt. %) from Indofine Chemical Company (Hillsborough, NJ, USA), and chrysoeriol (≥ 95 wt. %) from Extrasynthese (Genay, France). Ascorbic acid (≥ 99 wt. %) was obtained from VWR International (Radnor, PA, USA). Dimethylsulfoxide (DMSO) was obtained from Merck Millipore (Billerica, MA, USA). DMSO- d_6 was purchased from Euriso-top (Saint-Aubin, France). ULC-MS grade acetonitrile (ACN) and water, both containing 0.1 vol. % formic acid, and *n*-hexane (≥ 99 vol. %) were purchased from Biosolve (Valkenswaard, The Netherlands). Water for other purposes than UHPLC was prepared using a Milli-Q water purification system (Merck Millipore, Billerica, MA, USA).

4.2.2. Extraction of phenolics from bouillon and herbs

Phenolics were extracted from the chicken bouillon cubes and dried herbs. First, 2.5 g of bouillon cube or dried herb was ground with a mortar and pestle and defatted by extraction with 50 mL *n*-hexane. To assist the extraction, the samples were vortexed and incubated in an ultrasonic bath (15 min, RT). Subsequently, the samples were centrifuged (10 min, $5000 \times g$), the *n*-hexane supernatants were discarded, and the pellets were subjected to two more identical extraction cycles. Any remaining *n*-hexane was removed from the pellet by flushing it with nitrogen. The defatted pellets were subjected to four extraction cycles, each with 50 mL methanol (MeOH), using the same procedure as described for *n*-hexane. MeOH was evaporated by flushing with nitrogen, and the MeOH extracts were diluted to 1 mg mL^{-1} prior to analysis by reversed phase ultra-high performance liquid chromatography coupled to electrospray ionisation ion trap mass spectrometry (RP-UHPLC-PDA-ESI-ITMSⁿ; section 4.2.6).

4.2.3. Large-scale extraction of phenolics from celery

Lyophilised celery leaves were bead milled (Cryomill MM440; Retsch GmbH, Haan, Germany) into a fine powder with stainless steel beads ($\varnothing 20 \text{ mm}$) at a frequency of

30 s⁻¹, for 30 s. For the large-scale extraction, we optimised the extraction conditions and extracted the celery powder with 80 vol. % MeOH (5 mL g⁻¹), as described elsewhere.^[25] Samples were subjected to sonication for 15 min. The suspensions were filtered over a paper filter under reduced pressure and the retentate celery powders were subjected to four more identical extraction cycles. The MeOH extracts were combined and concentrated to 25 % of the initial volume under reduced pressure. Liquid-liquid partitioning with *n*-hexane (*n*-hexane:concentrated extract, 1:2.5 [v:v]) was performed three times to remove lipids and chlorophyll. The remaining MeOH in the cleaned MeOH extracts was evaporated under reduced pressure. Samples were resolubilised using *tert*-butanol and lyophilised to yield the cleaned extracts. Cleaned extracts were bead milled (ø 20 mm beads, 30 s⁻¹, 30 s).

4.2.4. Pre-purification and purification by preparative RP-HPLC

Cleaned extracts were pre-purified with a Büchi Pure C-850 FlashPrep system, operated in flash mode, and equipped with a UV detector (Büchi, Flawil, Switzerland). Fractionation was performed on a Büchi FlashPure C18 cartridge (column size 80 g; particle size 40 µm) that was eluted with water (A) and acetonitrile (B), both acidified with 1 vol. % formic acid, at room temperature at a flow rate of 60 mL min⁻¹. The settings and elution profiles can be found in **Method S4.1**. The pre-purified pools were subjected to evaporation under reduced pressure to remove acetonitrile, and were subsequently resolubilised using *tert*-butanol prior to lyophilisation. Four flavone-enriched pools were further separated by preparative RP-HPLC, as described in **Method S4.2**, to obtain 9 purified compounds. The purified compounds were analysed by reversed-phase ultra-high performance liquid chromatography coupled to either electrospray ionisation ion trap mass spectrometry or electrospray ionisation hybrid quadrupole Orbitrap mass spectrometry (RP-UHPLC-PDA-ESI-ITMSⁿ or RP-UHPLC-PDA-ESI-FTMS²), and nuclear magnetic resonance (NMR) spectroscopy (**section 4.2.6**).

4.2.5. Incubation of flavones with iron

Stock solutions of each flavone were prepared by dissolving them in DMSO to a 20 mM concentration. Subsequently, each flavone stock solution was diluted either in water (flavone blank; final concentration flavone 1 mM; pH 6.0-7.5) or a freshly prepared FeSO₄ solution (iron-flavone; final concentration flavone 1 mM; final concentration Fe(II) 1 mM; pH 4.5-5.0). The final volume of all samples was 1.50 mL, containing 5 vol. % DMSO. Samples were placed in a 15 mL Greiner tube, and no measures were taken to reduce oxygen levels in the headspace. Aliquots of 0.25 mL were taken from the samples immediately after adding the flavone (*t*₀). Subsequently, each sample was adjusted to pH 6.5 and during the experiment the pH was maintained at 6.5 by titration with 0.05 M HCl and 0.05 M NaOH using a pH-stat device (Metrohm, Herisau, Switzerland). This approach of maintaining pH with concentrated HCl and NaOH was previously used,^[8] and is preferred over the use of buffers to minimise interference of buffer compounds with complexation and oxidation reactions. After

pH adjustment to 6.5 (t_0), the samples were incubated at 40 °C under magnetic stirring (300 rpm) and aliquots (0.25 mL) were taken after 24 h (t_{24}). Immediately after sampling, the samples were frozen in liquid nitrogen to stop any reactions. Samples were thawed on the day of analysis. The 0.25 mL samples were centrifuged (5 min, 15,000 × g) and the supernatants were separated to obtain the water soluble (WS) fraction. The pellets were solubilised in DMSO and centrifuged once more (5 min, 15,000 × g) and the supernatants were separated to obtain the DMSO soluble (DS) fraction. The DMSO insoluble pellets were freeze-dried to remove the remaining DMSO. Subsequently, 100 µL of 25 mM aqueous ascorbic acid was added to the freeze-dried pellets, which were then sonicated for 15 min, diluted 20 times with DMSO for a final DMSO concentration of 95 vol. %, and sonicated for an additional 15 min. After sonication, the samples were centrifuged (5 min, 15,000 × g) and the supernatants were collected as the ascorbic acid soluble (AAS) fractions. The remaining pellets were not analysed further. DS, WS, and AAS fractions were immediately analysed by RP-UHPLC-PDA-ESI-ITMS (section 4.2.6). Quantification of the recovery of each flavone in the WS, DS, and AAS fraction was performed based on PDA peak area (280 nm) and a calibration curve of the corresponding purified flavone (0.03–1 mM, in duplicate, $R^2 \geq 0.99$). The relative quantity of flavone over time was defined as recovery, in which the starting concentration of flavone (1 mM) was set as 100 %. To test if the trend in flavone decrease over time was statistically significant, ANOVA analysis was performed using IBM SPSS Statistic v23 software (SPSS Inc., Chicago, IL, USA). Tukey's *post hoc* comparisons (significant at $p < 0.05$) were carried out to evaluate differences per time point in the total flavone recovery and recovery of flavone in the WS, DS, and AAS fraction.

4.2.6. Identification of phenolics

RP-UHPLC-ESI-ITMS/FTMS analysis

The extracts, pools, purified flavones, and flavones after incubation with iron were analysed using a Thermo Vanquish UHPLC system (Thermo Scientific, San Jose, CA, USA). The UHPLC was equipped with an autosampler, a pump, a degasser, and a photodiode array (PDA) detector. The UHPLC was coupled to an LTQ Velos Pro ion trap mass spectrometer (ESI-ITMSⁿ) or a Thermo Q Exactive Focus hybrid quadrupole Orbitrap mass spectrometer (ESI-FTMS²). The injection volume, column temperature, gradient elution program, and MS settings were used as described in **Method S4.3**.

NMR spectroscopy

The purified compounds were dissolved in DMSO- d_6 (1 mg/0.5 mL). NMR spectra of the purified compounds were recorded on a Bruker Avance-III-700 spectrometer at a probe temperature of 300 K. ^1H , HMBC, and HSQC spectra were acquired. Due to their limited solubility in DMSO- d_6 and various other deuterated solvents, no HMBC and HSQC NMR spectra were obtained for compounds with a luteolin backbone. For luteolin 7-*O*-(6''-*O*-malonyl)-apiosylglucoside in D_2O /DMSO- d_6 , the ^1H spectrum could be acquired, which was solely used for purity determination.

4.2.7. Monitoring complexation, oxidation, and discolouration by UV-Vis spectroscopy

The effect of FeSO_4 addition on complexation and oxidation reactions, and their effect on discolouration was monitored using UV-Vis spectroscopy. The UV-Vis spectra of the WS and DS fractions were obtained after sampling and centrifugation, samples (50 μL) were diluted two times in water (WS fraction) or DMSO (DS fraction) and transferred to a Corning UV-transparent flat bottom polystyrene 96 well-plate (Sigma Aldrich, St. Louis, MO, USA). Spectra were recorded in the range from 230 to 750 nm in a SpectraMax iD3 (Molecular Devices, Sunnyvale, CA, USA) at room temperature. The combined absorbance spectra (WS and DS) were normalised to the maximum absorption intensity. The colour of the samples was recorded and assessed by spectrophotometric analysis and by taking pictures (OnePlus 7T, Shenzhen, China) using a ring light to cast a uniform light onto the subject against a white background.

4.2.8. Determination of iron concentration in solution by ferrozine-based colourimetric assay

The total amount of iron in the WS, DS, and AAS fractions obtained at the different time points was quantified using a ferrozine-based colourimetric assay.^[26] Binding of ferrous iron by ferrozine results in the formation of a ferrous-ferrozine complex with λ_{max} at 565 nm.^[27] To ensure the reduction of ferric iron to its ferrous state, an excess of ascorbic acid (50 μL , 100 mM) was added to 50 μL sample (*i.e.* WS, DS, AAS fractions). After 1 h incubation, an excess of ferrozine (50 μL , 40 mM) was added. Samples were transferred to 96-well microplates and the absorbance at 565 nm was measured in a SpectraMax iD3 at room temperature. All measurements were performed in duplicate. Quantification of total iron was performed based on a calibration curve of FeSO_4 (0.00625 – 0.5 mM, in duplicate, $R^2 \geq 0.99$). Measurements were corrected for the flavone blank and it was confirmed that the presence of DMSO did not interfere with the quantification of total iron.

4.3. Results & discussion

4.3.1. Purification and structural elucidation of (acylated) flavone glycosides

Eleven (acylated) flavone glycosides, six (acylated) phenolic acid glycosides, and three curcuminoids were tentatively identified in chicken bouillon methanol extract by RP-UHPLC-PDA-MS (**Fig. S4.1**, **Table S4.1**). The chromatographic profile of the extract of bouillon showed similarities with the extracts of celery and parsley, which are the main herbs present in the bouillon cubes. To get more insight into the effect of flavone glycosylation and acylation on the interaction of flavones with iron, these compounds had to be purified. Phenolic acids, especially those with a catechol moiety, and curcuminoids may also form dark-coloured complexes with Fe(III) .^[14,28] However, only one minor peak in the bouillon extract was identified as a phenolic acid

that possesses a catechol moiety (i.e. caffeoyl quinic acid), thus we do not expect that the phenolic acids affect discolouration. As the focus of this work was on the effect of flavone glycosylation and additional acylation, we did not further purify the phenolic acids and curcuminoids. The flavones were purified from celery extract as its flavone profile was most similar to that of bouillon extract and it contained fewer impurities than the bouillon extract itself (**Fig. S4.1**). Pre-purification by flash chromatography yielded four pools enriched in flavones (**Fig. S4.2**). Further purification by preparative RP-HPLC yielded nine purified flavones.

The purity and structure of the purified compounds were further elucidated by ITMS and FTMS, of which the spectrometric and spectroscopic data are shown in **Table 4.1**. The peaks were tentatively annotated based on the UV-visible absorbance (λ_{max}), the exact mass of the parent ions, product ions in positive and negative modes, and a comparison of these data with literature.^[7,12,29] Based on the product ions in CID MS², the purified compounds consisted of three different flavone backbones; apigenin, luteolin, and chrysoeriol or diosmetin. Neutral losses (NL) of 132 amu (i.e. pentose) and 294 amu (i.e. pentose + hexose) in the MS² fragmentation spectra indicate substitution with a pentosylhexoside (**Fig. S4.3**).^[29] Common glycosylation positions of flavones are C6, C8, or O7. Formation of ions with NL of 294 amu upon fragmentation indicates preferential cleavage at the glycosidic bond rather than cross-ring cleavage of the glycosyl moiety, thereby confirming O-glycosylation.^[12] In a previous study on parsley, the glycosides of apigenin were confirmed to be apiosylglucosides.^[9] Because parsley and celery both belong to the Apiaceae family and based on the neutral losses observed in UHPLC-MS, it is suggested that the pentosylhexoside substitutions on celery flavones are also apiosylglucosides.^[7,30] The additional neutral losses of 42 and 44 amu that we observed in the MS² spectra of the acylated flavone glycosides (**Fig. S4.3**) are indicative for the substitution with acetyl or malonyl.^[12] The selective loss of apiose as evidenced by a NL of 132 in the MS² data of the acetylated flavones confirms that acylation is not occurring on the apiosyl moiety and must, therefore, occur on the glucosyl moiety (**Fig. S4.3**).

Moreover, the initial annotations based on UHPLC-MS were verified by 2D NMR using HMBC and HSQC (**Fig. S4.4** to **Fig. S4.10**). NMR spectra provided additional proof of glycosylation on the O7 position since the signals of *H*6 and *H*8 were present with a downfield shift compared to the flavone aglycon (**Fig. S4.4**). Additionally, the downfield shift of the *H*6'' upon acylation also indicated that acetyl and malonyl were linked to O6'' of the glucosyl moiety. These spectral features are in line with previously reported results for apigenin 7-O-(6''-O-acetyl)-apiosylglucoside and apigenin 7-O-(6''-O-malonyl)-apiosylglucoside.^[9] For the methoxylated flavone, the chemical shifts of C5' (**Fig. S4.8** to **Fig. S4.10**) confirmed that the methoxy group was present on the C3' position (i.e. chrysoeriol) and not on the C4' position (i.e. diosmetin).^[31]

Table 4.1. Purity, spectrometric, and spectroscopic data of the purified compounds as determined by UHPLC-PDA coupled to ESI-ITMS or ESI-FTMS, and ^1H -NMR.

Compound name	λ_{max} (nm)	Molecular Formula	Ion	m/z calc.	m/z obs.	Error (ppm)	CID MS ² product ions (<i>r.a.</i>) ^a	HCD MS ² product ions (<i>r.a.</i>)	Purity (%) ^b UV ₂₈₀ MS (NI)	^1H NMR
apigenin 7- <i>O</i> - apiosylglucoside (<i>apiin</i>)	266, 338	$\text{C}_{26}\text{H}_{28}\text{O}_{14}$	[M-H] ⁻ [M+H] ⁺	563.14063 565.15519	563.14044 565.15564	-0.34 0.80	269, 431 (19) 271, 433 (67)	269.04535 271.06073	100 96	92
apigenin 7- <i>O</i> -(6''- <i>O</i> -acetyl)- apiosylglucoside (6''-acetylapiin)	266, 338	$\text{C}_{28}\text{H}_{30}\text{O}_{15}$	[M-H] ⁻ [M+H] ⁺	605.15120 607.16575	605.15106 607.16559	-0.23 -0.27	269, 563 (38), 473 (28) 271, 475 (96)	269.04532 271.06046	99 99	90
apigenin 7- <i>O</i> -(6''- <i>O</i> - malonyl)-apiosylglucoside (6''-malonylapiin)	266, 338	$\text{C}_{29}\text{H}_{30}\text{O}_{17}$	[M-H] ⁻ [M+H] ⁺	649.14103 651.15558	649.14154 651.15497	0.79 -0.94	605 271, 519 (81)	269.04535 271.06088	88 86	81
chrysoeriol 7- <i>O</i> - apiosylglucoside	250, 350	$\text{C}_{27}\text{H}_{30}\text{O}_{15}$	[M-H] ⁻ [M+H] ⁺	593.15120 595.16575	593.15106 595.16486	-0.23 -1.50	299, 284 (23), 461 (14) 301, 463 (46)	299.05582, 284.03232 (15) 301.07126	94 87	82
chrysoeriol 7- <i>O</i> -(6''- <i>O</i> - acetyl)-apiosylglucoside	250, 346	$\text{C}_{29}\text{H}_{32}\text{O}_{16}$	[M-H] ⁻ [M+H] ⁺	635.16176 637.17632	635.16144 637.17639	-0.51 0.12	299, 593 (59), 284 (31), 575 (15), 503 (15)	299.05585, 284.03232 (20) 301.07092	99 98	90
chrysoeriol 7- <i>O</i> -(6''- <i>O</i> - malonyl)-apiosylglucoside	250, 346	$\text{C}_{30}\text{H}_{32}\text{O}_{18}$	[M-H] ⁻ [M+H] ⁺	679.15159 681.16615	679.15192 681.16724	0.48 1.61	535 301, 549 (60)	299.05582, 284.03226 (12) 301.07135	87 79	76

n.d., not defined; CID, collision-induced dissociation; HCD, higher energy collisional dissociation; ^a *r.a.*, relative abundance. The threshold for fragments was ≥ 10 %. The most intense fragment is underlined; ^b UV₂₈₀, purity expressed as a percentage of total peak area in UHPLC-PDA at 280 nm; MS (NI), purity expressed as a percentage of total peak area in UHPLC-ESI-MS negative ionisation mode; ^1H NMR, purity expressed as a percentage of the total peak area of the aromatic region in proton NMR spectroscopy.

Table 4.1. Continued

Compound name	λ_{max} (nm)	Molecular Formula	Ion	<i>m/z</i> calc.	<i>m/z</i> obs.	Error (ppm)	CID MS ² product ions (<i>r.a.</i>) ^a	HCD MS ² product ions (<i>r.a.</i>)	Purity (%) ^b UV ₂₈₀ MS (NI)	¹ H NMR	
luteolin 7- <i>O</i> -apiosylglucoside	254, 350	C ₂₆ H ₂₈ O ₁₅	[M-H] ⁻	579.13555	579.13562	0.12	<u>285</u> , 447 (75)	285.04013, 579.13525 (29), 447.09311 (10)	96	95	n.d.
								287.05576			
luteolin 7- <i>O</i> -(6''- <i>O</i> -acetyl)- apiosylglucoside	250, 346	C ₂₈ H ₃₀ O ₁₆	[M-H] ⁻	621.14611	621.14655	0.70	<u>489</u> , 285 (65), 579 (23)	285.04019, 621.14600 (23) 489.10364 (10)	45	50 ^c	n.d.
								n.d.			
luteolin 7- <i>O</i> -(6''- <i>O</i> -malonyl)- apiosylglucoside	250, 346	C ₂₉ H ₃₀ O ₁₈	[M-H] ⁻	665.13594	665.13641	0.70	<u>621</u>	285.04007, 621.14569 (28), 489.10342 (11)	90	66 ^d	65
								287.05518			

n.d., not defined; CID, collision-induced dissociation; HCD, higher energy collisional dissociation; ^a *r.a.*, relative abundance. The threshold for fragments was ≥ 10 %. The most intense fragment is underlined; ^b UV₂₈₀, purity expressed as a percentage of total peak area in UHPLC-PDA at 280 nm; MS (NI), purity expressed as a percentage of the total peak area of the aromatic region in proton NMR spectroscopy; ^c main impurities are apigenin glucoside and apigenin malonyl glucoside; ^d main impurity is luteolin 7-*O*-apiosylglucoside.

Annotations of the compounds with a luteolin backbone could not be confirmed by NMR due to their limited solubility. Considering the identification of the other apigenin- and chrysoeriol-glycosides, and the fact that the putative luteolin-glycosides are produced via the same biosynthetic pathways, their structural elucidation based on ITMS and FTMS is very likely. The purity of all purified compounds was determined by UV₂₈₀, MS in negative ionisation mode, and the aromatic region in the proton NMR spectrum and is shown in **Table 4.1**. Most purified compounds were very pure (~ 90 %) except for luteolin 7-*O*-(6"-*O*-acetyl)-apiosylglucoside and luteolin 7-*O*-(6"-*O*-malonyl)-apiosylglucoside. Nevertheless, these compounds still have respective purities of ~ 65 % and ~ 50 %, with the impurities being other (acylated) flavone glycosides. Thus, these compounds could be used to obtain a better insight into the interaction with iron, as long as the impurity is taken into account for data interpretation. To conclude this section, purification yielded nine differentially (acylated) flavone glycosides that were used in the next part of this study to identify the effect of flavone 7-*O*-glycosylation and 6"-*O*-acylation on the interactions with iron.

4.3.2. Effect of substitution and flavone backbone on recovery and solubility

The purified (acylated) flavone glycosides and their commercial aglycons were incubated in the aqueous solution in the absence and presence of FeSO₄ (equimolar concentration) at pH 6.5. The recovery of flavone in the water soluble (WS), DMSO soluble (DS), and ascorbic acid soluble (AAS) fraction in absence and presence of equimolar concentration FeSO₄ before pH adjustment (*t*₀'), after adjustment of the pH to 6.5 (*t*₀), and after incubation for 24 h at 40 °C (*t*₂₄) was quantified by RP-UHPLC-PDA-MS.

For the blank flavones in absence of iron it was observed that the order of water solubility was malonyl apiosylglucoside > acetyl apiosylglucoside > apiosylglucoside > aglycon (**Fig. S4.11A**). Interestingly, after 24 h incubation of the flavones in absence of iron, most of the (acylated) flavone glycosides were recovered in the pellet (DS) and no longer in the supernatant (WS) (**Fig. S4.11A**). The precipitation of these acylated glycosylated flavones in water over this time indicates the possible formation of larger self-associated aggregates or micelle-like aggregates because of their pronounced hydrophobic and hydrophilic moieties (**Fig. S4.11B**). The recovery of malonylated glycosylated flavones in the WS fraction was higher than that of the (acetylated) flavone glycosides. We suggest that the negatively charged malonyl group prevents the formation of self-associated or micellar-like aggregates via repulsion.

The addition of FeSO₄ resulted in fast precipitation of the acylated flavone glycosides in water, and a steep decrease in recovery for all flavones with the luteolin backbone (**Fig. 4.2**).

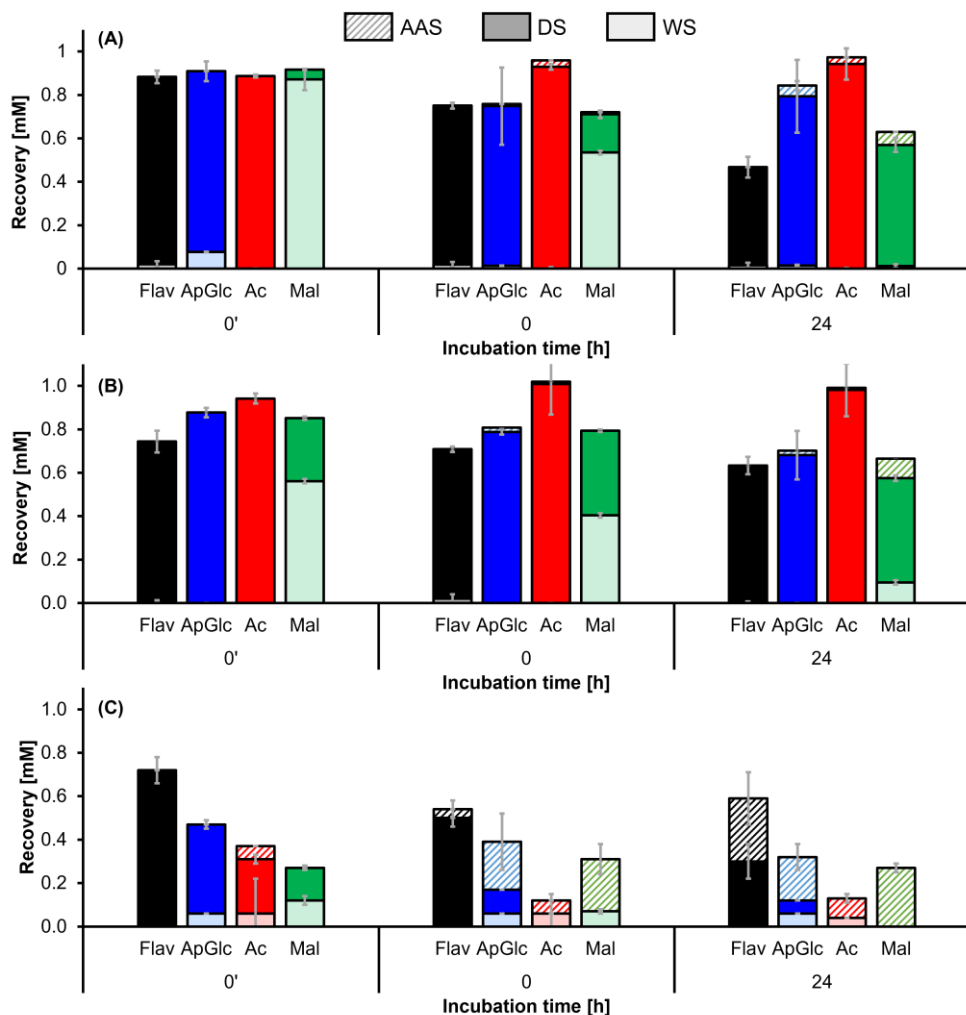


Figure 4.2. Recovery of the flavone aglycons (Flav; black) and apiosylglucoside (ApGlc; blue) with additional acetylation (Ac; red) or malonylation (Mal; green) for (A) apigenin, (B) chrysoeriol, and (C) luteolin in the water soluble (WS), DMSO soluble (DS), and ascorbic acid soluble (AAS) fractions in presence of equimolar concentration FeSO_4 . Time points shown are before the adjustment of the pH (t_0) and after 0 or 24 h of incubation at pH 6.5 in an aqueous solution. Error bars indicate the standard deviation of independent duplicates. Significance (Tukey's test, $p < 0.05$) of differences in the total recovery are indicated in Table S4.2.

This decreased recovery after iron addition may be due to degradation reactions or the formation of insoluble metal-phenolic networks (MPNs), which is more likely for luteolin derivatives because the aglycon possesses two iron-binding sites whereas apigenin and chrysoeriol only possess one iron-binding site.^[8] For the luteolin aglycon and its glycosides in particular, a significant proportion could be recovered in the AAS fraction, indicating that they are likely involved in the formation of MPNs.

For the apigenin and chrysoeriol samples at 24 h, the malonylated flavone glycosides were also recovered in the AAS fraction. We suggest that malonylation provides an extra iron binding site and therefore allows for the formation of larger insoluble networks. Thus, the flavones are only recovered after the disruption of these networks by the addition of ascorbic acid.

Besides the solubility of the flavones, the total iron solubility [*i.e.* sum of Fe(II), Fe(III) and soluble products of Fe(II) and Fe(III)]^[8] was also assessed (**Fig. S4.12**). Before pH adjustment (t_0) and complex formation, iron was mainly recovered in the WS fractions. After pH adjustment (t_0), the (acylated) flavone glycosides showed higher iron recovery in the WS fraction than the aglycons, for which most iron was recovered in the DS fraction. In line with the decreased water solubility of the flavones in presence of iron over time, after 24 h most of the iron was recovered in the DS or AAS fractions for all samples.

4.3.3. Colour and spectral properties of (acylated) flavone glycosides as iron complexes

Absorbance spectra of the flavones in the absence or presence of FeSO_4 (equimolar concentration) were obtained by UV-Vis. For the samples incubated in absence of iron (**Fig. 4.3A**), we observed that the λ_{max} values of the benzoyl (A-ring, 260–280 nm) and cinnamoyl (B-ring, 340–350 nm) bands were not affected by glycosylation and additional acylation. However, we did see that substitution resulted in the formation of a shoulder around 400 nm. First, we investigated whether this bathochromic shift was a result of self-association of the (acylated) flavone glycosides via π - π or CH- π stacking.^[20,32] However, our results indicate that self-association was unlikely to be the underlying mechanism, as is further explained by **Fig. S4.13**. It is more likely that this bathochromic shift is observed because the pH of the aqueous solution is close to the first pK_a of the flavone backbone,^[33–35] resulting in (partial) deprotonation of the (acylated) flavone glycosides in the WS fraction. Formation of a new band ~ 400 nm was previously also observed for deprotonated species of other flavonoids.^[36,37] For the aglycons, this bathochromic shift was not observed because they were poorly soluble in water, thus the spectra were measured in DMSO. The pK_a of the flavone backbone in DMSO is increased, due to the lower dielectric constant of DMSO compared to water.^[38] Therefore, the aglycons are fully protonated and no shoulder at 400 nm is observed. This reasoning was confirmed by measuring the flavones in 50 vol. % aqueous ACN with 0.1 vol. % formic acid, which resulted in identical UV-Vis spectra of the aglycons and (acylated) flavone glycosides (data not shown).

The addition of equimolar concentration FeSO_4 to the flavones and adjustment of the pH to 6.5 resulted in a bathochromic shift for all samples (**Fig. 4.3B**). This bathochromic shift indicates that Fe(III)-flavone complexes are present in the solutions. Complexes of Fe(II) with phenolics in absence of oxygen were previously demonstrated to show

no bathochromic shift of the spectra to the visible range and were colourless.^[39-41] In the presence of oxygen these Fe(II)-phenolic complexes show fast autooxidation to Fe(III)-phenolic complexes because of the higher stability of the Fe(III)-phenolic complexes.^[42,43]

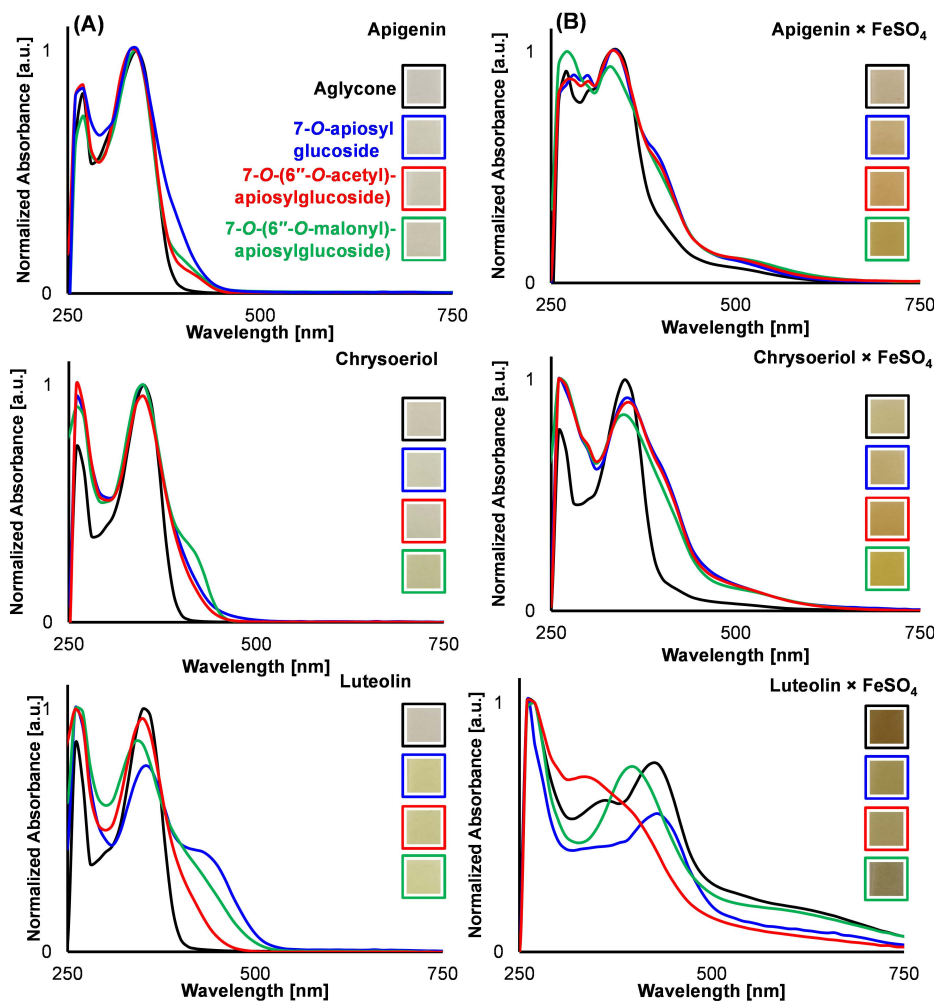


Figure 4.3. Normalised UV-Vis absorbance spectra of the combined WS and DS spectra of the flavones at pH 6.5 (t_0) in (A) absence and (B) presence of FeSO_4 at equimolar concentration. Insets show pictures of the aqueous solutions/dispersions of the flavones in absence and presence of FeSO_4 at pH 6.5. Separate absorbance spectra for the WS and DS fraction are shown in Fig. S4.14 and Fig. S4.15.

For the samples with an apigenin or chrysoeriol backbone the cinnamoyl band was shifted to the visible range, resulting in a light yellow-brown colour (Fig. 4.3B). For luteolin samples, additional formation of a broad absorbance band at 550–750 nm was observed due to ligand-to-metal charge transfer (LMCT), resulting in a darker

brownish or blackish colour (**Fig. 4.3B**). It is as expected that only the flavones with a luteolin backbone show an LMCT band, because it is the only tested flavone backbone with a catechol moiety on the B-ring.^[8]

Slightly more discolouration and a bathochromic shift of the cinnamoyl bands were observed for the (acylated) glycosides of apigenin and chrysoeriol samples in presence of FeSO_4 compared to the aglycons. All (acylated) glycosides and aglycons in presence of FeSO_4 were mainly recovered in the DS fraction (**Fig. 4.2, Fig. S4.14, Fig. S4.15**). Thus, the observed bathochromic shift is not a result of solvent effects, as described above for the samples in absence of FeSO_4 but is apparently caused by the presence of the (acylated) apiosylglucosyl moiety. To verify that the lower relative polarity of DMSO (0.44) in comparison to water (1.00) did not affect the electronic transitions and absorbance spectra, we compared the WS and DS spectra for chrysoeriol 7-*O*-(6''-*O*-malonyl)-apiosylglucoside in the presence of FeSO_4 . These spectra were almost identical, thereby confirming that the impact of the selected solvents (water and DMSO) on the obtained spectra was minimal (**Fig. S4.16**). Interestingly, no difference in absorbance was observed between the acylated glycosides and the non-acylated glycosides. Contrary to our hypothesis that malonylation would affect the stability of iron-flavonoid complexes, this indicates that the increase in discolouration is solely due to the presence of the 7-*O*-apiosylglucosyl moiety and is not enhanced by additional malonylation. The increased discolouration and more pronounced bathochromic shift for the apigenin and chrysoeriol 7-*O*-apiosylglucosides, compared to the aglycon, indicates that the ability of the 4–5 site to coordinate iron at pH 6.5 is increased by 7-*O*-glycosylation.

For luteolin, we observed less discolouration for the (acylated) glycosides compared to the aglycon. It should be noted that the acylated glycosides are of lower purity (**Table 4.1**) and may therefore show less absorbance. However, luteolin apiosylglucoside ($\geq 95\%$ purity) also showed a decrease in discolouration in presence of FeSO_4 compared to the aglycon, which indicates that the decrease in discolouration is due to the addition of (acylated) 7-*O*-apiosylglucosyl moieties and not due to lower purity. Besides the 4–5 site, the luteolin backbone also possesses the 3'–4' site, which is generally regarded as the strongest Fe(III) binding site.^[44] Increased ability of iron to coordinate to the 4–5 site of luteolin 7-*O*-glycosides allows it to compete with coordination at the 3'–4' site, which decreases discolouration.^[8] We expect that when equimolar concentrations of iron and luteolin apiosylglucoside are present, a mixture of the 4–5 and the 3'–4' complexes will exist in solution. We expected this effect to diminish at a 1:2 ratio of flavone:iron, as sufficient iron would be present to bind at the 3'–4' site and 4–5 site simultaneously. However, upon testing this experimentally, much more precipitation was observed in both the DS and WS fraction, which hindered further in-depth analysis. Increased precipitation suggested that increasing the relative amount of iron leads to the formation of insoluble metal-phenolic networks.

4.3.4. Increased iron coordination to the flavone 4–5 site by 7-*O*-glycosylation

There are several possible explanations why coordination to the 4–5 site is preferred for the flavone 7-*O*-apiosylglucosides compared to the aglycons. Our first hypothesis was that the apiosyl residue can stabilise the iron bound to the 4–5 site of the flavone by additional coordination of the glycosyl –OH groups to iron. However, in an additional experiment we also observed a bathochromic shift for apigenin 7-*O*-glucoside, which lacks the apiosyl moiety, compared to the apigenin aglycon (results not shown). This indicates that involvement of the apiosyl moiety is not the (sole) mechanism stabilising iron bound to the 4–5 site. Another possible explanation for the increased ability of iron to coordinate to the 4–5 site is a lower pK_a of the 5-OH group due to 7-*O*-glycosylation and thus increased deprotonation of the 5-OH at pH 6.5, thereby enhancing its ability to coordinate iron.

The pK_a can either be lowered due to the absence of the free 7-OH group or because glycosylation introduces a bulky, electron-withdrawing group on the *O*7 position, thereby making the 5-OH slightly more acidic.^[22,45] The last possible explanation for the increased ability of iron to coordinate to the 4–5 site is related to the lower planarity of the glycosylated flavones, compared to the flavone aglycons, which can decrease the hydrophobic π - π stacking interactions of the aromatic nuclei.^[46] The π - π stacking interactions play an important role in metal-ligand complexes.^[47] A decrease in stacking for the flavone 7-*O*-glycosides may potentially increase the ability of the 4–5 site to coordinate iron. It can be concluded that the ability of the 4–5 site to coordinate iron is increased by 7-*O*-glycosylation, yet the underlying mechanism remains unclear and should be investigated in future experimental studies, and confirmed by additional *in silico* modelling.

4.3.5. Effect of glycosylation and additional acylation on flavone stability in presence of iron

It is known that, depending on the flavonoids' aglycon structural features, complexation with Fe(III) can be followed up by electron transfer reactions, that cause oxidation of the flavonoid.^[8,48] The formation of degradation and polymerisation products was investigated by RP-UHPLC-PDA-MS. The chromatograms of the flavones in presence of FeSO₄ before pH adjustment (t_0), after adjustment of the pH to 6.5, and after incubation for 24 h (t_{24}) are shown in **Fig. S4.17**. None of the characteristic degradation products of iron-mediated oxidative degradation of flavonoid aglycons, such as 4-hydroxybenzoic acid, 3,4-dihydroxybenzoic acid, and 2,4,6-trihydroxyphenylglyoxilic acid,^[8,48] were found in extracted ion chromatograms of the samples after 24 h incubation. Moreover, we also did not observe formation of other oxidative degradation products, dimers, or larger oxidative coupling products in any of the obtained chromatograms, including full MS (negative and positive mode) and PDA (190 to 680 nm). We also investigated the stability of the apiosylglucosyl,

acetylapiosylglucosyl, and malonylapiosylglucosyl moieties in presence of iron **Fig. S4.18**. No deglycosylation was observed for any of the flavones in the absence or presence of iron. Deacetylation was observed in minor amounts (< 1 %) in the absence and presence of iron. For the malonylated flavone glycosides, 10 to 20 % cleavage of the malonyl group was observed after 24 h incubation in an aqueous solution at pH 6.5, regardless of the presence of iron. Thus, our results indicate that iron did not affect deglycosylation, deacetylation, and demalonylation reactions. Additionally, glycosylation and additional acylation did not affect the degradation of the flavone backbone.

4.3.6. The effect of the structural features of flavones on their interaction with iron

An overview of the effect of 7-*O*-apiosylglucosylation and additional 6"-*O*-acetylation or 6"-*O*-malonylation of the flavone backbone on its reactivity with iron is provided in **Fig. 4.4**.

Flavone 7- <i>O</i> -apiosylglucoside			Flavone 7- <i>O</i> -apiosylglucoside		
Spectral properties	bathochromic shift $\pi \rightarrow \pi^*$		Spectral properties	decreased absorbance $\pi \rightarrow d_\pi$	
Color	aglycon	glycoside	Color	aglycon	glycoside
Solubility	DMSO and ascorbic acid		Solubility	DMSO and ascorbic acid	
Stability	stable against oxidation		Stability	stable against oxidation	
Acylation	Acetyl			Malonyl	
	$R_3 =$ 			$R_3 =$ 	
Spectral properties	no effect		Spectral properties	no effect	
Color	glycoside	acetyl glycoside	Color	glycoside	malonyl glycoside
Solubility	DMSO and ascorbic acid		Solubility	t_0 in water, t_{24} DMSO and ascorbic acid	
Stability	<1% deacetylation no effect of iron		Stability	10-20% demalonylation no effect of iron	

Figure 4.4. Structure-reactivity relationships highlighting the influence of flavone backbone, glycosylation, and additional acylation on the reactivity (*i.e.* complexation, oxidation, discolouration) with iron at equimolar concentration.

Overall, our findings show that 7-*O*-apiosylglucosylation of flavones affects the formed iron-flavone complex and the resulting colour. For the flavones that only possess the 4–5 binding site (i.e. apigenin and chrysoeriol), more bathochromic shifting and discolouration was observed for the (acylated) glycosides compared to the aglycon due to an increased ability of iron to coordinate to the 4–5 site. At equimolar iron:flavone concentration, the increased ability of iron to coordinate to the 4–5 site of (acylated) luteolin glycosides competes with binding to the 3'–4' site, reducing observed discolouration compared to the aglycon. This is the result of lower intensity of the LMCT absorbance band that is typically observed for iron-catecholate complexes.

The additional presence of the malonyl or acetyl moieties did not lead to changes in the absorbance spectra or colour. The Fe(III)-complexes with the malonylated flavone glycosides were water soluble at t_0 , but precipitation occurred after incubation for 24 h. We suggest that this is due to the formation of MPNs, as the presence of malonyl creates an additional binding site allowing the formation of MPNs over time. The presence of iron did not increase the (oxidative) degradation of the backbones or (acylated) apiosylglucosyl moieties of the tested flavones.

4.4. Conclusion

In conclusion, the findings of this work indicate that 7-*O*-apiosylglucosylation of flavones affects their iron complexation behaviour by increasing the ability of iron to coordinate to the 4–5 binding site. The presence of iron does not affect the oxidative degradation of the flavone backbone. These results demonstrate that outcomes of iron interaction studies with flavonoid aglycon model systems cannot be directly extrapolated to iron-fortified food systems containing (acylated) flavonoid glycosides. Thus, to understand discolouration in iron-fortified foods, model systems should also comprise (acylated) glycosides of relevant flavonoids. Our results indicate that (acylated) flavone glycosides show less intense discolouration than what was previously reported for flavonoid aglycons and curcuminoids. Therefore, we expect that discolouration in fortified bouillon cubes is not only caused by the complexation of iron with natural flavones.

4.5. Acknowledgements

The authors thank the MAGNEFY facility at Wageningen University for access to the NMR instrument. The authors are grateful to Annemiek van Zadelhoff (Laboratory of Food Chemistry, Wageningen University & Research) for her help with the NMR measurements. Part of the presented results were obtained using a Thermo Scientific Velos Pro MS system, a Thermo Scientific Q Exactive Focus Orbitrap MS system, and a Waters auto purification system which are owned by WUR-Shared Research Facilities. Investment by WUR-Shared Research Facility was made possible by the 'Regio Deal Foodvalley' of the province of Gelderland, The Netherlands.

4.6. References

- 1 Allen, L. H., De Benoist, B., Dary, O., Hurrell, R., & (Eds.). (2006) *Guidelines on food fortification with micronutrients*. Geneva, Switzerland: World Health Organization.
- 2 Hurrell, R. F. (1997). Preventing iron deficiency through food fortification. *Nutrition Reviews*, 55(6), 210-222.
- 3 Moretti, D., Hurrell, R. F., & Cercamondi, C. I. (2018). Bouillon cubes. In M. G. V. Mannar & R. F. Hurrell (Eds.), *Food fortification in a globalized world*, (pp. 159-165): Elsevier.
- 4 Habeych, E., van Kogelenberg, V., Sagalowicz, L., Michel, M., & Galaffu, N. (2016). Strategies to limit colour changes when fortifying food products with iron. *Food Research International*, 88, 122-128.
- 5 Caponio, F., Gomes, T., & Bilancia, M. T. (2003). Bouillon cubes: Assessment of the state of degradation of the lipid fraction. *Journal of the Science of Food and Agriculture*, 83(13), 1331-1336.
- 6 Hostettler, G. L., Ralston, R. A., & Schwartz, S. J. (2017). Flavones: Food sources, bioavailability, metabolism, and bioactivity. *Advances in Nutrition*, 8(3), 423-435.
- 7 Hostettler, G. L., Riedl, K. M., & Schwartz, S. J. (2012). Endogenous enzymes, heat, and pH affect flavone profiles in parsley (*Petroselinum crispum* var. *neapolitanum*) and celery (*Apium graveolens*) during juice processing. *Journal of Agricultural and Food Chemistry*, 60(1), 202-208.
- 8 Bijlsma, J., de Bruijn, W. J. C., Velikov, K. P., & Vincken, J.-P. (2022). Unravelling discolouration caused by iron-flavonoid interactions: Complexation, oxidation, and formation of networks. *Food Chemistry*, 370, 131292.
- 9 Eckey-Kaltenbach, H., Heller, W., Sonnenbichler, J., Zetl, I., Schäfer, W., Ernst, D., & Sandermann, H. (1993). Oxidative stress and plant secondary metabolism: 6'-O-malonylapiin in parsley. *Phytochemistry*, 34(3), 687-691.
- 10 Yoshikawa, M., Uemura, T., Shimoda, H., Kishi, A., Kawahara, Y., & Matsuda, H. (2000). Medicinal foodstuffs. XVIII. Phytoestrogens from the aerial part of *Petroselinum crispum* Mill. (parsley) and structures of 6'-acetylapiin and a new monoterpene glycoside, petroside. *Chemical and Pharmaceutical Bulletin*, 48(7), 1039-1044.
- 11 Markham, K., Chari, V., & Mabry, T. (1982). The flavonoids: Advances in research. London: Chapman and Hall, 19-134.
- 12 Cuyckens, F., & Claeys, M. (2004). Mass spectrometry in the structural analysis of flavonoids. *Journal of Mass Spectrometry*, 39(1), 1-15.
- 13 Lin, L.-Z., Lu, S., & Harnly, J. M. (2007). Detection and quantification of glycosylated flavonoid malonates in celery, Chinese celery, and celery seed by LC-DAD-ESI/MS. *Journal of Agricultural and Food Chemistry*, 55(4), 1321-1326.
- 14 Mellican, R. I., Li, J., Mehansho, H., & Nielsen, S. S. (2003). The role of iron and the factors affecting off-color development of polyphenols. *Journal of Agricultural and Food Chemistry*, 51(8), 2304-2316.
- 15 Perron, N. R., & Brumaghim, J. L. (2009). A review of the antioxidant mechanisms of polyphenol compounds related to iron binding. *Cell Biochemistry and Biophysics*, 53(2), 75-100.
- 16 McGee, E. J. T., & Diosady, L. L. (2018). Prevention of iron-polyphenol complex formation by chelation in black tea. *LWT - Food Science and Technology*, 89, 756-762.
- 17 Bijlsma, J., de Bruijn, W. J. C., Hageman, J. A., Goos, P., Velikov, K. P., & Vincken, J.-P. (2020). Revealing the main factors and two-way interactions contributing to food discolouration caused by iron-catechol complexation. *Scientific Reports*, 10(1), 8288.
- 18 Ren, J., Meng, S., Lekka, C. E., & Kaxiras, E. (2008). Complexation of flavonoids with iron: Structure and optical signatures. *The Journal of Physical Chemistry B*, 112(6), 1845-1850.
- 19 Yoshida, K., Mori, M., & Kondo, T. (2009). Blue flower color development by anthocyanins: From chemical structure to cell physiology. *Natural Product Reports*, 26(7), 884-915.
- 20 Trouillas, P., Sancho-Garcia, J. C., De Freitas, V., Gierschner, J., Otyepka, M., & Dangles, O. (2016). Stabilizing and modulating color by copigmentation: Insights from theory and experiment. *Chemical Reviews*, 116(9), 4937-4982.
- 21 Alluis, B., & Dangles, O. (1999). Acylated flavone glucosides: Synthesis, conformational investigation, and complexation properties. *Helvetica Chimica Acta*, 82(12), 2201-2212.
- 22 Alluis, B., & Dangles, O. (2001). Quercetin (=2-(3,4-dihydroxyphenyl)-3,5,7-trihydroxy-4h-1-benzopyran-4-one) glycosides and sulfates: Chemical synthesis, complexation, and antioxidant properties. *Helvetica Chimica Acta*, 84(5), 1133-1156.
- 23 Escandar, G. M., & Sala, L. F. (1991). Complexing behavior of rutin and quercetin. *Canadian Journal of Chemistry*, 69(12), 1994-2001.
- 24 Nowak, D., Kuźniar, A., & Kopacz, M. (2010). Solid complexes of iron(II) and iron(III) with rutin. *Structural Chemistry*, 21(2), 323-330.
- 25 Nguyen Thu, H., Nguyen Van, P., Ngo Minh, K., & Le Thi, T. (2021). Optimization of extraction conditions of flavonoids from celery seed using response surface methodology. *Journal of Food Measurement and Characterization*, 15(1), 134-143.
- 26 Stookey, L. L. (1970). Ferrozine: A new spectrophotometric reagent for iron. *Analytical Chemistry*, 42(7), 779-781.
- 27 Berker, K. I., Güçlü, K., Demirata, B., & Apak, R. (2010). A novel antioxidant assay of ferric reducing capacity measurement using ferrozine as the colour forming complexation reagent. *Analytical Methods*, 2(11), 1770-1778.

- 28 Hieu, T. Q., & Thao, D. T. T. (2019). Enhancing the solubility of curcumin metal complexes and investigating some of their biological activities. *Journal of Chemistry*, 2019, 8082195.
- 29 Lin, L.-Z., & Harnly, J. M. (2007). A screening method for the identification of glycosylated flavonoids and other phenolic compounds using a standard analytical approach for all plant materials. *Journal of Agricultural and Food Chemistry*, 55(4), 1084-1096.
- 30 Kaiser, A., Carle, R., & Kammerer, D. R. (2013). Effects of blanching on polyphenol stability of innovative paste-like parsley (*Petroselinum crispum* (Mill.) Nym ex A. W. Hill) and marjoram (*Origanum majorana* L.) products. *Food Chemistry*, 138(2), 1648-1656.
- 31 Park, Y., Moon, B. H., Yang, H., Lee, Y., Lee, E., & Lim, Y. (2007). Complete assignments of NMR data of 13 hydroxymethoxyflavones. *Magnetic Resonance in Chemistry*, 45(12), 1072-1075.
- 32 Montalvillo-Jiménez, L., Santana, A. G., Corzana, F., Jiménez-Osés, G., Jiménez-Barbero, J., Gómez, A. M., & Asensio, J. L. (2019). Impact of aromatic stacking on glycoside reactivity: Balancing CH/ π and cation/ π interactions for the stabilization of glycosyl-oxocarbenium ions. *Journal of the American Chemical Society*, 141(34), 13372-13384.
- 33 Bitew, M., Desalegn, T., Demissie, T. B., Belayneh, A., Endale, M., & Eswaramoorthy, R. (2021). Pharmacokinetics and drug-likeness of antidiabetic flavonoids: Molecular docking and DFT study. *PloS one*, 16(12), e0260853.
- 34 Voirin, B., Sportouch, M., Raymond, O., Jay, M., Bayet, C., Dangles, O., & El Hajji, H. (2000). Separation of flavone C-glycosides and qualitative analysis of *Passiflora incarnata* L. By capillary zone electrophoresis. *Phytochemical Analysis*, 11(2), 90-98.
- 35 Lemańska, K., van der Woude, H., Szymusiak, H., Boersma, M. G., Gliszczyńska-Świgto, A., Rietjens, I. M. C. M., & Tyrakowska, B. (2004). The effect of catechol O-methylation on radical scavenging characteristics of quercetin and luteolin—a mechanistic insight. *Free Radical Research*, 38(6), 639-647.
- 36 Zhang, L., Song, L., Zhang, P., Liu, T., Zhou, L., Yang, G., Lin, R., & Zhang, J. (2015). Solubilities of naringin and naringenin in different solvents and dissociation constants of naringenin. *Journal of Chemical & Engineering Data*, 60(3), 932-940.
- 37 Zhang, L., Liu, Y., Wang, Y., Xu, M., & Hu, X. (2018). UV-Vis spectroscopy combined with chemometric study on the interactions of three dietary flavonoids with copper ions. *Food Chemistry*, 263, 208-215.
- 38 El-Sherif, A. A., Shoukry, M. M., & Abd-Elgawad, M. M. A. (2013). Protonation equilibria of some selected α -amino acids in DMSO–water mixture and their Cu(II)-complexes. *Journal of Solution Chemistry*, 42(2), 412-427.
- 39 Kipton, H., Powell, J., & Taylor, M. C. (1982). Interactions of iron(II) and iron(III) with gallic acid and its homologues: A potentiometric and spectrophotometric study. *Australian Journal of Chemistry*, 35(4), 739-756.
- 40 Perron, N. R., Hodges, J. N., Jenkins, M., & Brumaghim, J. L. (2008). Predicting how polyphenol antioxidants prevent DNA damage by binding to iron. *Inorganic Chemistry*, 47(14), 6153-6161.
- 41 Jewett, S. L., Egglings, S., & Geller, L. (1997). Novel method to examine the formation of unstable 2: 1 and 3: 1 complexes of catecholamines and iron (III). *Journal of Inorganic Biochemistry*, 66(3), 165-173.
- 42 Perron, N. R., Wang, H. C., DeGuire, S. N., Jenkins, M., Lawson, M., & Brumaghim, J. L. (2010). Kinetics of iron oxidation upon polyphenol binding. *Dalton Transactions*, 39(41), 9982-9987.
- 43 Chvátalová, K., Slaninová, I., Březinová, L., & Slanina, J. (2008). Influence of dietary phenolic acids on redox status of iron: Ferrous iron autooxidation and ferric iron reduction. *Food Chemistry*, 106(2), 650-660.
- 44 Kasprzak, M. M., Erxleben, A., & Ochocki, J. (2015). Properties and applications of flavonoid metal complexes. *RSC Advances*, 5(57), 45853-45877.
- 45 Zheng, Y.-Z., Deng, G., Liang, Q., Chen, D.-F., Guo, R., & Lai, R.-C. (2017). Antioxidant activity of quercetin and its glucosides from propolis: A theoretical study. *Scientific Reports*, 7(1), 1-11.
- 46 Hamzeh-Mivehroud, M., Rahmani, S., Rashidi, M.-R., Hosseinpour Feizi, M.-A., & Dastmalchi, S. (2013). Structure-based investigation of rat aldehyde oxidase inhibition by flavonoids. *Xenobiotica*, 43(8), 661-670.
- 47 Janiak, C. (2000). A critical account on π - π stacking in metal complexes with aromatic nitrogen-containing ligands. *Dalton Transactions*, 21, 3885-3896.
- 48 Malacaria, L., Bijlsma, J., Hilgers, R., de Bruijn, W. J. C., Vincken, J.-P., & Furia, E. (2023). Insights into the complexation and oxidation of quercetin and luteolin in aqueous solutions in presence of selected metal cations. *Journal of Molecular Liquids*, 369, 120840.
- 49 Narváez-Cuenca, C.-E., Vincken, J.-P., & Gruppen, H. (2012). Identification and quantification of (dihydro) hydroxycinnamic acids and their conjugates in potato by UHPLC-DAD-ESI-MSⁿ. *Food Chemistry*, 130(3), 730-738.
- 50 Plazonić, A., Bucar, F., Maleš, Ž., Mornar, A., Nigović, B., & Kujundžić, N. (2009). Identification and quantification of flavonoids and phenolic acids in burr parsley (*Caucalis platycarpus* L.), using high-performance liquid chromatography with diode array detection and electrospray ionization mass spectrometry. *Molecules*, 14(7), 2466-2490.
- 51 Fernández-Poyatos, M. D. P., Ruiz-Medina, A., Zengin, G., & Llorent-Martínez, E. J. (2019). Phenolic characterization, antioxidant activity, and enzyme inhibitory properties of *Berberis thunbergii* DC. Leaves: A valuable source of phenolic acids. *Molecules*, 24(22).
- 52 Cavaliere, C., Foglia, P., Pastorini, E., Samperi, R., & Laganà, A. (2005). Identification and mass spectrometric characterization of glycosylated flavonoids in *Triticum durum* plants by high-

- performance liquid chromatography with tandem mass spectrometry. *Rapid Communications in Mass Spectrometry*, 19(21), 3143-3158.
- 53 Munekata, P. E. S., Alcántara, C., Žugčić, T., Abdelkebir, R., Collado, M. C., García-Pérez, J. V., Jambrak, A. R., Gavahian, M., Barba, F. J., & Lorenzo, J. M. (2020). Impact of ultrasound-assisted extraction and solvent composition on bioactive compounds and in vitro biological activities of thyme and rosemary. *Food Research International*, 134, 109242.
- 54 Ma, Y., Kosińska-Cagnazzo, A., Kerr, W. L., Amarowicz, R., Swanson, R. B., & Pegg, R. B. (2014). Separation and characterization of phenolic compounds from dry-blanched peanut skins by liquid chromatography–electrospray ionization mass spectrometry. *Journal of Chromatography A*, 1356, 64-81.
- 55 Bresciani, L., Favari, C., Calani, L., Francinelli, V., Riva, A., Petrangolini, G., Allegrini, P., Mena, P., & Del Rio, D. (2020). The effect of formulation of curcuminoids on their metabolism by human colonic microbiota. *Molecules*, 25(4), 940.
- 56 Momin, R. A., & Nair, M. G. (2002). Antioxidant, cyclooxygenase and topoisomerase inhibitory compounds from *Apium graveolens* Linn. seeds. *Phytomedicine*, 9(4), 312-318.
- 57 Boulton, R. (2001). The copigmentation of anthocyanins and its role in the color of red wine: A critical review. *American Journal of Enology and Viticulture*, 52(2), 67-87.

4.7. Supplementary information

Method S4.1. Pre-purification by RP-flash chromatography

Pre-purification of the celery extract was performed by use of a Büchi Pure C-850 FlashPrep system, operated in flash mode and equipped with a UV detector (Büchi, Flawil, Switzerland). The cleaned celery extracts (4 g) were dissolved in 100 % MeOH and 8 g of C18 bulk sorbent was added (Bondesil, particle size 40 µm). Subsequently, the MeOH was evaporated under reduced pressure. The remaining powder was dry-loaded in 15 g cartridges (Grace, Columbia, USA) on the FlashPrep system with a solid loader plunger. The fractionation was performed at room temperature on a Büchi FlashPure C18 cartridge (column size 80 g; particle size 40 µm). Water and ACN (ULC/MS grade), both acidified with 1 vol. % formic acid, were used as eluent A and B, respectively. The flow rate was 60 mL min⁻¹ and UV detection was set from 254 to 400 nm. The following elution profile was used: 0 – 7.3 min, isocratic at 20 vol. % B; 7.3 – 36.6, linear gradient from 20 to 30 vol. % B; 36.6 – 38.1, linear gradient from 30 to 100 vol. % B; 38.1 – 45.4, isocratic at 100 vol. % B; 45.4 – 46.9, linear gradient from 100 to 20 vol. % B; 46.9 – 54.3, isocratic at 20 vol. % B. Several runs were performed to pre-purify a total of 44.5 g of celery extract. The collected fractions were analysed by RP-UHPLC-PDA-ESI-ITMSⁿ and those containing similar compounds were pooled. The ACN was removed under reduced pressure at 45 °C using a rotavapor (Büchi, Fawil, Switzerland) and the remaining water was removed by lyophilisation. Afterwards the flavone-enriched pools were solubilised in DMSO for analysis on RP-UHPLC-PDA-ITMSⁿ.

Method S4.2. Preparative RP-HPLC-ESI-MS

Purification of the flavone-enriched pools was performed using a Waters preparative HPLC, equipped with a 2545 quaternary gradient module, 2767 sample manager, fluid organiser, and 2998 photodiode array detector. The pools (~10 mg in 1 mL 20 % ACN) were injected on a Waters XBridge Prep C18 OBD column (19 × 250 mm, 5 µm particle size) (Waters, Milford, MA, USA) and eluents used were water (A) and ACN (HPLC-R grade) (B), both acidified with 1 vol. % formic acid. The elution programs for the different pools were as follows: **Pool 1:** Isocratic at 13 vol. % B for 5.65 min, linear gradient to 18 vol. % B from 5.65 to 40.48 min, linear gradient to 100 vol. % B from 40.48 to 43.97 min, isocratic at 100 vol. % B from 43.97 to 61.39 min, linear gradient to 13 vol. % B from 61.39 to 64.87 min, isocratic at 13 vol. % B from 64.87 to 82.29 min. **Pool 2:** Isocratic at 15 vol. % B for 5.65 min, linear gradient to 20 vol. % B from 5.65 to 40.48 min, linear gradient to 100 vol. % B from 40.48 to 43.97 min, isocratic at 100 vol. % B from 43.97 to 61.39 min, linear gradient to 15 vol. % B from 61.39 to 64.87 min, isocratic at 15 vol. % B from 64.87 to 82.29 min. **Pool 3:** Isocratic at 19 vol. % B for 5.65 min, linear gradient to 24 vol. % B from 5.65 to 40.48 min, linear gradient to 100 vol. % B from 40.48 to 43.97 min, isocratic at 100 vol. % B from 43.97 to 61.39 min, linear gradient to 19 vol. % B from 61.39 to 64.87 min, isocratic at 19 vol. % B from 64.87 to 82.29 min. **Pool 4:** Isocratic at 22 vol. % B for 5.65 min, linear gradient to 27 vol. % B from 5.65 to 40.48

min, linear gradient to 100 vol. % B from 40.48 to 43.97 min, isocratic at 100 vol. % B from 43.97 to 61.39 min, linear gradient to 22 vol. % B from 61.39 to 64.87 min, isocratic at 22 vol. % B from 64.87 to 82.29 min. The purified fractions were subjected to evaporation under reduced pressure to remove acetonitrile, and were subsequently resolubilised using *tert*-butanol prior to lyophilisation.

Method S4.3. Identification and quantification of phenolics in the extract by RP-UHPLC-PDA-ITMS/FTMS

Samples were separated on a Thermo Vanquish UHPLC system (Thermo Scientific, San Jose, CA, USA) equipped with an autosampler, a pump, a photodiode array (PDA) detector. A sample (1 μ L) was injected on an Acquity UPLC BEH C18 column (150 mm \times 2.1 mm i.d., 1.7 μ m) with a VanGuard (5 mm \times 2.1 mm i.d., 1.7 μ m) guard column of the same material (Waters, Milford, MA). Water (A) and acetonitrile (B), both acidified with 0.1 vol. % formic acid, were used as eluents. The flow rate was 400 μ L min⁻¹, and the temperature of the column oven was 45 °C with the post column cooler set to 40 °C. Various elution profiles were used, depending on the type of sample. *For the extracts and the enriched pools*: 0.00 – 1.09 min, isocratic on 1 vol. % B; 1.09 – 33.26 min, linear gradient from 1 to 60 vol. % B; 33.26 – 34.35 min linear gradient from 60 to 100 vol. % B; 34.35 – 39.80 min isocratic on 100 vol. % B; 39.80 – 40.89 min linear gradient from 100 to 1 vol. % B; 40.89 – 46.35 min isocratic on 1 vol. % B. *For the purified compounds*: 0.00 – 1.09 min, isocratic on 1 vol. % B; 1.09 – 22.54 min, linear gradient from 1 to 55 vol. % B; 22.54 – 23.63 min linear gradient from 55 to 100 vol. % B; 23.63 – 29.08 min isocratic on 100 vol. % B; 29.08 – 30.17 min linear gradient from 100 to 1 vol. % B; 30.17– 35.62 min isocratic on 1 vol. % B. *For the reactivity of the purified compounds with iron*: 0.00 – 1.09 min, isocratic on 1 vol. % B; 1.09 – 20.72 min, linear gradient from 1 to 55 vol. % B; 20.72 – 21.81 min linear gradient from 55 to 100 vol. % B; 21.81 – 27.26 min isocratic on 100 vol. % B; 27.26 – 28.35 min linear gradient from 100 to 1 vol. % B; 28.35– 33.81 min isocratic on 1 vol. % B. The PDA detector was set to measure spectra in the wavelength range of 190 – 680 nm. The temperature of the autosampler was controlled at 10 °C, except the samples dissolved in DMSO, where the temperature was set at 25 °C to prevent solidification of DMSO (T_m = 18.5 °C).

Electrospray ionisation ion trap mass spectrometry (ESI-ITMSⁿ)

Mass spectrometric data of the extracts, pools, and purified compounds were acquired using an LTQ Velos Pro linear ion trap mass spectrometer (Thermo Scientific) equipped with a heated electrospray ionisation probe (ESI-ITMSⁿ) and coupled to the Vanquish UHPLC system. Nitrogen was used as a sheath gas (50 arbitrary units) and auxiliary gas (13 arbitrary units). Data were collected over the *m/z* range of 150 – 1,500 in negative and positive ionisation mode by using source voltages of 2.5 and 3.5 kV, respectively. For both modes, the S-lens RF level was set at 67 %, the ion transfer tube temperature was 263 °C, and the source heater temperature 425 °C. Data-dependent MSⁿ analysis was performed on the most intense ion by collision-induced dissociation (CID) with normalised collision energy of 35 %. A dynamic mass exclusion approach

was used, in which the most intense ion was fragmented 3 times and was subsequently excluded from fragmentation for the following 5 seconds, allowing data-dependent MSⁿ of less intense co-eluting compounds. Data acquisition and processing were performed using Xcalibur version 4.1 (Thermo Scientific).

Electrospray ionisation hybrid quadrupole Orbitrap mass spectrometry (ESI FTMS²)

Accurate mass data of the purified compounds were acquired using a Thermo Q Exactive Focus hybrid quadrupole-Orbitrap Fourier transform mass spectrometer (FTMS) (Thermo Scientific) equipped with a heated ESI probe coupled to the Vanquish UHPLC system. Prior to analysis, the mass spectrometer was calibrated in the negative and positive ionisation mode using Tune 2.11 (Thermo Scientific) by injection of Pierce negative and positive ion calibration solutions (Thermo Scientific). Gas flows and source conditions were the same as for ESI-ITMS. Full MS and higher energy collisional dissociation (HCD) fragmentation data were recorded at 70.000 FWHM and 35.000 FWHM resolution, respectively. Normalised collision energy was 35 %. MS² fragmentation was performed on the most intense product ion in the MS spectrum and the exact masses of the purified compounds were inserted in an inclusion list. Data acquisition and processing were performed using Xcalibur version 4.1 (Thermo Scientific).

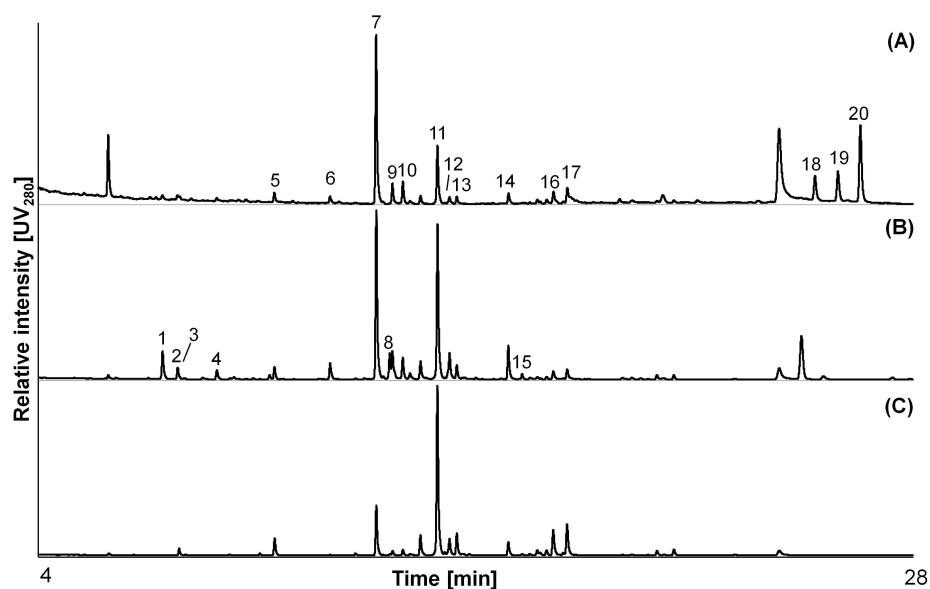


Figure S4.1. RP-UHPLC-UV profile (280 nm) of the phenolic extracts from chicken bouillon (A), celery (B), and parsley (C). Peak numbers refer to the compounds in [table S4.1](#).

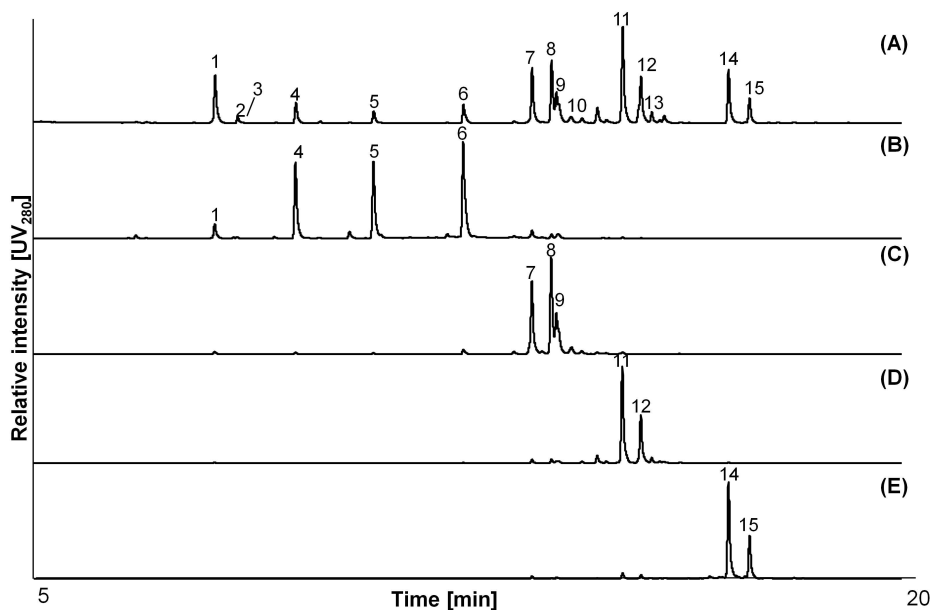


Figure S4.2. RP-UHPLC-UV profile (280 nm) of the celery extract (A), and pools derived from flash chromatographic separation; Pool 1 (B), Pool 2 (C), Pool 3 (D), and Pool 4 (E). Peak numbers refer to the compounds in [table S4.1](#).

Table S4.1. Spectrometric and spectroscopic data of phenolic compounds in extracts as determined by UHPLC-PDA coupled to ESI-ITMS.

Peak no.	T _R (min)	λ _{max} (nm)	[M-H] ⁻		[M+H] ⁺		Tentatively identified compound
			m/z	CID MS ² fragments (r.a.) ^a	m/z	CID MS ² fragments (r.a.)	
1	7.27	322, 398	353	191 127, 85 (95), 173 (84), 93 (60), 111 (44), 171 (27), 87 (21), 109 (20)	355	163 -	Caffeoyl quinic acid ^[29, 49, 50]
2	7.64	286	325	163 119	-	-	Coumaric acid hexoside A ^[49]
3	7.82	278	325	163, 119 (67), 161 (53), 101 (13)	-	-	Coumaric acid hexoside B ^[49]
4	8.81	350	447	285 285, 241 (45), 199 (37), 175 (37), 217 (32), 151 (17), 257 (15), 201 (12)	449	287 287	Luteolin 7-O-glucoside (Cynaroside) ^[50]
5	10.28	310	337	191 127	339	147	Coumaroyl quinic acid ^[51]
6	11.96	350	579	285, 447 (67), 284 (11) 285, 460 (58), 543 (37), 559 (29), 463 (22), 403 (17), 515 (13), 461 (13)	581	287, 449 (67) 287, 153 (13)	Luteolin 7-O-apiosylglucoside ^[7, 13, 29, 52]
7	13.24	266, 338	563	269, 431 (18) 269, 225 (22)	565	271, 433 (73) 271	Apigenin 7-O-apiosylglucoside ^[2-5] (Aplin) ^[7, 13, 29, 52]
8	13.56	346	665	621 489, 285 (60), 579 (22), 284 (10)	667	287, 535 (85) 287, 258 (11)	Luteolin 7-O-malonyl Apiosylglucoside ^[7, 13, 29, 52, 53]
9	13.67	346	593	299, 284 (23), 461 (12) 284	595	301, 463 (50) 286, 301 (24)	Chrysoeriol 7-O-apiosylglucoside A ^[7, 13, 29, 52, 53]
10	13.94	254, 346	593	299, 284 (17) 284	595	301, 463 (51) 286, 301 (20)	Chrysoeriol 7-O-apiosylglucoside B ^[7, 13, 29, 52, 53]

CID, collision-induced dissociation; HCD, higher energy collisional dissociation; r.a., relative abundance. The threshold for fragments was ≥ 10 %. The most intense fragment is underlined; ^a The parent ion of the MS³ fragmentation is the fragment with 100 % relative abundance in MS² fragmentation.

Table S4.1. continued Spectrometric and spectroscopic data of phenolic compounds in extracts as determined by UHPLC-PDA coupled to ESI-ITMS.

Peak no.	T _R (min)	λ _{max} (nm)	<i>m/z</i>	CID MS ² fragments (<i>r.a.</i>) ^a	[M-H] ⁺ CID MS ³ fragments (<i>r.a.</i>)	<i>m/z</i>	CID MS ² fragments (<i>r.a.</i>)	[M+H] ⁺ CID MS ³ fragments (<i>r.a.</i>)	Tentatively identified compound
11	14.87	266, 338	649	<u>605</u>	545, 563 (37)	651	<u>519</u> , 271 (80)	<u>271</u>	Apigenin 7-O-malonyl (Malonylapiin apiosylglucoside) ^[7, 13, 29, 52]
12	15.20	346	679	<u>635</u>	<u>575</u> , 593 (50), 299 (28), 473 (16)	681	<u>301</u> , 549 (80), 286 (10)	<u>286</u> , 301 (24)	Chrysoeriol 7-O-malonyl apiosylglucoside A ^[7, 13, 29, 52, 53]
13	15.38	346	679	<u>635</u>	<u>299</u> , 593 (58), 284 (29), 575 (14), 503 (13)	681	<u>301</u> , 549 (58), 595 (12)	<u>286</u> , 301 (21)	Chrysoeriol 7-O-malonyl apiosylglucoside B ^[7, 13, 29, 52, 53]
14	16.81	266, 338	605	<u>563</u> , 545 (57)	<u>269</u> , 431 (20)	607	<u>271</u> , 475 (64)	<u>271</u>	Apigenin 7-O acetyl apiosylglucoside (Acetylapiin) ^[7, 13, 29, 52]
15	17.17	346	635	<u>299</u> , 593 (55), 284 (27), 503 (14), 575 (13)	<u>284</u>	637	<u>301</u> , 505 (74)	<u>286</u> , 301 (20)	Chrysoeriol 7-O-apiosylglucoside ^[7, 13, 29, 52, 53]
16	17.95	282	557	<u>513</u>	<u>349</u> , 469 (40), 163 (30)	-	-	-	Malonyl coumaroyl feruloyl tartaric acid A ^[54]
17	18.32	282	557	<u>513</u>	<u>349</u> , 469 (40), 163 (30), 325 (12)	-	-	-	Malonyl coumaroyl feruloyl tartaric acid B ^[54]
18	24.56	418	307	<u>187</u> , 143 (30)	<u>143</u>	-	-	-	Bisdemethoxycurcumin ^[55]
19	25.57	422	337	<u>217</u> , 187 (24), 173 (21), 143 (11)	<u>173</u>	-	-	-	Demethoxycurcumin ^[55]
20	26.15	426	367	<u>217</u> , 173 (33)	<u>173</u>	-	-	-	Curcumin ^[55]

CID, collision-induced dissociation; HCD, higher energy collisional dissociation; ^a*r.a.*, relative abundance. The threshold for fragments was ≥ 10 %. The most intense fragment is

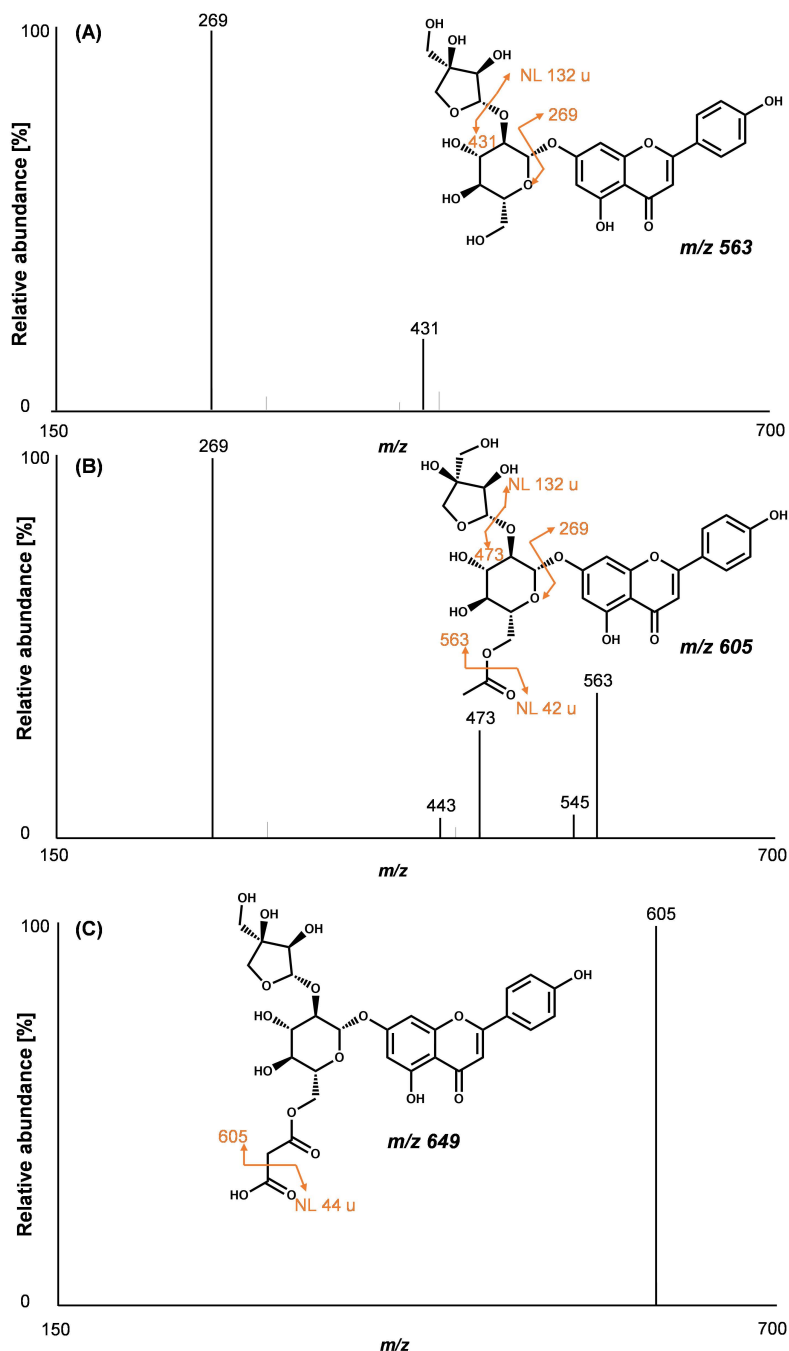


Figure S4.3. Negative mode CID MS² fragmentation spectra of (A) apigenin 7-O-apiosylglucoside; (B) apigenin 7-O-(6''-O-acetyl)-apiosylglucoside; and (C) apigenin 7-O-(6''-O-malonyl)-apiosylglucoside. The cut-off value for fragment labelling was 10 % of the relative abundance.

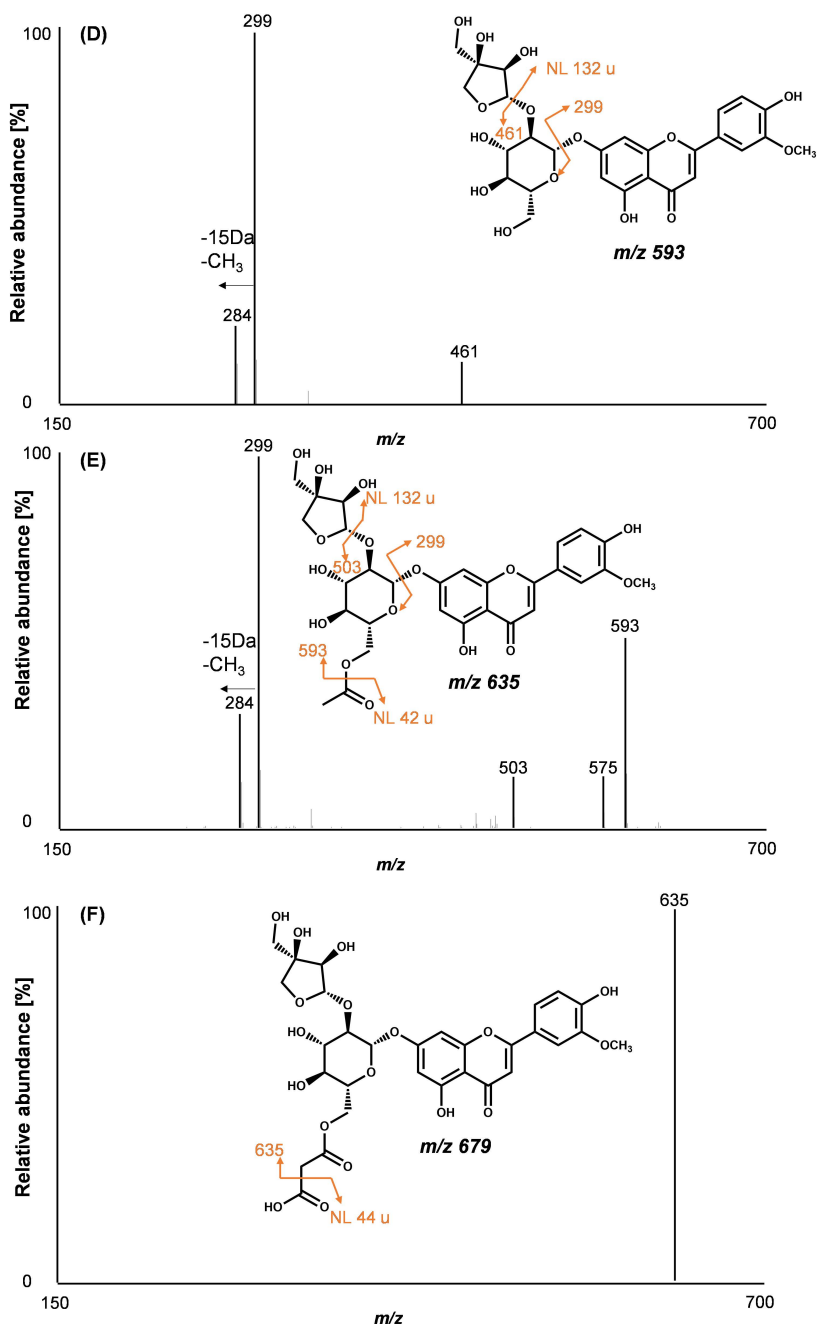


Figure S4.3. continued. Negative mode CID MS² fragmentation spectra of **(D)** chrysoeriol 7-O-apiosylglucoside; **(E)** chrysoeriol 7-O-(6''-O-acetyl)-apiosylglucoside; and **(F)** chrysoeriol 7-O-(6''-O-malonyl)-apiosylglucoside. The cut-off value for fragment labelling was 10 % of the relative abundance.

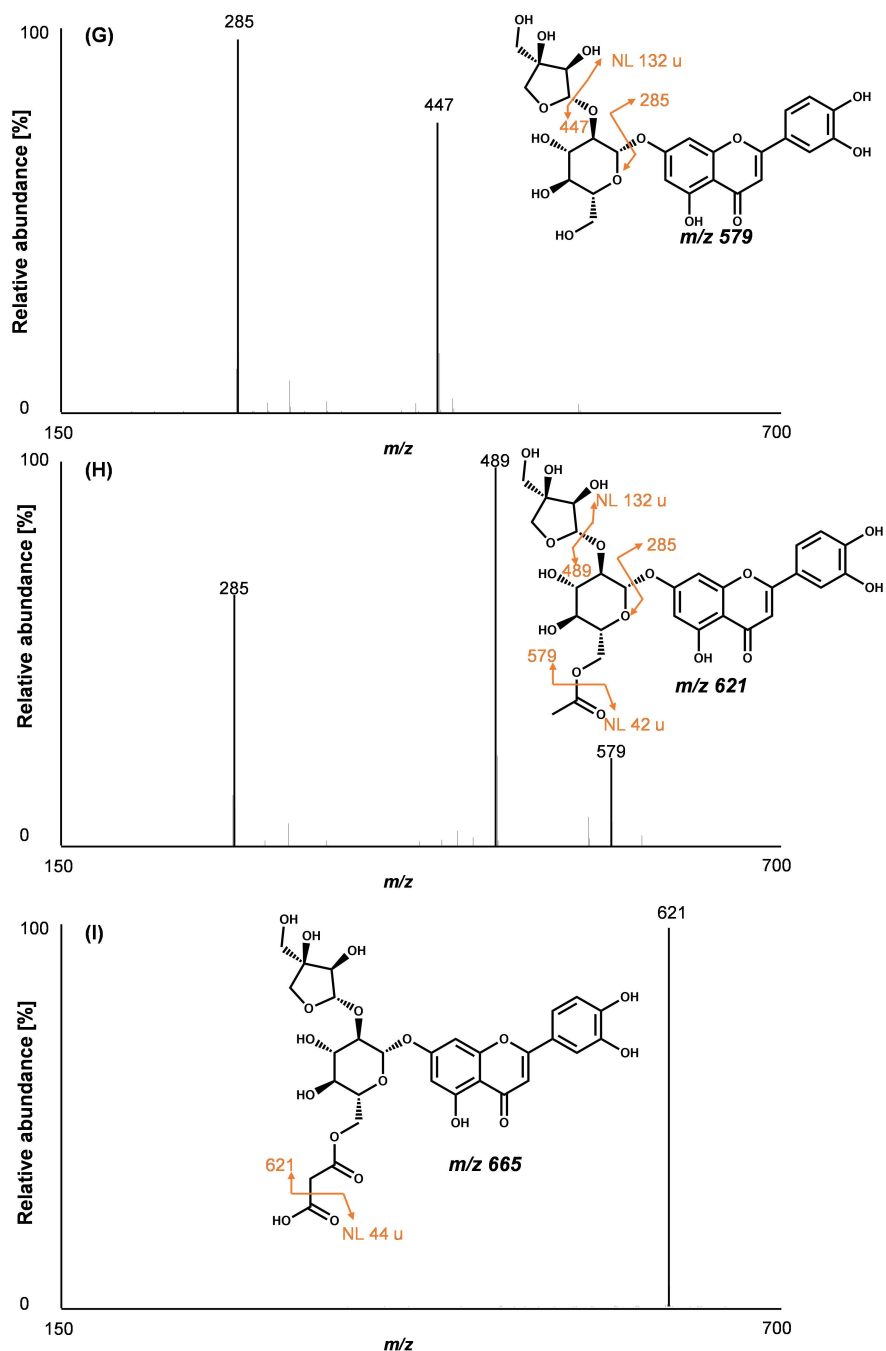


Figure S4.3. continued. Negative mode CID MS² fragmentation spectra of (G) luteolin 7-O-apiosylglucoside; (H) luteolin 7-O-(6''-O-acetyl)-apiosylglucoside; and (I) luteolin 7-O-(6''-O-malonyl)-apiosylglucoside. The cut-off value for fragment labelling was 10 % of the relative abundance.

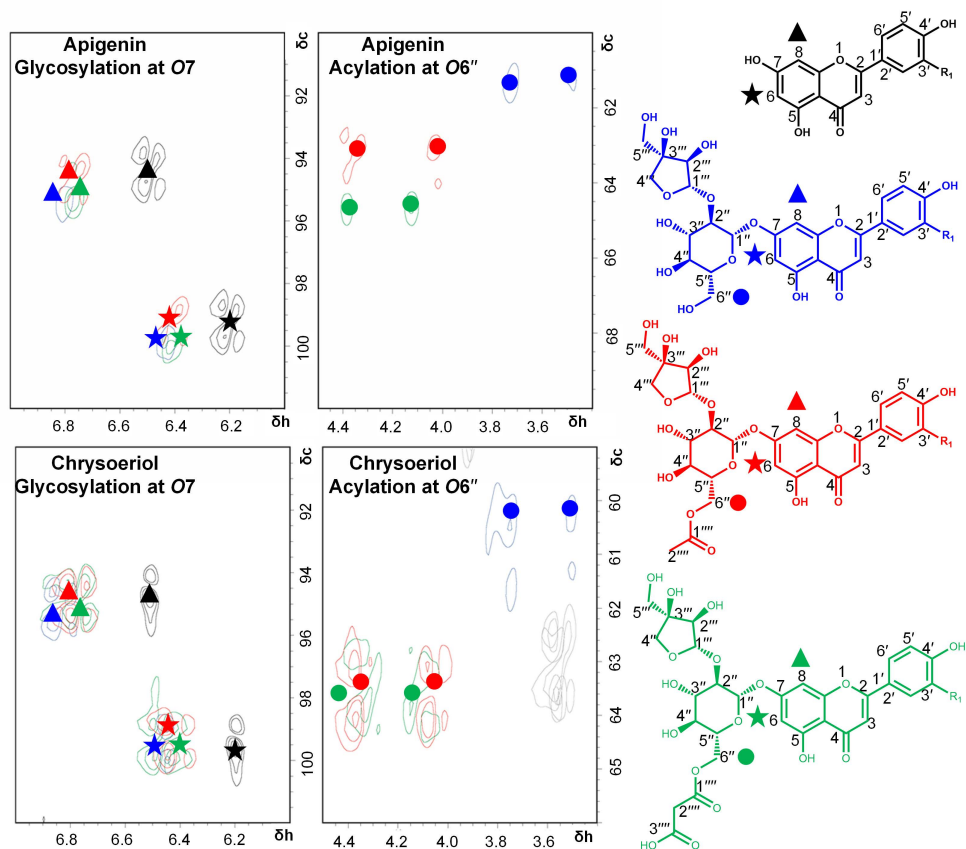


Figure S4.4. Overlaid 2D HSQC NMR spectra of the C₆-H₆ (star) and C₈-H₈ (triangle) region (δ_c 90-102, δ_h 6.0-7.0) and the C_{6''}-H_{6''} (circle) region (δ_c 58-70, δ_h 3.4-4.5) of the apigenin and chrysoeriol aglycone (black), apiosylglucoside (blue), acetyl apiosylglucoside (red), and malonyl apiosylglucoside (green). Spectra confirm glycosylation at the O₇ position due to the downfield shifts of C₆-H₆ and C₈-H₈, and acylation at the O_{6''} position due to the downfield shift of C_{6''}-H_{6''}.

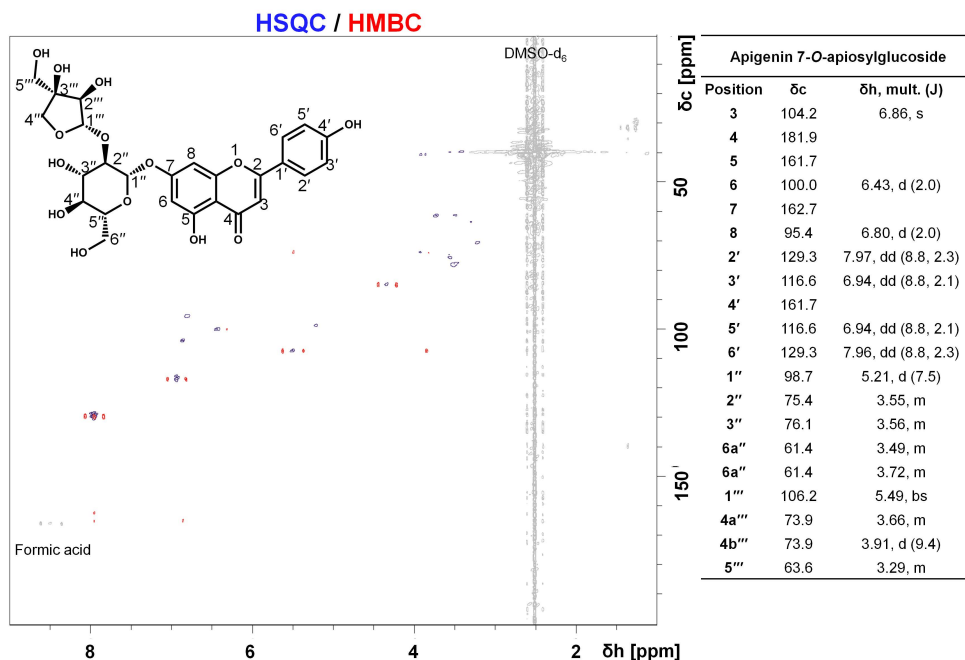


Figure S4.5. 2D HSQC (blue) and HMBC (red) NMR spectra and peak annotations of apigenin 7-*O*-apiosylglucoside (apiin) measured in DMSO- d_6 . The signal assignment of the ^1H NMR spectra matches with the chemical shifts of apiin reported by Eckey-Kaltenbach and co-authors.^[9] The HSQC and HMBC correlations also confirmed the structure of apiin. Grey correlations are unassigned signals originating from the solvent or impurities.

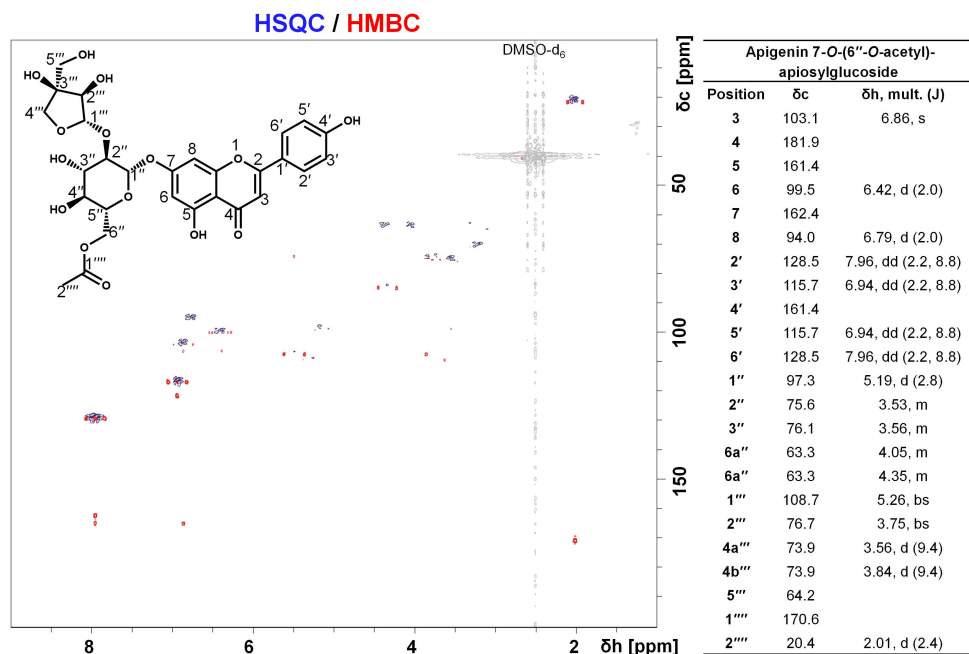


Figure S4.6. 2D HSQC (blue) and HMBC (red) NMR spectra and peak annotations of apigenin 7-O-(6''-O-acetyl)-apiosylglucoside (6''-acetylapiin) measured in DMSO-d₆. The signal assignment of the ¹H and ¹³C NMR spectra matches with the chemical shifts of 6''-acetylapiin reported by Yoshikawa et al.^[10] The HSQC and HMBC correlations also confirmed the structure of acetylapiin. Grey correlations are unassigned signals originating from the solvent or impurities.

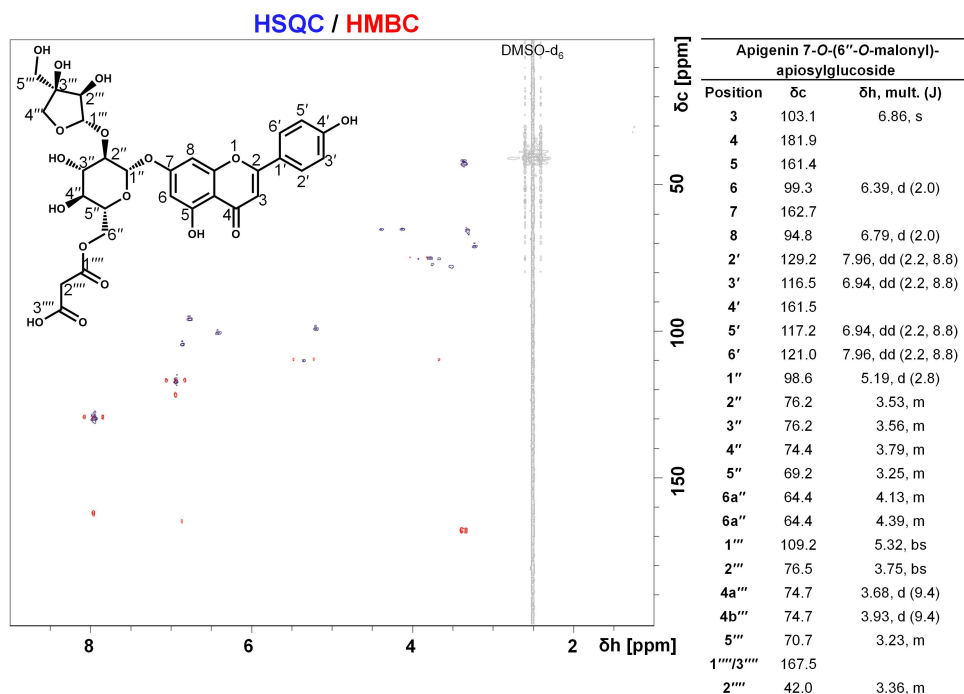


Figure S4.7. 2D HSQC (blue) and HMBC (red) NMR spectra and peak annotations of apigenin 7-O-(6''-O-malonyl)-apiosylglucoside (6''-malonylapiin) measured in DMSO- d_6 . The signal assignment of the ^1H NMR spectra matches with the chemical shifts of 6''-malonylapiin reported by Eckey-Kaltenbach et al.^[9] The HSQC and HMBC correlations also confirmed the structure of malonylapiin. Grey correlations are unassigned signals originating from the solvent or impurities.

4

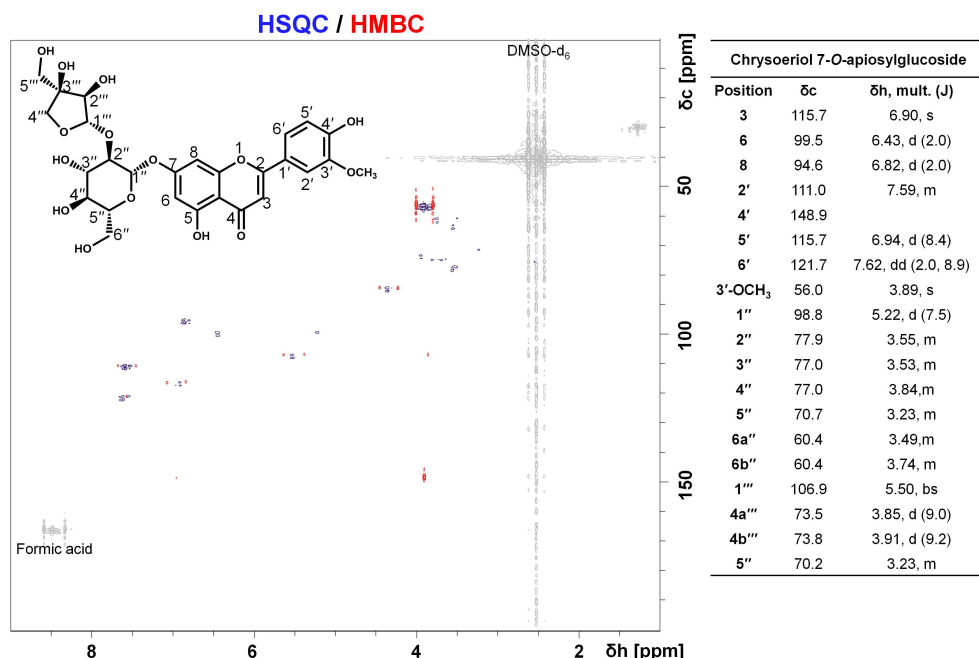


Figure S4.8. 2D HSQC (blue) and HMBC (red) NMR spectra and peak annotations of chrysoeriol 7-*O*-apiosylglucoside measured in DMSO- d_6 . The signals for the phenolic backbone of this compound were similar to chrysoeriol as reported by Park et al.^[31] Different from the signals reported by Park et al., *H*6 and *H*8 showed an downfield shift which is due to the presence of the apiosylglycoside on the *O*7 position similar to what was seen for compound A compared to the apigenin aglycon. Presence of the methoxy group at *C*3' was evidenced by the new signals at $\delta_{3.89}$ (s) in H and δ_{56} in C and the HMBC and HSQC spectra.^[56] Grey correlations are unassigned signals originating from the solvent or impurities.

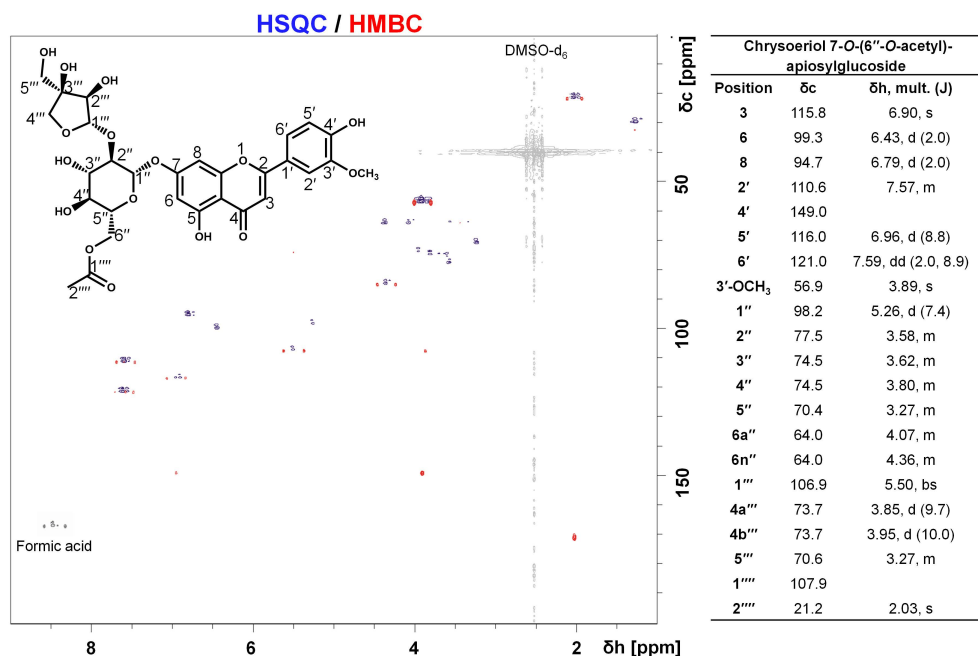


Figure S4.9. 2D HSQC (blue) and HMBC (red) NMR spectra and peak annotations of chrysoeriol 7-O-(6''-O-acetyl)-apiosylglucoside measured in DMSO- d_6 . The signals for the phenolic backbone of this compound were similar to chrysoeriol as reported by Park et al.^[31] Different from the signals reported by Park et al., *H*6 and *H*8 showed an downfield shift which is due to the presence of the apioglycoside on the *O*7 position. Presence of the methoxy group at *C*3' was evidenced by the new signals at δ 3.89 (s) in H and δ 56 in C and the HMBC and HSQC spectra.^[56] This compound showed similar signals as compound G which was identified as a chrysoeriol 7-O-apiosylglucoside but the diagnostic differences of 42 in RP-UHPLC-MS indicated the presence of an acetyl substitution. Presence of the acetyl was evidenced by the new signal for the 2'''' position at δ 2.03 in H and δ 21.2 in C for acetyl. Grey correlations are unassigned signals originating from the solvent or impurities.

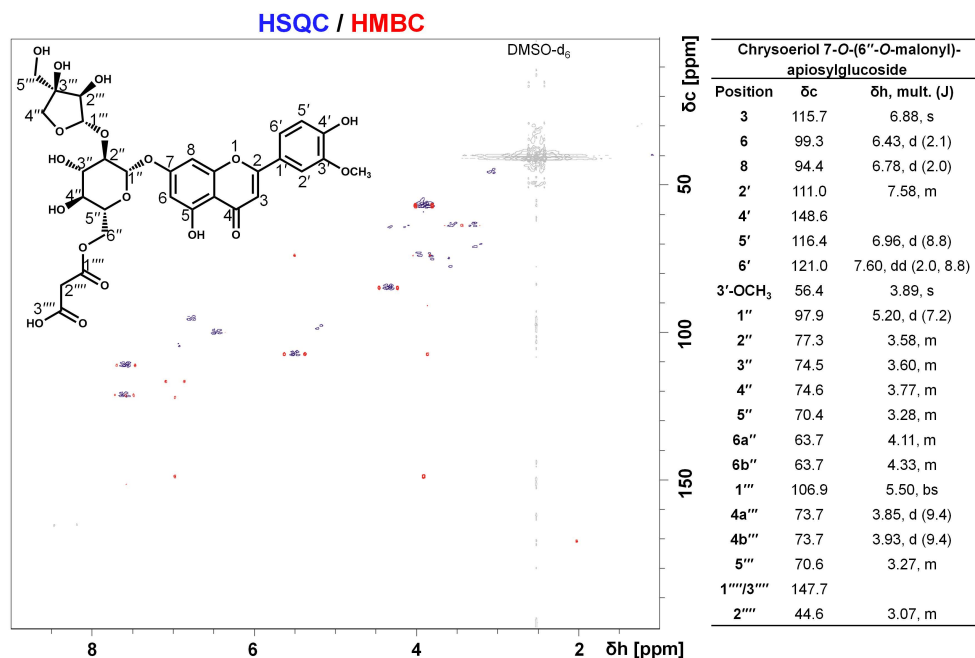


Figure S4.10. 2D HSQC (blue) and HMBC (red) NMR spectra and peak annotations of chrysoeriol 7-*O*-(6''-*O*-malonyl)-apiosylglucoside measured in DMSO-*d*₆. The signals for the phenolic backbone of this compound were similar to chrysoeriol as reported by Park et al.^[33] Different from the signals reported by Park et al., *H*6 and *H*8 showed an downfield shift which is due to the presence of the apioglycoside on the *O*7 position. Presence of the methoxy group at *C*3' was evidenced by the new signals at $\delta_{3.89}$ (s) in H and δ_{56} in C and the HMBC and HSQC spectra.^[56] This compound showed similar signals as compound G which was identified as a chrysoeriol 7-*O*-apiosylglucoside but the diagnostic differences of 86 in RP-UHPLC-MS indicated the presence of an malonyl substitution. Presence of the malonyl was evidenced by the new signal for the 2''' position at $\delta_{3.07}$ in H and $\delta_{44.6}$ in C. Grey correlations are unassigned signals originating from the solvent or impurities.

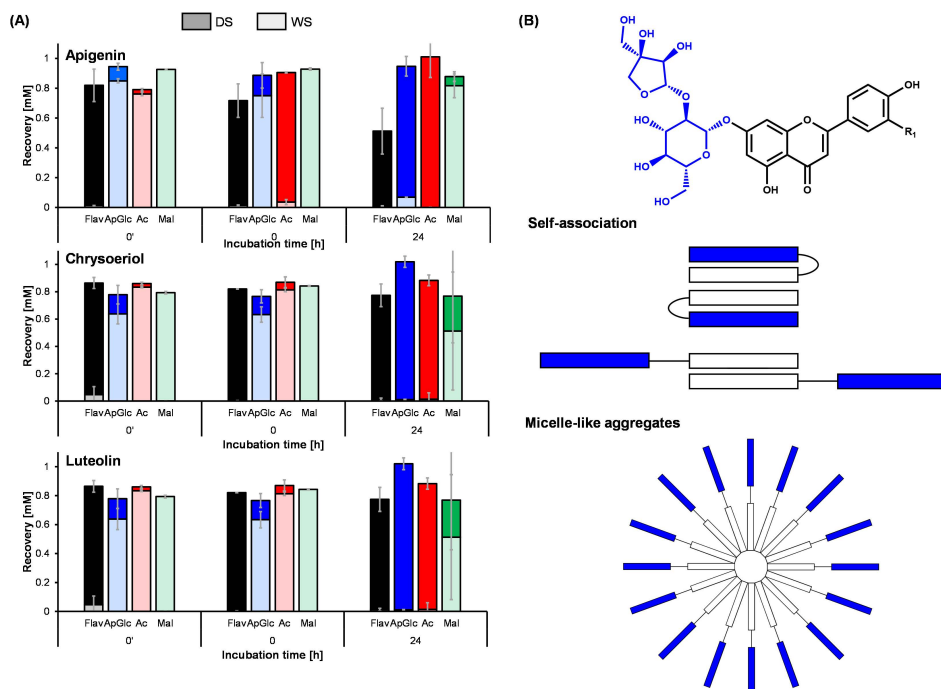


Figure S4.11. (A) Recovery of the flavone aglycons (Flav; black) and apiosylglucoside (ApGlc; blue) with additional acetylation (Ac; red) or malonylation (Mal; green) in the WS and DS fractions in absence of FeSO_4 . Time points shown are before the adjustment of the pH (t_0') and after 0 or 24 h of incubation at pH 6.5 in an aqueous solution. Error bars indicate the standard deviation of independent duplicates. Significance (Tukey's test, $p < 0.05$) of differences in the total recovery are indicated in **Table S4.2**. (B) Proposed self-association or micelle-like aggregate formation of flavone glycosides, the hydrophilic moieties are indicated in blue and hydrophobic moieties in white.

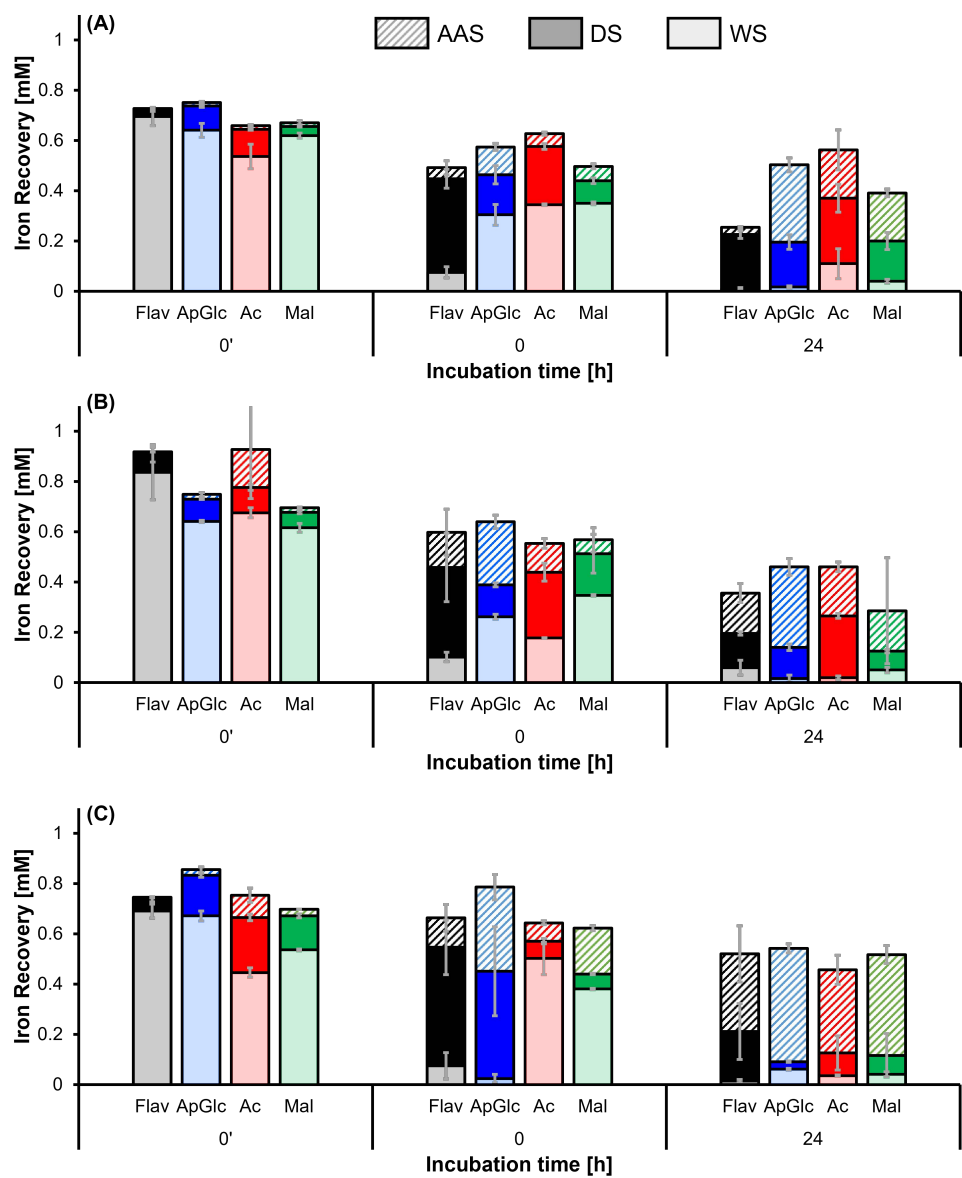


Figure S4.12. Recovery of iron in presence of equimolar concentration of the flavone aglycons (Flav; black) and apiosylglucoside (ApGlc; blue) with additional acetylation (Ac; red) or malonylation (Mal; green) for (A) apigenin, (B) chrysoeriol, and (C) luteolin in the WS, DS, and AAS fractions. Time points shown are before the adjustment of the pH (t_0) and after 0 or 24 h of incubation at pH 6.5 in an aqueous solution. Error bars indicate the standard deviation of independent duplicates. Significance (Tukey's test, $p < 0.05$) of differences in the total recovery are indicated in Table S4.2.

Table S4.2. Statistical analysis of the flavone and iron recovery in total and for the recovery in each of the three different fractions: water soluble (WS), DMSO soluble (DS), and ascorbic acid soluble (AAS) fractions. The quantitative differences were assessed by Tukey's *post hoc* comparison ($p < 0.05$). Significant differences in recovery compared to the other time points for the same flavone and of the three individual fractions (*i.e.* WS, DS, and AAS) are indicated with a different letter.

Flavone	t (h)	Flavone recovery in presence of FeSO ₄				Flavone recovery in absence of FeSO ₄				Iron recovery in presence of flavone			
		Tot	WS	DS	AAS	Tot	WS	DS	AAS	Tot	WS	DS	AAS
apigenin	0'	a	a	a	a	a	a	a	n.a.	a	a	a	a
	0	ab	a	a	a	a	a	a	n.a.	b	b	b	a
	24	b	a	b	a	a	a	a	n.a.	c	b	c	a
apigenin 7-O-apiosylglucoside	0'	a	a	a	a	a	a	a	n.a.	a	a	a	a
	0	a	b	a	a	a	a	a	n.a.	b	b	a	b
	24	a	b	a	b	a	b	b	n.a.	b	c	a	c
apigenin 7-O-(6''-O-acetyl)-apiosylglucoside	0'	a	a	a	a	a	a	a	n.a.	a	a	a	a
	0	a	a	a	a	a	b	b	n.a.	a	b	a	a
	24	a	a	a	b	a	b	b	n.a.	a	c	a	a
apigenin 7-O-(6''-O-malonyl)-apiosylglucoside	0'	a	a	a	a	a	a	a	n.a.	a	a	a	a
	0	ab	b	a	a	a	a	a	n.a.	b	b	ab	a
	24	b	c	b	b	a	a	a	n.a.	c	c	b	b
chrysoeriol	0'	a	a	a	a	a	a	a	n.a.	a	a	a	a
	0	a	a	a	a	a	a	a	n.a.	ab	b	a	a
	24	a	a	a	a	b	a	a	n.a.	b	b	a	a
chrysoeriol 7-O-apiosylglucoside	0'	a	a	a	a	a	a	a	n.a.	a	a	a	a
	0	a	a	a	a	a	a	a	n.a.	b	b	b	b
	24	a	a	a	a	a	b	b	n.a.	c	c	b	b
chrysoeriol 7-O-(6''-O-acetyl)-apiosylglucoside	0'	a	a	a	a	a	a	a	n.a.	a	a	a	a
	0	a	a	a	a	a	a	a	n.a.	a	b	b	a
	24	a	a	a	a	a	b	b	n.a.	a	c	b	a
chrysoeriol 7-O-(6''-O-malonyl)-apiosylglucoside	0'	a	a	a	a	a	a	a	n.a.	a	a	a	a
	0	ab	b	b	a	a	a	a	n.a.	a	b	a	a
	24	b	c	c	b	a	a	a	n.a.	a	c	a	a
luteolin	0'	a	a	a	a	a	a	a	n.a.	a	a	a	a
	0	a	a	ab	ab	a	a	a	n.a.	a	b	b	a
	24	a	a	b	b	a	a	a	n.a.	a	b	b	a
luteolin 7-O-apiosylglucoside	0'	a	a	a	a	a	a	a	n.a.	a	a	a	a
	0	a	a	b	a	a	a	a	n.a.	ab	b	a	b
	24	a	a	b	a	a	a	a	n.a.	b	b	a	b
luteolin 7-O-(6''-O-acetyl)-apiosylglucoside	0'	a	a	a	a	a	a	a	n.a.	a	a	a	a
	0	a	a	b	a	a	a	a	n.a.	a	a	a	ab
	24	a	a	b	a	a	a	a	n.a.	b	b	a	b
luteolin 7-O-(6''-O-malonyl)-apiosylglucoside	0'	a	a	a	a	a	a	a	n.a.	a	a	a	a
	0	a	ab	b	ab	a	a	a	n.a.	ab	b	a	b
	24	a	b	b	b	a	a	a	n.a.	b	c	a	c

n.a. not applicable, no ascorbic acid soluble fraction was present.

Possible self-association of the flavones was tested using a dilution series of the (acylated) apigenin glycosides in phosphate buffer at pH 6.5. Self-associated complexes that are formed by π - π or CH- π stacking show a nonlinear relationship between the intensity of self-association induced absorbance and concentration of the flavones, because the complexes are disrupted below a certain concentration threshold (*i.e.*, < 1 mM).^[57] In our system, we observed a linear relationship between the concentration and absorbance at 400 nm (**Fig. S4.13**). This is an indication that the bathochromic shift of the (acylated) glycosides is not caused by self-association.

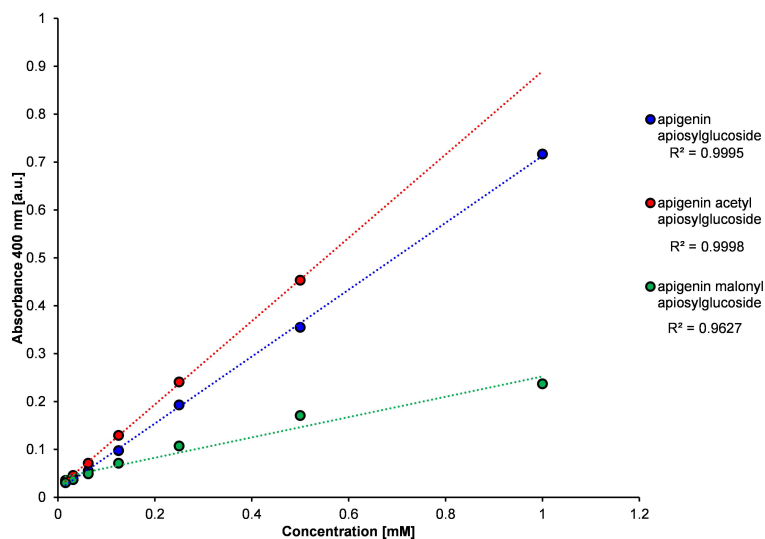


Figure S4.13. Absorbance at 400 nm of apigenin 7-*O*-apiosylglucoside, apigenin 7-*O*-(6''-*O*-acetyl)-apiosylglucoside, apigenin 7-*O*-(6''-*O*-malonyl)-apiosylglucoside at different concentrations of flavone and measured in phosphate buffer at pH 6.5. For apigenin 7-*O*-(6''-*O*-acetyl)-apiosylglucoside the point at 1 mM could not be taken into account because of precipitation at this concentration.

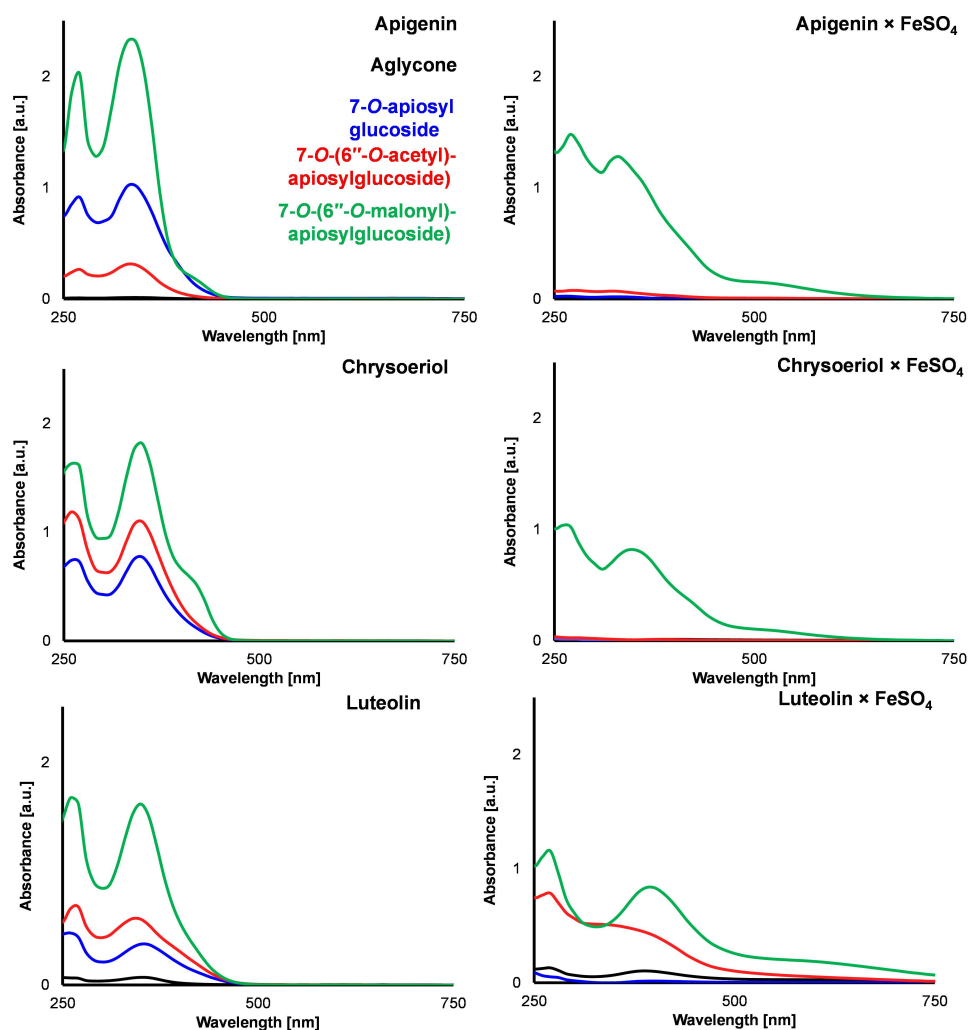


Figure S4.14. UV-Vis absorbance spectra of the WS fraction of acylated flavone glycosides at pH 6.5 (t=0) in absence and presence of equimolar concentration FeSO₄.

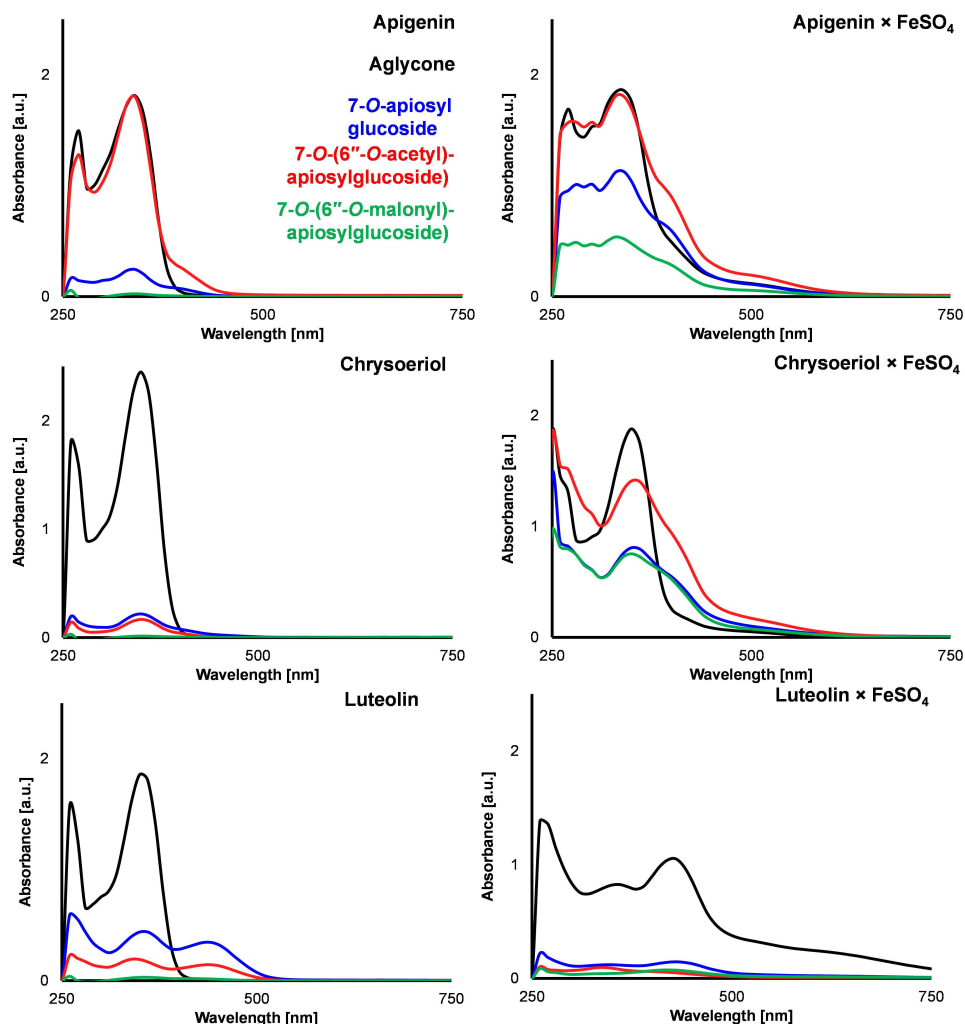


Figure S4.15. UV-Vis absorbance spectra of the DS fraction of acylated flavone glycosides at pH 6.5 ($t=0$) in absence and presence of equimolar concentration FeSO_4 .

The spectra of luteolin 7-O-apiosylglucoside and luteolin 7-O-(6''-O-acetyl)-apiosylglucoside in absence of iron show a shoulder band at 450 nm in the DS fraction. We suggest that the shoulder band that is observed here is probably caused by impurities that were present in the sample and not because of oxidation of the parent molecule. This is further confirmed by the fact that the new bands were also observed in the sample at t_0 , which was the sample before pH adjustment and incubation.

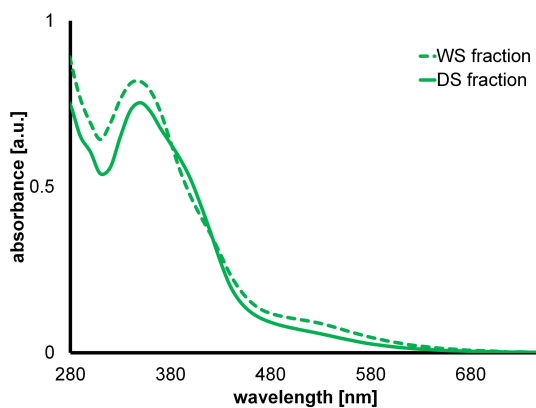


Figure S4.16. UV-Vis absorbance spectra of the WS fraction (dashed line) and DS fraction (solid line) of chrysoeriol 7-*O*-(6''-*O*-malonyl)-apiosylglucoside at pH 6.5 ($t=0$) in the presence of equimolar concentration FeSO_4 .

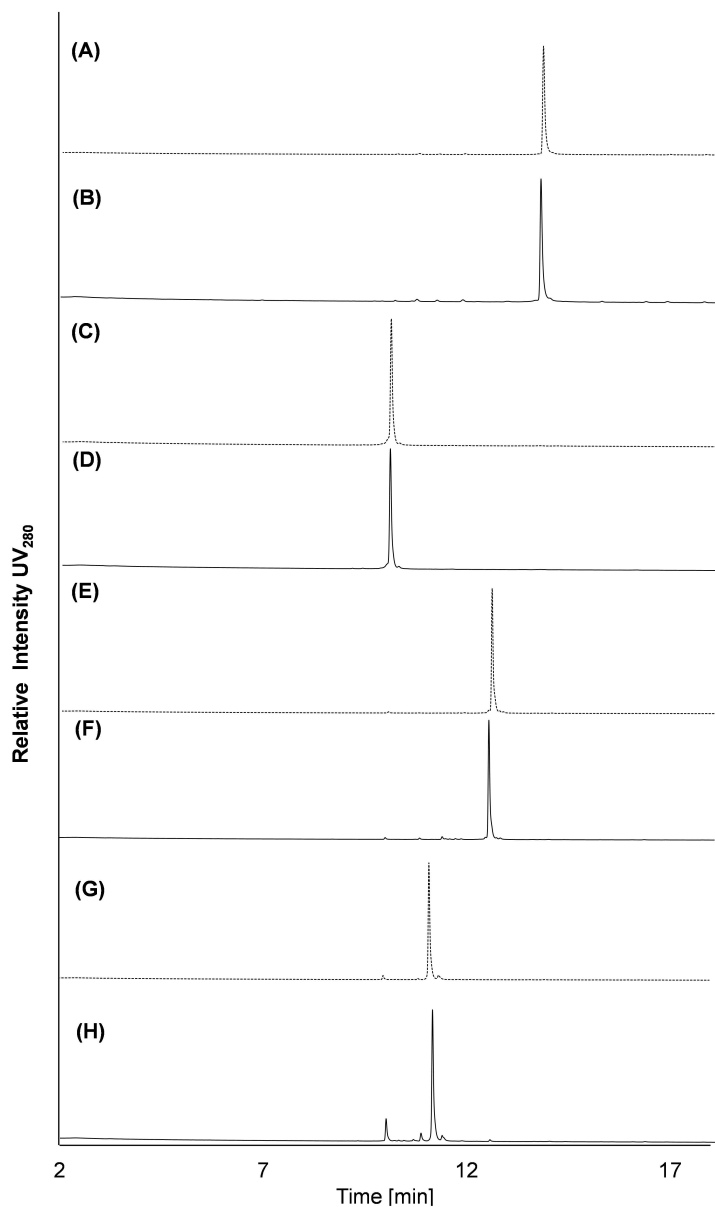


Figure S4.17. Combined RP-UHPLC-PDA (280 nm) chromatograms from the WS and DS fractions of (A) apigenin \times FeSO₄ (t_0); (B) apigenin \times FeSO₄ (t_{24}); (C) apigenin 7-*O*-apiosylglucoside \times FeSO₄ (t_0); (D) apigenin 7-*O*-apiosylglucoside \times FeSO₄ (t_{24}); (E) apigenin 7-*O*-6''-acetyl apiosylglucoside \times FeSO₄ (t_0); (F) apigenin acetyl 7-*O*-6''-apiosylglucoside \times FeSO₄ (t_{24}); (G) apigenin 7-*O*-6''-malonyl apiosylglucoside \times FeSO₄ (t_0); and (H) apigenin 7-*O*-6''-malonyl apiosylglucoside \times FeSO₄ (t_{24}).

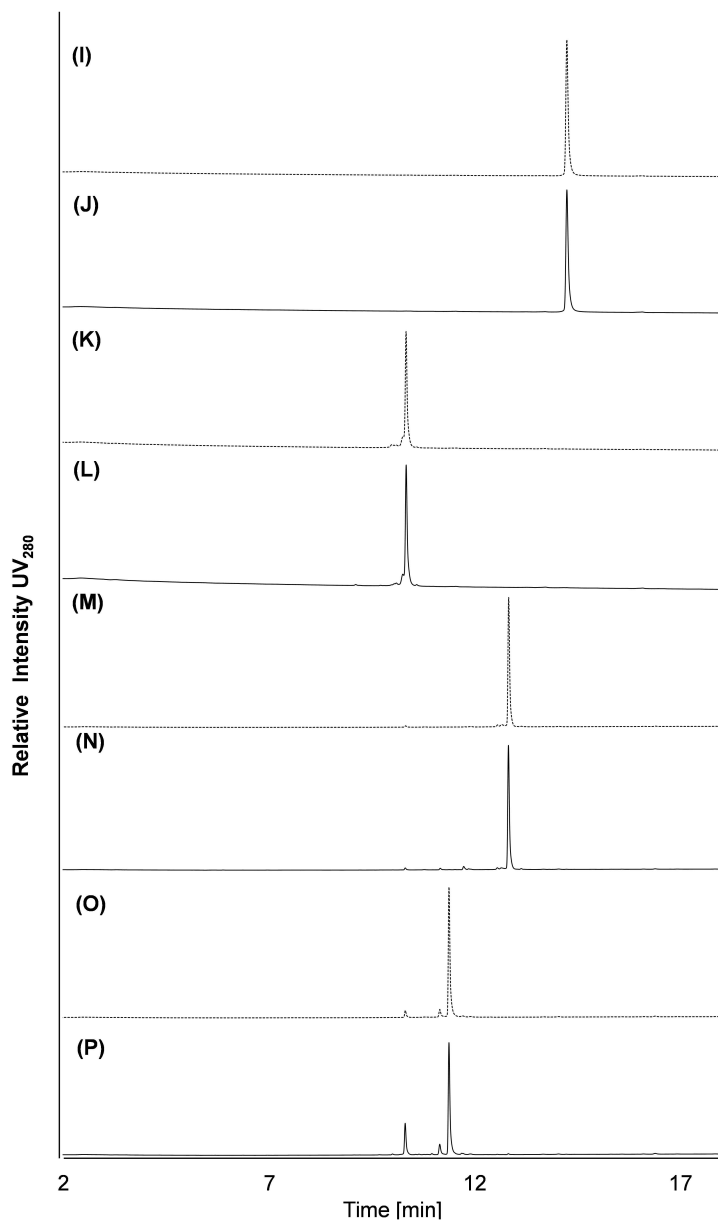


Figure S4.17. continued Combined RP-UHPLC-PDA (280 nm) chromatograms from the WS and DS fractions of (I) chrysoeriol \times FeSO_4 (t_0); (J) chrysoeriol \times FeSO_4 (t_{24}); (K) chrysoeriol 7-*O*-apiosylglucoside \times FeSO_4 (t_0); (L) chrysoeriol 7-*O*-apiosylglucoside \times FeSO_4 (t_{24}); (M) chrysoeriol 7-*O*-6''-acetyl apiosylglucoside \times FeSO_4 (t_0); (N) chrysoeriol 7-*O*-6''-acetyl apiosylglucoside \times FeSO_4 (t_{24}); (O) chrysoeriol 7-*O*-6''-malonyl apiosylglucoside \times FeSO_4 (t_0); and (P) chrysoeriol 7-*O*-6''-malonyl apiosylglucoside \times FeSO_4 (t_{24}).

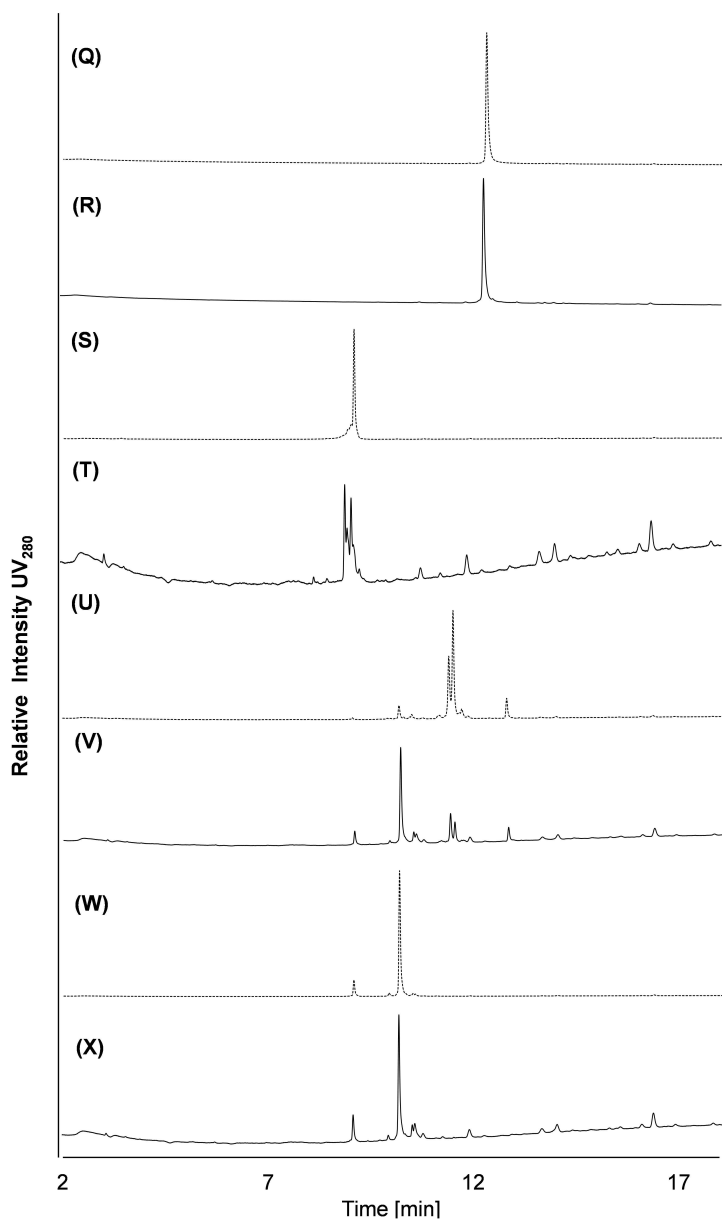


Figure S4.17. continued Combined RP-UHPLC-PDA (280 nm) chromatograms from the WS and DS fractions of **(Q)** luteolin \times FeSO_4 (t_0); **(R)** luteolin \times FeSO_4 (t_{24}); **(S)** luteolin 7-*O*-apiosylglucoside \times FeSO_4 (t_0); **(T)** luteolin 7-*O*-apiosylglucoside \times FeSO_4 (t_{24}); **(U)** luteolin 7-*O*-6''-acetyl apiosylglucoside \times FeSO_4 (t_0); **(V)** luteolin 7-*O*-6''-acetyl apiosylglucoside \times FeSO_4 (t_{24}); **(W)** luteolin 7-*O*-6''-malonyl apiosylglucoside \times FeSO_4 (t_0); and **(X)** luteolin 7-*O*-6''-malonyl apiosylglucoside \times FeSO_4 (t_{24}).

We also investigated the stability of the malonyl, acetyl, and apiosylglucosyl substituents in presence of iron. For the malonyl apiosylglucosides, we investigated the effect of iron on demalonylation and decarboxylation by screening for formation of the corresponding apiosylglucosides and acetyl apiosylglucosides over time in presence and absence of iron (**Fig. S4.18A**). In all tested samples demalonylation (~ 14 %) occurred more extensively than decarboxylation (~ 1 %) after 24 h incubation. For the acetyl apiosylglucosides, we investigated the effect of iron on deacetylation by screening for formation of the corresponding apiosylglucosides (**Fig. S4.18B**). The acetyl group was more stable than the malonyl group, as < 1 % of deacetylation was observed. No relationship between the presence of iron and demalonylation or deacetylation was observed. Moreover, no deglycosylation of the samples in absence or presence of iron was observed.

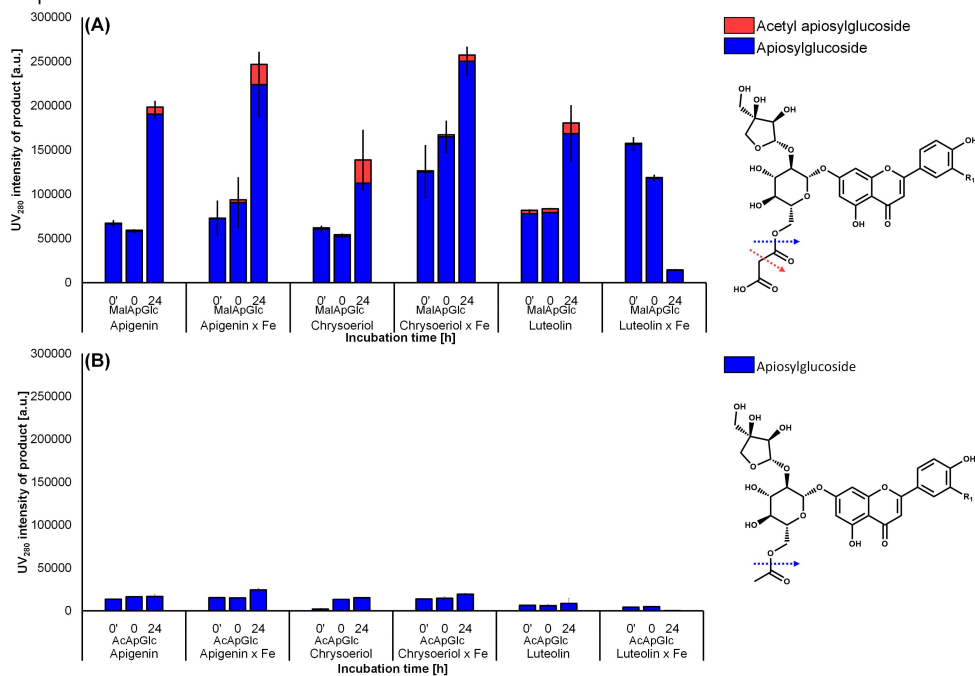


Figure S4.18. Stability of the malonylated (A) and acetylated (B) flavone 7-O-apiosylglucosides in presence or absence of equimolar concentration FeSO_4 before adjustment of the pH (t_0) and after 0 and 24 h of incubation at pH 6.5 in aqueous solution on product formation was investigated. Error bars indicate the standard deviation of independent duplicates.

PART II

Strategies to limit iron-phenolic mediated discolouration

Chapter 5

Chapter 6

Chapter 7

CHAPTER 5

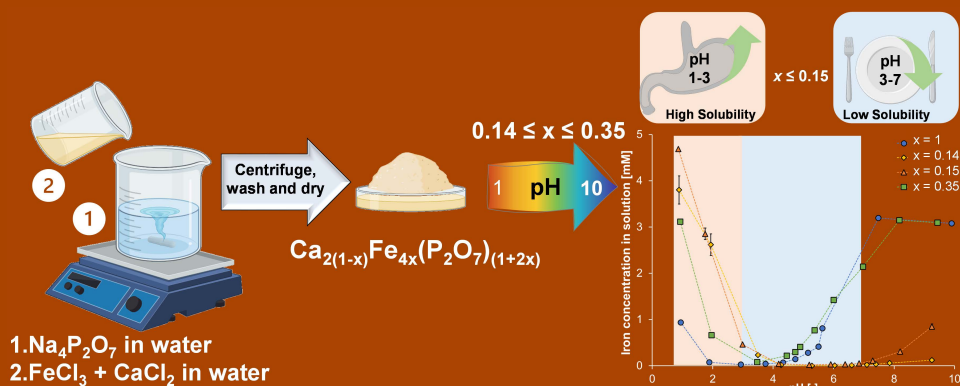
Design and characterisation of Ca-Fe(III) pyrophosphate salts with tuneable pH-dependent solubility for dual-fortification of foods

Judith Bijlsma, Neshat Moslehi, Wouter J.C. de Bruijn, Krassimir P. Velikov, Jean-Paul Vincken, and Willem K. Kegel

Based on: *Journal of Functional Foods*, 2022, 92:105066.

Abstract

Food-fortification using poorly water soluble mineral-containing compounds is a common approach to deliver iron. However, it comes with the challenge of ensuring iron bio-accessibility and limiting iron-phenolic interactions that can change sensory properties. Mixed Ca-Fe(III) pyrophosphate salts with the general formula $\text{Ca}_{2(1-x)}\text{Fe}_{4x}(\text{P}_2\text{O}_7)_{(1+2x)}$ were designed as a system for simultaneous delivery of iron and calcium. The salts were synthesised via a co-precipitation method and characterised by TEM-EDX, XRD, and FT-IR. All mixed salts with $0.14 \leq x \leq 0.35$ yielded homogenous amorphous particles. The iron dissolution from these mixed salts showed a fourfold increase at gastric pH compared to iron(III) pyrophosphate (Fe_4PP_3). In the food-relevant pH range, the salts with $x \leq 0.15$ showed up to an eight-fold decrease in iron solubility. Despite this, reactivity of the mixed salts in tea was similar to that of Fe_4PP_3 . Our results indicate that these mixed salts are potential dual-fortificants with tuneable iron content and solubility.



5.1. Introduction

Micronutrient fortification of foods can effectively overcome mineral and vitamin deficiencies.^[1,2] Among minerals, particularly iron receives significant attention since one-quarter of the world's population is affected by iron deficiency anaemia.^[3] However, iron is a challenging mineral to introduce to food products due to the high reactivity of 'free' iron ions.^[4] Iron compounds are highly reactive with food products because of the complexation and oxidation of iron with phenolics that are abundant in plants and vegetables.^[5-7] This reactivity of iron with phenolics is responsible for a change in the sensory properties of the food and compromises iron bioavailability.^[8,9] Several physical and chemical approaches are currently being used to control the reactivity of iron ions by limiting their exposure to reactive phenolics.^[4] One strategy is the micro-encapsulation of soluble iron-containing salts.^[10] However, encapsulated iron can lead to undesirable higher prices and therefore less acceptance by customers.^[11] Another approach for fortification of food products with iron is the use of strong molecular complexes such as FeEDTA (Ferrazone) which reduces the reactivity of Fe ions while providing similar relative bioavailability as ferrous sulphate.^[12] However, the relatively high costs and the concern that EDTA compounds may negatively influence the metabolism of other essential minerals, or increase absorption of potentially-toxic minerals limit consumer acceptance.^[3] Another commonly used strategy is the use of water insoluble, or poorly soluble salts such as iron (III) pyrophosphate (FePP; Fe_4PP_3).^[13-15]

In food research, Fe_4PP_3 receives extensive attention and it is often used in iron fortification of food products such as infant cereal and chocolate drink powders.^[16-18] The low solubility of iron from Fe_4PP_3 reduces the impact of Fe_4PP_3 on the sensory properties of the fortified food but also results in low iron bioavailability.^[9] Micronisation (*i.e.* downsizing the particle size to the micron range, *e.g.* 0.3 to 0.5 μm) and emulsification techniques have been used to improve the bioavailability of Fe_4PP_3 . The high costs of micronised Fe_4PP_3 currently limit its use.^[19,20] Even though the solubility of (micronised) Fe_4PP_3 is limited in the pH range of 3-6, the addition of Fe_4PP_3 to phenolic-rich foods or model systems still results in discolouration.^[4,21]

Iron (III) pyrophosphate has also been incorporated with secondary minerals for higher efficiency and multipurpose applications.^[22,23] An example of this is the co-fortification of Fe_4PP_3 with zinc sulphate in extruded rice.^[24] Furthermore, Fe_4PP_3 has been used in combination with citric acid or trisodium citrate in rice grains and with sodium pyrophosphate in bouillon cubes for relatively higher storage stability.^[25,26] Inspired by nature, the main goal of this work is to integrate iron ions in an inorganic poorly water soluble matrix of another mineral as a carrier. For example, anastaseite ($\text{CaFe}^{\text{II}}\text{P}_2\text{O}_7$)^[27] and anapaite ($\text{Ca}_2\text{Fe}^{\text{II}}(\text{PO}_4)_2 \cdot 4\text{H}_2\text{O}$)^[28,29] are naturally occurring but not necessarily edible mixed phosphates of multivalent metal salts.^[29,30] We particularly focus on pyrophosphate salts because pyrophosphate anions form colourless and/or

white and water insoluble compounds with most metals.^[14,15,31] To maintain the sensory properties and (chemical) stability of the iron-fortified food, iron dissolution from the iron-containing compound should ideally be limited in the pH range from 3-7, which is the pH range of most common food and beverages.^[4] The insolubility of the iron ions in the pH range from 3-7 will suppress iron-mediated reactivity in the food.^[21] Additionally, to ensure bio-accessibility of iron, dissolution of iron from the iron-containing compound should be fast in gastric (*i.e.* pH 1-3) and/or intestinal (*i.e.* pH 6-8) conditions.^[32-34] It should be noted that although bio-accessibility (*i.e.* the quantity of iron in solution and available for absorption in the gastrointestinal tract) is a prerequisite for bioavailability, it cannot directly be correlated to iron bioavailability, which also includes digestion, absorption, and metabolism.^[34] Fe_4PP_3 salt has low solubility (< 5 %) at pH 3 with increased solubility to > 99 % at pH 7-8.^[14] whereas the pyrophosphate salts of divalent metals, such as calcium pyrophosphate (Ca_2PP), dissolve well (> 99 %) at pH 3 but are poorly soluble (< 5 %) at pH 7-8.^[35] Doping of iron (III) oxide with calcium has previously shown improved iron solubility in dilute acid and sensory characteristics in fortified foods.^[23,36] Additionally, van Leeuwen and co-authors have shown that incorporation of an excess of Mg in Fe_4PP_3 (*i.e.* Mg:Fe(III) ratio 50:1), reduced its reactivity towards phenolics.^[22] Due to the reversed solubility character of Ca_2PP and Fe_4PP_3 salts, it is expected that the combination of Ca and Fe(III) in one matrix will result in unique pH-dependent dissolution behaviour. Although any non-iron divalent metal (*e.g.* Zn, Ca, Mg, or Mn) could be used, Ca is selected due to its higher recommended nutrient intake and consequently less risk of overdosing compared to the other divalent metals.^[3,37] Besides decreasing the reactivity of iron by embedding it in another less chemically reactive mineral carrier, the main advantage of these systems is that they can be used for simultaneous delivery of another essential mineral along with iron, in this case calcium.

In this study, we explore the possibility to design mixed Ca-Fe(III) pyrophosphate salts with the general formula, $\text{Ca}_{2(1-x)}\text{Fe}_{4x}(\text{P}_2\text{O}_7)_{(1+2x)}$ ($0 \leq x \leq 1$), as a potential delivery system for two essential minerals. To this end, we develop a detailed synthesis for and perform in-depth characterisation of such mixed salts. The range of the ratios of iron to calcium is guided by the Recommended Dietary Allowance (RDA). Co-precipitation is used as a synthesis method to embed iron (III) ions homogenously into the calcium pyrophosphate matrix structure. After characterisation of the salts, the pH dependence of the dissolution behaviour of the mixed Ca-Fe(III) pyrophosphate salts with various Ca:Fe(III) ratios are investigated. Then, the effect of three food-relevant temperatures (23, 37, and 90 °C), as well as the dissolution time, are investigated. Finally, the designed salts are tested for their reactivity using a black tea model solution. The main aim of this study is to design mixed Ca-Fe(III) pyrophosphate salts with three main properties: (i) maximum iron content in which no physical segregation occurs, (ii) increased solubility at gastric/intestinal pH, and (iii) reduced iron solubility at food pH and thus decreased reactivity compared to iron (III) pyrophosphate.

5.2. Materials & methods

5.2.1. Materials

Iron (III) chloride hexahydrate ($\text{FeCl}_3 \cdot 6\text{H}_2\text{O}$, > 99 wt. %), tetrasodium pyrophosphate decahydrate ($\text{Na}_4\text{P}_2\text{O}_7 \cdot 10\text{H}_2\text{O}$, > 99 wt. %), calcium dichloride (CaCl_2 , > 93 wt. %), nitric acid (HNO_3 , 65 wt. %), 3-(2-pyridyl)-5,6-diphenyl-1,2,4-triazine-*p,p'*-disulfonic acid monosodium salt hydrate (*i.e.* ferrozine; ≥ 97 wt. %), hydrochloric acid (HCl , 37 wt. %), sodium hydroxide (NaOH , ≥ 98 wt. %), and iron (II) sulphate heptahydrate ($\text{FeSO}_4 \cdot 7\text{H}_2\text{O}$, ≥ 99 wt. %) were obtained from Sigma Aldrich (St. Louis, MO, USA). Ethanol absolute (≥ 99 wt. %) and ascorbic acid (≥ 99 wt. %) were obtained from VWR International (Radnor, PA, USA). The Milli-Q (MQ) water used was deionised by a Millipore Synergy water purification system (Merck Millipore, Billerica, MA, USA). The tea used for preparing the tea solutions was an Original English tea blend from Pickwick (Amsterdam, The Netherlands).

5.2.2. Preparation of pure and mixed salts

Pure salts

Pure salts were synthesised as references for comparative purposes. The preparation procedure was a co-precipitation method similar to the methods described elsewhere.^[15,31] Firstly, solutions of 0.857 mmol $\text{FeCl}_3 \cdot 6\text{H}_2\text{O}$ and 1.286 mmol CaCl_2 in 50 mL of MQ water were prepared independently. Following this, the solutions were added quickly (within 5 seconds) to a solution of 0.643 mmol $\text{Na}_4\text{P}_2\text{O}_7 \cdot 10\text{H}_2\text{O}$ (Na_4PP) in 100 mL of MQ water to prepare iron (III) pyrophosphate ($\text{Fe}_4(\text{P}_2\text{O}_7)_3$, Fe_4PP_3) and calcium pyrophosphate ($\text{Ca}_2\text{P}_2\text{O}_7$, Ca_2PP), respectively. This was done while the Na_4PP solution was stirred vigorously (~ 400 rpm) with a magnetic stir bar. In both cases, a turbid white dispersion was formed a few seconds after the addition. The samples were then centrifuged at $3273 \times g$ for 15 minutes in 50 mL volume polypropylene conical centrifuge tubes using an Allegra X-12R Centrifuge (Beckman Coulter, Brea, CA, USA). This was followed by washing the precipitate with MQ water twice. The sediment was then post-treated by ultrasonication at 40 kHz for 10 minutes using a CPX8800H ultrasonic cleaning bath (Branson Ultrasonics™, Brookfield, CT, USA), after which they were dried overnight in an oven at 45 °C (Fe_4PP_3 : 59 % yield, Ca_2PP : 74 % yield).

Mixed metal salts

The mixed Ca-Fe(III) salts were prepared by the same procedure as the pure salts, by the addition of 50 mL of a mixed solution of $\text{FeCl}_3 \cdot 6\text{H}_2\text{O}$ and CaCl_2 in MQ water to a solution of Na_4PP with a fixed concentration of pyrophosphate ions (6.43 mM, 100 mL). Eight different salts containing different Ca to Fe(III) ratios were prepared, generally coded as $\text{Ca}_{2(1-x)}\text{Fe}_{4x}(\text{P}_2\text{O}_7)_{(1+2x)}$ ($0 < x < 1$), for different theoretical *x*-values (*i.e.* 0.005, 0.006, 0.007, 0.011, 0.021, 0.051, 0.100 and 0.260, coded as Mix1 to Mix8). After adding the mixed solution to Na_4PP the eight solutions were stirred vigorously (~ 400 rpm) with a magnetic stir bar (final concentration of Na_4PP : 4.29 mM). In all ratios, a turbid

white or off-white dispersion was formed a few seconds after the addition. The samples were then centrifuged, washed, post-treated in an ultrasonic bath, and dried in an oven following the same procedures as explained for the pure salts, see **section 5.2.2**. It is worth recalling here that the x-values in the general formula indicate the mineral composition of the salts. These values were chosen based on average nutritional requirements for the human body (*i.e.* 1000 mg calcium and 15 mg iron intake per day.^[38] Consequently, the mole ratios were calculated based on which the x-value was found in the structural formula. The molar ratio of total metal ions (*i.e.* [Ca] + [Fe], final concentration: 8.573 mM) to pyrophosphate ions was based on the stoichiometry of Ca₂PP. The average yield of the prepared mixed salts was 67.3 ± 4.2 %. Standard deviation was calculated based on three independent syntheses of all the mixed salts.

5.2.3. Characterisation methods

Transmission electron microscopy (TEM) and energy-dispersive X-ray spectroscopy (EDX)

Water dispersions of the salts were dried on a carbon-coated copper grid and analysed by transmission electron microscopy (TEM) and energy-dispersive X-ray spectroscopy (EDX). This was performed on a Talos™ F200X (Thermo Fisher Scientific, San Jose, CA, USA) operated at 200 kV. The elemental composition of the mixed salts was obtained from EDX and used for finding the experimental x-value based on the general formula of the mixed salts. The ratios of the atomic percentages (*i.e.* Ca/Fe = $2(1-x)/4x$, Ca/P = $2(1-x)/2(1+2x)$, Fe/P = $4x/2(1+2x)$) were used to find x in the structural formula Ca_{2(1-x)}Fe_{4x}(P₂O₇)_(1+2x). The average x-value for each mixed salt was reported with a standard deviation based on 3 replicate preparations of the salts and 3 independent measurements. The average x-values were incorporated in the general formula of the mixed Ca-Fe(III) pyrophosphate salts to obtain the final chemical formula of the salts. For the salts with heterogeneous morphology, this procedure was done separately on the different morphological phases.

High-angle annular dark field scanning TEM (HAADF-STEM)

High-angle annular dark-field scanning TEM (HAADF-STEM) was performed on a Talos™ F200X (Thermo Fisher Scientific, San Jose, CA, USA) operated at 200 kV. The elemental mapping was recorded by use of assigning a colour to each element. Colour indications are as follows: calcium: green, iron: red, and phosphorus: blue.

X-Ray diffraction (XRD) spectroscopy

The dried powders of the salts were analysed at room temperature with an AXS D2 Phaser powder X-ray diffractometer (Bruker, Billerica, MA, USA), which was equipped with a LYNXEYE detector in Bragg-Brentano mode. The radiation used was cobalt K α 1,2, λ = 1.79026 Å, operated at 30 kV, 10 mA for 2 θ = 5 to 70 degrees. A silicon holder was used and the measurements were repeated twice on the salts from independent synthesis batches.

Fourier transform infrared (FT-IR) spectroscopy

FT-IR measurements were done on dried powders of the samples by an FT-IR spectrometer (PerkinElmer, Waltham, MA, USA), using the KBr pellet technique.^[39] 2.5 mg of each salt was mixed thoroughly with 250 mg of KBr (FT-IR grade) and dried in an oven at 60 °C overnight. Pellets were prepared using a press and the measurements were done in independent duplicates. The interferograms were accumulated over the spectral range of 1600 – 400 cm⁻¹ using a nominal resolution of 4 cm⁻¹, with a background spectrum recorded before each measurement.

5.2.4. Dissolution behaviour of iron in Fe₄PP₃ and the mixed Ca-Fe(III) pyrophosphate salts

To perform the iron dissolution measurements, the synthesis of the pure Fe₄PP₃ and Ca₂PP as well as the mixed Ca-Fe(III) pyrophosphate salts with measured $0.14 \leq x \leq 0.35$ were up-scaled, **Method S5.1**. The dried powders of the salts were then redispersed by stirring (~250 rpm) with a magnetic stir bar in MQ water (final concentrations: 10 mg mL⁻¹). Next, the pH of the dispersions was adjusted using a pH-stat device (Metrohm, Herisau, Switzerland) by the addition of 0.1 M HCl or 0.1 M NaOH. Subsequently, all dispersions were incubated at 1000 rpm using an Eppendorf Thermomixer F1.5 (Eppendorf, Hamburg, Germany) at pH values ranging from one to eleven (steps of one pH unit), over time (1, 2, and 48 h), and at three different temperatures (23, 37, and 90 °C). After incubation, the pH of each sample was measured again to determine the final pH. Finally, the samples were centrifuged at 15,000 × *g* for 10 minutes using an Eppendorf Centrifuge 5415R and the supernatants were separated to quantify the dissolved iron concentration.

Iron concentration measurement by ferrozine-based colourimetric assay

Total iron in solution was quantified using a ferrozine-based colourimetric assay.^[40] Binding of Fe(II) to 3-(2-pyridyl)-5,6-diphenyl-1,2,4-triazine-*p,p'*-disulfonic acid (*i.e.* ferrozine) results in the formation of a complex with absorbance at 565 nm.^[6] To ensure the reduction of Fe(III) to Fe(II), first an excess of ascorbic acid (50 µL, 100 mM) was added to 50 µL sample (supernatant). After 30 min incubation of the sample with ascorbic acid, ferrozine (50 µL, 10 mM) was added. Samples were transferred to 96-well microplates and the absorbance at 565 nm was measured at room temperature in a SpectraMax iD3 (Molecular Devices, Sunnyvale, CA, USA). All measurements were performed in duplicate and quantification of total dissolved iron was performed based on intensity (*A*_{565 nm}) with a calibration curve of FeSO₄ (0.0078 – 1 mM, *R*² > 0.99). It was confirmed that the presence of the Ca ion did not interfere with the quantification of total iron (**Fig. S5.1**). The pH of the samples was measured after the addition of ascorbic acid and ferrozine. Most samples had a pH of 2.7, except for the samples that were prepared at very acidic conditions (*i.e.* pH < 2). The pH of these samples after the addition of ascorbic acid and ferrozine was 1.7 ± 0.3. At this pH, less Fe(II)-ferrozine complex is formed.^[40] We corrected the absorbances of these acidic samples using the pH-dependent absorbance factors previously reported for the Fe(II)-ferrozine

complex formation.^[40] The iron quantification by the ferrozine assay was verified independently using inductively coupled plasma–atomic emission spectroscopy (ICP-AES), **Method S5.2**.

To test if the trend in iron dissolution was statistically significant, ANOVA analysis was performed using IBM SPSS Statistic v23 software (SPSS Inc., Chicago, IL, USA). Tukey's *post hoc* comparisons (significant at $p < 0.05$) were carried out to evaluate the significance of differences in iron concentration.

5.2.5. Assessment of the reactivity of selected mixed salts in a black tea solution

To assess the reactivity of the iron in the mixed Ca-Fe(III) pyrophosphate salts, a black tea solution was used as a model system. Ground tea leaves of Original English blend (Pickwick) were added to boiling MQ water (1 g of tea leaves in 100 mL of water). After stirring for 3 minutes, the tea leaves were filtered out using 1541-125 cellulose filter papers (Whatman, Maidstone, UK). Selected mixed and pure Fe_4PP_3 salts with a normalised concentration of iron (*i.e.* 1.05 mg Fe in 100 mL tea) were added to the tea solution ($\text{pH } 5.13 \pm 0.13$). For comparison, Ca_2PP with a normalised concentration of 2.31 mg Ca in 100 mL tea (*i.e.* the concentration of Ca in the salt with the highest calcium content) was added as well. After stirring for 10 minutes using an RCT basic stirrer (IKA-Werke, Staufen, Germany), the tea solutions were filtered first over Whatman cellulose filter papers and second over a 17845-ACK Minisart NY polyamide (nylon) filter with 0.2 micron pore size, (Sartorius, Göttingen, Germany). During the procedure, the temperature was kept constant at approximately 90 °C in all steps. The residues on the filter papers were washed with ethanol to remove any unbound phenolics from the particle surface. The discolouration of the filtered tea solutions was quantified by ultraviolet-visible light (UV-Vis) spectroscopy at room temperature. UV-Vis spectra of the tea solutions were recorded on a Lambda-35 spectrophotometer (PerkinElmer, Waltham, MA, USA), using quartz cuvettes. The increase in absorbance at 550 nm compared to the blank black tea solution was used to quantify the iron-phenolic complexation.^[13] All the measurements were done in independent triplicates and the average values along with standard deviations were reported. The colours of the tea solutions were visualised by taking an image of all tea solutions standing next to each other illuminated with a uniform light source at room temperature. The images were evaluated using an online colour conversion tool (<https://imagecolorpicker.com>) and converted to the $L^*a^*b^*$ colour space (*i.e.* L^* dark or light, a^* red vs green, b^* yellow vs. blue) (**Table S5.1**).

The concentration of the iron released from the salts in the tea solutions was measured by elemental analysis using ICP-AES. ICP-AES was performed on the tea solutions using an Optima 8300 instrument (PerkinElmer, Waltham, MA, USA). Electrodeposited samples were dissolved in 10 mL of a 2 % HNO_3 solution to achieve

optimal measurement concentration ranges. The measurements were performed in triplicates. Statistical analysis was carried out to evaluate the significance of differences in iron concentration (significant at $p < 0.05$).

5.3. Results & discussion

5.3.1. Characterisation of the pure calcium and iron(III) pyrophosphate salts

The morphology of the pure Ca_2PP and Fe_4PP_3 salts was analysed by electron microscopy (**Fig. 5.1**). The dried dispersions of Ca_2PP and Fe_4PP_3 showed noticeably different morphologies. The TEM images for Ca_2PP showed large micron-sized needle-shaped aggregates (**Fig. 5.1A**), which is in line with a previous study.^[41] However, the TEM image results for Fe_4PP_3 showed formation of large interconnected aggregates of roughly 25 nm irregularly shaped particles, see **Fig. 5.1B**.

It has been previously shown that the degree of crystallinity in metal pyrophosphate particles can strongly depend on the valence of the metal ion.^[15] This has been confirmed by XRD and FT-IR spectra of the pure Ca_2PP and Fe_4PP_3 salts in this work as well. The X-ray diffraction pattern for Ca_2PP indicated clear signals of crystallinity, while the spectrum for Fe_4PP_3 showed only noise and a broad peak indicating an amorphous structure for this salt (**Fig. 5.1C**). The XRD patterns of Ca_2PP and Fe_4PP_3 are consistent with previous studies.^[15,31] However, we observed a strong, sharp signal at approximately $2\theta = 9.2$ degree for Ca_2PP (**Fig. 5.1C**) that was not observed previously.^[15,31] This could be because of different crystalline structures from the fast co-precipitation method compared to the preparation of colloidal particles,^[15] or solid-state preparation at high temperatures.^[42] Moreover, ultrasonication treatment on the salts could have led to induced crystallinity and heterogenous nucleation.^[43] The observed amorphous structure of Fe_4PP_3 is suggested to be a result of the so-called valence mismatch of the metal (Fe^{3+}) and pyrophosphate ($\text{P}_2\text{O}_7^{4-}$) ions.^[31] Therefore, the complicated stoichiometry to reach neutrality results in an amorphous matrix for Fe_4PP_3 in a fast co-precipitation process, while calcium and pyrophosphate ions can form electroneutral crystalline unit cells more easily.^[15]

The details of chemical bonding in both the Ca_2PP and Fe_4PP_3 were investigated by FT-IR spectrometry (**Fig. 5.1D**). The FT-IR spectrum for Ca_2PP showed sharp and well-defined bands, whereas the peaks appeared broad and smooth for Fe_4PP_3 at the same wavenumbers. The sharper and well-defined bands were expected for crystalline materials. Spectral broadening in Fe_4PP_3 was a result of the pyrophosphates having to accommodate more types of bonding to reach neutrality,^[44] and indicates the amorphous nature of Fe_4PP_3 .^[15,45] Despite different broadness, the peak positions of the main peaks matched with each other because the pyrophosphate groups are the main vibrationally active species. The characteristic peaks attributed to bending for O-P-O bonds in the P_2O_7 groups appeared around $500\text{--}600\text{ cm}^{-1}$. The signals observed

at 745 and 945 cm^{-1} were assigned to symmetric and asymmetric vibrations in P-O-P, respectively, and the peaks in the range of 1000 to 1200 cm^{-1} corresponded to P-O stretching vibration frequencies. All the peaks observed for the $\text{P}_2\text{O}_7^{4-}$ anion are similar to previous reports.^[45-47]

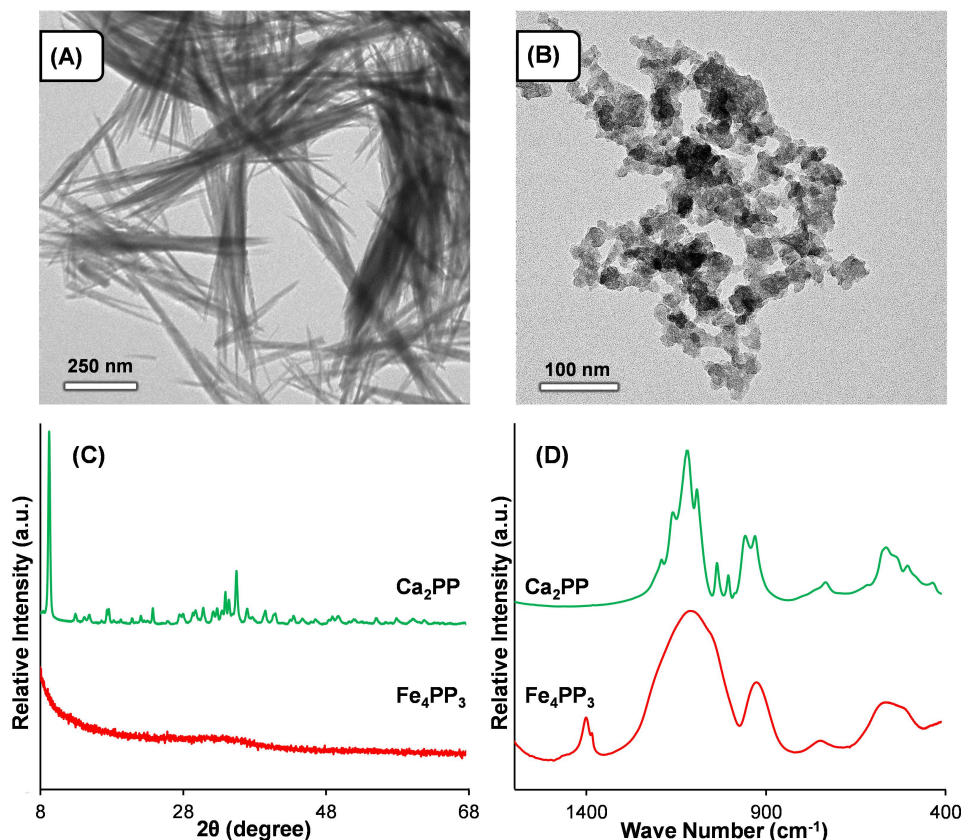


Figure 5.1. TEM images of (A) Ca_2PP and (B) Fe_4PP_3 , representing the difference between calcium and iron(III) pyrophosphate salt morphologies. Ca_2PP forms large aggregates of micron-sized needles whereas Fe_4PP_3 yields large interconnected aggregates of approximately 25 nm irregularly shaped particles. (C) Comparison between XRD patterns of the two pure pyrophosphate salts shows that Ca_2PP is crystalline, whereas Fe_4PP_3 is amorphous. (D) For the same reason, the FT-IR absorbance of the chemical bonds in the pyrophosphate ions appears sharp and strong for Ca_2PP , and broad and smooth for Fe_4PP_3 .

5.3.2. Characterisation of the mixed Ca-Fe(III) pyrophosphate salts

The morphology and chemical composition of the mixed metal salts, designed with $0.005 \leq x \leq 0.260$ in the general formula $\text{Ca}_{2(1-x)}\text{Fe}_{4x}(\text{P}_2\text{O}_7)_{(1+x)}$, (coded as Mix1-Mix8) were characterised by electron microscopy (Fig. 5.2). TEM images of the salt with the lowest iron content, Mix1, indicated a single phase of micron-sized needle-shaped aggregates (Fig. 5.2A). The measured x -value was 0.009, as determined from EDX measurements, (Fig. 5.2B).

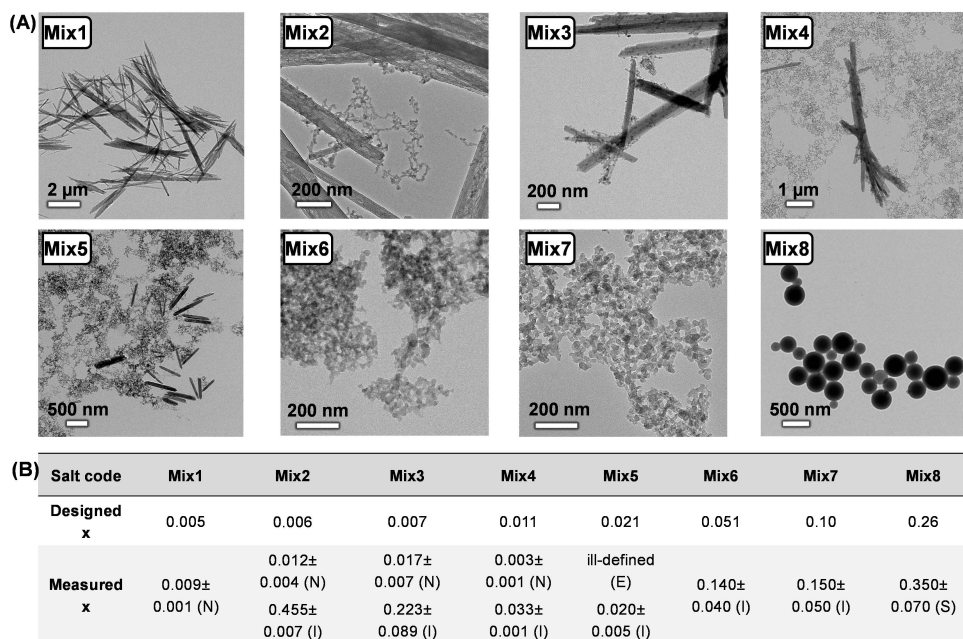


Figure 5.2. (A) Morphology of the mixed Ca-Fe(III) pyrophosphate salts with the general formula $\text{Ca}_{2(1-x)}\text{Fe}_x(\text{P}_2\text{O}_7)_{(1+2x)}$, coded as Mix1 to Mix8, obtained from TEM imaging. Comparison indicates that the iron-containing salts Mix1 and Mix6 to Mix8 are present in identical homogenous morphologies, whereas the samples Mix2 to Mix5 show segregation into two coexisting structural phases. (B) The measured x-value for the mixed Ca-Fe(III) pyrophosphate salts obtained from EDX quantification. Salts Mix2 to Mix5 show different measured x-values for the coexisting morphologies, while the salts Mix1 and Mix6 to Mix8 have identical x-values. The morphology of the aggregates is indicated by (N) needle-shaped, (I) irregularly shaped, (E) ellipse-shaped, and (S) spherical.

Detailed analysis of the TEM images and EDX results suggest that integrating Fe(III) as a second metal in the Ca_2PP matrix can yield local segregation and coexistence of two morphological phases: a crystalline needle-shaped phase with relatively low Fe content, and amorphous irregularly shaped aggregates with higher Fe content (*i.e.* higher x-value). Samples Mix2 to Mix5 appeared to be a mixture of an iron-rich phase (mostly irregularly shaped particles) and a calcium-rich phase (needle-shaped particles) (Fig. 5.2A). EDX quantification indicated that the sample Mix2 is a mixture of micron-sized needles with $x = 0.012$ and irregularly shaped aggregates with $x = 0.455$ (Fig. 5.2B). Similarly, in both samples, Mix3 and Mix4, micron-sized needles and irregularly shaped aggregates were in coexistence, and the latter yielded higher x-values. In the case of the sample Mix5, the measured x-value was equal to 0.020 for the irregularly shaped aggregates, while the ellipse-shaped aggregates remained ill-defined in this salt. These ill-defined particles can be oxide or hydroxide sediments of iron (III) formed during the synthesis or drying procedures (Fig. 5.2A and Fig. S5.2). The formation of the Ca-rich and Fe-rich phases of particles, resulting in different

measured x -values (from EDX quantification), might be explained by the possibility of phase separation in the resulting solid solutions.^[48,49] The salts Mix6 to Mix8 showed uniform morphologies and chemical compositions. For Mix6 and Mix7, irregularly shaped aggregates of 50 to 80 nm in size were observed, (**Fig. 5.2A**). These morphologies were similar to the Fe_4PP_3 particle morphology and the x -values corresponding to these two salts were measured to be 0.140 and 0.150, respectively (**Fig. 5.2B**). Interestingly, TEM images of the mixed salt with the highest iron content, Mix8, showed almost perfect spherical particles (**Fig. 5.2A**), for which the x -value was measured to be 0.350 from EDX quantification (**Fig. 5.2B**). The formation of well-defined needle-shaped or spherical particles can be caused by the ultrasonication treatment in the preparation method. Ultrasound energy fields have been shown to aid shape changes in particles by locally overcoming energy barriers for specific structures (**Fig. S5.3**).^[50] The possible effects of ultrasonication are currently being studied separately.

The elemental distribution in the mixed Ca-Fe(III) pyrophosphate salts with uniform morphologies (*i.e.* measured $0.14 \leq x \leq 0.35$) was explored by HAADF-STEM. Homogenous distribution of the elements Ca, Fe and P was observed by elemental mapping of the mixed salts Mix6 to Mix8 (**Fig. 5.3A**). The corresponding dark-field scanning TEM images of each elemental mapping are shown in **Fig. 5.3B** as well.

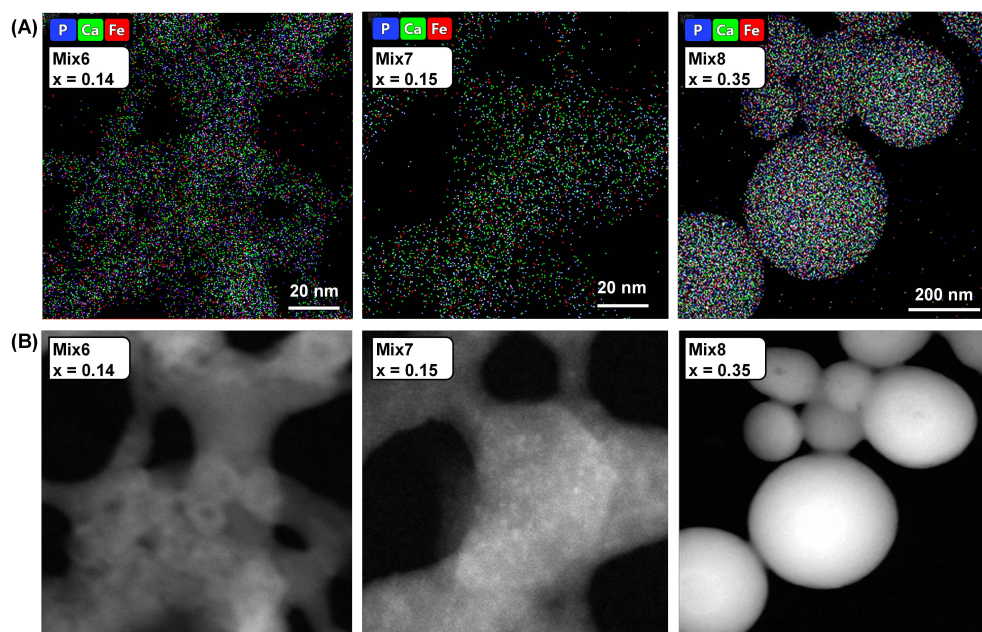


Figure 5.3. (A) Elemental mapping performed by HAADF-STEM on Mix6 ($x = 0.14$), Mix7 ($x = 0.15$) and Mix8 ($x = 0.35$). Colour indications are as follows: calcium (Ca): green; iron (Fe): red; and phosphorous (P): blue. Elemental mapping clearly shows homogeneous distribution of the elements in these salts. (B) The corresponding dark-field images.

The crystallinity of the mixed Ca-Fe(III) pyrophosphate salts was investigated by X-ray powder diffraction analysis (Fig. 5.4A). The XRD patterns of the mixed salts were not in agreement with any existing XRD reference patterns in the international centre for diffraction data (ICDD, <https://www.icdd.com>). In general, comparing the XRD patterns of the mixed salts to the diffraction peaks of the Ca_2PP specified the gradual transformation of crystalline structures upon increasing iron content in these samples. Similar to the Ca_2PP , the XRD patterns of the mixed Ca-Fe(III) pyrophosphate salts Mix1 to Mix5 (*i.e.* measured $0 \leq x < 0.14$), show consistent sharp signals which were clear signs of crystalline structures in these salts.^[15] The intensity of the diffraction peak at 9.2 degree (peak a), which appeared sharp and strong for Ca_2PP , decreased in the mixed Ca-Fe(III) pyrophosphate salts. Ultimately, this peak disappeared in the salt Mix4.

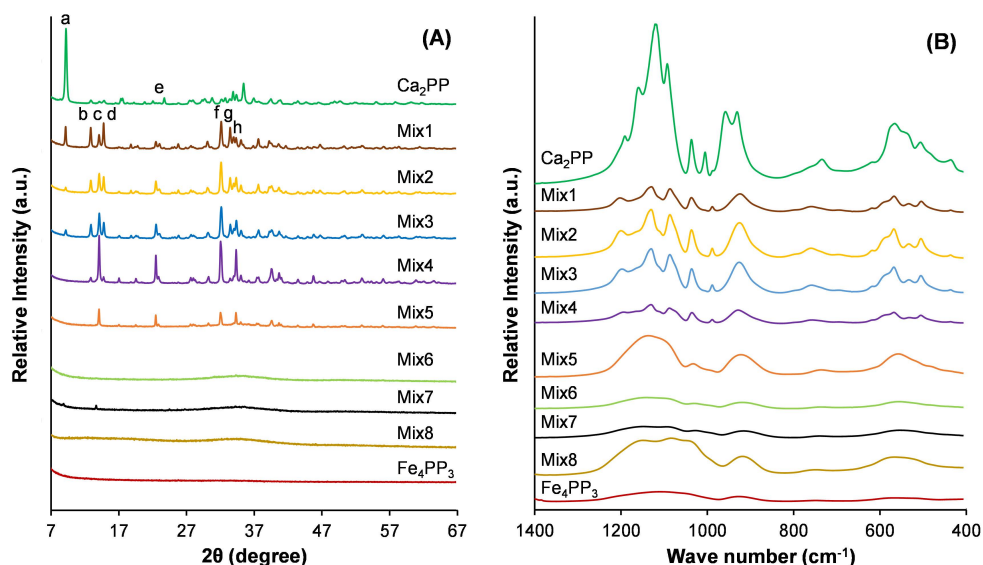


Figure 5.4. (A) XRD and (B) FT-IR spectra of the mixed Ca-Fe(III) pyrophosphate salts with the general formula $\text{Ca}_{2(1-x)}\text{Fe}_x(\text{P}_2\text{O}_7)_{(1+2x)}$ ($0 < x < 1$). The spectra of the pure Ca_2PP ($x = 0$) and Fe_4PP_3 ($x = 1$) are shown for comparison. (A) For the salts Mix1-Mix5 and Ca_2PP ($0 \leq x < 0.14$) samples show clear signals for crystalline structure. The spectra for the salts Mix6-Mix8 and Fe_4PP_3 ($0.14 \leq x \leq 1$) exhibit broad smooth peaks which indicate amorphous structures. (B) Positions of the peaks correspond to the chemical bonds in the pyrophosphate ions coincide between the mixed salts. Sharp and strong peaks are observed for the crystalline pyrophosphate salts Mix1-Mix5 and Ca_2PP ($0 \leq x < 0.14$), whereas broad and smooth peaks are obtained for the amorphous salts Mix6-Mix8 and Fe_4PP_3 ($0.14 \leq x \leq 1$).

The diffraction patterns of the mixed salts in the range of 13-15 degrees (peaks b-d), 22.5 degree (peak e), and 32-34 degrees (peaks f-h) indicate the presence of distinct crystalline phases and polymorphs in their structures. Peaks b, d, and g appeared with maximum intensity in the salt Mix1. A gradual decrease was observed upon increasing iron content in the salts Mix2, Mix3, and Mix4, and eventually, the peaks disappeared in the salt Mix5. Furthermore, the reflections c, e, f, and h slightly grew and reached a

maximum at Mix4. However, the intensity of these peaks was drastically reduced in the salt Mix5 and reached zero in the samples Mix6-Mix8 ($0.14 \leq x \leq 0.35$).

Finally, the mixed Ca-Fe(III) pyrophosphate salts Mix6 to Mix8 ($0.14 \leq x \leq 0.35$) and Fe_4PP_3 ($x = 1$) showed no distinct diffraction peaks in their X-ray diffraction spectra which was a clear indication of amorphous structure in these salts. The one exception to this was in the sample Mix7 ($x = 0.15$) which showed two weak absorbance peaks at 10 and 14 degree. This could be related to the ultrasonication-induced crystallisation of the pyrophosphate salts resulting from the preparation method in this work,^[15,43] which is out of the scope of the present work. Nonetheless, no sign of crystalline needle-shaped aggregates with iron or calcium dominant regions was observed in the TEM images of this sample (Fig. 5.2A).

The details of chemical bonds in the structure of the mixed Ca-Fe(III) pyrophosphate salts were explored by FT-IR spectroscopy (Fig. 5.4B). The analysis of the FT-IR spectra of the mixed salts showed that peak positions coincided between the salts because the vibrations only correspond to the chemical bonds present in the pyrophosphate ions. Pyrophosphate vibrations showed sharp and strong peaks for the crystalline salts with measured $0 \leq x < 0.14$, while the same peaks appeared broad and smooth for amorphous samples with measured $0.14 \leq x \leq 1$. The peak positions coincided with the values observed for pyrophosphate in the individual Ca_2PP and Fe_4PP_3 salts as discussed in section 5.3.1.

5.3.3. Dissolution behaviour of iron in Fe_4PP_3 and the mixed Ca-Fe(III) pyrophosphate salts

The challenge of novel iron-containing salts is to ensure appropriate pH-dependent dissolution behaviour of the iron compound. To limit iron-mediated reactions while ensuring bio-accessibility the iron dissolution should be limited at food pH (3-7) and fast at gastric pH (1-3) and/or intestinal pH (6-8). Therefore, we investigated the pH-dependent dissolution behaviour of Fe_4PP_3 and mixed Ca-Fe(III) pyrophosphate salts. According to what was discussed above, the mixed Ca-Fe(III) pyrophosphate salts Mix6-Mix8 were most desirable for the main application of this study as they presented uniform morphologies and homogenous distribution of the elements (*i.e.* Ca, Fe, P). On the contrary, the samples Mix2-Mix5 with two coexisting phases were not further investigated for their solubility or reactivity. This is because of the presence of multiple structural phases and hence different chemical compositions can result in unpredictable dissolution or reactivity behaviour of the salts. Furthermore, despite having a homogeneous morphology, sample Mix1 is not particularly suitable for food application because of the crystalline form and specific shape and size of its aggregate, besides having a very low iron content.^[15,51] The amorphous form of the mixed minerals is generally preferred over the crystalline form due to faster dissolution and higher bioavailability.^[52]

The three selected mixed Ca-Fe(III) pyrophosphate salts were prepared using the up-scaled synthesis method (Method S5.1). Up-scaling the synthesis did not affect the morphology or the elemental homogeneity in the salts (results not shown). The dissolution behaviour of Fe_4PP_3 ($x = 1$) and the three mixed Ca-Fe(III) salts Mix6 to Mix8 ($x = 0.14, 0.15$, and 0.35), was evaluated as a function of pH by UV-Vis spectroscopy using the ferrozine assay.^[40] Quantification of the accuracy of total iron determination by the ferrozine assay was verified by comparison with the ICP-AES method (Fig. S5.4). The iron concentrations measured by both methods were found to be in good agreement ($R^2 = 0.99$). Due to the affordability, availability, and high throughput of the ferrozine assay it was decided to use the ferrozine assay for further experiments. The aqueous dissolution behaviour of iron from Fe_4PP_3 and the three mixed Ca-Fe(III) pyrophosphate salts was evaluated in the pH range from 1-10 (Fig. 5.5A).

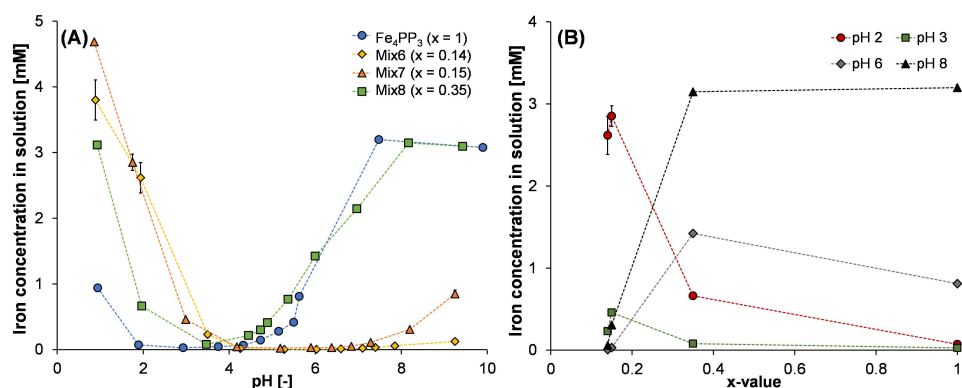


Figure 5.5. (A) Dissolution of iron from Fe_4PP_3 and mixed Ca-Fe(III) pyrophosphate salts Mix6 ($x = 0.14$), Mix7 ($x = 0.15$), and Mix8 ($x = 0.18$) as a function of pH. (B) Dissolution of iron from the salts as a function of x -value at pH 2, pH 3, pH 6, and pH 8. (A) Compared to Fe_4PP_3 , Mix6 ($x = 0.14$) and Mix7 ($x = 0.15$) have a lower iron solubility at food-relevant pH (3-7), whereas at gastric pH (1-3), the salts show enhanced iron dissolution up to a four-fold increase. (B) Lower x -values (*i.e.* ≤ 0.15) have higher iron dissolution at low pH (*i.e.* 2 and 3). However, the salts with higher x -values (*i.e.* 0.35 and 1.0) yielded the highest iron concentrations in solution at high pH (*i.e.* 6 and 8).

In the pH range 2-5.5, soluble iron concentrations from Fe_4PP_3 were below 0.50 mM (Fig. 5.5A). The limited solubility in this pH range is likely due to the presence of the solid species $\text{Fe}_4(\text{P}_2\text{O}_7)_3$.^[14,53] Below pH 2, iron dissolution from Fe_4PP_3 increased to 1 mM due to the presence of ionic Fe(III) and the formation of soluble ferric pyrophosphate complexes (*i.e.* $\text{FeH}_3\text{P}_2\text{O}_7^{2+}$ and $\text{FeH}_2\text{P}_2\text{O}_7^+$).^[53,54] Increased dissolution to 3.0 mM at pH > 5.5 could be explained by the formation of $\text{Fe}(\text{HP}_2\text{O}_7)_2^{3-}$, which is one of the soluble Fe(III)-pyrophosphate species.^[53,55]

For Mix6 ($x = 0.14$) and Mix7 ($x = 0.15$) lower dissolved iron concentration (< 0.25 mM) was observed at the food-relevant pH values (*i.e.* pH 3-7). This indicated that the

ternary complex of $\text{Ca}_{2(1-x)}\text{Fe}_x\text{P}_2\text{O}_7(1+2x)$ with $x = 0.14$ and 0.15 shows lower solubility at pH 3-7 compared to Fe_4PP_3 . The lower amounts of dissolved iron at pH 3-7 for the mixed salts are desirable for application in food, as it could potentially lead to reduced iron-mediated reactivity of the food products upon iron fortification. For Mix8 ($x = 0.35$), similar or even higher dissolution of iron was observed in the food-relevant pH range compared to Fe_4PP_3 . These results indicate that in the mixed Ca-Fe(III) pyrophosphate salts the x -value should be ≤ 0.15 to reduce iron dissolution at pH 3-7.

Interestingly, as the calcium content in the mixed salts increased, the salts showed enhanced iron solubility in the gastric pH range (1-3). For Mix6 ($x = 0.14$) and Mix7 ($x = 0.15$), an increase in dissolved iron of at least a four-fold compared to Fe_4PP_3 was observed at pH 1. Higher quantities of total soluble iron at pH 1-3 and/or pH 6-9 are indicative of better bio-accessibility in the gastric and intestinal environment, respectively.^[14,32-34,56] At pH > 6, the opposite behaviour was observed compared to acidic pH, with the highest iron dissolution for Fe_4PP_3 and Mix8 ($x = 0.35$) salts, and lowest for Mix6 ($x = 0.14$). Even though the dissolution of iron from Mix6 ($x = 0.14$) and Mix7 ($x = 0.15$) was decreased compared to Fe_4PP_3 at intestinal pH, the poor iron solubility of these salts at pH 3-7 and increased dissolution at pH 1-3 (Fig. 5.5A) indicates that these salts likely cause less sensory changes in food and are expected to show adequate bio-accessibility in the stomach.^[32,56] It has previously been shown that *in vitro* solubility of Fe-containing salts at pH 1 is a good indicator for *in vivo* Fe uptake by rats.^[33]

Overall, these results indicate that increasing the proportion of calcium in the mixed pyrophosphate salts promotes dissolution at low pH (1-3), whereas increasing the proportion of iron promotes dissolution at high pH (6-9). This is in line with previous results obtained for pure pyrophosphate salts, in which pure Ca_2PP and Fe_4PP_3 salts showed inverse pH-dependent solubility.^[35] The dissolution behaviour of iron from Fe_4PP_3 and mixed Ca-Fe(III) pyrophosphate salts was evaluated as a function of the x -value in $\text{Ca}_{2(1-x)}\text{Fe}_x\text{P}_2\text{O}_7(1+2x)$. Fig. 5.5B shows the dissolution of iron from the salts as a function of x -value at four representative pH values (*i.e.* pH 2 for gastric conditions, pH 3 and 6 for food, and pH 8 for intestinal conditions). Lower x -values (*i.e.* ≤ 0.15) tend to have higher iron dissolution at low pH (*i.e.* 2 and 3). Furthermore, the salts with higher x -values (*i.e.* 0.35 and 1.0) yielded the highest iron concentrations in solution at high pH (*i.e.* 6 and 8). These findings show that the mixed Ca-Fe(III) pyrophosphate salts possess pH-dependent dissolution behaviour which can be finetuned to the desired application by changing the x -value.

5.3.4. Effect of temperature and time on dissolution behaviour of iron in the Ca-Fe(III) pyrophosphate salts

To effectively apply the Ca-Fe(III) pyrophosphate salts in fortified food products the pH-dependent dissolution at pH 3-7 must be limited during storage (23 °C),

consumption (37 °C), and cooking (90 °C). Therefore, the effect of temperature on iron dissolution from Fe_4PP_3 and the mixed Ca-Fe(III) pyrophosphate salts was investigated by incubating the samples at different temperatures (23, 37, and 90 °C) (Fig. 5.6A). Overall, no significant change ($p > 0.05$) in iron dissolution in the pH range 1-10 was observed upon elevating the temperature from 23 °C to 37 °C. This is in line with a previous study, that observed no change in the dissolution of Fe(III) from Fe_4PP_3 upon elevating the temperature from 23 °C to 50 °C.^[57] Increasing the incubation temperature to 90 °C resulted in a significant ($p < 0.05$) increase in dissolved iron from Fe_4PP_3 at pH 1 and 5.5 (Fig. 5.6A). The iron dissolution for Mix8 ($x = 0.35$) at pH ~7 also increased at 90 °C.

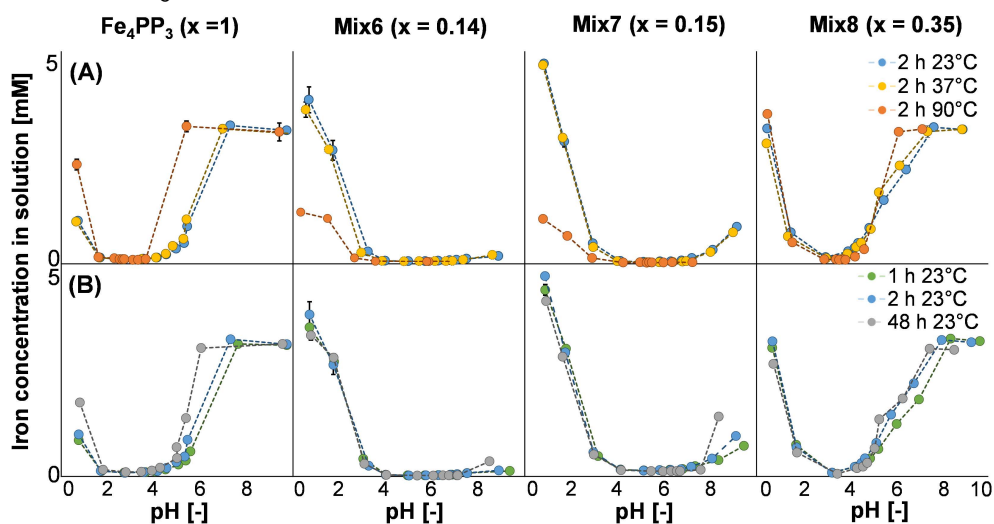


Figure 5.6. Effect of (A) temperature and (B) time on pH-dependent dissolution behaviour of iron in Fe_4PP_3 and mixed Ca-Fe(III) pyrophosphate salts. (A) No significant change in iron dissolution ($p > 0.05$) was observed upon increasing the temperature from 23 °C to 37 °C in the studied pH range (1-10). Upon elevating the temperature to 90 °C, an increase in dissolved iron from Fe_4PP_3 at pH 1 and 5.5 and from Mix8 ($x = 0.35$) at pH ~7 was observed. (B) Iron dissolution pointed to no remarkable difference between iron dissolution for one and two hours of incubation. After 48 h, dissolution remained constant at all pH ranges for all salts except for Fe_4PP_3 with a significant increase at pH < 2 and pH 5-6.

The iron dissolution of Mix6 ($x = 0.14$) and Mix7 ($x = 0.15$) decreased at pH 1-2 after heating at 90 °C. Possibly the ionic Fe(III) that is present in solutions of these mixed salts at pH < 3 underwent hydrolysis to insoluble species, which has been well-documented for Fe(III) at elevated temperatures.^[54,58] For the mixed salts with $x \leq 0.15$, iron concentration in the solution remained similar at elevated temperatures at pH 3-7. Therefore, these mixed salts could potentially be used for cooking without an increase in reactivity. Monitoring time-dependent iron concentration in the solutions pointed to no remarkable difference between iron dissolution for one and two hours of incubation (Fig. 5.6B). Over 48 hours of incubation, dissolution remained constant

at all pH ranges for all salts except for Fe_4PP_3 with a significant ($p < 0.05$) increase at $\text{pH} < 2$ and $\text{pH} 5\text{--}6$ after 48 h.

5.3.5. Assessment of the reactivity of selected mixed salts by discolouration of a black tea solution

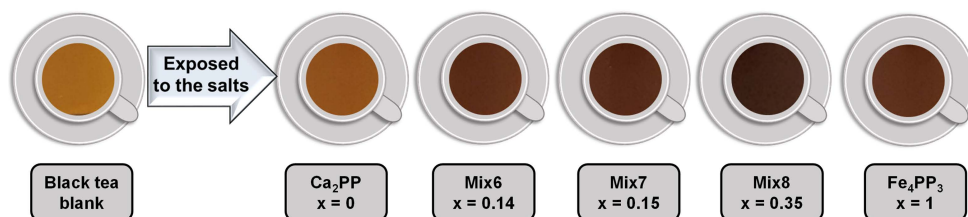
Black tea was chosen as a model system to investigate the reactivity of the mixed Ca-Fe(III) pyrophosphate salts in foods as, after water, it is the most widely consumed beverage in the world.^[59] Black tea contains a considerable amount of phenolics that can trigger discolouration in the presence of iron ions, via iron-mediated complexation and oxidation.^[6,9,60] The black tea model solution was exposed to the three selected mixed Ca-Fe(III) pyrophosphate salts (*i.e.* Mix6, Mix7, and Mix8), as well as the pure Ca_2PP and Fe_4PP_3 salts (final pH of the solutions: 5.13 ± 0.13). Because the mixed salts Mix6 ($x = 0.14$) and Mix7 ($x = 0.15$) showed poor solubility at food-relevant pH, they were expected to show less reactivity and therefore less discolouration upon food fortification. The discolouration of the tea solution, caused by iron ions released from the salts after filtration is shown in **Fig. 5.7A**.

Exposing the tea solutions to 1.05 mg Fe in the form of the pure Fe_4PP_3 and mixed Ca-Fe(III) pyrophosphate salts for 10 minutes, resulted in the darkening of the tea solutions compared to the reference, the pure black tea solution. The visual colour comparison between tea solutions showed that surprisingly, the discolouration induced by these salts was a non-monotonic function of their iron content. The salts Mix6 ($x = 0.14$), Mix7 ($x = 0.15$), and Fe_4PP_3 ($x = 1$) resulted in visually similar discolouration in the black tea solution. However, exposing the tea solution to Mix8 ($x = 0.35$) increased the discolouration and resulted in the darkest tea solution compared to all other salts.

The results obtained from the UV-Vis absorbance of the tea solutions are shown in **(Fig. 5.7B)**. The UV-Vis absorbance of the tea solutions was consistent with the discolouration (**Fig. 5.7A**) and showed the same non-monotonic relation between absorbance at 550 nm and iron content of the salts. Using the mixed salt Mix6 ($x = 0.14$) resulted in equal absorbance compared to Fe_4PP_3 , whereas for the salt Mix7 ($x = 0.15$) a slightly darker colour and higher absorbance was observed (**Table S5.1**). After being exposed to Mix8 ($x = 0.35$), which had the highest iron content, the darkness of the tea solution increased significantly with an approximate 1.5-fold increase in the UV-Vis absorbance compared to pure Fe_4PP_3 ($p < 0.05$). The discolouration induced by Ca_2PP , shown for comparative purposes, caused slight darkening of the tea solution (lightness $L^* = 40$ for Ca_2PP versus $L^* = 49$ for blank). It was previously reported in the literature that complexation of calcium with phenolics does not lead to a change in colour.^[4] However, the slight discolouration observed in the tea solution in presence of calcium is suggested to be due to interaction and oxidation of polyphenols with calcium at elevated temperatures, which is also responsible for tea stains on the

surface of teacups.^[61] The concentration of the dissolved iron from the salts in the tea solutions was measured by ICP-AES (Fig. 5.7B).

(A)



(B)

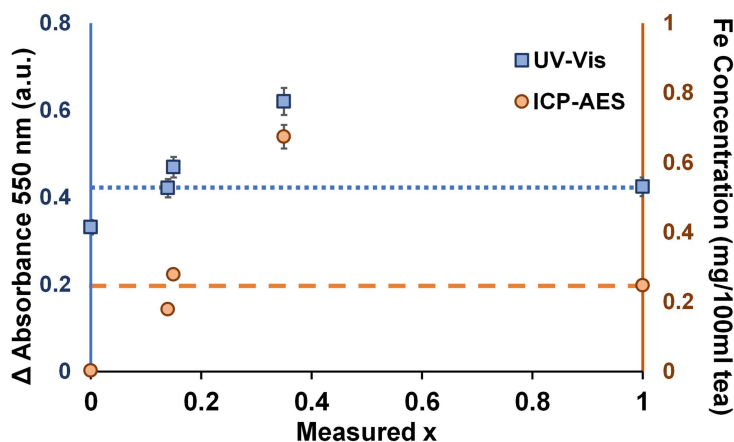


Figure 5.7. The results of the reactivity assessment by exposure to a black tea solution. (A) Images show discolouration of the black tea solution after 10 minutes exposure to the pure salts Ca_2PP ($x = 0$), Fe_4PP_3 ($x = 1$), and the mixed Ca-Fe(III) pyrophosphate salts with $x = 0.14$, 0.15 , and 0.35 compared to the blank tea solution ($\text{pH } 5.13 \pm 0.13$). (B) Increase in absorbance of the tea solutions compared to the blank black tea solution measured at 550 nm by UV-Vis spectroscopy (blue squares, primary y-axis) and concentration of the dissolved Fe in the tea solution is determined by ICP-AES (orange circles, secondary y-axis). The horizontal lines correspond to the absorbance of the tea solution (blue, dotted) and the Fe concentration (orange, dashed) obtained for the tea solution exposed to Fe_4PP_3 .

ICP-AES analysis of the pure black tea solution before the addition of any salts showed that it contained on average $2.7 \pm 0.2 \mu\text{g}$ of iron per 100 mL of tea. Results showed that exposure to Fe_4PP_3 increased the iron concentration in the tea solution to 0.25 mg per 100 mL tea. Exposure to Mix6 ($x = 0.14$) resulted in a 28 % lower iron concentration compared to the Fe_4PP_3 . In the tea solution tested with the salt Mix8 ($x = 0.35$), the dissolved iron concentration was almost 2.7-fold (0.67 mg per 100 mL tea) higher than in the tea exposed to Fe_4PP_3 . Consequently, exposure to Mix8 ($x = 0.35$) resulted in significantly higher discolouration compared to the other samples ($p < 0.05$). Despite the observed discolouration of tea upon exposure to the salts, the

highest measured iron concentration was only 64 % of the total amount of iron added. This indicates that a considerable amount of iron was retained in the salt matrix. Interestingly, discolouration was also observed on the surface of the insoluble proportion of the salt that was recollected as a residue upon filtration of the black tea solutions (Fig. S5.5). All salt powders were either white or off-white before performing the reactivity experiment. The colour of the residues of all iron-containing pyrophosphate salts changed to dark brown or black after being in contact with the tea solution, whereas the residue of Ca_2PP remained white. We suggest that the iron-containing salts show darkening due to the complexation of the iron ions on the surface of the salts with the phenolics present in the black tea solution.

Although the main intention of the performed black tea experiment in this work is not to fortify tea, we used tea solution to investigate the reactivity of iron from the designed mixed salts, to show their potential for food fortification. Contrary to our expectations based on the pH-dependent dissolution assay, the mixed salts did not show noticeably less reactivity in black tea solution compared to Fe_4PP_3 . In future experiments, the reactivity and surface interactions of the iron-containing pyrophosphate salts with phenolic compounds should be further explored using model systems of selected pure phenolic compounds to get more insights into the mechanism for phenolic-mediated discolouration by complexation and oxidation in the presence of the mixed Ca-Fe(III) pyrophosphate salts. Even though the mixed salts show similar reactivity compared to Fe_4PP_3 in foods, the increased dissolution at pH 1-3 indicates that these salts likely possess improved bio-accessibility compared to Fe_4PP_3 . Assessment of the effect of these mixed salts on other sensory properties, such as taste, and the required safety clearance, which can be product-specific are beyond the scope of this manuscript.

5.4. Conclusion

In the present study, we report the design, synthesis, and characterisation of mixed calcium and iron (III) pyrophosphate salts with the general formula $\text{Ca}_{2(1-x)}\text{Fe}_{4x}(\text{P}_2\text{O}_7)_{(1+2x)}$ ($0 \leq x \leq 1$). Mixed salts with $0.14 \leq x \leq 0.35$ were amorphous and uniform in terms of their morphology. We demonstrate for the first time the tuneable pH-dependent solubility of mixed Ca-Fe(III) pyrophosphate salts. Our results indicate that the mixed salts with $x = 0.14$ and 0.15 have a lower iron solubility at food-relevant pH (3-7) compared to Fe_4PP_3 . Furthermore, at gastric pH (1-3), the salts show enhanced iron dissolution with up to a four-fold increase of soluble iron compared to Fe_4PP_3 . Assessment of the reactivity of the selected mixed Ca-Fe(III) pyrophosphate salts in a black tea solution showed that the concentration of the dissolved iron ions released from the salts was a non-monotonic function of the x -values and that none of the salts could reduce the development of discolouration compared to Fe_4PP_3 . The present findings indicate that the mixed Ca-Fe(III) pyrophosphate salts with experimental $x \leq 0.15$ in the general formula $\text{Ca}_{2(1-x)}\text{Fe}_{4x}(\text{P}_2\text{O}_7)_{(1+2x)}$ can be potential food fortificants with tuneable iron composition and dissolution behaviour. The main benefit of these salts

is improved bio-accessibility resulting from increased dissolution at gastric pH (1-3) compared to Fe_4PP_3 . Furthermore, our results demonstrate that the pyrophosphate salts can be used as a carrier for iron and as a potential delivery system for dual-fortification.

5.5. Acknowledgements

Hans Meeldijk from Inorganic Chemistry, Utrecht University, is thanked for TEM-EDX and HAADF-STEM measurements. Coen Mulder from Geo-Science group of Utrecht University is thanked for ICP-AES measurements (black tea experiment). K. P. V. acknowledges the stimulating discussion with Roumen Tsekov. The authors are grateful to Arjen Reichwein, Raymond Nijveld, and Teun de Bruin of Nouryon specialty chemicals B.V. for performing the ICP-AES measurements (dissolution behaviour). The graphical abstract was made with content from BioRender.com.

5.6. References

- 1 Diaz, J. R., de las Cagigas, A., & Rodriguez, R. (2003). Micronutrient deficiencies in developing and affluent countries. *European Journal of Clinical Nutrition*, 57(1), S70-S72.
- 2 Saha, S., & Roy, A. (2020). Whole grain rice fortification as a solution to micronutrient deficiency: Technologies and need for more viable alternatives. *Food Chemistry*, 326, 127049.
- 3 Allen, L. H., De Benoist, B., Dary, O., & Hurrell, R. (2006). Guidelines on food fortification with micronutrients. World Health Organization.
- 4 Habeych, E., van Kogelenberg, V., Sagalowicz, L., Michel, M., & Galaffu, N. (2016). Strategies to limit colour changes when fortifying food products with iron. *Food Research International*, 88, 122-128.
- 5 Ashwin, K., Pattanaik, A. K., & Howarth, G. S. (2021). Polyphenolic bioactives as an emerging group of nutraceuticals for promotion of gut health: A review. *Food Bioscience*, 44, 101376.
- 6 Bijlsma, J., de Bruijn, W. J. C., Velikov, K. P., & Vincken, J.-P. (2022). Unravelling discolouration caused by iron-flavonoid interactions: Complexation, oxidation, and formation of networks. *Food Chemistry*, 370, 131292.
- 7 Bolade, O. P., Williams, A. B., & Benson, N. U. (2020). Green synthesis of iron-based nanomaterials for environmental remediation: A review. *Environmental Nanotechnology, Monitoring & Management*, 13, 100279.
- 8 Bovell-Benjamin, A. C., & Guinard, J.-X. (2003). Novel approaches and application of contemporary sensory evaluation practices in iron fortification programs. *Critical Reviews in Food Science and Nutrition*, 43(4), 379-400.
- 9 McGee, E. J. T., & Diosady, L. L. (2018). Prevention of iron-polyphenol complex formation by chelation in black tea. *LWT - Food Science and Technology*, 89, 756-762.
- 10 Zimmermann, (2004). The potential of encapsulated iron compounds in food fortification: A review. *International Journal for Vitamin and Nutrition Research*, 74(6), 453-461.
- 11 Zuidam, N. J. (2012). An industry perspective on the advantages and disadvantages of iron micronutrient delivery systems. In N. Garti & D. J. McClements (Eds.), *Encapsulation technologies and delivery systems for food ingredients and nutraceuticals*, (pp. 505-540): Woodhead Publishing.
- 12 Bothwell, T. H., & Macphail, A. P. (2004). The potential role of NaFeEDTA as an iron fortificant. *International Journal for Vitamin and Nutrition Research*, 76(6), 421-434.
- 13 McGee, E. J. T., & Diosady, L. L. (2018). Development of spectrophotometric quantification method of iron-polyphenol complex in iron-fortified black tea at relevant pH levels. *Food Analytical Methods*, 11(6), 1645-1655.
- 14 Tian, T., Blanco, E., Smoukov, S. K., Velez, O. D., & Velikov, K. P. (2016). Dissolution behaviour of ferric pyrophosphate and its mixtures with soluble pyrophosphates: Potential strategy for increasing iron bioavailability. *Food Chemistry*, 208, 97-102.
- 15 van Leeuwen, Y. M., Velikov, K. P., & Kegel, W. K. (2012). Morphology of colloidal metal pyrophosphate salts. *RSC Advances*, 2(6), 2534-2540.
- 16 Baars, R. J., van Leeuwen, Y. M., Hendrix, Y., Velikov, K. P., Kegel, W. K., & Philipse, A. P. (2015). Morphology-controlled functional colloids by heterocoagulation of zein and nanoparticles. *Colloids and Surfaces A: Physicochemical and Engineering Aspects*, 483, 209-215.
- 17 Salgueiro, M. J., & Boccio, J. (2013). Ferric pyrophosphate as an alternative iron source for food fortification. In V. R. Preedy, R. Srirajskanthan & V. B. Patel (Eds.), *Handbook of food fortification and health*, (pp. 91-97): Springer.
- 18 Srinivasu, B. Y., Mitra, G., Muralidharan, M., Srivastava, D., Pinto, J., Thankachan, P., Suresh, S., Shet, A., Rao, S., Ravikumar, G., Thomas, T. S., Kurpad, A. V., & Mandal, A. K. (2015). Beneficiary effect of

- nanosizing ferric pyrophosphate as food fortificant in iron deficiency anemia: Evaluation of bioavailability, toxicity and plasma biomarker. *RSC Advances*, 5(76), 61678-61687.
- 19 Moretti, D., Zimmermann, M. B., Wegmüller, R., Walczyk, T., Zeder, C., & Hurrell, R. F. (2006). Iron status and food matrix strongly affect the relative bioavailability of ferric pyrophosphate in humans. *The American Journal of Clinical Nutrition*, 83(3), 632-638.
- 20 Shubham, K., Anukiruthika, T., Dutta, S., Kashyap, A. V., Moses, J. A., & Anandharamkrishnan, C. (2020). Iron deficiency anemia: A comprehensive review on iron absorption, bioavailability and emerging food fortification approaches. *Trends in Food Science & Technology*, 99, 58-75.
- 21 Bijlsma, J., de Bruijn, W. J. C., Hageman, J. A., Goos, P., Velikov, K. P., & Vincken, J.-P. (2020). Revealing the main factors and two-way interactions contributing to food discolouration caused by iron-catechol complexation. *Scientific Reports*, 10(1), 8288.
- 22 van Leeuwen, Y. M., Velikov, K. P., & Kegel, W. K. (2014). Colloidal stability and chemical reactivity of complex colloids containing Fe^{3+} . *Food Chemistry*, 155, 161-166.
- 23 Zimmermann, M. B., & Hilty, F. M. (2011). Nanocompounds of iron and zinc: Their potential in nutrition. *Nanoscale*, 3(6), 2390-2398.
- 24 Hackl, L., Zimmermann, M. B., Zeder, C., Parker, M., Johns, P. W., Hurrell, R. F., & Moretti, D. (2017). Iron bioavailability from ferric pyrophosphate in extruded rice cofortified with zinc sulfate is greater than when cofortified with zinc oxide in a human stable isotope study. *The Journal of Nutrition*, 147(3), 377-383.
- 25 Gupta, A., Pratt, R., & Mishra, B. (2018). Physicochemical characterization of ferric pyrophosphate citrate. *Biomaterials*, 31(6), 1091-1099.
- 26 Cercamondi, C. I., Duchateau, G. S., Harika, R. K., van den Berg, R., Murray, P., Koppenol, W. P., Zeder, C., Zimmermann, M. B., & Moretti, D. (2016). Sodium pyrophosphate enhances iron bioavailability from bouillon cubes fortified with ferric pyrophosphate. *British Journal of Nutrition*, 116(3), 496-503.
- 27 Miyawaki, R., Hatert, F., Pasero, M., & Mills, S. J. (2020). IMA commission on new minerals, nomenclature and classification (CNMNC)-newsletter 52. *European Journal of Mineralogy*, 32(1), 1-11.
- 28 Catti, M., Ferraris, G., & Ivaldi, G. (1979). Refinement of the crystal structure of anapaite $\text{Ca}_2\text{Fe}(\text{PO}_4)_2 \cdot 4\text{H}_2\text{O}$: Hydrogen bonding and relationships with the bihydrated phase. *Bulletin de Minéralogie*, 102(4), 314-318.
- 29 Lafuente, B., Downs, R. T., Yang, H., & Jenkins, R. A. (2014). Calcioterrite with composition $(\text{Ca}_{3.94}\text{Sr}_{0.06})\text{Mg}_{1.01}(\text{Fe}_{2.93}\text{Al}_{1.07})(\text{PO}_4)_6(\text{OH})_4 \cdot 12\text{H}_2\text{O}$. *Acta Crystallographica Section E: Structure Reports Online*, 70(3), i16-i17.
- 30 Ravet, N., Chouinard, Y., Magnan, J. F., Besner, S., Gauthier, M., & Armand, M. (2001). Electroactivity of natural and synthetic triphylite. *Journal of Power Sources*, 97-98, 503-507.
- 31 Rossi, L., Velikov, K. P., & Philipse, A. P. (2014). Colloidal iron (III) pyrophosphate particles. *Food Chemistry*, 151, 243-247.
- 32 Hurrell, R. (2002). How to ensure adequate iron absorption from iron-fortified food. *Nutrition Reviews*, 60, S7-S15.
- 33 Rohner, F., Ernst, F. O., Arnold, M., Hilbe, M., Biebinger, R., Ehrensperger, F., Pratsinis, S. E., Langhans, W., Hurrell, R. F., & Zimmermann, M. B. (2007). Synthesis, characterization, and bioavailability in rats of ferric pyrophosphate nanoparticles. *The Journal of Nutrition*, 137(3), 614-619.
- 34 Wienk, K., Marx, J., & Beynen, A. (1999). The concept of iron bioavailability and its assessment. *European Journal of Nutrition*, 38(2), 51-75.
- 35 van Leeuwen, Y. M. (2013). *Colloidal metal pyrophosphate salts: Preparation, properties and applications*. Ph.D. Thesis. Utrecht University, Utrecht.
- 36 Hilty, F. M., Knijnenburg, J. T. N., Teleki, A., Krumeich, F., Hurrell, R. F., Pratsinis, S. E., & Zimmermann, M. B. (2011). Incorporation of Mg and Ca into nanostructured Fe_2O_3 improves Fe solubility in dilute acid and sensory characteristics in foods. *Journal of Food Science*, 76(1), N2-N10.
- 37 Joint FAO/WHO expert consultation: Vitamin and mineral requirements in human nutrition. (2004). World Health Organization and Food and Agriculture Organization of the United Nations.
- 38 Ross, A. C., Taylor, C. L., Yaktine, A. L., & Del Valle, H. B. (2011). Dietary reference intakes for adequacy: Calcium and vitamin D. In A. C. Ross, C. L. Taylor, A. L. Yaktine & H. B. Del Valle (Eds.), *Dietary reference intakes for calcium and vitamin D*. (pp. 345-402). National Academies Press: Washington, D.C.
- 39 Drenchev, N. L., Chakarova, K. K., Lagunov, O. V., Mihaylov, M. Y., Ivanova, E. Z., Strauss, I., & Hadjivanov, K. I. (2020). *In situ* FTIR spectroscopy as a tool for investigation of gas/solid interaction: Water-enhanced CO_2 adsorption in UiO-66 metal-organic framework. *JoVE (Journal of Visualized Experiments)*(156), e60285.
- 40 Stookey, L. L. (1970). Ferrozine: A new spectrophotometric reagent for iron. *Analytical Chemistry*, 42(7), 779-781.
- 41 Gras, P., Rey, C., Marsan, O., Sarda, S., & Combes, C. (2013). Synthesis and characterisation of hydrated calcium pyrophosphate phases of biological interest. *European Journal of Inorganic Chemistry*, 2013(34), 5886-5895.
- 42 El Kady, A. M., Mohamed, K. R., & El-Bassouini, G. T. (2009). Fabrication, characterization and bioactivity evaluation of calcium pyrophosphate/polymeric biocomposites. *Ceramics International*, 35(7), 2933-2942.
- 43 Luque de Castro, M. D., & Priego-Capote, F. (2007). Ultrasound-assisted crystallization (sonocrystallization). *Ultrasonics Sonochemistry*, 14(6), 717-724.

- 44 Lai, Y., Liang, X., Yin, G., Yang, S., Wang, J., Zhu, H., & Yu, H. (2011). Infrared spectra of iron phosphate glasses with gadolinium oxide. *Journal of Molecular Structure*, 1004(1), 188-192.
- 45 Singh, R. K., Srivastava, M., Prasad, N. K., Awasthi, S., Dhayalan, A., & Kannan, S. (2017). Iron doped β -tricalcium phosphate: Synthesis, characterization, hyperthermia effect, biocompatibility and mechanical evaluation. *Materials Science and Engineering: C*, 78, 715-726.
- 46 Kosova, N. V., Rezepova, D. O., Podgornova, O. A., Slobodyuk, A. B., Petrov, S. A., & Avdeev, M. (2017). A comparative study of structure, air sensitivity and electrochemistry of sodium iron pyrophosphates $\text{Na}_{2-x}\text{Fe}_{1+x/2}\text{P}_2\text{O}_7$ ($x=0; 0.44$). *Electrochimica Acta*, 235, 42-55.
- 47 Zheng, J.-c., Ou, X., Zhang, B., Shen, C., Zhang, j.-f., Ming, L., & Han, Y.-d. (2014). Effects of Ni^{2+} doping on the performances of lithium iron pyrophosphate cathode material. *Journal of Power Sources*, 268, 96-105.
- 48 Li, Y. (2018). A review of recent research on nonequilibrium solid solution behavior in Li_xFePO_4 . *Solid State Ionics*, 323, 142-150.
- 49 Tan, H. J., Dodd, J. L., & Fultz, B. (2009). Thermodynamic and kinetic stability of the solid solution phase in nanocrystalline Li_xFePO_4 . *The Journal of Physical Chemistry C*, 113(48), 20527-20530.
- 50 Suslick, K. S., Fang, M., & Hyeon, T. (1996). Sonochemical synthesis of iron colloids. *Journal of the American Chemical Society*, 118(47), 11960-11961.
- 51 Marian, N. M., Giorgetti, G., Magrini, C., Capitani, G. C., Galimberti, L., Cavallo, A., Salvini, R., Vanneschi, C., & Viti, C. (2021). From hazardous asbestos containing wastes (ACW) to new secondary raw material through a new sustainable inertization process: A multimethodological mineralogical study. *Journal of Hazardous Materials*, 413, 125419.
- 52 Velikov, K. P., & Pelan, E. (2008). Colloidal delivery systems for micronutrients and nutraceuticals. *Soft Matter*, 4(10), 1964-1980.
- 53 Jiang, C., Wang, X., Parekh, B., & Leonard, J. (1998). Pyrite depression by phosphates in coal flotation. *Mining, Metallurgy & Exploration*, 15(1), 1-7.
- 54 Flynn, C. M. (1984). Hydrolysis of inorganic iron(III) salts. *Chemical Reviews*, 84(1), 31-41.
- 55 Sun, Y., Zhao, L., & Teng, Y. (2020). Effect of soil type on the degradation of polychlorinated biphenyls in a pyrophosphate-chelated Fenton-like reaction. *Chemical Engineering Journal*, 390, 124574.
- 56 Swain, J. H., Newman, S. M., & Hunt, J. R. (2003). Bioavailability of elemental iron powders to rats is less than bakery-grade ferrous sulfate and predicted by iron solubility and particle surface area. *The Journal of Nutrition*, 133(11), 3546-3552.
- 57 Wilhelmy, R. B., Patel, R. C., & Matijevic, E. (1985). Thermodynamics and kinetics of aqueous ferric phosphate complex formation. *Inorganic Chemistry*, 24(20), 3290-3297.
- 58 Dousma, J., & De Bruyn, P. (1976). Hydrolysis-precipitation studies of iron solutions. I. Model for hydrolysis and precipitation from Fe(III) nitrate solutions. *Journal of Colloid and Interface Science*, 56(3), 527-539.
- 59 Dueik, V., Chen, B. K., & Diosady, L. L. (2017). Iron-polyphenol interaction reduces iron bioavailability in fortified tea: Competing complexation to ensure iron bioavailability. *Journal of Food Quality*, 2017, 1-8.
- 60 Wang, Z., Fang, C., & Mallavarapu, M. (2015). Characterization of iron-polyphenol complex nanoparticles synthesized by sage (*Salvia officinalis*) leaves. *Environmental Technology & Innovation*, 4, 92-97.
- 61 Yamada, K., Abe, T., & Tanizawa, Y. (2007). Black tea stain formed on the surface of teacups and pots. Part 2-study of the structure change caused by aging and calcium addition. *Food Chemistry*, 103(1), 8-14.
- 62 Allen, L. H., Carriquiry, A. L., & Murphy, S. P. (2019). Perspective: Proposed harmonized nutrient reference values for populations. *Advances in Nutrition*, 11(3), 469-483.

5.7. Supplementary information

Method S5.1. Up-scaled synthesis of pure and mixed Ca-Fe(III) pyrophosphate salts

The synthesis of the pure and mixed pyrophosphate salts described in this study was up-scaled. Iron (III) pyrophosphate ($\text{Fe}_4(\text{P}_2\text{O}_7)_3$, Fe_4PP_3) and calcium pyrophosphate ($\text{Ca}_2\text{P}_2\text{O}_7$, Ca_2PP) were separately prepared using a fast coprecipitation method similar to what was described in [section 5.2.2](#). In short, 0.5 L solutions of 17.14 mM $\text{FeCl}_3 \cdot 6\text{H}_2\text{O}$ and 25.72 mM CaCl_2 in water were made. The solutions were quickly added to an aqueous solution of $\text{Na}_4\text{P}_2\text{O}_7 \cdot 10\text{H}_2\text{O}$ (6.43 mM, 1 L) while stirring vigorously (~ 500 rpm) by an IKA RW16 basic electronic overhead stirrer (IKA-Werke, Staufen, Germany). A turbid white dispersion formed after a couple of seconds during addition. The samples were then centrifuged using an Avanti J-26 XP centrifuge (Beckman Coulter, Brea, CA, USA) using JLA-9.1000 rotor, at $6000 \times g$ and 25°C for 45 min in 1000 mL volume polycarbonate centrifuge bottles (95×191 mm-2Pk) with caps followed by washing the precipitates twice with water. The sediments were dried in an oven at 45°C overnight. The mixed Ca-Fe(III) pyrophosphate salts were prepared by the same procedure as the pure salts, at a fixed concentration of $\text{Na}_4\text{P}_2\text{O}_7 \cdot 10\text{H}_2\text{O}$ (6.43 mM, 1 L) and by addition of a mixed solution of $\text{FeCl}_3 \cdot 6\text{H}_2\text{O}$ and CaCl_2 in 0.5 L of water. Three different mixed salts were synthesised with the general formula $\text{Ca}_{2(1-x)}\text{Fe}_{4x}(\text{P}_2\text{O}_7)_{(1+2x)}$ ($0 < x < 1$), containing low to high Fe(III) content corresponding to three different theoretical x-values (*i.e.* 0.05, 0.10, 0.26). The x-values were chosen based on the recommended nutrient intake of iron and calcium (respectively 20 and 833 mg for adult females, assuming 15 % bioavailability of Fe and 30 % of Ca in the salt).^[37,62] The molar ratio of total metal to pyrophosphate ion was based on the stoichiometry of calcium pyrophosphate (final concentration of $[\text{Ca}] + [\text{Fe}] = 8.57 \text{ mM}$). The average yield of the prepared salts was $73.3 \pm 5.5 \%$.

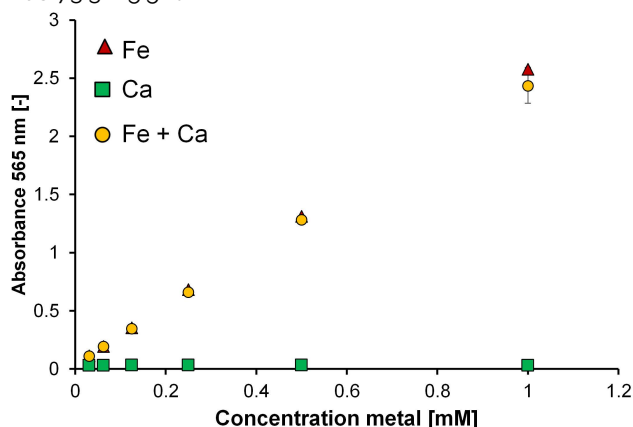


Figure S5.1. Absorbance of the ferrozine complex at 565 nm in presence of increasing concentrations of iron, calcium, or a mixture containing equimolar concentrations of iron and calcium. Presence of the calcium ion (Ca) does not result in absorbance at 565 nm or interfere with the absorbance of the Fe-ferrozine complex.

Method S5.2. Iron concentration measurement by inductively coupled plasma – optical emission spectroscopy (ICP-AES)

Inductively coupled plasma–atomic emission spectroscopy (ICP-AES) was used for independent verification of the iron quantification by the ferrozine assay. For ICP-AES measurements, powders of pure Fe_4PP_3 and Ca_2PP , as well as mixed Ca-Fe(III) pyrophosphate salts were dispersed in water to obtain final concentrations of 10 mg mL^{-1} . pH was set to reach a target pH 3, 6, or 8 after 2 hours of incubation at 23°C while mixing at 1000 rpm using an Eppendorf Thermomixer F1.5. Samples were five times diluted in 0.14 M HNO_3 , before injection in the ICP-AES system (Agilent 5110 VDV; Agilent Technologies, Tokyo, Japan). Independent duplicate samples were taken from the salt at each pH point by independent titrations. The concentration of iron, calcium, and phosphorus was determined using scandium as an internal standard. The limit of detection (LOD) values of iron, calcium, and phosphorus were respectively 0.05, 0.05, and 0.20 mg/L , the limit of quantification (LOQ) values were 0.15, 0.15, and 0.61 mg/L , respectively.

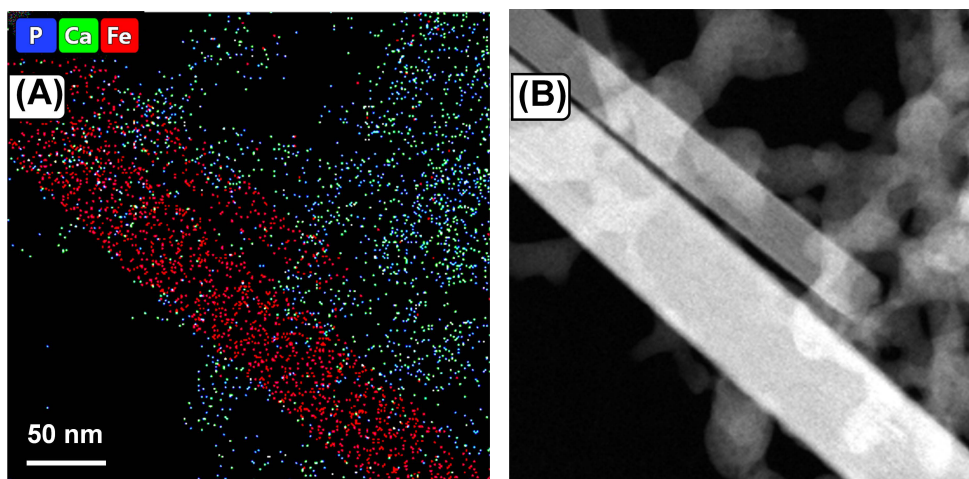


Figure S5.2. (A) Heterogenous distribution of iron and calcium in the salt Mix5 obtained by elemental mapping using HAADF-STEM. Colour indications are as follows: calcium (Ca): green; iron (Fe): red; and phosphorous (P): blue. The chemical composition of the needle-shaped particles in the salt Mix5 remains ill-defined (atomic percentages: O: 43.00 %, P: 0.98 %, Ca: 2.36 %, Fe: 53.64 %). (B) The corresponding-dark-field images.

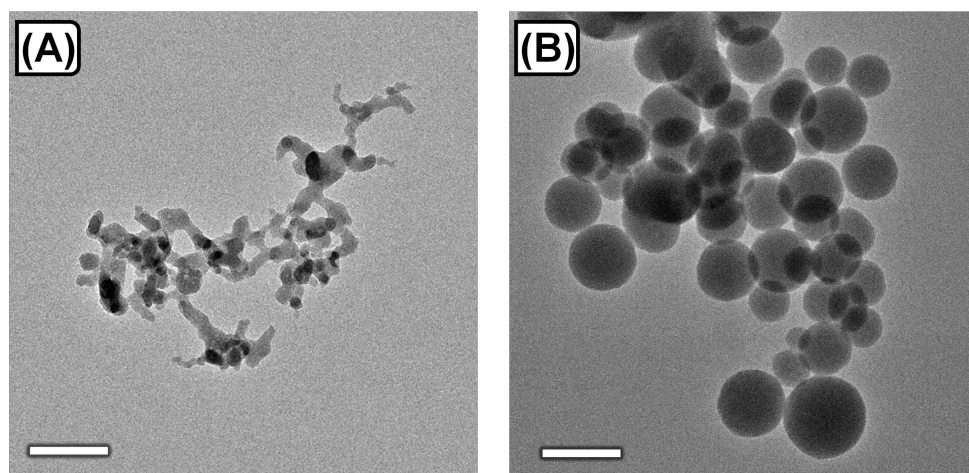


Figure S5.3. The mixed Ca-Fe(III) pyrophosphate salt Mix8 ($x = 0.35$), (A) before ultrasonication treatment and (B) after ultrasonication 10 minutes. The scale bar represents 200 nm. TEM images indicate the effect of ultrasonication treatment on the shape and size of the precipitates.

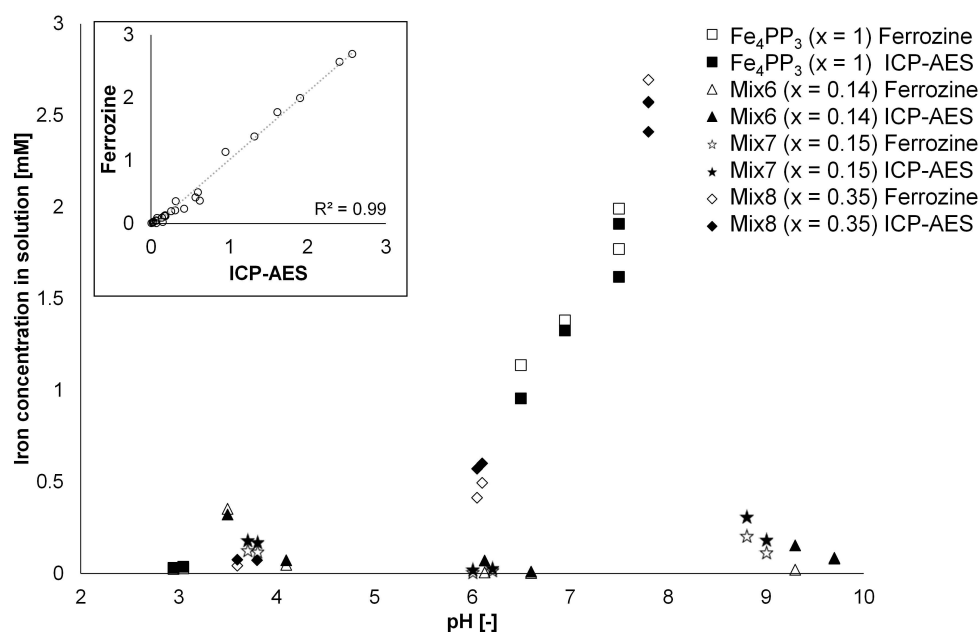








Figure S5.4. Dissolution of iron from Fe_4PP_3 and mixed Ca-Fe(III) pyrophosphate salts as a function of pH determined by ICP-AES (filled markers) and by the ferrozine (open markers) methods. The inset depicts the correlation between the iron concentration measured using both methods. The iron concentrations in solution measured by the two different methods are found to be in good agreement ($R^2 = 0.99$).

Table S5.1. The details of colour conversion of the black tea solutions obtained by an online colour measurement tool; <https://imagecolorpicker.com>. After exposing the tea solutions to the pure Ca_2PP and Fe_4PP_3 , and the selected mixed Ca-Fe(III) pyrophosphate salts, an image including all the solutions was taken while they were illuminated with a uniform light source. The image was then used to extract the colours. Using the mixed salt Mix6 ($x = 0.14$) results in equal darkness compared to Fe_4PP_3 (*i.e.* $L^* = 25$), whereas for the salt Mix7 ($x = 0.15$) a slightly darker colour is observed (*i.e.* $L^* = 22$). Interestingly, exposing the tea solution to Mix8 ($x = 0.35$) increases the discolouration and results in the darkest tea solution compared to all other salts

Colour Conversion	Black tea	Ca_2PP $x = 0$	Mix6 $x = 0.14$	Mix7 $x = 0.15$	Mix8 $x = 0.35$	Fe_4PP_3 $x = 1$
Shade						
$L^*a^*b^*$	49, 20, 49	40, 24, 40	25, 19, 23	22, 18, 21	16, 12, 13	25, 19, 22

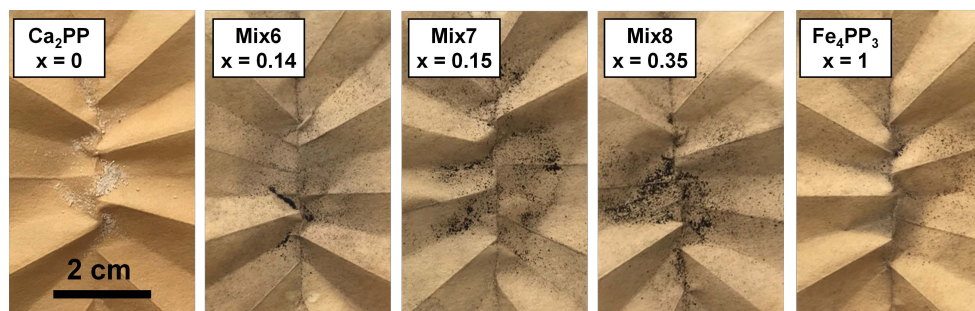


Figure S5.5. Images of residue of the black tea solution after being exposed to Ca_2PP ($x = 0$), Fe_4PP_3 ($x = 1$), and the mixed Ca-Fe(III) pyrophosphate salts Mix6 ($x = 0.14$), Mix7 ($x = 0.15$), and Mix8 ($x = 0.35$) on filter papers (background). All filtrates were washed with ethanol and then dried. The Ca_2PP powder remained white. Darkening at the surface of the iron-containing salts is observed after being exposed to the tea solution.

CHAPTER 6

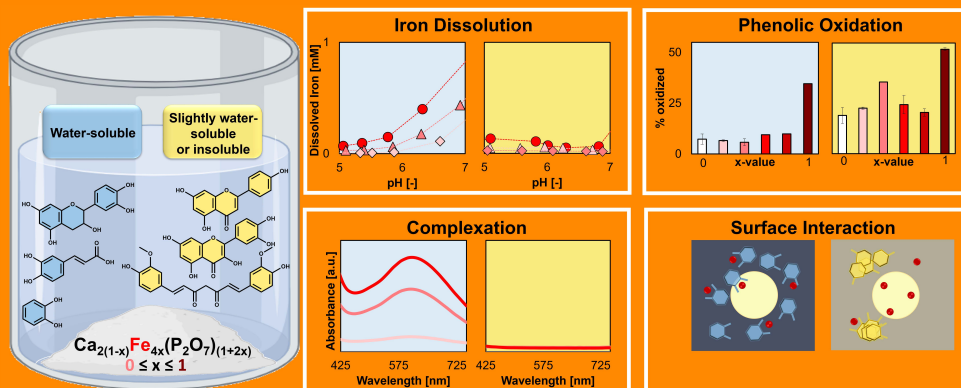
Reactivity of Fe(III)- containing pyrophosphate salts with phenolics: complexation, oxidation, and surface interaction

Judith Bijlsma, Neshat Moslehi, Krassimir P.
Velikov, Willem. K. Kegel, Jean-Paul Vincken, and
Wouter J.C. de Bruijn

Based on: *Food Chemistry*, 2023, 407:135156.

Abstract

Mixed pyrophosphate salts with the general formula $\text{Ca}_{2(1-x)}\text{Fe}_{4x}(\text{P}_2\text{O}_7)_{(1+2x)}$ potentially possess less iron-phenolic reactivity compared to ferric pyrophosphate (Fe_4PP_3), due to decreased soluble Fe in the food-relevant pH range 3-7. We investigated reactivity (*i.e.* complexation, oxidation, and surface interaction) of Fe_4PP_3 and mixed salts (with $x = 0.14, 0.15, 0.18$, and 0.35) in presence of structurally diverse phenolics. At pH 5-7, increased soluble iron from all salts was observed in presence of water soluble phenolics. XPS confirmed that water soluble phenolics solubilise iron after coordination at the salt surface, resulting in increased discolouration. However, colour changes for mixed salts with $x \leq 0.18$ remained acceptable for slightly water soluble and insoluble phenolics. Furthermore, phenolic oxidation in presence of mixed salts was significantly reduced compared to Fe_4PP_3 at pH 6. In conclusion, these mixed Ca-Fe(III) pyrophosphate salts with $x \leq 0.18$ can potentially be used in designing iron-fortified foods containing slightly water soluble and/or insoluble phenolics.



6.1 Introduction

Fortification of food with iron is an effective approach to overcome the global iron deficiency.^[1] However, the addition of iron to foods is problematic due to its high reactivity with phenolic compounds present in the food. Complexation and oxidation of phenolics in the presence of iron ions cause an undesirable change in the sensory properties of the food products such as discolouration resulting from dark brown or black colour formation upon iron-phenolic complexation.^[2-4] Moreover, the reactivity of iron with phenolic compounds can hinder iron bioavailability and can consequently reduce iron uptake in the human body.^[5] One strategy to limit reactivity is to use a poorly water soluble iron-containing salt such as iron(III) pyrophosphate (FePP; Fe_4PP_3).^[2,6] However, even addition of iron as Fe_4PP_3 cannot fully prevent discolouration in phenolic-rich foods.^[7,8] Moreover, the poor solubility of Fe_4PP_3 in the gastrointestinal tract results in limited iron bioavailability.^[7,8]

Our previous study indicated that including calcium as a divalent metal, alongside iron, in the pyrophosphate salt matrix can be utilised to design potential dual-fortificants. The soluble iron concentration from these mixed salts, with the general formula of $\text{Ca}_{2(1-x)}\text{Fe}_{4x}\text{P}_2\text{O}_{7(1+2x)}$, was reduced by up to eight-fold at food-relevant pH ranges, whereas it was enhanced up to four-fold in gastric relevant pH ranges, compared to Fe_4PP_3 .^[9] Additionally, the inclusion of calcium as the second metal in the mixed Ca-Fe(III) pyrophosphate salt is expected to lower the iron content at the surface of these salts and therefore lead to a decrease in reactivity, with respect to Fe_4PP_3 . Despite much lower soluble iron concentration and the expected lower iron content at the surface, the mixed Ca-Fe(III) pyrophosphate salts previously did not show noticeably less reactivity compared to Fe_4PP_3 in a black tea system.^[9] To create a clear link between the dissolution behaviour of iron from these mixed salts and the observed reactivity of the salts, the current work aims to investigate the soluble iron from the Ca-Fe(III) pyrophosphate salts in the presence of phenolics as representative food matrix compounds that can react with iron.

We previously observed that the solubility of flavonoids affects the soluble iron concentration.^[14] Therefore, a set of six model phenolic compounds with different chemical properties, most notably different water solubilities, were selected (**Fig. 6.1**) to investigate their interaction behaviour with the mixed Ca-Fe(III) pyrophosphate salts. The chosen phenolic compounds also differ in the most likely Fe(III)-complexation sites, as is highlighted in **Fig. 6.1**.^[4,10-12] The solubility values are calculated and shown as $\log S$ (i.e. the logarithm of water solubility in molar) in **Fig. 6.1**. Catechol, caffeic acid, and epicatechin show $\log S$ values ranging from 0 to -2, which was previously classified as water soluble by Sorkun and co-authors.^[13] Accordingly, quercetin and apigenin ($-4 < \log S < -2$) are slightly soluble, and curcumin ($\log S < -4$) is insoluble. These phenolics were chosen because they are common in food

products,^[2,14] except for catechol which was selected as a model for *o*-dihydroxybenzenes.

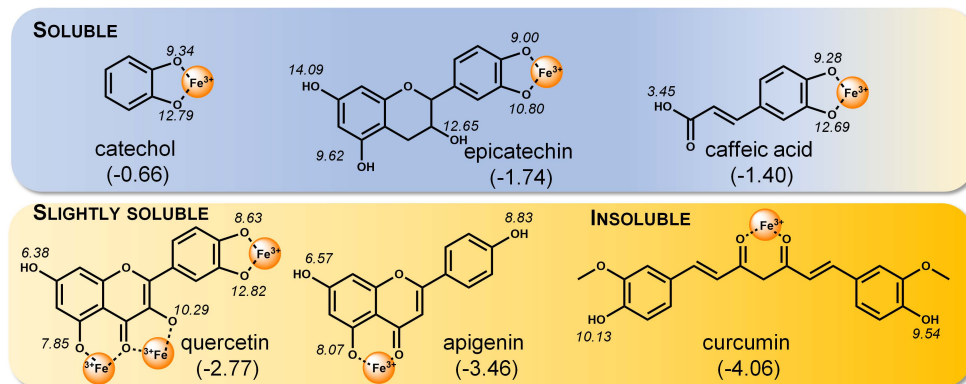


Fig. 6.1. Structure of phenolic compounds used in this study, and the most likely Fe(III)-complexation sites. The *pK_a* values for hydroxyl groups of the phenolics are shown in italic, and *logS* values of the phenolic compounds are given in brackets. *LogS* values were calculated using MarvinSketch 22.3 (ChemAxon). Based on the *logS* values, the water solubility of the phenolics was classified as soluble, slightly soluble, and insoluble.

Deprotonation of the hydroxyl substituents is a prerequisite for iron coordination.^[12] The *pK_a* values of the hydroxyl groups are indicated in **Fig. 6.1**. It should be noted that in the presence of iron ions the deprotonated state of the phenolics is stabilised and that the apparent *pK_a* values will therefore be lowered to values in the range of pH 5–8 for the phenol moiety.^[15] The actual *pK_a* lowering effect is dependent on the structural features of the phenolic compound and the stabilisation of the resulting anion.^[16] The stoichiometry and colour of iron-phenolic complexes (*e.g.* 1:1, 1:2, 2:1, *etc.*) and the preferred iron-binding sites are dependent on the solvent, the pH of the sample, iron salt, and the phenolic structure.^[17,18] For caffeic acid, coordination of metals to the catecholate moiety is suggested to be preferred over coordination to the carboxylate moiety, because of the higher electron density of the catecholate oxygens and the stable five-membered ring that is formed upon coordination.

We hypothesise that mixed Ca-Fe(III) pyrophosphate salts will show decreased reactivity towards phenolic compounds at food-relevant pH values compared to Fe₄PP₃ due to (i) decreased soluble iron concentration from the salts at pH 3–7, and (ii) decreased iron content at the surface of these salts. To this end, we evaluate iron dissolution behaviour, spectral changes indicating iron-mediated complexation, oxidation of the phenolic compounds, and reactions at the surface of these salts.

6.2 Materials & methods

6.2.1 Materials

Hydrochloric acid (37 wt. %), sodium hydroxide (≥ 98 wt. %), nitric acid (65 wt. %), iron(II) sulfate heptahydrate (≥ 99 wt. %), 3-(2-pyridyl)-5,6-diphenyl-1,2,4-triazine-*p,p'*-disulfonic acid monosodium salt hydrate (≥ 97 wt. %; ferrozine), ferric chloride hexahydrate ($\text{FeCl}_3 \cdot 6\text{H}_2\text{O}$, ≥ 99 wt. %), tetrasodium pyrophosphate decahydrate ($\text{Na}_4\text{P}_2\text{O}_7 \cdot 10\text{H}_2\text{O}$, ≥ 99 wt. %, Na_4PP), calcium dichloride (CaCl_2 , ≥ 93 wt. %), quercetin hydrate (≥ 95 wt. %), 1,2-dihydroxybenzene (≥ 99 wt. %; catechol), caffeic acid (≥ 98 wt. %), and curcumin (≥ 94 wt. %), were obtained from Merck Life Science (Darmstadt, Germany). (–)-Epicatechin (≥ 97 wt. %) was purchased from TCI Europe NV (Zwijndrecht, Belgium), apigenin (≥ 98 wt. %) from Indofine Chemical Company (Hillsborough, NJ, USA), and ascorbic acid (≥ 99 wt. %) was obtained from VWR International (Radnor, PA, USA). ULC-MS grade acetonitrile (ACN) and water, both containing 0.1 vol. % formic acid (FA) were purchased from Biosolve (Valkenswaard, The Netherlands). Water for other purposes than UHPLC was prepared using a Milli-Q (MQ) water purification system (Merck Millipore, Billerica, MA, USA).

6.2.2 Preparation of the Ca_2PP , Fe_4PP_3 , and mixed Ca-Fe(III) pyrophosphate salts

Iron (III) pyrophosphate ($\text{Fe}_4(\text{P}_2\text{O}_7)_3$, Fe_4PP_3), calcium pyrophosphate ($\text{Ca}_2\text{P}_2\text{O}_7$, Ca_2PP), and mixed Ca-Fe(III) pyrophosphate salts with different iron to calcium ratios according to the general formula $\text{Ca}_{2(1-x)}\text{Fe}_{4x}(\text{P}_2\text{O}_7)_{(1+2x)}$ with $x = 0.14, 0.15, 0.18$, and 0.35 were prepared using a coprecipitation method as described elsewhere.^[9] Uniformity in morphology was confirmed by transmission electron microscopy (TEM). Bulk morphology and chemical compositions of the mixed salts, obtained by energy-dispersive spectroscopy (TEM-EDX) are reported in **Fig. S6.1**.

6.2.3 Reactivity of the Ca_2PP , Fe_4PP_3 , and mixed Ca-Fe(III) pyrophosphate salts with phenolics

The Ca_2PP , Fe_4PP_3 , and the mixed Ca-Fe(III) pyrophosphate salts were redispersed in water by stirring (~ 250 rpm) with a magnetic stir bar (final amount of salt 10 mg mL^{-1}) followed by the addition of aqueous solutions (*i.e.* catechol, caffeic acid, and epicatechin) or dispersions (*i.e.* quercetin, apigenin, and curcumin) of the phenolics to reach a final concentration of 5 mM phenolic. Next, the pH of the dispersions was adjusted using a pH-stat device (Metrohm, Herisau, Switzerland) by automatic titration using 0.1 M HCl or 0.1 M NaOH . Subsequently, the dispersions with pH values ranging from one to eleven (steps of one) were incubated for 2 h at 23°C under continuous stirring at 1000 rpm . After incubation, the pH of each sample was measured again to determine the final pH. Finally, the samples were centrifuged at $15,000 \times g$ for 10 min , and the supernatants were separated to quantify the dissolved iron concentration and obtain the absorbance spectra.

6.2.4 Iron concentration measurement by ferrozine-based colourimetric assay

The total iron in the solution was quantified using a ferrozine-based colourimetric assay,^[19] with slight adaptations as described elsewhere.^[9] In short, the absorbance of the iron(II)-ferrozine complex at 565 nm was measured at room temperature in a SpectraMax iD3 (Molecular Devices, Sunnyvale, CA, USA). All measurements were performed in duplicate and quantification of the total dissolved iron was performed with a calibration curve of FeSO_4 (0.0078 – 1 mM, $R^2 > 0.99$). The relative change in soluble iron concentration after addition of phenolics was defined according to **equation 6.1**.

$$\text{Relative change} = \frac{\text{iron solubility with phenolics} - \text{iron solubility blank}}{\text{iron solubility blank}} \quad (\text{Eq. 6.1})$$

The iron quantification in presence of phenolics by the ferrozine assay was verified independently using inductively coupled plasma–atomic emission spectroscopy (ICP-AES) (**Method S6.1**).

6.2.5 Monitoring reactivity and discolouration by UV-Vis spectroscopy

The reactivity of the pure Fe_4PP_3 and Ca_2PP , as well as the mixed Ca-Fe(III) pyrophosphate salts in the presence of the different phenolic compounds, was monitored using ultraviolet-visible light (UV-Vis) spectroscopy. After centrifugation, 200 μl sample was transferred to a Corning UV-transparent flat-bottom polystyrene 96-well plate (Sigma Aldrich, St. Louis, MO, USA). Spectra were recorded in the range from 250 to 750 nm in a SpectraMax iD3 (Molecular Devices, Sunnyvale, CA, USA), at room temperature. The colour of the samples was visualised by taking an image (OnePlus 7T, Beijing, China) of the Eppendorf tubes with a uniform light source against a white background. The images were evaluated using the $L^*a^*b^*$ colour space (*i.e.* L^* dark or light, a^* red vs. green, b^* yellow vs. blue). The values were extracted using the standard image analysis software (Photoshop CC 2021, Adobe). In this procedure, the $L^*a^*b^*$ value was taken at five different spots in the supernatant and five spots in the precipitate (**Fig. S6.2**). The degree of difference between the phenolic blank and the samples of phenolics in presence of the iron-containing salts, ΔE_{ab} , corresponds to the distance between two points within the $L^*a^*b^*$ colour space. The ΔE_{ab} value (*e.g.* the absolute value of the colour difference, not the direction) was calculated according to **equation 6.2**.^[20,21]

$$\Delta E_{ab} = [(L_0^* - L_x^*)^2 + (a_0^* - a_x^*)^2 + (b_0^* - b_x^*)^2]^{1/2} \quad (\text{Eq. 6.2})$$

Where L_0^* , a_0^* , b_0^* and L_x^* , a_x^* , b_x^* are the colour space values for the blank phenolic and the phenolic exposed to the iron-containing salts, respectively.

6.2.6 Monitoring phenolics solubility and oxidation by RP-UHPLC-PDA-ESI-ITMSⁿ

The water solubility of the blank phenolics at pH 3, 6, and 8, and oxidation of epicatechin and quercetin at pH 3, 6, and 8 after incubation with the iron-containing salts, were analysed by reversed-phase ultra-high performance liquid chromatography coupled to electrospray ionisation ion trap mass spectrometry (RP-UHPLC-PDA-ESI-ITMSⁿ). Here, pH 3, 6, and 8 were chosen as they respectively represent gastric, food, and intestinal conditions.^[2,22]

To test the oxidation of epicatechin and quercetin after incubation with the iron-containing salts, the supernatants from **section 6.2.3** were separated from the precipitate to obtain the water soluble fractions. The precipitates were then solubilised in DMSO (100 vol. %), which is known to be a suitable solvent for metal:ligand systems.^[4,23] The resulting suspensions were centrifuged once more (at $15,000 \times g$ for 5 min) and the supernatants were separated to obtain the DMSO-soluble fractions. Phenolics' recovery and their oxidation products in the water soluble and DMSO-soluble fractions were separated on a Thermo Vanquish UHPLC system (Thermo Scientific, San Jose, CA, USA) equipped with an autosampler, a pump, and a photodiode array (PDA) detector. A sample (1 μ l) was injected on an Acquity UPLC BEH C18 column (150 mm \times 2.1 mm i.d., 1.7 μ m) with a VanGuard (5 mm \times 2.1 mm i.d., 1.7 μ m) guard column of the same material (Waters, Milford, MA). Water (A) and acetonitrile (B), both acidified with 0.1 vol. % formic acid, were used as eluents. The flow rate was 400 μ l min⁻¹, and the temperature of the column oven was 45 °C with the post-column cooler set to 40 °C. The elution profiles can be found in **Method S6.2**. The PDA detector was set to measure the wavelength range of 190 – 680 nm. Mass spectrometric data were acquired using a Velos Pro ion trap mass spectrometer (Thermo Scientific) equipped with a heated electrospray ionisation probe (ESI-ITMSⁿ) coupled in line to the Vanquish UHPLC system. Nitrogen was used as a sheath gas (50 arbitrary units) and auxiliary gas (13 arbitrary units). Data were collected over the m/z range of 100 – 1,500 in negative and positive ionisation mode by using source voltages of 2.5 and 3.5 kV, respectively. For both modes, the S-lens RF level was set at 67 %, the ion transfer tube and the source heater temperatures were 263 and 425 °C, respectively. Data-dependent MS² analysis was performed on the most intense ion by collision-induced dissociation (CID) with a normalised collision energy of 35 %. A dynamic mass exclusion approach was used, in which the most intense ion was fragmented 3 times and was subsequently excluded from fragmentation for the following 5 seconds, allowing data-dependent MS² of less intense co-eluting compounds. Data acquisition and processing were performed using Xcalibur (version 4.1, Thermo Scientific). Quantification of phenolic was performed based on PDA peak area (280 nm) and an external calibration curve of the corresponding authentic standard (0.003 – 0.5 mM, in duplicate, $R^2 = 1.00$). To assess whether the change in phenolic recovery was statistically significant, ANOVA analysis was performed using

IBM SPSS Statistic v23 software (SPSS Inc., Chicago, IL, USA). Tukey's *post hoc* comparisons (significant at $p < 0.05$) were carried out to evaluate the total concentration of the phenolics at different pH values in presence of the different salts.

6.2.7 Surface composition of the Ca_2PP , Fe_4PP_3 , and mixed Ca-Fe(III) pyrophosphate salts by X-ray photoelectron spectroscopy

The surface composition of Ca_2PP , Fe_4PP_3 , and Ca-Fe(III) pyrophosphate particles was determined by X-ray photoelectron spectroscopy (XPS), the sampling depth of XPS is 3-10 nm.^[24] The salts were also analysed after incubation with epicatechin (pH 6) using the same incubation setup as in **section 6.2.3**. After incubation, the samples were centrifuged at $5,000 \times g$ for 10 min and the precipitate was washed twice with water. Complete removal of water from the samples was ensured by overnight drying in a vacuum oven at 50 °C. Samples were prepared on indium foil. XPS measurements were performed using a JPS-g200 photoelectron spectrometer (JEOL Ltd., Japan). All samples were analysed using a focused monochromated Al K α X-ray source (spot size of 300 μm), wide scans were recorded at a constant dwelling time of 50 ms and pass energies of 50 eV. The power of the X-ray source was 240 W (20 mA and 12 kV). The charge compensation was used during the XPS scans with an accelerating voltage of 2.8 eV and a filament current of 4.8 A. XPS wide-scan were obtained under ultrahigh-vacuum conditions (base pressure, 3×10^{-7} Pa). The spectra were fitted with symmetrical Gaussian/Lorentzian (GL(30)) line shapes using CasaXPS (version 2.3.22PR1.0). All spectra were referenced to the C 1s peak attributed to C-C and C-H atoms at 285.0 eV.

6.3 Results & discussion

6.3.1 Dissolution behaviour of iron from Fe_4PP_3 and the mixed Ca-Fe(III) pyrophosphate salts in the presence of phenolics

The dissolution of total iron from Fe_4PP_3 and the mixed Ca-Fe(III) pyrophosphate salts in the presence of phenolic compounds was studied as a function of pH, using the ferrozine assay.^[19] This assay was verified for the combination of epicatechin and all salts by comparison with the ICP-AES method (**Fig. S6.3**). The soluble iron concentration from 10 mg mL⁻¹ dispersions of Fe_4PP_3 and the four mixed salts in the presence of the six different phenolics was evaluated in water in the food-relevant pH range 3-7 (**Fig. 6.2A**). The dispersions were prepared based on an equal amount of the salts (10 mg mL⁻¹). No direct relationship was observed between the theoretical maximum iron concentration of the dispersion and the measured iron concentration in solution (**Table S6.1**). The soluble iron concentrations presented here were determined after two hours incubation of the salt dispersions, and are therefore not necessarily equal to the solubilities (*i.e.* the equilibrium saturation concentrations). We assume that the iron dissolution from the mixed salt was complete at that time point.^[9]

We confirmed experimentally that at pH 3, 6, and 8 epicatechin, caffeic acid, and catechol showed good water solubility and that quercetin, apigenin, and curcumin were slightly soluble or insoluble in water in the absence of iron (**Fig. S6.4**). At food-relevant pH values (3-7), the mixed salts with $x \leq 0.18$ exhibit a lower soluble iron concentration than Fe_4PP_3 (**Fig. 6.2A**, blank). Additionally, the soluble iron concentration from the mixed salts with $x \leq 0.18$ depended on the pH and water solubility of the phenolic compound as well.

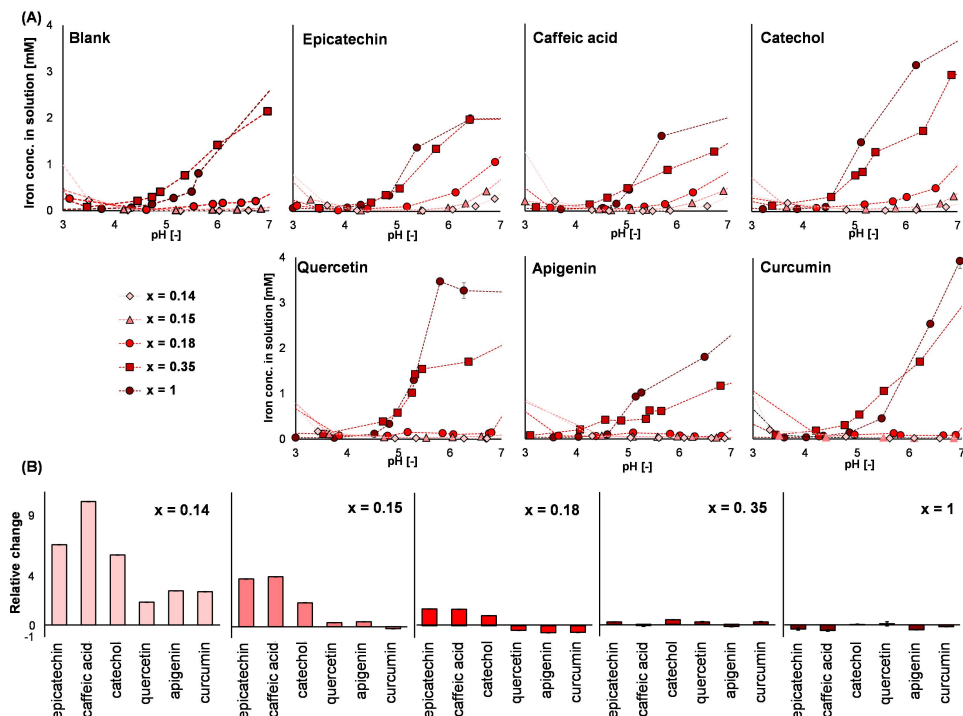


Figure 6.2. (A) Dissolution behaviour of iron at pH 3-7 from Fe_4PP_3 ($x = 1$) and mixed Ca-Fe(III) pyrophosphate salts with $x = 0.14$, $x = 0.15$, $x = 0.18$, and $x = 0.35$, in the absence of phenolics (blank), and in presence of catechol, caffeic acid, epicatechin, quercetin, apigenin, and curcumin at 23 °C. (B) Relative change (equation 6.1, section 6.2.4) in the soluble iron concentration from the salts in presence of the phenolic compound compared to the salts in absence of phenolic compound at pH 6-6.5.

In the range from pH 3 to 5, iron from the mixed Ca-Fe(III) pyrophosphate salts with $x \leq 0.18$ was (practically) insoluble regardless of the presence of phenolics, *i.e.* iron concentration in solution was $< 0.18 \text{ mM}$ which equals $< 0.1 \text{ g L}^{-1}$.^[25] In the pH range from 3 to 5, the phenolics did not affect the iron dissolution because all hydroxyl groups are protonated (the apparent pK_a range of phenolate is 5-8) and therefore do not coordinate iron.^[15] Upon increasing the pH from 5 to 7 the hydroxyl groups of the phenolics are deprotonated, leading to differential iron dissolution from the pyrophosphate salts for the different categories of phenolics (**Fig. 6.2A**). For the water

soluble phenolics (*i.e.* catechol, caffeic acid, and epicatechin), an up to 11-fold increase in soluble iron concentration from the mixed Ca-Fe(III) pyrophosphate salts with $x \leq 0.18$ was observed at pH 6-6.5 compared to the iron salt in the absence of the phenolics (**Fig. 6.2B**). However, in the presence of the slightly water soluble (*i.e.* quercetin and apigenin) and insoluble phenolics (*i.e.* curcumin), the relative change in soluble iron concentration was lower compared to water soluble phenolics and the iron remained practically insoluble. Interestingly, a higher dissolved iron concentration was measured for the salts with $x = 0.35$ and $x = 1$ in the presence of quercetin, compared to apigenin, despite the similar pK_a and $\log S$ values for these flavonoids (**Fig. 6.1A**). We suggest that the observed difference in the measured iron concentration in solution is because a charged, and therefore soluble, iron-phenolic complex is more likely for quercetin than for apigenin. This is expected to be due to the multiple iron-binding sites in the case of quercetin and the relatively high reported stability constant of iron-quercetin complexes resulting from the presence of a catecholate moiety (**Table S6.2**).^[26] Furthermore, the salt with $x = 0.35$ showed the highest absolute soluble iron concentration among the mixed salts and was similar to Fe_4PP_3 ($x = 1$) in the presence of all phenolics over the food-relevant pH range (3-7) (**Fig. 6.2A**). At pH 6-6.5 the soluble iron concentration from the salts with $x = 0.35$ and $x = 1$ was not affected by the solubility of the phenolic (**Fig. 6.2B**).

At pH < 3, in the blank and in presence of all phenolics, an increase in soluble iron concentration was observed from all mixed Ca-Fe(III) pyrophosphate salts compared to pure Fe_4PP_3 (**Fig. S6.5**). No clear trend was observed below pH 3 between the category of the phenolic and the soluble iron. At pH > 7, which includes the intestinal pH range, irrespective of the phenolic compound, lower iron concentrations in solution were measured for all the mixed Ca-Fe(III) pyrophosphate salts compared to Fe_4PP_3 . There was only one exception to this observation: For the salt with $x = 0.35$, at pH > 8 in the presence of epicatechin and caffeic acid, the soluble iron concentration was measured to be equal to and higher than that of Fe_4PP_3 , respectively (**Fig. S6.5**). Finally, the soluble iron from the mixed salts with $x = 0.14$ and 0.15 remained low (*i.e.* < 0.15 mM) and in line with the blank (no phenolics) in the presence of apigenin and curcumin at pH > 8. The effect of temperature on the dissolution behaviour of iron from the pyrophosphate salts in the presence of epicatechin was also investigated. The soluble iron concentration from the salts with $x \leq 0.18$ was observed to be similar at 23, 37, and 90 °C in the gastric and food-relevant pH ranges (**Fig. S6.6**). These results suggest that the soluble iron does not change in gastric conditions (37 °C), and after cooking (90 °C).^[27]

6.3.2 Discolouration of Ca_2PP , Fe_4PP_3 , and mixed Ca-Fe(III) pyrophosphate salts with phenolics

The total absorbance in the visible light spectra of the Ca_2PP , Fe_4PP_3 , and the mixed Ca-Fe(III) pyrophosphate salts in the presence of all phenolics was assessed at pH 6-

6.5 (**Fig. 6.3A**). This pH range was explored as it is in the range of most food products, and more particularly bouillon cubes, which is one of the preferred foods for iron fortification.^[28] The pH of three commercial bouillon cubes was measured to be 6.27 ± 0.59 . The colour of the supernatants and the precipitates were evaluated visually (**Fig. 6.3B**) and according to the *CIELab** colour space. The $L^*a^*b^*$ values were used to calculate the ΔE_{ab} as a qualitative tool for the colour difference between the supernatant and precipitate after exposing the phenolics to the iron-containing salts (**Fig. 6.3C**). It was assumed that when the ΔE_{ab} value is 3-5, the colour difference can be observed by an average consumer.^[29] An ΔE_{ab} value of up to 10 is considered to indicate an acceptable colour change for iron-fortified salts.^[30] For all samples the ΔE_{ab} value was > 5 , indicating that a colour difference could be observed (**Fig. 6.3C**).

For the samples in the presence of the water soluble phenolics (*i.e.* epicatechin, caffeic acid, and catechol), an absorbance band was observed with $\lambda_{\max} \sim 580$ nm (**Fig. 6.3A**). This broad absorbance band is due to the ligand-to-metal charge transfer (LMCT) phenomenon. This absorbance band with $\lambda_{\max} \sim 580$ nm is typically observed for Fe(III)-catechol complexes with a stoichiometry of 1:2 at pH ranging from 5-7 and causes the bluish to purplish appearance of the supernatants (**Fig. 6.3B**).^[18,31] Moreover, in the presence of the water soluble phenolics, the precipitate changed from white to a greyish/bluish colour. We hypothesised previously that the discolouration of the precipitates at pH 6.5 can be due to the formation of Fe(III)-phenolic complexes at the surface of the salts,^[9] which is further discussed in **section 6.3.4**. In line with these colour changes in the supernatant and precipitate, the ΔE_{ab} differences for water soluble phenolics in presence of the Fe(III)-containing salts were unacceptable and much larger than for the slightly water soluble and insoluble phenolics (quercetin, apigenin, and curcumin) (**Fig. 6.3C**). In the case of quercetin, increased absorbance in the visual spectra was observed in the presence of Fe_4PP_3 and the mixed salt with $x = 0.35$ (**Fig. 6.3A**). The absorbance band with $\lambda_{\max} \sim 570$ nm is due to the LMCT phenomenon and the increase in the intensity of absorbance at 450 nm is due to the bathochromic shift of the cinnamoyl band of quercetin.^[4] In the absence of any of the iron-containing salts or in the presence of the mixed salts with $x \leq 0.18$, the supernatant of the quercetin sample did not show any absorbance due to the poor solubility of quercetin in water. The increased absorbance observed in the supernatant in presence of the salts with $x = 0.35$ and $x = 1$ is suggested to be a result of the formation of a charged Fe(III)-quercetin complex that improves the solubility of quercetin.^[32] For apigenin and curcumin, no increase in absorbance was observed in the presence of iron-containing salts (**Fig. 6.3A**), in line with the transparent supernatants of these samples (**Fig. 6.3B**). For the supernatants of quercetin in the presence of Ca_2PP and the mixed salts (with $x \leq 0.18$) and for apigenin and curcumin in presence of all salts the ΔE_{ab} value was at maximum around 10. The images of apigenin indicate that the precipitates in the presence of Fe_4PP_3 and the mixed salt with $x = 0.35$ turned dark brown.

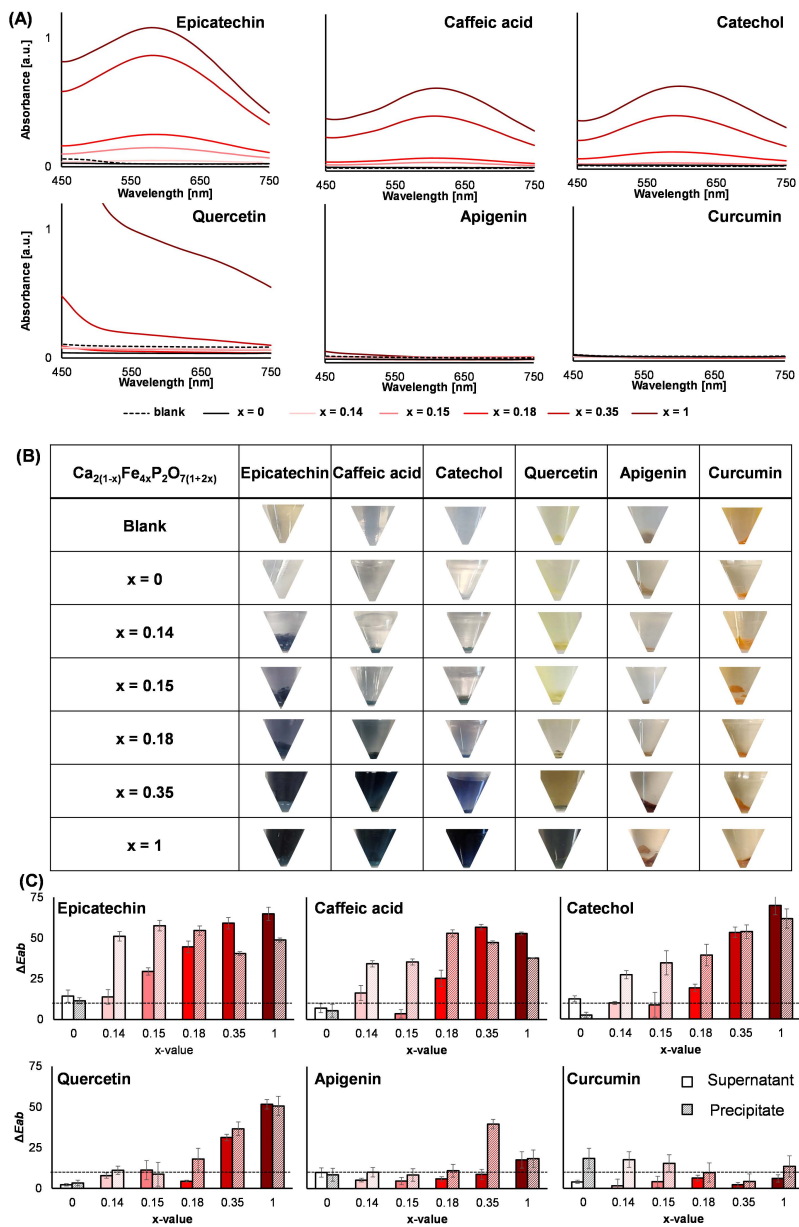


Figure 6.3. (A) Absorbance spectra of the supernatants of Ca_2PP ($x=0$), Fe_4PP_3 ($x=1$), and mixed Ca-Fe(III) pyrophosphate salts with 0.14, 0.15, 0.18, and 0.35 in the presence of the different phenolics at pH 6. The dashed lines indicate the absorbance of the pure phenolics (in the absence of the salts). (B) Pictures of the supernatants and precipitates in the Eppendorf tubes. (C) The values of ΔE_{ab} correspond to the colour changes in the supernatant (filled bar) and precipitate (striped bar) after being exposed to Ca_2PP , Fe_4PP_3 , and the mixed Ca-Fe(III) pyrophosphate salts, compared to no salts (*i.e.* blank phenolics). The dashed line indicates the maximum acceptable colour change (*i.e.* $\Delta E_{ab} = 10$).

Additionally, for curcumin a slightly darker layer was observed on the precipitate in the presence of Fe_4PP_3 (Fig. 6.3B). This indicates that complexation reactions between iron and apigenin or curcumin occurred, but the formed products remained insoluble. This is most likely for one or a combination of the following three reasons: (i) Fe(III)-phenolic complexation at the surface of the undissolved salt particles, (ii) the formation of neutral and/or insoluble complexes of iron with these phenolics,^[32] or (iii) the inherently poor solubility of these phenolics (Fig. S6.4). In line with the observed discolouration in the precipitate (Fig. 6.3B), the ΔE_{ab} value of quercetin and apigenin in the presence of Fe_4PP_3 or the salt with $x = 0.35$ was unacceptable (> 10). The ΔE_{ab} value for the precipitate of curcumin in the presence of the salts with $x \leq 0.15$ was also > 10 . This apparent colour change to lighter shades of orange (lightness $L^* = 48$ for blank versus $L^* = 64$ for Ca_2PP) is resulting from the presence of white or off-white insoluble pyrophosphate salts in these precipitates that mix with curcumin, compared to the orange colour of pure curcumin (blank), rather than from dark-colour formation.

We observed that the intensity of the LMCT absorbance band (Fig. 6.3A) increased monotonically with the x -value of the mixed Ca-Fe(III) pyrophosphate salts. For the mixed salts with $0 \leq x \leq 0.35$ in presence of catechol, caffeic acid, epicatechin, and quercetin, the area under the curve in the visible range ($\text{AUC}_{380-750}$) showed a linear relationship with the iron concentration in solution ($R^2 > 0.97$) (Fig. S6.7). For epicatechin and quercetin the R^2 value decreased from 0.995 to 0.970 and from 0.990 to 0.872, respectively, if the point corresponding to Fe_4PP_3 ($x = 1$) was included, because the slope of $\text{AUC}_{380-750}$ suddenly increased from $x = 0.35$ to $x = 1$. It has previously been shown that the inclusion of the divalent metals (*i.e.* M(II)), such as calcium, can change the dark-coloured iron-phenolic complexation product towards a colourless M(II)-phenolic reaction product via metal competition for complexation with phenolics.^[33] If this competition would occur in these samples, then we would expect this relation between $\text{AUC}_{380-750}$ and iron concentration to be non-linear, because the samples at lower x -value contain relatively more Ca compared to higher x -values (*i.e.* for $x = 0.14$ $\text{Ca}/\text{Fe} = 3.1$ and for $x = 0.35$ the $\text{Ca}/\text{Fe} = 0.93$). However, our findings show a direct linear relationship between the iron concentration and colour, thus, we conclude that the effect of metal competition on colour was likely very limited in these samples. We suggest that competition is limited because Fe(III) is a harder Lewis acid compared to Ca, and therefore a much larger excess of Ca (*i.e.* $\text{Ca}/\text{Fe} \geq 10$) should be present to effectively limit colour change via metal competition.^[2]

Overall, for water soluble phenolics, the use of mixed Ca-Fe(III) pyrophosphate salts did not protect against adverse colour changes that are caused by iron-phenolic complexation, as is indicated by the observed colour change and presence of the LMCT band in the absorbance spectra. For quercetin, apigenin, and curcumin, the colour change was limited to acceptable values ($\Delta E_{ab} \sim 10$) in the presence of salts with $x \leq 0.18$. These outcomes show that the mixed Ca-Fe(III) pyrophosphate salts are

more suitable for fortification of food products that do not contain water soluble phenolic compounds. Moreover, these findings explain why the mixed salts show comparable reactivity to Fe_4PP_3 in a model black tea solution, which mainly contains water soluble phenolics.^[9]

6.3.3 Oxidation rate of phenolics in the presence of the Ca_2PP , Fe_4PP_3 , and mixed Ca-Fe(III) pyrophosphate salts

Complexation reactions can be succeeded by oxidation reactions of phenolics because the complexation can be followed by an electron transfer from the ligand to Fe(III).^[34] Subsequent reactions of the oxidised phenolics yield a plethora of products that can arise from phenolic degradation and oxidative coupling. Because of the extended conjugated system of phenolics after oxidative coupling, these products may also contribute to discolouration.^[35] To date, the effect of Fe_4PP_3 and mixed Ca-Fe(III) pyrophosphate salts on phenolic oxidation is unknown. Therefore, we quantified the recovery of phenolics after incubation in the presence of the studied pyrophosphate salts at selected pH values (*i.e.* 3, 6, and 8) by RP-UHPLC-PDA-MSⁿ (Fig. 6.4). Epicatechin and quercetin were chosen as representatives for water soluble and slightly soluble/insoluble categories of the studied phenolics, respectively.

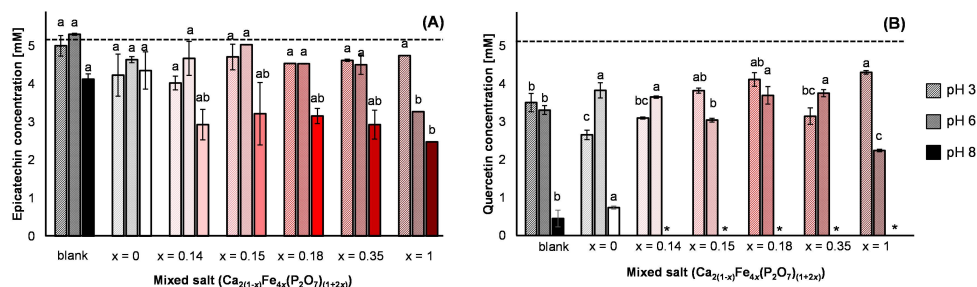


Figure 6.4. Recovery of (A) epicatechin and (B) quercetin in the absence and presence of Ca_2PP ($x = 0$), Fe_4PP_3 ($x = 1$), and mixed Ca-Fe(III) pyrophosphate salts with $x = 0.14$, 0.15 , 0.18 , and 0.35 at pH 3 (striped bar), 6 (dotted bar), and 8 (filled bar) after incubation for 2 h at 23 °C. The error bars indicate the standard deviation of independent duplicates. The dashed line indicates the initial concentration of the phenolics (5 mM). Different letters indicate a significant difference in the concentration compared to the other x -values for the same pH value (Tukey's test, $p < 0.05$). * indicates that the concentration was below the limit of quantification.

At pH 3, no significant difference ($p > 0.05$) was observed in the recovery of epicatechin in the presence of the different pyrophosphate salts (Fig. 6.4A). Because the hydroxyl groups are protonated at pH 3 (Fig. 6.1), no complexation and subsequent oxidation reactions occurred at pH 3. In the case of quercetin at pH 3, a significant decrease in recovery was observed for the blank and in presence of the different salts. (Fig. 6.4B). These differences could not be linked to the x -value of the salts, and because no oxidation products were detected in these samples (results not shown) it remains unclear why significantly different recoveries were observed at pH 3. Possibly

some quercetin was lost due to the poor solubility and adsorption on the electrode during pH adjustment.

At pH 6, a significant decrease ($p < 0.05$) in the recovery of epicatechin and quercetin in the presence of Fe_4PP_3 ($x = 1$) was observed compared to the blank, Ca_2PP , and all mixed Ca-Fe(III) pyrophosphate salts. The significant decrease in intact epicatechin and quercetin by 35 % and 55 % of their initial amount, respectively, after 2 hours of exposure to the Fe_4PP_3 is suggested to be due to oxidation of the phenolic compounds. This was supported by an increase in peak areas of the main oxidation products from epicatechin (δ -type dehydrocatechin) and quercetin (2,4,6-trihydroxyphenyl glyoxylic acid and 3,4-dihydroxybenzoic acid) upon increasing x -value (**Fig. S6.8**, and **Fig. S6.9**).^[4,35] For quercetin, more oxidative degradation products rather than oxidative coupling products were observed compared to epicatechin due to the presence of the 3-OH group in conjugation with the C2-C3 double bond, which enables formation of the highly reactive quinone methides as intermediates in the degradation of quercetin.^[36] Faster oxidation of the phenolics in the presence of Fe_4PP_3 at pH 6 can be linked to a higher degree of complexation as shown in **section 6.3.2**. Exposure to Fe_4PP_3 resulted in the most intense discolouration caused by more complex formation of quercetin and epicatechin with iron ions.

After 2 h incubation of epicatechin at pH 8 in the presence of Fe_4PP_3 , the epicatechin concentration significantly decreased compared to incubation of the blank or in the presence of Ca_2PP ($p < 0.05$) (**Fig. 6.4A**). The concentration of recovered epicatechin was not significantly different in the presence of the various mixed Ca-Fe(III) pyrophosphate salts. Similarly, no significant difference between the salts could be found for quercetin because its fast oxidation in the presence of the Fe(III)-containing pyrophosphate salts at pH 8 resulted in concentrations being below the limit of quantification. However, in the blank or in presence of Ca_2PP , a significantly higher amount of quercetin was recovered compared to all iron-containing salts.

At food-relevant pH (*i.e.* 6), the inclusion of calcium in the Fe(III)-containing pyrophosphate salts resulted in less oxidation of the phenolic compound compared to pure Fe_4PP_3 . This is the first indication that fortification of foods with mixed Ca-Fe(III) pyrophosphate salts instead of pure Fe_4PP_3 can potentially limit the extent of iron-mediated food oxidation. Even though oxidation is already limited to a certain extent in the presence of Fe_4PP_3 compared to FeSO_4 , because of the decreased soluble iron concentration,^[30,37] inclusion of calcium in the Ca-Fe(III) pyrophosphate salts further lowers the soluble iron concentration, thereby limiting phenolic oxidation as well. Another added benefit of the limited phenolic oxidation in the presence of the mixed Ca-Fe(III) pyrophosphate salts is inhibition of the formation of the potentially toxic or mutagenic oxidative degradation products of quercetin upon iron fortification.^[38] Besides oxidation of phenolics, oxidation of fatty acids, amino acids, and other micronutrients may also occur in presence of Fe(III).^[37] It should be further

investigated whether these iron-mediated oxidation reactions are also limited in the presence of the mixed Ca-Fe(III) pyrophosphate compared to Fe_4PP_3 .

6.3.4 Surface composition of Ca_2PP , Fe_4PP_3 , and mixed Ca-Fe(III) pyrophosphate salts in the absence and presence of phenolics

The mixed Ca-Fe(III) pyrophosphate salts based on the general formula, $\text{Ca}_{2(1-x)}\text{Fe}_x(\text{P}_2\text{O}_7)_{(1+2x)}$ with a theoretical x -value < 0.33 contain a lower percentage of Fe compared to Ca in bulk. This $\text{Ca/Fe} > 1$ has previously been confirmed for the salts with $x \leq 0.18$ by TEM-EDX,^[9] and is indicated by the ratios of Fe/P and Ca/P for the salts as shown in **Fig. 6.5A**.

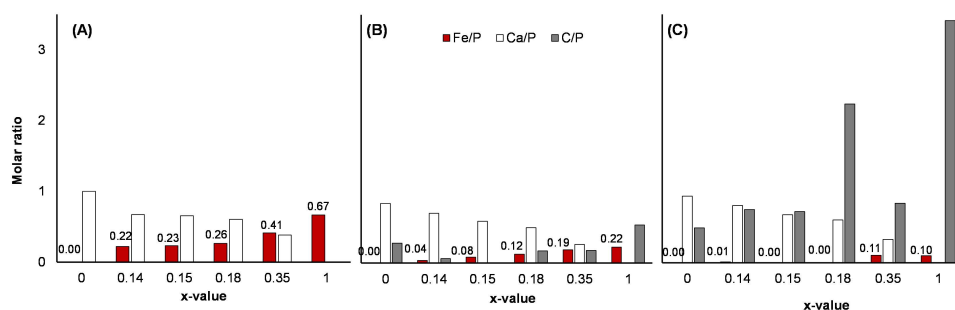


Figure 6.5. Analysis of the elemental composition of the Ca_2PP ($x = 0$), Fe_4PP_3 ($x = 1$), and mixed Ca-Fe(III) pyrophosphate salts with $x = 0.14$, 0.15 , 0.18 , and 0.35 , **(A)** in the bulk by TEM-EDX obtained from,^[9] **(B)** at the surface by XPS, and **(C)** at the surface after reactivity with epicatechin at pH 6. The data labels on the bars indicate the Fe/P ratios.

We hypothesised that the incorporation of calcium as a second mineral along with iron in the pyrophosphate matrix would reduce the iron content at the surface of the mixed Ca-Fe(III) pyrophosphate salts and thereby lower the soluble iron concentration and iron-mediated reactivity. XPS measurements were employed to find the elemental composition at the surface of these salts (**Fig. 6.5B**, wide scan XPS spectra in **Fig. S6.10**). To interpret the data, the elemental percentages of the salts obtained from XPS were normalised with respect to phosphorus. It was confirmed that Fe_4PP_3 and all the mixed salts contained a lower iron to phosphorus ratio (Fe/P) at the surface than in the bulk, with up to a 5.5-fold decrease in the case of the mixed salt with $x = 0.14$. This variation in distribution of iron elements in the salt matrix (*i.e.* surface vs. bulk) can be caused by the higher dissolution of Fe ions than Ca ions from the surface of the pyrophosphate salts in water at the pH of the reaction mixture which results in higher Fe solubilisation from the salts during the washing steps for purification.^[9,39] This solubilisation of Fe from the surface of the salts can be experimentally linked to the negative surface charge of the salts particles in their colloidal state (before drying to powder) at this pH range as well (**Fig. S6.11**). However, comparing the calcium to phosphorus ratio (Ca/P) in the bulk and at the surface of the salts showed that this ratio was the same or slightly lower (on average 1.18 ± 0.18 fold). These results suggest that the mixed pyrophosphate salts have a lower iron to calcium ratio at their surface

compared to their bulk composition, despite having homogeneous elemental distribution throughout their aggregates.^[9]

The XPS measurements were also utilised to obtain the carbon to phosphorus ratio (C/P) as an indication of the presence of phenolics on the surface of the salts. Accurate determination of elemental ratios of carbon in the bulk using TEM-EDX was not possible due to the carbon film on the TEM grids. The XPS measurements indicated that after exposing the salts to epicatechin and removal of the free epicatechin by washing with water, C/P at the surface of the salts increased noticeably, by up to 13-fold (Fig. 6.5C, wide scan XPS spectra in Fig. S6.12. Although the minor amounts of carbon present in XPS spectra are inevitable (e.g. due to the presence of atmospheric carbon dioxide impurities), this considerable increase in the carbon content at the surface of the Fe(III)-containing iron salts is additional confirmation, besides the colour of the precipitates, for the presence of epicatechin at the surface of the insoluble pyrophosphate salts. In addition, Fe/P at the surface of the iron-containing salts decreased substantially, up to a 3.2-fold, after incubation with epicatechin, whereas the Ca/P ratio remained similar (Fig. 6.5C). This indicates that besides binding of Fe at the surface of the salt by epicatechin, a significant proportion of Fe was released into the solution after complexation with epicatechin, which is in line with the increased soluble iron concentration in the presence of epicatechin (Fig. 6.2, and Fig. S6.13). Furthermore, it is possible that a fraction of Fe at the surface of these salts is covered by the bound epicatechin and therefore the detection intensity of iron can be decreased in XPS measurements due to this spatial hindrance.

6.3.5 Possible mechanism for reactivity of iron from Fe₄PP₃ and mixed Ca-Fe(III) pyrophosphate salts

This study demonstrated that the dissolution behaviour of iron from Fe₄PP₃ and mixed Ca-Fe(III) pyrophosphate salts depends on the x-value of the salt, the pH, the solubility of the phenolic compound, and the Fe(III)-coordinating group(s) of the phenolic compound. Fig. 6.6 schematically summarises the fate of the Fe(III)-containing pyrophosphate salts with different x-values in the absence and presence of phenolics at pH 6-6.5 (representative for food products).

In the absence of phenolics, the salts with $x \leq 0.18$ show up to an eight-fold decrease in soluble iron concentration compared to Fe₄PP₃. In the presence of water soluble phenolics, the colour of both the supernatant and the precipitate is negatively affected. Firstly, the precipitate turns dark due to interactions of the water soluble phenolic with iron present at the surface of the salts. Secondly, after binding the water soluble phenolic to the iron at the surface, the iron-phenolic complex releases into solution and becomes soluble, causing discolouration of the supernatant. For slightly water soluble and insoluble phenolics with an *ortho*-diphenolic group, we suggest that the soluble iron can form stable charged complexes that are solubilised in water,

leading to discolouration in both the supernatant and precipitate. For slightly water soluble and insoluble phenolics without the *ortho*-diphenolic group, there is no interaction between the iron and the phenolic for the mixed salts with $x \leq 0.18$. If iron is already present in the solution (*i.e.* $x = 0.35$ and 1), it can coordinate to the insoluble phenolic and cause discolouration in the precipitate but these Fe(III)-phenolic coordinates remain insoluble. The schematic overview in **Fig. 6.6** only applies when the pH is above the apparent pK_a of the phenolic compounds, as deprotonation of the phenolic hydroxyl groups is a prerequisite for these interactions.

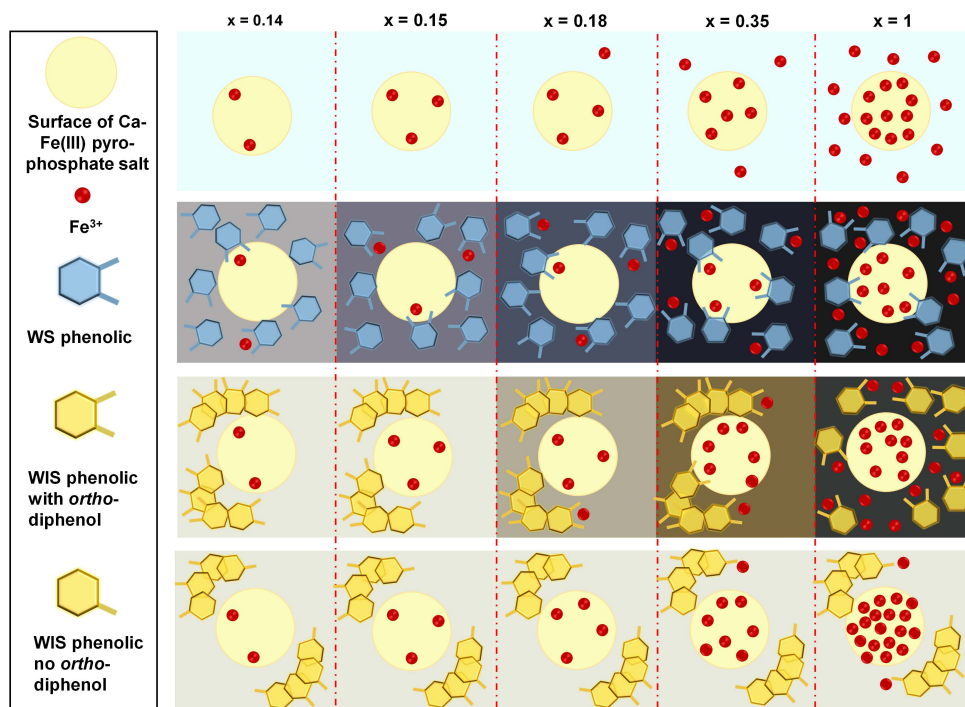


Figure 6.6. Schematic overview of the proposed mechanism underlying the observed dissolution behaviour of iron at the surface of the Fe₄PP₃ ($x = 1$) and mixed Ca-Fe(III) pyrophosphate salts with $x = 0.14$, 0.15 , 0.18 , and 0.35 , and the reactivity of iron from these salts in the presence of phenolics at pH 6. The colours in the squares are in line with the experimentally observed colour of the supernatant, a dark outline on the salt surface indicates the discolouration observed in the precipitate. WS = water soluble, WIS = slightly water soluble or water insoluble.

This is the first study to report that the reactivity of Fe(III)-containing pyrophosphate salts in the presence of phenolic compounds is dependent on the solubility and iron-coordinating groups of the phenolic. Understanding the reactivity of the mixed pyrophosphate salts with phenolics is helpful for the application of these salts in the design of iron-fortified food products. The present findings show that these salts are potential iron-fortificants for application in food products that mainly contain poorly

water soluble phenolic compounds, such as bouillon cubes. In future studies, the reactivity of the mixed salts can be assessed in real food products and in the presence of product-specific mixtures of phenolic compounds.

6.4 Conclusion

In this study, we investigated the reactivity of Fe_4PP_3 and mixed Ca-Fe(III) pyrophosphate salts (based on the general formula $\text{Ca}_{2(1-x)}\text{Fe}_{4x}(\text{P}_2\text{O}_7)_{(1+2x)}$ with $0 \leq x \leq 1$) in the presence of six different phenolic compounds. Besides iron-phenolic reactivity, which results in complexation and oxidation, the effect of the presence of phenolic compounds on iron solubility from the salts was also assessed. At pH 5-7, the water soluble phenolics (*i.e.* catechol, caffeic acid, and epicatechin) increased iron solubility from the mixed pyrophosphate salts by up to 11-fold, by solubilisation of iron from the surface of the salts. This led to unacceptable discolouration as a result of Fe(III)-phenolic complexation. In the presence of the slightly water soluble (*i.e.* quercetin and apigenin) and insoluble phenolics (*i.e.* curcumin), iron from the salts remained practically insoluble. Furthermore, for the salts with $x \leq 0.18$, the colour change after exposure to these poorly water soluble phenolics remained acceptable for application. In addition, all mixed Ca-Fe(III) pyrophosphate salts resulted in significantly less oxidation of epicatechin and quercetin at pH 6 compared to Fe_4PP_3 . In conclusion, mixed pyrophosphate salts with $x \leq 0.18$ cause limited iron-mediated discolouration and oxidation. Thereby, they can potentially be used in designing iron-fortified foods containing slightly water soluble and/or water insoluble phenolics. In future studies, the reactivity of these salts in real food products, along with associated changes in other sensory properties should be investigated. Additionally, the *in vivo* iron bioavailability and the potential of these salts as dual-fortificants have to be investigated in future work.

6.5 Acknowledgements

The authors are grateful to Barend van Lagen (Organic Chemistry, Wageningen University & Research) for performing the XPS measurements. Arjen Reichwein, Raymond Nijveld, and Teun de Bruin of Nouryon Chemicals B.V. are thanked for performing the ICP-AES measurements. The graphical abstract was made with content from BioRender.com. Part of the presented results were obtained using a Thermo Scientific Velos Pro MS system and X-ray photoelectron spectroscopy which are owned by WUR-Shared Research Facilities. Investment by WUR-Shared Research Facility was made possible by the 'Regio Deal Foodvalley' of the province of Gelderland, The Netherlands.

6.6 References

- 1 Allen, L. H., De Benoist, B., Dary, O., Hurrell, R., & (Eds.). (2006) *Guidelines on food fortification with micronutrients*. Geneva, Switzerland: World Health Organization.
- 2 Habeych, E., van Kogelenberg, V., Sagalowicz, L., Michel, M., & Galaffu, N. (2016). Strategies to limit colour changes when fortifying food products with iron. *Food Research International*, 88, 122-128.
- 3 Janssen, R. H., Canelli, G., Sanders, M. G., Bakx, E. J., Lakemond, C. M., Fogliano, V., & Vincken, J.-P. (2019). Iron-polyphenol complexes cause blackening upon grinding *Hermetia illucens* (black soldier fly) larvae. *Scientific Reports*, 9(1), 2967.
- 4 Bijlsma, J., de Bruijn, W. J. C., Velikov, K. P., & Vincken, J.-P. (2022). Unravelling discolouration caused by iron-flavonoid interactions: Complexation, oxidation, and formation of networks. *Food Chemistry*, 370, 131292.
- 5 Andre, C. M., Evers, D., Ziebel, J., Guignard, C., Hausman, J.-F., Bonierbale, M., zum Felde, T., & Burgos, G. (2015). In vitro bioaccessibility and bioavailability of iron from potatoes with varying vitamin C, carotenoid, and phenolic concentrations. *Journal of Agricultural and Food Chemistry*, 63(41), 9012-9021.
- 6 Hurrell, R. (2002). How to ensure adequate iron absorption from iron-fortified food. *Nutrition Reviews*, 60, S7-S15.
- 7 Hurrell, R. F., Lynch, S., Bothwell, T., Cori, H., Glahn, R., Hertrampf, E., Kratky, Z., Miller, D., Rodenstein, M., Streekstra, H., Teucher, B., Turner, E., Yeung, C. K., & Zimmermann, M. B. (2004). Enhancing the absorption of fortification iron. *International Journal for Vitamin and Nutrition Research*, 74(6), 387-401.
- 8 Dueik, V., Chen, B. K., & Diosady, L. L. (2017). Iron-polyphenol interaction reduces iron bioavailability in fortified tea: Competing complexation to ensure iron bioavailability. *Journal of Food Quality*, 2017, 1-8.
- 9 Moslehi, N., Bijlsma, J., De Bruijn, W. J. C., Velikov, K. P., Vincken, J.-P., & Kegel, W. K. (2022). Design and characterization of Ca-Fe(III) pyrophosphate salts with tunable pH-dependent solubility for dual-fortification of foods. *Journal of Functional Foods*, 92, 105066.
- 10 Mohammed, F., Rashid-Doubell, F., Cassidy, S., & Henari, F. (2017). A comparative study of the spectral, fluorometric properties and photostability of natural curcumin, iron-and boron-complexed curcumin. *Spectrochimica Acta Part A: Molecular and Biomolecular Spectroscopy*, 183, 439-450.
- 11 Nkhili, E., Loonis, M., Mihai, S., El Hajji, H., & Dangles, O. (2014). Reactivity of food phenols with iron and copper ions: Binding, dioxygen activation and oxidation mechanisms. *Food & Function*, 5(6), 1186-1202.
- 12 Perron, N. R., & Brumaghim, J. L. (2009). A review of the antioxidant mechanisms of polyphenol compounds related to iron binding. *Cell Biochemistry and Biophysics*, 53(2), 75-100.
- 13 Sorkun, M. C., Khetan, A., & Er, S. (2019). AqSolDB, a curated reference set of aqueous solubility and 2D descriptors for a diverse set of compounds. *Scientific Data*, 6(1), 143.
- 14 Delgado, A. M., Issaoui, M., & Chammem, N. (2019). Analysis of main and healthy phenolic compounds in foods. *Journal of AOAC International*, 102(5), 1356-1364.
- 15 Hider, R. C., Liu, Z. D., & Khodr, H. H. (2001). Metal chelation of polyphenols. *Methods in Enzymology*, 335, 190-203.
- 16 Silva, A., Kong, X., & Hider, R. C. (2009). Determination of the pKa value of the hydroxyl group in the α -hydroxycarboxylates citrate, malate and lactate by ^{13}C NMR: Implications for metal coordination in biological systems. *Biometals*, 22(5), 771-778.
- 17 Kasprzak, M. M., Erxleben, A., & Ochocki, J. (2015). Properties and applications of flavonoid metal complexes. *RSC Advances*, 5(57), 45853-45877.
- 18 Bijlsma, J., de Bruijn, W. J. C., Hageman, J. A., Goos, P., Velikov, K. P., & Vincken, J.-P. (2020). Revealing the main factors and two-way interactions contributing to food discolouration caused by iron-catechol complexation. *Scientific Reports*, 10(1), 8288.
- 19 Stookey, L. L. (1970). Ferrozine: A new spectrophotometric reagent for iron. *Analytical Chemistry*, 42(7), 779-781.
- 20 Poynton, C. (2012). The CIE system of colorimetry. In M. Kaufmann (Ed.), *Digital video and HD: Algorithms and interfaces*, vol. 2 (pp. 266-285). Waltham, MA, USA: Elsevier.
- 21 Araki, H., Kim, J., Zhang, S., Banks, A., Crawford, K. E., Sheng, X., Gutruf, P., Shi, Y., Pielak, R. M., & Rogers, J. A. (2017). Materials and device designs for an epidermal UV colorimetric dosimeter with near field communication capabilities. *Advanced Functional Materials*, 27(2), 1604465.
- 22 Tian, T., Blanco, E., Smoukov, S. K., Velez, O. D., & Velikov, K. P. (2016). Dissolution behaviour of ferric pyrophosphate and its mixtures with soluble pyrophosphates: Potential strategy for increasing iron bioavailability. *Food Chemistry*, 208, 97-102.
- 23 El-Sherif, A. A., Shoukry, M. M., & Abd-Elgawad, M. M. A. (2013). Protonation equilibria of some selected α -amino acids in DMSO-water mixture and their Cu(II)-complexes. *Journal of Solution Chemistry*, 42(2), 412-427.
- 24 Giesbers, M., Marcelis, A. T. M., & Zuilhof, H. (2013). Simulation of XPS C1s spectra of organic monolayers by quantum chemical methods. *Langmuir*, 29(15), 4782-4788.
- 25 Liangou, A., Florou, K., Psichoudaki, M., Kostenidou, E., Tsiligiannis, E., & Pandis, S. N. (2022). A method for the measurement of the water solubility distribution of atmospheric organic aerosols. *Environmental Science & Technology*, 56(7), 3952-3959.

- 26 Malacaria, L., Corrente, G. A., Beneduci, A., Furia, E., Marino, T., & Mazzone, G. (2021). A review on coordination properties of Al(III) and Fe(III) toward natural antioxidant molecules: Experimental and theoretical insights. *Molecules*, 26(9), 2603.
- 27 Swain, J. H., Newman, S. M., & Hunt, J. R. (2003). Bioavailability of elemental iron powders to rats is less than bakery-grade ferrous sulfate and predicted by iron solubility and particle surface area. *The Journal of Nutrition*, 133(11), 3546-3552.
- 28 Moretti, D., Hurrell, R. F., & Cercamondi, C. I. (2018). Bouillon cubes. In M. G. V. Mannar & R. F. Hurrell (Eds.), *Food fortification in a globalized world*, (pp. 159-165): Elsevier.
- 29 Ghidouche, S., Rey, B., Michel, M., & Galaffu, N. (2013). A rapid tool for the stability assessment of natural food colours. *Food Chemistry*, 139(1), 978-985.
- 30 Wegmüller, R., Zimmermann, M. B., & Hurrell, R. F. (2003). Dual fortification of salt with iodine and encapsulated iron compounds: Stability and acceptability testing in Morocco and Côte d'Ivoire. *Journal of Food Science*, 68(6), 2129-2135.
- 31 Elhabiri, M., Carrër, C., Marmolle, F., & Traboulsi, H. (2007). Complexation of iron(III) by catecholate-type polyphenols. *Inorganica Chimica Acta*, 360(1), 353-359.
- 32 Malacaria, L., La Torre, C., Furia, E., Fazio, A., Caroleo, M. C., Cione, E., Gallelli, L., Marino, T., & Plastina, P. (2022). Aluminum(III), iron(III) and copper(II) complexes of luteolin: Stability, antioxidant, and anti-inflammatory properties. *Journal of Molecular Liquids*, 345, 117895.
- 33 Guo, J., Ping, Y., Ejima, H., Alt, K., Meissner, M., Richardson, J. J., Yan, Y., Peter, K., Von Elverfeldt, D., & Hagemeyer, C. E. (2014). Engineering multifunctional capsules through the assembly of metal-phenolic networks. *Angewandte Chemie International Edition*, 53(22), 5546-5551.
- 34 Ryan, P., & Hynes, M. J. (2008). The kinetics and mechanisms of the reactions of iron(III) with quercetin and morin. *Journal of Inorganic Biochemistry*, 102(1), 127-136.
- 35 Tan, J., de Bruijn, W. J. C., van Zadelhoff, A., Lin, Z., & Vincken, J.-P. (2020). Browning of epicatechin (EC) and epigallocatechin (EGC) by auto-oxidation. *Journal of Agricultural and Food Chemistry*, 68(47), 13879-13887.
- 36 Stepanic, V., Gasparovic, A. C., Troselj, K. G., Amic, D., & Zarkovic, N. (2015). Selected attributes of polyphenols in targeting oxidative stress in cancer. *Current Topics in Medicinal Chemistry*, 15(5), 496-509.
- 37 Zuidam, N. J. (2012). An industry perspective on the advantages and disadvantages of iron micronutrient delivery systems. In N. Garti & D. J. McClements (Eds.), *Encapsulation technologies and delivery systems for food ingredients and nutraceuticals*, (pp. 505-540): Woodhead Publishing.
- 38 Harwood, M., Danielewska-Nikiel, B., Borzelleca, J. F., Flamm, G. W., Williams, G. M., & Lines, T. C. (2007). A critical review of the data related to the safety of quercetin and lack of evidence of in vivo toxicity, including lack of genotoxic/carcinogenic properties. *Food and Chemical Toxicology*, 45(11), 2179-2205.
- 39 van Leeuwen, Y. M. (2013). *Colloidal metal pyrophosphate salts: Preparation, properties and applications*, Ph.D. Thesis. Utrecht University, Utrecht.
- 40 Avdeef, A., Sofen, S. R., Bregante, T. L., & Raymond, K. N. (1978). Coordination chemistry of microbial iron transport compounds. 9. Stability constants for catechol models of enterobactin. *Journal of the American Chemical Society*, 100(17), 5362-5370.
- 41 Hynes, M. J., & O'Coinceanainn, M. n. (2004). The kinetics and mechanisms of reactions of iron(III) with caffeic acid, chlorogenic acid, sinapic acid, ferulic acid and naringin. *Journal of Inorganic Biochemistry*, 98(8), 1457-1464.
- 42 Escandar, G. M., & Sala, L. F. (1991). Complexing behavior of rutin and quercetin. *Canadian Journal of Chemistry*, 69(12), 1994-2001.
- 43 Borsari, M., Ferrari, E., Grandi, R., & Saladini, M. (2002). Curcuminoids as potential new iron-chelating agents: Spectroscopic, polarographic and potentiometric study on their Fe(III) complexing ability. *Inorganica Chimica Acta*, 328(1), 61-68.

6.7 Supplementary information

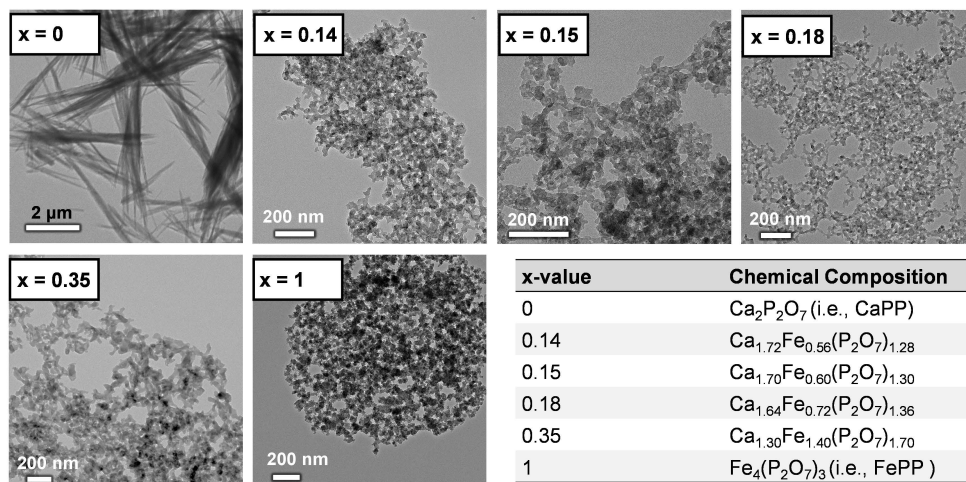


Figure S6.1. TEM images of the Ca_2PP ($x = 0$), Fe_4PP_3 ($x = 1$), and mixed Ca-Fe(III) pyrophosphate salts with $x = 0.14$, 0.15 , 0.18 , and 0.35 prepared by coprecipitation. The x -values and chemical formula of the pure and mixed salts were obtained from the elemental composition determined by EDX.

Method S6.1. Dissolution of Ca_2PP , Fe_4PP_3 , and mixed Ca-Fe(III) pyrophosphate salts in the presence of phenolics by inductively coupled plasma – atomic emission spectroscopy (ICP-AES)

Inductively coupled plasma–atomic emission spectroscopy (ICP-AES) was used for independent verification of the iron quantification by the ferrozine assay. For ICP-AES measurements, Ca_2PP , Fe_4PP_3 , and the mixed Ca-Fe(III) pyrophosphate salts were redispersed in water by stirring ($\sim 250 \text{ rpm}$) with a magnetic stir bar (final amount of salt 10 mg mL^{-1}) followed by the addition of aqueous solutions (*i.e.* catechol, caffeic acid, and epicatechin) or dispersions (*i.e.* quercetin, apigenin, and curcumin) of the phenolics at a final concentration of 5 mM . pH was set to reach a target pH 3, 6, or 8 after 2 h of incubation at 23°C while mixing at 1000 rpm . Samples were five times diluted in 0.14 M HNO_3 , before injection in the ICP-AES system (Agilent 5110 VDV; Agilent Technologies, Tokyo, Japan). Independent duplicate samples were taken from the salt at each pH point. The concentration of iron, calcium, and phosphorus was determined using scandium as an internal standard. The limit of detection values of iron, calcium, and phosphorus were respectively 0.05 , 0.05 , and 0.20 mg/L , the limit of quantification values were 0.15 , 0.15 , and 0.61 mg/L respectively.

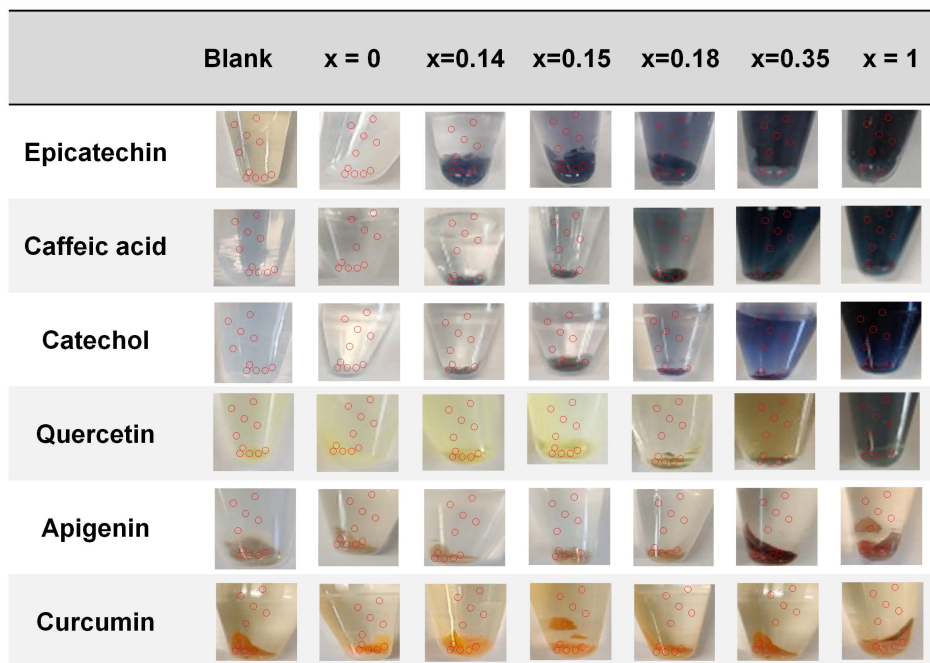


Figure S6.2. Images of Eppendorfs containing phenolics in combination with Ca_2PP ($x = 0$), Fe_4PP_3 ($x = 1$), and mixed Ca-Fe(III) pyrophosphate salts with $x = 0.14, 0.15, 0.18$, and 0.35 at pH 6. The red spots indicate the positions where the $L^*a^*b^*$ values were extracted using a standard image analysis software (Photoshop CC2021, Adobe)

Method S6.2. Elution profiles reversed-phase chromatography

The following elution profile was used to measure the solubility of the phenolics at pH 3, 6, and 8: 0.00 – 1.09 min, isocratic on 1 vol. % B; 1.09 – 20.72 min, linear gradient from 1 – 55 vol. % B; 20.72 – 21.81 min linear gradient from 55 – 100 vol. % B; 21.81 – 27.26 min isocratic on 100 vol. % B; 27.26 – 28.35 min linear gradient from 100 – 1 vol. % B; 28.35 – 33.81 min isocratic on 1 vol. % B.

The following elution profile was used to monitor the oxidation of epicatechin and quercetin: 0.00 – 1.09 min, isocratic on 1 vol. % B; 1.09 – 13.45 min, linear gradient from 1 – 35 vol. % B; 13.45 – 14.54 min linear gradient from 35 – 100 vol. % B; 14.54 – 19.99 min isocratic on 100 vol. % B; 19.99 – 21.08 min linear gradient from 100 – 1 vol. % B; 21.08 – 26.54 min isocratic on 1 vol. % B.

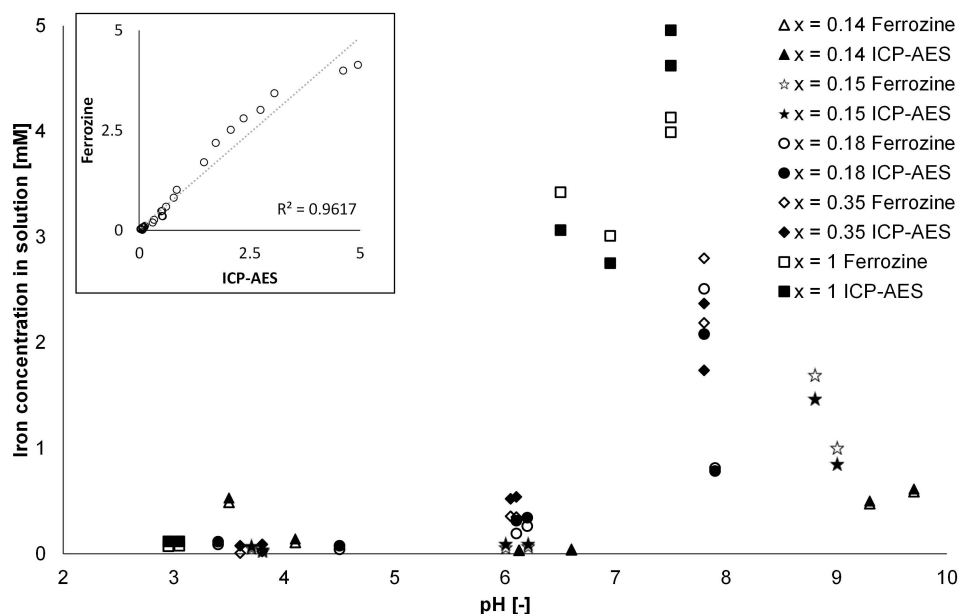


Figure S6.3. Soluble iron concentration from Fe_4PP_3 ($x = 1$) and mixed Ca-Fe(III) pyrophosphate salts with $x = 0.14$, 0.15 , 0.18 , and 0.35 in the presence of epicatechin as a function of pH determined by ICP-AES (filled markers) and by the ferrozine (open markers) methods. The inset depicts the correlation between the iron concentration measured using both methods. The iron concentrations in solution measured by the two different methods were found to be in good agreement ($R^2 = 0.96$).

Table S6.1. Iron content (%), theoretical maximum concentration (mM), and measured iron concentration (mM) from Fe_4PP_3 ($x = 1$) and mixed Ca-Fe(III) pyrophosphate salts with $x = 0.14$, 0.15 , 0.18 , and 0.35 , based on the iron content of the salt and the amount of salt in the starting dispersion (10 mg mL^{-1} for all salts).

x-value	Iron content (Mole %)	Theoretical maximum iron concentration (mM)	Measured iron concentration (mM)		
			pH 3	pH 6	pH 8
0.14	4.06	17.35	0.232 ± 0.000^a	0.006 ± 0.000	0.059 ± 0.001
0.15	4.29	17.75	0.365 ± 0.017	0.032 ± 0.003	0.307 ± 0.014
0.18	4.93	21.03	0.265 ± 0.005	0.147 ± 0.002	0.608 ± 0.009
0.35	7.78	32.87	0.080 ± 0.004	1.422 ± 0.037	3.148 ± 0.037
1	12.90	53.69	0.028 ± 0.001	0.810 ± 0.029	3.198 ± 0.016

^a standard deviation of independent duplicates

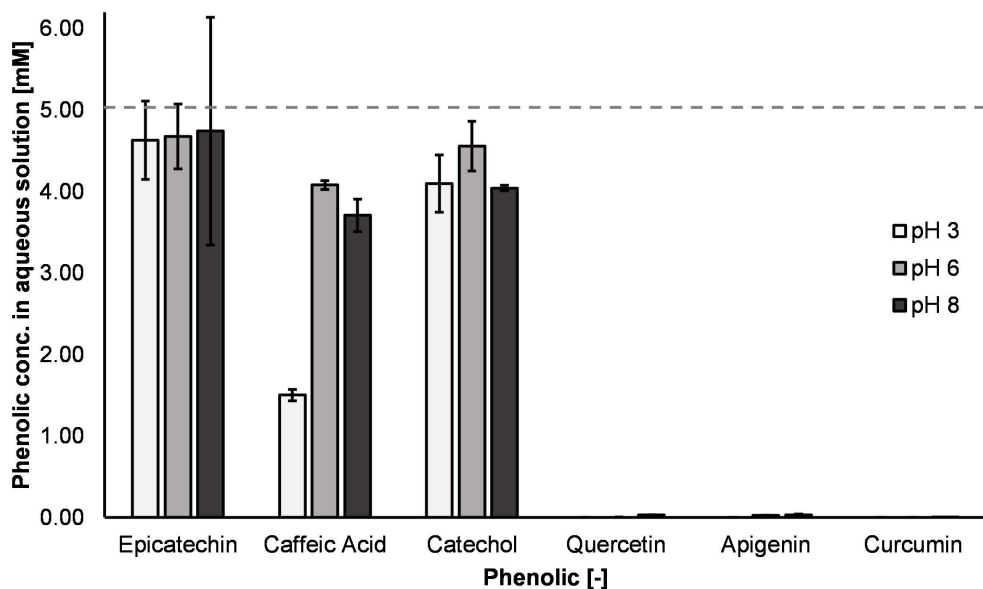


Figure S6.4. Water solubility of the phenolics in absence of any iron- or calcium-containing salts at pH 3, 6, and 8 as quantified by RP-UHPLC-PDA-MS. The dashed line indicates the prepared concentration of the phenolic solution.

Table S6.2. Reported stability constants of Fe(III) with the phenolic compounds tested in this study.

Phenolic	Log β	Reference
Catechol	43.8	[40]
Caffeic acid	18.9	[41]
Catechin	47.4	[12]
Quercetin	44.2	[42]
Apigenin	Not reported	
Curcumin	22.1	[43]

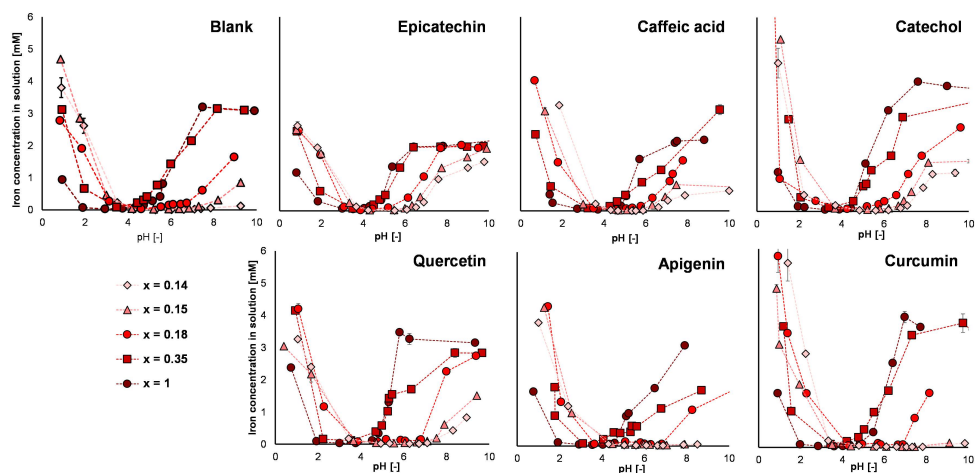


Figure S6.5. Dissolution behaviour of iron from Fe_4PP_3 ($x = 1$) and the mixed Ca-Fe(III) pyrophosphate salts with $x = 0.14$, $x = 0.15$, $x = 0.18$, and $x = 0.35$ at pH 1-10; in the absence of phenolics (blank), and in presence of catechol, caffeic acid, epicatechin, quercetin, apigenin, and curcumin at 23 °C.

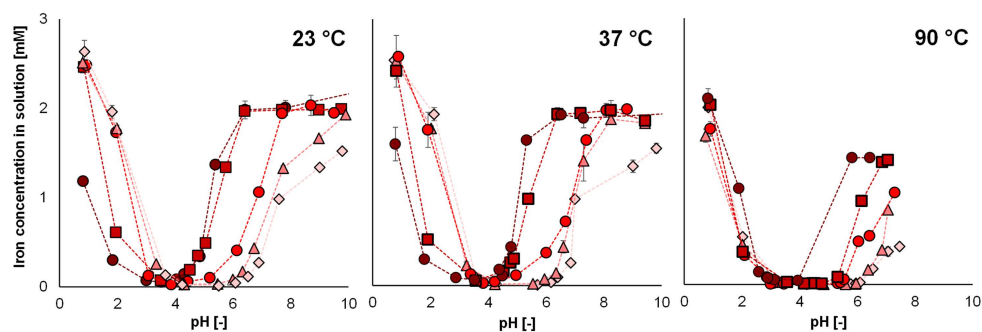


Figure S6.6. Dissolution behaviour of iron from Fe_4PP_3 ($x = 1$) and the mixed Ca-Fe(III) pyrophosphate salts with $x = 0.14$, $x = 0.15$, $x = 0.18$, and $x = 0.35$ at pH 1-10 in the presence of epicatechin at 23, 37, and 90 °C.

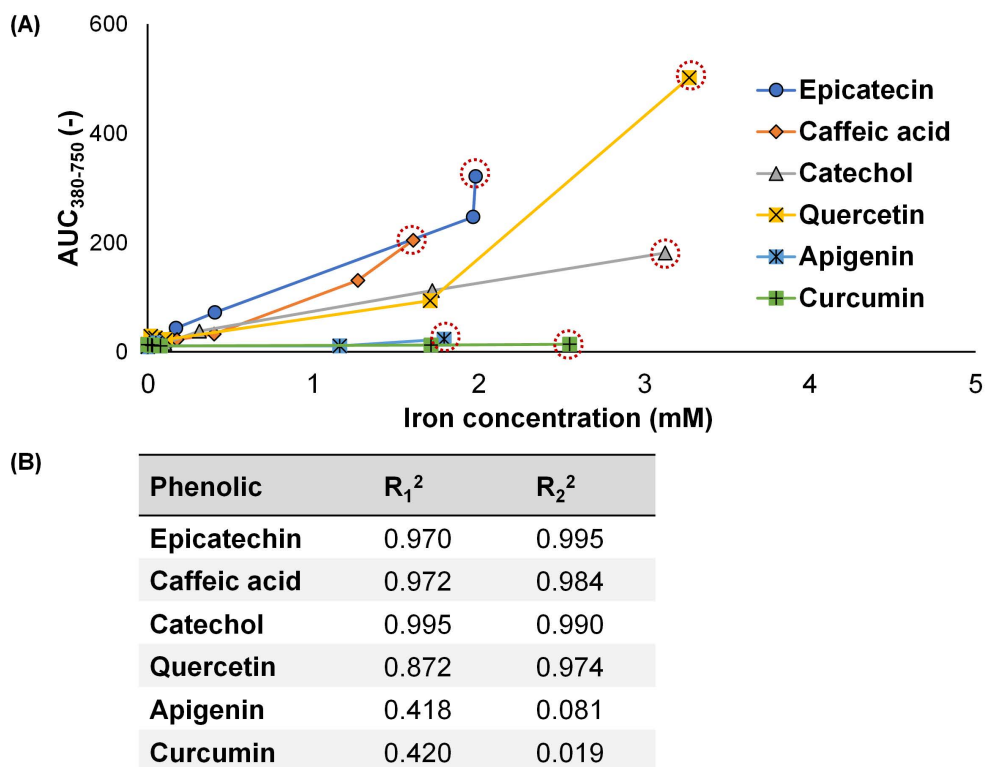


Figure S6.7. (A) Relationship between the area under the curve in the visible light spectra ($\text{AUC}_{380-750}$) versus the iron concentration in solution and (B) R_1^2 the regression value from the mixed salts and Fe_4PP_3 (including the red dashed point from A), and R_2^2 the regression value of the mixed salts only (excluding the red dashed point from A).

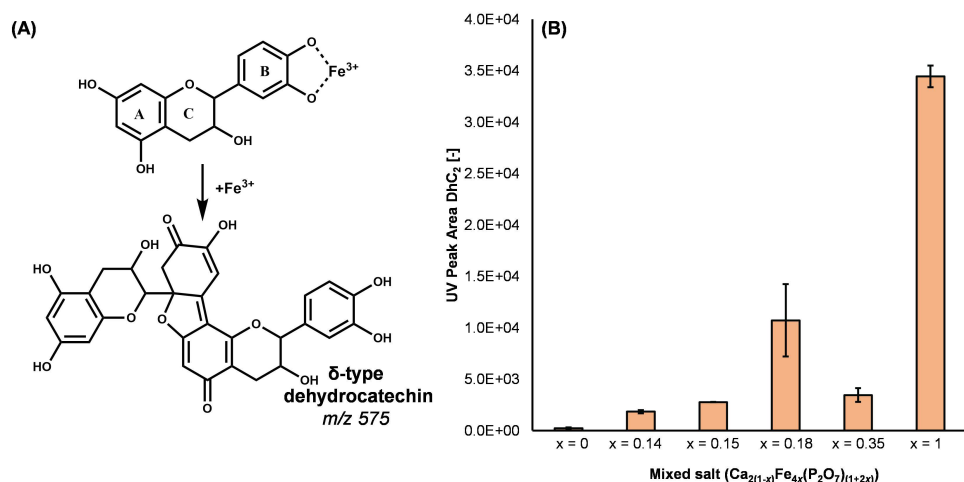


Fig. S6.8. (A) Proposed main oxidation compound (δ -type dehydrocatechin; δ -type DhC2) of Fe(III)-mediated oxidation of epicatechin.^[4,35] (B) Bar graph indicating the peak area of δ -type DhC2 after incubation of Ca_2PP ($x = 0$), Fe_4PP_3 ($x = 1$), and mixed Ca-Fe(III) pyrophosphate salts with epicatechin at pH 6.

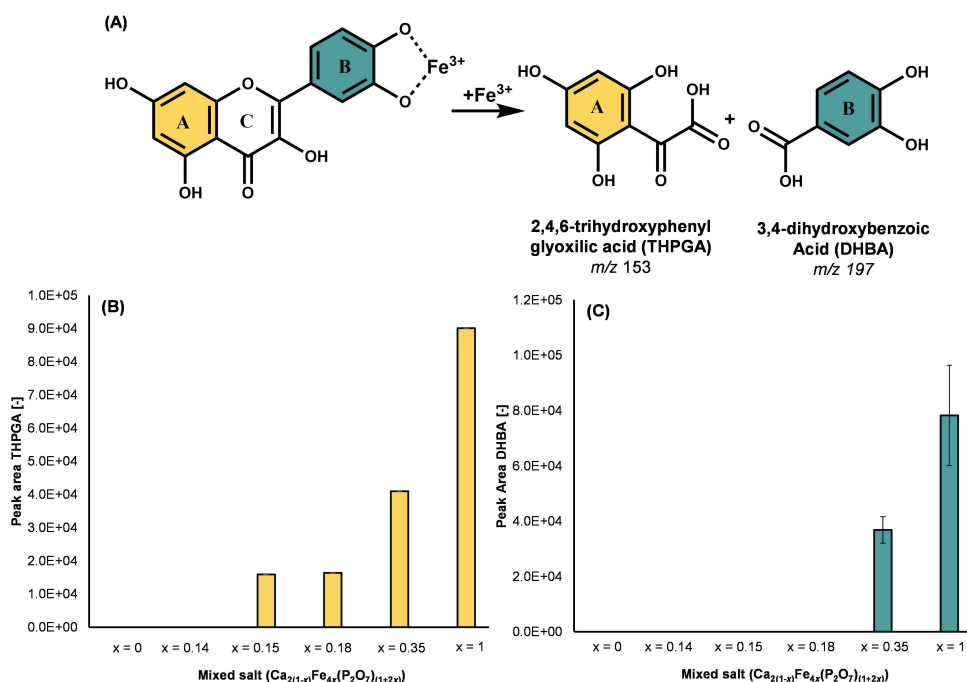


Fig. S6.9. (A) Main oxidation compounds of Fe(III)-mediated oxidation of quercetin.^[4] (B) Bar graph indicating the peak area of THPGA and (C) of DHBA after incubation of Ca_2PP ($x = 0$), Fe_4PP_3 ($x = 1$), and mixed Ca-Fe(III) pyrophosphate salts with $x = 0.14, 0.15, 0.18$, and 0.35 , with quercetin at pH 6.

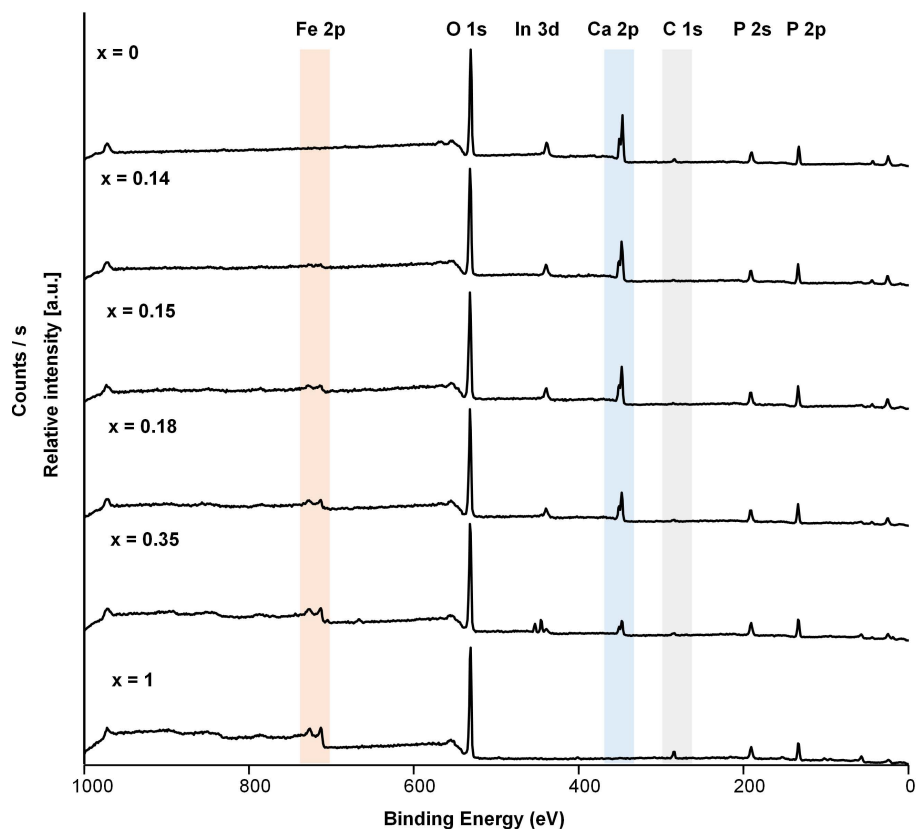


Fig. S6.10. XPS Wide scan spectrum of Ca_2PP ($x = 0$), Fe_4PP_3 ($x = 1$), and mixed Ca-Fe(III) pyrophosphate salts with $x = 0.14, 0.15, 0.18$, and 0.35 . The salts were measured on a indium (In) surface.

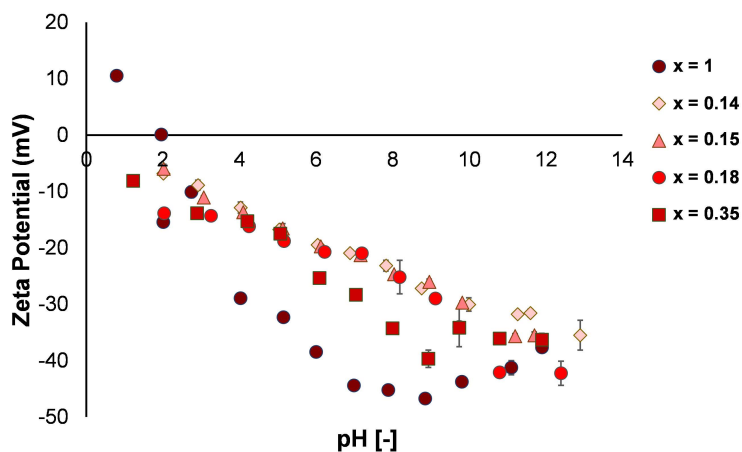


Fig. S6.11. Zeta potential of Ca_2PP ($x = 0$), Fe_4PP_3 ($x = 1$), and mixed Ca-Fe(III) pyrophosphate salts with $x = 0.14, 0.15, 0.18$, and 0.35 as a function of the pH of their dispersions.

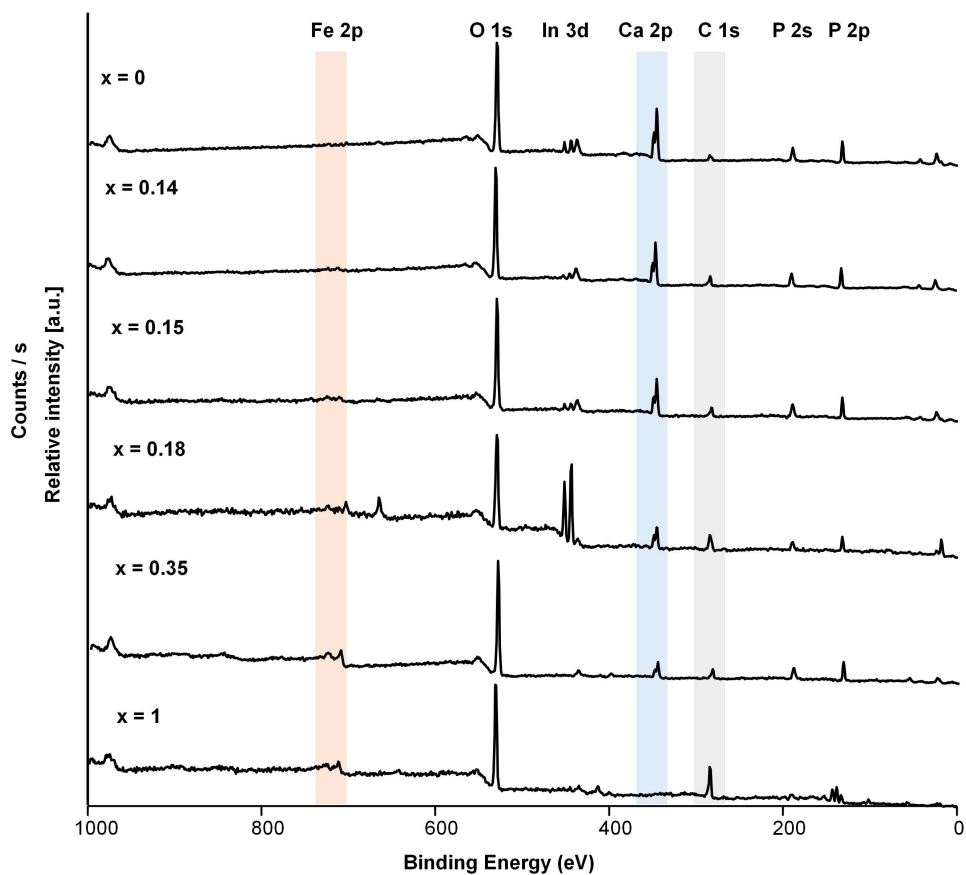


Fig. S6.12. XPS Wide scan spectrum of Ca_2PP ($x = 0$), Fe_4PP_3 ($x = 1$), and mixed Ca-Fe(III) pyrophosphate salts with $x = 0.14, 0.15, 0.18$, and 0.35 after incubation with epicatechin (pH 6). The salts were measured on a indium (In) surface.

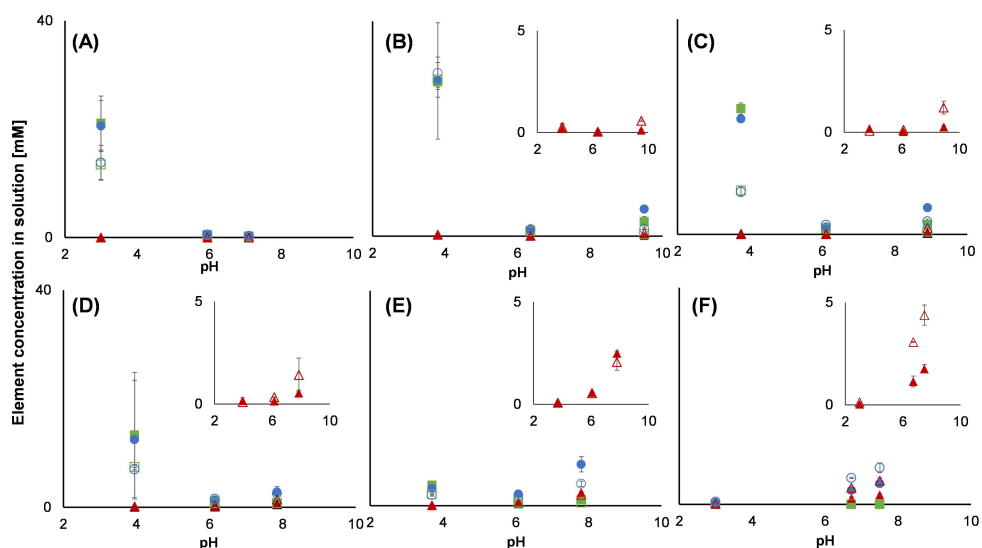


Fig. S6.13. Concentration of iron (red triangle), calcium (green square), and phosphorus (blue circle) quantified by ICP-AES in aqueous supernatant for (A) Ca_2PP ($x = 0$) and the mixed Ca-Fe(III) pyrophosphate salts with (B) $x = 0.14$; (C) $x = 0.15$; (D) $x = 0.18$; (E) $x = 0.35$; and (F) Fe_4PP_3 ($x = 1$) in the absence (filled markers) and presence (open markers) of epicatechin. The insets show the corresponding iron concentration in solution.

CHAPTER 7

Interaction of iron(III) with taste enhancers:

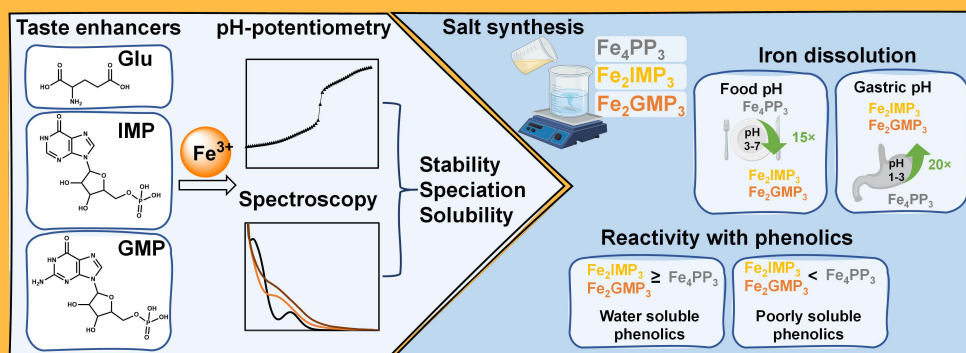
potential of Fe(III) salts with inosine monophosphate or guanosine monophosphate for food fortification

Judith Bijlsma, Péter Buglyó, Etelka Farkas,
Krassimir P. Velikov, Jean-Paul Vincken, and
Wouter J.C. de Bruijn

Based on: *LWT – Food Science and Technology*,
2023, 184:115024

Abstract

Iron interactions in iron-fortified bouillon cubes lead to undesirable discolouration, even when poorly-water soluble iron salts such as ferric pyrophosphate (Fe_4PP_3) are used. This is the first study to comprehensively investigate the interaction of Fe(III) with three common taste enhancers: glutamate (Glu), inosine monophosphate (IMP), and guanosine monophosphate (GMP). The stability of the complexes of Fe(III) with IMP or GMP is higher compared to that with Glu. Neutrality of IMP or GMP species with Fe(III) at pH 3-8 resulted in precipitation. This property was exploited to synthesise Fe(III) salts of IMP or GMP (*i.e.* Fe_2IMP_3 and Fe_2GMP_3) by aqueous chemical precipitation. Iron dissolution from Fe_2IMP_3 and Fe_2GMP_3 was up to twenty-fold higher at gastric pH (1-3), indicative of better bio-accessibility, and up to fifteen-fold lower at food pH (3-7), indicative of decreased reactivity in food, compared to Fe_4PP_3 . Consequently, Fe_2IMP_3 and Fe_2GMP_3 , compared to Fe_4PP_3 , led to less discolouration in combination with the poorly soluble phenolics similarly to those that are commonly present in bouillon cubes. We conclude that Fe(III) salts of IMP or GMP can potentially serve as iron fortificants due to their increased solubility at gastric pH and decreased reactivity at food pH.



7.1. Introduction

Fortification of savoury concentrates (e.g. bouillon cubes) with iron can effectively reduce the global prevalence of iron deficiency.^[1-3] Bouillon cubes are typically composed of salt, fat, carbohydrates, proteins, herbs, and spices. Additionally, they may contain taste enhancers. The most widely used taste enhancer in food is the monosodium salt of glutamate (MSG, NaGlu; E621), which is often used in combination with the disodium salts of 5'-ribonucleotides such as guanosine 5'-monophosphate (Na₂GMP; E626) and inosine 5'-monophosphate (Na₂IMP; E630), to further boost the umami taste.^[4,5] For example, dry bouillon cubes from different local supermarkets in Argentina contained 38 ± 17 wt. % MSG, 0.23 ± 0.16 wt. % IMP, and 0.06 ± 0.05 wt. % of GMP.^[4]

When bouillon cubes are fortified with iron, the product colour and iron bioavailability can be compromised due to iron-phenolic interactions.^[6-8] These phenolics are naturally present in the herbs. To limit these iron-phenolic interactions, insoluble iron fortificants, such as ferric pyrophosphate (*i.e.* ferric diphosphate; Fe₄PP₃), are used for the fortification of bouillon cubes.^[8,9] Fe₄PP₃ is practically insoluble (< 0.1 mg L⁻¹) in aqueous solution at pH 3-5 and sparingly soluble (10 - 33 mg L⁻¹) at pH 1-2.^[10-12] Despite its water insolubility at food pH discolouration with phenolics can still be observed in presence of Fe₄PP₃.^[10,13-15]

The presence of glutamate (Glu) was previously associated with increased discolouration in an iron-phenolic model system and iron-fortified bouillon cubes.^[16,17] Ferric iron (Fe(III)) was previously reported to coordinate to glutamate via the carboxylate oxygen atoms.^[18] Additionally, nucleotides strongly coordinate metals, although the metal binding preference is metal and nucleobase dependent.^[19-21] Metal ions may be coordinated to nucleotides via the oxygen donor atoms of the phosphate group, the nitrogen atom in the nucleobase, the oxygen atoms of the sugar moiety, or a combination thereof.^[22-24] As hard Lewis metals prefer to coordinate to hard Lewis ligands such as the phosphate group, it is expected that Fe(III) primarily coordinates to the phosphate groups of the nucleotides.^[25-27] The pH strongly influences the coordination of metals to ligands because it affects the ligand protonation state and the hydrolytic processes of the metal ions. Despite this, little is known about the effect of pH on the coordination and speciation of Fe(III) in presence of IMP or GMP.

Here we comprehensively study the interaction of Fe(III) and all taste enhancers in aqueous solution at different pH. IMP and GMP are expected to coordinate Fe(III) via their phosphate group, therefore, we also included monophosphate (MP) and pyrophosphate (PP) for comparison. Fe₄PP₃ is one of the most commonly used salts in iron fortification but, despite its wide use, data regarding the basic properties, formed complexes, stability constants, and solubility are inconsistent.^[11,28-32] In general Fe(III) phosphates form neutral insoluble complexes in aqueous solution in the food



pH range (3-7).^[10-12] Since IMP and GMP also coordinate Fe(III) via the phosphate group, we expect that their complexes with iron will also be insoluble in aqueous solution at food pH (3-7).

This work aims to provide more insights into the interaction of Fe(III) with Glu, IMP, GMP, MP, and PP. To this end, pH-potentiometric and UV-Vis spectrophotometric methods in model systems were utilised to determine stability constants and to study the speciation over a wide pH range. We hypothesised that (i) all taste enhancers coordinate Fe(III) but that, due to the hard Lewis nature of the phosphate groups, IMP, GMP, MP, and PP form more stable complexes with Fe(III) compared to Glu, and (ii) that complexes of Fe(III) with IMP or GMP possess limited solubility at food pH (3-7) due to coordination via the phosphate group.

7.2. Materials and methods

7.2.1. Materials

Ferric chloride hexahydrate ($\text{FeCl}_3 \cdot 6\text{H}_2\text{O}$; a.r. grade) was purchased from Reanal (Budapest, Hungary). Pyrophosphate (PP) tetrasodium salt decahydrate (Na_4PP , $\text{Na}_4\text{P}_2\text{O}_7 \cdot 10\text{H}_2\text{O}$, ≥ 99 wt. %), dihydrogen phosphate (MP) monosodium salt monohydrate (NaH_2MP , $\text{NaH}_2\text{PO}_4 \cdot \text{H}_2\text{O}$, ≥ 99 wt. %), L-glutamate (Glu) monosodium salt monohydrate (NaHGlU , $\text{NaC}_5\text{H}_8\text{NO}_4 \cdot \text{H}_2\text{O}$, ≥ 98 wt. %), inosine 5'-monophosphate (IMP) disodium salt hydrate (Na_2IMP , $\text{Na}_2\text{C}_{10}\text{H}_{11}\text{N}_4\text{O}_8\text{P} \cdot x\text{H}_2\text{O}$, ≥ 99 wt. %), guanosine 5'-monophosphate (GMP) disodium salt hydrate (Na_2GMP , $\text{Na}_2\text{C}_{10}\text{H}_{12}\text{N}_5\text{O}_8\text{P} \cdot x\text{H}_2\text{O}$, ≥ 99 wt. %), ferric chloride (FeCl_3 , ≥ 97 wt. %, for synthesis), quercetin hydrate (≥ 95 wt. %), 1,2-dihydroxybenzene (≥ 99 wt. %; catechol), caffeic acid (≥ 98 wt. %), curcumin (≥ 94 wt. %), 3-(2-pyridyl)-5,6-diphenyl-1,2,4-triazine-*p,p'*-disulfonic acid monosodium salt hydrate (≥ 97 wt. %; ferrozine), hydrochloric acid (HCl), and potassium hydroxide (KOH) were obtained from Merck Life Science (Darmstadt, Germany). (-)-Epicatechin (≥ 97 wt. %) was purchased from TCI Europe NV (Zwijndrecht, Belgium), apigenin (≥ 98 wt. %) from Indofine Chemical Company (Hillsborough, NJ, USA), and ascorbic acid (≥ 99 wt. %) was obtained from VWR International (Radnor, PA, USA). ULC-MS grade acetonitrile (ACN) and water both containing 0.1 vol. % formic acid, and pure formic acid (FA, ≥ 99 vol. %) were purchased from Biosolve (Valkenswaard, The Netherlands). Water for other purposes than UHPLC was prepared using a Milli-Q water purification system (Merck Millipore, Billerica, MA, USA).

7.2.2. Potentiometric and spectrophotometric studies

The metal ion stock solutions for pH-potentiometric and spectrophotometric measurements were prepared from $\text{FeCl}_3 \cdot 6\text{H}_2\text{O}$ (Reanal, Hungary), the stock solution also contained 0.10 M hydrochloric acid to prevent hydrolysis. Metal ion concentrations were determined by complexometric titration. The acid content of Fe(III) stock solution and the purity and exact concentration of the ligand stock solutions were determined by Gran's method.^[33] Due to the limited water solubility of

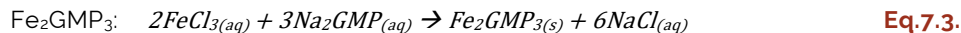
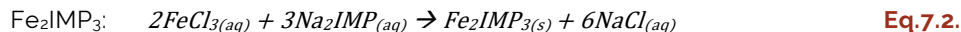
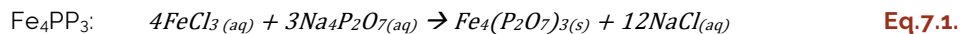
some of the Fe(III) complexes, pH-potentiometric and spectrophotometric measurements were carried out in aqueous solution (water) and also in DMSO/water 70/30 wt. % at an ionic strength of 0.20 M (KCl) and at 25.0 ± 0.1 °C. A carbonate-free 0.20 M KOH solution of known concentration in water or the solvent mixture was used as titrant. HCl stock solutions in water or the solvent mixture were prepared and their concentrations were determined by potentiometric titrations. A Mettler T50 instrument equipped with a Metrohm combined electrode (type 6.0234.100) and Metrohm T5 instrument with Metrohm combined electrode (type DG1114-SC) were used for the pH-potentiometric measurements. The IUPAC recommendations were employed to perform the measurements in the DMSO/water 70/30 wt. % solvent mixture. The combined glass electrode was conditioned for three days before the measurements in the solvent mixture.^[34] The electrode system was calibrated according to Irving *et al.*^[35] pH-metric readings could therefore be converted into hydrogen ion concentration. The water ionisation constant (pK_w) was 13.74 ± 0.01 in the aqueous system and 17.01 ± 0.01 in the solvent mixture. The titrations in aqueous solution were performed in the pH range 2.0-11.0 and in solvent mixture in the pH range 3.0-15.0 or until precipitation occurred. The initial volume of the samples was 15.0 mL. Ligand concentrations were kept constant at 4.0 mM and the Fe(III) to ligand ratios were 1:1, 1:2, 1:4 and 1:10. All samples were completely deoxygenated by bubbling with purified argon for ca. 15 min before the measurements. The protonation constants of the ligands were determined with the computer program SUPERQUAD.^[36] Standard deviations are indicated as 3σ values (*i.e.* data within three standard deviations from the mean so covering 99.7 % of the data), the standard deviations over the last decimal are indicated in parentheses; *i.e.* 9.49(1) equals 9.49 ± 0.01 . Potentiometric data were used to find the stoichiometry of the species and calculate their stability constants. The calculations were performed using the PSEQUAD^[37] computer program and the literature data ($\log \beta$) for hydrolytic Fe(III) species, taking into account the different ionic strengths by the Davies equation. The following values were used in the calculations: $[\text{FeH}_{-1}]^{2+} = -3.21$; $[\text{FeH}_{-2}]^+ = -6.73$; $[\text{Fe}_2\text{H}_{-2}]^{4+} = -4.09$; and $[\text{Fe}_3\text{H}_{-4}]^{5+} = -7.58$; H_{-1} relates to the metal induced ionisation of the coordinated water.^[38,39] Titration points with a waiting time of 10 min or more were omitted from the calculations and about 200 titration points were used for each system.

A Perkin-Elmer Lambda 25 spectrophotometer was used to record the UV-Vis spectra over the range 200-800 nm with a path length of 1 cm. Measurements were carried out by preparing individual samples in which the 0.20 M KCl was partially or completely replaced by HCl. pH values, varying in the range ca. 0.7-1.6 were calculated from the HCl content. Iron(III) ion concentrations were in the range 0.025-0.10 mM and the metal ion to ligand ratios were in the range 1:3-1:6.

7.2.3. Preparation of Fe_4PP_3 , Fe_2IMP_3 , and Fe_2GMP_3 salts

Iron(III)-IMP ($\text{Fe}_2(\text{C}_{10}\text{H}_{11}\text{N}_4\text{O}_8\text{P})_3$; Fe_2IMP_3) and iron(III)-GMP ($\text{Fe}_2(\text{C}_{10}\text{H}_{12}\text{N}_5\text{O}_8\text{P})_3$; Fe_2GMP_3) salts were separately prepared using an aqueous chemical precipitation

method as described elsewhere.^[12] Iron(III)-pyrophosphate ($\text{Fe}_4(\text{P}_2\text{O}_7)_3$, Fe_4PP_3) was also prepared for comparison. The precipitation reactions of the three different salts are indicated by **equations 7.1-7.3**.



The reactions were performed at room temperature by mixing the following stoichiometric ratios of the reactants: 4:3:1 for Fe_4PP_3 and 2:3:1 for Fe_2IMP_3 and Fe_2GMP_3 . A small excess of the ligand solution was added to ensure binding of all iron, *i.e.* 3.1 times instead of 3 in **equations 7.1-7.3**. For Fe_2IMP_3 and Fe_2GMP_3 , solutions of 2.07 mmol FeCl_3 in 250 mL MQ water (*i.e.* 8.30 mM) were prepared. Subsequently, they were quickly added to solutions of 3.22 mmol Na_2IMP or Na_2GMP in 500 mL of MQ water (*i.e.* 6.43 mM) while stirring at 500 rpm. For Fe_4PP_3 , a solution of 4.15 mmol FeCl_3 in 250 mL MQ water (*i.e.* 16.59 mM) was quickly added to a solution of $\text{Na}_4(\text{P}_2\text{O}_7)$ (3.22 mmol, 500 mL) while stirring at 500 rpm. For all three systems, a turbid dispersion was rapidly formed upon mixing. Freshly prepared solutions were used for every synthesis and two independent syntheses were performed for each salt. The dispersions were then centrifuged ($6,000 \times g$, 25 °C, 45 min) in 500 mL centrifuge bottles followed by washing the precipitates twice with Milli-Q water to remove the aqueous NaCl. The sediments were dried in a vacuum oven at 50 °C overnight (Fe_2IMP_3 : 27±2 % yield; Fe_2GMP_3 : 50±0 % yield; Fe_4PP_3 : 46±10 % yield). The salts were characterised by XRD, TEM, SEM-EDX, and by elemental analysis (CHNS, ICP-AES) (**Method S7.1**). Results on characterisation, dissolution, and reactivity are displayed as one of the duplicate salts after a reproducibility check.

7.2.4. Iron dissolution and reactivity of Fe_4PP_3 , Fe_2IMP_3 , and Fe_2GMP_3 salts

Iron dissolution from Fe_4PP_3 , Fe_2IMP_3 , and Fe_2GMP_3

The Fe_4PP_3 , Fe_2IMP_3 , and Fe_2GMP_3 salts were redispersed in Milli-Q water to obtain final concentrations of 10 mg mL⁻¹. The pH of the dispersions was adjusted by automatic titration with 0.1 M HCl or 0.1 M NaOH in a pH-stat device (Metrohm, Herisau, Switzerland). The dispersions were incubated at 1,000 rpm using an Eppendorf Thermomixer F1.5 (Eppendorf, Hamburg, Germany) at pH values ranging from one to eleven (steps of one), for 2 h at 23 °C. After incubation, the pH of each sample was measured again to determine the final pH. The samples were centrifuged at $15,000 \times g$ for 10 min and supernatants were isolated to measure the dissolved iron concentrations. Total iron in solution was quantified using a ferrozine-based colourimetric assay as reported previously.^[12]

Reactivity of Fe_4PP_3 , Fe_2IMP_3 , and Fe_2GMP_3 with phenolics

The reactivity of Fe_4PP_3 , Fe_2IMP_3 , and Fe_2GMP_3 salts with phenolics was assessed according to our previously published method with slight modifications.^[15] To this end,

three water soluble phenolics (*i.e.* catechol, caffeic acid, and epicatechin) and three poorly water soluble phenolics (*i.e.* quercetin, apigenin, and curcumin) were investigated. The reactivity of Fe_4PP_3 , Fe_2IMP_3 , and Fe_2GMP_3 in the presence of the different phenolic compounds after incubation at pH 6.5 for 2 h at 23 °C, was monitored using ultraviolet-visible light (UV-Vis) spectroscopy and the dissolved iron resulting from phenolic interactions was quantified using a ferrozine-based colourimetric assay.^[12]

7.2.5. Nucleotide and nucleoside quantification by HILIC-PDA-ESI-ITMSⁿ

To investigate if dephosphorylation occurred we analysed the nucleotides and nucleosides by hydrophilic interaction liquid chromatography coupled to electrospray ionisation ion trap mass spectrometry (HILIC-PDA-ESI-ITMSⁿ). The injection volume, column information, temperature, gradient elution program, and MS settings were used as described in **Method S7.2**.

7.3. Results & discussion

7.3.1. Interaction of iron(III) with taste enhancers and phosphates

Proton equilibria of the ligands

The fully protonated ligands H_3MP and $\text{H}_3(\text{Glu})^+$ have three dissociable protons and H_4PP , $\text{H}_3(\text{IMP})^+$, and $\text{H}_3(\text{GMP})^+$ have four dissociable protons (**Fig. 7.1**).

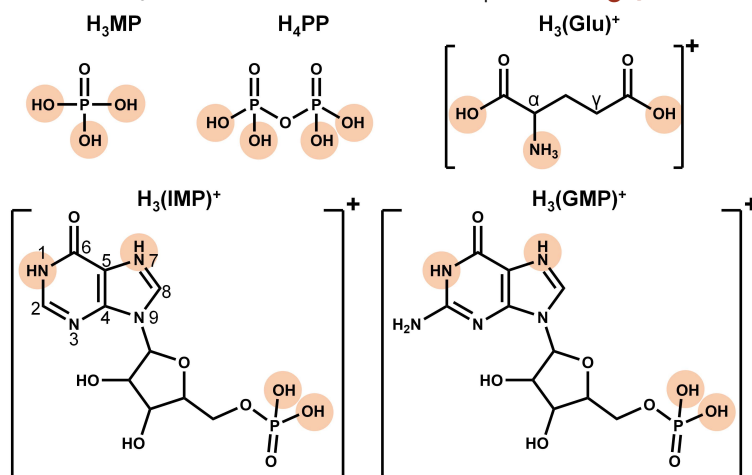


Figure 7.1. Chemical structure of monophosphate (MP), pyrophosphate (PP), glutamate (Glu), inosine 5'-monophosphate (IMP), and guanosine 5'-monophosphate (GMP) in their protonated state. The orange circles highlight the dissociable protons.

The corresponding dissociation constants of the ligands in aqueous solutions were determined by pH-potentiometric titrations at the same conditions as used to investigate the interaction with Fe(III) (25 °C, 0.20 M KCl) (**Table 7.1**).

Table 7.1. Dissociation constants of the studied ligands determined by pH-potentiometric titrations ($T = 25.0\text{ }^{\circ}\text{C}$, $I = 0.20\text{ M}$ (KCl) in aqueous solution).

	$\text{H}_3(\text{Glu})^+$	$\text{H}_3(\text{IMP})^+$	$\text{H}_3(\text{GMP})^+$	H_3MP	H_4PP
pK_1	2.11(2) ^a	< 1 ^b	< 1	1.78(1)	< 1
pK_2	4.08(1)	1.19(2)	2.18(3)	6.64(1)	1.54(1)
pK_3	9.49(1)	6.09(1)	6.08(2)	11.57(1)	5.84(1)
pK_4		8.94(1)	9.39(1)		8.19(1)

^a Standard deviations (3σ values) of the last decimal are given in parentheses; ^b it was not possible to measure at $\text{pH} < 1$ using the potentiometric setup but it is known that the first pK_a of these compounds is at very acidic pH.^[18,30,40,41]

Since the pH-effect of the deprotonation processes is not sensitive for the dissociation sites, if a compound has more than one dissociable proton, the dissociation constants (so called macro-constants) determined by pH-potentiometric method cannot be assigned to the individual sites; assumptions can only be made based on chemical evidence. For the compounds in this study, the acidity orders are known from literature. It was previously described that for $\text{H}_3(\text{IMP})^+$ and $\text{H}_3(\text{GMP})^+$ the first proton is released from the phosphate, the second from *N*7 on the nucleobase, the third one from the phosphate, and the fourth proton in the alkaline pH range from *N*1.^[40,42] For H_3Glu^+ it was previously reported that the first proton is released from the α -carboxylate, the second from the γ -carboxylate, and the third from the α -amino group.^[43] Taking the different experimental conditions into account, the dissociation constants of the ligands are in reasonable agreement with the reported data in literature.^[18,30,40,41]

The hydrolytic stability of IMP, GMP, and PP was monitored by a second titration similar to what was done previously.^[44,45] After the titration of IMP, GMP, and PP with KOH titrant up to pH around 12, HCl was added to set the pH at 2 again after which the sample was titrated with KOH again. The obtained titration curves were superimposed (results not shown) and therefore indicate that IMP, GMP, and PP do not hydrolyse in aqueous solution in the measured pH-range during the run time of one titration (*i.e.* several hours).

Investigation of Fe(III) complexes of the ligands by potentiometric titration

The pH-potentiometric titrations of Fe(III) with all ligands were performed in aqueous solution (water) and in the solvent mixture (DMSO/water 70/30 wt. %) and were terminated when precipitation occurred. For the system of Fe(III) in presence of MP at a 1:4 ratio precipitation occurred at $\text{pH} > 3.5$ (**Fig. S7.1**). The Fe(III) systems with PP displayed white precipitate from the start (*i.e.* pH 2) for all measured ratios (*i.e.* 1:1, 1:2, and 1:4). Due to the low dissociation constants (**Table 7.1**) and bidentate binding, PP already forms stable chelates with Fe(III) at acidic pH.

The pH-potentiometric titration curves of the taste enhancers Glu, IMP, and GMP with Fe(III) are provided in **Fig. 7.2**. The investigation of the Fe(III) complexes with all the taste enhancers was hindered by the very low solubility of the iron complexes and/or by the formation of iron hydrolysis products.

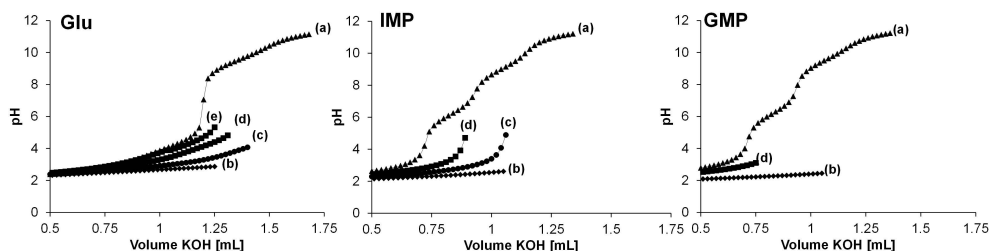


Figure 7.2. pH-potentiometric titration curves in aqueous solution for 4.0 mM Glu, IMP, and GMP in (a) absence and in presence of Fe(III) at a ratio of Fe(III):ligand (b) 1:1, (c) 1:2, (d) 1:4, and (e) 1:10 at $I = 0.20$ M (KCl), and $T = 25.0$ °C.

For the Fe(III) systems with Glu, orange-red precipitate was observed for all ratios. We suggest this is due to the formation of iron hydrolysis products which were previously reported to have this colour.^[46] When more ligand was present (1:4 ratio), precipitation occurred at a higher pH. These outcomes indicate that Glu competes with hydroxide for iron coordination. This was further confirmed by the 1:10 ratio sample, in which iron precipitated at an even higher pH. For IMP or GMP the titrations were terminated upon the formation of a white precipitate, we suggest that precipitation is a result of the coordination of Fe(III) to the phosphate anion in the nucleotides. For Fe(III) in presence of GMP the precipitate at 1:4 ratio was formed at $pH > 3.0$ and for IMP at $pH > 4.7$. It is interesting that for GMP the precipitation occurs at lower pH compared to IMP because the only structural difference between these ligands is the presence of $-NH_2$ for GMP, and this amine is unlikely to coordinate Fe(III).^[20] We tried to describe the Fe(III) complexes in the pH-range in which no precipitation was observed by fitting the experimental data using the PSEQUAD program. The stability constants of Fe(III) complexes with Glu and MP are given in **Table 7.2**.

Table 7.2. Protonation constants of Glu and MP and stability constants (Log β) of the Fe(III) complexes of Glu and MP determined by pH-potentiometric titrations ($T = 25.0$ °C, $I = 0.20$ M (KCl) in aqueous solution).

Log β	Glu ^a	MP ^a
H ₃ L	15.68(2)	19.99(1)
H ₂ L	13.57(1)	18.21(1)
HL	9.49(1)	11.57(1)
[FeHL]	12.90(2)	-
[FeL]	10.82(6)	19.92(9)
[FeH ₂ L]	7.92(3)	-
Fitting ^b	0.0362	0.0305

^a Standard deviations (3 σ values) are in parentheses.

^b Average difference between experimental and calculated titration curves expressed in cm³ of titrant.

The model and the stability constants of the 1:1 species with different protonation degree obtained in the Fe(III)-Glu system were similar to those previously reported.^[18] Calculations with MP indicated the formation of a 1:1 FePO₄ species. Including the previously reported 1:1 complexes FeH₂PO₄²⁺ and FeHPO₄⁺,^[28] into the model resulted in lower fitting parameters. It should be noted that stoichiometries of the species in

Table 7.2 may cover mixed hydroxido complexes (e.g. $\text{FeL} = [\text{Fe}(\text{HL})(\text{OH})]$) in which, besides the differently protonated ligand, hydroxide ion(s) can also be found in the coordination sphere of the metal ion due to the high tendency of $\text{Fe}(\text{III})$ to hydrolyse. Due to the precipitation reactions, no acceptable fitting was obtained for complexes of $\text{Fe}(\text{III})$ with PP, IMP, and GMP. Thus, it was not possible to obtain quantitative data about the stoichiometries and stability of the complexes in these systems.

Previously, stoichiometric data and stability constants of poorly water soluble ligands could be measured in DMSO/water mixtures.^[47,48] So, we also investigated if stability data of combinations of $\text{Fe}(\text{III})$ with the ligands could be obtained in a mixture of DMSO/water 70/30 wt. %. The dissociation constants of Glu, IMP, and MP in DMSO/water 70/30 wt. % are given in (**Table S7.1**). Although the 1:1 combinations of $\text{Fe}(\text{III})$ with Glu, IMP, and GMP indicated slightly improved solubility in the solvent mixture, precipitation still occurred at pH 5.2, 3.9, and 3.4, respectively. Thus, the titration curves could not be acceptably fitted in PSEQUAD. These results implied that investigation of the systems of $\text{Fe}(\text{III})$ in presence of PP, IMP, or GMP by pH-potentiometric titrations was not possible due to the poor solubility of these ligands and their ready complexation at very acidic pH. Therefore, the speciation was further investigated by spectrophotometric analysis.

Investigation of $\text{Fe}(\text{III})$ complexes of the ligands by spectrophotometry

Qualitative information about the speciation was obtained by spectrophotometry (**Fig. 7.3**). With spectrophotometric measurements the acidic pH region in aqueous solution can be extended to a pH around 0.7 and measurements can be carried out at a lower concentration of metal and ligand, thus precipitation is less likely.

At pH 0.7-1.5 monochloro complexes of $\text{Fe}(\text{III})$ (i.e. $[\text{FeCl}]^{2+}$) were identified by the typical absorption band with a λ_{max} of 334-336 nm both for FeCl_3 without ligands and in the systems in presence of MP, Glu, IMP, or GMP.^[49,50] FeCl_3 solution without ligand or in presence of MP and Glu also showed the typical $[\text{FeCl}]^{2+}$ band at 223 nm, which was not observed in presence of IMP or GMP, most likely due to overlap with the intense absorbance of the nucleotides at < 280 nm.

In absence of ligand or in presence of Glu, a band with $\lambda_{\text{max}} \sim 300$ nm was observed at pH 3.4-3.5, corresponding to the hydrolytic products $[\text{Fe}(\text{OH})]^{2+}$ or $[\text{Fe}_2(\text{OH})_2]^{4+}$.^[51] At pH > 3.5, in absence of ligand and in the presence of Glu, a broad band from 200-600 nm was observed. This band is a result of the formation of the red-orange coloured (hydr)oxide species.^[46] Formation of this band for $\text{Fe}(\text{III})$ (hydr)oxide species was hindered by the presence of the ligands with a phosphate group (MP, PP, IMP, and GMP) until pH > 10. However, it cannot be ruled out that other (colourless) mixed (hydr)oxide species are present.

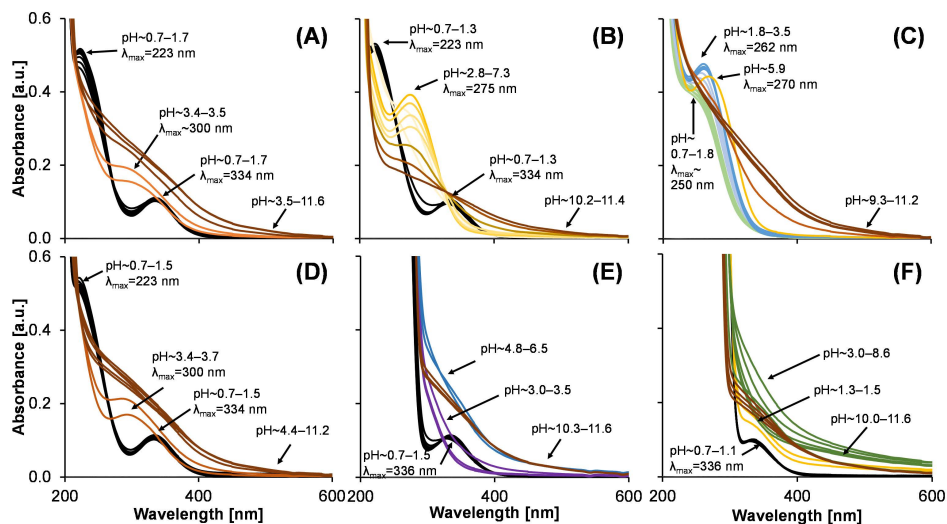


Figure 7.3. Representative UV-Vis absorption spectra of the Fe(III) system in (A) absence of ligand and in presence of (B) MP, (C) PP, (D) Glu, (E) IMP, and (F) GMP at different pH values ($C_{\text{Fe(III)}} = 0.1 \text{ mM}$, $C_{\text{Ligand}} = 0.4 \text{ mM}$, and $I = 0.20 \text{ M}$ (KCl)).

In the presence of MP a band with a λ_{max} at 275 nm was observed from pH 2.8 to 7.3, this corresponds to the 1:1 species of Fe(III) with MP (*i.e.* $[\text{FeH}_2\text{PO}_4]^{2+}$).^[52] In presence of PP a band with a shoulder at 250 nm was present at pH 0.7, which indicates that at pH 0.7 the complexation of Fe(III) by PP is already complete. In presence of PP a band with a λ_{max} at 262 nm was formed at pH 1.8–3.5 and at pH ~ 5.9 a band with λ_{max} at 270 nm was present. We suggest that these bands correspond to the formation of $[\text{FeH}_3\text{P}_2\text{O}_7]^{2+}$, $[\text{FeH}_2\text{P}_2\text{O}_7]^+$, and $\text{Fe}_4(\text{P}_2\text{O}_7)_3$, respectively.^[32]

The fact that similar spectra were obtained in presence of Glu as for FeCl_3 in absence of ligand, indicates that there were only weak interactions of Glu with Fe(III) at these concentrations. Previously, at higher concentrations of Fe(III) and Glu, a change in absorbance was reported at a λ_{max} of 450 nm.^[18] We confirmed that in a more highly concentrated Fe(III) and Glu system (*i.e.* 30 mM Glu and 3 mM Fe(III)) a species with a poorly defined maximum around 450 nm at pH ~ 3 was formed (Fig. S7.2). Formation of this species indicates that at higher Glu and Fe(III) concentrations there is a competition between the carboxylate moieties of glutamic acid and hydroxide for iron coordination. The interaction of Fe(III) with carboxylate is weaker than that of Fe(III) with hydroxide due to the lower electron density of the conjugated base pair of the carboxylate compared to the hydroxide. If present in high concentrations, as in some bouillon cubes (*e.g.* 38 wt. % MSG),^[4] the carboxylate moieties of Glu may be able to compete with hydroxide and coordinate Fe(III) at low pH.

In presence of IMP or GMP, the formation of a soluble species at pH ~ 3 was followed by the formation of a second poorly soluble species as indicated by the increase of the baseline around 700–800 nm. Based on the dissociation constants of IMP and GMP (**Table 7.1**) we suggest that the soluble species of IMP or GMP at pH ~ 3 could be due to the formation of a soluble macrochelate of Fe(III) with GMP or IMP via coordination to the deprotonated phosphate and *N*7, as previously reported for these ligands in the presence of divalent metals.^[40] Alternatively, these species may be stabilised by secondary interactions such as hydrogen bonding or stacking when *N*7 is deprotonated. The insoluble species that are formed at pH > 4.8 for IMP and pH > 3 for GMP are more likely to result from the formation of charge neutral coordination complexes of Fe(III) with the phosphate group. These spectrophotometric results are in line with the potentiometric titrations in which precipitation of Fe(III) with GMP was also observed at lower pH compared to Fe(III) with IMP.

The stability of the complexes of Fe(III) with IMP or GMP is higher compared to Glu, as they form species at lower ratios of ligand (1:1), whereas for Glu higher concentrations ligand (1:10) are needed to compete with the hydroxide for coordination. Moreover, our results indicate that the presence of IMP or GMP can hinder the formation of the red-orange coloured Fe(III) (hydr)oxide species up to pH > 10. The fact that IMP or GMP can form water soluble Fe(III) species at pH < 3 (*i.e.* gastric pH) but insoluble Fe(III) species at pH 3–7 (*i.e.* food pH) makes them promising iron salts for fortification of foods.^[10–12] Therefore, we decided to synthesise and characterise salts of Fe(III) and IMP or GMP.

7.3.2. Synthesis and characterisation of Fe₄PP₃, Fe₂IMP₃, and Fe₂GMP₃ salts

To investigate the potential of insoluble salts of Fe(III) with IMP, GMP, and PP as iron fortificants with a decreased reactivity we synthesised Fe₄PP₃, Fe₂IMP₃, and Fe₂GMP₃ salts using an aqueous chemical precipitation method. The Fe₄PP₃, Fe₂IMP₃, and Fe₂GMP₃ salts were characterised by XRD, TEM, SEM-EDX, ICP-AES, and the elemental analyser (see **supplementary information** for a detailed description of the results per analysis). The dried Fe(III) salts had different colours (**Fig. 7.4A**); Fe₄PP₃ was white, Fe₂IMP₃ was yellow, and Fe₂GMP₃ orange. XRD analyses of the Fe₄PP₃, Fe₂IMP₃, and Fe₂GMP₃ salts indicated that they were all amorphous (**Fig. 7.4B**).

With TEM analysis, these amorphous particles were confirmed, although different types of shapes and particle sizes were observed (**Fig. 7.4C**, **Fig. S7.3**). Fe₄PP₃ consisted of aggregates of colloidal particles typical for precipitation with sizes from 5–30 nm, which is in line with previous reports.^[29,53] Fe₂IMP₃ consisted of aggregates of spherical particles with an average size of 100 nm, whereas Fe₂GMP₃ aggregates consisted of more elongated primary particles with an average size of 50 nm. We suggest that differently shaped particles were created for GMP because it can form G-quadruplexes that are crosslinked by Fe(III) to assemble into larger coordination polymers (**Fig. S7.4** and **Fig. S7.5**).^[54–57]

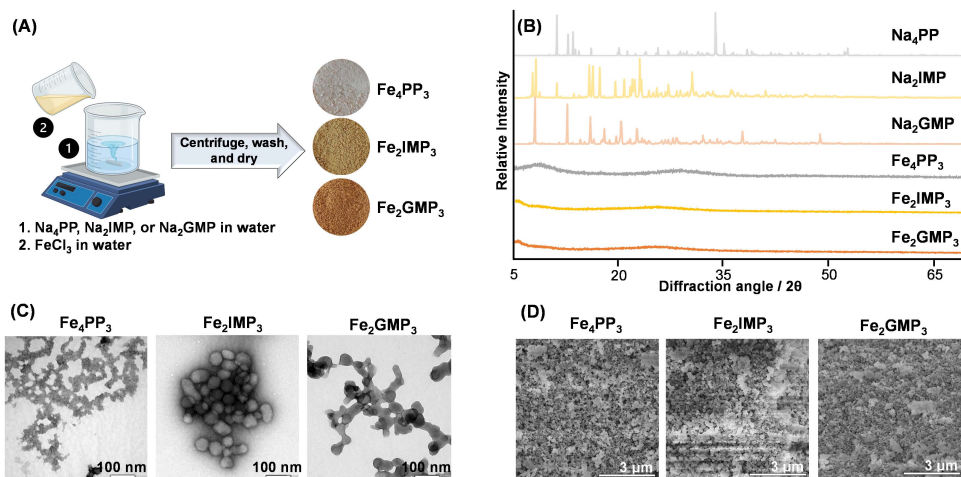


Figure 7.4. (A) Synthesis of iron-containing salts via an aqueous chemical precipitation procedure and colour of the dried salts; (B) Powder XRD patterns of the ligands before and after reacting with iron; (C) TEM and (D) SEM images of Fe_4PP_3 , Fe_2IMP_3 , and Fe_2GMP_3 .

Homogenous distribution of the elements in the salts was confirmed by SEM-EDX (Fig. S7.6). A high abundance of H as detected in the elemental analysis (Table S7.2) indicated that the salts were hydrated. Furthermore, the analysed elemental ratios were in good agreement with the calculated elemental ratios (Table S7.3) based on the molecular formulas for stoichiometric ratios as provided in Method 7.2.3.

7.3.3. pH-dependent dissolution behaviour and iron-phenolic reactivity

pH-dependent iron dissolution from Fe_4PP_3 , Fe_2IMP_3 , and Fe_2GMP_3

For food fortification purposes it is important that iron salts possess pH-dependent dissolution behaviour. To limit iron-mediated reactions, while maximising bio-accessibility, iron dissolution from the iron salts should be limited in the pH range of food (3-7) and fast at gastric (1-3) and/or intestinal pH (6-8). Therefore the pH-dependent dissolution behaviour of iron from Fe_4PP_3 , Fe_2IMP_3 , and Fe_2GMP_3 salts was investigated (Fig. 7.5). It can be observed that Fe_4PP_3 possessed low solubility in the acidic pH range (1-4), whereas the iron dissolution increases around pH 4. For Fe_2IMP_3 , iron dissolution from the salt was observed at pH < 3 and pH > 6. Similarly, Fe_2GMP_3 also possessed iron dissolution at pH < 3 and at pH > 6.5.

Up to a fifteen-fold decrease of soluble iron for Fe_2IMP_3 and Fe_2GMP_3 at food pH (3-7) was observed compared to Fe_4PP_3 . This dissolution behaviour makes Fe_2IMP_3 and Fe_2GMP_3 desirable as fortification salts for food, as it could potentially lead to reduced iron-mediated reactivity in the food products since less iron is in solution. Moreover, the up to a twenty-fold increase in iron solubility of Fe_2IMP_3 and Fe_2GMP_3 salts in the gastric pH range (1-3), compared to Fe_4PP_3 , are indicative of better bio-accessibility in the gastric environment.^[11,12,58,59] At intestinal pH (6-8) the Fe_2IMP_3 and Fe_2GMP_3 salts

show a decrease in solubility compared to Fe_4PP_3 . However, the solubility in acid is the common measure used to indicate bio-accessibility,^[10] and was shown to be a good indication for *in vivo* iron uptake.^[59]

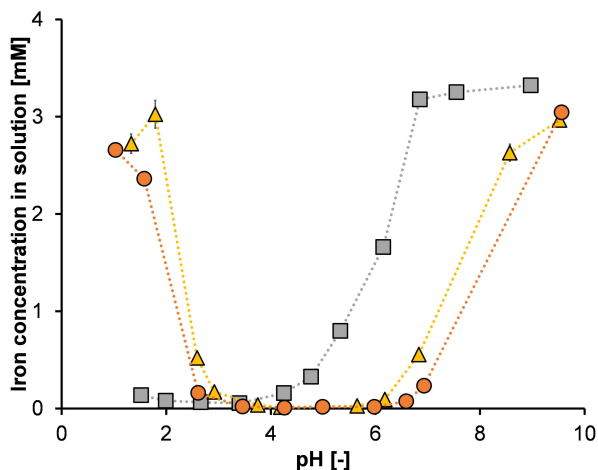


Figure 7.5. Iron dissolution from Fe_4PP_3 (grey square), Fe_2IMP_3 (yellow triangle), and Fe_2GMP_3 (orange circle) as a function of pH.

Reactivity of Fe_4PP_3 , Fe_2IMP_3 , and Fe_2GMP_3 with phenolics

Besides the iron dissolution from the iron salts, we also evaluated the reactivity of the iron salts with phenolics. Prevention of iron-phenolic interactions is important to ensure iron bio-accessibility and limit discolouration.^[60] For these phenolic reactivity measurements, we applied a set of six model phenolic compounds with different chemical properties, most notably different water solubilities, as previously reported.^[15] **Fig. 7.6** shows the total absorbance, colour, and iron in a solution of the three salts after incubation with different phenolics at pH 6.5 (2 h, 23 °C). This pH was chosen as it is in the pH range of bouillon cubes. For the water soluble phenolics (*i.e.* catechol, caffeic acid, and epicatechin) an absorbance band at $\lambda_{\text{max}} \sim 580$ nm was observed for all three salts (**Fig. 7.6A**). This absorbance at 580 nm is indicative for 1:2 complexes of Fe(III) from the salts with the catecholate moiety of the phenolic, and is responsible for the bluish to purplish appearance (**Fig. 7.6B**).^[17,61]

It was observed that in presence of the water soluble phenolics the total absorbance and discolouration in the Fe_2IMP_3 and Fe_2GMP_3 samples was equal or even showed a slight increase compared to Fe_4PP_3 . This was contrary to our expectations, because much lower iron solubilities for Fe_2IMP_3 and Fe_2GMP_3 salts in aqueous solution were observed at pH 6.5 in **Fig. 7.5**. However, we also measured the iron solubilities of the salts in presence of the phenolics and noticed a fast increase in iron dissolution from the salt in presence of the water soluble phenolics compared to the insoluble phenolics (**Fig. 7.6C**).

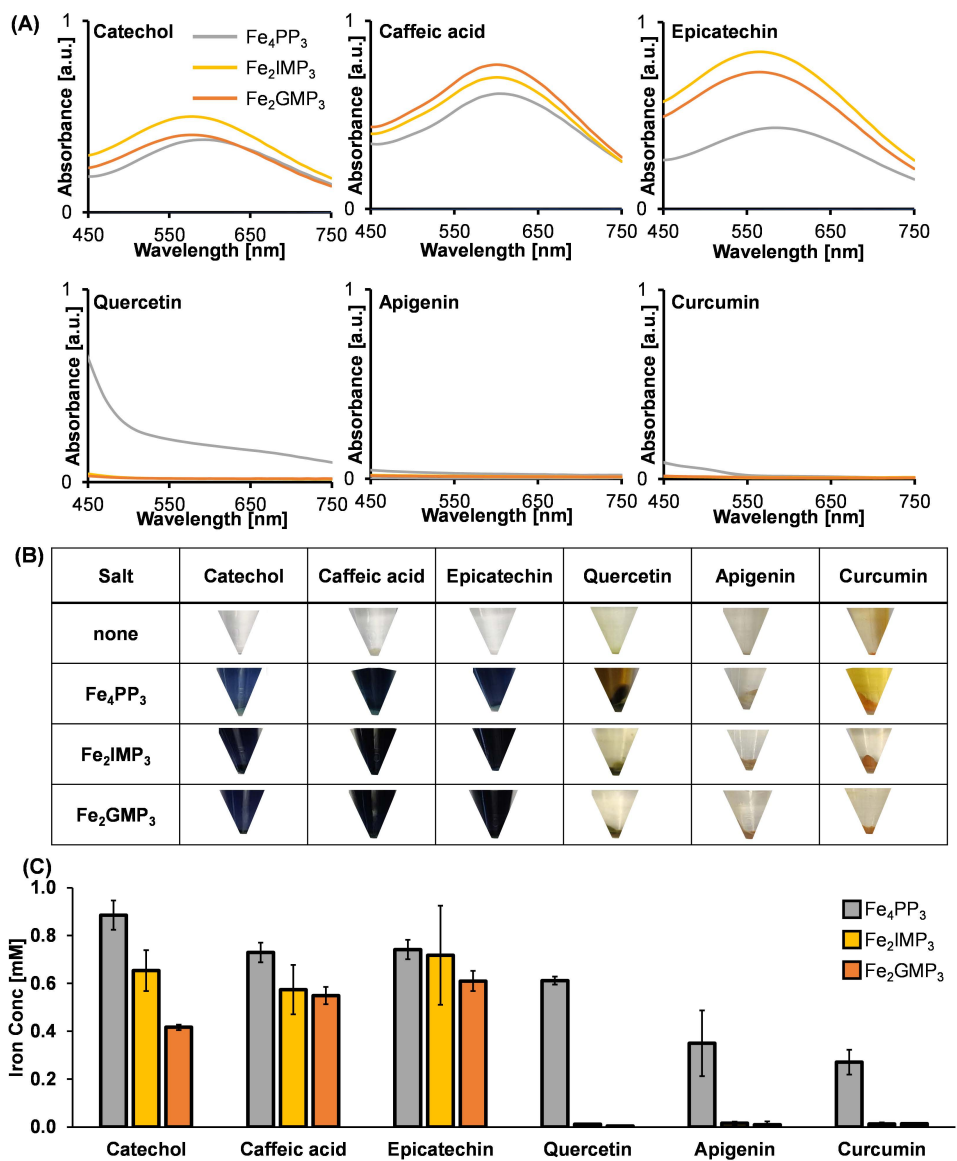


Figure 7.6. (A) Absorbance spectra of the supernatants of Fe_4PP_3 , Fe_2IMP_3 , and Fe_2GMP_3 in the presence of different phenolics at pH 6.5. (B) Pictures of the samples in the Eppendorf tubes after incubation and centrifugation. (C) Soluble iron concentration in solutions of Fe_4PP_3 , Fe_2IMP_3 , and Fe_2GMP_3 after incubation (2 h, pH 6.5) with different phenolics.

As suggested previously, the water soluble phenolics may coordinate Fe(III) on the surface of the insoluble salt particles and thereby bring it in solution, forming soluble coloured complexes.^[15] This interaction of Fe(III) with phenolics can compete with the Fe(III) interactions with PP, IMP, and GMP at neutral pH because the phenolate oxygens are more electron-rich compared to the phosphate oxygens. In general, very strong coordinate bonds with Fe(III) are formed for highly electron-rich binding sites.^[62]

In presence of quercetin and curcumin, absorbance in the visible spectra increased and discolouration of the samples was observed in presence of Fe_4PP_3 (**Fig. 7.6A** and **6B**). For Fe_2IMP_3 and Fe_2GMP_3 with these phenolics, no increased absorbances of the supernatants were observed. The precipitate changed from a yellow to brownish colour. We hypothesised previously that the discolouration of these precipitates can be due to formation of Fe(III)-phenolic complexes on the surface of the salts.^[15] For apigenin, no absorbance was observed with any of the Fe(III) salts. These poorly water soluble phenolics do not increase the Fe(III) dissolution (**Fig. 7.6C**) from the surface of the salts and therefore no discolouration was observed for Fe_2IMP_3 and Fe_2GMP_3 in aqueous solutions at pH 6.5. These findings indicate that Fe_2IMP_3 and Fe_2GMP_3 are promising salts for the fortification of food products containing poorly soluble phenolic compounds, such as the phenolics that are commonly present in bouillon cubes.

7.3.4. Dephosphorylation of GMP and IMP in presence of Fe(III)

Dephosphorylation of nucleoside 5'-mono-, -di-, and -triphosphates was previously reported to be catalysed by metal coordination.^[45,63,64] To check if dephosphorylation occurred in the Fe(III) salts of the nucleotides, we separated and quantified the amounts of nucleotides and nucleosides in the synthesised salts of Fe_2IMP_3 and Fe_2GMP_3 using HILIC-PDA-MSⁿ (**Fig. S7.7**). We observed a small peak for inosine and guanosine but for both salts > 98 % of the total peak area was still the intact nucleotide. This indicates that the nucleotides are stable in a coordination complex with Fe(III).

7.3.5. Implications of iron fortification using Fe_2IMP_3 and Fe_2GMP_3

The Fe(III) salts of IMP or GMP can potentially serve as food fortificants because of their pH-dependent iron dissolution and decreased reactivity with poorly soluble phenolics similarly to those that are commonly present in bouillon cubes. The implications of Fe(III) coordination to IMP and GMP on the umami perception has to be confirmed in future sensory studies. We expect that the coordination of Fe(III) to IMP or GMP may affect their interaction with the umami receptor because the negatively charged phosphate group is normally involved in stabilisation of that interaction.^[65]

Previously, we have also synthesised mixed Ca-Fe(III) pyrophosphate salts that already possessed very promising dissolution behaviour.^[12] Compared to the Ca-Fe(III) pyrophosphate salts, these nucleotide salts are even five times more soluble in the

gastric pH range and two times less soluble in the food pH range. Additionally, the presence of dietary nucleotides has already been demonstrated to enhance the intestinal absorption of iron in rats.^[66,67] However, additional experiments have to be performed to confirm the bioavailability of iron from the Fe_2IMP_3 and Fe_2GMP_3 salts. Based on the increased dissolution of Fe_2IMP_3 and Fe_2GMP_3 at gastric pH, these salts may be preferred over Fe_4PP_3 and Ca-Fe(III) pyrophosphate salts as iron fortificant.

7.4. Conclusion

This work reports the pH-dependent interaction of taste enhancers (Glu, IMP, and GMP) and phosphates (MP and PP) with Fe(III) in aqueous solutions. All three taste enhancers can coordinate Fe(III), however, coordination was more stable with the phosphate moiety of the nucleotides (IMP and GMP) than with the carboxylate moieties of glutamate (Glu). Similar to complexes of Fe(III) with PP, complexes of Fe(III) with IMP or GMP possess limited solubility in aqueous solution at pH 3–8, leading to their precipitation. The precipitation of these species with Fe(III) was utilised to synthesise salts of Fe(III) with IMP, GMP, and PP using an aqueous chemical precipitation method. The synthesised Fe(III) salts of IMP or GMP possessed increased iron dissolution at gastric pH (1–3), decreased iron dissolution at food pH (3–7), and less discolouration with poorly soluble phenolics compared to the currently used fortification salt Fe_4PP_3 . In conclusion, these Fe(III) salts with IMP or GMP have the potential to be used to design more stable iron-fortified foods.

7.5. Acknowledgements

We would like to thank Orsolya Bogdányi-Fekete for her support with the potentiometric measurements, and the Department of Inorganic and Analytical Chemistry at the University of Debrecen for hosting JB. We are thankful to the Graduate School VLAG for granting the PhD fellowship to visit Debrecen University. We thank Neshat Moslehi (Utrecht University) for the fruitful discussion on the synthesis of the Fe(III) salts. We would like to thank Jelmer Vroom from the Wageningen Electron Microscopy Centre (WEMC) for carrying out TEM and SEM data collection and Ilse Gerrits (Wageningen University & Research) for her help with the X-Ray powder diffraction measurements. The authors are grateful to Arjen Reichwein, Johan Hoekstra, and Ewout Otto of Nouryon Specialty Chemicals B.V. for performing the elemental analysis. Part of the presented results were obtained using advanced microscopy, mass spectrometry, and XRD equipment which is owned by WUR-Shared Research Facilities. Investment by WUR-Shared Research Facility was made possible by the 'Regio Deal Foodvalley' of the province of Gelderland, The Netherlands.

7.6. References

- 1 Hurrell, R. F. (1997). Preventing iron deficiency through food fortification. *Nutrition Reviews*, 55(6), 210-222.
- 2 Moretti, D., Zimmermann, M. B., Wegmüller, R., Walczyk, T., Zeder, C., & Hurrell, R. F. (2006). Iron status and food matrix strongly affect the relative bioavailability of ferric pyrophosphate in humans. *The American Journal of Clinical Nutrition*, 83(3), 632-638.
- 3 de Mejia, E. G., Aguilera-Gutiérrez, Y., Martín-Cabrejas, M. A., & Mejia, L. A. (2015). Industrial processing of condiments and seasonings and its implications for micronutrient fortification. *Annals of the New York Academy of Sciences*, 1357(1), 8-28.
- 4 Acebal, C. C., Lista, A. G., & Fernández Band, B. S. (2008). Simultaneous determination of flavor enhancers in stock cube samples by using spectrophotometric data and multivariate calibration. *Food Chemistry*, 106(2), 811-815.
- 5 Chiang, P.-D., Yen, C.-T., & Mau, J.-L. (2007). Non-volatile taste components of various broth cubes. *Food Chemistry*, 101(3), 932-937.
- 6 Habeych, E., van Kogelenberg, V., Sagalowicz, L., Michel, M., & Galaffu, N. (2016). Strategies to limit colour changes when fortifying food products with iron. *Food Research International*, 88, 122-128.
- 7 Bijlsma, J., de Bruijn, W. J. C., Velikov, K. P., & Vincken, J.-P. (2022). Unravelling discolouration caused by iron-flavonoid interactions: Complexation, oxidation, and formation of networks. *Food Chemistry*, 370, 131292.
- 8 Gupta, S., Habeych, E., Scheers, N., Merinat, S., Rey, B., Galaffu, N., & Sandberg, A.-S. (2020). The development of a novel ferric phytate compound for iron fortification of bouillons (part I). *Scientific Reports*, 10(1), 1-10.
- 9 Martínez-Navarrete, N., Camacho, M. M., Martínez-Lahuerta, J., Martínez-Monzó, J., & Fito, P. (2002). Iron deficiency and iron fortified foods—a review. *Food Research International*, 35(2), 225-231.
- 10 Allen, L. H., De Benoist, B., Dary, O., & Hurrell, R. (2006). Guidelines on food fortification with micronutrients. World Health Organization.
- 11 Tian, T., Blanco, E., Smoukov, S. K., Velez, O. D., & Velikov, K. P. (2016). Dissolution behaviour of ferric pyrophosphate and its mixtures with soluble pyrophosphates: Potential strategy for increasing iron bioavailability. *Food Chemistry*, 208, 97-102.
- 12 Moslehi, N., Bijlsma, J., De Bruijn, W. J. C., Velikov, K. P., Vincken, J.-P., & Kegel, W. K. (2022). Design and characterization of Ca-Fe(III) pyrophosphate salts with tunable pH-dependent solubility for dual-fortification of foods. *Journal of Functional Foods*, 92, 105066.
- 13 Hurrell, R. F., Lynch, S., Bothwell, T., Cori, H., Glahn, R., Hertrampf, E., Kratky, Z., Miller, D., Rodenstein, M., Streekstra, H., Teucher, B., Turner, E., Yeung, C. K., & Zimmermann, M. B. (2004). Enhancing the absorption of fortification iron. *International Journal for Vitamin and Nutrition Research*, 74(6), 387-401.
- 14 Dueik, V., Chen, B. K., & Diosady, L. L. (2017). Iron-polyphenol interaction reduces iron bioavailability in fortified tea: Competing complexation to ensure iron bioavailability. *Journal of Food Quality*, 2017, 1-8.
- 15 Bijlsma, J., Moslehi, N., Velikov, K. P., Kegel, W. K., Vincken, J.-P., & de Bruijn, W. J. C. (2023). Reactivity of Fe(III)-containing pyrophosphate salts with phenolics: Complexation, oxidation, and surface interaction. *Food Chemistry*, 407, 135156.
- 16 Jansen, F. J. H. M., & Velikov, K. P. (2014). Fortified savoury food concentrate. *European Patent Office*, EP2774497B1(131577314).
- 17 Bijlsma, J., de Bruijn, W. J. C., Hageman, J. A., Goos, P., Velikov, K. P., & Vincken, J.-P. (2020). Revealing the main factors and two-way interactions contributing to food discolouration caused by iron-catechol complexation. *Scientific Reports*, 10(1), 8288.
- 18 Djurdjević, P., & Jelić, R. (1997). Solution equilibria in L-glutamic acid and L-serine+ iron(III) systems. *Transition Metal Chemistry*, 22(3), 284-293.
- 19 Thakur, N., Sharma, B., Bishnoi, S., Mishra, S. K., Nayak, D., Kumar, A., & Sarma, T. K. (2018). Multifunctional inosine monophosphate coordinated metal-organic hydrogel: Multistimuli responsiveness, self-healing properties, and separation of water from organic solvents. *ACS Sustainable Chemistry & Engineering*, 6(7), 8659-8671.
- 20 Lopez, A., & Liu, J. (2017). Self-assembly of nucleobase, nucleoside and nucleotide coordination polymers: From synthesis to applications. *ChemNanoMat*, 3(10), 670-684.
- 21 Zhou, P., Shi, R., Yao, J.-F., Sheng, C.-F., & Li, H. (2015). Supramolecular self-assembly of nucleotide-metal coordination complexes: From simple molecules to nanomaterials. *Coordination Chemistry Reviews*, 292, 107-143.
- 22 Aoki, K. (1976). Crystallographic studies of interactions between nucleotides and metal ions. II. The crystal and molecular structure of the 1:1 complex of cadmium (II) with guanosine 5'-phosphate. *Acta Crystallographica Section B: Structural Crystallography and Crystal Chemistry*, 32(5), 1454-1459.
- 23 Aoki, K., Clark, G. R., & Orbell, J. D. (1976). Metal-phosphate bonding in transition metal-nucleotide complexes. The crystal and molecular structures of the polymeric copper(II) complex of guanosine 5'-monophosphate. *Biochimica et Biophysica Acta (BBA) - Nucleic Acids and Protein Synthesis*, 425(3), 369-371.
- 24 Alabart, J. R., Moreno, V., Labarta, A., Tejada, J., & Molins, E. (1990). Electronic structure determination and dynamical properties of iron (II)-guanosine-5'-monophosphate complex via mossbauer and magnetic susceptibility measurements. *The Journal of Chemical Physics*, 92(10), 6131-6139.

- 25 Moreno, V., Terrón, A., Vicens, M., Molins, E., Labarta, A., Caubet, A., Pereda, J. A., Fernández, A., & Tejada, J. (1985). Synthesis, spectroscopic and magnetic characterization of some iron(III)-nucleotide compounds. *Transition Metal Chemistry*, 10(3), 90-93.
- 26 Richter, Y., & Fischer, B. (2003). Characterization and elucidation of coordination requirements of adenine nucleotides complexes with Fe(II) ions. *Nucleosides, Nucleotides & Nucleic Acids*, 22(9), 1757-1780.
- 27 Zhelyaskov, V., & Yue, K. T. (1992). A Raman study of the binding of Fe(III) to ATP and AMP. *Biochemical Journal*, 287(2), 561-566.
- 28 Lemire, R., Taylor, P., Schlenz, H., & Palmer, D. (2020). *Chemical thermodynamics of iron, part 2* (Vol. 13a). Boulogne-Billancourt, France Nuclear Energy Agency of the OECD (NEA).
- 29 Rossi, L., Velikov, K. P., & Philipse, A. P. (2014). Colloidal iron (III) pyrophosphate particles. *Food Chemistry*, 151, 243-247.
- 30 Atkari, K., Kiss, T., Bertani, R., & Martin, R. B. (1996). Interactions of aluminum(III) with phosphates. *Inorganic Chemistry*, 35(24), 7089-7094.
- 31 Sun, Y., Zhao, L., & Teng, Y. (2020). Effect of soil type on the degradation of polychlorinated biphenyls in a pyrophosphate-chelated Fenton-like reaction. *Chemical Engineering Journal*, 390, 124574.
- 32 Jiang, C., Wang, X., Parekh, B., & Leonard, J. (1998). Pyrite depression by phosphates in coal flotation. *Mining, Metallurgy & Exploration*, 15(1), 1-7.
- 33 Gran, G., Dahlenborg, H., Laurell, S., & Rottenberg, M. (1950). Determination of the equivalent point in potentiometric titrations. *Acta Chemica Scandinavica*, 4(4), 559-577.
- 34 Mussini, T., Covington, A., Longhi, P., & Rondinini, S. (1985). Criteria for standardization of pH measurements in organic solvents and water + organic solvent mixtures of moderate to high permittivities. *Pure and Applied Chemistry*, 57(6), 865-876.
- 35 Irving, H., Miles, M., & Pettit, L. (1967). A study of some problems in determining the stoichiometric proton dissociation constants of complexes by potentiometric titrations using a glass electrode. *Analytica Chimica Acta*, 38, 475-488.
- 36 Sabatini, A., Vacca, A., & Gans, P. (1974). MINQUAD —a general computer programme for the computation of formation constants from potentiometric data. *Talanta*, 21(1), 53-77.
- 37 Gans, P., Sabatini, A., & Vacca, A. (1996). Investigation of equilibria in solution. Determination of equilibrium constants with the HYPERQUAD suite of programs. *Talanta*, 43(10), 1739-1753.
- 38 Baes, C. F., & Mesmer, R. S. (1977). The hydrolysis of cations. *Berichte der Bunsengesellschaft für Physikalische Chemie*, 81(2), 245-246.
- 39 Farkas, E., Buglyó, P., Enyedy, É. A., Gerlei, V. A., & Santos, A. M. (2002). Factors affecting the metal ion-hydroxamate interactions: Effect of the position of the peptide function in the connecting chain on the Fe(III), Mo(VI) and V(V) complexation of some new desferrioxamine B (DFB) model dihydroxamic acids. *Inorganica Chimica Acta*, 339, 215-223.
- 40 Sigel, H., Massoud, S. S., & Corfu, N. A. (1994). Comparison of the extent of macrochelate formation in complexes of divalent metal ions with guanosine (GMP²⁻), inosine (IMP²⁻), and adenosine 5'-monophosphate (AMP²⁻). The crucial role of N-7 basicity in metal ion-nucleic base recognition. *Journal of the American Chemical Society*, 116(7), 2958-2971.
- 41 Kiss, T., Buglyó, P., Sanna, D., Micera, G., Decock, P., & Dewaele, D. (1995). Oxovanadium(IV) complexes of citric and tartaric acids in aqueous solution. *Inorganica Chimica Acta*, 239(1), 145-153.
- 42 Gogia, S., Jain, A., & Puranik, M. (2009). Structures, ionization equilibria, and tautomerism of 6-oxopurines in solution. *The Journal of Physical Chemistry B*, 113(45), 15101-15118.
- 43 Bastug, A. S., Goz, S. E., Talman, Y., Gokturk, S., Asil, E., & Caliskan, E. (2011). Formation constants and coordination thermodynamics for binary complexes of Cu(II) and some α -amino acids in aqueous solution. *Journal of Coordination Chemistry*, 64(2), 281-292.
- 44 Enyedy, É. A., Pöcsi, I., & Farkas, E. (2004). Complexation of desferrioxamine with trivalent Fe, Al, Ga, In and divalent Fe, Ni, Cu, Zn metal ions: Effects of the linking chain structure on the metal binding ability of hydroxamate based siderophores. *Journal of Inorganic Biochemistry*, 98(11), 1957-1966.
- 45 Oivanen, M., & Lonnberg, H. (1990). Kinetics of reactions of pyrimidine nucleoside 2'-and 3'-monophosphates under acidic and neutral conditions: Concurrent phosphate migration, dephosphorylation and deamination. *Acta Chemica Scandinavica*, 44, 239-242.
- 46 Flynn, C. M. (1984). Hydrolysis of inorganic iron(III) salts. *Chemical Reviews*, 84(1), 31-41.
- 47 Enyedy, É. A., Primik, M. F., Kowol, C. R., Arion, V. B., Kiss, T., & Keppler, B. K. (2011). Interaction of triapine and related thiosemicarbazones with iron (III)/(II) and gallium (III): a comparative solution equilibrium study. *Dalton Transactions*, 40(22), 5895-5905.
- 48 Enyedy, É. A., May, N. V., Pape, V. F., Heffeter, P., Szakács, G., Keppler, B. K., & Kowol, C. R. (2020). Complex formation and cytotoxicity of triapine derivatives: A comparative solution study on the effect of the chalcogen atom and NH-methylation. *Dalton Transactions*, 49(46), 16887-16902.
- 49 Heistand, R. N., & Clearfield, A. (1963). The effect of specific swamping electrolytes upon the formation constant of the monochloroiron (III) complex. *Journal of the American Chemical Society*, 85(17), 2566-2570.
- 50 Bjerrum, J., & Lukes, I. (1986). The iron (III)-chloride system. A study of the stability constants and of the distribution of the tetrachloro species between organic solvents and aqueous chloride solutions. *Acta Chemica Scandinavica* 40a, 31-40.
- 51 Lente, G., & Fábrián, I. (2001). A simple test to confirm the ligand substitution reactions of the hydrolytic iron(III) dimer. *Reaction Kinetics and Catalysis Letters*, 73(1), 117-125.

- 52 Lente, G., Magalhães, M. E. A., & Fábíán, I. (2000). Kinetics and mechanism of complex formation reactions in the iron(III)-phosphate ion system at large iron(III) excess. Formation of a tetranuclear complex. *Inorganic Chemistry*, 39(9), 1950-1954.
- 53 van Leeuwen, Y. M., Velikov, K. P., & Kegel, W. K. (2012). Morphology of colloidal metal pyrophosphate salts. *RSC Advances*, 2(6), 2534-2540.
- 54 Thakur, N., Sharma, B., Bishnoi, S., Jain, S., Nayak, D., & Sarma, T. K. (2019). Biocompatible Fe³⁺ and Ca²⁺ dual cross-linked G-quadruplex hydrogels as effective drug delivery system for pH-responsive sustained zero-order release of doxorubicin. *ACS Applied Bio Materials*, 2(8), 3300-3311.
- 55 Bhattacharyya, T., Saha, P., & Dash, J. (2018). Guanosine-derived supramolecular hydrogels: Recent developments and future opportunities. *ACS Omega*, 3(2), 2230-2241.
- 56 Sutyak, K. B., Zavali, P. Y., Robinson, M. L., & Davis, J. T. (2016). Controlling molecularity and stability of hydrogen bonded G-quadruplexes by modulating the structure's periphery. *Chemical Communications*, 52(74), 11112-11115.
- 57 Xiao, S., & Davis, J. T. (2018). G₄-quartet hydrogels from 5'-hydrazino-guanosine for the non-covalent and covalent remediation of contaminants from water. *Faraday Discussions*, 209(0), 97-112.
- 58 Hurrell, R. (2002). How to ensure adequate iron absorption from iron-fortified food. *Nutrition Reviews*, 60, S7-S15.
- 59 Rohner, F., Ernst, F. O., Arnold, M., Hilbe, M., Biebing, R., Ehrensperger, F., Pratsinis, S. E., Langhans, W., Hurrell, R. F., & Zimmermann, M. B. (2007). Synthesis, characterization, and bioavailability in rats of ferric phosphate nanoparticles. *The Journal of Nutrition*, 137(3), 614-619.
- 60 McGee, E. J. T., & Diosady, L. L. (2018). Prevention of iron-polyphenol complex formation by chelation in black tea. *LWT - Food Science and Technology*, 89, 756-762.
- 61 Elhabiri, M., Carrér, C., Marmolle, F., & Traboulsi, H. (2007). Complexation of iron(III) by catecholate-type polyphenols. *Inorganica Chimica Acta*, 360(1), 353-359.
- 62 Athira, S., Mann, B., Sharma, R., Pothuraju, R., & Bajaj, R. K. (2021). Preparation and characterization of iron-chelating peptides from whey protein: An alternative approach for chemical iron fortification. *Food Research International*, 141, 110133.
- 63 Sigel, H. (1990). Mechanistic aspects of the metal ion promoted hydrolysis of nucleoside 5'-triphosphates (NTPs). *Coordination Chemistry Reviews*, 100, 453-539.
- 64 Buisson, D. H., & Sigel, H. (1974). Significance of binary and ternary copper(II) complexes for the promotion and protection of adenosine 5'-di- and triphosphate toward hydrolysis. *Biochimica et Biophysica Acta (BBA) - General Subjects*, 343(1), 45-63.
- 65 Zhang, F., Klebansky, B., Fine, R. M., Xu, H., Pronin, A., Liu, H., Tachdjian, C., & Li, X. (2008). Molecular mechanism for the umami taste synergism. *Proceedings of the National Academy of Sciences*, 105(52), 20930-20934.
- 66 Faelli, A., & Esposito, G. (1970). Effect of inosine and its metabolites on intestinal iron absorption in the rat. *Biochemical Pharmacology*, 19(9), 2551-2554.
- 67 Cosgrove, M. (1998). Nucleotides. *Nutrition*, 14(10), 748-751.
- 68 Liang, H., Liu, B., Yuan, Q., & Liu, J. (2016). Magnetic iron oxide nanoparticle seeded growth of nucleotide coordinated polymers. *ACS Applied Materials & Interfaces*, 8(24), 15615-15622.
- 69 Zhou, J., Han, H., & Liu, J. (2022). Nucleobase, nucleoside, nucleotide, and oligonucleotide coordinated metal ions for sensing and biomedicine applications. *Nano Research*, 15(1), 71-84.

7.7. Supplementary information

Method S7.1. Characterisation of Fe_4PP_3 , Fe_2IMP_3 , and Fe_2GMP_3 salts

X-ray diffraction (XRD)

XRD measurements of the dried salts were performed with a Bruker D8 Advance diffractometer (Bruker, Karlsruhe, Germany). The source consisted of Cu $K\alpha$ radiation ($\lambda = 1.54 \text{ \AA}$). XRD patterns were recorded from 5° to 70° 2θ , with a step size of 0.01° and a scan speed of 0.1 s/step . The XRD data was processed using the Bruker DIFFRAC.EVA software and the obtained patterns were compared with reference patterns in the Crystallography Open Database (COD).

Electron microscopy and energy dispersive X-ray spectroscopy (EDX)

Optical analysis was carried out at the Wageningen Electron Microscopy Centre (WEMC). The transmission electron microscopy (TEM) analysis, was done on the dispersions after washing but before the drying step. Dispersions ($5 \mu\text{L}$) were added to a 400 mesh formvar/carbon grid (after discharging the grid) and incubated for 2 min at room temperature. The grid was washed with $5 \mu\text{L}$ MQ, and after 2 min the excess water was removed with a blotting paper. Next, the sample was negatively stained with $5 \mu\text{L}$ of 2% uranyl acetate, and after 30 s the excess was removed with a blotting paper and the sample was air-dried before measurement using a JEM-1400Plus (JEOL, MA, USA), operating at 120 kV. The particle size distribution was obtained by analysis of TEM images using the ImageJ software (Version 1.53t, Wayne Rasband, National Institutes of Health, USA).

For scanning electron microscopy (SEM), the dried salts were applied to a carbon adhesive tab attached to a sample holder and the excess powder was removed with compressed air. The sample was sputter-coated with 12 nm tungsten using a Leica SCD 500 (Vienna, Austria). SEM analysis was performed on FEI Magellan 400 (FEI, Eindhoven, The Netherlands), operating at 2 kV and 13 pA. Energy dispersive X-ray (EDX) analysis was performed using a SEM equipped with an EDX system (SEM-EDX). The measurements were performed on the thick powder sediments to obtain information about the samples' homogeneity and the elemental composition.

Elemental analysis

The dried salts were milled and homogenised and weighed into a tin foil cup (2–10 mg). Carbon, nitrogen, and hydrogen contents of the samples were measured in duplicate using the Thermo Flash 2000 CHNS elemental analyser based on the modified Dumas method.

For the determination of phosphorus and iron 0.1 g of sample was weighed and digested in 70 vol. % nitric acid (HNO_3) at medium pressure and 185°C in the microwave digestion system (Multiwave Go, Anton Paar, Graz, Austria). Inductively coupled plasma atomic emission spectroscopy (ICP-AES; Agilent 5110 VDV; Agilent



Technologies, Tokyo, Japan), was used to quantify the amount of P and Fe in the digestates using scandium as an internal standard. The limit of detection (LOD) values of iron and phosphorus were respectively 0.05 and 0.20 mg L⁻¹, and the limit of quantification (LOQ) values were respectively 0.15 and 0.61 mg L⁻¹.

Method S7.2. Identification and quantification of nucleotides by HILIC-PDA-ITMSⁿ

The salts were dissolved at 0.1 mg mL⁻¹ in 50 vol. % ACN + 0.2 vol. % FA and separated on a Thermo Vanquish UHPLC system (Thermo Scientific, San Jose, CA, USA) equipped with an autosampler, a pump, a degasser, and a photodiode array (PDA) detector. A sample (1 µL) was injected on an Acquity UPLC BEH amide column (150 mm × 2.1 mm i.d., 1.7 µm) with a VanGuard (5 mm × 2.1 mm i.d., 1.7 µm) guard column of the same material (Waters, Milford, MA, USA). Water (A) and acetonitrile (B), both acidified with 0.2 vol. % formic acid, were used as eluents. The flow rate was 400 µL min⁻¹, and the temperature of the column oven was 35 °C. The following elution profile was used: 0.00 – 1.09 min, isocratic on 95 vol. % B; 1.09 – 13.81 min, linear gradient from 95 to 60 vol. % B; 13.81 – 14.90 min linear gradient from 60 to 50 vol. % B; 14.90 – 20.36 min isocratic on 50 vol. % B; 20.36 – 21.45 min linear gradient from 50 to 95 vol. % B; 21.45 – 26.90 min isocratic on 95 vol. % B. The PDA detector was set to measure the wavelength range of 190 – 680 nm. Mass spectrometric data were acquired using an LTQ Velos Pro linear ion trap mass spectrometer (Thermo Scientific) equipped with a heated electrospray ionisation probe (ESI-ITMSⁿ) and coupled *in-line* to the Vanquish UHPLC system. Nitrogen was used as a sheath gas (50 arbitrary units) and auxiliary gas (13 arbitrary units). Data were collected over the *m/z* range of 150 – 1,500 in negative and positive ionisation mode by using source voltages of 2.5 and 3.5 kV, respectively. For both modes, the S-lens RF level was set at 67 %, the ion transfer tube temperature was 263 °C and the source heater temperature was 425 °C. Data-dependent MSⁿ analysis was performed on the most intense ion by collision-induced dissociation (CID) with a normalised collision energy of 35 %. A dynamic mass exclusion approach was used, in which the most intense ion was fragmented 3 times and was subsequently excluded from fragmentation for the following 5 seconds, allowing data-dependent MSⁿ analysis of less intense co-eluting compounds. Data acquisition and processing were performed using Xcalibur version 4.1 (Thermo Scientific). Quantification of the nucleotides and nucleosides was performed based on PDA peak area (280 nm) and an external calibration curve of the corresponding authentic standards (0.06–1 mM, in duplicate, R² ≥ 0.99).

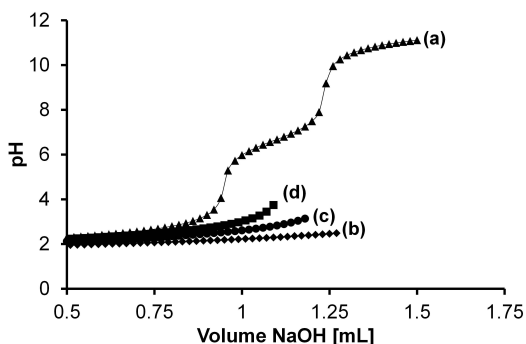


Figure S7.1. pH-potentiometric titration curves for 4.0 mM MP in (a) absence and in presence of Fe(III) at a ratio of Fe(III):ligand (b) 1:1, (c) 1:2, and (d) 1:4 at $I = 0.20$ M (KCl), and $T = 25.0$ °C.

Table S7.1. Dissociation constants of the studied ligands determined by pH-potentiometric titrations ($T = 25.0$ °C, $I = 0.20$ M (KCl) in DMSO/water 70/30 wt. %).

	Glu	IMP	GMP	MP	PP
pK_1	3.71(2) ^a	< 3 ^b	n.d. ^c	4.40(6)	n.d.
pK_2	5.94(1)	4.62(4)	n.d.	8.70(5)	n.d.
pK_3	10.25(1)	8.91(3)	n.d.	13.76(4)	n.d.
pK_4		14.12(2)	n.d.		n.d.

^a Standard deviations (3σ values) of the last decimal are given in parentheses; ^b it was not possible to measure at $pH < 3$ in DMSO/water 70/30 wt. % using the potentiometric setup; ^c dissociation constants could not be obtained due to precipitation of the ligand in absence of iron in the solvent mixture.

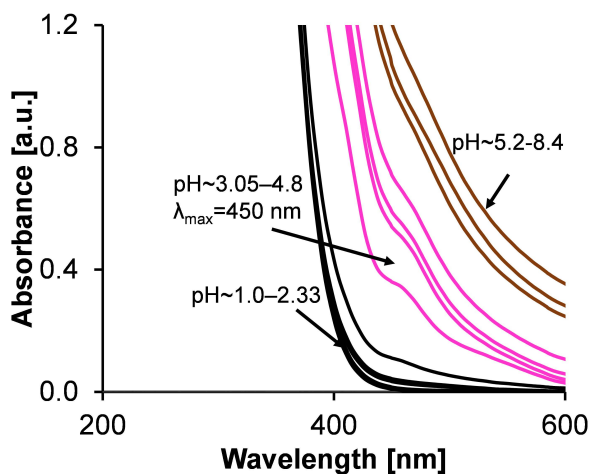


Figure S7.2. UV-Vis absorption spectra of $FeCl_3$ alone and in presence of Glu at different pH values ($C_{Fe(III)} = 3$ mM, $C_{Ligand} = 30$ mM, and $I = 0.20$ M (KCl)).

Characterisation of Fe_2IMP_3 and Fe_2GMP_3 salts

XRD analysis

The starting material (*i.e.* sodium salt of PP, IMP, and GMP) had clear XRD signals, indicating the crystalline nature of these materials. After the chemical precipitation with Fe(III) , the XRD patterns only showed noise, indicative for amorphous materials. The amorphous nature of these salts is suggested to be a result of the valence mismatch between iron (Fe^{3+}) and pyrophosphate ($\text{P}_2\text{O}_7^{4-}$), IMP ($\text{C}_{10}\text{H}_{13}\text{N}_4\text{O}_8\text{P}^{2-}$), and GMP ($\text{C}_{10}\text{H}_{12}\text{N}_5\text{O}_8\text{P}^{2-}$). Due to this valence mismatch, a more complicated stoichiometry is required to reach charge neutrality, resulting in formation of an amorphous matrix during the fast aqueous chemical precipitation process.^[12,29,53]

TEM analysis

We also used TEM analysis to compare the influence of the ligand on the particles that were formed during chemical precipitation (**Fig. 7.4C**). TEM analysis showed amorphous particles for all three systems although different types of shapes and particle sizes were observed. For Fe_4PP_3 , typical colloidal particles were observed for chemical precipitation using stoichiometric ratios of iron and pyrophosphate ions. The primary particle sizes ranged from 5 to 30 nm (**Fig. S7.3**), and were in line with the previously reported particle sizes.^[29,53]

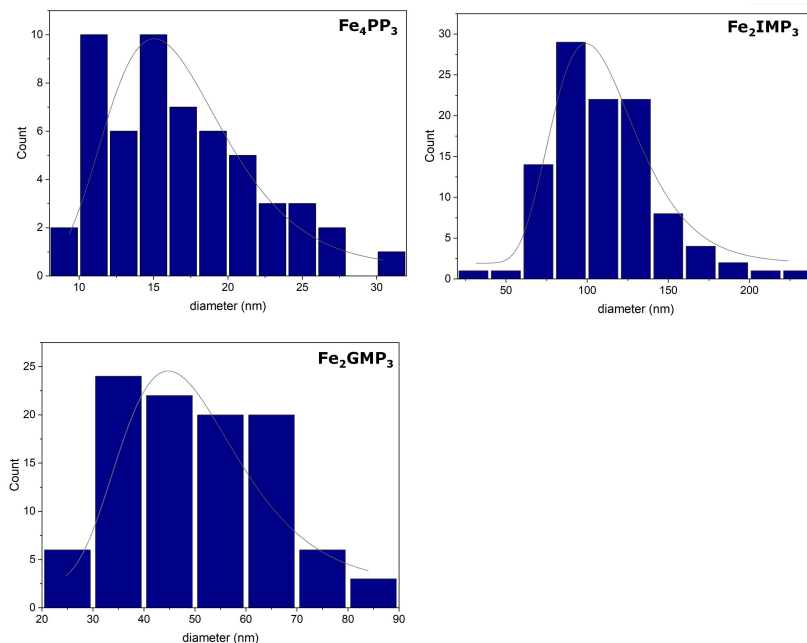


Figure S7.3. Particle size distribution of the primary particles in the amorphous aggregates as obtained from TEM images using ImageJ. The number (*n*) of primary particles that were measured by ImageJ were; Fe_4PP_3 *n*=57; Fe_2IMP_3 *n*=107; Fe_2GMP_3 *n*=102.

For Fe_2IMP_3 and Fe_2GMP_3 , different morphologies were observed with TEM. Fe_2IMP_3 consisted of spherical particles with an average size of 100 nm, whereas Fe_2GMP_3 consisted of more elongated primary particles with an average diameter of 50 nm. This elongation is an indication for interactions between the particles. These chain-like aggregated structures for Fe_2GMP_3 were previously reported to be the result of the formation of coordination polymers.^[20,68,69] Based on these differences in particle shape, we suggest that complexes of IMP with Fe(III) formed mononuclear species in which the phosphate coordinates Fe(III) (**Fig. S7.4A**). For GMP we suggest that a coordination polymer was formed (**Fig. S7.4B**). The only structural difference between IMP or GMP is the amine group on the guanine nucleobase at the C2 position, this amine is unlikely to coordinate metals.^[20] However, the presence of these amine groups is responsible for Hoogsteen type-hydrogen bonding that can lead to formation of planar aromatic G-quartet structures from the guanosine bases.^[55] Stacking of these G-quartets in presence of small amounts of potassium or sodium leads to the formation of G-quadruplexes.^[56,57] Therefore, we suggest that the elongated polymer observed for Fe_2GMP_3 in comparison to Fe_2IMP_3 is because of the formation of G-quadruplexes that are further crosslinked by Fe(III). Crosslinked G-quadruplexes by Fe(III) were discussed previously.^[54]

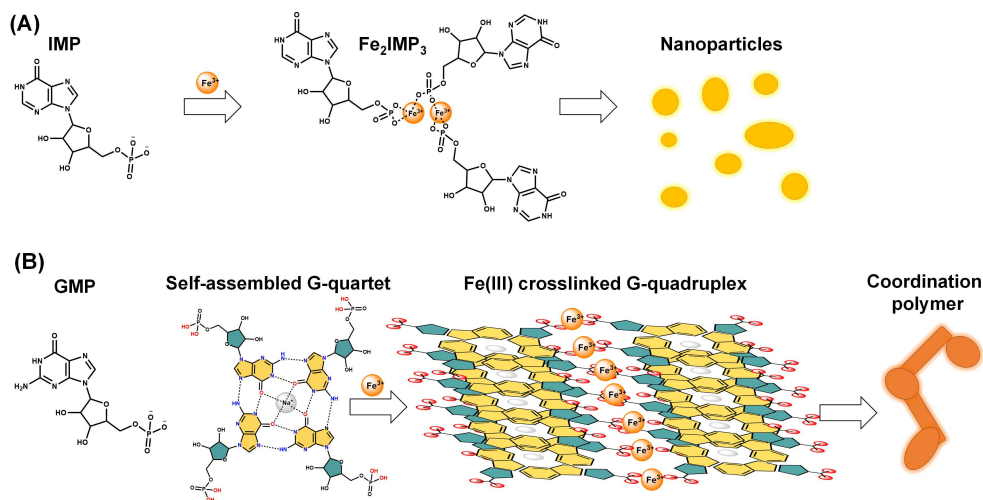


Figure S7.4. (A) Scheme for the self-assembly of IMP and Fe(III) to form nanoparticles; (B) Scheme for the self-assembly of GMP and Fe(III) into Fe(III) crosslinked G-quadruplexes that form coordination polymers, based on literature.^[54,55]

Additional proof for these G-quadruplexes is gel formation observed in the Fe(III)-GMP solutions at acidic (**Fig. S7.5**). Gel formation was not observed for Fe_2IMP_3 . The formation of this coordination polymer may also explain the low solubility of the Fe(III)-GMP species as was shown in **section 7.3.1**.

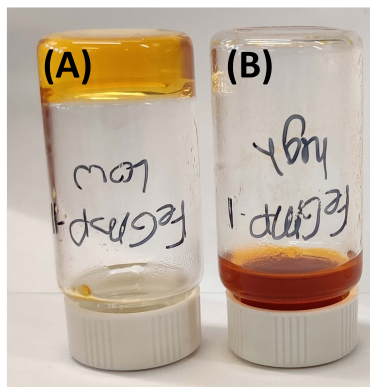


Figure S7.5. (A) Gel formation in a 10 mg mL^{-1} solution of Fe_2GMP_3 at pH 2; (B) no gel is formed at pH 9.

Elemental analysis

SEM-EDX was performed on the particle sediment to obtain qualitative information on the elemental ratios. With SEM-EDX we confirmed homogeneous distribution of the elements O, P, and Fe for Fe_4PP_3 and O, P, C, N, and Fe for Fe_2IMP_3 and Fe_2GMP_3 (Fig. S7.6). Quantitative information on the elemental ratios was obtained by elemental analysis using ICP-AES (Fe, P) and the elemental analyser (H, C, N, S) (Table S7.3). The abundance of H in all samples indicated that all salts were hydrated. Because we did not know the degree of hydration for each of the salts, H could not be taken into account to determine the elemental ratios, thus we compared the relative ratios of C, N, P, and Fe instead. These elemental ratios were in good agreement with the elemental ratios calculated based on the molecular formulas (Table S7.4).

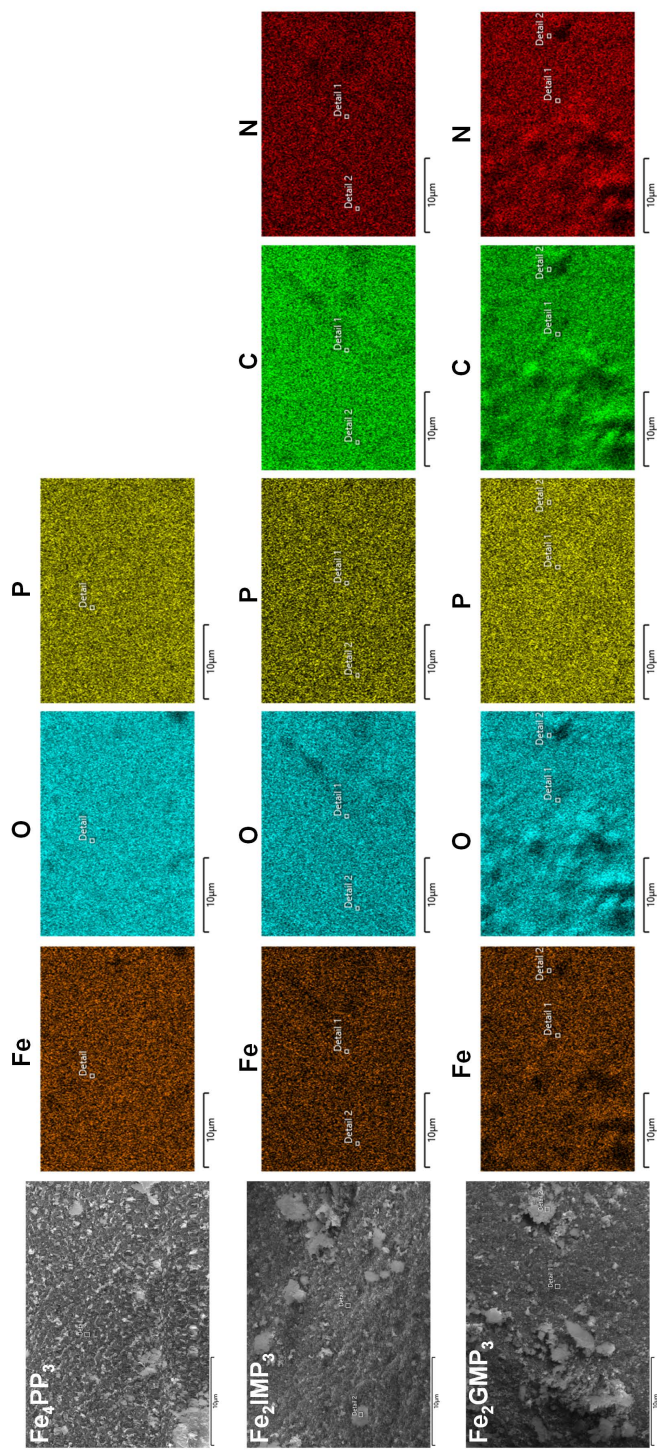


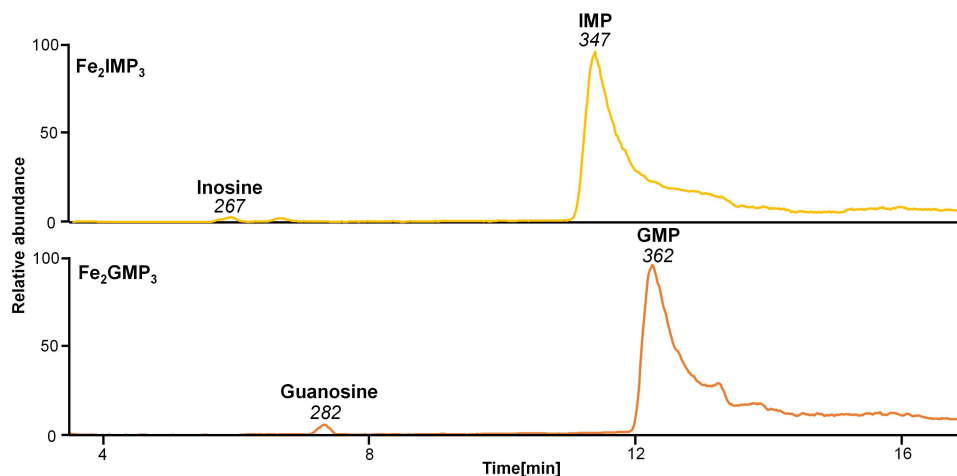
Figure S7.6 SEM images of Fe_4PP_3 , Fe_2IMP_3 , and Fe_2GMP_3 in grey and the elemental mapping performed by scanning electron microscopy energy dispersive X-ray (SEM-EDX) on Fe_4PP_3 , Fe_2IMP_3 , and Fe_2GMP_3 .

Table S7.2. Elemental composition of Fe_4PP_3 , Fe_2IMP_3 , and Fe_2GMP_3 .

Sample/Element	N (% m/m)	C (% m/m)	H (% m/m)	Fe (% m/m)	P (% m/m)
Fe_4PP_3	n.d.	n.d.	3 ± 0.1	21 ± 0.6	16 ± 0.0
Fe_2IMP_3	12 ± 0.6	25 ± 0.0	4 ± 0.1	11 ± 0.6	6 ± 0.0
Fe_2GMP_3	14 ± 0.0	24 ± 0.6	4 ± 0.2	10 ± 0.1	6 ± 0.0

Table S7.3. Comparison of analysed and calculated relative ratios of C, N, P, and Fe in Fe_4PP_3 , Fe_2IMP_3 , and Fe_2GMP_3 .

Salt	Molecular formula	Analysed elemental ratios % (calc.)			
		C	N	P	Fe
Fe_4PP_3	$\text{Fe}_4(\text{P}_2\text{O}_7)_3$	n.d.	n.d.	58 ± 0.8 (59)	42 ± 0.8 (41)
Fe_2IMP_3	$\text{Fe}_2(\text{C}_{10}\text{H}_{13}\text{N}_4\text{O}_8\text{P}_3)_3$	63 ± 0.7 (64)	25 ± 1 (26)	6 ± 0.1 (6)	6 ± 0.4 (4)
Fe_2GMP_3	$\text{Fe}_2(\text{C}_{10}\text{H}_{12}\text{N}_5\text{O}_8\text{P}_3)_3$	59 ± 0.8 (59)	30 ± 0.5 (27)	6 ± 0.1 (5)	5 ± 0.2 (4)

**Figure S7.7.** HILIC-MS base peak chromatograms (negative ionisation mode) of the Fe_2IMP_3 and Fe_2GMP_3 salt, the nucleoside and nucleotide are indicated. Peak labels show the base peak m/z value, identification of inosine, IMP, and GMP was based on commercially available standards.

CHAPTER 8

General discussion

Outline of the general discussion

Iron fortification of food is an effective solution to counter iron malnutrition but is often compromised by the reactivity of the iron ion with phenolics in the food. The main aims of this thesis were to gain insights into the chemistry of iron-phenolic interaction at the molecular level and to explore potential strategies to limit the discolouration mediated by Fe(III)-phenolic interactions.

In this chapter, the main findings of the previous chapters on the insights into the chemistry of iron-phenolic interactions ([section 8.1](#)), and strategies to limit iron-phenolic interactions ([section 8.2](#)) will be discussed and placed in perspective alongside other (unpublished) results. We also explore how our new insights into iron-phenolic interactions can be extrapolated to applications beyond fortified food ([section 8.3](#)), and provide an outlook on future opportunities for iron fortification of food ([section 8.4](#)).

8.1. Unravelling iron-phenolic interactions

This research aimed to unravel the chemistry of iron-phenolic interactions at the molecular level. In this section, we depict and discuss the main parameters and mechanism responsible for the discolouration mediated by iron-phenolic interactions. We also reflect on the analysis of the interaction products and colour.

8.1.1. Main parameters defining Fe(III)-phenolic mediated discolouration

This PhD study comprehensively maps the key factors affecting discolouration mediated by iron-phenolic interactions, an overview of which is shown in **Fig. 8.1**. This overview offers a route towards the selection of the parameters for the design of iron-fortified food products to limit discolouration mediated by iron-phenolic interactions.

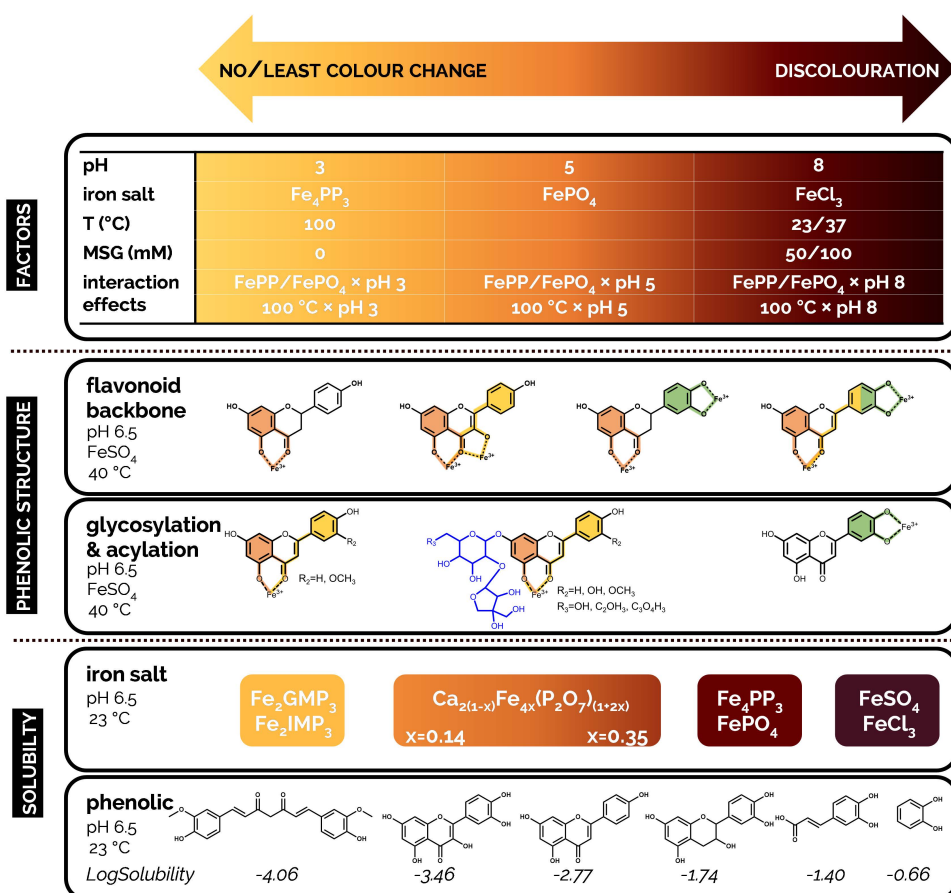


Figure 8.1. Schematic overview of the parameters affecting the discolouration mediated by Fe(III)-phenolic interactions, according to the main findings of this thesis.

In **Chapter 2** we revealed that the pH, type of iron salt, temperature, and presence of the taste enhancer MSG were the main factors that affected the discolouration of Fe(III)-catecholate systems. Additionally, the interplay of iron salt \times pH and temperature \times pH were demonstrated, amongst others, to significantly affect discolouration. In **Chapters 3** and **4**, we investigated the effect of phenolic structure on discolouration mediated by Fe(III)-phenolic interactions. The results of **Chapter 3** indicated that complexation of iron (*i.e.* Fe(II) and/or Fe(III)) to the 3–4 or 4–5 site of flavonoid aglycons instantly resulted in bathochromic shifting of the $\pi \rightarrow \pi^*$ transition band and a red-brown colour, and that complexation to the 3'–4' site induced a $\pi \rightarrow d_{\pi}$ transition band (LMCT) and resulted in a purplish appearance. The combination of $\pi \rightarrow \pi^*$ and $\pi \rightarrow d_{\pi}$ transitions resulted in intense black colour. As the majority of flavones that are present in nature and in bouillon cubes (and other savoury concentrates) are acylated and glycosylated, we also investigated the effect of the (acylated) 7-*O*-apiosylglucosyl moiety on the interaction with iron in **Chapter 4**. The 7-*O*-apiosylglucosyl moiety increased the ability of iron to coordinate to the 4–5 site, and thereby affected iron complexation. The presence of the 7-*O*-apiosylglucosyl moiety led to an increase of absorbance in the visible light region of the spectra and discolouration for flavones that possessed solely the 4–5 binding site, whereas it led to a decrease in absorbance and colour for flavones with an additional 3'–4' site. Additional substitution of the 7-*O*-apiosylglucosyl moiety by 6"-*O*-acetyl or 6"-*O*-malonyl did not affect the discolouration mediated by Fe(III)-phenolic interactions.

Two results of **Chapter 2** in particular offered opportunities for further studies: (i) the poorly water soluble ferric (pyro)phosphate salt (Fe_4PP_3 and FePO_4) showed less discolouration compared to soluble iron salt (FeCl_3); and (ii) presence of the taste enhancer MSG affected discolouration. As confirmed by (i), fortification with poorly soluble iron salts is a promising approach to limit discolouration. Nonetheless, even Fe_4PP_3 induced colour changes at the pH of interest (6.5) due to partial iron dissolution via interactions with catechol at this pH (see **section 8.2.1**), thus this approach needs further development. The second result demonstrated that the interaction between iron and taste enhancers warrants further investigation.

In **Chapters 5** and **7**, mixed Ca-Fe(III) pyrophosphate salts ($\text{Ca}_{2(1-x)}\text{Fe}_{4x}(\text{P}_2\text{O}_7)_{(1+2x)}$) and Fe(III)-nucleotide salts (Fe_2GMP_3 and Fe_2IMP_3) were synthesised, respectively. These salts exhibited decreased solubility at pH 6.5 and less discolouration with water insoluble phenolic compounds compared to Fe_4PP_3 . Compared to the Ca-Fe(III) pyrophosphate salts with the lowest *x*-value (*i.e.* 0.14), the Fe(III) nucleotide salts were even two times more insoluble at pH 6.5. However, the findings of **Chapters 6** and **7** indicated that when these insoluble salts were combined with water soluble phenolics ($\text{LogS} \geq -2$) discolouration could still be observed because the phenolics solubilised iron from the surface of the salts. To limit discolouration mediated by Fe(III)-phenolic interactions upon iron fortification, it is preferred to use low pH, a water insoluble iron salt (*e.g.* Fe_2GMP_3), and a fortification vehicle that does not contain water soluble

flavonoids (aglycons) with a 3'-4' site. The development of proof-of-concept iron-fortified bouillon cubes should be the next step to confirm these selected parameters.

8.1.2. Analysis of iron-phenolic interaction products and colour

In this research the contribution of three different iron-phenolic interaction products (*i.e.* complexation, oxidation, metal-phenolic networks) to discolouration in aqueous solutions were investigated using the approach as depicted in **Fig. 8.2**. This approach allowed us, for the first time, to unravel the combined contribution of these different interaction products.

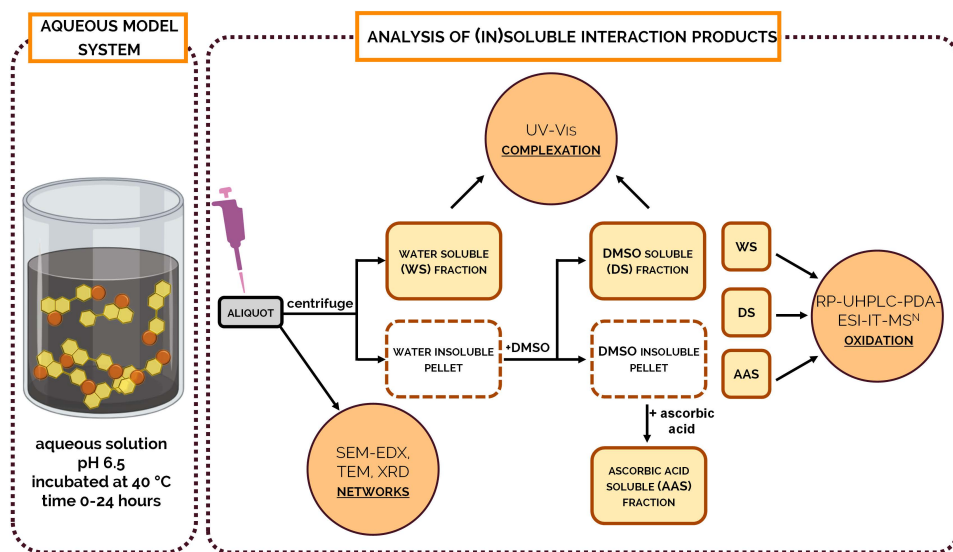


Figure 8.2. Schematic representation of the general approach that was used in this thesis to analyse iron-phenolic complexation, oxidation, formation of networks, and the resulting colour after incubation in aqueous solutions.

Incubation of iron with phenolics in aqueous model systems

The iron-phenolic interactions were studied after incubation in aqueous model systems at the approximate pH of bouillon cubes (pH 6.5). The pH was adjusted using concentrated acid (HCl) or base (NaOH) instead of buffers, to avoid interference of buffer compounds with the iron-phenolic interactions.^[1] Compared to the organic solvent solutions that were previously used in most studies on iron-phenolic interactions (**Chapter 1**), the incubation in aqueous solutions allowed for a better representation of real food systems. These aqueous model systems do not represent a real food product and the translation of the present findings to food products, and the influence of the products' matrix effects, should be confirmed. Nevertheless, our results provided direct information about how a parameter, or a set of parameters, affected the mechanism of iron-phenolic interaction and iron dissolution, as well as the colour.

Analysis of (in)soluble iron-phenolic interaction products

Water solubility varied widely between the different iron-flavonoid interaction products observed in **Chapters 3** and **4**. Therefore, we decided to separate the reaction mixture after incubation into an aqueous solution to obtain a water soluble (**WS**) fraction, and a water insoluble pellet (**Fig. 8.2**). The latter was solubilised in DMSO to obtain a DMSO soluble (**DS**) fraction. As the initial incubations were still performed in aqueous solutions, and the interaction products were immediately measured after solubilisation in DMSO we minimised the influence of organic solvent on the formation of Fe(III)-phenolic complexes and Fe(III)-mediated oxidation products. DMSO was preferred over other organic solvents because it is a solvent that is known to be suitable for metal:ligand systems.^[2-4] Despite this, it may still influence the colour of Fe(III)-phenolic complexes via solvatochromism.^[5] In **Chapters 3** and **4** we verified that this only had a very limited influence on the absorbance spectra, resulting in a maximum bathochromic shift of 30 nm in the presence of DMSO, but no change in the type of transition ($\pi \rightarrow \pi^*$ and $\pi \rightarrow d_n$) or observed colour. Furthermore, DMSO can act as a hydroxyl radical scavenger,^[6] but as incubations were done in aqueous solution in absence of DMSO this effect on oxidation is expected to be negligible.

This approach allowed us to observe that in absence of iron, all phenolics were recovered in the WS or DS fractions. In contrast, in presence of iron, a DMSO insoluble pellet was obtained, which was suggested to be due to the formation of metal-phenolic networks (MPNs). To quantify the amount of phenolic that was insoluble in DMSO after incubation with iron, we solubilised this pellet with 25 mM ascorbic acid solution to obtain an ascorbic acid soluble (**AAS**) fraction. Additional checks with concentrated HCl confirmed that lowering the pH was sufficient to disrupt the MPNs and solubilise the pellet. The remaining pellet after removal of the AAS fraction could not be analysed further and is suggested to be insoluble iron (hydr)oxides.

After fractionation of the iron-phenolic interaction products to the WS, DS, and AAS fractions, several analytical tools were used to obtain more information about the iron-phenolic interactions and their contribution to colour. Firstly, UV-Vis spectroscopy was used to get insight into the electronic transitions of phenolics in presence of Fe(III). These transitions were used to shed light on the colour and the preferred iron binding site. Secondly, intact phenolics and oxidation products were identified and (semi)quantified using RP-UHPLC-PDA-ESI-IT-MSⁿ. Unfortunately, UHPLC did not allow for the identification and quantification of iron-phenolic complexes as these dissociated during chromatographic separation. Thirdly, the nature, and morphology of MPNs was investigated by SEM-EDX, TEM, and XRD analyses of the sample. Overall, the strength of our approach is that it allows identification of iron-phenolic complexes, oxidation products, and networks after separation of the WS, DS, and AAS fractions. In this way, we were able to unravel the combined contribution of these different interaction products to the discolouration mediated by iron-phenolic interactions in aqueous solutions.

8.1.3. Flavonoid oxidation by iron revisited

In **Chapter 3** a putative pathway for Fe(III)-mediated oxidation of quercetin was proposed. This pathway did not take into consideration the different possible origins of the oxygen atom (*e.g.* H₂O or O₂), that were previously proposed for (metal-mediated) oxidation of flavonoids.^[7–10] In additional work, we further refined the oxidation mechanism we first proposed in **Chapter 3**. Herein, we investigated the origin of the oxygen atom by performing an incubation of quercetin with Fe(III) in H₂¹⁸O in presence of atmospheric oxygen (*i.e.* ¹⁶O).^[11] A more comprehensive understanding of the role of iron in the oxidation mechanism can facilitate the development of future strategies to limit Fe(III)-mediated oxidation of flavonoids. The proposed oxidation pathways, involving oxygenation and/or hydroxylation, and expected degradation products formed after incubation in H₂¹⁸O are presented in **Fig. 8.3**.

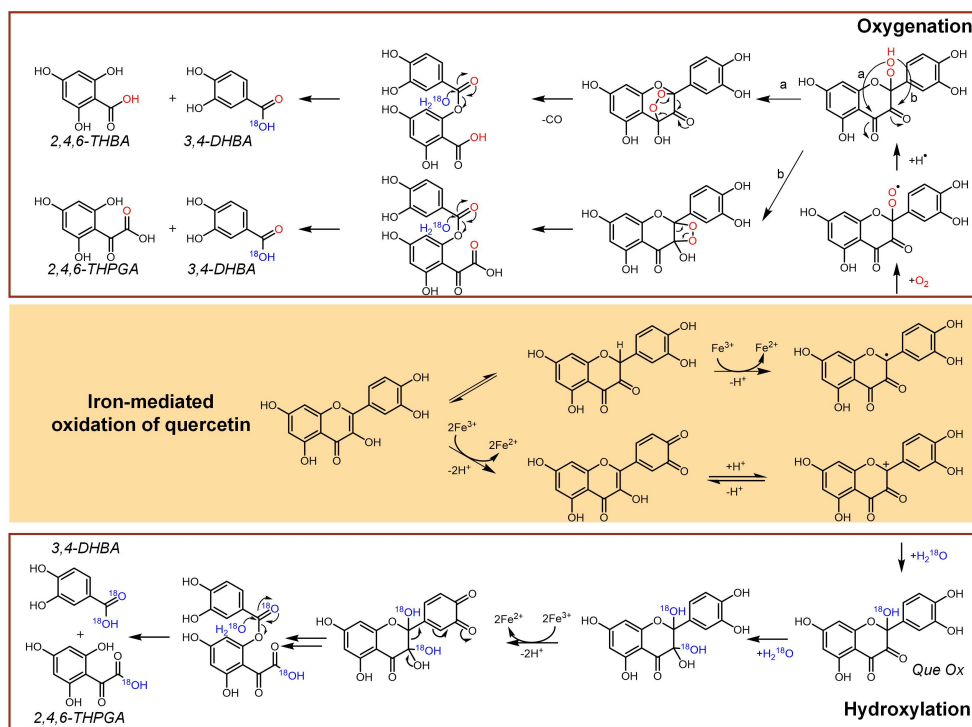


Figure 8.3. Putative pathways of Fe(III)-mediated quercetin oxidation in H₂¹⁸O labelled water, including the oxygenation reaction pathway involving incorporation of an oxygen atom from molecular oxygen and the hydroxylation reaction pathway involving incorporation of oxygen from water, adapted from Malacaria and Bijlsma *et al.*^[11]

While the two putative oxidative pathways via oxygenation or hydroxylation yield similar oxidation products (*i.e.* 3,4-DHBA, 2,4,6-THBA, and 2,4,6-THPGA) they will demonstrate a distinct ¹⁸O-labelling pattern (**Fig. 8.3**). We calculated the theoretical abundance of the ¹⁸O isotopes in 3,4-DHBA, 2,4,6-THBA, and 2,4,6-THPGA expected from the oxygenation and hydroxylation mechanism and compared these to the

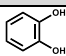
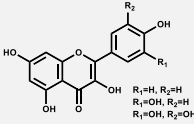
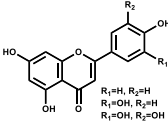
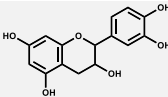
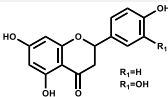
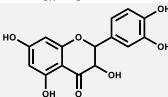
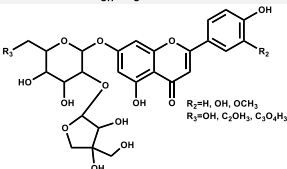
experimentally obtained abundances of these oxidation products. Based on the results of this experiment, we conclude that in presence of Fe(III) both mechanisms seem to occur simultaneously rather than exclusively. Future work should investigate the fate and rate of phenolic oxidation in presence of Fe(III) and (^{18}O) atmospheric oxygen but in absence of water.

8.1.4. Main mechanism responsible for Fe(III)-phenolic discolouration

With the integrated approach used in **Chapters 2, 3, and 4** of this thesis we have, for the first time, unravelled the combined contribution of complexation, oxidation, and the additional formation of iron-phenolic networks to the discolouration mediated by Fe(III)-phenolic interactions in food model systems. **Table 8.1** provides an overview of the contribution of these interactions on the iron-phenolic mediated discolouration for a set of structurally diverse phenolics.

For simple phenolics such as catechol, the discolouration is caused by rapidly occurring complexation (**Chapter 2**). For flavonoid aglycons, complexation was also the main contributor to discolouration (**Chapter 3**). Depending on the flavonoid's structural features, however, oxidation and the formation of networks could further affect discolouration. For flavonols, degradation of the 2-phenylchromen-4-one backbone resulted in the formation of oxidative degradation products that still produced $\pi \rightarrow d_{\pi}$ transitions but no additional $\pi \rightarrow \pi^*$ transitions and were therefore slightly lighter in colour. Although some flavonol dimers were also identified, the overall colour of the flavonols incubated with iron decreased over time. For flavanols, the formation of coloured oxidative coupling products that were also able to undergo $\pi \rightarrow d_{\pi}$ and $\pi \rightarrow \pi^*$ transitions resulted in a darker colour. Depending on the flavone, oxidative degradation and/or oxidative coupling were observed. The overall colour difference of flavones incubated with iron after 24 h did not demonstrate a positive or negative correlation with the amount of oxidation product. Additionally, it was observed that MPNs were formed for flavonoids with multiple binding sites, which produced a black precipitate. For the (acylated) flavone glycosides that are naturally present in bouillon cubes, no Fe(III)-mediated oxidation was observed after 24 h incubation (**Chapter 4**). This indicates that the discolouration of these substituted flavones in iron-fortified bouillon cubes is exclusively caused by the complexation and formation of MPNs. Nevertheless, (accelerated) shelf-life tests for a longer time (e.g. 6 months) should be performed to assess possible oxidation-mediated discolouration during storage of fortified foods.^[12] Overall, the findings of this study reveal that the main contributor to fast discolouration is complexation, which leads to rapid and intense discolouration of the solution. Simultaneously, the formation of MPNs can lead to the additional development of dark precipitates for phenolics with multiple iron binding sites, whereas oxidation is a much slower process that can lead to either a darkening or gradual loss of colour over time.

Table 8.1. Overview of the contribution of iron-phenolic complexation, oxidation, and formation of networks to discolouration based on the results of **Chapters 2, 3, and 4**. + indicates a positive correlation of the interaction and colour, – a negative correlation, ± no clear correlation, n.d. that this interaction was not detected for this phenolic and n.i. that this interaction was not investigated for this phenolic.

Type of Phenolic	Structure	Correlation with discolouration			
		Complexation	Oxidation	Iron-Phenolic Networks	
Catechol		+	n.d.	n.i.	
Flavonol	 R ₁ =H, R ₂ =H R ₁ =OH, R ₂ =H R ₁ =OH, R ₂ =OH	+	—	+	(if R ₁ = OH)
Flavone	 R ₁ =H, R ₂ =H R ₁ =OH, R ₂ =H R ₁ =OH, R ₂ =OH	+	±	+	(if R ₁ = OH)
Flavanol		+	+	n.d.	
Flavanone	 R ₁ =H R ₁ =OH	+	n.d.	n.d.	
Flavanonol		+	n.d.	+	
(Acylated) Flavone Glycosides	 R ₂ =H, OH, OCH ₃ R ₃ =OH, C ₂ H ₅ , C ₃ O ₄ H ₅	+	n.d.	+	(if R ₁ = OH) (if R ₃ = C ₃ O ₄ H ₅)

8.2. Strategies to limit iron-phenolic interactions

In **Chapters 5** and **7** of this thesis, we designed insoluble iron salts to limit iron-phenolic interactions. In the first part of this section, we discuss the reactivity of insoluble iron salts and the evaluation of iron bioavailability from these salts. In the second part, we explore the potential of sulphur-containing compounds and iron chlorophyllin as alternative approaches to limit iron-phenolic interactions.

8.2.1. Challenges of insoluble iron salts for fortification

The reactivity of water insoluble iron salts

Despite the very poor solubility of Fe₄PP₃ in water, discolouration with phenolics was still observed upon iron fortification of bouillon cubes with Fe₄PP₃.^[13-15] In **Chapters 6** and **7**, we described, for the first time, how water soluble phenolics coordinate Fe(III)

on the surface of water insoluble iron salts, thereby solubilising iron and causing discolouration of the salt surface and/or the aqueous solution. Furthermore, in agreement with our results from **Chapter 2**, brownish or blackish discolouration of fortified bouillon cubes (containing both iron and phenolics) was previously reported to be significantly increased when glutamate was present.^[16] This led us to the hypothesis that the increased discolouration in the presence of glutamate was due to the formation of soluble Fe(III)-glutamate complexes^[17] from the surface of insoluble Fe_4PP_3 , thereby making iron available to react with phenolics.

To better understand the mechanism underlying the discolouration mediated by Fe(III)-phenolic interactions in presence of glutamate, we performed an additional experiment. Here, we measured the solubility of iron from Fe_4PP_3 in the presence of catechol (1:1), an excess of glutamate (1:25) or a combination thereof (1:1:25) (**Fig. 8.4**). The molar ratios were chosen to represent the molar ratios of phenolic:iron:glutamate in fortified bouillon cubes.

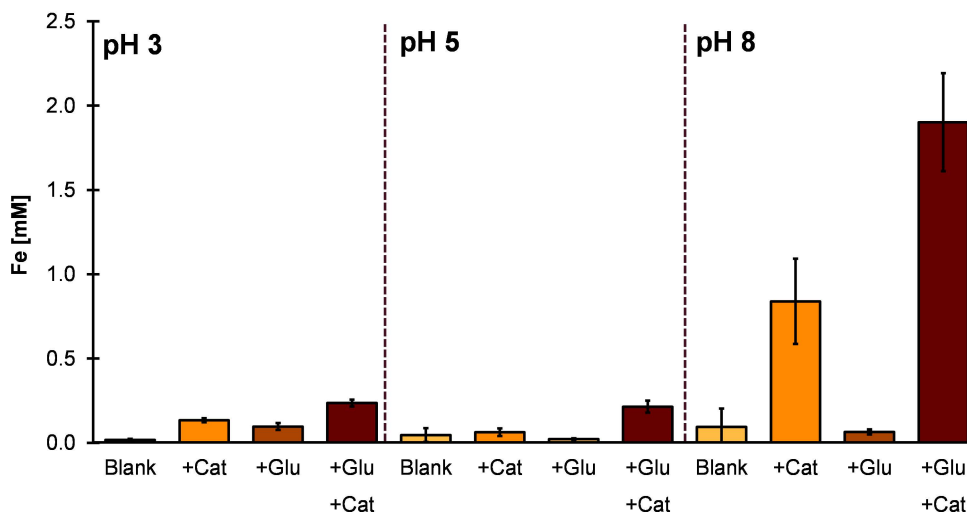


Figure 8.4. Soluble iron in aqueous dispersions of Fe_4PP_3 ($C_{\text{Fe(III)}}=10$ mM) in absence of ligand (blank), presence of catechol (+Cat), glutamate (+Glu), or a combination thereof (+Glu +Cat) ($C_{\text{Catechol}}=10$ mM, $C_{\text{Glutamate}}=250$ mM) at pH 3, 5, and 8. The pH was adjusted using concentrated HCl and NaOH. Subsequently, the aqueous solutions were incubated for 1 hour at 23 °C, centrifuged for 10 min at 5,000 *g* and finally the supernatants were 20 × diluted in nitric acid before determination of soluble iron concentration by ICP-AES.

For Fe_4PP_3 salts, the presence of catechol increased the Fe dissolution, especially at pH 8, when deprotonated catechol could solubilise Fe from the salt. Compared to the blank, the presence of glutamate alone did not increase the Fe dissolution from the insoluble salts. Interestingly, the combination of glutamate and catechol did result in an increase in the dissolution of iron at pH 3, 5, and 8 with higher iron solubility than with catechol alone. Likely this is a result of the formation of a ternary complex as identified in **Chapter 2**. The increased discolouration of Fe_4PP_3 fortified bouillon cubes

in the presence of glutamate,^[16] is thus potentially a result of dissolution of iron via the formation of ternary complexes of iron, phenolics, and glutamate (**Fig. 8.4**), whereby glutamate contributes to discolouration (**Chapter 2**).

These results indicate that even when an iron salt is water insoluble and poorly soluble in dilute (non-iron complexing) acid, its reactivity with phenolic compounds can be influenced by the presence of other ingredients in the food matrix. Recent work has investigated the addition of the complexing and solubilising agents EDTA, NaPP, and citric acid/trisodium citrate to improve the bioavailability of Fe₄PP₃.^[18-20] These solubilising agents can form soluble complexes from the insoluble salts, yet, it is important to keep in mind that the addition of these compounds to improve the bioavailability may unintentionally lead to more iron-phenolic interactions and undesired discolouration of the fortified food product.

Evaluation of iron bioavailability in water insoluble iron salts

In general, iron from water insoluble salts is considered to be less reactive but also less bioavailable (especially when the particles are large). In this thesis, we demonstrated that the newly synthesised mixed Ca-Fe(III) pyrophosphate salts (**Chapter 5**) and Fe(III)-nucleotide salts (**Chapter 7**) exhibited promising iron solubility at gastric pH. In these chapters, we linked the increased Fe solubility at gastric pH to improved bio-accessibility of these salts compared to Fe₄PP₃. Herein, iron bio-accessibility was defined as the quantity of total iron in solution at gastric pH (1-3), which is thus assumed to be available for absorption in the gastro-intestinal tract. Bio-accessibility cannot directly be correlated to iron bioavailability because the latter also includes digestion, absorption, and metabolism.^[21] Nevertheless, in previous studies, the solubility of iron at pH 1 (0.1 M HCl) was confirmed to be a good indicator for *in vivo* bioavailability.^[22-25] Our results on *in vitro* iron solubility, therefore, demonstrate the potential of the Ca-Fe(III) pyrophosphate salts and Fe(III)-nucleotide salts with improved iron solubility at acidic pH. The main pitfall of *in vitro* solubility measurements is that they can under- or overestimate iron availability because the effect of the food matrix is not taken into account. Future studies should confirm the iron bioavailability and the effect of the food matrix. The established *in vitro* Caco-2 cell model is similarly affected by the food matrices as *in vivo* studies,^[26-28] and can therefore be used to assess whether the presence of divalent metals (**Chapter 5**) or nucleotides (**Chapter 7**) is affecting the iron uptake by the DMT1 receptor prior to *in vivo* bioavailability testing.

8.2.2. Exploring (alternative) approaches to limit iron-phenolic interactions

Aside from the use of poorly soluble iron salts, the addition of reducing agents and/or competing ligands and metals were mentioned in **Chapter 1** as possible approaches to limit iron-phenolic interactions in fortified foods. Constraints of the currently used approaches to limit iron-phenolic interactions are the pH range in which they are limiting discolouration, oxidation of the reducing agents which decreases their activity,

and the high costs. In the following sections, some other alternative approaches to limit iron-phenolic interactions that were assessed in this PhD study are discussed.

Inhibition of iron-phenolic interactions by sulphur-containing compounds

As mentioned in **Chapter 1**, sulphur-containing compounds are mild reducing agents that inhibit discolouration caused by (enzymatic) oxidative coupling reactions of phenolics, and may additionally act as competing ligands for Fe(III)-phenolic complexation. One study reports prevention of Fe(III)-phenolic mediated discolouration by sodium bisulphite,^[29] which is likely due to the reducing activity of bisulphite or prevention of oxidative coupling but the exact mechanism has not specifically been investigated. Examples of sulphur-containing compounds that inhibit enzymatic oxidative coupling of phenolics are sodium bisulphite, cysteine, and glutathione.^[30]

The effect of cysteine and glutathione on iron-phenolic interactions was, to date, not reported. Additionally, methyl propyl trisulphide and diallyl sulphide are natural sulphur-containing compounds from onion and garlic that were previously reported to coordinate metals,^[31,32] and can be inherently present in bouillon cubes. In additional experiments, we tested whether these sulphur-containing compounds could inhibit iron-phenolic interactions. Fe(II) (1 mM) was incubated with flavonoids (1 mM) and sulphur-containing compounds at different pH (2-8) and different concentrations of the sulphur compound (0-100 mM). After incubation for 1 or 24 hours, the mixtures were compared visually and by UV-Vis spectroscopy. The presence of sodium bisulphite or cysteine decreased the absorbance in the visible region of the spectrum and limited the discolouration caused by iron-flavonoid interaction (**Fig. 8.5**). The other sulphur-containing compounds could not inhibit the iron-flavonoid mediated discolouration.

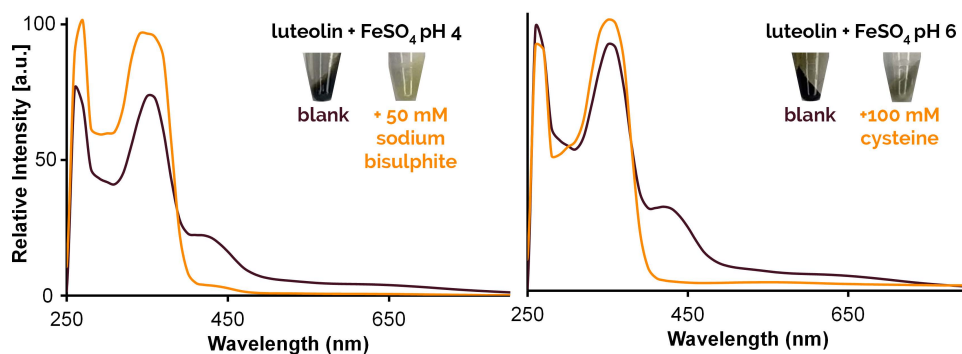


Figure 8.5. Combined absorbance spectra of the water soluble and DMSO soluble fractions of mixtures of luteolin and iron ($C_{\text{Fe(II)}}=1$ mM; $C_{\text{Luteolin}}=1$ mM) at pH 4 and 6 in the absence (brown) and presence of sulphur compound (yellow). Note that these mixtures vary in more than one parameter because they were selected from a fractional factorial design (similarly to the design used in **Chapter 2**), nonetheless they are two representative and comparable examples.

Potential mechanisms for the observed inhibition are: (i) competition of the flavonoid and sulphur-containing compound for iron binding; (ii) reduction of Fe(III) to Fe(II) by the sulphur-containing compound; and/or (iii) the formation of sulphur-flavonoid addition products, after a nucleophilic attack from a thiol group on a quinone that is formed as intermediate in phenolic oxidation, which prevents the formation of coloured coupling products and/or iron complexation.

In our samples, no sulphur-flavonoid addition products were detected by RP-UHPLC-MS, making proposed mechanism iii unlikely. Inhibition of iron-phenolic interactions only occurred at an excess of the sulphur-containing compound and $\text{pH} \leq 6$. Furthermore, inhibition primarily occurred for flavonoids that do not possess the 3'-4' site (results not shown), which is the most stable iron binding site. These observations support proposed mechanism i. However, a potential contribution of Fe(III) reduction to inhibition of complexation cannot yet be ruled out. For cysteine in presence of Fe(III), the cysteine oxidation product cystine was formed as a white precipitate. Formation of this product in the presence of iron was previously reported to be accompanied by reduction of Fe(III) to Fe(II), thus this observation supports proposed mechanism ii.^[33,34] Although cysteine may oxidise to cystine in this process, its inhibitory activity is likely not completely lost because cystine can also compete for iron binding.^[35] We conclude that addition of an excess of sodium bisulphite or cysteine could be a potential alternative approach to limit the discolouration mediated by Fe(III)-phenolic interactions via competition and reduction of Fe(III) to Fe(II).

Iron chlorophyllin: a plant-based haem alternative?

Generally, foods are fortified using non-haem iron sources, as they are cheap and readily available. The use of natural haem analogues from plant origin is an interesting alternative iron source due to its acceptance by consumers with a plant-based diet.^[36-38] Previously, chlorophyll derivatives have been explored as natural haem analogues (Fig. 8.6).^[39] These so-called iron chlorophyllin molecules are commercially available and able to deliver bioavailable iron.^[36]

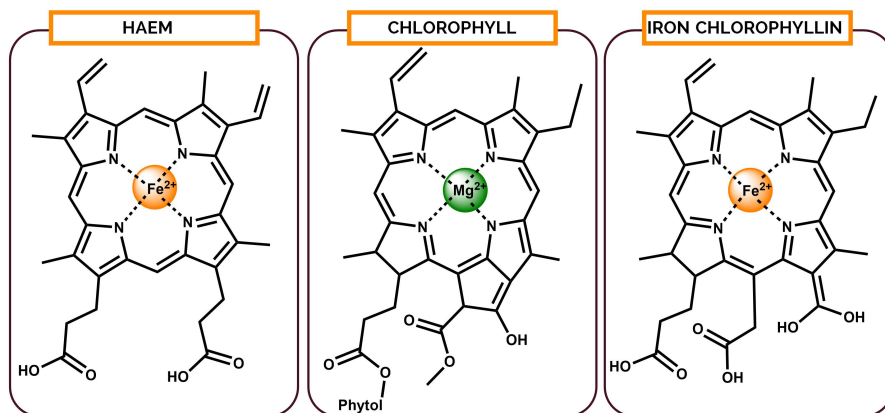


Figure 8.6. The porphyrin ring structure of haem, chlorophyll, and iron chlorophyllin.

The iron chlorophyllin compounds were hypothesised to be less reactive because iron is bound in the porphyrin ring. To date, the reactivity of these iron chlorophyllins with phenolics present in the food matrix has not yet been tested. We performed a preliminary study in which we tested the reactivity of iron chlorophyllin with model phenolics (*i.e.* quercetin, apigenin, and epicatechin) and in bouillon solutions. More oxidation of the flavonoids was observed with iron chlorophyllin compared to FeSO_4 or Fe_4PP_3 . Additionally, it resulted in an unacceptable green colour change of the bouillon solution. These findings indicated that iron chlorophyllins are not a good plant-based alternative for iron fortification of bouillon cubes. Nevertheless, other future applications of iron chlorophyllin may be of interest (**text box 8.1**).

Text box 8.1 Creating the 'real' Popeye spinach

The general consensus is that Popeye gets his strength from spinach, due to the high reported iron content of spinach. However, this is highly unlikely. In fact, spinach does not contain outstandingly high amounts of iron compared to other vegetables.^[42] With an additional experiment, in which iron chlorophyllin was added to (chopped) spinach, we observed that addition of iron chlorophyllin to spinach is a way to create the 'real' *Popeye spinach* without any adverse discolouration.

8.3. Lessons learned from iron-phenolic interactions: extrapolation to other applications

This research project aimed to explore strategies to limit iron-phenolic interactions as they lead to undesirable colour changes in iron-fortified foods. In other cases, purposefully inducing controlled interactions of phenolics with iron, or other metals, may be beneficial for various applications. In this section, we explore how our knowledge of iron-phenolic interactions could be applied to frontiers in science.

8.3.1. Therapeutic agents

Metal complexes of flavonoids and curcuminoids have been explored as a novel class of therapeutic agents.^[41-45] Due to their unique structural characteristics, metal-phenolic complexes may exhibit antioxidant, antimicrobial, antitumor, anticancer, anti-inflammatory, and antidiabetic activities.^[46-49] Our results on the factors that affect Fe(III) -phenolic complexation (**Chapter 2**), phenolic oxidative stability (**Chapter 3**), and water solubility of the interaction products (**Chapters 3 and 4**) give direction to future work on the use of complexes as therapeutic agents.

Potential of flavonoids for metal chelation therapy

Chelation therapy is the preferred treatment to reduce the accumulation of (toxic) metals in the body and the resulting metal intoxication.^[50] Flavonoids are promising natural chelators,^[51] however, to be used for chelation therapy it should first be investigated whether they form thermodynamically stable complexes that are

resistant to transformations (*i.e.* hydrolysis, reduction, and oxidation), water soluble, and are excreted from the body as such.^[49,52-54] To this end, we performed an additional experimental study, which revealed that the flavonoids quercetin and luteolin can form stable chelates in aqueous solutions at physiological pH (*i.e.* pH 7.4) with a set of first-row transition metal cations.^[11] Luteolin showed to be a more suitable chelating agent than quercetin due to its higher oxidative stability. Based on the outcomes of **Chapter 3**, we suggest further investigation of eriodictyol and taxifolin for metal chelation therapy, as they form stable complexes, undergo limited metal-mediated oxidation, and demonstrate improved water solubility compared to luteolin.

8.3.2. Natural colouring agents

Fe(III)-phenolic complexes have been used as natural dyes and pigments since ancient times. Until the beginning of the 20th century, dark black iron gall inks, that contained Fe(III)-phenolic complexes, were used for hand-written documents and painting sketches.^[55,56] The disadvantages of these inks are that their black colour fades due to hydrolysis and oxidation reactions, and that the inks degrade the paper.^[57,58] The results presented in this thesis constitute an improved understanding of the factors that affect Fe(III)-phenolic complexation and oxidation, its analysis, and its effect on colour. Thus, our results could be useful for characterisation of iron gall complexes and improvement of the conservation of these inks. Additionally, the colour of yellow or orange metal-flavonoid dyes can fade in time due to oxidation reactions.^[59] The outcomes of **Chapter 3** indicated that the use of flavonoids without the C2–C3 double bond, the catechol moiety, and the 4-carbonyl or 3-hydroxyl group results in improved oxidative stability of the metal complexes. Thus, to improve the oxidative stability of these dyes, it is recommended to incorporate flavonoids that meet these requirements.

8.3.3. Iron mobilisation in plants

Iron is also an essential micronutrient for plants, but its bioavailability is limited as a result of the poor solubility of iron (hydr)oxides in (alkaline) soils.^[60,61] Coumarins (1-benzopyran-2-one), another class of phenolics, have been recently demonstrated to be important molecules for iron uptake in plants by mobilisation of iron due to complexation of the coumarin with iron.^[62] Especially the coumarins that contain a catecholate moiety were able to mobilise iron.^[61,62] Upon complexation, the coumarins can be oxidised by Fe(III).^[63] Our integrated approach to analyse iron-phenolic complexation, oxidation, and formation of networks in aqueous solutions (**section 8.1.2**), allows for an in-depth analysis of iron-coumarin interactions and the coumarin oxidation products that are relevant for iron mobilisation in plants.

8.3.4. Isotopic labelling of catecholates

Upon the elucidation of the Fe(III) mediated oxidation of quercetin in H₂¹⁸O (**section 8.1.3**), we observed unexpected rapid ¹⁶O/¹⁸O exchange on the catecholic hydroxyl groups. This exchange occurred at mild conditions (37 °C, neutral or slightly acidic pH)

and in absence of Fe(III) no exchange was observed. We have, in an additional study, further investigated this isotopic exchange under mild conditions and found near-to-complete (> 90 %) ^{18}O labelling for some catecholates in presence of Fe(III) within 30 min.^[64] A proposed mechanism for catalysis of this $^{16}\text{O}/^{18}\text{O}$ exchange via Fe(III)-catechol complex formation is depicted in **Fig. 8.7**.

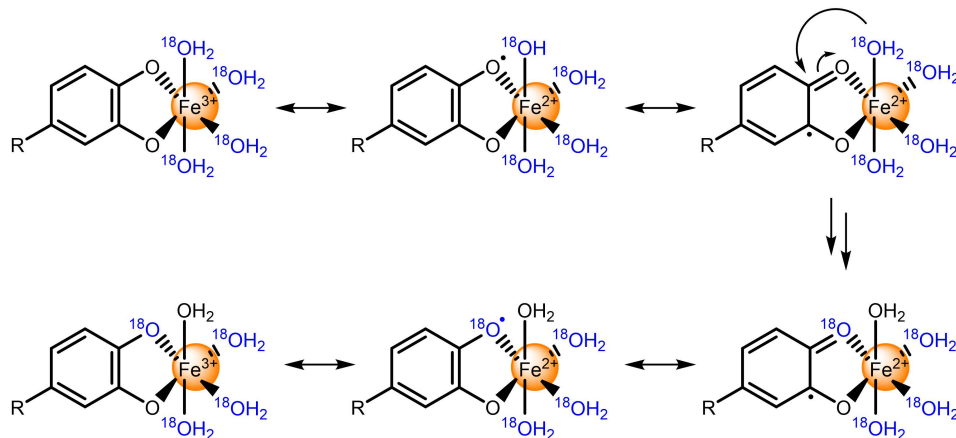


Figure 8.7. Proposed mechanism for Fe(III) catalysed $^{16}\text{O}/^{18}\text{O}$ exchange of catechol motifs, from Hilgers, Bijlsma *et al.*^[64] The H_2^{18}O attacking the catecholato ligand may also originate from the bulk. Examples of valence tautomerism as a mechanism underlying catalysis in Fe-catechol complexes have been reported in earlier research.^[65]

These isotopically labelled compounds can be used in many fields of chemistry^[66–73] and to follow the metabolic fate of biologically active compounds in human or animal studies.^[74,75] Fe(III)-phenolic complexation can catalyse the $^{16}\text{O}/^{18}\text{O}$ exchange of catechol motifs with H_2^{18}O under mild conditions and provides a new route for the facile production of ^{18}O -labelled catechol derivatives.

8.3.5. Extrapolation to other metals

Although this research focussed on the interaction of phenolics with iron, some of the present findings on the complexation, oxidation, and discolouration can be extrapolated to other first-row transition metals, including zinc as a 3d-block metal. All of these metals are hard or borderline Lewis acids and form stable complexes with phenolics.^[76,77] The oxidation rate of phenolics by these first-row transition metals depends on the metals' redox activity and the ability for electron transfer with the ligand. Iron, copper, cobalt, and manganese are known to exhibit rich redox chemistry, whereas zinc is not redox-active due to the completely filled d-orbitals.^[78] In terms of complexation and oxidation the charge of the metal cation is an important characteristic. In another study, we investigated the interaction of flavonoids with transition metals and demonstrated that trivalent transition metal cations formed complexes at lower pH with more oxidation products compared to divalent transition metals.^[111] Although most first-row transition metals, except for zinc, form coloured

complexes with phenolics, the colour of Fe(III) complexes is the most intense.^[11,79] The outcomes of our additional study indicate that the fortification of phenolic-rich food with other important dietary minerals, such as zinc, will likely be less challenging, in terms of discolouration, than iron fortification.

8.4. Designing iron-fortified foods

8.4.1. Translating iron-phenolic model systems to bouillon cubes

The outcomes of this study can be used to answer some fundamental questions of the food industry to improve the design of iron-fortified products. First of all, the outcomes of **Chapter 5** indicated that (acylated) flavone glycosides, derived from celery and parsley, are present in bouillon cubes and interact with iron to form coloured interaction products. The quantities of flavone glycosides in celery and parsley may differ depending on their origin and time of purchase.^[80-82] One approach that could be explored to limit iron-phenolic discolouration is to screen raw materials for flavone content during sourcing. Selecting raw ingredients with low flavone glycoside, especially luteolin glycoside, content could limit discolouration in the final product.

The discolouration caused by (acylated) flavone glycosides (**Chapter 4**) was not as intense as for the flavonoid aglycons (**Chapter 3**). Possibly, the flavone glycosides may not be the only phenolics causing iron-mediated discolouration in bouillons. Besides the flavone glycosides, bouillon cubes also contain phenolic acids and curcuminoids. The phenolic acids that were present in bouillon (*i.e.* primarily *p*-coumaric acid derivatives) are not expected to lead to intense discolouration as they lack an *ortho*-diphenol moiety that can serve as an iron chelation site. Coordination of Fe(III) to the β -diketone moiety of curcumin was previously reported to result in a dark-coloured complex.^[42,83] Thus, it was hypothesised that the discolouration observed in fortified bouillons was additionally caused by complexation of iron with curcuminoids.

Complementing the outcomes of **Chapter 5** we performed an additional experiment in which we compared the colour of solutions of iron with (acylated) flavone glycosides or curcumin (**Fig. 8.8**). This confirmed that iron-curcumin interactions indeed cause more intense absorbance in the visible range of the spectra and a darker colour compared to the flavone glycosides at the same molar concentrations. In future work, the interactions (*e.g.* complexation, oxidation, formation of networks) of iron with curcumin and the mixed phenolic bouillon extract have to be explored.

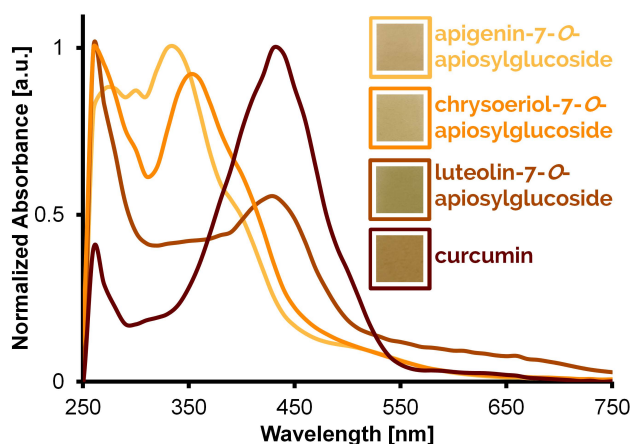


Figure 8.8. Normalised UV-Vis absorbance spectra of the combined WS and DS spectra of flavone glycosides and curcumin at pH 6.5 ($C_{Fe}=1$ mM; $C_{Ligand}=1$ mM).

Curcuminoids in bouillon cubes are derived from turmeric, which is added as one of the main spices and as a natural yellow-orange colourant. We suggest exploring whether the replacement of curcuminoids by carotenoids as orange colourants (*i.e.* β -carotene or zeaxanthin) results in less discolouration, while maintaining a similar flavour. These carotenoids do not contain a phenolate moiety or a diketone moiety and are therefore not expected to form coloured complexes with Fe(III). Nevertheless, β -carotene can be oxidised in presence of iron, which may result in the formation of off-flavours.^[84-86]

8.4.2. Design guidelines for iron-fortified foods

The knowledge that is generated in this thesis regarding the factors that affect the colour of iron-fortified foods can also be extrapolated to other types of food vehicles beyond bouillon cubes. The most effective strategy to prevent iron-phenolic interactions and discolouration of fortified foods depends on the phenolic compounds and other ingredients that are present in the food matrix. Thus, solutions should be tailored to the specific food product selected as an iron fortification vehicle to effectively limit iron-phenolic interactions and discolouration. **Fig. 8.9** depicts design guidelines based on the outcomes of this thesis that can help direct the choice of the most suitable iron salt and optimal conditions to limit discolouration mediated by Fe(III)-phenolic interactions.

In our research, all phenolics with a bidentate binding site demonstrated discolouration upon iron complexation. Some food phenolics (*e.g.* ferulic acid, *p*-coumaric acid) coordinate to iron in a monodentate fashion and do not result in the fast complexation mediated discolouration.^[29] However, monodentate coordination can be followed by electron transfer reactions, leading to formation of larger oxidative

coupling products that may contribute to discolouration.^[87] Therefore, interaction of these phenolic compounds with iron should also be prevented to limit discolouration.

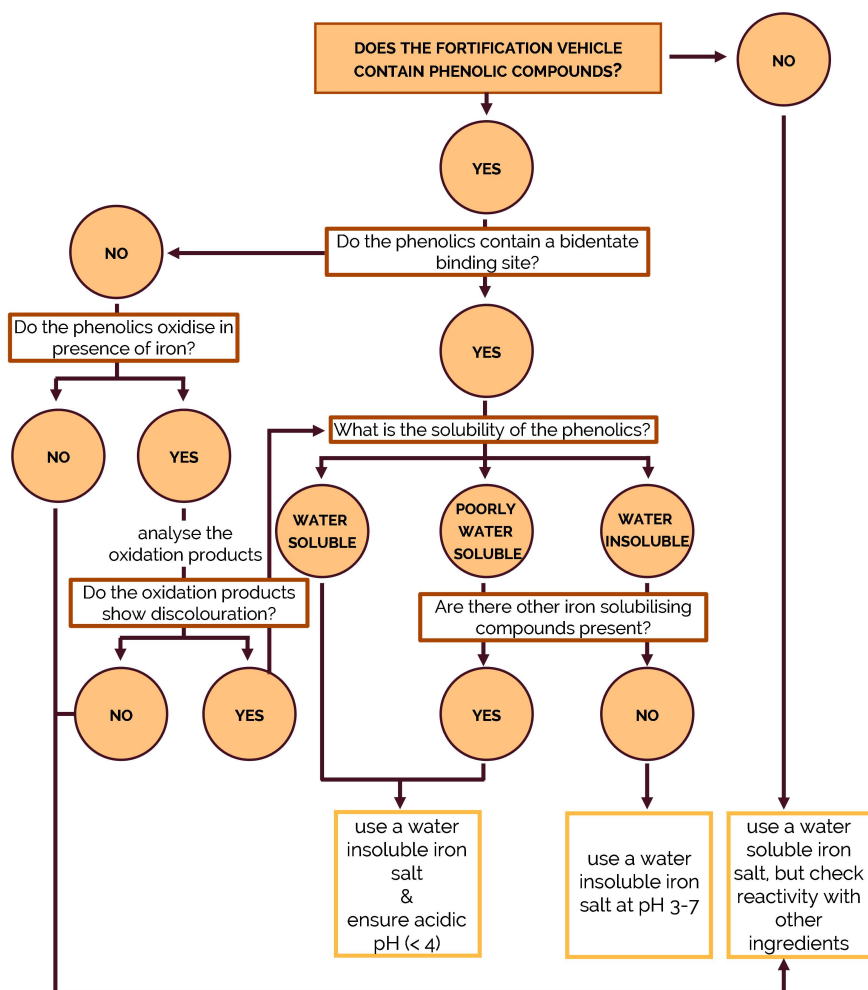


Figure 8.9. Design guidelines for iron fortification of foods to ensure limited discolouration mediated by Fe(III)-phenolic interactions, based on the outcomes of this thesis.

These design guidelines have to be confirmed in suitable fortification vehicles and are especially suitable for (semi-)solid foods as for liquid products (e.g. tea) care should be taken that the water insoluble iron salt remains suspended in the solution. To design iron-fortified bouillon cubes that contain slightly water soluble phenolics (e.g. apiin $\log S$ -2.5) and insoluble phenolics (e.g. curcumin $\log S$ -4.06) that contain a bidentate binding site, it is recommended to use a water insoluble salt at pH 3-7. To ensure iron bio-accessibility and limit reactivity we recommend using an iron salt with increased dissolution at gastric pH but very poor water solubility at food pH (e.g. Ca-Fe(III) pyrophosphate or Fe(III)-nucleotide salts).

8.4.3. Future outlook on product development of iron-fortified foods

As fortification of food with iron is technologically more difficult than fortification with other micronutrients, it is important to carefully follow iron fortification recommendations. Following these recommendations and the design guidelines as depicted in **section 8.3.2** facilitates design of a product with an acceptable colour and good iron bioavailability. In a recent study by Hurrell,^[88] a typical development procedure was laid out for fortified food products. In **textbox 8.2** we provide a short overview of this framework. With the work of **Chapter 5, 6, and 7 (part 2)** of this thesis we covered step two of the product development framework. Future investigation should focus on the next steps, starting with an investigation of the relative bioavailability of the iron compounds (*i.e.* Ca-Fe(III) pyrophosphate and Fe(III)-nucleotides) that were developed in this study.

Text box 8.2. Steps in the product development of iron-fortified foods, based on Hurrell^[81]

1. Select food fortification vehicle
2. Select the iron fortification compound
3. Test the compound for relative bioavailability
4. Multimeal stable isotope study
5. Ensuring stability of ascorbic acid
6. Nutrient retention studies
7. Sensory studies
8. Consumer acceptability
9. Long-term, well-controlled, efficacy studies
10. Noncontrolled effectiveness studies

8.5. Closing remarks & highlights

The current thesis set out to understand the chemistry of iron-phenolic interactions and the resulting discolouration, and to explore strategies to limit the discolouration of fortified food mediated by Fe(III)-phenolic interactions. The outcomes of this thesis shed light on the effect of intrinsic and extrinsic factors, as well as the structural features of flavonoids, and on the discolouration mediated by Fe(III)-phenolic interactions. We confirmed that the main contributor to fast discolouration in aqueous solutions is the complexation of Fe(III) to phenolics, simultaneously the formation of MPNs can lead to dark precipitates for phenolics with multiple iron binding sites, whereas oxidation can slowly lead to a darkening or gradual loss of colour over longer time. The newly developed Ca-Fe(III) pyrophosphate and Fe(III)-nucleotide salts demonstrate interesting pH-dependent dissolution behaviour, with decreased reactivity at food pH and increased dissolution at gastric pH compared to Fe(III) pyrophosphate. Food products comprising these salts have the potential to contribute to countering the global problem of iron deficiency.

8.6. References

- 1 Ferreira, C. M., Pinto, I. S., Soares, E. V., & Soares, H. M. (2015). (Un)suitability of the use of pH buffers in biological, biochemical and environmental studies and their interaction with metal ions—a review. *RSC Advances*, 5(39), 30989–31003.
- 2 EL-Sherif, A. A., Shoukry, M. M., & Abd-Elgawad, M. M. A. (2013). Protonation equilibria of some selected α -amino acids in DMSO–water mixture and their Cu(II)-complexes. *Journal of Solution Chemistry*, 42(2), 412–427.
- 3 Enyedy, É. A., Primik, M. F., Kowol, C. R., Arion, V. B., Kiss, T., & Keppler, B. K. (2011). Interaction of triapine and related thiosemicarbazones with iron (III)/II and gallium (III): a comparative solution equilibrium study. *Dalton Transactions*, 40(22), 5895–5905.
- 4 Enyedy, É. A., May, N. V., Pape, V. F., Heffeter, P., Szakács, G., Keppler, B. K., & Kowol, C. R. (2020). Complex formation and cytotoxicity of triapine derivatives: A comparative solution study on the effect of the chalcogen atom and NH-methylation. *Dalton Transactions*, 49(46), 16887–16902.
- 5 Reichardt, C., & Welton, T. (2011). *Solvents and solvent effects in organic chemistry*. New York: John Wiley & Sons.
- 6 Napolitano, A., Pezzella, A., & Prota, G. (1999). New reaction pathways of dopamine under oxidative stress conditions: Nonenzymatic iron-assisted conversion to norepinephrine and the neurotoxins 6-hydroxydopamine and 6,7-dihydroxytetrahydroisoquinoline. *Chemical Research in Toxicology*, 12(11), 1090–1097.
- 7 Photiades, A., Grigorakis, S., & Makris, D. P. (2020). Kinetics and modeling of L-cysteine effect on the Cu(II)-induced oxidation of quercetin. *Chemical Engineering Communications*, 207(2), 139–152.
- 8 Osman, A., & Makris, D. P. (2010). Comparison of fisetin and quercetin oxidation with a cell-free extract of onion trimmings and peel, plant waste, containing peroxidase enzyme: A further insight into flavonol degradation mechanism. *International Journal of Food Science & Technology*, 45(11), 2265–2271.
- 9 Zenkevich, I. G., Eshchenko, A. Y., Makarova, S. V., Vitenberg, A. G., Dobryakov, Y. G., & Utsal, V. A. (2007). Identification of the products of oxidation of quercetin by air oxygen at ambient temperature. *Molecules* 12(3), 654–672.
- 10 Brown, S., Rajananda, V., Holroyd, J., & Evans, E. (1982). A study of the mechanism of quercetin oxygenation by ^{18}O labelling. A comparison of the mechanism with that of haem degradation. *Biochemical Journal*, 205(1), 239.
- 11 Malacaria, L., Bijlsma, J., Hilgers, R., de Bruijn, W. J. C., Vincken, J.-P., & Furia, E. (2023). Insights into the complexation and oxidation of quercetin and luteolin in aqueous solutions in presence of selected metal cations. *Journal of Molecular Liquids*, 369, 120840.
- 12 Klassen-Wigger, P., Geraets, M., Messier, M. C., Detzel, P., Lenoble, H. P., Barclay, D. V., Mannar, M. G. V., & Hurrell, R. F. (2018). Micronutrient fortification of bouillon cubes in Central and West Africa. In M. G. V. Mannar & R. F. Hurrell (Eds.), *Food fortification in a globalized world*, (pp. 363–372): Elsevier.
- 13 Allen, L. H., De Benoist, B., Dary, O., & Hurrell, R. (2006). Guidelines on food fortification with micronutrients. World Health Organization.
- 14 Dueik, V., Chen, B. K., & Diosady, L. L. (2017). Iron-polyphenol interaction reduces iron bioavailability in fortified tea: Competing complexation to ensure iron bioavailability. *Journal of Food Quality*, 2017, 1–8.
- 15 Hurrell, R. F., Lynch, S., Bothwell, T., Cori, H., Glahn, R., Hertrampf, E., Kratky, Z., Miller, D., Rodenstein, M., Streekstra, H., Teucher, B., Turner, E., Yeung, C. K., & Zimmermann, M. B. (2004). Enhancing the absorption of fortification iron. *International Journal for Vitamin and Nutrition Research*, 74(6), 387–401.
- 16 Jansen, F. J. H. M., & Velikov, K. P. (2014). Fortified savoury food concentrate. *European Patent Office*, EP2774497B1(13157731.4).
- 17 Djurdjević, P., & Jelić, R. (1997). Solution equilibria in L-glutamic acid and L-serine+ iron(III) systems. *Transition Metal Chemistry*, 22(3), 284–293.
- 18 Scheuchzer, P., Syryamina, V. N., Zimmerman, M. B., Zeder, C., Nyström, L., Yulikov, M., & Moretti, D. (2023). Ferric pyrophosphate forms soluble iron coordination complexes with zinc compounds and solubilizing agents in extruded rice and predicts increased iron solubility and bioavailability in young women. *The Journal of Nutrition*, 153(3), 636–644.
- 19 Hackl, L., Cercamondi, C. I., Zeder, C., Wild, D., Adelman, H., Zimmermann, M. B., & Moretti, D. (2016). Cofortification of ferric pyrophosphate and citric acid/trisodium citrate into extruded rice grains doubles iron bioavailability through in situ generation of soluble ferric pyrophosphate citrate complexes. *The American Journal of Clinical Nutrition*, 103(5), 1252–1259.
- 20 Cercamondi, C. I., Duchateau, G. S., Harika, R. K., van den Berg, R., Murray, P., Koppenol, W. P., Zeder, C., Zimmermann, M. B., & Moretti, D. (2016). Sodium pyrophosphate enhances iron bioavailability from bouillon cubes fortified with ferric pyrophosphate. *British Journal of Nutrition*, 116(3), 496–503.
- 21 Wienk, K., Marx, J., & Beynen, A. (1999). The concept of iron bioavailability and its assessment. *European Journal of Nutrition*, 38(2), 51–75.
- 22 Björn-Rasmussen, E., Hallberg, L., & Rossander, L. (1977). Absorption of 'fortification' iron: Bioavailability in man of different samples of reduced Fe, and prediction of the effects of Fe fortification. *British Journal of Nutrition*, 37(3), 375–388.

- 23 Swain, J. H., Newman, S. M., & Hunt, J. R. (2003). Bioavailability of elemental iron powders to rats is less than bakery-grade ferrous sulfate and predicted by iron solubility and particle surface area. *The Journal of Nutrition*, 133(11), 3546-3552.
- 24 Lynch, Bothwell, & Campbell, L. (2007). A comparison of physical properties, screening procedures and a human efficacy trial for predicting the bioavailability of commercial elemental iron powders used for food fortification. *International Journal for Vitamin and Nutrition Research*, 77(2), 107-124.
- 25 Rohner, F., Ernst, F. O., Arnold, M., Hilbe, M., Biebinger, R., Ehrensperger, F., Pratsinis, S. E., Langhans, W., Hurrell, R. F., & Zimmermann, M. B. (2007). Synthesis, characterization, and bioavailability in rats of ferric phosphate nanoparticles. *The Journal of Nutrition*, 137(3), 614-619.
- 26 Glahn, R. P., Lee, O. A., Yeung, A., Goldman, M. I., & Miller, D. D. (1998). Caco-2 cell ferritin formation predicts nonradiolabeled food iron availability in an in vitro digestion/Caco-2 cell culture model. *The Journal of Nutrition*, 128(9), 1555-1561.
- 27 Glahn, R. (2009). The use of Caco-2 cells in defining nutrient bioavailability: Application to iron bioavailability of foods. In D. J. McClements & E. A. Decker (Eds.), *Designing functional foods*. (pp. 340-361): Woodhead Publishing.
- 28 Pynaert, I., Armah, C., Fairweather-Tait, S., Kolsteren, P., van Camp, J., & Henauw, S. D. (2006). Iron solubility compared with in vitro digestion-Caco-2 cell culture method for the assessment of iron bioavailability in a processed and unprocessed complementary food for Tanzanian infants (6-12 months). *British Journal of Nutrition*, 95(4), 721-726.
- 29 Mellican, R. I., Li, J., Mehansho, H., & Nielsen, S. S. (2003). The role of iron and the factors affecting off-color development of polyphenols. *Journal of Agricultural and Food Chemistry*, 51(8), 2304-2316.
- 30 Kuijpers, T. F., Narváez-Cuenca, C.-E., Vincken, J.-P., Verloop, A. J., van Berkel, W. J., & Gruppen, H. (2012). Inhibition of enzymatic browning of chlorogenic acid by sulfur-containing compounds. *Journal of Agricultural and Food Chemistry*, 60(13), 3507-3514.
- 31 Kamyabi, M. A., Soleymani-Bonoti, F., & Zakavi, S. (2016). Voltammetric determination of stability constants of lead complexes with diallyl disulfide, dimethyl disulfide, and diallyl sulfide. *Chinese Chemical Letters*, 27(1), 71-76.
- 32 Osipova, V., Polovinkina, M., Gracheva, Y., Shpakovsky, D., Osipova, A., & Berberova, N. (2021). Antioxidant activity of some organosulfur compounds in vitro. *Arabian Journal of Chemistry*, 14(4), 103068.
- 33 Jameson, G. N. L. (2011). Iron, cysteine and parkinson's disease. *Monatshefte für Chemie - Chemical Monthly*, 142(4), 325-329.
- 34 McAuliffe, C., & Murray, S. (1972). Metal complexes of sulphur-containing amino acids. *Inorganica Chimica Acta Reviews*, 6, 103-121.
- 35 Furia, E., & Sindona, G. (2010). Complexation of L-cystine with metal cations. *Journal of Chemical & Engineering Data*, 55(9), 2985-2989.
- 36 Miret, S., Tascioglu, S., van der Burg, M., Frenken, L., & Klaffke, W. (2010). In vitro bioavailability of iron from the heme analogue sodium iron chlorophyllin. *Journal of Agricultural and Food Chemistry*, 58(2), 1327-1332.
- 37 Zhong, S., Bird, A., & Kopec, R. E. (2021). The metabolism and potential bioactivity of chlorophyll and metallo-chlorophyll derivatives in the gastrointestinal tract. *Molecular Nutrition & Food Research*, 65(7), 2000761.
- 38 Shayeghi, M., Latunde-Dada, G. O., Oakhill, J. S., Laftah, A. H., Takeuchi, K., Halliday, N., Khan, Y., Warley, A., McCann, F. E., & Hider, R. C. (2005). Identification of an intestinal heme transporter. *Cell*, 122(5), 789-801.
- 39 Nelson, R., & Ferruzzi, M. (2008). Synthesis and bioaccessibility of Fe-pheophytin derivatives from crude spinach extract. *Journal of Food Science*, 73(5), H86-H91.
- 40 USDA. (2021). Fooddata central. Retrieved from: <https://fdc.nal.usda.gov/index.html> Accessed 19/04/2023.
- 41 Selvaraj, S., Krishnaswamy, S., Devashya, V., Sethuraman, S., & Krishnan, U. M. (2014). Flavonoid-metal ion complexes: A novel class of therapeutic agents. *Medicinal Research Reviews*, 34(4), 677-702.
- 42 Hieu, T. Q., & Thao, D. T. T. (2019). Enhancing the solubility of curcumin metal complexes and investigating some of their biological activities. *Journal of Chemistry*, 2019, 8082195.
- 43 Khater, M., Ravishankar, D., Greco, F., & Osborn, H. M. (2019). Metal complexes of flavonoids: Their synthesis, characterization and enhanced antioxidant and anticancer activities. *Future Medicinal Chemistry*, 11(21), 2845-2867.
- 44 Bravo, A., & Anaconda, J. R. (2001). Metal complexes of the flavonoid quercetin: Antibacterial properties. *Transition Metal Chemistry*, 26(1), 20-23.
- 45 Wanninger, S., Lorenz, V., Subhan, A., & Edelmann, F. T. (2015). Metal complexes of curcumin-synthetic strategies, structures and medicinal applications. *Chemical Society Reviews*, 44(15), 4986-5002.
- 46 Malešev, D., & Kuntić, V. (2007). Investigation of metal-flavonoid chelates and the determination of flavonoids via metal-flavonoid complexing reactions. *Journal of the Serbian Chemical Society*, 72(10), 921-939.
- 47 Pereira, R. M., Andrades, N. E., Paulino, N., Sawaya, A. C., Eberlin, M. N., Marcucci, M. C., Favero, G. M., Novak, E. M., & Bydlowski, S. P. (2007). Synthesis and characterization of a metal complex containing naringin and Cu, and its antioxidant, antimicrobial, antiinflammatory and tumor cell cytotoxicity. *Molecules*, 12(7), 1352-1366.

- 48 Cazarolli, L. H., Zanatta, L., Jorge, A. P., de Sousa, E., Horst, H., Woehl, V. M., Pizzolatti, M. G., Szpoganicz, B., & Silva, F. R. M. B. (2006). Follow-up studies on glycosylated flavonoids and their complexes with vanadium: Their anti-hyperglycemic potential role in diabetes. *Chemico-Biological Interactions*, 163(3), 177-191.
- 49 Meng-zhen, S., Ju, L., Lan-chun, Z., Cai-feng, D., Shu-da, Y., Hao-fei, Y., & Wei-yan, H. (2022). Potential therapeutic use of plant flavonoids in AD and PD. *Heliyon*, 8(11), e11440.
- 50 Flora, S. J. S., & Pachauri, V. (2010). Chelation in metal intoxication. *International Journal of Environmental Research and Public Health*, 7(7), 2745-2788.
- 51 Wang, X., Li, Y., Han, L., Li, J., Liu, C., & Sun, C. (2021). Role of flavonoids in the treatment of iron overload. *Frontiers in Cell and Developmental Biology*, 9, 685364.
- 52 Malacaria, L., Corrente, G. A., Beneduci, A., Furia, E., Marino, T., & Mazzone, G. (2021). A review on coordination properties of Al(III) and Fe(III) toward natural antioxidant molecules: Experimental and theoretical insights. *Molecules*, 26(9), 2603.
- 53 Corrente, G. A., Malacaria, L., Beneduci, A., Furia, E., Marino, T., & Mazzone, G. (2021). Experimental and theoretical study on the coordination properties of quercetin towards aluminum(III), iron(III) and copper(II) in aqueous solution. *Journal of Molecular Liquids*, 325, 115171.
- 54 Malacaria, L., La Torre, C., Furia, E., Fazio, A., Caroleo, M. C., Cione, E., Gallelli, L., Marino, T., & Plastina, P. (2022). Aluminum(III), iron(III) and copper(II) complexes of luteolin: Stability, antioxidant, and anti-inflammatory properties. *Journal of Molecular Liquids*, 345, 117895.
- 55 Teixeira, N., Nabais, P., de Freitas, V., Lopes, J. A., & Melo, M. J. (2021). In-depth phenolic characterization of iron gall inks by deconstructing representative iberian recipes. *Scientific Reports*, 11(1), 8811.
- 56 Espina, A., Cañamares, M. V., Jurašeková, Z., & Sanchez-Cortes, S. (2022). Analysis of iron complexes of tannic acid and other related polyphenols as revealed by spectroscopic techniques: Implications in the identification and characterization of iron gall inks in historical manuscripts. *ACS Omega*, 7(32), 27937-27949.
- 57 Kolar, J., Stolf, A., Strlič, M., Pompe, M., Pihlar, B., Budnar, M., Simčič, J., & Reissland, B. (2006). Historical iron gall ink containing documents — properties affecting their condition. *Analytica Chimica Acta*, 555(1), 167-174.
- 58 Rouchon, V., & Bernard, S. (2015). Mapping iron gall ink penetration within paper fibres using scanning transmission X-ray microscopy. *Journal of Analytical Atomic Spectrometry*, 30(3), 635-641.
- 59 Kasprzak, M. M., Erxleben, A., & Ochocki, J. (2015). Properties and applications of flavonoid metal complexes. *RSC Advances*, 5(57), 45853-45877.
- 60 Lindsay, W. L. (1979). *Chemical equilibria in soils* (Vol. 28) John Wiley and Sons Ltd.
- 61 Connorton, J. M., Balk, J., & Rodríguez-Celma, J. (2017). Iron homeostasis in plants—a brief overview. *Metallomics*, 9(7), 813-823.
- 62 Stringlis, I. A., De Jonge, R., & Pieterse, C. M. (2019). The age of coumarins in plant-microbe interactions. *Plant and Cell Physiology*, 60(7), 1405-1419.
- 63 Baune, M., Kang, K., Schenkeveld, W. D. C., Kraemer, S. M., Hayen, H., & Weber, G. (2020). Importance of oxidation products in coumarin-mediated Fe(hydroxide) mineral dissolution. *Biometals*, 33(6), 305-321.
- 64 Hilgers, R., Bijlsma, J., Malacaria, L., Vincken, J.-P., Furia, E., & de Bruijn, W. J. C. (2022). Transition metal cations catalyze $^{16}\text{O}/^{18}\text{O}$ exchange of catechol motifs with H_2^{18}O . *Organic & Biomolecular Chemistry*, 20(46), 9093-9097.
- 65 Shaikh, N., Goswami, S., Panja, A., Wang, X.-Y., Gao, S., Butcher, R. J., & Banerjee, P. (2004). New route to the mixed valence semiquinone-catecholate based mononuclear Fe^{III} and catecholate based dinuclear Mn^{III} complexes: First experimental evidence of valence tautomerism in an iron complex. *Inorganic Chemistry*, 43(19), 5908-5918.
- 66 Jašíková, L., Anania, M., Hybelbauerová, S., & Roithová, J. (2015). Reaction intermediates kinetics in solution investigated by electrospray ionization mass spectrometry: Diaurated complexes. *Journal of the American Chemical Society*, 137(42), 13647-13657.
- 67 Hilgers, R., Yong Teng, S., Briš, A., Pereverzev, A. Y., White, P., Jansen, J. J., & Roithová, J. (2022). Monitoring reaction intermediates to predict enantioselectivity using mass spectrometry. *Angewandte Chemie International Edition*, 61(36), e202205720.
- 68 Liuni, P., Olkhov-Mitsel, E., Orellana, A., & Wilson, D. J. (2013). Measuring kinetic isotope effects in enzyme reactions using time-resolved electrospray mass spectrometry. *Analytical Chemistry*, 85(7), 3758-3764.
- 69 Singleton, D. A., & Thomas, A. A. (1995). High-precision simultaneous determination of multiple small kinetic isotope effects at natural abundance. *Journal of the American Chemical Society*, 117(36), 9357-9358.
- 70 Hilgers, R., van Dam, A., Zuilhof, H., Vincken, J.-P., & Kabel, M. A. (2020). Controlling the competition: Boosting laccase/HBT-catalyzed cleavage of a β -O-4' linked lignin model. *ACS Catalysis*, 10(15), 8650-8659.
- 71 Arsene, C. G., Ohlendorf, R., Burkitt, W., Pritchard, C., Henrion, A., O'Connor, G., Bunk, D. M., & Güttler, B. (2008). Protein quantification by isotope dilution mass spectrometry of proteolytic fragments: Cleavage rate and accuracy. *Analytical Chemistry*, 80(11), 4154-4160.
- 72 Tretyakova, N., Goggin, M., Sangaraju, D., & Janis, G. (2012). Quantitation of DNA adducts by stable isotope dilution mass spectrometry. *Chemical Research in Toxicology*, 25(10), 2007-2035.

- 73 Villanueva, J., Carrascal, M., & Abian, J. (2014). Isotope dilution mass spectrometry for absolute quantification in proteomics: Concepts and strategies. *Journal of Proteomics*, 96, 184-199.
- 74 Neinast, M. D., Jang, C., Hui, S., Murashige, D. S., Chu, Q., Morscher, R. J., Li, X., Zhan, L., White, E., Anthony, T. G., Rabinowitz, J. D., & Arany, Z. (2019). Quantitative analysis of the whole-body metabolic fate of branched-chain amino acids. *Cell Metabolism*, 29(2), 417-429.e414.
- 75 Kluger, B., Bueschl, C., Neumann, N., Stücker, R., Doppler, M., Chassy, A. W., Waterhouse, A. L., Rechthaler, J., Kampleitner, N., Thallinger, G. G., Adam, G., Krska, R., & Schuhmacher, R. (2014). Untargeted profiling of tracer-derived metabolites using stable isotopic labeling and fast polarity-switching LC-ESI-HRMS. *Analytical Chemistry*, 86(23), 11533-11537.
- 76 Pearson, R. G. (1963). Hard and soft acids and bases. *Journal of the American Chemical Society*, 85(22), 3533-3539.
- 77 Atkins, P. W., Overton, T. I., Rourke, J. P., Weller, M. T., & Armstrong, F. A. (2014). d-Metal complexes: Electronic structure and properties. In D. Shriver, M. Weller, T. Overton, J. Rourke & F. Armstrong (Eds.), *Inorganic chemistry 6th edition*. New York, NY: W.H. Freeman and Company.
- 78 Crans, D. C., & Kostenkova, K. (2020). Open questions on the biological roles of first-row transition metals. *Communications Chemistry*, 3(1), 104.
- 79 Guo, J., Ping, Y., Ejima, H., Alt, K., Meissner, M., Richardson, J. J., Yan, Y., Peter, K., Von Elverfeldt, D., & Hagemeyer, C. E. (2014). Engineering multifunctional capsules through the assembly of metal-phenolic networks. *Angewandte Chemie International Edition*, 53(22), 5546-5551.
- 80 Sakakibara, H., Honda, Y., Nakagawa, S., Ashida, H., & Kanazawa, K. (2003). Simultaneous determination of all polyphenols in vegetables, fruits, and teas. *Journal of Agricultural and Food Chemistry*, 51(3), 571-581.
- 81 Justesen, U., Knuthsen, P., & Leth, T. (1998). Quantitative analysis of flavonols, flavones, and flavanones in fruits, vegetables and beverages by high-performance liquid chromatography with photo-diode array and mass spectrometric detection. *Journal of Chromatography A*, 799(1), 101-110.
- 82 Haytowitz, D. B., Wu, X., & Bhagwat, S. (2018). USDA database for the flavonoid content of selected foods, release 3.3. *US Department of Agriculture*, 173.
- 83 Gordon, O. N., Luis, P. B., Sintim, H. O., & Schneider, C. (2015). Unraveling curcumin degradation autoxidation proceeds through spiroepoxide and vinyl ether intermediates en route to the main bicyclopentadione. *Journal of Biological Chemistry*, 290(8), 4817-4828.
- 84 Stutz, H., Bresgen, N., & Eckl, P. M. (2015). Analytical tools for the analysis of β -carotene and its degradation products. *Free Radical Research*, 49(5), 650-680.
- 85 Roland, W. S. U., Pouvreau, L., Curran, J., van de Velde, F., & de Kok, P. M. T. (2017). Flavor aspects of pulse ingredients. *Cereal Chemistry*, 94(1), 58-65.
- 86 Falconer, M. E., Fishwick, M. J., Land, D. G., & Sayer, E. R. (1964). Carotene oxidation and off-flavour development in dehydrated carrot. *Journal of the Science of Food and Agriculture*, 15(12), 897-901.
- 87 Vuillemin, M. E., Michaux, F., Adam, A. A., Linder, M., Muniglia, L., & Jasniewski, J. (2020). Physicochemical characterizations of gum arabic modified with oxidation products of ferulic acid. *Food Hydrocolloids*, 107, 105919.
- 88 Hurrell, R. F. (2021). Iron fortification practices and implications for iron addition to salt. *The Journal of Nutrition*, 151, 3S-14S.

Summary

Fortification of food (e.g. bouillon cubes) with iron is an effective solution to counter the global health problem of iron deficiency but is often compromised by the reactivity of iron with phenolics (e.g. flavonoids) that are naturally present in foods. Iron-phenolic interactions can result in unwanted discolouration of the fortified food product and can impair iron bioavailability. However, systematic knowledge of iron-phenolic chemistry and the main factors that influence iron-phenolic interactions and the resulting discolouration is lacking. Furthermore, current strategies to limit iron reactivity in fortified foods are not yet sufficiently effective at preventing discolouration and typically involve the use of insoluble iron compounds that are also less bioavailable. This thesis aims to create insights into the chemistry of iron-phenolic interactions at the molecular level and to explore strategies to limit iron-phenolic mediated discolouration.

In **Chapter 1**, we delineated the rationale behind this research project. We explained why food fortification is a good solution to treat iron deficiency and what challenges can be encountered upon iron fortification of foods. The underlying chemistry of iron, phenolics, and iron-phenolic interactions was discussed. Building on this information, we described how these interactions can induce colour changes in food. Moreover, we summarised commonly used methods to analyse iron-phenolic interactions. Most of the iron-phenolic complexes of interest have been studied in organic solvents, whereas water is the preferred solvent because we are interested in iron-phenolic complexes in food products. Lastly, the limitations of existing strategies to inhibit iron-phenolic mediated discolouration in fortified foods were discussed.

Part I of this work comprehensively mapped the effect of pH, temperature, salt strength, type of iron salt, and the phenolic structure on complexation, oxidation, and discolouration.

In **Chapter 2**, we studied the interplay between several factors (e.g. iron salt, pH, temperature, ionic strength, concentration iron, iron:catechol ratio, and presence of monosodium glutamate (MSG)) on discolouration caused by iron-catechol complexation. To this end, a three-level fractional factorial design was implemented, and UV-Vis spectrophotometry was used to measure colour formation. We analysed the absorbance spectra using statistical methods and revealed that the main factors affecting discolouration were the type of iron salt, pH, and temperature. Additionally, several two-way interactions significantly affected iron-catechol complexation. We also observed black precipitation in several aqueous samples, depending on intrinsic and extrinsic factors. These results indicated that further research on the parallel occurrence of iron-phenolic complexation, oxidation, and formation of networks was required.

Thus, in **Chapter 3**, we created an integrated approach to analyse iron-flavonoid complexation, oxidation, and formation of metal-phenolic networks (MPNs) in aqueous solutions at food pH (i.e. 6.5). Samples were taken over time and fractionated

to water soluble, DMSO soluble, and ascorbic soluble fractions that were measured by spectrophotometric, mass spectrometric, and microscopic techniques. This allowed us, for the first time, to unravel the combined contribution of three different iron-flavonoid interactions (*i.e.* complexation, oxidation, and the formation of networks) to discolouration. We observed that iron complexation to the 3–4 or 4–5 site instantly resulted in bathochromic shifting of the $\pi \rightarrow \pi^*$ transition bands, and complexation to the 3'-4' site (*i.e.* B-ring catechol moiety) induced a $\pi \rightarrow d_\pi$ (LMCT) transition band. Simultaneously, the formation of MPNs led to dark precipitates for the flavonoids with multiple iron binding sites. Oxidation on the other hand occurred more slowly over time with oxidative coupling leading to a darkening of colour, whereas oxidative degradation led to a loss of colour. Our work indicated that the presence of the C2–C3 double bond in combination with the catechol moiety and either the 4-carbonyl or 3-hydroxyl group increased the intensity of discolouration, the extent of flavonoid oxidation, and the formation of MPNs. The work described in this chapter provides insights into the reactivity of iron with flavonoid aglycons. However, in nature and in bouillon cubes, most flavonoids are glycosylated. Thus further research was required to investigate the effect of flavonoid glycosylation on their interaction with iron.

In **Chapter 4**, we purified nine differentially (acylated) flavone glycosides that are present in bouillon cubes. We comprehensively investigated the effect of (acylated) 7-*O*-apiosylglucosyl substitution on the interaction with iron. Our work revealed that the presence of the 7-*O*-apiosylglucosyl moiety increased the ability of iron to coordinate to the 4–5 site, and thereby affected iron-flavone complexation. As a result, increased discolouration was observed for flavones possessing solely the 4–5 binding site, whereas decreased discolouration was observed for flavones with an additional 3'-4' site. Additional 6''-*O*-acylation did not affect the colour.

Overall, the outcomes of **Part I** of this thesis contributed to a more systematic understanding of the main factors affecting iron-phenolic interactions. With the integrated approach used here, we demonstrated that rapid complexation was the main contributor to fast and intense discolouration in solution. Simultaneously, the formation of MPNs led to the additional development of dark precipitates for phenolics with multiple iron binding sites, whereas oxidation was a much slower process that led to either a darkening or gradual loss of colour over time.

Part II of this thesis aimed to find solutions to limit iron-phenolic mediated discolouration. The use of water insoluble or very poorly soluble iron salts such as Fe(III) pyrophosphate (Fe_4PP_3) is one of the current approaches to deliver iron. Despite the very poor solubility of Fe_4PP_3 resulting in limited reactivity, it still causes discolouration in fortified bouillons. Moreover, its poor solubility also leads to reduced iron bio-accessibility. When using poorly soluble iron salts, it is challenging to ensure sufficient iron bio-accessibility while limiting the iron-phenolic interactions to an acceptable level. Ideally, these salts should have limited dissolution at food pH (*i.e.* 3–7), to limit iron-phenolic reactivity leading to sensorial changes in food, and fast

dissolution at gastric pH (*i.e.* 1-3), to ensure iron bio-accessibility. To achieve this we synthesised different insoluble iron salts, where iron was integrated into an (in)organic matrix to reduce its reactivity, and characterised their pH-dependent dissolution, as well as their reactivity with phenolics.

In **Chapter 5**, we reported the design and synthesis of, nature-inspired, mixed Ca-Fe(III) pyrophosphate salts with tuneable pH-dependent dissolution. The salts with the general formula $\text{Ca}_{2(1-x)}\text{Fe}_x(\text{P}_2\text{O}_7)_{(1+2x)}$ and $0 \leq x \leq 1$ were synthesised by a co-precipitation method and characterised by TEM(-EDX), XRD, and FT-IR. It was confirmed that iron in these salts, with $0.14 \leq x \leq 0.35$, was homogeneously distributed and that the salts had an amorphous nature. Iron dissolution from these mixed salts was increased four-fold at gastric pH (1-3) and decreased eight-fold at food pH (3-7) compared to Fe_4PP_3 . By changing the x -value, the dissolution behaviour of iron could be tuned. These findings indicated that mixed Ca-Fe(III) pyrophosphate salts are potentially more bioavailable due to increased iron dissolution at gastric pH and less reactive due to decreased iron dissolution at food pH.

In **Chapter 6**, we aimed to provide insights into the reactivity of these mixed Ca-Fe(III) pyrophosphate salts with structurally diverse phenolics. Iron-phenolic complexation, oxidation, and surface interactions of Fe_4PP_3 and $\text{Ca}_{2(1-x)}\text{Fe}_x(\text{P}_2\text{O}_7)_{(1+2x)}$ with $x = 0.14, 0.15, 0.18$, and 0.35 were studied. We confirmed that at $\text{pH} > 5$, water soluble phenolics coordinated iron on the salt surface and thereby solubilised iron, which resulted in discolouration. However, for the mixed salts with $x \leq 0.18$ the colour changes remained acceptable in the presence of slightly water soluble and insoluble phenolics similarly to those that are commonly present in bouillon cubes. Additionally, phenolic oxidation was significantly reduced in the presence of the mixed salts compared to Fe_4PP_3 .

In **Chapter 7**, we investigated the interaction of Fe(III) with three different taste enhancers (*i.e.* MSG, inosine monophosphate (IMP), and guanosine monophosphate (GMP)). We demonstrated that complexes of the nucleotides IMP and GMP with Fe(III) are more stable compared to Fe(III)-MSG complexes, but also precipitated at pH 3-8 due to charge neutrality. This latter property was exploited to synthesise Fe(III) salts of IMP or GMP (*i.e.* Fe_2IMP_3 and Fe_2GMP_3) using an aqueous precipitation method. The resulting salts demonstrated promising iron dissolution behaviour, as they were even more soluble at gastric pH and less soluble at food pH than the mixed Ca-Fe(III) pyrophosphate salts. The solubility of Fe_2IMP_3 and Fe_2GMP_3 salts was up to twenty-fold increased at gastric pH (1-3) and fifteen-fold decreased at food pH (3-7) compared to Fe_4PP_3 . Additionally, the presence of Fe_2IMP_3 and Fe_2GMP_3 led to less discolouration in the presence of poorly soluble phenolics.

The newly developed Ca-Fe(III) pyrophosphate with $x \leq 0.18$ and Fe(III)-nucleotide salts possessed the desired pH-dependent dissolution behaviour for food fortification with decreased reactivity at food pH and increased dissolution at gastric pH compared to Fe(III) pyrophosphate, thus they can potentially serve as iron fortificants for food.

In **Chapter 8**, the main findings presented in this thesis were discussed and placed in perspective alongside other (unpublished) results. We discuss the main parameters affecting Fe(III)-phenolic mediated discolouration, the main mechanism responsible for discolouration, and the integrated approach that we developed and used in this thesis for the analysis of iron-phenolic interactions in aqueous model systems. Additionally, we discuss various strategies to limit iron-phenolic interactions, including those described in **part II** of this thesis. The challenges associated with using insoluble iron salts for fortification are addressed and alternative or complementary approaches to limit discolouration are described. We explore how our new insights into iron-phenolic interactions can be extrapolated to applications beyond fortified food. Lastly, we provide an outlook on future opportunities for iron fortification of food and present design guidelines for the iron fortification of foods based on the outcomes of this thesis. These guidelines can direct the choice of the most suitable iron salt and optimal conditions to limit discolouration mediated by Fe(III)-phenolic interactions. For the design of iron-fortified bouillon cubes that contain slightly water soluble and insoluble phenolics, we recommend to use an iron salt with increased dissolution at gastric pH but very poor water solubility at food pH (e.g. Ca-Fe(III) pyrophosphate or Fe(III)-nucleotide salts) and ensure pH 3-7 in the food.

Acknowledgements

En toen was het tijd om het allerlaatste, en meest gelezen, hoofdstuk van mijn boekje te schrijven. En misschien daarom wel een van de moeilijkste. Ondanks dat het hele proces van een PhD soms eenzaam kan zijn mag ik van geluk spreken met alle mensen om mij heen en voor de begeleiding, samenwerking, het luisterende oor, de tolerantie en de afleiding. Ik wil iedereen bedanken die hieraan een bijdrage heeft geleverd!

Allereerst wil ik mijn (co-)promotoren bedanken voor de supervisie de afgelopen jaren en de vrijheid en het vertrouwen dat jullie mij in mijn onderzoek hebben gegeven! **Jean-Paul**, bedankt dat je mij aan de andere kant van de wereld wist te overtuigen om een PhD onderzoek te starten bij FCH. Ik waardeer je betrokkenheid zowel binnen mijn project als ook op persoonlijk gebied. Jouw positieve instelling en creatieve denkwijze op vraagstukken, resultaten, en figuren hebben erg geholpen binnen mijn onderzoek en je stond altijd klaar voor nieuwe 'gekleurde' ideeën. Wanneer ik ergens mee zat had je dit altijd snel door, en bood je een luisterend oor om mij vervolgens weer op de juiste manier te enthousiasmeren en motiveren om verder op onderzoek uit te gaan. **Wouter**, ik had al het voorrecht gehad om als MSc student mijn afstudeeronderzoek bij jou te mogen doen, en toen jij na een jaar betrokken raakte bij mijn PhD onderzoek als co-promotor was ik daar dan ook erg blij mee. Bedankt dat je altijd benaderbaar was en bent voor mijn vragen en er tijdens onze meetings ook altijd nog ruimte was voor de nodige dosis humor. Jouw betrokkenheid bij mijn onderzoek, enthousiasme voor de wetenschap, analytische kennis en scherpe blik op resultaten en mijn (lange) teksten zijn van groot belang geweest voor het werk in dit boekje. Bedankt dat je mij af en toe ook wist af te remmen en af te leiden. **Krassi**, thank you for initiating the IronTech project and for sharing your broad knowledge and passion about chemistry, food formulation, industry, innovation, and especially about iron! Meetings with you always helped me to see things from a new perspective for which I am very grateful.

I would like to thank all collaborators from the **IronTech** consortium. Dear **Neshat**, thank you for being my iron-partner in crime!! You have been a big support during my PhD and I am very grateful for our collaboration on the mixed calcium-iron salts and of course for all the talk/gossip/complaints about the difficulties with iron, the PhD, or life in general. I am very happy with the friendship that grew out of our collaboration and to have you by my side as my paranymphe! **Willem**, bedankt voor de samenwerking op de gemengde zouten en de positieve e-mails die altijd in mijn inbox verschenen na het indienen van documenten voor de clearance. Thank you **Arjen**, **Alexey**, **Noushine**, **Daniel**, and **Simon** for your input during our project meetings and for performing the elemental analysis.

I am also very grateful to our other collaborators! Bedankt **Jos** en **Peter** voor jullie hulp met de statistische opzet en analyses en data interpretatie van het werk in

hoofdstuk 2. Nagyön szépen köszönöm to **Péter** for hosting me in Debrecen and thank you for providing me with insights on coordination chemistry and the analytical methodology. Köszönöm to **Etelka, Orsi** and the rest of the people from the Department of Inorganic and Analytical Chemistry for the warm welcome. Grazie mille to **Luana** and **Emilia** from the University of Calabria for broadening my horizon and letting me step away from iron for once!

Roelant, bedankt voor al je chemische kennis die je met mij hebt willen delen! Of het nu ging over errors met berekeningen, het uittekenen van reactie mechanismes, de MS, of wat extra experimenten die konden worden uitgevoerd om nieuw inzicht te creëren, jij stond altijd open om te helpen en mee te denken, zo nu en dan onder het genot van een biertje. Super dat dit ook nog heeft geresulteerd in twee gemeenschappelijke publicaties! **Bianca** bedankt voor de gezelligheid en goede gesprekken bij LFOTMs & wandelingen, sorry voor de rondslingerende papieren met chemische reacties en mijn kieskeurige dieren...

Elsemieke, Rosanne, Margot, Aafke, Cas, Jamie, Milan, Romy, David, and **Vinay**, you have all contributed in your own way to the work presented in this thesis and my development. Thank you for the hard work and fresh energy you brought, I enjoyed supervising you for your BSc and MSc thesis projects!

Jolanda, dankjewel voor alles wat je voor FCH doet, en alles wat je de afgelopen jaren voor mij hebt gedaan! Wat was het fijn om altijd even bij jou binnen te kunnen lopen voor praatje, roddel, gezelligheid, snoep, stickers, data, etc. Ik hoop dat je mij het kapot gooien van de snoeppot en de adrenaline kick rond het boeken van de datum voor mijn verdediging zult vergeven.

Ik wil graag alle **FCH technicians** bedanken voor het draaiende houden van de labs en de analytische apparatuur. **René**, dankjewel voor de geordendheid in ons lab en het bestellen van de chemicaliën. **Mark**, dankjewel voor het delen van jouw kennis op het gebied van LC-MS analyses en preparatieve chromatografie! **Edwin**, dankjewel voor je hulp met de direct injection van de metaal complexen op de Synapt! **Margaret**, bedankt voor de discussies over de BZV poll ;-). **Giovanni** bedankt voor de hulp met de pH-Stat en **Peter** bedankt voor de prettige samenwerking bij het AMG practicum. Also many thanks to all other FCH staff!

To all my lab mates of X0222: **René, Carolina, Gijs, Maud, Madelon, Abel, Cas, Thore**, and **Adrian** thank you for creating the nice lab atmosphere! Even though we were all working on different topics and we often had visitors in our lab we always managed to be the cleanest lab! Thanks to my **office mates** for providing such a comfortable office environment. **Carolina** thank you for being my office mate for such a long time and for sharing all your ins and outs about the PhD and for all the good talks. You are an amazing scientist, and I am sure they are very happy to have you in Switzerland!



Also a big thanks to you for finally breaking the office curse!! **Abel** jouw komst naar ons kantoor zorgde voor veel levendigheid, groen, positiviteit en dragibus. Bedankt voor je blijdschap, goede gesprekken, en dat je mij hebt leren delegeren (en sorry daarvoor!). **Pim** and **Nan** thank you for letting me experience some Thai and Chinese foods! To all the **phyto(activities)**: thank you for sharing your phyto knowledge and for all the helpful input in my research! **Eva** and **Maud** talking with you in the lab, office, or on the corridor always brought a smile to my face! I hope I can once join the two of you and your veggies and animals on your plan B. I am also very happy that I had the opportunity to engage in some other tasks at FCH far away from iron or phenolics. **Wouter, Roelant, Gijs, Eva, Annemiek, Anne, & Jan Willem** it was great to organise the FCH activities with all of you. Thanks for all the laughter during the preparation of our first conference on degradation analysis, recording sounds for the pubquiz, or with pipette pooping and parafilm pulling. **Sarah, Katharina, Gijs, Jianli, and Lorenz** organising the PhD trip together with you was a great experience for me! We were unlucky that due to Covid our plans to South Korea were cancelled but luckily we could enjoy the North of the Netherlands all together - er gaat niets boven...! Thanks to everyone else at **FCH** for all the coffee breaks, lunches, LFOTMs, TTTs, activities, winterwalks, WeDay, and VeluweLoop, and for creating such a nice work atmosphere.

Lieve **Sarah**, we hebben heel wat meegemaakt bij FCH de afgelopen jaren, een MSc scriptie, AMG, het wijn- en bierproeven, LC-MS injecties (volgende keer toch maar niet de cone karamelliseren), en het gezamenlijke begeleiden van een student! Bedankt voor al je analytische input, input over figuren, de gezellige gesprekken, het luisterend oor, de 4daagse feesten, en de Bob-talk! Dankjewel dat je mijn paranymphtje wilt zijn!

Lieve **Annemiek**, bedankt voor al je hulp met de NMR, van het aanzetten van de machine tot het uitleggen van de spectra. Sorry dat je door mijn metalen bijna op de zwarte lijst kwam! De bezoeken aan CHAINS & ICP en Lowlands waren samen met jou een groot feest. Het was fijn dat we altijd even samen jouw project partner konden sponsoren! Bedankt dat je mijn paranymphtje wilt zijn!

Óók buiten FCH hebben vele mensen mij de afgelopen jaren gesteund met een luisterend oor en de nodige afleiding. Lieve **Lappers** bedankt voor alle etentjes, feestjes, en logeerpartijen die ook na onze studententijd doorgingen! Lieve **Tien**, ik ben dankbaar dat ik zo'n pittige moid ben tegengekomen toen we in Wageningen gingen studeren, bedankt voor je interesse en betrokkenheid! Lieve **Fien** bedankt voor onze fijne tijd in Uut, voor je blijdschap, en dat je me leert reflecteren! Aan mijn medelappers **As** en **Frans** fijn dat jullie mij altijd zo goed begrepen en bedankt voor de tips en PhD talk. Lieve **Chaoten**, bedankt voor de ontspanning in de vorm van de wijntjes, weekendjes weg, en op avontuur in Montenegro, Israël en Jordanië! Ik ben heel blij met jullie vriendschap, gezelligheid & humor! Lieve **Veronie**, bedankt voor je luisterend oor, blijdschap & knuffels en je tips voor dit boekje, zelfs in tijden van cats & dogs. Lieve **Charlotte**, bedankt voor de lunchwandelingen over de campus &

bucketlist activiteiten! Lieve **Sjaps++**, de met muziek gevulde avondjes en Lowlands weekenden waren altijd een welkome reset knop om er daarna weer volop tegen aan te kunnen. Lieve **Floor**, ik ben blij dat we vanaf ons 7^e levensjaar al zoveel samen hebben mogen beleven, en nu heb je ook nog de cover voor mijn thesis geschilderd! Zonder jou had dit proefschrift toch wat minder kleur gehad, bedankt!! **WHoffers**, een PhD schrijven in de polder was zeker niet zo gezellig geweest zonder Ria, de BZV avondjes, schuurfeesten, en jullie mooie werk!

Lieve **de Jong's** dankjewel voor de gezelligheid en (letterlijke) warmte die ik in jullie familie mag ontvangen, hoe druk jullie ook zijn, er is altijd ruimte voor gezelligheid en de nodige humor. **Nico en Margriet** bedankt voor alle maaltijden, ijs, ijsvitjes, en zorg de afgelopen vier jaar. Ik heb veel respect voor jullie flexibiliteit en bedrijvigheid op de zorgboerderij! **Lotte, Klaas, Judi, Arjan, Toon, Cato** en **Fiene** bedankt voor de gezelligheid, lekkere baksels, meters bier, en plantverzorging!

Lieve **Alja & Marlou**, ik ben dankbaar dat ik jullie mijn zussen mag noemen! Lieve **Lou** na onze studie in Wageningen zijn we beiden een andere richting ingeslagen, maar gelukkig weten we elkaar nog altijd goed te vinden als we advies nodig hebben, moeten ventileren, of een rondje willen rennen of fietsen. Lieve **La**, ik vind het erg leuk dat jij ook aan het avontuur van een PhD bent begonnen en dat ik af en toe mijn grote zus van insider-PhD advies of Excel tips mag voorzien. **Jorge** muchas gracias for your interest and for always making sure that there was enough good coffee in the Netherlands to fuel the writing of this thesis. **Gijs** bedankt voor je betrokkenheid, interesse en het delen van handige IT-tips! **Jente** mag blij zijn met jou en La! Lieve **pake**, bijzonder om deze mijlpaal te mogen delen! Lieve **papa** en **mama** bedankt voor jullie onvoorwaardelijke support en liefde. Ik ben blij dat jullie mij van jongs af aan de vrijheid hebben gegeven om mijn eigen pad te kiezen, nieuwsgierig te zijn, op onderzoek uit te gaan, en mijn eigen fouten te maken. Jullie noordelijke nuchterheid met de uitspraken zoals *'as it net kin sa't it moat, dan moat it mar sa't it kin'* heeft mij op vele vlakken sterker in mijn schoenen laten staan, en maken het leven een stukje gemakkelijker. De ontspannen weekenden in het hoge Noorden en gezamenlijke wintersport- en wandelvakanties met familie doen me altijd weer veel goed.

Lieve **Pip**, onze gezamenlijke rondjes door het bos en vele knuffels hebben zeker positief bijgedragen aan mijn gemoedsrust en gezondheid tijdens het schrijven van deze thesis! Lieve **Joep**, ook voor jou zit het er nu op! Ik hoop dat het een beetje vol te houden was om samen te zijn met een PhD'er de afgelopen paar jaar. Bedankt voor je steun, liefde, en geduld! Thuis is altijd een blijde plek voor mij geweest, en ondanks dat het werk in en rondom de boerderij nooit klaar is heb jij toch - meestal - de gouden gave om mij tot rust te brengen. Ik ben blij dat we de afgelopen jaren geen uitdagingen en avonturen uit de weg zijn gegaan en als team samen sterk stonden. Ik kijk uit naar onze toekomst en hoop dat we samen nog heel veel mooie dingen durven te doen!



About the author

Curriculum vitae

Judith Bijlsma was born on May 11th 1994 in Groningen, the Netherlands. After graduating high school with an atheneum diploma in Nature & Health, and Nature & Technology (Maartenscollege, Haren), she enrolled in the Bachelor program Food Technology at Wageningen University in 2012. During her BSc she did a minor about the interaction between Food, Medicine, and the Human Body at Lund University, Sweden. Her BSc degree was completed with a thesis on the polysaccharide architecture in the carrot cell wall at the laboratory of Food Chemistry. In 2015 she continued her Master studies in Food Technology at Wageningen University with Ingredient Functionality as her specialisation. Her master thesis at the laboratory of Food Chemistry focused on structure-activity relationships of antibacterial prenylated stilbenoids against methicillin-resistant *S. aureus*. She conducted her MSc internship at the Riddet Institute (Palmerston North, New Zealand), where she developed milk protein-quercetin complexes as a neutral delivery system for improved bioavailability of quercetin. After obtaining her MSc degree (Cum Laude), Judith worked as research and education officer at the laboratory of Food Chemistry for 6 months. After that, she started as PhD candidate at the Laboratory of Food Chemistry under the supervision of Prof. Dr. Jean-Paul Vincken, Dr. Wouter de Bruijn, and Prof. Dr. Krassimir Velikov. This research was performed in the public-private partnership 'IronTech' in collaboration with Unilever Innovation Centre Wageningen B.V., Nouryon Chemicals B.V., Nobian Industrial Chemicals B.V., Utrecht University and the University of Amsterdam. The results of her PhD research are presented in this thesis. Judith continues to work as a postdoctoral researcher at the Laboratory of Food Chemistry.



LinkedIn: www.linkedin.com/in/judithbijlsma

Publications

Judith Bijlsma, Péter Buglyó, Etelka Farkas, Krassimir P. Velikov, Jean-Paul Vincken & Wouter J.C. de Bruijn. Interaction of iron(III) with taste enhancers: Potential of Fe(III) salts with inosine monophosphate or guanosine monophosphate for food fortification. *LWT - Food Science and Technology*. 2023, 184: 115024. DOI: 10.1016/j.lwt.2023.115024

Judith Bijlsma, Wouter J.C. de Bruijn, Jamie Koppelaar, Mark G. Sanders, Krassimir P. Velikov, & Jean-Paul Vincken. Interactions of natural flavones with iron are affected by 7-O-glycosylation, but not by additional 6"-O-acylation. *ACS Food Science & Technology*. 2023, 3: 1111-1121. DOI: 10.1021/acsfoodscitech.3c00112

Judith Bijlsma¹, Neshat Moslehi¹, Wouter J.C. de Bruijn, Krassimir P. Velikov, Willem K. Kegel & Jean-Paul Vincken. Reactivity of Fe(III)-containing pyrophosphate salts with phenolics: complexation, oxidation, and surface interaction. *Food Chemistry*. 2023, 407: 135156. DOI: 10.1016/j.foodchem.2022.135156

Luana Malacaria¹, **Judith Bijlsma**¹, Roelant Hilgers, Wouter J.C. de Bruijn, Jean-Paul Vincken, Emilia Furia. Insights into the complexation and oxidation of quercetin and luteolin in aqueous solutions in presence of selected metal cations. *Journal of Molecular Liquids*. 2023, 369: 120840. DOI : 10.1016/j.molliq.2022.120840

Roelant Hilgers, **Judith Bijlsma**, Luana Malacaria, Wouter J.C. de Bruijn, Emilia Furia, Jean-Paul Vincken. Transition metal cations catalyze ¹⁶O/¹⁸O exchange of catechol motifs with H₂¹⁸O. *Organic & Biomolecular Chemistry*. 2022, 20: 9093-9097. DOI: 10.1039/D2OB01884E

Neshat Moslehi¹, **Judith Bijlsma**¹, Wouter J.C. de Bruijn, Krassimir P. Velikov, Jean-Paul Vincken & Willem K. Kegel. Design and characterization of Ca-Fe(III) pyrophosphate salts with tunable pH-dependent solubility for dual-fortification of foods. *Journal of Functional Foods*. 2022, 92: 105066. DOI: 10.1016/j.jff.2022.105066

Judith Bijlsma, Wouter J.C. de Bruijn, Krassimir P. Velikov & Jean-Paul Vincken. Unravelling discolouration caused by iron-flavonoid interactions: complexation, oxidation, and formation of networks. *Food Chemistry*. 2022, 370: 131292. DOI: 10.1016/j.foodchem.2021.131292

Judith Bijlsma, Wouter J.C. de Bruijn, Jos A. Hageman, Peter Goos, Krassimir P. Velikov & Jean-Paul Vincken. Revealing the main factors and two-way interactions contributing to food discolouration caused by iron-catechol complexation. *Scientific Reports*. 2020, 10: 8288. DOI: 10.1038/s41598-020-65171-1

¹These authors contributed equally to this work.



Wouter J.C. de Bruijn, Carla Araya-Cloutier, **Judith Bijlsma**, Anne de Swart, Mark G. Sanders, Pieter de Waard, Harry Gruppen & Jean-Paul Vincken. Antibacterial prenylated stilbenoids from peanut (*Arachis hypogaea*). *Phytochemistry letters*. 2018, 28: 13-18. DOI: 10.1016/j.phytol.2018.09.004

Patents

Provisional patent application (23153405.8), filed at the European Patent Office on 26 January 2023. "Mineral-fortified food product". Inventors: **Judith Bijlsma**, Wouter J.C. de Bruijn, Krassimir P. Velikov, Jean-Paul Vincken. Applicant: Unilever IP Holdings B.V.

Patent application (WO 2022/048952 A1) (10 March 2022). "Iron-fortified food product". Inventors: **Judith Bijlsma**, Willem K. Kegel, Neshat Moslehi & Krassimir P. Velikov. Applicant: Unilever IP Holdings B.V.

Overview of completed training activities

Discipline specific activities	
Courses	
Chemometrics	VLAG, Wageningen, 2019
Advanced Organic Chemistry	VLAG, ORC, Wageningen, 2021-2022
Conferences & Symposia	
International Symposium on Metal Complexes	University of Debrecen, Hungary, 2019
CHAINS, the Dutch Chemistry Conference	NWO, Veldhoven, 2019
Wageningen Food Symposium	VLAG, Wageningen, 2020
Micronutrient Forum 5 th Global Conference CONNECTED	Micronutrient Forum, Online, 2020
CHAINS, the Dutch Chemistry Conference	NWO, Online, 2020
International Symposium on Metal Complexes	University of Białystok, Online, 2021
International Conference on Polyphenols ^a	Natural Chemistry Research Group Turku, Groupe Polyphenol, Online, 2021
Edible Soft Matter Workshop & Conference ^a	Wageningen University & Research, 2022
CHAINS, the Dutch Chemistry Conference ^a	NWO, Veldhoven, 2022
International Conference on Polyphenols ^b	INRAE Institute, BIA Research Unit, Groupe Polyphenol, Nantes, France, 2023
General courses	
VLAG PhD Week	VLAG, Baarlo, 2019
Project and Time Management	WGS, Wageningen 2019
Introduction to R	VLAG, Wageningen, 2019
Competence Assessment	WGS, Wageningen, 2019
Brain Friendly Working and Writing	WGS, Wageningen, 2020
Scientific Writing	Wageningen in'to Languages, Wageningen, 2021
Career Perspectives	WGS, Wageningen, 2022
Optional courses and activities	
Preparation of PhD research proposal	FCH, Wageningen, 2018
Food Chemistry PhD trip ^a	FCH, Italy and Austria, 2018
Food Chemistry PhD trip ^{a,b,c}	FCH, the Netherlands, 2021
BSc and MSc thesis student supervision, presentations and colloquia	FCH, Wageningen, 2018-2022
PhD presentations	FCH, Wageningen, 2018-2022
PhytoActive meetings	FCH, Wageningen, 2018-2022
IronTech project meetings ^b	UICW, Nouryon, Nobian, UU, UvA, WUR, 2018-2022

^a Poster presentation. ^b Oral presentation. ^c Organising committee

Abbreviations: FCH, Laboratory of Food Chemistry, Wageningen University; VLAG, Graduate School (Biobased, Biomolecular, Chemical, Food and Nutrition Sciences); ORC, Laboratory of Organic Chemistry; UICW, Unilever Innovation Centre Wageningen B.V.; UU, Utrecht University; UvA, University of Amsterdam; WGS, Wageningen Graduate Schools.

*Success is a mixture of having a flair
for the thing that you are doing;
knowing that it is not enough,
that you have got to have hard work
and a certain sense of purpose.*

Margaret Thatcher

The work described in this thesis was performed at the Laboratory of Food Chemistry, Wageningen University & Research, the Netherlands. This work was performed in the public-private partnership "IRONTECH" and was financed by participating industrial partners Unilever Innovation Centre Wageningen B.V., Nouryon Chemicals B.V., Nobian B.V., and allowances of The Netherlands Organization for Scientific Research (NWO) in the framework of the Innovation Fund for Chemistry and from the Ministry of Economic Affairs in the framework of the "TKI/PPS-Toeslagregeling" (Grant 731017205).

Financial support from Wageningen University for printing this thesis is gratefully acknowledged.

Copyright © **Judith Bijlsma**, 2023. All rights reserved. No part of this publication may be reproduced or transmitted in any form or by any means without permission from the author.

Cover artwork by Floor ter Haar (Instagram: @floorninetyfour)

Layout and design: Judith Bijlsma

Printed by ProefschriftMaken, the Netherlands, on FSC-certified paper

Edition: 150 copies